RELEVANCE OF FRACTURE MECHANICS TO CREEP CRACK GROWTH

by

Kamran Mohammad-Pour Nikbin, B.Sc.(Eng.)

December 1976

A thesis submitted for the degree of Doctor of Philosophy of the University of London and for the Diploma of Imperial College

Mechanical Engineering Department
Imperial College
LONDON, S.W 7. 2AZ

Acknowledgments

I am grateful for the facilities provided at Imperial College to carry out this work and extend my deepest appreciation to Professor C.E Turner and Dr. G.A. Webster for all their help and useful advice.

I would also like to thank the staff at the computer centre and the technical staff in particular Mr. D.K. Willis for all their assistance.

ABSTRACT

The integrity of components containing crack like defects at high temperatures has been under close scrutiny in recent years. Many authors have tried, with varying degrees of success, to use fracture mechanics as a tool to describe the creep crack growth behaviour in laboratory test-pieces. Many have claimed that creep crack growth rate å can be expressed in terms of the stress intensity factor K in the form

$$\mathring{a} = AK^m$$

whereas others claim better correlations with the net section stress, σ_{net}, remaining on the uncracked ligament or with a reference stress concept. It is found generally that creep fracture ranges from a creep brittle to a creep ductile mode. The present work assesses the significance of a defect in a particular situation in terms of the creep properties of the material, specimen geometry, physical size, and the extent of constraint.

In reviewing the work on uniaxial data it is shown that creep failure in uniaxial tests is nucleation controlled rather than due to creep crack propagation and therefore it is expected that creep fracture will behave differently in geometries containing a dominant crack. Extensive cracking tests were carried out on an aluminium alloy (RR58) (in the temperature range of 100° - 200°C) and a heat treated bainitic $\frac{1}{2}$Cr - $\frac{1}{2}$Mo - $\frac{1}{4}$V steel (at 565, and 615°C) using various geometries and test conditions. The results of over a hundred tests were analysed with the aid of a computer

and the data were correlated with various fracture mechanics parameters. The stress intensity factor K fails to describe crack growth rate with increase in material ductility and reduction in specimen thickness and also shows a distinct geometry dependence.

Due to the non-linear effects in creep it may be expected that an extension of the J contour integral could be used to describe the crack tip behaviour. An energy rate line integral C* is described and an analytical derivation presented for the DCB assuming creep strains are dominant in the specimens. The displacement at the loading pin measured during each test showed that both elastic and creep strains were incorporated at the crack tip and that the extent of these were both material and geometry dependent. Using experimental displacement rate $\dot{\Delta}$ an approximate experimental method is put forward to evaluate a total C^*_T incorporating both the elastic and creep strains giving

$$C^*_T = \frac{1}{B_n} \frac{dw^*}{da} = \frac{\eta P \dot{\Delta}}{a B_n}$$

The data correlated with C^*_T show no geometry dependence and is shown to describe creep crack growth rate over a range of creep ductilities.

INDEX

Chapter 1		Page
1.1	Concepts of Fracture Mechanics	1
1.2.1	The Griffith Concept	2
1.2.2	Introduction of Non-linear effects to the elastic concept	4
1.3	Yielding Fracture mechanics	9
1.3.1	Crack Opening Displacement (C.O.D.)	9
1.3.2	The J Contour Integral	11
1.4.1	Stable Crack Growth	15
1.4.2	Slow crack growth due to stress corrosion, fatigue and creep	16
Chapter 2		
2.1.1	Phenomenon of Creep	19
2.1.2	Equation for Creep	20
2.1.3	Stress dependence of a steady state creep rate	21
2.1.4	The temperature dependence of a steady state creep rate	21
2.1.5	Specific Creep Theories	22
2.2.1	Creep fracture of Uniaxial tests	24
2.2.2	Correlation of time to rupture	24
2.2.3	Theories of rupture related to the Uniaxial creep tests	26
2.2.4	Kachanov's Brittle rupture Theory	27
2.2.5	Theories of rupture related to the nucleation and growth of cavities	30
2.2.6	Parametric approach to creep damage	33
Chapter 3		
3	Relevance of Fracture mechanics to Creep Crack growth (C.C.G.)	36
3.1	Introduction	36

		Page
3.1.1	Specimen Geometries used in high temperature crack growth tests	36
3.1.2	Specimen Side grooving	38
3.1.3	Methods of Crack measurement	39
3.2.1	Application of stress intensity factor K to creep crack growth	41
3.3.1	Correlation of Creep Crack growth rate with Net section stress	47
3.4.1	Application of Non-linear Fracture Mechanics to creep cracking	49
3.4.2	Recent models to creep crack initiation and growth	54
3.4.3	Use of C.O.D. as a parameter	55
3.4.4	The Use of C* as the Correlating parameter	57
3.4.5	The Theoretical method of evaluating C* for the DCB Test-piece	61
Chapter 4		
4.1	Choice of Materials, Heat treatment and Geometries	65
4.1.1	Material Selection	65
4.1.2	Heat Treatment prior creep cracking tests	66
4.1.3	Specimen geometries	67
4.2.1	Description of the apparatus	68
4.3.1	Experimental Procedure	72
4.3.2	Crack tip preparation prior testing	73
4.3.3	Uniaxial Creep tests	74
4.3.4	Metallurgical Investigations	74
4.4	Derivation of experimental and theoretical formulae used to evaluate the stress intensity factor K for different geometries	74
4.4.1	Experimental evaluation of K	74
4.4.2	Theoretical evaluation of K	76

Page

Chapter 5

5.1 Experimental Results 79

5.1.1 Results and Analysis of the Uniaxial Creep deformation tests 79

5.2.1 Results of the Creep Cracking tests obtained from Different Geometries, Thicknesses and Side grooving 84

5.2.2 The general trends of the experimental graphs 87

5.2.3 The shape of the DCB-C graphs 87

5.2.4 The shape of the DCB-P graphs 89

5.2.5 The shape of the DT graphs 90

5.2.5 The shape of the CT graphs 90

5.2.6 Constant C* (Analytical) tests performed on DCB-C test-pieces 91

5.2.7 The effect of load change on crack growth of different geometries 92

5.2.8 The effect of temperature on crack growth 94

5.2.9 The Relationship between transducer Displacement and crack growth 95

5.2.10 Creep Deformation tests using the DCB-C geometries 99

5.3.1 Metallurgical Observations 101

5.3.2 Fracture Surfaces of RR58 and Steel 101

5.3.3 The effect of geometry on the mode of fracture 104

5.3.4 Hardness Measurements 106

Chapter 6

6.1 Correlation of Creep crack growth data with various fracture mechanics parameters 109

6.1.1 Correlation of the data with the L.E.F.M. Parameter K 110

6.1.2 Individual trends of cracking rate versus K for each test-piece 110

		Page
6.1.3	The effect of Heat treatment, Thickness, and side grooving on the crack growth rate of the DCB test-piece	115
6.1.4	The Effect of Different geometries on the crack growth rate of RR58, and steel	117
6.1.5	The Effect of temperature on the creep cracking rate	120
6.2.1	Correlation of creep cracking with a non-linear fracture mechanics parameter	121
6.2.2	Proposal for an experimental evaluation of C^*_T to correlate the creep crack growth data	123
Chapter 7		
7.1	Conclusions	131
7.2	Further Work	135
Appendix		137
References		139
Tables 1 - 5		146
Figures 1 - 145		182
LIST OF PUBLISHED PAPERS		313.

SYMBOLS AND NOTATION

a	crack length
$\dot{a}$	crack growth rate
B	thickness
B_n	net thickness after sidegrooving
C	compliance
C^*	energy rate line integral
E	Young's modulus
G	energy release rate or crack extension force
G_c	critical value of G
i,j	subscripts in cartesian tensor notation
J	value of Rice's contour integral
J_{Ic}	critical value of J
K	stress intensity factor
K_I K_{II} K_{III}	stress intensity factors for three loading modes
K_{IC}	critical value of K for mode I (plane strain stress intensity factor)
K_{ICC}	critical value of K required to propagate a creep crack
m	yield ratio for a crack body
P	load
P_L	limit load
Q	activation energy for creep
r	radial distance (polar co-ordinate)
r_y	radius of plastic zone
R	gas constant
t	time
t_R	time to rupture
T_m	melting point in degrees absolute

u	displacement at the crack tip
U	stored strain energy density
U^*	stored strain energy density rate
v	displacement at loading pin ($2v = \Delta$)
w	total potential work
w^*	total potential work rate
W	strain energy density
X, Y, Z	Cartiesian co-ordinates
η	crack length factor (dependent on the geometry)
δ	crack opening displacement C.O.D.
Δ	total transducer displacement
$\dot{\Delta}$	total transducer displacement rate
Δ_e	elastic transducer displacement
Δ_{cr}	creep transducer displacement
$\dot{\Delta}_e$	elastic transducer displacement rate
$\dot{\Delta}_{cr}$	creep transducer displacement rate
ϵ	creep strain
$\dot{\epsilon}$	creep strain rate
$\dot{\epsilon}_s$	secondary creep rate
ω	creep damage factor
γ	surface energy
ν	Poisson's ratio
σ	applied stress
σ_{net}	net section stress
σ_{ref}	reference stress

σ_y	yield stress
τ	shear stress
λ	P/P_L
C.C.G.	creep crack growth
C.O.D.	crack opening displacement
L.E.F.M.	linear elastic fracture mechanics
DCB-C	contoured double cantilever beam
DCB-P	parallel edge double cantilever beam
DT	double torsion
CT	compact tension
SEN	single edge notch

CHAPTER 1

1.1. THE CONCEPTS OF FRACTURE MECHANICS

The basic principle of fracture mechanics is the analysis of the rupture of cohesive atomic bonding using the general laws of continuum mechanics and the physical macroscopic properties of the material. The prediction of fracture behaviour in laboratory test pieces through theoretical analysis is essential if the final objective is the establishment of improved design codes for complex engineering structures subjected to various forms of stress and environmental attacks.

Although the microscopic properties of the material will determine the nature of atomic separation by means of cleavage, shear void growth, fracture mechanics will describe quantitatively the macroscopic behaviour of the material fracture in terms of universal parameters. Continuum mechanics analysis presupposes the existence of a crack within a homogenous and isotropic material. Irrespective of the mode of cracking and the extent of deformation, the techniques of fracture mechanics provide boundary conditions for the regions in which the fracture processes are taking place and, if the boundary conditions govern the fracture behaviour at the crack tip, it is expected that given various types of geometries and loading conditions the crack tip will effectively show a similar behaviour in all the cases, for the same boundary conditions.

The relevant continuum mechanics parameter to describe the crack tip behaviour will depend on the extent of deformation that occurs with cracking. Ideally, linear elastic concepts would be relevant in cases where there is

no plastic deformation but this approach along with refinements is used consistently to relate to conditions where the degree of deformation, with respect to the absolute size of the crack and geometry, is severely restricted. In cases where extensive deformation and plasticity occur yielding fracture mechanics may become the relevant criterion for fracture. In other words, the relative extent of non-linear deformation in a test piece will determine the selection of the fracture mechanics parameter to describe the crack tip characteristic.

1.2. LINEAR-ELASTIC FRACTURE MECHANICS

1.2.1. The Griffith Concept

The original work by Griffith (1) in 1921 laid the basis for the present concepts of linear elastic fracture mechanics (L.E.F.M.). By using the elastic analysis of the stress field around an elliptical hole, developed earlier by Inglis (2), he argued that macroscopicly homogenous materials will contain inherent flaws which enable the ideal theoretical fracture strength of the solid to be overcome in small localized regions of the sample. Griffith used an energy balance criterion to suggest that the strain energy stored in a body decreased with the increase in crack length i.e. the elastic energy released was equal to or greater than the energy absorbed by crack propagation. In fact this is a statement of the first law of thermodynamics describing a system in equilibrium.

In explaining the fracture behaviour of glass he (1) found the difference in strain energy between a cracked plate and an uncracked plate, both having the same loading

conditions. The difference between this strain energy U_E and the energy absorbed by forming the cracked surface U_S was then differentiated to give the equilibrium condition, hence:

$$U_E = - \frac{\pi a^2 B \sigma^2}{E} \qquad (1.1)$$

$$U_S = 4 a B \gamma \qquad (1.2)$$

where 2a is the crack length, B is the plate thickness, γ is the surface energy, E is the elastic modulus and σ is the remotely applied stress normal to the crack plane.

Thus for an increase δa in the crack length the requirements for unstable equilibrium, i.e. no change in the net energy U of the system with an incremental increase in crack length, is given by:

$$\frac{\delta U}{\delta a} = \frac{\delta (U_E + U_S)}{\delta a} = 0 \qquad (1.3)$$

Substituting (1.1) and (1.2) in (1.3) gives:

$$\frac{\delta U}{\delta a} = - \frac{2\pi a \sigma^2}{E} + 4\gamma = 0 \qquad (1.4)$$

which gives a critical remote stress for fracture σ_F as:

$$\sigma_F = \sqrt{\frac{2\gamma E}{\pi a}} \qquad (1.4)$$

or more appropriately

$$\sigma_F \geqslant \sqrt{\frac{2\gamma E}{\pi a}} \simeq \sqrt{\frac{E\gamma}{a}} \qquad (1.5)$$

which predicts the fracture load for a particular crack length.

This classical expression obtained specifically for brittle solids can be taken as a starting point in relating L.E.F.M. to the more practical cases.

The rate of release of strain energy with increasing crack length was expressed by Irwin and Kies (7) as the crack extension force G and the critical value of G_c for fracture of a centre cracked infinite plate figure (1) subjected to a remote stress of σ is given by:

$$\frac{\delta U_E}{\delta a} = G_c = \frac{2\pi\ a\ \sigma^2}{E'} \qquad (1.6)$$

where, $E' = E$ for plane stress

$$E' = \frac{E}{1 - \nu^2} \quad \text{for plane strain}$$

Figure (2) shows a graphical description of the Griffith energy balance, a_o is the critical crack length below which work, by way of remote loading, must be put into the system and above which catastrophic fracture will occur.

However, the basic problem is that engineering materials do not act in such an ideal elastic manner. Where the Griffith Theory concerns itself with the surface energy, in real material there are many contributions to the total energy loss in terms of heat, sound, the kinetic energy of the moving crack and the energy of plastic deformation. In engineering materials there is rarely a case of an ideal brittle fracture and this to a great extent is the major restriction in the use of L.E.F.M.

1.2.2. Introduction of Non-linear effects to the elastic Concept

Irwin et. al. (3) and Orowan (4,5) suggested modifications to the basic Griffith Theory and allowed for work done on

the system to cause fracture and a limited amount of plastic deformation, changing the basic Griffith formula for a centre cracked plate to:

$$\sigma = \left[\frac{E(2\gamma + p)}{\pi a}\right]^{\frac{1}{2}} \qquad (1.7)$$

where p is the work of plastic deformation at the crack tip. In fact Orowan (6) noted that the energy absorbed by plastic distortion is much greater than the energy needed to create a new surface thus changing the previous equation (1.7) to:

$$\sigma = \left[\frac{Ep}{\pi a}\right]^{\frac{1}{2}} \qquad (1.8)$$

where $p >> \gamma$

In quantifying G in terms of real materials, it was argued that provided the plastic zone was small and was contained within a small region with respect to the crack size, fracture would occur at a critical value of G regardless of geometry. Irwin and Kies (7) showed that the value of the strain energy release rate G can be determined experimentally. They did this by making use of results produced by Love (8) relating the stored strain energy density to the applied load.

$$U_e = \frac{P^2 C}{2} \qquad (1.9)$$

where $C = \frac{\Delta}{P}$, is the compliance of the body in terms of a measurable quantity of displacement Δ with respect to a load P at a particular crack length, illustrated in figure (3). From equation (1.9) they (7) developed

$$G = \frac{\partial U}{\partial a} = \frac{P^2}{2B} \cdot \frac{\partial C}{\partial a} \qquad (1.10)$$

where G is the energy release rate for crack extension per limit thickness B.

The experimental procedure is quite general and subsequently a considerable number of tests have been carried out to determine the compliance of common specimen geometries.

Later Irwin (9) continued by analysing the effect of stress level at the crack tip. Since he had previously argued (7) that the criterion for unstable fracture in materials with limited ductility is a critical value of strain energy rate G_c (equation (1.6)) he (9) suggested that this parameter could be made equivalent to another universal parameter, in L.E.F.M., which identifies the stress environment at the crack tip , namely the stress intensity factor K. By making use of the analyses by Westergaard (10), Irwin (9) showed that the stress field ahead of the crack tip in a linear elastic material is characterized by a stress singularity which can be described in general (for the coordinate system in figure (4)) for small values of r as:

$$\begin{bmatrix} \sigma_{xx} \\ \sigma_{yy} \\ \sigma_{xy} \end{bmatrix} = \frac{K \cos\frac{\theta}{2}}{2\pi r} \begin{bmatrix} 1 - \sin\frac{\theta}{2}\sin\frac{3\theta}{2} \\ 1 + \sin\frac{\theta}{2}\sin\frac{3\theta}{2} \\ \sin\frac{\theta}{2}\cos\frac{3\theta}{2} \end{bmatrix} + \left[O(r^0)\right] \quad (1.11)$$

With K being a parameter dependent only on geometry and loading, in general given as

$$K = f(P, \text{geometry})$$

For the case of the central crack of crack length 2a in an infinite plate subjected to a tensile stress σ, K is given by:

$$K = \sigma\sqrt{\pi a}$$

Quantifying the relationship between K and G Irwin (9) went on to show that

$$G = \frac{K^2}{E'} \qquad (1.12)$$

Or more specifically in terms of the different modes of cracking shown in figure (5):

$$G_I = \frac{K_I^2}{E'}$$

$$G_{II} = \frac{K_{II}^2}{E'}$$

$$G_{III} = \frac{K_{III}^2}{E'}$$

where K_I is for the tensile opening mode of fracture K_{II} is the shear mode and K_{III} is the anti-plane mode. Irwin (9) went on to suggest that the criterion for predicting the crack path is that the crack would move along a path normal to the direction of greatest tension so that the component of shear stress resolved on the line of the expected extension of the crack would be zero.

Thus the philosophy of L.E.F.M. was established when the equivalence of G and K was demonstrated. Therefore taking suitably shaped test pieces it was postulated that a critical K_c or G_c existed at the point of fracture independent of the geometry. But it is clearly apparent that in real situations plasticity cannot be avoided. Irwin and Kies (11) found that a relationship existed between the fracture toughness of the material and the plate thickness figure (6). They (11) suggested that below a critical thickness the fracture mode will be mixed and that to describe

a minimum K_C in terms of a cleavage fracture i.e. K_{IC}. The plate thickness B must be greater than a critical value given by:

$$B > 2.5 \left(\frac{K_{IC}}{\sigma_y}\right)^2 \qquad (1.13)$$

where K_{IC} is the plane strain value of K_C and σ_y is yield stress of the material.

For very thin specimens the large plastic zone developed prior to fracture will reduce the crack tip singularity, but with the increase in thickness the bulk of the material inhibits the growth of the plastic zone especially at the centre of the specimen, where essentially the conditions of plane strain prevail. The plastic zone size gradually increases towards the specimen surface suggesting a transition from plane strain to plane stress. The term thick and thin are relative and only the fracture behaviour will determine the prevailing stress conditions. Thus if a plate fails by a shear mode it is described as a thin plate and where cleavage fracture dominates the plate is termed as thick.

Various limits have been set for the validity of L.E.F.M. (12-14) based primarily on two main conditions:

1) The deviation from linear-elastic behaviour must not be greater than 5% from the elastic load-deflection graph of the specimen or structure.

2) The size of the plastic zone must be small compared to the thickness, i.e. plane strain conditions must dominate. Quantitatively (12-13) show:

$$B \geqslant 2.5 \left(\frac{K_{IC}}{\sigma_y}\right)^2$$

$$a \geq 2.5 \left(\frac{K_{IC}}{\sigma_y}\right)^2$$

and from the L.E.F.M. analysis a valid limit of plastic zone size (r_y) can be derived:

$$r_y = \frac{1}{6\pi} \left(\frac{K_I}{\sigma_y}\right)^2 \qquad (1.14)$$

1.3. YIELDING FRACTURE MECHANICS CONCEPTS

The necessary extension to L.E.F.M. is the development of general yielding fracture mechanics. In the literature importance has been laid on two aspects, the crack opening displacement and the crack tip contour integral. Both appear to be related and describe the conditions at the crack tip in terms of a strain controlled parameter.

1.3.1. Crack Opening Displacement (C.O.D.)

The original concepts of C.O.D. were put forward independently by authors (15-17) following Irwin's (9) definition of a plastic zone size for the case of limited plasticity at the crack tip. C.O.D. is defined as the opening separation at the tip of a real crack which has yielded in a plastic zone. The displacement u within an elastic crack may be shown to be

$$2u = \delta = \frac{4K}{E'} \sqrt{\frac{2r}{\pi}} \qquad (1.15)$$

where δ is the C.O.D. near the elastic crack tip and r is the crack length within the coordinate system of figure (4). Now using the general formula for the plastic zone size $r_y = \frac{1}{2\pi} \left(\frac{K}{\sigma_y}\right)^2$ and equation (1.15) a value for C.O.D. at the real crack tip within the equivalent elastic zone can be found.

Hence for the condition of a small plastic zone r_y at the crack tip using equation (1.15) it can be shown that:

$$\delta = \frac{4K}{E'} \sqrt{\frac{2r_y}{\pi}} = \frac{4K^2}{\pi\sigma_y E'} \qquad (1.16)$$

Wells (15) further suggested that the following relationship should be valid between δ and crack extension force G.

$$G = \sigma_y \delta \qquad (1.17)$$

Since in elastic behaviour $K^2 = E'G$, Wells (15) also suggested that given constant conditions it would be reasonable to expect fracture to occur at a critical value of C.O.D.

Dugdale (18) carried out an analysis of the size of the plastic zone extending along the plane of the crack for the model of an infinite plate containing a central crack. He obtained a relationship for the plastic zone size :

$$r_y = a\left\{\sec\left(\frac{\pi\sigma}{2\sigma_y}\right) - 1\right\}$$

A similar model was used by Burdekin and Stone (19), to evaluate the C.O.D. in relation to the applied loading and material constant, giving the relationship:

$$\delta = \frac{8\sigma_y a}{\pi E} \log \sec . \left(\frac{\pi\sigma}{2\sigma_y}\right)$$

which is very similar to the result obtained by Dugdale (18). Bilby et al (20) also obtained comparable results from an analysis in anti-plane strain conditions.

The applicability of these models to experimental data have been examined (19). A certain amount of success

has been achieved up to the region of 0.5% yield strain, but for the range beyond the yield strain no logical patterns can be found to relate to either C.O.D./crack length ratios or the theoretical prediction of C.O.D. models. Nevertheless the experimental observations are used by Harrison et al (21) and Burdekin and Dawes (22) as a basis for a design curve giving a working relationship between the applied stress crack size and C.O.D. for conditions beyond yield.

Attempts have also been made to find a critical C.O.D. at fracture analogous to the L.E.F.M. K_{IC} testing. Testing techniques have been standardized (23) and extensive tests have been carried out at the Welding Institute to examine the effects of different materials, welding processes, as well as geometrical effects on fracture toughness measured by K_I or C.O.D. techniques as appropriate. The results generally indicate the importance that, specimen thickness, initial crack sharpness and test temperature play in affecting the critical C.O.D. value at fracture. Therefore it is clear that there can be no unique one term description of the whole plastic region and that all field values are not identical for the various geometries (24,25). These differences are ascribed to the effects of in-plane constraint which hitherto the concept of C.O.D. has failed to explain.

1.3.2. The J Contour Integral

A theoretical extension of the C.O.D. concept to characterize the crack tip behaviour in an elastic-plastic stress field to complement the L.E.F.M. parameter is the J Contour Integral developed by Rice (26). The existence

of plasticity does not destroy the singularity in stress or strain at tip of a sharp crack but merely redefines it in relation to the degree of work-hardening of the material. By considering the behaviour of a linear or non-linear elastic body containing a crack, Rice (26) developed a useful relationship associated with the change in energy of the body due to crack growth. This relationship is expressed in terms of a path independent line integral. This integral may be regarded as the most general statement of a single parameter describing the crack tip environment and in fact all the other important fracture mechanics parameters such as K and G may be deduced from Rice's J Contour integral.

For the purpose of this work, only a general descriptive explanation of this model is sufficient. Rice considered the variation in potential energy of a non-linear elastic body in which a void grew an amount ΔV introducing a new traction free surface ΔS. He showed that the difference in the potential energy ΔU consisted of two terms:

$$-\Delta U = \int_{\Delta V} W(\epsilon_o)dV - \int_{\Delta S}\left\{\int_{u_o T_o}^{u_f T_f} T_i \, du_i\right\}dx \quad (1.18)$$

where $W(\epsilon_o)$ is the strain energy density given by:

$$W(\epsilon_o) = \int_o^{\epsilon_o} \sigma_{ij}, d\,\epsilon_{ij} \quad (1.19)$$

and $T_i\, du_i$ are the work terms when the surface tractions T_i move through displacements du_i, S is the surface of the body and ΔS the new free surface exposed as the void grows, and on which the original displacements and tractions u_o, T_o change to u_f, T_f respectively with $T_f = 0$ for a free surface

He pointed out that the two terms are the difference between the strain energy in the volume removed and the negative work done in freeing the surface of tractions.

By considering the limits of equation (1.18) for infinitessimal extension in two dimensional bodies Rice derived the rate of change of potential energy with void growth. For the case of a crack this was found, as illustrated in figure (7), to be

$$-\frac{dU}{da} = \int_{\Gamma} W dy - T_i \frac{du_i}{dx} dS \qquad (1.20)$$

where Γ is any continuous contour surrounding the crack tip starting from the lower crack face and proceeding in an anti-clockwise sense to terminate at the upper crack face.

Hence for a general interpretation of the path independent integral the symbol J is used to give

$$J = -\frac{dU}{da} \qquad (1.21)$$

where for a linear elastic body $-\frac{dU}{da}$ is identical to G the strain energy release rate, giving J = G for the L.E.F.M. case. In the analysis elastic (linear or non-linear) behaviour is assumed and a strain energy function W is taken as a single valued function of strain. Thus materials following a total (deformation) theory of plasticity with no unloading would give the same results as non-linear elasticity. In essence, in the unloading of the elastic body, be it linear or non linear-elastic, the line retraces the loading line, which means that the potential energy U evaluated from the loading process remains available for further work (figure (9a)). Whereas for the unloading of the non-linear plastic case the line follows the elastic loading line which means that the energy term evaluated would

not represent energy available for further work, since most of it has been absorbed in plastic work during loading (figure (9b)).

For a monotonic process i.e. no unloading, a pseudo-compliance interpretation of J can be considered for both elastic and the plastic circumstance. The total work done w on a size of crack of length a and a similar loading process on another test piece with a slightly longer crack length will give an energetic interpretation of $J = \frac{\partial w}{\partial a}$. This term does not result from the increase of the crack length whilst holding the load and does not equal the potential energy release rate $\frac{\partial U}{\partial a}$, except for the elastic circumstance. It is merely the difference in energy input to the successively longer crack under monotonic loading which may possibly be used as a measure of the damage done to the crack tip region and hence a characterizing term. This method is clearly illustrated in figure (8) both for the case of constant load and constant displacement rate.

Using the compliance technique attempts have been made by Begley and Lanes (27) and Landes and Begley (27) to measure a J_{IC} value for fracture. They conclude that the J integral is an average measure of the near tip stress-strain environment of cracked elastic-plastic bodies and that (27) failure occurred at a critical value of J, termed J_{IC} to denote a critical plane strain value. It is unwise to draw a clear conclusion from the limited data available and only extensive fracture tests will help to justify the eventual acceptance of J_{IC} as a fracture mechanics correlating parameter.

1.4.1. Stable Crack Growth

The success with which fracture mechanics has been used to relate the final fracture event in a flawed structure is terms of the applied stress and flaw size, has led to attempts to empirically characterize slow crack growth rate by the same methods. Initiation and controlled crack growth are two important events that may occur before a catastrophic fracture of a structure. These effects are found to occur in two distinct circumstances. Firstly, initiation and crack propagation are found to occur, prior to rapid failure in fracture toughness test, in materials and geometries which exhibit an increasing amount of plastic deformation at the crack tip. In the second circumstance, which may be of more practical importance, is when external factors help to create and propagate the crack at stresses which are well below the fracture stresses of the material.

The consideration of energy changes occurring in a cracked body during incremental crack growth can be described in the elastic body simply by the energy balance criteria proposed by Griffith (1) and later developed by Irwin (9). More recently the problem has been treated more rigorously by Rice (29) and Cherapanov (30) which is fundamentally in agreement with the basic principles of (1,9). Experimentally crack propagation in an elastic body can therefore be defined with respect to the elastic compliance of the structure and hence the stress intensity factor K.

The plasticity analysis of growing cracks is more complex and much less developed. The non-reversible deformation occurring at the crack tip suggests that a one parameter

description of the crack tip field may not be possible (24). The use of experimental C.O.D. and the energy interpretation of the J contour integral (27,28) gives the most promising opening to experimentally determine emperical values which may be useful to design against crack propagation in an elastic body. Analytically only a few contiuum plasticity solutions for growing cracks have been developed (31-33) all using an anti-plane strain (mode III) elastic-plastic model. McClintock (34) has also obtained solutions for plane strain crack advance in rigid-plastic material by methods of slip line field theory, but only Rice (32) has analysed the nature of the crack tip strain singularity under conditions of steady state crack advance in an elastic-plastic case. Essentially these analysis are not precise but serve, for the present, to reveal the important features of the problem.

1.4.2. Slow Crack Growth due to Stress Corrosion, Fatigue and Creep

The problems of stress corrosion, and fatigue crack growth have received considerable attention. A full review of the current findings are given by Knott (38).

The most widely accepted fracture mechanics parameter that has been used to correlate the results is the stress intensity factor K, hence the general assumption being that controlled crack growth will predominantly occur in a brittle manner. If these failures occur at stresses well below the yield stress the use of L.E.F.M. is acceptable, therefore it is expected that the high cycle low stress fatigue at room temperature will give a better correlation with K. Paris and Erdogan (35) in reviewing this work found that generally

$$\frac{da}{dN} = C(\Delta K)^n$$

where ΔK is the range of stress intensity factor, C and n are material constants, a is the crack length and N is the number of cycles. For low-cycle high stress fatigue test the above equation may not hold and the most recent work by Dowling (36) and Mowbray (37) have extended with some success the correlation of the low cycle fatigue data by using the energy interpretation of the J contour integral in non-linear fracture mechanics.

Crack growth in an inert environment has been observed under plane stress conditions (39) and mixed plane strain conditions (40). This contrasts with the environmentally induced crack which occurs mainly under plane strain. Landes and Wei (41) testing AISI 4340 steel found sustained crack growth at room temperature (20°C) to 140°C in a chemically inert environment (dehumidified argon). They concluded that the calculated thermal activation energies for these tests were in the range of creep activation energies.

In recent years considerable attention has been placed on the slow creep crack gorwth behaviour of engineering materials. Initially it was assumed that the L.E.F.M. concepts would be sufficient to correlate the laboratory results. Creep fracture being predominantly intergranular, it was expected that fracture would occur in a quasi-brittle manner. The relative effect of L.E.F.M. concepts on a time-dependent process of creep crack growth will be discussed fully in chapter three, but from the general observation of the literature on this subject it seems that the complex interaction of non-recoverable creep deformation with crack propagation needs a non-linear fracture mechanics approach.

A possible problem in the use of plasticity solutions for a time dependent creep crack growth is the difficulty in defining the creep yield stress, therefore basic assumptions will be needed to relate the creep deformation to plasticity concepts. These will be discussed in chapter three section (4.4.3).

CHAPTER 2

2. CREEP DEFORMATION AND RUPTURE OF METALS

2.1.1. Phenomenon of Creep

When a static tensile force is applied to a solid, the atomic lattice will accordingly adjust itself to oppose the applied force in order to maintain equilibrium. Depending on the circumstances and the intrinsic material behaviour this adjustment will either be observed as deformation when the atomic lattice remains macroscopically continuous or as fracture when the metal is pulled apart. Therefore the measurement of displacement in time will determine the deformation characteristics and this value is converted into a dimensionless quantity called the strain (ϵ). The response of the strain to the applied stress varies with the magnitude of stress, temperature and strain rate. Figure (10) shows an idealized creep curve showing the effect of creep strain with time. This involves three main regions. In region (1), known as the primary region, the continual decrease in the creep strain rate represents a period of work-hardening in the material. In the secondary region, which exhibits a constant rate of deformation, a balance is reached between the thermal activation process to deform the material and the work-hardening processes at the atomistic level. Region (3) is associated with a period of acceleratd creep rate, called tertiary creep, resulting in the final fracture of the metal. The cause of fracture is directly related to the growth and coalescence of cavities which were initiated in the secondary region.

2.1.2. Equations for Creep

Creep-time relation

A simple way of describing the creep deformation in terms of the infuencing factors is given by the equations:-

$$\epsilon_C = f(\sigma, t, T) \qquad (2.1)$$

where ϵ_C is the creep strain, t is time, σ is stress, and T is the temperature. Each stage of the creep process can be described effectively by an extension of equation (2.1).

For example the primary region can be described in two principle forms:-

$$\epsilon = \alpha \ln t + C \qquad (2.2)$$

$$\epsilon = \epsilon_o + \beta t^q \qquad (2.3)$$

where α, β, C, and q are all material constants and ϵ_o is the elastic loading strain. Equation (2.2), known as logarithmic creep, describes a continually decreasing creep rate found at low temperatures (T) for $\left(\frac{T}{T_m} < 0.3\right.$ of the melting temperature (T_m) of the material), and also at low stresses. For the secondary creep a linear term is added and the strain-time function becomes:-

$$\epsilon = \epsilon_o + \beta t^q + \dot{\epsilon}_s t \qquad (2.4)$$

where $\dot{\epsilon}$ is the secondary creep rate. Within certain limitations, these two relations satisfy experimental results. An equation which has been found to satisfy a wide range of deformation rates is of the form:

$$\epsilon = \epsilon_o + \epsilon_t(1 - e^{-rt}) + \dot{\epsilon}_s t \qquad (2.5)$$

where ϵ_t is the limiting transient creep strain, r is the ratio of transient creep rate to the transient creep strain. Equation (2.5) is called the 'exponential creep'. Further

refinements of the creep time equation are given by Kennedy (42) Garofalo (43). Kennedy (42) suggests that by choosing idealized mechanisms to represent the basic material it is often possible to derive many of these line functions.

2.1.3. Stress Dependence of a Steady State Creep Rate

In the recovery creep range the secondary creep rate is extremely stress sensitive for most metals. The basic and the most commonly used function suggested by Norton (44) is in the form of a power law:

$$\dot{\epsilon}_s = C\,\sigma^n \qquad (2.6)$$

where C and n are material constants independent of stress. A full summary of the other forms of stress function are given by (42,45). Garofalo (43), in conclusion notes that the range of the exponent n for anealed metals and alloys is around 1 - 7. These values are the most common for simple materials, but n values of as high as 20 are not uncommon for engineering alloys.

Equation (2.6) is the most commonly used stress function and as Penny and Marriot (45) point out it is the simplicity of its application in stress analysis that has made it acceptable. In some circumstances such as for example at high stresses the power law might not give the best fit but, given the large extent of scatter found in the creep data, equation (2.6) will always give a very good approximation.

2.1.4. The Temperature-Dependence of the Steady State Creep Rate

Experimentally the creep rate of a simple material (single phase) obeys an Arrhenius equation,

$$\dot{\varepsilon} = \dot{\varepsilon}_o \exp. \left[- \frac{\Delta H_C}{RT} \right] \qquad (2.7)$$

where $\dot{\varepsilon}$ is the creep rate, $\dot{\varepsilon}_o$ is the stress dependent constant of the material, ΔH_C is the activation enthalpy for creep, R is the gas constant and T is the absolute temperature. In the recovery controlled creep range (between 0.4 - 0.6 T/T_m) it is found that ΔH_C is independent of stress since in this range the complex processes of dislocation movements and temperature induced diffusion are the rate controlling factors. The applied stress forms a pile up of dislocations which produce a stress build up, the thermal process of diffusion will induce dislocation climb which relaxes the internal stress built up by the dislocations. Equation (2.7) which is fundamental to the thermally controlled processes will give a good quantitative assessment of the data in the recovery creep range.

2.1.5. Specific Creep Theories

In the previous sections the basic dependence of deformation on time, stress and temperature for uniaxial creep tests was discussed. The development of creep theories needs to include varying effects of stress and temperature. It is outside the range of the present work to discuss the unlimited number of theories put forward, many of them predicting widely different results under the same stress histories, but a comparison ot two of the important uniaxial creep theories will be discussed here.

The Time-Hardening and the strain-hardening are the simplest form of creep theories. A combination of these extend the emperical refinements to obtain a better fit to

experimental data. The implication of the Time-Hardening hypothesis is that the only influence on strain rate, besides stress is a time dependent change of the material giving:

$$\dot{\varepsilon} = f(\sigma, t, T)$$

or in a simpler form:

$$\dot{\varepsilon} = f_1(\sigma) \frac{df_2(t)}{dt} f_3(T)$$

whereas the strain hardening theory is based on the assumption that the creep strain is a function of stress temperature and accumulated creep strain ε_c

$$\dot{\varepsilon} = f(\sigma, \varepsilon_c, T)$$

or in the more confined form

$$\dot{\varepsilon} = g_1(\sigma)\, g_2(\varepsilon_c)\, g_3(T)$$

Figure (11) illustrates the differences in the theories. Two creep curves at stresses σ_1 and σ_2 ($\sigma_2 > \sigma_1$) are shown. At the stress σ_1 the load is increased suddenly to σ_2 at point A, ignoring the elastic increase in displacement, Time-Hardening Theory predicts the curve AD will be obtained by shifting the upper curve downwards parallel to itself until C coincides with A, whilst strain-hardening theory predicts the curve AE which will be obtained by shifting the upper curve parallel to itself to the right until B coincides with A. In general strain-hardeing is consistent with a primary form of creep and time-hardening may be associated with recovery and similar time dependent processes

Penny and Marriot (45) have comprehensively analysed a number of other creep theories. In general they conclude that for variable loading none of the theories are totally satisfactory, but in the absence of thermal softening and

metallurgical changes, test results indicate that strain-hardening is the most accurate of the simple theories.

2.2.1. Creep Fracture of Uniaxial Tests

A direct consequence of the primary and secondary stages of creep deformation is the formation of cavities leading to necking and macroscopic fracture during tertiary creep. This fracture may occur at some finite strain which may be as little as 0.1%. Therefore, from a design point of view the possibility of failure due to rupture is often considered to be more important than excessive deflection. For example a steam turbine can be designed to keep its initial shape in service, but the safeguard against creep deformation will not necessarily mean protection against creep fracture. Hence the conventional methods of measuring creep deformation rates to relate to creep theories will be completely unsatisfactory and in some cases even the rupture time and rupture strain data of uniaxial tests cannot be used to adequately describe the fracture of components which are affected by different states of stress and complex creep histories. However, given the extensive amount of uniaxial test data that has been gathered over the years, attempts have been made to correlate the time to rupture data to the applied stress, creep strain, and creep temperature.

2.2.2. Correlation of Time to Rupture

The conventional form of plotting rupture data is log stress against log time to rupture, illustrated in figure (12) for different temperatures ($T_1 > T_2 > T_3$), giving the common relationship at constant temperature:-

$$t_R \propto \frac{1}{\sigma^m} \qquad (2.8)$$

where t_R is the time to rupture and m is a constant. Often

m varies over a range of t_R which may be due to the brittle-ductile transition of the fracture mode. Figure (13) illustrates an idealized log t_R versus log σ graph which shows that at high stress and temperatures and short rupture times the fracture is predominantly ductile and accompanied by large creep strains, whereas at low stresses the tendency is towards a more intergranular quasi-brittle fracture with a smaller amount of creep deformation. Therefore, it appears that a brittle behaviour is governed by the cohesive strength of the grain boundaries and this is seriously affected by both temperature and strain rate. This means that at high temperatures there is a rapid decrease in the grain boundary strength with respect to the grain matrix and at low stresses the reduction in the creep strain rate tends to reduce the extent of creep deformation. Both of these factors will help to produce a quasi-brittle intergranular creep fracture. From equation (2.8) and the relationship $\dot{\epsilon} = C\,\sigma^n$ it can be seen that the following emperical expression holds:

$$t_R \propto \frac{1}{\dot{\epsilon}} \qquad (2.9)$$

Indicating the interrelationship that exists between creep deformation rates, where cavities nucleate and grow, and the tertiary stage of creep when final failure occurs. More extensive time to rupture functions are described in references (43,45), producing better correlation of the experimental data making them more useful in predicting the service life of components. However, the lack of knowledge of the effects of complicated interactions between stress, temperature and rupture life, as well as changes in stress patterns and metallurgical instabilities, such as overaging,

forces the designer to adopt over-conservative safety factors in component design (46,47). Such design procedures may reduce the level of permanent deformation but do not ensure protection from a sudden catastrophic failures of components resulting from a non-homogeneous formation of cavities and their growth at a stress concentration.

2.2.3. Theories of Rupture Related to the Uniaxial Creep Tests

To describe the tertiary process of creep in a quantitative manner, initial emphasis was laid on the mechanics of growth of the microcracks and cavities and their relationship with creep deformation. Robinson (48) proposed a practical solution of estimating life under variable conditions of temperature, but it has since been widely used to deal with varying stress problems (49,50). The life fraction rule is in fact an extension of the strain-hardening principle discussed in section (2.1.5).

The basis of Robinson's life fraction rule is that creep damage under steady conditions is proportional to the fraction of total rupture life under those conditions:

$$D_1 = \frac{t_1}{t_{R_1}} \qquad (2.10)$$

where D_1 is the damage under the condition σ_1, T_1, t_1 is the period spent at σ_1, T_1 and t_{R_1} is the rupture life for σ_1, T_1. If the stress and temperature are changed so that a second period of time t_2 is spent at σ_2 and T_2 then the second amount of damage incurred is

$$D_2 = \frac{t_2}{t_{R_2}} \qquad (2.11)$$

Assuming that the damage resulting from each loading period is independent of all other periods the total damage D for all the periods will be:

$$D = \sum\left(\frac{t_i}{t_{R_i}}\right) = \sum D_i \qquad (2.12)$$

And when D reaches unity rupture occurs putting equation (2.12) in an integral form:

$$\int \frac{dt}{t_R} = 1 \text{ for rupture} \qquad (2.13)$$

The advantage of this method is that it is capable of using steady load rupture data as it exists to-day requiring no knowledge of strain history to predict rupture times under variable conditions.

2.2.4. Kachanov's Brittle Rupture Thoery

Kachanov (52) proposed a phenomenological theory which reflects the deterioration and damage occurring in the tertiary region of creep. For uniaxial tension he suggested the relation of the form:

$$\dot{\epsilon} = f(\sigma,\omega) \;\&\; \dot{\omega} = g(\sigma,\omega) \qquad (2.14)$$

where $\dot{\epsilon}$ is the creep strain rate, ω is a state variable which is in some sense a measure of cracking or damage in the material. By selecting suitable functions of f, and g it is possible to represent the tertiary section of the creep curve and to produce stress-rupture life relations which are consistent with experimental observations. Odquist and Hult (51) showed that Kachanov's low stress rupture theory is consistent with Robinson's life fraction rule.

Kachanov called ω the continuity of the material and

as time passes damage accumulates and reduces the proportion of material available to carry load. If the load is constant the average stress is increased with the amount of damage until eventually continuity is destroyed by rupture. Therefore if a specimen, of initial cross-sectional area of A_o, is subjected to load P the initial stress σ_o is:

$$\sigma_o = \frac{P}{A_o} \qquad (2.15)$$

after a time t the creep damage reduces the cross-sectional area to:

$$A_t = A_o(1 - \omega) \qquad (2.16)$$

so that the stress at time t is:

$$\sigma_t = \frac{P}{A_t} = \frac{\sigma_o}{1 - \omega} \qquad (2.17)$$

To enable the variation of damage with time to be calculated Kachanov assumed that the rate of decrease in material continuity is a function of stress in the following form:

$$\frac{d\omega}{dt} = C\,\sigma_t^{\nu} \qquad (2.18)$$

where C and ν are assumed to be constants:

Substituting from (2.17) and (2.18) a differential equation is obtained:

$$\frac{d\omega}{dt} = C\,\sigma_o^{\nu}\,(1 - \omega)^{-\nu} \qquad (2.19)$$

For an initially damage free area equation (2.19) can be integrated subject to the conditions; $\omega = 0$ at $t = 0$ and $\omega = 1$ at $t = t_R$. Thus it follows that at time t_R:

$$t_R = \frac{1}{C(1 + \nu)\, \sigma_o^{\nu}} \qquad (2.20)$$

which is the relationship that follows the usual log σ versus log t plot. Rabotnov (53) later generalized these consepts to make predictions of creep strain accumulation as well as rupture times assuming negligible primary creep. Penny (47) in reviewing the usefulness of an engineering approach to creep damage, originated by Kachanov (52) and later extended by Rabotnov (53), notes that the approach appears to bear promise in relation to their use in real component operations. Other applications of spinning discs, beams and tubes are discussed by Rabotnov (55), and Odquist (54) has considered the effects of initial plasticity on the damage parameter. It is clear that the inclusion of a damage relationship for use in structural calculations presents no conceptual or computational difficulties in uniaxial stress conditions. So far as multiaxial stress conditions and the influence of stress concentrations are concerned, it is not viable to use the damage concept to define a general description of the problem. The approach is only useful in cases when intensive creep and damage accumulation spread across the structural member and the influence of a crack tip singularity can be neglected. Therefore it is apparent that the analysis of the growth of a major crack due to creep at stress concentrations is of importance and could well be described by a fracture mechanics parameter. The review of this subject will be discussed in chapter three.

2.2.5. Theories of Rupture related to the Nucleation and Growth of Cavities

In the previous section no attempt was made to describe the precise nature of the damage parameter, which plays the role of a hidden state variable in the manner described by Onat (56). However extensive metallurgical and fractographic investigation by metal physicists of the growth mechanism of voids in creep provides the insight to interpret and develop theories which may be suitable for the purpose of structural mechanics. Greenwood et al (57) noted that rupture resulted from the growth and coalescence of voids and grain boundaries. Hull and Rimmer (58) tried to develop a theory in which voids on the grain boundary grow as a result of the diffusion of vacancies along the grain boundary. The rate of growth of the void radius is governed by the magnitude of the stress acting normal to the surface and the surface tension of the voids. If ω is the cross-sectional area of void per unit area then the void growth equation of Hull and Rimmer (58) can be written in the form:

$$\frac{d\omega}{dt} \alpha \left[\frac{\sigma}{1 - \omega} - \frac{\nu}{l} \sqrt{\frac{\pi}{\omega}} \right]$$

where ν is the specific surface energy and l is the void spacing. Since void growth and creep strain occur at comparitively small stresses the effect of the surface tension of the holes is small so that the second term in the damage rate equation may be neglected. In this form the physical theory can be described by the Kachanov's Theory with the damage parameter ω representing the cross-sectional area of voids per unit area. Ratcliffe and

Greenwood (59) eliminated the creep cavitation in magnesium by superimposing a hydrostatic pressure equal in magnitude to the stress under which creep occurs. This indicates that cavity growth depends on a supply of vacancies from grain boundaries approximately perpendicular to the applied stress, hence substantiating the growth mechanism developed by (58). Greenwood (57) further infers that the cavity nucleation at the grain boundaries is predominantly dependent on creep strains and that the growth of these cavities will be due to a diffusion mechanism.

The creep failure has also been described in terms of a wedge crack growth mechanism (60-63). They suggest that cavities nucleate by grain boundary sliding and that final fracture occurs when these wedge cracks at grain boundaries join up in sufficient numbers to reach a critical size. Figure(14a) shows a graphical description of the generation of a wedge-type crack at a grain corner and figure(14b) shows generation of a cavity at a grain boundary ledge. The existence of a second phase particle or voids due to creep diffusion will assist the grain boundary sliding to initiate cavities. Therefore Heald and Williams (64) proposed a model to include both grain boundary sliding process and the vacancy diffusion process (58,65). The number of approximations in the analysis make this method only useful as a qualitative assessment of creep fracture. More recently Weertman (66), Raj and Ashby (67) have proposed similar models for the nucleation and the subsequent growth of these defects.

Lindborg (68) suggested a statistical model for the linking of separately nucleated grain boundary cracks into

large cracks. He derived a relationship which gave the fraction of cracked grains P in terms of the number of microcracks n required for fracture:

$$P = 0.2 \left(\frac{2n}{N}\right)^{\frac{1}{2}}$$

where N is the number of grains. Thus there exists a limiting value of P of 0.2. The details of the linking are complicated and using this method it is not necessary to study the kinetics of the process in detail. The author claims consistency with experimental evidence in predicting the percentage of area that have been cracked due to creep prior to final fracture. Lindborg (69) considered the growth rate of sharp intercrystalline cracks, and suggested that fracture occurred when one of the cracks reached a critical size. It was proposed that this was the "Damage" crack and a suitable measure of the damage concept used in Kachanov's (52) brittle rupture theory. He (69) put forward the relationship:

$$(1 - \omega)^{\nu+1} = e^{-h(1-1)}$$

where ν and h are factors which possibly are material constant for a given temperature. For such a case damage builds up only if the applied stress field is able to cause a crack.

Taplin (70) has suggested that creep fracture would take place when the largest crack is long enough for a Griffith type fracture criterion to be satisfied. He found an approximate value of the fracture toughness of α-brass from the fracture strength and the largest crack length. Söderberg (71) found in fast tensile tests of an austenitic

steel a direct proportionality between the fracture stress and the maximum crack length and suggested that the Griffith-Orowan relation $\sigma\sqrt{a}$ = constant also holds for the slow quasi-brittle fracture in creep tests.

Generally the evidence from the literature shows that after the development of voids and triple point cracks, the final failure occurs by ligament tearing when the U.T.S. of the undamaged material is approached. The amount of creep ductility will determine the extent of stress concentration that builds up at each individual cavity and this stress built up will in turn determine the critical flow size required for final fracture. Brittle creep failures will occur at values well below the U.T.S. but for ductile fractures where there is very little stress intensification at the microcrack, fracture is likely to occur at values near the U.T.S. of the damaged material.

2.2.6. Parametric Approach to Creep Damage

Other methods of predicting deterioration occurring during creep life are by means of density changes and the measurement of the number of cavities found per unit area. Such data are corrleated with stress, strain, time and Kachanov's damage parameter and although they can be subjective in experimental techniques, in a limited sense they can attain satisfactory conclusions. Since such predictions depend on a knowledge of both elongation and rupture and specific void sizes they are unlikely to be of any use for the purpose of extrapolation. An extensive experimental study was carried out by Boettner and Robertson (72) to measure the precise density change in an oxygen-free high conductivity copper, tested at creep temperatures. They

were able to determine the volume of voids per unit weight at four different temperatures and stresses following creep to various strains. Woodford (73) expressed a functional relationship for V the void volume per unit weight:

$$V = f(\epsilon, t, \sigma, T)$$

The equation was determined experimentally with no assumptions on the mechanism of cavity nucleation and growth. He concluded that the number of voids was determined by the amount of strain rather than the time at creep and suggested that the continuous nucleation of cavities may be associated with grain boundary sliding (associated with large creep strains), but that the growth of the cavities was due to a time dependent diffusion process. Hence this denotes that failure is essentially nucleation controlled.

The number of cavities per unit area is a parameter which is also used to predict the fracture life of uniaxial test pieces (74,135). By measuring the number of cavities under an optical microscope, Dyson and Mclean (74) proposed a method of predicting the service life of a component. This is a similar concept to the density measurements by Woodford (73) and can be used as a possible measure of the extent of damage in a material. More recently Dyson et al (75) using a 1 MV electron microscope to measure the cavity density at the grain boundaries of plastically prestrained Nimonic 80A alloy suggested a direct relationship between the cavity density and the effective plastic strain. Creep tests of different levels of prestraining showed that the larger the plastic prestrain and hence the larger the void density,

effectively reduced the creep life by a factor of about 8 suggesting that the fracture life in a uniaxial test is strongly dependent on the nucleation of cavities rather than creep crack growth.

CHAPTER 3

3. RELEVANCE OF FRACTURE MECHANICS TO CREEP CRACK GROWTH

3.1 Introduction

As data have accumulated in recent years, through investigations of crack growth under creep conditions, it has become obvious that various approaches are possible to the interpretation of these results. Attempts to rationalize them (75 - 77, 138) show that as yet there are many differences of opinion about the available methods of data analysis. Success in the correlation of the results is essential if the long term aim of the laboratory investigation is the prediction of the behaviour of engineering materials in service conditions. An intermediate step to this aim would be the correlation of creep crack growth (from here on termed as C.C.G) rate in differing geometries and specimen sizes. The fracture mechanics parameter used to describe the results, can only be accepted as a viable criterion for design if it shows uniformity over a wide spectrum of test variables. In this chapter a comprehensive review of the work done on this subject in recent years will be made by taking into consideration the specimen geometry and size, the fracture mechanics correlating parameters and the differences between the theoretical and the experimental approaches.

3.1.1. Specimen Geometries Used in High Temperature Crack Growth Tests

Listed below and shown in figure (15) are the types of specimen used for high temperature tests. Table (1)

shows a list of authors (79-95) that have undertaken investigation of creep crack growth in the presence of a dominant crack using these test-pieces.

1. Single Edge Notch (Tension) SEN-T.
2. Double Edge Notch (Tension) DEN-T.
3. Centre Crack (Tension) CCT.
4. Compact Tension CT.
5. Wedge Opening Loading WOL.
6. Single Edge Notch (BEND) SEN-B.
7. Double Cantilever Beam: (Parallel edge) DCB-P.
8. (Contoured) DCB-C.
9. Double Torsion DT.

The first six types of specimens have been primarily developed to test the fracture toughness of materials and differ greatly to the last two in terms the length of crack over which a stable range of crack growth can be measured. The typical crack length over which the most number of tests have been done is in the region of $0.4 < \frac{a}{W} < 0.7$ which in terms of the first six specimens shown in figure (15) is not more than 15 mm for a standard 25 mm wide testPiece, whereas, the DCB and the DT specimens of similar thicknesses have a useful crack growth region of around 100 mm. There are also important differences in the nature of the applied stress at the crack tip, varying from simple tension in the first three specimens to a mixture of bending and tension in the CT and WOL and primarily bending in the SEN-B and DCB geometries. The loading of the DT test piece is radically different and it's constant compliance characteristics is such that it allows for the stress intensity factor to be constant at a constant load over the entire depth of the crack. This means that, similar to a DCB-C

testpiece which is especially contoured to achieve a constant compliance independent of crack length, the DT specimens can also be used as constant K specimen. Outwater et al (96) have suggested that the DT is a useful specimen for use as a universal fracture toughness test but as yet, defined by ASTM (97) the DCB and DT testpieces are non-standard for use in valid K_{1C} tests. The contour of the DCB-C specimens used by Kenyon (78) and in the present study were derived by Srawley and Gross (98) and the testpieces were checked experimentally for constant compliance (78), and the variation of the experimental compliance with crack length was found to be within 5%. The instability factor (i.e. increasing compliance with crack length) inherent in all other testpieces is therefore eliminated in the DCB-C and DT specimens.

3.1.2. Specimen Side-Grooving

The extent of side-grooving is an important factor in high temperature C.C.G. tests, since not only does the side-grooving control the crack route along a crack plane perpendicular to the loading axis, but it also helps to provide sufficient constraint to help introduce plane-strain conditions at the crack tip. The amount of side grooving is found to be more important for the DCB and DT geometries, where the tendency is for the crack to deviate and break off the arms of the test-piece. Many of the authors table (1) have not used side-grooving and it is clearly evident from the literature that a small percentage (10 - 20%) of side-grooving will greatly reduce the shear lip formed in creep crack growth tests. The modifications introduced to take into

account the extent of side-grooving has followed the practice suggested by Freed and Kraft (99). They showed that in terms of the stress intensity factor K:

$$K_n = K\left(\frac{B}{B_n}\right)^{\frac{1}{2}} \qquad (3.1)$$

where B and K are the thickness and the actual stress intensity factor for an ungrooved specimen and B_n and K_n are the corresponding values for the grooved specimen.

3.1.3. Methods of Crack Measurement

C.C.G. tests present a problem of measuring the crack length in high temperature envirobments. Usually, except for aluminium, this means attempting to observe a crack covered by oxidation. Therefore direct visual measurements at high temperature is ruled out. There are two main methods available, the first is the potential drop technique which is used almost universally and the second method is the visual observation, through a window in the furnace, of the crack surface coated by a high temperature paint which cracks with the cracking of the specimen. Both methods have their inherent inaccuracies but on the whole they have given consistent results in a majority of tests.

The potential drop technique is ideally suited to the first six test pieces (figure (15)), since the crack length over which the data are collected is generally found to be less than 10 mm. Gilby and Pearson (100) produced a method to relate the length of a crack in a specimen to the change in its electrical resistance. The calibration curve they produced show the importance of the positioning of the potential points with respect to the geometry and the

plane of cracking. Neate (101) testing ferritic steel noted the difficulties encountered by this method. He found that there was an actual potential increase in the early stages of the tests, similar observations were made by Harper (95), both concluding that the reason for this may be due to the shorting of the current between the crack surfaces by oxide wedging. Furthermore Neate (101) suggested that this phenomenon was even more apparent in the brittle steels, suggesting that oxide wedging can be more easily established for smaller deflections. He also indicated that where the crack front is bowed, leading at the centre, the positioning of the current leads will give different values of crack length and only calibration curves for the different lead position will help to reduce the error involved. There is also the added problem of possible resistance changes if metallurgical and structural changes occur due to overaging, or if slight changes occur in the furnace temperature. These factors along with the fact that crack growths have been measured in the region of around 10 mm. or less give rise to some doubts as regards the level of accuracy that authors claim $\pm$ 0.25 mm. (95), $\pm$ 0.05 mm. (85). Therefore keeping in mind that there are inherent scatters existing in any creep related tests, greater care must be taken in accepting the conclusions that are reached through the evaluation of such data.

The second means of crack measurement is the visual observation of the crack, through a window in a furnace, using a telescope. This method has been used successfully by Kenyon (78) and in the present work. It is ideal for

the particular geometries of DCB and DT where the measurable crack growth is in the region of approximately 80 mm. The degree of accuracy ($\pm$ 1.0 mm) claimed is well below the capabilities of a potential drop method but this loss in accuracy is compensated for by the large length of crack growth.

3.2.1. Application of Stress Intensity Factor K to Creep Crack Growth

Several authors shown in table (1) have used the L.E.F.M. concepts to describe C.C.G. by the relationship:

$$\dot{a} = \frac{da}{dt} = AK^m \qquad (3.2)$$

where $\dot{a}$ is the C.C.G. rate, A and m are the material constants for any particular geometry and temperature, and K is the stress intensity factor. This directly infers the major assumption that L.E.F.M. is applicable for high temperature applications.

Robson (83), testing CT and SEN-T specimens of steel of high plain bar rupture ductility (50% and 25%) at 400° - 500°C, concluded that equation (3.2) gives a reasonably good fit and the C.C.G. is not affected by the creep deformation characteristics of the material which in his case was creep ductile. Further he suggested that side-grooving and different forms of crack starter (e.g. fatigue, machine notches) did not affect the C.C.G. rate significantly. He also found a wide range of scatter in the experimental data (similar observation made later by others (76,86)). Thornton (84) testing three types of Cr-Mo-V steels in cast and wrought conditions at 565°C

also found correlations of his data with K, for SEN-B test-pieces, but only showed results from a single specimen. James (82) working on 316 steel in 20% cold worked condition at 538°C used CT and CCP test-pieces, claimed a good fit of equation (3.2). None of these results mentioned above can be conclusive proof that the rate controlling parameter for C.C.G. is the stress intensity factor K, since over limited ranges of stress intensity, cracking rate and specimen geometries it would be comparatively simple to achieve some form of correlation of the data.

Neate and Siverns (88) and later Neate (91) using various geometries of different sizes of two types of low alloy steel with various heat treatments, attempted to distinguish between the creep brittle and creep ductile modes of fracture. Materials with rupture ductilities of 2% - 30% and grain sizes of 600 - 30 μm were tested. The bainitic heat treatment simulating heat affected zone (H.A.Z.) material adjacent to welds gave a range of large grains and lowest rupture ductilities and the normalized and tempered specimens had a grain size of around 30μm and the highest creep ductility. For both the heat treatments the correlation of cracking rate with K showed a scatter factor of 15, figure (16,17), with the bainitic material having approximately ten times the cracking rate of the ferritic steel. They (88) also compared the data in terms of the net-section stress and found that there was little improvement in the scatter. They concluded that the extrapolation of the data should not be for more than a decade and that crack growth rate data for very low values

of stress intensities are required in order to relate them to real service environment and conditions. This is a fallacy since at the normal service stress intensities, which are usually less than 10-15 $MPa.m^{\frac{1}{2}}$, the problem is not one of crack growth, rather one of creep crack initiation. The vital region of C.C.G. is the transition stages from the initiation > 10^{-7} - 10^{-6} m/H to fast fracture speeds. In any case the normal service stresses are not the sole cause for creep cracking, since there are inherent forms of stress concentrations, such as thermal, residual or metallurgical which form stress intensities far above the normal service levels and certainly in the region of K where most of the C.C.G. data are obtained, hence one important reason for testing geometries containing a dominant crack. Another point that emerges from the experiment by Neate and Siverns (88) is that the cracking rate for the bainitic low alloy steels is in the region of 10^{-5} - 10^{-2} m/H and the range for the normalized and tempered material is between 10^{-6} - 10^{-4} m/H. This is a similar trend in all available data. At high stresses the creep ductility of the material in the creep range of the normalized steel act as a controlling factor in the growth of the crack, i.e. there is a limit of loading above which stress relaxation at the crack tip suppresses further crack growth. Therefore, in the slower region of cracking, if it is assumed that K has been moderately successful in correlating the data it would be feasible to suggest that at very low stresses and low crack rates creep ductility does not strongly effect the stress singularity.

Ellison and Walton (86) and later Harper (95) testing

1 Cr-Mo-V steel in the normalized condition at 565°C using SEN-T and SEN-B and CT specimens found no correlation with the stress intensity factor and the comparison of the crack rates with K for differing geometries was worse. They (86) suggested a variation to equation (3.2) containing a non-linear function of time:

$$\dot{a} = At^{l} K^{m} \qquad (3.3)$$

the ferritic 1 Cr-Mo-V steel they used had a grain size of approximately 30 μm with tensile ductilities in the region of 60%. The crack tip profile of the specimens without side grooving was highly convex leading at the centre all suggesting that at high loads there would be a large rate of relaxation of the elastic stress singularity. They noted an incubation period for such a material suggesting that final rapid crack propagation would take place when the damage, observed in micrographs as extensive disconnected cracking, ahead of the crack has reached a critical level. In these circumstances it is perhaps not surprising that they could not correlate the data with the stress intensity factor K. Furthermore they found that the use of net section stress did little to improve the correlation.

Popp and Coles (79) and later Floreen (92) working on the creep rupture behaviour of nickel base alloys considered the propagation rates in terms of net-section stress and L.E.F.M. basis. Floreen found a consistent result with the application of the stress intensity and noted an incubation time of around 10-15% of the total test time. There was no excessive tunnelling in his C.T. specimens suggesting a more creep-brittle behaviour. Comparing this incubation

period to that of a creep ductile cracking (86,95) it is found that the incubation covers a considerably larger period of the test time in the ductile specimen (greater than 70% of time to rupture). This suggests an initial blunting of the crack tip which slows down the crack propagation. Harper (95) specifically tested a blunt notch SEN-B specimen of a normalized low alloy steel and found that over 80% of the test time was taken up in the incubation stage. It is here suggested that such forms of creep rupture take place as a result of general material degradation and creep damage ahead of the crack reaching a critical limit.

Floreen (92) also compared the crack growth rates of a C.T. specimen to the tensile creep test of the material in terms of:

$$\dot{a}_s \, t_{f_1} = \dot{\varepsilon}_s \, t_{f_2} \qquad (3.4)$$

where t_{f_1} is the time to rupture of the CT specimen

t_{f_2} is the time to rupture of a tensile creep specimen

$\dot{a}_s$ is the secondary (or minimum) cracking rate

and $\dot{\varepsilon}_s$ is the secondary (or minimum) creep rate.

This is another way of considering the CT as a more complicated creep specimen. This method is likely to be more feasible for creep ductile materials where the increased rate of stress relaxation could be described more accurately by a net-section stress concept rather than K.

Kaufman et al (94) testing aluminium alloys at 150° - 200°C used, fracture crack started, CT specimens of considerably larger size (W = 100 mm) than the usual (W = 50 mm). This increase in size gives a measurably bigger length of controlled

crack growth for the inherently unstable CT specimens. This extra crack length is needed for the aluminium alloys which are very stress sensitive and reach unstable fracture extremely rapidly (78,94). They found a good correlation with K over a range of crack growth rates. The thick specimens with no side-grooving had markedly bowed crack front and the crack reached rapid propagation after approximately 15-20 mm of C.C.G. Similar problems to these have been found by Kenyon (78) and in the present study. The strain rate sensitivity to cracking in aluminium alloys is such that sudden rapid fracture will occur from a steadily growing creep crack. Kaufmann et al have found a divergence from equation (3.2) at the lower stress intensities where the crack growth is slow, similar effects have been found in the present study testing an aluminium RR 58 alloy. They (94) conclude that it is due to the effect of the primary creep behaviour of the material, but it is suggested that the likely reason for this behaviour could be due to over-aging of the alloy. They (94) also note a dependence of crack rate on crack length, especially at crack length values of $\frac{a}{W} > 0.7$. This effect is also observed by most authors shown in table (1). A possible reason for this is that by nearing the end of the specimen the stress analysis of the geometry begins to break down giving an over-conservative estimate of the stress intensity for the particular crack length. Kaufmann et al suggest a K_{ICC} (critical K_I for creep crack initiation) as a percentage of room temperature K_{1C}. They found that C.C.G. occurred at stress intensities of 40% K_{IC} values in the CT specimens of 75 mm thickness and that creep, and not as suggested by some authors envir-

onmental corrosion, is the controlling factor for cracking. Kenyon (78) observed larger values of around 70% of K_{1C} testing aluminium (RR 58) 25 mm thick DCB test-piece. This suggests that a thickness as well as a geometry effect is controlling the behaviour of C.C.G.

3.3.1. Correlation of Creep Crack Growth Rate with Net Section Stress

Simply, net section stress is the applied load divided by the remaining uncracked area. For a test-piece loaded in tension the normal crack tip stress is the stress on the net section remaining as the crack progresses:

$$\sigma_{net} = \frac{\sigma W}{W - a} \qquad (3.4)$$

where W is the specimen width and a is the crack length. It is more difficult to imagine a σ_{net} in bending since the average crack tip stress in this case is not the net section. Instead the simple beam equation can be used:

$$\sigma_{net} = \frac{Md}{I} \qquad (3.5)$$

where M is the bending moment, d is the distance from the neutral axis of net section to crack tip and I is the moment of inertia of the net-section. Many authors, shown in table (1) have used this simple method to correlate their data, but only a few claimed it to be successful (81,87,93). The concept of the net section stress may be more acceptable for the creep ductile rupture of test-pieces where the sharp crack will become blunted and the test may tend to simulate a uniaxial creep test. There exists no relationship as such between C.C.G. and net section stress, but since incubation and deformation play the more

important role in the failure of creep ductile specimens it is postulated that the relaxation of the stress singularity occurring at the crack tip may be better described by this parameter.

Harrison and Sandor (81) in relating this principle to low cycle fatigue at high temperatures claimed a better correlation than by using the stress intensity factor K. Nicholson and Formby (103) using AISI 360 steel at 740°C found that the results from the SEN-T and C.C.P. specimens were described well with the net section stress. The specimens tested were 0.78 mm thick and therefore likely to be under plane stress. The crack in such a circumstance will hardly act as a stress raiser and as Lẹkie and Hayhurst (104), testing soft copper plates, have pointed out the average stress is the more plausible explanation to describe the failure of such test-pieces. In fact these tests (103) can be accepted as a form of uniaxial creep test and in such circumstances it is doubtful to accept that the failure criterion is due to the growth of one dominant crack. Kachanov's (52) damage parameter may also give a good correlation in this case and the apparent crack growths for these tests may be termed as the amount of damage accumulated in time. In a later paper Nicholson (93) using similar size DEN-T (Double Edge Notch Tension) specimen at temperature between 600° - 850°C, reached similar conclusions to those of his earlier work (103) and suggested that net section stress describes the data for over a range of testing temperatures.

3.4.1. Application of Non-Linear Fracture Mechanics to Creep Cracking

The interplay of creep ductility and creep crack growth in creep ductile materials is complex and cannot simply be related to L.E.F.M. A qualitative understanding of the cracking behaviour of the material in terms of K may be reached but it is doubtful whether the values calculated would be useful for the purpose of component design. A possible opening in terms of a better crack tip controlling parameter may be through the use of a reference stress σ_{ref} concept. As the creep exponent (n) increases the net section stress will degenerate to a reference stress (at $n = \infty$). Therefore according to the deformation mode and particular test conditions the use of a particular value of the stress index n should ideally describe the rate of stress relaxation. Anderson (107) and Mackenzie (108) have shown that the reference stress is only weakly dependent on n since it is found from calculations (107) that there is a point in a body where the stress is approximately constant for all values of the stress index. This point is called the skeletal point (107,77) and the reference stress can be defined to be equivalent to the stress at that point. Reference stresses have been evaluated by some authors (106-108) by taking advantage of the weak dependence of σ_{ref} upon n. William's and Price (77) have derived a form of reference stress or a so-called skeletal stress for SEN-T, SEN-B and CT test-pieces from the point of intersection of the stress redistribution ahead of the crack for n of 4 and 7. They (77) also categorize the creep

behaviour of the materials into creep brittle ($n < 5$) where L.E.F.M. is applicable and creep ductile ($n > 5$) where reference stress and creep deformation properties are the controlling factors.

It is interesting to point out that Williams and Price (77) go on to show that the inherent amount of scatter in a creep crack growth test will not clearly distinguish between K or σ_{ref} for the commonly used test-piece geometries and therefore in order to distinguish unambiguously between the two criteria, test-pieces of widely different geometries should be used.

Marriot (105) indicated a possible reference stress arising from Sim's (106) work:

$$\sigma_D\Big]_{n\to\infty} = \frac{P}{P_L}\,\sigma_y \qquad (3.6)$$

where $\sigma_D\Big]_{n\to\infty}$ is the limit of deformation reference stress as the creep index n tends to infinity, P_L is the limit load, P is the applied load and σ_y is the yield stress assuming rigid perfectly plastic material. In essence this reference describes only the creep deformation in a particular geometry and can be used only to predict creep life only, but for materials of high creep index it is assumed that the stress distribution and the strain conditions are very similar for a cracked and an uncracked body when their particular reference strain values are the same.

Leckie et al (109) and Hayhurst et al (110) have found similar relationships to equation (3.6) and have also attempted (104) to differentiate between the reference stress for creep deformation σ_D and the reference stress for creep

rupture σ_R in terms of the different behaviours that occur in the secondary and the tertiary stages of the creep test. σ_D is defined in terms of the creep energy dissapation rate in the absence of damage and σ_R is the stress at which damage begins to appear. Porter and Leckie (111) have shown how to obtain an upper bound on the deformation reference stress σ_D by means of an approximate stress field:

$$\sigma_D = \lambda \sigma_y \qquad (3.7)$$

where $\lambda = \frac{P}{P_L}$. Leckie and Hayhurst (104) further found the reference stress for rupture of a simpler structure in terms of Kachanov's (52) damage concept. From a simple damage and strain rate equation they showed that the uni-axial behaviour of low stress brittle rupture are given by:

$$\frac{\dot{\varepsilon}}{\dot{\varepsilon}_o} = f(\sigma,\omega,t) = \left(\frac{\sigma}{(1-\omega)\sigma_o}\right)^n = \left(\frac{\sigma}{\psi\,\sigma_o}\right)^n \qquad (3.8)$$

$$\dot{\omega} = g(\sigma,\omega,t) = \left(\frac{A\,\sigma}{(1-\omega)\sigma_o}\right)^\nu = A\left(\frac{\sigma}{\psi\,\sigma_o}\right)^\nu \qquad (3.9)$$

where $\dot{\varepsilon}_o$, σ_o, A, ν, n are material constants. The transformation $\psi = (1 - \omega)$ is introduced for convenience and ω is some dimensionless measure of material deterioration. It follows that rupture should occur when $\omega = 1$ or $\psi = 0$ giving the relation between the applied stress and time to rupture as:

$$t_R = \frac{\sigma_o{}^\nu}{A(1+\nu)\sigma^\nu} \qquad (3.10)$$

The rupture behaviour of materials when subjected to multi-axial stress-states can differ considerably from the uni-axial behaviour (112), and failure to include these effects in the structural design calculations can lead to

estimates of rupture life which are non-conservative (114). The Kachanov-Rabotnov theory has been used (113) to obtain lower bounds on the rupture lives of a number of structures, but the effect of multiaxial stress rupture were not included in the calculations. In general these methods can be used under homogeneous states of stress distribution which are markedly lower than the initial elastic stress level and cannot be applied to a dominant crack growth situation in which the extent of constraint has effectively contained the material deterioration, due to creep, to a very small zone at the crack tip.

Haigh (115,76) attempted to relate plasticity concepts to the C.G.G. problem by defining a yield ratio m in a cracked body where:

$$m = \frac{\text{Load to yield a cracked body}}{\text{load to yield an uncracked body}} = \frac{P_{LC}}{BW\,\sigma_y} \qquad (3.11)$$

assuming perfectly plastic behaviour. For specimen geometries which do not have bending components the yield load of the cracked member can be found from the product of the uncracked area and the yield stress. For specimens with mainly a bending component yield point loads can be found from the slip-line field analysis (116). One important assumption of slip line field theory is that of no work-hardening. Engineering materials do exhibit work-hardening and therefore stress relaxation at the crack tip is not so rapid. Haigh (115) using this concept defined an equivalent stress σ_e in terms of m:

$$\sigma_e = \frac{P}{m\ B\ W} \qquad (3.12)$$

It follows from the definition of m:

$$P_{LC} = m(B\ W\ \sigma_y)$$

$$\sigma_e = \frac{P}{P_{LC}}\ \sigma_y \qquad (3.13)$$

Williams and Price (77) note that their skeletal stress was identical to Haigh's equivalent stress and that both can be defined as a reference stress when the creep index n tends to infinity. Haigh also suggested that his σ_e can be directly related to C.O.D., but this is unlikely since the latter is clearly a time dependent parameter whereas σ_e is evaluated from a time-independent plasticity concept.

In a later paper Haigh (76) developed the idea in order to relate it to the K analysis of the data by previous authors (table (1)). Having assumed that the tests with which the stress intensity factor K had been correlated exhibited large amounts of creep deformation he related the apparent strain intensity factor K_A to the equivalent stress σ_e by

$$K_A = \frac{PY}{BW^{\frac{1}{2}}} \qquad (3.14)$$

where Y is a function related to the compliance and by earlier definition of equation (3.12) eliminating P gives

$$mY = \frac{K_A}{\sigma_e\ W^{\frac{1}{2}}} \qquad (3.15)$$

Figure (18) shows the relationship of mY for differing specimen geometries versus $\frac{a}{W}$. It is clearly seen from the graph that mY remains constant or changes very little over

the important range of cracking $\frac{a}{W}$, thus a similar problem to that of Williams and Price (77) arises, which is the inability to distinguish between the two parameters using conventional test-pieces. It is unlikely that the cracking behaviour in a creep ductile situation should behave in a similar manner to the other extreme case of a quasi-brittle essentially elastic C.C.G. and therefore doubt must be placed on the factor m and its derivation from the slip-line field theory.

3.4.2. Recent Models for Creep Crack Initiation and Growth

More recently Goodall and Chubb (117) used a continuum method of examining the damage front of a propagating crack in a creep ductile situation. They used a similar method used by Goodall et al (137) in studying the creep rupture of uncracked components. The theory assumes that failure occurs when a damage front has propagated across a structure so that a mechanism is formed to produce at a specific time an infinite deflection (i.e. rupture time). They suggest that the creep damage spreads well ahead, effectively blunting the physically identifiable crack and final fracture occurs when the load carrying capacity of the structure is exceeded. Goodall examined the propagation of cracks in the creep range by obtaining a relationship for the available energy to form a new surface. He suggested that during creep the apparent surface energy of the material ahead of the crack falls due to the matrix deterioration and therefore the observed correlation of the crack growth rate with the stress intensity factor is to be expected for creep cracking situations. This is unlikely to be true since it

has been found that where the stress intensity concept has worked there has been no damage ahead of the crack tip (91,118) and conversely where the material used has been creep ductile (95) then the data did not correlate with K.

For the more creep ductile situations initiation times are more relevant (95). Vietek (119) produced a computer simulation of the time-dependent development of the plastic zone ahead of a crack loaded in uniform tension. This plastic zone was based on a model of Bilby et al (120) consisting of an array of edge dislocation coplanar with the crack. The dislocation distribution ahead of the crack will change with time and the stress redistribution is dependent on it. This dependence can be governed by Norton's (44) creep law, and then by using a critical value of the J integral as the criterion for the onset of crack growth an initiation time can be evaluated. In relating this micromechanical aspect of creep damage to the contiuum properties of the structure there are dangers that the models based on the atomic level of the material will usually be too simplified in describing the complex creep behaviours at the structural level. The usefulness of these methods (some of which were discussed in section (2.2.5) for uniaxial tests) is to provide a qualitative understanding of the subjects.

3.4.3. Use of C.O.D. as a Parameter

On the assumption that C.O.D. is a material characteristic (in general yielding fracture mechanics) and that indirect measurement of overall strain, notch region extension or the angle of bend are directly related to the C.O.D. it may be possible to use C.O.D. as a relevant crack tip parameter.

Wells and Mcbride (121) suggested that this is such a parameter. They used a low carbon steel BS 15 as 25 mm. plate, in the form of large non-conventional specimens shaped like a DCB test-piece but with the taper on the inside, so as to allow the C.O.D. transducer paddle to protrude from the furnace for better access. They found that a proportionality exists between the loading point displacement and the C.O.D. transducer opening and that their measured C.O.D. showed the predicted pattern of the value obtained from the simple hinging mechanism. Later work on creep cracking, most of the authors (in table (1)) used the simultaneous measurements of creep crack growth and the loading pin displacement during the tests. Many authors (85, 87, 90) have commented on the interrelationship of C.O.D. and crack growth and have noted a linear relationship between the C.O.D. rate and cracking rate. Nicholson and Formby (87) testing this SEN specimens in relating their results to the net section stress used the notch region extension method, in which the C.O.D. is used as a measure of crack growth, to derive the crack length for a particular time and found that this method of crack measurements correlated well with the potential drop technique. But this is unlikely to be of any use for large specimens, in which the notch region extension will be extremely small. Haigh (76) comparing the mechanism of macroscopic high temperature crack growth of a ferritic and bainitic steel found agreement with Pilkington's (85) results that a proportionality existed between the crack growth rate and the C.O.D. opening rate for each test. He (76) suggested

that WOL specimens used deformed by rigid rotation at the plastic hinge-point;

$$\frac{y}{2(W - D)} = \tan \frac{\alpha}{2} \qquad (3.16)$$

where D is the distance from the hinge-point to the back face of the specimen, y is the displacement at the loading pin, α is the angle of rotation. He obtained estimates of C.O.D. from a knowledge of the hinge-point position D which he had obtained from the slipline field theory (116) for the WOL test-piece. By similar triangles from figure (19);

$$\frac{\delta}{y} = \frac{W - (a + D)}{W - D} \qquad (3.17)$$

He concluded that a substantial C.O.D. was needed to develop a creep crack in the ferritic steel and that cracking started at a lower value of C.O.D. for the brittle bainitic steel. He notes that since the range of applicability of K and net section stress is strictly limited, C.O.D. may be a better proposition for defining failure in a range of materials of varying ductility. It is suggested here that the important parameter is C.O.D. rate rather than C.O.D. since this parameter will also contain the time dependence factor which is very important in a creep test.

3.4.4. The Use of C* as the Correlating Parameter

A relatively recent approach to the application of non-linear fracture mechanics to creep cracking has been in the use of an energy rate line integral defined by the term C*. For the two-dimensional case C* is given by:-

$$C^* = \int_\Gamma W^* \, dy - T_i \left(\frac{\partial \dot{u}_i}{\partial x}\right) ds \qquad (3.18)$$

where

$$W^* = \int_0^{\dot{\varepsilon}_{mn}} \sigma_{ij} \, d \, \dot{\varepsilon}_{ij} \qquad (3.19)$$

As shown in figure (20) Γ is the line contour taken from the lower crack surface in a counter-clockwise direction to the upper crack surface. W^* is the strain energy rate density associated with the point stress σ_{ij} and the creep strain rate $\dot{\varepsilon}_{ij}$. T_i is the traction vector defined by the outward normal n_j along , $T_i = \sigma_{ij} n_j$. $\dot{u}_i$ is the displacement vector and S is the arc length .

C^* is an extension of the J contour integral developed by Rice (Section (1.3.2.)). Where ε_{ij} and u_i are replaced by their rates $\dot{\varepsilon}_{ij}$ and $\dot{u}_i$. Since C.C.G. reflects an interplay between non-linear stress-strain behaviour and geometry C^* could prove a possible improvement as a correlating parameter. Goldman and Hutchinson (122) noted that this parameter could apply to secondary creep in the form of the basic creep law:

$$\frac{\dot{\varepsilon}}{\varepsilon_o} = C\left(\frac{\sigma}{\sigma_o}\right)^n \qquad (3.20)$$

where ε_o, C, σ_o and n are constants,

and generalized to a multiaxial state of stress to:

$$\frac{\dot{\varepsilon}_{ij}}{\varepsilon_o} = \frac{3}{2} C\left(\frac{\sigma_e}{\sigma_o}\right)^{n-1} \frac{S_{ij}}{\sigma_o} \qquad (3.21)$$

where σ_e is an effective stress, and S_{ij} is the stress deviator.

For linear elastic behaviour K characterizes the near-

tip stress and strain field. For crack propagation behaviour of materials following equation (3.20) it is reasonable to assume that C* will correlate the data.

An energy rate interpretation of J discussed in section (1.3.2.) and the relationship between J and C* may suggest a means of measuring C* experimentally. J can be interpreted as the energy difference between two identically loaded bodies having incrementally differing crack length:

$$J = -\frac{1}{B_n}\frac{dU}{da} \qquad (3.22)$$

where U is the potential energy and a is the crack length given by:

$$U = U(\sigma_{ij}, \epsilon_{ij}) \qquad (3.23)$$

By analogy for the case of steady state creep rate:

$$U^* = U(\sigma_{ij}, \dot{\epsilon}_{ij}) \qquad (3.24)$$

Such that:

$$C^* = -\frac{1}{B_n}\frac{dU^*}{da} \qquad (3.25)$$

where U* is the power or energy rate associated with displacement rate. Since U has no meaning in the creep sense i.e. there is no unique value of the strain field for a given applied stress it can be said that:

$$C^* \neq \frac{dJ}{dt} \qquad (3.26)$$

Landes and Begley (89) tested CCP and CT specimens of discaloy super alloys in constant strain rate machines, used a form of data reduction technique shown in figure (21) to derive C* experimentally. Basically they derive C* from a pseudo-compliance technique from a family of experimental $\dot{\Delta}$ curves for different loads and different

crack lengths. They found that C* correlated the crack growth rates for both the geometries and also indicated that this experimental data reduction method of evaluating C* inherently reduced the scatter in the data.

Harper (95) suggested another means of deriving C* from the limit load analysis. He derived an expression for C* from ideas discussed by Haigh (76) in considering a limit load stress of a cracked body in terms of plasticity concepts. By using Ewing and Richards (116) and Haigh and Richards (124) yield load values of m and assessing by analogy that the load P to cause a particular displacement rate $\dot{\Delta}$ is m times the load P' to cause the similar displacement rate in an uncracked specimen, from the basic creep law of equation (3.20) he states that

$$\dot{\Delta} = C(P')^n \qquad (3.27)$$

and further finds the relationship:

$$C^* = -\frac{1}{B_n}\frac{dU^*}{da} = -\frac{n}{n+1}\frac{P\dot{\Delta}}{B_n W}\left[\frac{1}{m}\frac{dm}{d\left(\frac{a}{W}\right)}\right] \qquad (3.28)$$

and for large creep index approximating to:

$$C^* \triangleq -\frac{P\dot{\Delta}}{BW}\left[\frac{1}{m}\frac{dm}{d\left(\frac{a}{W}\right)}\right] \qquad (3.29)$$

Using this method he claims a good correlation of the raw data of Landes and Begley (89), Robson's (83) and his own and suggests that C* is a useful parameter for a limited range of material behaviour at high temperatures, where neither K nor reference stress would correlate the data. Also his correlation of time to rupture of the CT and SEN test-pieces with σ_{ref} derived from Haigh and Richards (124)

m factor was still not satisfactory.

It would appear that the basic assumptions of equation (3.20) has not been fulfilled in the two cases of C^* determination mentioned. In both cases the authors claim that the $\dot{\Delta}$ measured is essentially the deformation $\dot{\Delta}$ due to creep damage whereas it is suggested that $\dot{\Delta}$ measured incorporates the important factor of the elastic $\dot{\Delta}$ due to the crack extension. This basic shortcoming will be discussed in Chapter Six in the light of the new results from the present work.

3.4.5. The Theoretical Method of Evaluating C^* for the DCB Test-Piece

Following the work done by Kenyon (78) and discussed by Kenyon et al (125) on testing constant K DCB-C test-pieces of an aluminium alloy. It was noted that regions of primary, secondary and tertiary cracking existed which could not be explained by basic L.E.F.M. arguments. Turner and Webster (126) suggested that a non-linear argument may be needed to describe this. By analogy from the material obeying the work-hardening law:

$$\epsilon = A\sigma^n \qquad (3.30)$$

it can be said that for the creep situation:

$$\dot{\epsilon} = A\sigma^n \qquad (3.31)$$

which is identical to equation (3.20) and the argument put forward by Landes and Begley (89). Where the J contour integral describes equation (3.30) then a potential power rate $\dot{J}$, by analogy, could describe the creep process. Turner and Webster (126) found an approximate theoretical calculation of J using non-linear beam theory for the DCB-C:

$$J \propto \frac{B\, P^{n+1}}{a^{\left(\frac{n-1}{3}\right)}} \qquad (3.32)$$

where a is measured from the loading pins of the contoured profile and P is the applied load. Hence for creep by analogy:

$$\dot{J} \propto \frac{B\, P^{n+1}}{a^{\left(\frac{n-1}{3}\right)}} \qquad (3.33)$$

The derivation predicted a drop in $\dot{J}$ as a function of crack length and it was suggested (127,118) that this could possibly explain the fall in the crack rate of DCB-C specimens tested by Kenyon (78). Nikbin et al (128) found a good correlation of $\dot{J}$ with the C.C.G. data for particular creep index n.

The principles of C^* used by authors (89,95,123) are similar to $\dot{J}$ used by Nikbin et al (128) and it was suggested in a later paper by Nikbin et al (129) that the C^* should be used as the notation for this parameter since $\dot{J}$ may mistakenly be taken as a J contour integral rate.

The full theoretical derivation of J, using non-linear beam theory, for the DCB test pieces of any contour is shown in appendix (A), but the principles of its use will be discussed here. For an energy interpretation of J it has already been shown from equation (3.22) that

$$J = -\frac{1}{B_n}\frac{du}{da} \qquad (3.22)$$

In elasticity this energy is available to grow the crack, with plasticity, equation (3.22) may be used as a means of defining a unique crack tip parameter J which is no longer the energy potentially available to grow the crack.

For a non-linear material obeying the law

$$\epsilon = A\,\sigma^n \qquad (3.30)$$

it can be shown (128,129) that for DCB test-piece subjected to a constant load P

$$J = \frac{P}{B_n\,(n+1)}\,\frac{d\Delta}{da} \qquad (3.34)$$

where Δ is the deflection at the loading pin. Evaluation of $\frac{d\Delta}{da}$ as the crack propagates along the length of the test-piece will give J as a function of crack length. From the final equation in Appendix (A) the value of J can be evaluated as a function of crack length for any DCB contour:

$$J = \frac{2A}{B_n\,(n+1)}\left[\frac{(2n+1)}{2nB}\right]^n \frac{(aP)^{n+1}}{\left(\frac{h}{2}\right)^{2n+1}} \qquad (3.35)$$

For linear elasticity n = 1, $A = \frac{1}{E'}$ and J = G (the elastic strain energy release rate) and for plane strain

$$G = \frac{K^2}{E} \qquad (3.36)$$

and for plane stress

$$G = \frac{(1-\nu^2)\,K^2}{E} \qquad (3.37)$$

where ν is Poisson's ratio.

Now consider a material obeying the secondary creep law:

$$\dot{\epsilon}_s = C\,\sigma^n \qquad (3.38)$$

where $\dot{\epsilon}_s$ is the secondary creep rate.

It can be argued that the stress distribution around the crack tip characterized by

$$\sigma \alpha \left(\frac{J}{A}\right)^{\frac{1}{(n+1)}} \qquad (3.39)$$

$$\epsilon \alpha A\left(\frac{J}{A}\right)^{\frac{n}{(n+1)}} \qquad (3.40)$$

for the case of plasticity is the same as the stress and strain rates around a crack tip of a material following the steady state creep equation (3.38) giving

$$\sigma \alpha (C^*/C)^{\frac{1}{(n+1)}} \qquad (3.41)$$

$$\dot{\epsilon}_s \alpha C(C^*/C)^{\frac{n}{(n+1)}} \qquad (3.42)$$

where C^* is the characterizing parameter for creep. Therefore the non-linear analysis for the DCB can be rep eated with ϵ replaced by $\dot{\epsilon}_s$ and A by C leaving Δ having to be replaced by $\dot{\Delta}$, and equation (3.35) becomes

$$C^* = \frac{2C}{B_n(n+1)} \left(\frac{(2n+1)}{2nB}\right)^n \frac{(aP)^{n+1}}{\left(\frac{h}{2}\right)^{2n+1}} \qquad (3.43)$$

Figure (22) shows, for the DCB-C test-piece, the effect of increasing the value of n on a graph of normalized C^*/C^*_i versus crack length, where C^*_i is the value of C^* at a crack length of 75 mm. The final increase of the C^*/C^*_i value at a crack length of approximately 150 mm is due to the limit of the contour of the actual specimens used, restricted by the plate thickness (about 75 mm) from which the specimens were machined. This increase in effect predicts an accelerating C.C.G. rate when the crack nears the end of the test-piece.

The correlation of the data, from the present test program, with this parameter will be discussed in Section (6.2.1.).

CHAPTER 4

EXPERIMENTAL PROGRAM

4.1. Choice of Materials, Heat Treatment and Geometries

4.1.1. Material Selection

Tests were carried out on two alloys which have two completely different uses in industry, but the service conditions in which they are used make them liable to fail by high temperature creep cracking. The precipitation hardenable aluminium alloy RR 58 used in the aircraft industry which was previously tested in the C.C.G. range by Kenyon (78) was chosen for the continuity of the test program and to re-asses the effects of change of geometry and other variables on the high temperature fracture of the alloy. The second material chosen was a $\frac{1}{2}$%Cr, $\frac{1}{2}$% Mo, $\frac{1}{4}$%V steel, predominantly used in the power industry in pressure vessels, steam chests and numerous items of turbine components and associated pipeworks all operating in the creep range.

Table (2a) shows the compositions and the mechanical properties of the RR58 alloy, which was received in the form of 75 mm thick rolled plate solution treated at 530°C, water quenched and subsequently strained 2$\frac{1}{2}$%. Previous uniaxial creep tests (78,130) suggested that failure in this aluminium alloy occurred with a limited ductility of around 1% for test times greater than 1000 hours and to a maximum of around 8% for short term tests, in the creep range of 100 - 175°C. The low alloy steel was received in five blocks from English Electric-AEI Turbine Generators Limited, all given an identical normalizing and tempering treatment. Tables (2b) show the composition of the blocks and the mechanical properties of the steels. The

compositions are predominantly similar with grain sizes in the as received condition ranging from 30 - 40 μm.

4.1.2. Heat Treatments Prior Creep Cracking Tests

The standard heat treatment for each specimen of RR58 was 30 hours in a salt bath at 190°C ± 1°C in order to reach peak hardness (of approximately 150 V.H.N.). Some specimens were further heat treated to observe the effects of prolonged times at temperature on C.C.G. and material hardness. Specimen hardness was checked before and after each test, figure (95) shows the effect of test duration on hardness. It is seen that at 150°C there is very little change in the hardness value and therefore attention was primarily centred on testing the RR58 at 150°C and thus hoping to reduce the effect of overaging during the test.

The five blocks of ½% Cr, ½% Mo, ¼% V steel received in the normalized and tempered condition with ferritic grain size of 30 - 40 μm had rupture ductilities in excess of 40%. Initial tests carried out on this as received condition only succeed in extensively deforming the arm of the DCB-C test-piece and it was noted that for specimens with predominantly bending stresses only materials with limited creep ductilities would be suitable for testing. Therefore an embrittling heat treatment was used to simulate the heat affected zone (H.A.Z.) of welds in steam pipes. The first block tested was 3F and it was heat treated for half an hour at 1250°C ± 1%, in a Gallenkamp furnace, and oil quenched to room temperature. This produced a mixture of martensitic and bainitic structure with grain size of 250 - 350 μm and vickers hardness of around 250 VHN.

Testing at 565°C had the effect of continuously tempering the microstructure giving an initial sharp rise in hardness, followed by a continuing decrease in V.H.N.(figure (96)). In order to reduce the tempering effect subsequent block were given a standard tempering treatment of twenty four hours at 680°C followed by air cooling. It was found that the hardness had stabalized in the region of 230 - 250 V.H.N. and dropped slightly with time at the test temperature of 565°C (figure (96)). The tempering effectively introduced a tempered bainite structure and it is assumed that for longer term tests the C.C.G. is increasingly affected by the change in the metallurgical structure of the material.

4.1.3. Specimen Geometries

In Chapter Three section (3.1.1.) the different geometries used in C.C.G. tests were reviewed and compared. in this program only a selection of the different geometries and specimen sizes shown in figure (15) were tested. Most tests were carried out on DCB-C and DCB-P test-pieces but DT, CT and SEN-T specimens were also tests. In addition raw data available, in some published papers (table (1)), on differing geometries were also re-analysed and compared to the present results, in the hope of unifying the C.C.G. analysis on a broader front.

The CT and SEN-T tests on RR58 appeared fruitless since it was found that although small amounts of slow C.C.G. had occurred it was not sufficient to visually measure it and due to the stress sensitivity of the RR58 and the instability of the CT and the SEN-T test-piece there was a rapid acceleration from slow growth to unstable fast fracture. The possible use of the potential drop technique

to measure small amounts of crack growth would be ideal in this case. The DCB-P RR58 test-pieces showed an appreciable amount of crack growth but the onset of rapid unstable fracture as in the case of all the other RR58 specimens were unpredictable. Only the DT test-piece of RR58 were tested and the difficulties of testing steel DT specimens are outlined in the Section (4.2.1.).

The C.C.G. behaviour was more predictable for the steel. DCB-C, DCB-P of different sizes and side-grooving were tested. CT specimens were used in the latter stages of the test program and it was found that visual crack measurements on the steel CT test-pieces were easier than the RR58 CT specimens but it is suggested that for an increase in accuracy the potential drop would give more accurate readings over a small range of crack growth.

Table (3a) shows the representative dimensions of the DCB-C, DCB-P, DT and CT geometries that have been used in the C.C.G. tests. For the analysis of the results in Chapter Six the accurate values of each individual test-piece are incorporated in the computations.

4.2.1. Description of the Apparatus

The major portion of the test program was carried out on six machines specifically made to monitor crack growth at high temperature. The Instron testing machine and the standard Denison Creep deformation machines were also used but to a lesser degree.

The creep deformation machine was a standard Denison rig with a 10:1 lever ratio and vertical furnace wound in three zones to enable the temperature distribution to be

adjusted. The furnace temperature was measured by using two chromel-alumel thermocouples attached to the ends of the specimen and the temperature was kept constant to within $\pm$ 1°C using a CNS Trivect mark 1 three-zone temperature controller. The creep strain was measured continuously using a DC-LVDT (linear variable differential transformer) type transducer, shown in figures (23,25), with a sensitivity of 0.1 mm per mv.

For the C.C.G. tests a total of six machines were used. Three of the machines which were previously described by Kenyon (78) were used for testing DCB test-pieces, of RR58. Subsequently one of the rigs was converted to test DT specimens. The remaining three machines, figure (24) were constructed to test low alloy steels at temperatures of 500° - 600°C and apart from the pull rods which were made on nimonic 80A, these were in every way similar to the first three machines.

The machines used for the RR58 and steel to test DCB-C, DCB-P, and CT specimens, figure (24), had a 10:1 lever ratio and two pull-rods which were connected to the steel shackles via ball-bearings, in order to ensure that the pull-rods and therefore the specimen remained vertical throughout the test. The furnaces were rectangular in design and opened vertically in the middle. Figure (26) shows an open furnace with a tested steel specimen. The element windings were in three zones situated on the sides of the furnace, and the method of temperature control was similar to the Denison creep rig described earlier. Figure (25) in conjunction with figure (23) shows the arrangement of the extensometry, effectively the displacement at the

loading line was measured using this method and the values were continuously plotted on a 24-point recorder during all tests.

The crack growth was monitored using a telescope mounted on a shaft attached to the platform, figure (24). The crack reflection was viewed through two side windows using two mirrors clamped at an angle of 45^{o} to either side of the furnace. The crack length was measured from the loading line at convenient time intervals and the average was plotted versus time. For the RR58 test-piece tested between 100^{o} - 200^{o}C it was found that a thin spray of high temperature white matt paint on the base of the side-grooves improved the detectability of the crack. A powerful lamp was used to reflect light from the surface of the specimen and the view from the telescope showed a hairline crack tip as a dark line against a white background, consequently this length of crack was measured using a vernier scale mounted on the telescope.

Testing the low alloy steel at 565^{o}C presented a problem of oxidation which completely marred the view of the crack. Conventional high temperature paints did not adhere well enough to the notch base of the specimen and would not be reliable in monitoring C.C.G. After numerous trials of different combination of coatings such as high temperature aluminium paints, and different forms of glass cement a paint was found that was acceptable in determining, to a good degree of accuracy, the crack front. This coating was called the Delta-gaurd 130 (trade name) used to protect low alloy steels from surface oxidation at temperatures in excess of 1100^{o}C. The specimen side grooves were

sand blasted and degreased using trichloroethylene and a thin layer of Delta-gaurd 130 was applied using a pencil brush. The test temperature of 565° Delta-gaurd 130 forms a brilliant white matt surface which adheres extremely well to the specimen surface. If carefully applied the paint will crack as the specimen cracks and it will last up to 2500 hours at 565°C. Several specimens were stopped in the middle of the test and broken at room temperature to compare the measured value of the crack length to the actual value. The accuracy of the measurements were with $\pm$ 1.0 mm for the steel and $\pm$ 0.5 mm for the RR58 and given the crack length monitored for DCB test-pieces were usually in excess of 70 mm the error involved is acceptable.

The Double Torsion rig shown in figure (27) consisted of a lever arm ratio of 6:1 attached to a stainless steel compressive loading rod. The crack opening deflection was measured directly by attaching the transducer to the top of the loading rod. The rectangular DT specimens (figure (15)) were held up horizontally at each corner by four rods protruding from the base of the furnace and the compressive load was applied from the loading rod. The point of contact of the specimens with the rods were with ball-bearings slotted at the centre of the rods. The method of crack measurement was similar to the other machines but since the plane of the crack growth was parallel to the side windows the reflection of the crack was passed onto the outside mirror via another mirror clamped at 45° below the crack line figure (27) shows at DT specimen set up inside the furnace. The lighting needed to view the crack was a 12 v quartz lamp placed inside the furnace, below the

mirror. Only RR58 was tested in the shape of a DT geometry since there were problems involving crack monitoring of the steel at 565°C using the above method. The lighting and the reflective surface needed to withstand long times at 565°C could not be found. However it is suggested that the use of the potential drop technique will solve the problem of crack measurement.

4.3.1. Experimental Procedure

Apart from the specimen preparation for surface coating they were also, for ease of crack measurements, marked on both sides at intervals of 0.25 inches (6.35 mm), since the vernier on the telescope mounting was marked in fractions of an inch. Four chromel-alumel thermocouples were fixed in previously drilled holes along the specimen at intervals of 30 mm. In this way temperature gradient, if any, could be determined throughout the test.

The specimens were placed in the furnace and held at the testing temperature for approximately twenty hours prior loading. The loading of the specimen was performed manually for the steel and for the more stress sensitive RR58 a motorised jack was used to apply the load. The loading rate was kept to within one minute for the full laod in all cases. Once the load had been applied the initial crack reading and the zero value for the transducer was taken and the clock attached to the machine was switched on. Initially the crack length and the transducer readings were taken at short intervals and depending on the rate of crack growth, and at convenient times thereafter. During some of the tests load changes were performed simply by carefully adding or subtracting at the back of

the machines. In some earlier tests and more predominantly in tests performed by Kenyon (78), the temperature was altered during the test by resetting the temperature controller and it was found that the new temperature reached a stable level within a three hour period.

4.3.2. Crack Tip Preparation Prior Testing:

Different methods of crack starting were tried. For the RR58 sharp cracks were initiated using the instron machine at strain rates of 0.25 mm/min. Fatigue cracking was found to be unsuitable for RR58 since the crack direction deviated from a flat fracture. Later tests were carried out on RR58 (DCB and DT test-pieces) with a very fine flat saw cut as the crack starter. The crack growth data overall showed similar behaviour, irrespective of the mode of the crack starter.

The initial crack-starter for the steel specimens was less critical, since the heat treatment had reduced the creep ductility drastically making the metallurgical structure more creep-brittle. Tests 3F1-3F6 and 8F1 were fatigue precracked and the rest were given a fine flat saw cut as a crack starter. For long crack lengths in the DCB and DT test-pieces the method of precracking will have a small effect at the initial stage of crack growth but once the crack tip stresses have stabalized and the crack lines grown into the virgin material ahead, the C.C.G. behaviour will not be affected by the mode of the crack starter. For small specimens where the cracking range is usually less than 10 mm the method of crack initiation will be of importance. For example tests carried out by Ellison and Walton (86)

and Harper (95) on CT and SEN-B test-pieces of 1 Cr, Mo, V steel, had a standard precracking of 100,000 cycles of fatigue, which must ultimately effect the C.C.G. behaviour of the material in the vicinity of the crack tip.

4.3.3. Uniaxial Creep Tests

Standard high temperature creep deformation tests were carried out on the steel and a few on RR58 (extensive creep tests on RR58 were previously performed by Kenyon (78)). The overall gauge length of the creep specimens were 25.4 mm with a diameter of 4.76 mm.

4.3.4. Metallurgical Investigations

Metallurgical examination on some of the specimens were performed. The hardness values of the test-piece were recorded before and after each test-piece. The fracture surface of each specimen was analysed using a stereo microscope. Certain tests were stopped prior to rapid fracture and the specimens were cut perpendicular to the crack plane in order to observe the nature of C.C.G. and its relation to its geometry, thickness and loading history. Metallographic examinations of this nature were carried out on both RR58 and steel. Micrographs, using a Vicker's microscope were taken before and after etching and some of these are discussed in section (5.3.1.).

4.4. Derivation of Experimental and Theoretical Formulae used to evaluate the Stress Intensity Factor K for different Geometries

4.4.1. Experimental Evaluation of K

The DCB, DT and the CT specimens may be analysed by the general compliance method described in section (1.2.2.).

It was shown that for a body containing a crack a relationship exists between the stress intensity factor K and the energy release rate G. For plane strain conditions:

$$K^2 = \frac{EG}{(1 - \nu^2)} \qquad (4.1)$$

From equation (1.10) it follows that:

$$K^2 = \left(\frac{P^2}{2 B_n}\right) E\frac{dC}{da} \qquad (4.2)$$

where C is the compliance given by

$$C = \frac{\text{Extension}}{\text{Load}} = \frac{\Delta}{P}$$

and can be measured experimentally. Tests to evaluate the elastic compliance at room temperature were carried out on DCB-C, DCB-P and DT test-pieces. Since the displacement Δ for the evaluation of K must always be elastic it follows that tests performed for different materials and temperatures will give a constant value of $E\frac{dC}{da}$ giving the general equation

$$E_1 \left(\frac{dC}{da}\right)_1 = E_2 \left(\frac{dC}{da}\right)_2 \qquad (4.3)$$

where subscripts 1 and 2 can be for different temperatures or materials. The DCB and DT test-piece were sawn to consecutively longer crack lengths and the values of C for each crack length was evaluated. From the slope of the compliance versus crack length graph $\frac{dC}{da}$ was found and plotted versus crack legth. Figures (28,29) show the graphs of $\frac{dC}{da}$ versus crack length for the DCB and DT geometries used in the C.C.G. tests. It is seen that both the DCB-C and the DT have a constant compliance independent of crack length, giving from equation (4.2) a constant value of K

independent of crack length. The DCB-P test-pieces are inherently unstable and exhibit increasing $\frac{dC}{da}$ with crack length. The final increase in $\frac{dC}{da}$ in figures (28,29) for the DCB-C test-piece is due to the breakdown of the contour (since the maximum height of available material was limited to 75), and due to the crack length reaching the end of the specimen.

4.4.2. Theoretical Evaluation of K

Analytical methods for determining the elastic stress distribution around the crack tip for the geometries in figure (15) have been developed extensively in recent years. The general method of analysis consists of finding a stress function of two variables (X_1, X_2 or r, θ) figure (4) which will satisfy the compatibility equation $\nabla^4 = 0$ and also the boundary conditions at a finite number of stations along the boundary of a specimen.

Another common method of theoretically evaluating K is by the use of equation (4.2). The elastic value of Δ can be determined analytically using methods commonly described in texts on strength of materials and converted into $\frac{dC}{da}$.

From the boundary collocation computations performed by Srawley and Gross (98) the values for the contour of the DCB-C were chosen to give a constant compliance. Table (3a) shows the contour dimensions and table (3b), in conjunction with figure (30), gives the particular values of $\frac{H_p}{e}$, $\frac{W}{e}$ and $\frac{W}{H_p}$ which give:

$$\frac{KBW^{\frac{1}{2}}}{p} = \text{constant} \qquad (4.4)$$

Srawley and Gross (98) also formulated an approximate method of evaluating K for the DCB test-piece which is:

$$K = P \frac{3.46 \left(\frac{a}{h} + 0.7\right)}{Bh^{\frac{1}{2}}} \qquad (4.5)$$

and taking into account side grooving from equation (3.1) and for plane strain conditions

$$K = \frac{P \quad 3.46 \left(\frac{a}{h} + 0.7\right)}{\sqrt{B \; B_n (1 - \nu^2) \; h}} \qquad (4.6)$$

This method is increasingly inaccurate for increasing specimen taper.

Another means of evaluating K is from the non-linear beam theory discussed in section (3.4.5) and shown in appendix (A). From equation (3.35) for the case of n = 1 in linear elasticity J = G (the crack extension force, and using equation (4.2) gives for a side grooved specimen under plane strain conditions

$$K = \sqrt{\frac{P^2 \; 3 \; a^2}{2 \; B \; B_n \; (1 - \nu^2) \left(\frac{h}{2}\right)^3}} \qquad (4.7)$$

This calculation ignores shear stresses and assumes a built in beam.

Outwater et al (96) found an approximate expression of K for the DT test-piece by considering the torsional compliance C of one half of the DT specimen (figure 15):

$$C = \frac{\theta}{M_t} = \frac{a}{I_p \; E_s} \qquad (4.8)$$

where θ is the angular displacement, M_t is the torque, I_p is the polar moment and E_s is the shear modulus. Hence:

$$\frac{dC}{da} = \frac{1}{I_p E_s} \qquad (4.9)$$

which is a constant depending on the cross section and modulus of the specimen. I_p for a rectangular cross-section is given by Roark (131) as

$$I_p = \frac{hB^3}{32}\left(\left(\frac{16}{3}\right) - 6.72\,\frac{B}{h}\left(1 - \frac{4}{3}\left(\frac{t}{h}\right)^4\right)\right) \approx \frac{hB^3}{6} \qquad (4.10)$$

They derive the crack extension force G for the DT test-piece in terms of the torque M_t:

$$G = \frac{M_t^2}{hB_n}\,\frac{dC}{da} \qquad (4.11)$$

Substituting (4.9) and (4.11) into equation (4.2) gives an approximate formula for the stress intensity factor K:

$$K = P\left(\frac{h_m^2}{8\,B_n\,I_p(1-\nu)}\right)^{\frac{1}{2}} \qquad (4.12)$$

Equation (4.12) is crack length independent and K and G can now be determined from the knowledge of specimen dimensions, modulus and the applied load.

The stress intensity for the CT test-piece has been defined by A.S.T.M. (13) for valid K_{1C} tests and is universally accepted for calculating K in this geometry:

$$K = \frac{P}{B\sqrt{W}}\left[29.6\left(\frac{a}{W}\right)^{\frac{1}{2}} - 185.5\left(\frac{a}{W}\right)^{\frac{3}{2}} + 655.9\left(\frac{a}{W}\right)^{\frac{5}{2}} - 1017.0\left(\frac{a}{W}\right)^{\frac{7}{2}} + 638.9\left(\frac{a}{W}\right)^{\frac{9}{2}}\right] \qquad (4.13)$$

In Chapter Six a comparison of the theoretical and the experimental methods of evaluating K will be made by correlating them with the C.C.G. data.

CHAPTER 5

5.1. Experimental Results

The results will be presented in two major sections.

1. Uniaxial Creep deformation tests.
2. Crack growth data obtained from different geometries.

Tests were carried out on an aluminium alloy (RR58) and a low alloy steel ($\frac{1}{2}$% Cr, $\frac{1}{2}$% Mo, $\frac{1}{4}$% V). The RR58 used in the present tests was the same as used previously in an experimental program by Kenyon (78) who investigated the application of L.E.F.M. to C.C.G. In the third section metallurgical observations will be discussed in the light of the creep deformation and cracking behaviour of the RR58 and steel.

5.1.1. Results and Analysis of the Uniaxial Creep Deformation Tests

A selection of data of creep strain (ε) versus time (t) from the uniaxial creep tests are shown in figures (31-34) for the RR58 and Figures (35-38) for the steel. The general objectives of these tests were to evaluate the range of creep ductilities and also to establish any possible link that may exist between the creep deformation and the creep cracking results.

The bulk of the RR58 creep tests were carried out by Kenyon (78) and are shown in table (4a). Figures (31-34) show a comparison of the short and long term tests for temperatures of 100°, 150°, 200°C respectively. The essential features are the marked decrease in the primary region and the failure ductility with the increase in temperature. The creep strain at fracture varies with

temperature and loading. The creep strain at fracture (ε_f) drops from approximately 10 - 11% at 100°C to 3 - 4% at 200°C for short time tests of less than 100 hours and drops from 7 - 8% to 1 - 2% for the same temperature range and test times in excess of 500 hours. Therefore there is a relative transition from a ductile fracture at high stresses and low temperatures to a more creep brittle rupture at low stresses and high temperatures. The RR58 is heat treated at 190°C for 30 hours prior to testing in order to give a peak hardness of around 150 VHN. The extent of overaging is dependent on the length of test time and the testing temperature. Figure (34) shows the effect of overaging on the creep ductility and rupture of two RR58 specimens tested at 150°C with an applied stress of 232 MPa. There is a reduction in rupture life by a factor of four approximately and an increase in the rupture ductility by over a factor of two in the overaged specimen. The RR58 is received in 75 mm thick rolled plates which had been prestrained 2½%. The time of testing at temperature accelerates the metallurgical processes such as overaging and also reduces the residual stresses due to the prestraining. Both these factors reduce the material hardness and increase the creep ductility and the tertiary region of the creep curve.

Figures (35-36) show the creep strain versus time relationships for quenched and quenched and tempered low alloy bainitic steels tested at 565°C. Table (4b) gives a summary of the uniaxial creep data collected for the ½% Cr, ½% Mo, ¼% V steel. The steels were solution treated at 1250°C for half an hour and then oil quenched, giving

a predominantly martensitic and bainitic structure with a prior austenite grain size of 200 - 300 μm. This was followed by a tempering treatment of 24 hours at 680°C to reduce the residual stresses and temper the bainitic structure. Uniaxial creep tests were performed on the quenched and quenched and tempered material. The steel in the as received condition consists of a normalized ferritic structure with a hardness of approximately 130 V.H.N. Cummings and King (132) tested a similar ½% Cr, ½% Mo, ¼ V, steel in the ferritic condition and found that the creep curves showed an extended tertiary region with creep ductility decreasing from 40% to 20% in long term tests. In comparison figures (35-36) show the sharp reduction in the creep rupture ductility for bainitic heat treatments of the low alloy steel. Both show a predominantly primary region with extensive work hardening. The creep strain at fracture for the quenched material is in the region of 0.2% decreasing to 0.1% for long term tests and for the quenched and tempered steels, shown in figure (36), the creep strain at fracture drops from 1.6% to approximately 0.6% or less for long term tests. Figures (37) compares the effect of tempering on the creep curves of the two specimens tested at 565°C under a stress of 360 MN/m^2. The quenched and tempered steel shows an increase in ductility of a factor of ten and an increase in rupture life by a factor of over two. But generally compared to the ferritic low alloy steel tested by Cummings and King the bainitic heat treatment can be said to produce a relatively creep brittle structure.

The data collected on RR58 and the steel covers short term uniaxial creep tests (less than 1000 hours) and cannot be used for predicting accurately the creep behaviour beyond this range. But, by correlating strain, strain and times to rupture data, useful quantitative relationships can be formed. Figures (38-40) for RR58 and figures (41-43) for the steel show respectively the secondary creep rate ($\dot{\varepsilon}_s$) versus stress (σ), stress (σ) versus time to rupture (t_R) and secondary creep rate ($\dot{\varepsilon}_s$) versus time to rupture (t_R) of the uniaxial data. There is an increase in the amount of data scatter for the steel, which could be due to the marked reduction in creep ductility of the bainitic microstructure suggesting that it may be more useful to observe the creep crack propagation behaviour of this material in geometries containing a dominant crack, since in uniaxial creep tests the problem is one of crack initiation rather than creep crack propagation.

By using the creep data an estimate of the value of n can be found for the equation

$$\dot{\varepsilon}_s \alpha \sigma^n \qquad (5.1)$$

Figures (38,41) show the respective relationships for RR58 and steel. For the RR58 the range of values for n varies from 40 at 100°C to an average of 17 at 200°C. The increase in temperature effectively reduces the creep ductility and the material fractures in a more brittle manner. The stress dependence of n for the steel in the quenched state is around 5.6 and for the quenched and tempered material is about 7.7. It is seen from figure (41) that at lower strain rates, i.e. longer time tests, the quenched material

is also beginning to be tempered at 565°C and thus tending to behave like the quenched and tempered steel.

A more accepted form of correlating the data, specially for use in design codes (46) is to use the stress dependence of time to rupture. It is found (46) that in long duration tests approaching the times for service life fractures there can be a drastic loss in ductility which may invalidate the conventionally measured values of creep elongation used in design codes. This is specially true for engineering materials where the microstructure is specifically made to be creep resistant. From equation (2.8), figures (39,42) for RR58 and steel respectively can be correlated in the form

$$t_R \propto \sigma^{-m} \qquad (5.2)$$

The value of m for RR58 varies from 32 at 100°C to an average of 14 at 200°C. The time to rupture values drop by four decades in going from 100°C to 200°C emphasising the importance of the thermal activation processes on the rupture life of the material. For the steel the value of m is around 4.5 for both heat treatments but there is an increase by a factor of over two in the rupture life of the tempered steel compared to the quenched material. In comparison, the values of m derived by Cummings and King (132) for the ferritic low alloy steel were from 13→9→6 with decreasing stress over a time period of up to 20,000 hours. For the Cummings and King tests (132), which were within the same time period (less than 1000 hours) as the present tests, the values of m increase from about m = 4.5 for the bainitic material to m = 13 for the ductile ferritic steel.

Figures (40,43) show the relationship of the data, for RR58 and steel respectively, plotted in the form:

$$\dot{\varepsilon}_s \alpha \left(\frac{1}{t_R}\right)^p \qquad (5.3)$$

If the value of p = 1 then it is feasible to assume that a direct relationship exists between the creep deformation behaviour and creep fracture. Figure (40) shows that this relationship is temperature independent for RR58 but the slope p is found to 1.09 suggesting that at longer test times the effect of overaging coupled with a loss in creep ductility forces a departure from direct proportionality of equation (5.3). The test temperature does not drastically affect the creep rate and this is clearly illustrated in figure (40) for RR58 for test temperatures of 100°C to 200°C. Figure (43) shows the same correlation for the steel tests. The secondary creep rate measured in the case of the steel uniaxial data is effectively the minimum creep rate since the large primary exhibited by the steels extend in some instances right up to the tertiary region. The effect of tempering is to increase the time to rupture by a factor of 10 for the same secondary creep rate. The slopes of p drawn on the figure are both one but it is expected that similar to RR58 there will be a departure from linearity for longer term tests when the effect of tempering will become more pronounced.

5.2.1. Results of the Creep Cracking tests obtained from Different Geometries, Thicknesses and Side grooving

In section (3.1.1) various test-piece geometries used for C.C.G. tests were discussed. In this section the

representative curves of crack length versus time, transducer displacement versus time, and crack length versus transducer displacement for different geometries will be shown. Extensive crack growth data of RR58 were collected by Kenyon (78) using the DCB-C test-piece. His test temperature ranged between 100°C - 200°C and he predominantly used specimen thicknesses of 9.5 mm and 25 mm. In order to reach a broader understanding of the problem the present program was orientated to test other geometries (the dimensions of which are shown in table 3) and also a different material. Therefore simultaneous creep cracking tests were carried out using the specified material.

RR58	½% Cr, ½% Mo, ¼% V Steel
DCB-C	DCB-C
DCB-P	DCB-P
DT	CT
(CT,SEN)	

The CT and S.E.N. tests of RR58 were not successful since a small amount of crack growth was followed by a fast uncontrolled fracture. In such a circumstance the potential drop technique to monitor constantly the small amount of crack growth would be ideal. DT tests on the steel were not attempted since there were problems in finding a special mirror and light bulb to withstand long periods at 565°C. Once again where it is found that there are difficulties in visually recording the crack length, the use of the potential drop method will overcome these problems.

Table (5) gives a comprehensive list of all the crude

growth data for both RR58 and steel. The basic information such as crack length, applied load, test temperature, the type and size of geometry for each test-piece is shown. The values of crack growth rate, transducer displacement rate, the slope of transducer versus crack length, and finally the experimentally calculated elastic stress intensity factor K are also shown for the individual crack lengths and applied loads of each test-piece. It will serve no purpose to show all the experimental graphs and therefore only representative figures will be discussed.

Figures (44-67) show the experimental graphs of RR58 and steel, which will be discussed in the following section. The graphs of crack growth against time are simultaneously shown with the graph of the transducer displacement versus time. In this way, the extent of loading pin displacement in relation to the amount of crack growth can be compared for each test-piece. Figures (68-81) show the graphs of displacement (Δ) versus crack length (a) and the corresponding values of the elastic displacement due to crack growth are also plotted for comparison. The crack growth data show a jumpy nature which is due to the scatter produced by the visual method of crack reading ($\pm$ 1 mm). There is a further reduction in accuracy of the crack growth measurement of the steel specimens due to the high temperature oxidation, and therefore it is suggested that the crack growth behaviour of these geometries should not be considered over small ranges of crack lengths (i.e. less than 5 mm) since the amount of scatter will dominate in that range. However since the DCB and the DT test-pieces, forming 95% of the test data in this work, have measurably long crack growth regions

(around 100 mm), the extent of scatter should not affect the final analysis of the C.C.G. behaviour.

5.2.2. The General Trends of the Experimental Graphs

A qualitative understanding of the fracture behaviour can be reached by observing the shapes of the experimental graphs, without using a fracture mechanics correlating parameter.

The geometry of the test-piece inherently controls the shape of the crack growth curves. The test variables such as load, temperature, specimen size, crack length, material ductility and the extent of side grooving only modify these shapes. Therefore by using a particular geometry it is possible to observe the effects of the test variables and, following this, to compare the effects of different geometries.

5.2.3. The shape of the DCB-C Graphs

The DCB-C test-piece was designed to give a region of constant K over a range of crack lengths, a, (50 mm < a < 150 mm). Kenyon (78) testing DCB-specimens of RR58 expected to find a linear crack growth versus time relationship in order to relate the creep cracking rate to the L.E.F.M. parameter K. Instead he suggested that there existed regions of primary, secondary and tertiary cracking. Figures (44,45) show typical crack growth curves for RR58 and steel respectively. Kenyon (78) found that an increase in crack length, load and aging effectively reduced the primary region and that testing at higher temperatures tended to increase the primary region. It is misleading to separate the crack growth into three

distinct regions since this may suggest different cracking mechanisms for the different stages. A better explanation would be that there is a constant slowing down of the cracking rate with increase in crack length and that the rapid increase in crack rate in the final stage is only due to the effect of reaching the end of the test-piece. This reduction in the crack speed can be attributed to two main factors:

1. Metallurgical changes in the material during the test.
2. Non-applicability of L.E.F.M. for C.C.G.

If purely geometrical factors dominate, then the L.E.F.M. concept does not adequately describe the fracture process and non-linear mechanics may be more suitable (127-129). This will be discussed in section (6.2.1.) The metallurgical changes will help to reduce the C.C.G. rate and the extent of this slowing down will depend on the testing time, temperature and the materials metallurgical stability. The RR58 which is received in a 75 mm thick rolled plate is effectively prestrained $2\frac{1}{2}\%$. At creep temperatures metallurgical changes such as overaging as well as a reduction in the residual stress due to the prestraining will reduce the C.C.G. rate. The slowing down is still prevalent in a test lasting 500 hours shown in figure (46) compared to figure (44) which lasted for over 3000 hours, both tested at $150^{\circ}C$. Tests carried out on quenched steel at $565^{\circ}C$ showed a similar phenomenon. Figure (45) with a test time of 600 hours shows a decreasing rate of C.C.G. for steel. It could be argued that the heat treatment and oil quenching from $1250^{\circ}C$ would produce an unstable martensite-bainitic structure which rapidly tempers at $565^{\circ}C$. Unlike RR58 the steel is

less stress sensitive and therefore it was possible to measure a wider and faster range of controlled crack growth rates. A test lasting 30 hours for the quenched material, figure (47), shows a constant crack growth rate region. In effect the low creep ductility of this material together with short time at temperature has not allowed tempering to affect the crack growth which can therefore be described in terms of K. By tempering the quenched steel for 24 hours at 680°C prior to testing it was hoped that the metallurgical structure would be more stable for a longer test period. Figure (48) shows a relatively linear crack growth relationship with time for a test lasting 160 hours. Figure (49a) shows a tempered steel in a slower test (1300 hours) for which the effect of tempering could be more dominant. Figure (50) shows a comparison between a quenched and an quenched and tempered material at the same load and a very similar initial crack length. The quenched material shows a decreasing cracking rate but it is clear that the effect of tempering is not dominating the C.C.G. rate. An important comparison is figure (50) with the uniaxial creep curves of the quenched and quenched and tempered material shown in figure (37). Although the rupture life of the tempered material is increased by a factor of 2.5 in figure (37) the crack propagation behaviour in figure (50) of the two treatments are comparable, suggesting that geometry greatly influences C.C.G. behaviour.

5.2.4. The Shape of the DCB-P Graphs

Unlike the DCB-C test piece this specimen has an increasing compliance rate with an increase in crack length.

Figures (51,52) show typical crack growth data for RR58 and steel respectively. In every instance there is a slow increase in crack length followed by rapid crack growth, culminating in unstable fracture. The effects of metallurgical changes that were discussed with respect to the shape of DCB-C tests cannot be readily evaluated from the DCB-P graphs since inherent in the geometry is an increasing crack rate with crack length at constant load. Although the DCB-P is in every way similar to the DCB-C geometry, excepting for the contour, the crack growth behaviour is markedly different and only by using a relevant fracture mechanics parameter would one be able to correlate the data. This will be discussed fully in Chapter Six.

5.2.5. The Shape of the DT graphs

This specimen also shows a constant K characteristic independent of crack length. Tests were only carried out on RR58 at 150°C. Figure (53) shows a characteristic crack growth graph for a DT test-piece. There is still a slight slowing down associated with overaging. The load was dropped from 9607.7 N to 8273.3 N for 900 hours and when the test-piece was reloaded to the original load the cracking rate reduced by a factor of two, suggesting a possible effect due to overaging which was also seen in the behaviour of the DCB-C test-piece.

The Shape of the CT graphs

CT test-pieces along with SEN-T, SEN-B and W.O.L. geometries all show a similar behaviour to the DCB-P test-piece. Figure (54) shows a steel CT tested at 565°C. This is a typical behaviour of the crack growth of these

specimens all of which have a rapidly increasing stress intensity K with crack length. The steel tested in this case has a low creep ductility value of around 1%, but the advantage of the CT test-piece over the DCB specimens is that they can be used to test materials with very high creep ductilities. Harper (95) was able to test a 1 Cr. Mo. V steel in the ferritic condition using a 25 mm thick CT test-piece and found that the length of the incubation period prior to rapid crack growth was related to the materials creep ductility. He found that as much as 85% of the specimen life was taken up in incubation whereas for the bainitic CT, cracking will start almost immediately even though Harper (95) used a sharp fatigue crack starter and the test-piece in figure (54) had a flat saw-cut for the initial crack tip. Relatively few tests were performed using the CT specimens since it was found that the visual technique of crack measurement was not sufficiently accurate for such short ranges of crack growth.

5.2.6. Constant C* (Analytical) tests performed on DCB-C Test-pieces

From the discussion of the shape of the DCB-C graphs in section (5.2.3) it was concluded that a probable explanation for the slowing down phenomenon might be the non-applicability of L.E.F.M. In section (3.4.5) the concepts of non-linear mechanics for the DCB test-piece were discussed. It was found from equation (3.43) that the value of the analytical C* decreased with increasing crack length (figure (22)) as a function of the creep index n, possibly explaining the decrease in cracking rate. Using the same equation

(3.43)for the DCB-P test-piece it is found that C* analytical also increases with crack length. To explain the slowing down of the cracking, constant C* (analytical) tests were performed on some DCB-C specimens of RR58 and steel by evaluating from equation (3.43) the load needed to keep C* (analytical) constant along the specimen length at a particular creep index n (in this case values of n of 10 and 14 were selected for steel and RR58 respectively). It was found that approximately 20 - 25% load increase was needed to keep C* constant along the DCB-C test-piece. Figures (49b, 55, 56) show constants C* tests for RR58 and steel 25 mm thick specimens. The incremental load increases are also shown on the graphs. These two tests which are relatively short term (70, and 150 hours respectively) show a linear relationship of crack growth with time, but it was found that testing at lower loads (i.e. longer test duration) the slowing down of the cracking in the DCB-C test-piece was still prevalent suggesting that the formulation of C* (analytical) is still inadequate in explaining the reduction in crack speed. In Chapter Six all the DCB data will be plotted versus the C* (analytical) parameter and the possible weaknesses in the analysis will be pointed out.

5.2.7. The effect of Load Change on Crack Growth of Different Geometries

One advantage of the DCB and DT over CT and SEN test-pieces is that a number of load increases and/or decreases can be made during the test to achieve different rates of crack growth. In the bend type specimens the material further ahead of the crack is essentially unaffected by

stresses, especially for the more creep brittle materials which allow less stress redistribution to take place at the crack tip. From all the experimental graphs it is observed that at the start of the tests or during the initial stages following a load change there is a short time period (approximately 5% of the total test time) in which the crack tip stress and strains adjust to the changes in the applied stress level. This effect is hardly noticeable for the more creep brittle materials and also at lower loads. Figures (49a,53) show the initial rapid increase in the displacement for a DCB-C and a DT test-piece respectively. Both have relatively blunt (compared to fatigue pre-cracked materials) saw cut crack starters and once the crack has grown about 7-8 mm the condition is stabilized and creep cracking dominates.

In general a load increase will increase the cracking rate and a load decrease will reduce it. The extent of the relative crack rate increase with an incremental load change will depend on the geometry, thickness, side grooving and the creep ductility of the material and a quantitative assessment of these factors will be made using fracture mechanics correlating parameters in chapter six.

Figure (57) shows the effect of a short drop in load on a 25 mm thick steel DCB-C test-piece. The transducer displacement shows the marked drop at the load change associated with the elastic displacement. Figure (58) shows a 12 mm DCB-C test-piece with load increase at three different crack lengths. Similar trends are shown in DCB-P tests when the load is changed. Figure (59) shows an initial load decrease followed by an increase at a longer crack length for DCB-P RR58 test-piece. It should be noted that although

the load increase to 7117 N was less than the initial load of 8896 N the cracking rate was faster, this is because the compliance for the DCB-P geometry is a function of crack length. Figure (60) shows a similar trend for 25 mm thick DCB-P steel specimen. In this instance the load is dropped by about 40% and effectively there is no visible crack growth for 130 hours, but given sufficient time it would be expected that cracking would occur at this load. The load was subsequently increased to observe the cracking behaviour at a faster rate.

Various tests were performed on the quenched and tempered steel using DCB test-pieces of thickness (B) of 12 mm. to compare to the 25 mm thick specimens. Figures (58,61) show the shapes of crack growth and load change for thinner (12 mm) steel DCB-C with net thickness (B_n) of 3 and 6 mm respectively. Both show a marked increase in creep bending compared to figure (57) which is a 25 mm thick steel specimen. Similarly figures (62,63) show two thin DCB-P test-pieces of B_n = 3 and 6 mm respectively. The effect of the applied load on the C.C.G. rate observed in the different geometries can only be satisfactorily determined by using a fracture mechanics correlating parameter. Section (6.1.1) in chapter six will quantitatively compare the C.C.G. rate of each geometry, thickness, and side grooving in order to reach an understanding of the effect of triaxiality on creep cracking. The effect of the load histories will also be discussed in terms of the stress intensity factor K in the next chapter.

5.2.8. The Effect of Temperature on Crack Growth

Nearly all the tests in this program were performed

at the test temperature of 150°C for RR58 and 565°C for steel. Kenyon (78) tested DCB-C specimens in the range of 100° - 200°C. He found that at 100°C there was either a stoppage or a markedly reduced amount of crack growth, and an increase in temperature increased the cracking rate as well as the amount of creep deformation. He found that at temperatures above 175°C the extent of arm bending due to creep made it extremely difficult to achieve a steady cracking rate, since at high temperatures the creep deformation became dominant. Figures (64,65) show DCB-C tests at 175°C and 200°C respectively. It should be noted that for the first 30 mm of crack growth the transducer displacement for the tests at 200°C (figure (65)) was approximately double that of the test at 175°C. Figure (66) shows a test of DCB-C, RR58 during which there was a load increase and temperature increase from 150° to 175°C to 200°C. Clearly both the extent of creep cracking and the creep bending of the arms rapidly increases with the increase in temperature.

Only one single test at 615°C was attempted for steel on a DCB-P test-piece. Figure (67) compares the steel DCB-P specimens tested at 615°C and 565°C with the same initial crack length. The load on the test at 565°C is approximately 10% greater than the test at 615° but its crack rate is on average slower by a factor of more than two.

5.2.9. <u>The Relationship between Transducer Displacement and Crack Growth</u>

The transducer displacement (Δ) was monitored for each test. A selection of transducer displacement (Δ) versus

crack length (a) for different geometries and conditions are shown in figures (68-81). The respective plots of the elastic Δ_e, evaluated from the experimental elastic compliance, are also plotted against crack length in some instances. These show that the total displacement (Δ) recorded during a creep cracking test consists of:

$$\Delta = \Delta_e + \Delta_{cr} \qquad (5.4)$$

The elastic displacement is dominant in materials which are relatively creep-brittle and therefore for such cases it is expected that the Δ versus a graphs will reflect the shape of the elastic compliance graph. The amount of Δ_{cr} varies with material ductility as well as geometry, loading, size and the extent of side grooving.

From equation (5.5) it is seen that the elastic compliance C is given by

$$C = \frac{\Delta}{P} \qquad (5.5)$$

$$\frac{dC}{da} = \frac{1}{P} \frac{d\Delta}{da} \qquad (5.6)$$

and normalizing for all temperatures gives

$$E \frac{dC}{da} = \frac{E}{P} \frac{d\Delta}{da} \qquad (5.7)$$

Therefore by multiplying the elastic compliance C by the particular testing load P it is possible to evaluate the elastic $\frac{d\Delta}{da}$ at the relevant temperature. This can then be compared with the experimental $\frac{d\Delta}{da}$, shown for each test in table (5), derived from the creep cracking tests. Generally, as shown in figures (68-81) the amount of Δ_{cr} accumulates during the test, and this is reflected by the increased slope of the experimental $\frac{d\Delta}{da}$ compared to

the elastic $\frac{d\Delta}{da}$.

The shape of the Δ versus a graph from the C.C.G. tests is modified by the increase in the test temperature, loading, specimen size and test duration. Figures (68,69) show a linear relationship between Δ and a for RR58 and steel DCB-C specimens of thichness B = 25 mm. The plots show that the creep deformation for the RR58 tested at 150°C is almost negligible and for the steel in the region of 5 - 10% and therefore suggest that the respective $\frac{d\Delta}{da}$ slopes are reflecting the constant K nature of the DCB-C geometry. Figures (70,71) show, for the same test temperature and specimen size as figures (68-69) the Δ versus a graphs of DCB-P, RR58 and steel respectively. It is found that the extent of Δ_{cr} is less than 10% for both cases. Due to the increasing compliance with crack length the slopes of the $\frac{d\Delta}{da}$ also accelerate with respect to crack length. It is found that a decrease in specimen thickness and sidegrooving also increases the amount of creep deflection in a test-piece. This factor will be discussed in terms of C^* in chapter six but representative graphs of Δ versus a for different specimen thicknesses are shown in figures (72-74) for DCB-C test-pieces, figures (75-76) for steel DCB-P test-pieces. It is found that a load increase generally increases the amount of creep deflection, as is evident for the steel DCB-C graphs in figures (73,74), and that a reduction in load reduces the extent of creep deflection. Figures (75-76) for steel DCB-P test-pieces, show that after a decrease in load the experimental and the elastic slopes of $\frac{d\Delta}{da}$ are approximately the same suggesting a reduction is the creep deflection

with a decrease in load. Figure (77) shows a comparison between the experimental deflection of three RR58 test-pieces for different B and B_n values at different loads. Reduction in thickness and geometry increases the creep deflection (shown in the shaded areas). For the two 25 mm thick specimens of different B_n values the necessary load increase to induce cracking in the specimen with B_n = 20 mm has effectively changed the creep deformation rate. Comparing the two specimens with the same B_n/B ratios both specimens show larger amounts of creep deformation compared to the specimen with a higher ratio of B_n/B suggesting the importance of constraint in the creep cracking behavicur of materials.

An increase in the testing temperature is synonymous with an increase in creep deformation. Figure (78) shows the effect of increasing the temperature from 150°C to 200°C for an RR58 alloy. The rapid increase in the bending of the arms at 200°C is shown when compared to the elastic displacement. Figure (79) shows the Δ versus a for a steel DCB-P test-piece at 615°C. The steel DCB-P tested at 565°C (figure (71)), with 20% more load, has approximately a third of the creep deflection shown by the specimen tested at 615°C (figure (79)).

The DT test-piece of RR58 at 150°C show a linear fig 80 Δ v a relationship, except for the initial rapid increase which can be attributed to the application of the load and the creep crack initiation from the razor cut crack starter. The constant K nature of the test-piece makes it comparable to figure (72) which is a DCB-C RR58 tested at 150°C.

The slopes of the elastic $\frac{d\Delta}{da}$ are similar to the experimental $\frac{d\Delta}{da}$, suggesting very little creep deformation with crack growth. A significant point is that by measuring the displacement at the loading pins of widely different geometries, it is possible to compare their cracking behaviour under different conditions.

Figure (81) shows a typical Δ versus a graph for a CT specimen of the quenched and tempered steel. The initial rise is associated with the stress relaxation occurring at the crack tip when the load is added. After a period of stabilization there is a typical increasing rate of $\frac{d\Delta}{da}$ with crack length. The elastic Δ_e calculated from the boundary collocation results for the elastic loading of the CT test-piece used by (133,134) shows that the experimental $\frac{d\Delta}{da}$ is primarily elastic and this is expected for such a bainitic steel with low creep ductility. Using the CT geometry the very creep ductile materials exhibit incubation periods (76,95,101). There is initially a constant increase in the transducer displacement, associated with the creep deformation of the test-piece and the creep damage due to the growth of cavities in the region of the crack tip. This period can take up 90% of the specimen's life depending on the creep ductility and the extent of side grooving.

5.2.10. Creep Deformation Tests using the DCB-C Geometries

Experiments were performed in order to see the effect of creep bending of the DCB-C arms without allowing creep crack growth to occur. Blunt holes were drilled at different crack lengths in the 25 mm thick DCB-C RR58 and steel

specimens and the creep deflections were measured over different loads and time periods and the following observations were made:

(1) It was found that primary creep was dominant, and that the specimens never reached a steady state creep situation. Figures (82,83) show this for RR58 and steel respectively.

(2) For the proportional increase in loading and crack length there was no marked increase in the creep rate. Figure (83) shows this for the steel at a crack length of 100 mm. This suggests that the stiffening of the arms is also dependent on the loading history and time at temperature. Figure (84) shows this clearly with two RR58 tests at 150^{o}C with the same load at a crack length of 100 mm. One of the two specimens was previously untested but the other specimen was tested for creep bending of the arms for 2000 hours for shorter crack lengths of 50 and 75 mm.

(3) It is found that after a time at testing temperature with an applied load a creep crack initiated and propagated from the blunt starter hole, reflecting the relatively creep brittle nature of the RR58 and steel. Figures (82,84) show the incremental increase in the deflection from the point at which it is estimated that a creep crack has initiated and begun to propagate.

(4) An insight into the influence of creep ductility and specimen geometry on C.C.G. can be made by observing figures (83,85). Figure (83) shows the creep deformation of a DCB-C steel in the bainitic condition at a crack length of 100 mm. There is less than 0.075 mm of arm bending after 100 hours and the crack eventually began to propagate

from the blunt crack tip. For comparison figure (85), which was a DCB-C tested in the as received ferritic condition (and also fatigue precracked) showed no sign of crack growth and deformed by about 100 times faster than the bainitic material. This suggests that the DCB-C type specimens, of the present thicknesses (B = 25 mm), are not sufficiently constrained enough to produce C.C.G. in creep ductile materials, whereas authors (shown in table (1)) who have used CT and SEN-B test-pieces have successfully induced C.C.G. in materials with high creep ductility, which effectively means an increase in constraint at the crack tip with the CT and SEN-B test-pieces.

5.3.1. Metallurgical Observations

The fracture characteristics of the RR58 and the steel alloy were observed by two methods. Firstly the appearances of the fracture surfaces of the test-piece were observed using a stereo microscope and in a few cases photographed using a scanning electron microscope. The second method was to examine the fracture path by stopping a test prior to final fracture and polishing and etching the surface perpendicular to the crack path. In this way a better understanding of the behaviour of the mechanical tests can be reached. No attempt was made in this work to quantitatively relate the microscale observations to the macroproperties of the material since the objective of the present studies was to relate creep crack growth to the concepts of continuum mechanics.

5.3.2. Fracture Surfaces of RR58 and Steel

The metallurgy of creep fracture has been studied

in detail by many authors listed in table (1). Recent reports (78,135) have examined in detail the creep cracking process in RR58. They conclude that the fracture facets are formed during creep by the growth of wedge cracks at grain boundaries or at the second phase particles within the grains. The intergranular feature of the creep crack is also prevalent in steel (136). The extent of the intergranular fracture is dependent on the stress level and temperature. At low stresses, thermal activation causes creep cavities to initiate and coalesce at the grain boundaries. An increase in the temperature drastically reduces the grain boundary strength which in turn helps the formation of cavities by the sliding mechanism. Figures (86,87) compare the scanning electron fractrograph of a room temperature tensile fracture and creep fracture at 150°C in the RR58. In both cases there are dimples which are associated with ductile grain boundary damage and rupture. The extent of ductile tearing at room temperature, shown in figure (86), marked A, could be due to the relatively high strain rate (0.025 mm/min) used to fracture the specimen, but some grain boundary fracture is also (marked F) prevalent at room temperature. In both figures (86,87) there are extensive numbers of intermetallic particles lodged at the base of the dimples (marked C). These can be associated with void initiation prior to rapid crack propagation. Figure (88) shows a higher magnification of a grain boundary RR58 creep fracture at 150°C. The second phase particles on the surface are clearly visible and the fine dimple feature (marked D) are in complete contrast to

the larger more ductile dimples (marked B) induced by the presence of the second phase particles in the grain matrix. The comparison between the fracture surfaces of RR58 is more difficult at lower magnifications but the general trend is the increase in surface roughness with increase in test temperature. This is possibly due to the increase in a creep damage zone with increase in test temperature. This means that if creep cavities can be formed in a wider volume at the crack tip then their coalescence will produce a rougher fracture surface.

No scanning electron fractograph for the steel were taken since the cracking tests were performed in air thus rendering the fracture surface open to excessive oxidation. Figure (89) shows the magnified fracture surface of a quenched steel tested at 565°C. The clear intergranular fracture can be seen even with the presence of the oxide film. In this specimen the microstructure consisted of untempered martensite and bainite in prior austenite grains. This shows the high creep-deformation resistance of the quenched steel. The observation of the quenched and tempered fracture surfaces showsa less distinct intergranular fracture suggesting an increase in ductility as well as fracture occurring at the second phase carbide particles which would have nucleated at the tempering temperature of 680°C. Gooch (136) has observed the creep fracture of the $\frac{1}{2}$ Cr, $\frac{1}{2}$ Mo, $\frac{1}{4}$ V steel for different heat treatments. He shows that there is clear intergranular fracture for the fully bainitic structure (similar to figure (89)). The increase in the ferrite content decreased the clear intergranular

fracture and increased the ductile mode of fracture associated with dimples at the gtain boundaries similar to those observed in the RR58 (figures (86-88)). These findings indicate that the decrease in creep ductility observed in the above metals can be associated with an increase in intergranular mode of fracture. This is a relative effect since the increase in triaxiality and general reduction in the stress levels effectively produce low ductility and hence inter-granular creep fracture.

5.3.3. The Effect of Geometry on the Mode of Fracture

In analysing geometries with a dominant crack it is essential to know the extent of crack tip deformation which takes place at high temperatures. The brittle-ductile nature of a crack is relative and it is dependent on four factors; geometry, thickness, extent of constraint and the stress level.

In comparing the two thicknesses of the DCB-C RR58 and steel test-pieces it is concluded that the decrease in the extent of side grooving produces a curved fracture front leading at the centre, and an increase in the amount of cracking ahead of the crack tip as well as the tendency for a flat fracture to deviate from the cracking plane. Figure (90) shows the amount of unconnected cracking (around 2.5 mm) at the crack tip for a thin (B = 9.5 mm) DCB-C RR58 specimen tested at 150^{o}C. An increase in the size and side grooving of the test-piece reduces the amount of crack growth ahead of the crack tip.

The amount of constraint is also dependent on the creep ductility and size of the specimen. Thus in comparing

figures (91, 92) it is seen that for the tempered steel (figure (92)) of 12 mm thickness there is approximately 3 mm of disconnected cracking ahead of the main crack, whereas the low ductility quenched steel figure (89) shows a sharp inter-granular crack tip. Both appear to show that the cracking takes place at the prior austenite grain boundaries but the cracking of the tempered material appears to show a more complex behaviour. It is postulated that where voids initiate ahead of the main crack tip they will finally join up when their size and numbers reach a critical level so that the effective stress in that zone is greater than the local U.T.S. of that damaged area.

Figure (93) shows the side view of seven cracked D.C.B. specimen (1-4) are RR58 and (5-7) are steel test-pieces. Numbers (1,2,7) showing prominantly that the fracture surfaces are not flat, are respectively, a 25 mm thick RR58 specimen tested at 200^{o}C, a 9.5 mm thick DCB-C tested at 175^{o}C and number (7) a 12 mm thick DCB-P steel with B_n of 6 mm. Specimens (3-6) showing flat fracture surfaces are all 25 mm thick RR58 and steel DCB specimens all tested at 150^{o}C and 565^{o}C respectively. A graphical description of the fracture fronts and profiles are shown in figure (94). Generally a reduction in ductility, creep temperature, increase in side grooving and specimen size produces a flat fracture with a straight crack front and sometimes in the extreme cases fracture leading at the edges. Conversely an increase in ductility and stress level and a reduction in specimen thickness and side grooving produces a crack leading at the centre with cracking ahead of the main crack and a deviation of the fracture surface from the cracking plane. Specimen geometry will also effect the

crack tip behaviour. In general it can be stated that for a particular thickness, size and stress level the resistance to deformation, i.e. the increase in constraint, is greater in the CT and SEN geometries than in the DCB and DT test-pieces.

5.3.4. Hardness Measurements

One possible method of evaluating the metallurgical stability of the material, when subjected to long periods at high temperature, is to measure the hardness values of the specimens before and after each test. A stable Vicker's hardness value does not necessarily mean a stable creep property, but it can be used as an approximate measure of the material yield/tensile strength. For both RR58 and steel there was a general drop in hardness with increased time at temperature. Table (5) shows the duration of each test at the relevant temperature and figures (95,96) show the hardness drop with time at temperature. Figure (95) gives the drop in hardness for RR58 for test temperatures of 100°C to 200°C. The slight drop in hardness for over 3000 hours at 150°C and below suggested that the effect of overaging was possibly small and hence more importance was attached to the testing and analysing of RR58 C.C.G. data at 150°C. Figure (97) shows the effect of overaging at 200°C for 600 hours. Both DCB-C specimens were tested at 150°C and although the overaged specimen had about 20% more load its cracking rate was slower. Although the hardness values are relatively stable at 150°C both test-pieces in figure (97) show slowing down of cracking rates suggesting that the hardness decrease does not completely describe the cracking behaviour.

For the ½ Cr, ½ Mo, ¼ V steel in the as received condition, it was found that the normalized and tempered ferritic matrix gave an approximate hardness of 130 VHN with creep ductilities in the region of 20 - 50%. In such circumstances it was found that the arms of the DCB test-pieces bent rapidly due to creep deformation at 565°C (figure (86)) hence rendering the specimen useless for C.C.G., due to extensive deformation. The heat treatment chosen (given in section (4.1.2) essentially simulated the heat affected zone (H.A.Z.) of the weld metal. Figure (96) shows the hardness values of the 3F block after testing at 565°C. The initial values were in the region of 250 - 270 V.H.N. and after an initial peak hardness which is likely to be due to the precipitation of the second phase carbide there is constant drop in hardness. Block 8F, 10F, 7G and 4F were all oil quenched from 1250°C and then tempered for 24 hours at 680°C. The initial range of their hardness values lay between 225-245 V.H.N. with 10F, and 4F in the upper region and 8F and 7G in the lower values. It is found that after testing at 565°C there was a general drop in hardness value with increasing time at temperature. Figure (96) shows that after 2000 hours at 565°C the hardness values fall between V.H.N. of 205-225, suggesting that tempering is not negligible at 565°C. The harsh heat treatment of a rapid oil quench from 1250°C inevitably induces not only a large variation of hardness (figure (9.6)) from specimen to specimen but also a range of prior austenite greain sizes (200 μm - 400 μm) within each individual specimen. It is evident from these values that an inherent amount of scatter will exist in correlating creep

growth data, since there will be differences in the metallurgival properties for each specimen as well as the errors involved in experimental techniques. These factors suggest that the data should be analysed on a broad spectrum in order to achieve meaningful quantitative relationships for use in design. Chapter six will attempt to correlate all the data that has been individually discussed in this chapter.

CHAPTER 6

CORRELATION OF CREEP CRACK GROWTH DATA WITH VARIOUS FRACTURE MECHANICS PARAMETERS

6.1. Introduction

Creep cracking data collected from over one hundred tests at Imperial College have been analysed with the aid of a CDC 6400 computer. Table (5) gives the basic information relevant to each test, and it also gives the instantaneous cracking rate and the transducer displacement rate at different crack lengths for each test-piece. It is generally found that there is a large amount of experimental scatter in the data. This was found to be unavoidable since even under the most stringent test conditions the data did not exactly agree from test to test given the same initial conditions. The extent of scatter is found to be consistent with that found by other workers (table (1)) and for example shown in figures (16 - 17) for the data collected by Neate (88, 91).

In this chapter, the C.C.G. rate for the different specimens will be correlated initially in terms of the stress intensity factor K and subsequently an attempt will be made to describe creep cracking by a non linear fracture mechanics parameter called C*. The available data for the RR 58 and steel will not be discussed separately, but rather, by observing the cracking behaviour of both alloys together it is hoped that eventually a clearer picture will emerge as regards the applicability of Fracture Mechanics to C.C.G.

6.1.1. Correlation of the data with the L.E.F.M. Parameter K.

Before observing the behaviour of crack growth relation to K it is useful to understand the general range and cracking rate behaviour of the RR58 and steel. Figures (98,99) show the log crack growth versus log time results for a range of 25 mm thick DCB-C RR58 and steel test-pieces at various loads and temperatures. Clearly the RR58 is more stress sensitive and it was impossible experimentally to achieve creep cracking rates faster than 1.5 mm/H at any temperature. Also at lower loads, for cracking rates of less than 0.01 mm/H, problems of material overaging begin to dominate in RR58,inherently affecting the C.C.G. behaviour. Figures (99,100) show log crack growth versus log time graphs for DCB-C and DCB-P steel test-pieces. Controlled C.C.G. was achieved over a range of three decades in this bainitic material. For the low ranges of cracking rates (less than 0.01 mm/H) further tempering of the bainitic microstructure of the steel would effect the C.C.G. rate.

6.1.2. Individual trends of Cracking rate versus K for each test-piece

Figures (98,99) for the DCB-C test-pieces can be described by the equation

$$a \alpha t^{q} \qquad (6.1)$$

Since for these DCB-C specimens stress intensity is independent of crack length it follows that q should equal 1 to make the crack rate time independent. The value of q, for the RR58, is found to range between 0.5 - 0.8 over

a range of loads and temperatures and for the steel q varies between 0.95 - 0.7 over three decades of C.C.G. Kenyon (78) compared the value q to the exponent found in the creep strain - time relationship of uniaxial creep tests (equation (2.3)) and found that q for the uniaxial tests varied between 0.28 - 0.75 for the RR58. The lower ductilities (0.1% - 1%) for the steel made it more difficult to achieve consistent results in the steel uniaxial creep tests and further tests with larger creep specimens will be needed to determine accurately the exponent q, but the present data suggests that q for equation (2.3) for steel lies in a similar range to that for RR58. Figure (100) for the DCB-P specimens shows effectively an increasing cracking rate with time. In this case stress intensity is dependent on crack length and load level and for equation (6.1) to describe the cracking the value of q will need to be greater than unity.

Figures (101,105) show CCG rates versus the experimentally derived stress intensity factor for the 25 mm thick DCB specimens. These are shown specifically magnified and with lines drawn between the experimental points, in order to show the trends of the C.C.G. rate with K for different specimens and load changes. Figure (101) for the DCB-C, RR58 at 150^{o}C should ideally (provided that L.E.F.M. is applicable) show a single point for each specimen and each load change, but, as discussed earlier (section (5.2.3)). The slowing down of the cracking rate at a constant K produces in some instances a horizontal line within the general scatter band. These are more prominent in the

region of 0.01 - 0.1 mm/H producing a tail in the slower region of crack growth. The effect of overaging can be clearly demonstrated by observing the behaviour of specimen B9 in figure (101). An initial load of 3558.4 N produces slowing down of the crack growth rate and when the load is increased to 3736.3 N the cracking does not increase. Figures (102,103) for the quenched and the quenched and tempered steel show similar trends of horizontal lines within the general scatter band. The effect of tempering in this bainitic steel can be clearly indentified by the areas in which the scatter bands exist. In the quenched only material shown in figure (102) there is a slowing down of the crack in the region of 0.10 - 1.0 mm/H whereas in the quenched and tempered material the decreasing crack rate is one decade less. This is to be expected since the tempering at 680^{o}C prior to testing has relatively stabilized the microstructure so that for short term tests the effect of tempering at the test temperature of 565^{o}C will no longer dominate.

Figures (104,105) show the C.C.G. rates of the DCB-P test-pieces for the steel and RR58. As discussed earlier these specimens exhibit an increasing compliance rate with crack length. For both figures (104,105) the individual lines for each specimen show an increasing cracking rate with increasing crack length. Figure (104) shows the larger amount of scatter that is found in the DCB-P RR58 test-pieces compared to the DCB-C, RR58 at 150^{o}C (figure (101)). The effect of overaging is not so readily observed in the DCB-P specimens since the inherent increase of crack growth

with stress intensification tends to overide the relatively weaker effect of the decrease of cracking rate due to over-aging. Also apparent from figure (104) is the stress sensitivity of the RR58 which produces a scatter of about 10 within two decades of crack growth rate. Figure (105) for the steel DCB-P shows a more predictable material behaviour. The individual trends can be generally said to align with the total trend and any change in load also induces a crack growth rate within the scatter band.

Attempts were made to reduce the extent of scatter in the cracking data by reducing the test variables in order to see whether the C.C.G. rate correlated better with K. For exampe:

(a) the data were plotted for the first two hundred and fifty hours of the test or between 250 - 500 hours of test in order to reduce the period of overaging or tempering. Figure (106) shows all the DCB-C test data for RR58 at 150^{o}C and figure (107) shows only the data for the first 500 hours of the test. Comparison shows the only difference is a slight reduction in the scatter specially at the lower cracking rates.

(b) the data were plotted for a constant crack length (or for a limited range of crack length) so as to eliminate any crack lengths effects.

(c) the data for the specimens with the same load history and initial crack length were plotted to reduce the effect of different creep histories for different specimens.

All these factors provided no real improvements within the scatter band and therefore it was decided on this basis

to observe the general crack growth rate trends of each geometry separately.

Figure (106) shows all the available data points for the DCB-C, RR58 at 150°C. There is a fairly good correlation with K which can be described by the equation (3.2).

$$\dot{a} \alpha K^m \qquad (3.2)$$

By using the least squares method the values of m were computed and are shown on the relevant figures. The value of m for all the RR58 data at 150°C is found to be 13.5 and drops to 12.3 for the short term data (less than 500 hours) plotted in figure (107) suggesting an increasing sensitivity to K with increasing test time. Figures (108,109) for the DCB-C steel quenched, and quenched and tempered respectively show a better correlation with K which is to be expected since the creep ductility in these bainitic conditions are markedly reduced compared to the RR58. Comparing the values of m for the quenched m = 6.2 and for the quenched and tempered m = 8.0 shows that an increase in creep ductility increases the value of m for cracking. The creep index n (discussed in section (3.1.2.)) for the uniaxial creep deformation data was n = 5.6, and n = 7.8 respectively which compared well with these values of m suggesting that a relationship may exist between creep deformation and creep cracking.

Figures (110, 111) show the data for the 25 mm thick DCB-P, RR58 and steel respectively. The complexity of the cracking behaviour in the RR58 can be described less distinctly by K whereas the bainitic steel with generally lower values of m show a more predictable behaviour.

Figure (110) shows the large extent of scatter for the DCB-P RR58 data at 150°C and the statistically determined value of m for equation (3.2) is found to be 6.5 which is about half the value for the DCB-C RR58 specimens. Figure (111) shows the DCB-P graph for the steel at 565°C. The value of m for equation (3.2) was found to be 4.7 which is again lower than the DCB-C steel specimens. Both these results suggest that C.C.G. rate is strongly geometry dependent.

6.1.3. The Effect of Heat treatment, Thickness and Side grooving on the Crack Growth Rate of the D.C.B. Test-pieces

Figures (112,113) show the DCB-C data of different thicknesses and heat treatments for RR58 and steel respectively. The effect of extensive overaging is shown in Figure (112) for RR58. Specimen B41 was overaged at 200°C for 600 hours, during which time the hardness dropped from 150 to 128 V.H.N. The increase in creep ductility effectively increases the load needed for C.C.G. Figure (113) shows that the tempering prior to testing of the bainitic steel has had little effect on the cracking behaviour which still falls within the scatter band of the quenched material.

By far the biggest effect on the crack growth rate is due to the specimen thickness. Figures (112,113) for the DCB-C and figure (114) for the DCB-C show a range of specimen thicknesses. The trend shows that in general the cracking rate decreases markedly with decrease in thickness at constant K in the DCB-C specimens. It was shown in section (5.2.9) that the extent of creep

deflection Δ_{cr} in the DCB test-pieces increased with decrease in specimen thickness and this is synonymous with an apparent increase in stress intensity K for thinner test-pieces. It can be argued that the calculated K for the thinner specimens is an over estimate of the true stress singularity at the crack tip and that therefore the applicability of K begins to break down with decrease in specimen thickness. Figure (112) for the RR58 shows the complete lack of correlation for the 9.5 mm thick specimens. It is seen from figure (114) for the DCB-P steel data that there is a good correlation for the different thicknesses suggesting that specimen geometry also affects the critical thickness below which the correlation with K breaks down.

The extent of side grooving also affects the crack growth in a complex manner. It is essential for the DCB test-pieces to have side grooves in order to keep the crack path perpendicular to the load line and the centre of the specimen. Only one test (B2) in figure (112) was performed by Kenyon (78) to compare different side groove depths for 25 mm thick specimens and this shows that a decrease in side groove depth effectively increases the cracking area and produces a higher K for cracking. Once again this suggests that K is inapplicable since a load increase on the same thickness of test-piece increases the creep deformation rate of the test-piece and hence affects the rate of relaxation of the elastic stress singularity. The effect of side grooving for the steel is less distinct since ideally tests should have been carried out on different amounts of side grooving for the thicker (25 mm)

test-piece in the hope that the specimens would more likely be in a plane strain condition. The 12 mm thick steel specimens were tested with B_n values of 3 mm and 6 mm and figure (113) shows a reverse effect compared to the RR58 behaviour in figure (112). This is probably due to the fact that although the B_n = 3 mm is more constrained than the B_n = 6 mm The plane strain conditions do not prevail for these thicknesses. Once again it is observed in figure (114) for the DCB-P test-piece that side grooving has not affected the cracking behaviour suggesting that the DCB-P test-piece is more resistant to creep deformation in comparison to the DCB-C test-piece. Further tests on widely varying thicknesses and side groove depths are essential in order to produce a quantitative relationship between these factors and slow crack growth.

6.1.4. The Effect of Different Geometries on the Crack Growth Rate of RR58 and Steel

A comparison between the DCB-C and the DCB-P cracking rate is shown in figures (115,116) for 25 mm thick and 12 mm thick steel test-pieces respectively. The difference between the geometries is observed with an increase in specimen thickness but the DCB-P exhibits slower C.C.G. rate for the same instantaneous K. This is most pronounced in the 25 mm thick specimens at faster crack growth rates (figure (115)). Figure (116) shows a better correlation of K for the thinner specimens excepting for a very long term test (2000 hours) which would be affected by excessive tempering. The value of m from equation (3.2), not including the long term test, is 8.1. which is similar in

to that for 25 mm thick test-pieces of steel. Only two CT test-pieces of steel were tested but the results are compared in figure (117) with the results of Neate (91) and Harper (95). The scatter bands of figures (16,17) for the ferritic and bainitic ½% Cr ½% Mo ¼% V steel, tested by the authors (88,91), are plotted with the present CT data in figure (117). They (88,91) used various geometries (CT, SEN-T, SEN-B, WOL) and figure (117) shows that all the data for the bainitic material fall in a scatter band of a factor of 15 of C.C.G. rate. The figure also shows the data obtained by Harper (95) who tested a ductile CT test-piece of 1Cr-Mo-V ferritic steel at 565°C. Therefore figure (117) makes a comparison between various rising K geometries and also shows the effect of increased ductility in C.C.G. of similar geometries. Harper (95) claimed no correlation of his data with K which is acceptable, but looking at the whole spectrum his results fall in line with the general trend of Ductile/Brittle C.C.G. data. The better correlation achieved by Neate and Siverns (88) for the normalized ferritic steel can be attributed to the lower applied load producing crack rates of around 0.001 - 0.1 mm/H. The reduction in load effectively reduces the creep deformation rate and hence decreases the creep zone and the stress re-distribution at the crack tip and also since the normalized ferritic material is metallurgically more stable (compared to the quenched bainitic material) the lower cracking rate would be less affected by material tempering in long term tests. Where the cracking rate for the ductile material is faster (for example Harper

(95)) the rate of stress redistribution increases and hence the correlation with K breaks down.

Figures (118,119) show the graph of K versus cracking rate for various geometries and thicknesses of RR58 at 150°C and the bainitic steel at 565°C respectively. Figure (118) also includes the data from the 9.5 mm thick DT test-piece which also falls in line with the 9.5 thick DCB-C test-piece. The DCB-C 25 mm thick shows the fastest rate of cracking and the DCB-P test-pieces show a wide range of scatter covering a factor 20. the inability to achieve a wider range (about three decades) of controlled C.C.G. rate for the RR58 suggests that creep fracture in this material could be described by a critical value of K termed as K_{ICC} for plane strain creep fractures below which C.C.G. would not start. This concept was also suggested by Kaufmann et al (94) who tested CT aluminium test-pieces.

Figure (119) compares all the steel results and also includes the scatter band of the bainitic $\frac{1}{2}$Cr, $\frac{1}{2}$Mo, $\frac{1}{4}$V steel tested by (88,91) and shown in figure (17). Within the DCB scatter band the reduction in thickness reduces the C.C.G. rate for the same K. Also it is seen that at constant K DCB-C specimens crack faster than the DCB-P specimens. The scatter of all the DCB test-pieces of different thicknesses and side grooving is comparable to that of the unstable (rising K) test-pieces, but there is a factor of approximately 15 decrease in the C.C.G. rate for the DCB test-piece which strongly suggests that there is a dominant effect of geometry that cannot be explained in terms of K.

Finally a comparison of the different methods of

evaluating K is shown in figures (120,121) which show the same data as figures (118,119) for the RR58 and steel respectively. The stress intensities in figures (120,121) are evaluated using equations (4.6,4.12,4.13) for the DCB, DT, and the CT respectively. The values compare well with the experimentally evaluated K discussed in section (4.4.2). It is found that the values of K are approximately 5 - 10% lower using the theoretically evaluated K.

6.1.5. The Effect of Temperature on the Creep Cracking Rate

Variations in the testing temperatures affect C.C.G. in a complex manner. If the temperature is not high enough the thermal activation process that is needed for C.C.G. will not be sufficient. If the temperature is excessive creep bending of the arms will dominate and therefore the general statement that the cracking rate will increase with increase in temperature must be used with caution. Kenyon (78) tested the RR58 over a range of temperature (100 - 200°C) and found that at low temperature of 100 - 125°C he could not easily achieve stable crack growth and at high temperature 175° - 200° the extent of creep bending of the arms increased extensively. As discussed in section (5.2.9) the creep deflection of the RR58 at high temperature increases and this is illustrated in figure (122) showing the experimental $E_T\left(\frac{d\Delta}{da}\right)$ (where E_T is the modulus at the relevant test temperature) for the DCB-C specimens, increasing with test temperature. This suggests that the use of the K parameter becomes inappropriate for an increasing testing temperature. Figure (123) shows all the 25 mm thick RR58 tested from 100 - 200°C (not including the 150°C data which falls within

the scatter). There is no correlation of the data with K suggesting either a possible minimum K_{ICC} as a creep fracture criteria or the use of non linear fracture mechanics criteria which will be discussed in section (6.2.1). Only one test was performed for the steel at 615°C. This is shown in figure (111). The 50°C increase in testing temperature has produced a faster cracking rate since the data points are at the edges of the scatter band. Further tests at different temperatures may produce similar problems to those found in RR58 namely the complex interaction of creep deformation and fracture.

6.2.1. Correlation of Creep Cracking with a Non-Linear Fracture Mechanics Parameter.

It is clear from the last chapter that the apparent correlation of C.C.G. rate with K not only breaks down with increase in creep ductility but is also geometry depenent. From the arguments put forward in section (3.4.4) an attempt was made to describe the decreasing crack rate of the DCB-C test-piece by the use of the parameter C* estimated analytically(as shown in appendix (A)). The decrease in the crack growth rate with crack length can be due to overaging and/or tempering as described in section (5.2.3) or due to the inherent interaction of creep deformation with crack growth.

Equation (3.43) which is an approximate analytical evaluation of C* for the DCB was evaluated assuming steady state creep and ignoring primary creep and the elastic strains. Figure (124) shows the correlation of the 9.5 mm DCB-C RR58 specimens which exhibited decreasing cracking

rates and also from section (5.2.9) were shown to exhibit comparatively large amounts of creep deflection. As stated in section (6.1.1) and shown in figure (112) the thin (9.5 mm) DCB-C RR58 showed no correlation with K whereas figure (124) shows that each specimen follows the same general trend. Also in figure (124) the two specimens B2 (with B = 25 mm and B_n = 20 mm) and B41 (overaged for 600 hours at 200°C) both exhibiting extensive decrease in cracking rate show a good correlation with the analytical C*.

It was found that there was no improvement in the correlation with a change in the value of n (used in calculating C* in equation (3.43)) and therefore values of n = 5 and n = 10 for steel and RR58 respectively were chosen since these approximately gave a slope of unity for the C* versus C.C.G. rate graphs and these value of n were also the lower bound values of the creep exponent for the respective material. Figures (125,126) show the individual test-piece trends for the DCB-C, RR58 at 150°C and DCB-P steel, indicating a slight improvement compared to that with K (figures (101,105)). For figure (125) where at constant K constant C.C.G. rate produces a single point on the graph for C* a vertical scatter band is produced (since C* drops with crack length) but where a test has shown decreasing cracking rate C* describes it better than K.

Figures (127,128) show correlations of the crack growth rate with the analytical C* for all the DCB specimens of RR58 at 150°C and steel at 565°C respectively. Although

it is found that individually each specimen geometry and size shows a reasonable correlation versus C*, figures (127,128) there is little improvement in comparison to the correlation with K (figures 118,119), since they show both thickness and geometry dependence more especially for RR58 (figure (127)).

The assumption that sufficient creep occurs to allow a secondary creep stress distribution in the arms of the DCB test-piece is idealized and it is unlikely to happen in complex engineering materials. Also as described in section (5.2.9) in most instances, for both RR58 and steel, the elastic displacements were dominant remote from the crack and therefore it is suggested that the C* analysis is inadequate, and difficulty in including the time independent elastic strains will need to be incorporated into the non-linear bending beam analysis. This will probably involve the use of complex numerical and computational methods.

6.2.2. Proposal for an Experimental evaluation of C* to correlate the creep Crack Growth Data

As evident from section (5.2.9) the elastic strains recorded by the transducer displacement at the loading pins must be accounted for when characterizing the crack tip behaviour. The total displacement Δ has been shown in equation (5.4) to consist of

$$\Delta = \Delta_e + \Delta_{cr} \qquad (5.4)$$

And for a controlled cracking process the total instantaneous transducer displacement rate will consist of

$$\dot{\Delta} = \dot{\Delta}_e + \dot{\Delta}_{cr} \qquad (6.2)$$

It has been found that in tests where $\dot{\Delta}_e >> \dot{\Delta}_{cr}$ the L.E.F.M. parameter K gives an acceptable correlation of the data and this suggests that in such cases the crack propagates in a sharp distinct manner allowing only a very small amount of stress redistribution to take place. At the opposite end of the spectrum where $\dot{\Delta}_{cr} >> \dot{\Delta}_e$ there is rapid stress relaxation at the crack tip tending towards a homogenous state of stress in the crack tip region which effectively means that there is no single crack dominating and therefore fracture mechanics will not be applicable. Therefore it is postulated that where there is crack growth present regardless of the extent of the $\dot{\Delta}_e/\dot{\Delta}_{cr}$ ratio there must always exist a state of singularity at the crack tip although it will be modified by the extent of creep specimen geometry and thickness. The value of $\dot{\Delta}$ can be used to describe the crack growth behaviour for each individual test-piece as shown in figures (129-134) for various geometries and materials. Figures (129-133) show the individual test-piece trends with load change of the experimental $\dot{\Delta}$ for the DCB specimens. It can be seen clearly that $\dot{\Delta}$ adequately describes the cracking behaviour in all the cases. But the materials used in these tests are relatively creep brittle and have been shown (section (6.1.1) to correlate fairly well with K for individual geometries.

In order to see the behaviour of $\dot{\Delta}$ for a very creep ductile test two materials of different ductilities but the same geometry should be compared. Figure (134) shows this clearly by comparing the data from the tests performed

by Harper (95) on ferritic (high ductility) 1 Cr - Mo - V steel using Ct test-pieces at 565°C with the two tests performed on the CT specimens in the present test program. The $\dot{\Delta}$ for the bainitic material is relatively elastic as seen in figure (81) and the ferritic CT specimens show an increase of a factor of about 20 in the $\dot{\Delta}$ at constant C.C.G. rate and nearly all the increase is attributed to the $\dot{\Delta}_{cr}$ component. But for both cases the total $\dot{\Delta}$ describe the cracking rate. C* as evaluated by (89,95,123) makes the basic assumption that the measured $\dot{\Delta}$ is predominantly $\dot{\Delta}_{cr}$ which is not true since it has been shown that the elastic component $\dot{\Delta}_e$ plays an important part in the C.C.G. process. There must exist an interrelationship between $\dot{\Delta}$ and $\dot{\Delta}_{cr}$ but the governing description of cracking with crack length is mainly due to the elastic $\dot{\Delta}_e$. The variation of $\dot{\Delta}$ from an elastic $\dot{\Delta}_e$ to a creep $\dot{\Delta}_{cr}$ gives an insight to the use of the relevant correlating parameter. At the one extreme, when the total $\dot{\Delta} = \dot{\Delta}_e$ the L.E.F.M. concept is applicable and where the total $\dot{\Delta} = \dot{\Delta}_{cr}$ then there is no crack growth dominating circumstance and $\dot{\Delta}_{cr}$ will be equivalent to the uniaxial creep rate $\dot{\epsilon}$ and parameters such as a reference stress or a net section stress will be relevant in describing creep deformation and rupture.

Figures (135-137) show the experimental $\dot{\Delta}$ for various geometries, thicknesses and temperatures for the RR58 and steel. It is clear that the total $\dot{\Delta}$ does describe crack growth rate but unless taken as an indirect measure of C.O.D. it cannot be used to relate the various geometries, loadings and crack lengths. Therefore it is essential to attempt to describe it in terms of a fracture mechanics argument.

Following the description for an energetic interpretation of J from section (1.3.2) it can be numerically shown that

$$J = \frac{1}{B_n} \frac{dw}{da} \qquad (6.3)$$

where w is defined as the total work done.

Defining a term C^*_T as the total value of C^* containing the elastic (time independent) and creep (time dependent) terms in the creep cracking process then by analogy by dividing by time in equation (6.3)

$$C^*_T = \frac{1}{B_n} \frac{dw^*}{da} \qquad (6.4)$$

where w^* is defined as the rate of potential work done and differs from U^* except for the elastic circumstance where $w^* = U^*$. Therefore C^*_T can be split in concept into a linear elastic term C^*_e and a non-linear creep term C^*_{Cr} giving

$$C^*_T = C^*_{cr} + C^*_e \qquad (6.5)$$

where C^*_e can also be defined as the linear elastic term G (the elastic crack extension force) divided by time, and C^*_{cr} is the original concept of C^* based on creep deformation only. Accordingly the various ratios of C^*_{cr} to C^*_e will determine whether L.E.F.M. is applicable (where $C^*_e >> C^*_{cr}$) or whether the non-linear C^*_{cr} will define the crack tip singularity (where $C^*_{cr} >> C^*_e$). But the important point is that C^*_T inherently describes the crack tip over the wide spectrum of creep cracking behaviour i.e. from a creep brittle to a creep ductile circumstance.

The numerical estimates of C^*_T are possible in principle and can be computed numerically using incrementing crack programs. But by using the transducer displacement rate $\dot{\Delta}$, which inherently takes into account the complex combinations of the elastic and the creep terms, it is possible to evaluate an approximate experimental value for the C^*_T.

For a constant external work rate i.e. constant $\dot{\Delta}$ at constant load P

$$w^* = P\dot{\Delta} \qquad (6.5)$$

for any circumstances where bending displacements dominate it may be expected that $\dot{\Delta}$ can be written as:

$$\dot{\Delta} = \frac{1}{B} f(a)\, g(P) \qquad (6.6)$$

where f and g are functions. If at constant load the dependence on crack length can be approximated by a simple power law function as

$$f(a) = a^n \qquad (6.7)$$

equation (6.6) becomes

$$\frac{d\dot{\Delta}}{da} = \eta \frac{\dot{\Delta}}{a} \qquad (6.8)$$

Differentiating equation (6.5) at constant load with respect to a gives:

$$\frac{dw^*}{da} = P \frac{d\dot{\Delta}}{da} \qquad (6.9)$$

and substituting (6.9) in (6.8) and(6.4) gives:

$$C^*_T = \frac{1}{B_n} \frac{\eta P \dot{\Delta}}{a} \qquad (6.10)$$

Provided the η does not vary appreciably (by more than a factor of about 2) C^*_T will be proportional to $\frac{P\dot{\Delta}}{aB_n}$ giving

$$\dot{a} \quad \alpha \ (C^*_T)^{\varphi} \quad \alpha \left(\frac{P\dot{\Delta}}{aB_n}\right)^{\varphi} \qquad (6.11)$$

In figures (138 - 144) all the C.C.G. rate data for RR58 and steel are gathered from the different geometries and plotted, in various combinations versus the experimental C^*_T. The general trend shows that equation (6.11) is satisfied over a range of ductilities, temperatures and geometries with crack lengths varying from 15 mm to 150 mm (a factor of 10). The value of φ is found statistically to be between 0.8 - 0.9 for both the steel and RR58 tests of various geometries.

Figure (138 - 139) show the plots for the DCB geometry for thick and thin steel specimens respectively. There are no distinguishable differences for three decades of crack growth. Figure (140 - 141) show plots of C^*_T versus crack growth rate for various geometries and thicknesses and side groove depths for RR58 and steel respectively. Generally it is observed (more so for the steel) that reduction in specimen thickness produces a higher value of C^*_T for the same cracking rate suggesting that the extent of C^*_{cr} is affected by specimen thickness. As observed in section (6.1.1) the reduction in the thickness also showed an increase in the value of stress intensity factor, but it was shown that this was an apparent increase in the numerical value of K since stress relaxation at the

crack tip is profoundly affected by specimen thickness making the use of K invalid according to the principles of L.E.F.M. By the use of C^*_T which is strain rate based parameter the problem is overcome which directly suggests that creep crack growth rate is creep strain rate dependent.

Figure (142) shows the effect of temperature on the value of C^*_T for various DCB-C RR58 specimens tested from 100°C to 125°C. It is clear that the interaction between the thermal processes of creep to deform the geometry and/or to produce crack growth, are complex. At 100°C the load used to produce C.C.G. is relatively high to offset the reduction in thermal activation at the crack tip whereas as 200°C the value of C^*_T is higher due to the increase in the creep compoent C^*_{cr}. Values of C^*_T are lowest at around 125° - 150°C and rapidly increase in the region of 175°C - 200°C. It is postulated that a similar behaviour would occur in the C.C.G. of steel at various temperatures but insufficient time was available for this present work to allow complete verification of this statement. An increase in C^*_T is observed in figure (143) for the single steel DCB-P specimen tested at 615°C in comparison to the 25 mm thick DCB-P specimen tested at 565°C.

Finally figures (144,145) show the same data as figures (140,141) but include the calculated values of C^*_T from the raw data of two authors (94,95) shown in table (1). Four tests of Kaufmann et al (94) who tested large CT (B = 100 mm) aluminium specimens at 150°C with no side grooving are shown in figure (144). Although their specimens are not exactly the same as RR58 their chemical compositions

are very similar and only appreciably differ in the copper content. Kaufmann's material has about twice the amount of copper compared to RR58 and from the stated mechanical properties it is found to be slightly more ductile than RR58. The increase in ductility as well as the fact that Kaufmann et al used no side grooving on their CT test-piece is shown in figure (144) to give a slightly higher value of C^*_T compared to the RR58 tests at 150°C. Another factor that can be observed is that Kaufmann et al were easily able to achieve controlled C.C.G. rates at faster cracking rates suggesting their material was less stress sensitive than RR58.

A real test of C^*_T as a correlating parameter would be to compare the effects of increasing creep ductility at the crack tip. Unfortunately the present test program did not allow sufficient time for testing materials of different heat treatment and creep ductility but by using the raw data from Harper (95) who tested CT specimens of a ferritic 1 Cr - Mo - V steel of around 15% - 60% creep ductility at 565°C, Their value for the present C^*_T can be calculated and are plotted in figure (145) to compare with the bainitic heat treatments of different geometries of the $\frac{1}{2}$Cr, $\frac{1}{2}$Mo, $\frac{1}{4}$V steel. The correlation for Harper's data with crack growth is much improved, compared to the use of K (shown in figure (117)), and as expected the C.C.G. rate is appreciably reduced (by about a factor of 10 - 15) in comparison to the bainitic material. It is suggested that even for such a creep ductile material C^*_T still holds and although the extent of C^*_{cr} is appreciably increased the value of C^*_e cannot be disregarded.

CHAPTER 7

7.1. CONCLUSIONS

An attempt has been made to unify the C.C.G. problem by testing two engineering materials RR58 and a low alloy steel using various geometries each containing a dominant crack. The following conclusions have been reached.

1) The RR58 aluminium alloy was found to overage during testing within the creep range. The extent of overaging increased with test temperature and testing time thus explaining to some degree the decreasing cracking rate observed in DCB-C test-pieces. The second factor that affects the C.C.G. behaviour of this particular RR58 could be due to the initial cold rolling (giving it a $2\frac{1}{2}\%$ initial plastic strain) process which induces microcracks at the grain boundaries producing internal residual stress concentrations which are relaxed in the creep temperature range.

2) It was found that no crack growth initiated in the $\frac{1}{2}$Cr, $\frac{1}{2}$Mo, $\frac{1}{4}$V steel in the as received normalized ferritic condition using DCB-C specimens. The reason for this was due to the high creep ductility (> 40%) and the low hardness value (130 V.H.N.) of the ferritic steel. Consequently the steel specimens were solution treated and oil quenched giving a bainitic microstructure to simulate the heat affected zone (H.A.Z.) of welds, which gave a grain size of around 250 - 350 μm. Subsequent tests showed that tempering affected the creep ductility and C.C.G. In order to reduce the tempering effects during the tests at 565°C the specimens were given a tempering treatment of

680°C for 24 hours, after the solution treatment, in order to reduce the residual stresses and produce a more stable microstructure during the C.C.G. tests.

3) Uniaxial Creep data for RR58 and steel showed a range of ductilities dependent on the applied stress and temperature. For the RR58 the rupture elongation ranged from 4% to 12% and for the steel from 0.1% for the quenched specimens to about 1.5% maximum for the quenched and tempered condition.

4) The experimental slopes of the Δ versus a graph for both RR58 and steel showed a combination of elastic and creep components and the extent of each was found to vary for various test variables. Material ductility, reduction in side grooving and thickness of the test-piece geometry and an increase in the testing temperature increased the creep bending components of Δ suggesting an increased rate of stress redistribution.

5) Metallurgical observation of the two engineering materials showed that the analysis of the crack behaviour with respect to heat treatment and creep history is extremely complex but a general conclusion reached was that (a) the fracture surfaces showed predominently intergranular cracking with the RR58 (as expected from its better creep ductility) showing more ductile features than the steel and (b) the crack tip profiles for both RR58 and steel reflected the extent of creep deformation that had occurred during the cracking tests. Namely that a reduction in thickness and side grooving produced an increased amount of disconnected voids ahead of the crack tip, showing physically that there is increased stress redistribution due to creep at the crack tip.

6) Correlation of the data with the stress intensity factor K showed that for circumstances of reduced creep ductility and increased geometric constraint the equation $\dot{a} = AK^m$ aptly described C.C.G. rate for individual geometries. But a reduction in specimen thickness made the above equation more ineffective.

Controlled crack growth rate for the RR58 was only possible over a region of about two decades and it is suggested that a lower bound value of K_{ICC} as the critical value of creep fracture of RR58 could be a useful design tool. An increase in testing temperature (175° - $200^{\circ}C$) for the RR58 showed that no correlation existed with K for the cases where creep deformation increased.

It was possible to achieve C.C.G. rates in the steel for over a range of three decades and on the whole as expected, a better correlation with K was achieved.

7) Correlation of K for various geometries showed a distinct geometry effect for both the RR58 and steel. This suggests that extent of constraints i.e. resistance to deformation at the crack tip varies with geometry. Generally the constraints of fracture machanics geometries can be put in the following order DCB-C < DCB-P < DT < CCP < SEN < CT or more generally plane stress < plane strain. Therefore in any design procedure it is vital to choose the lower bound values to achieve conservative estimates.

8) A non linear fracture mechanics parameter C* which has been derived by analogy for J by relating the stress singularity within a plastically deforming crack

tip to the creep deformation process that occurs at the creep crack tip. An analytical estimate of C* for DCB specimens using non-linear beam theory was put forward and used to correlate the C.C.G. data.

9) Conclusions arrived at in (4) and the correlation of the data with the analytical C* mentioned in (8) suggested that the analysis of C* is inadequate in describing C.C.G. rate. A new method was put forward in section (6.2.2) in order to include both the elastic and the creep deformation components that are present at the crack tip. It was found that experimentally determined transducer displacement rate ($\dot{\Delta}$) which includes the elastic deflection and the creep deformation adequately described the C.C.G. rate and by using and energy rate interpretation of J it was suggested that a parameter C^*_T should describe the crack tip behaviour in terms of the potential work rate w*, such that:

$$C^*_T = \frac{1}{B_n} \frac{dw^*}{da}$$

and $C^*_T = C^*_e + C^*_{cr}$

such that C^*_T is the combination of the elastic C^*_e and the creep C^*_{cr} (previously defined as C*). An approximate experimental evaluation of C^*_T was put forward and the correlation of the data shows C.C.G. to be geometry independent. It is postulated that C^*_T will describe the crack tip behaviour over a range of creep ductilities from creep-brittle to a creep-ductile situation.

10) As a practical application it is suggested that a possible criterion for protecting components in service from rapid fracture is to choose a critical C.C.G. 'rate' $\dot{a}_{cc}$. By measuring the C.C.G. rate by the potential drop, ultrasonics, x-ray or if possible visually, over at ime period the component can be designated safe or unsafe depending on whether or not the value is greater than a previously selected $\dot{a}_{cc}$.

7.2. FUTURE WORK

1) The early estimates of C* were made analytically taking into account only the secondary creep rate and were only relevant to the DCB type geometries. The inclusion of the elastic component to produce C^*_T has been shown to be important. It is suggested that it is possible to arrive at better estimates of C^*_T for various geometries by using non-linear finite element techniques and computer programmes produced for incremental crack growth.

A critical evaluation of the calculations should be made by performing experiments on a wider range of DCB, CT, DT and other geometries of various size, thickness and depth of side groove.

The interplay of creep deformation and creep cracking and the effect of the specimens being held at temperature for long times suggest that a closer relationship must exist between the engineering aspects of C.C.G. and the metallurgical problems. This is of great importance if the results are to be related to the creep failure of components which have to exist in the creep temperature range for many years. A full metallographic study of the

cracking process should be made to develope quantitative estimates of the size of the creep deformation zone and possibly develope a microstructural model which could be related to the macro C.C.G. behaviour in metals.

Variable loading and temperature tests are also needed more especially for the creep ductile materials to observe the history effects and their relation to the incubation times that are observed in these materials. These history effects are known to exist in tensile creep experiments but which are not at first apparent in C.C.G.

Finally it is suggested that steps should be taken to relate the laboratory results to realistic practical situations. When designing and predicting the lives of components at high temperatures the present results suggest improvements can be made by taking into account the new C^*_T parameter.

APPENDIX A

Analysis of deflection of DCB test piece

Consider a cross section of the DCB test piece a distance $x < a$ from the loading line. Let the curvature at this section under load P be k. Then for plane sections to remain plane, the strain at any distance y from the neutral axis is

$$\epsilon = ky \qquad \text{(A1)}$$

For moment equilibrium;

$$M = \int_{-h/2}^{h/2} \sigma \, B \, y \, dy$$

.. Substituting from eqn. (3.30) and (A1)

$$M = B\left(\frac{k}{A}\right)^{1/n} \int_{-h/2}^{h/2} h^{1+1/n} \, dy$$

$$= \frac{2nB}{(2n+1)} \left(\frac{k}{A}\right)^{1/n} \left(\frac{h}{2}\right)^{2+1/n} \qquad \text{(A2)}$$

For small deflections v, eqn. (A2) can be re-arranged to give;

$$k = \frac{d^2v}{dx^2} \left[\frac{(2n+1)M}{2nB}\right]^n \frac{A}{(h/2)^{2n+1}}$$

But $M = Px$

$$\therefore \frac{d^2v}{dx^2} = \left[\frac{(2n+1)P}{2nB}\right]^n A \frac{x^n}{(h/2)^{2n+1}}$$

Integrating twice and using the boundary condition $\frac{d}{dx} = 0$ and $= 0$ at $x = a$, the crack tip, gives,

$$v = \left[\frac{(2n+1)P}{2nB}\right]^n A \left[I_x^{**} - I_a^{**} - I_a^{*} (x - a)\right] \qquad \text{(A3)}$$

where $I^* = \int \frac{x^n}{(h/2)^{2n+1}} \, dx$

and $I^{**} = \iint \frac{x^n}{(h/2)^{2n+1}} dx$

and the subscripts x and a indicate the values of the integrals at x and a, respectively. For the contoured geometry h is a function of x.

The loading pin displacement, Δ, required for the evaluation of J, Eqn. (3.39, 3.40), is given by

$$\Delta = 2v$$

evaluated at $x = 0$

$$\therefore \Delta = \left[\frac{(2n+1)P}{2nB}\right]^n \left[2A \; I_o^{**} - I_a^{**} + I_a^* \, a\right]$$

where I_o^{**} is the value of I^{**} at $x = 0$.

$$\therefore \frac{d\Delta}{da} = \left[\frac{(2n+1)P}{2nB}\right]^n 2A\left[- I_a^* + I_a^* + a\frac{dI_a^*}{da}\right]$$

$$= \left[\frac{(2n+1)P}{2nB}\right]^n 2A \frac{a^{n+1}}{(h/2)^{2n+1}} \qquad \text{(A4)}$$

This expression can be substituted into Eqn. (3.34) to give J.

REFERENCES

1. Griffith, A.A., Phil. Trans. of the Royal Soc. of London, 221(A), p 163-198, 1921.

2. Inglis,C.E. Proc. Inst. Nav. Archit., 60, 1, p 219, 1913.

3. Irwin, G.R., Kies, J.A. and Smith, H.L. Proc. A.S.T.M., 58, p 64, 1958.

4. Orowan, E. Trans. Inst. of Engineers and Shipbuilders in Scotland, 89, p 165-215, 1945-46.

5. Orowan, E. Reports on Progress in Physics, 12, p 185-232, 1948-49.

6. Orowan, E. J. Res. Suppl., 20, p 157-8, 1955.

7. Irwin, G.R., Kies, J.A. Weld. J. Res. Suppl., 31, p 953-1003, 1952.

8. Love, A.E. 'A Treatise on the Mathematical Theory of Elasticity', 4th Ed., Dover, N.Y. 1944.

9. Irwin, G.R. J. of Appl. Mech., 24, p 361-364, 1957.

10. Westergaard, H.M. J. of Appl. Mech., 61, p A49, 1939.

11. Irwin, G.R., Kies, J.A. Metal Prog., 78, p 73, 1960.

12. A.S.T.M., (a) S.T.P. No 381, 1965.
(b) S.T.P. No 410, 1966.

13. A.S.T.M., E 399, Annual Book A.S.T.M., standards Pt 31, 1973.

14. British Standards Publication, No DD3, 1971.

15. Wells, A.A. Symp. Crack Propagation, College of Aeronautics, Cranfield, Paper B4, 1961.

16. Cottrell, A.H., I.S.I. Spec. Rep. No. 69, p 281, 1961.

17. Bahrenblatt, G.I. Advances in Applied Mechanics, Academic Press, N.Y. 1962.

18. Dugdale, D.S. J. Mech. Phys. Solids, 8, p 100, 1960.

19. Burdekin, F.M., Stone, D.E.W. J. Strain Anal., 1, p 145, 1966.

20. Bilby, B., Cottrell, A.H., Smith, E., Swinden, K. Proc. Roy. Soc. (London), Ser. A 279, p 1, 1964.

21. Harrison, J.D., Burdekin, F.M., Young, J.G. 2nd Conf. 'Significance of Weld Defects', Welding Inst., London, 1968.

22. Burdekin, F.M., Dawes, M.G. 'Practical Application of Fracture Mechanics to Pressure Vessel Technology', Inst Mech. Eng., p 28, London, 1971.

23. British Standards Publication, DD19, 1972.

24. Sumpter, J.D.G. 'Elastic-Plastic Fracture Analysis and Design using the Finite Element Method'. Ph.D. Thesis, London University, 1974.

25. Sumpter, J.D.G., Turner, C.E., Proc 2nd Int Conf. Pressure Vessel Techniques, 3, A.S.M.E., San Antonio, 1974.

26. Rice, J.R. Trans. A.S.M.E., J. Appl. Mech., 35, p 379-386, 1968.

27. Begley, J.A., Landes, J.D. S.T.P. 514, A.S.T.M. Philadelphia, p 1-23, 1972.

28. Landes, J.D., Begley, J.A. S.T.P. 514, A.S.T.M. Philadelphia, p 24-39, 1972.

29. Rice, J.R. Proc. of 1st Int Conf on Fracture, 1, p 283-308, 1965.

30. Cherapanov, G.,Int. J. Solids and Structures, 4, p 811, 1968.

31. McClintock, F.A. J. Appl. Mech., 25, p 582, 1958.

32. Rice, J.R. 'Fracture: An Advanced Treatise' Vol. 2, edited by H. Liebowitz, Academic Press, N.Y. p 191, 1968.

33. Chitaley, A.D., McClintock, F.A. J. Mech. Phy. Solids, 19, p 147, 1971.

34. McClintock, F.A. Int. J. Fract. Mech., 4, p 101, 1969.

35. Paris, P.C., Erdogan, F.E. Trans A.S.M.E. J. Basic. Eng., 85, p 528, 1963.

36. Dowling, N.E., Westinghouse Research Laboratories Scientific Paper 75-1E7-Pal FA - P1. Pittsburgh, Pa 15235, 1975.

37. Mowbray, D.F. Materials and Processes Lab. General Electric Company, Schenectady, N.Y. 1975.

38. Knott, J.F. 'Fundamentals of Fracture mechanics', Butterworth, London, 1973.

39. Johnson, H.H., Paris, P.C. Eng. Fract. Mech., 1, p 3, 1968.

40. Hancock, G.G., Johnson, H.H. Mat. Res. and Stand., 6, p 431, 1966.

41. Landes, J.D., Wei, R.P. In. J. of Fract., 9, p 277, 1966.

42. Kennedy, A.J. 'Process of Creep and Fatigue in Metals', Oliver and Boyd, 1962.

43. Garofalo, F. 'Fundamentals of Creep and Creep-Rupture in Metals', McMillan, 1965.

44. Norton, F.H. 'The Creep of Steels at High Temperatures', McGraw-Hill, 1929.

45. Penny, R.K., Marriot, D.L. 'Design for Creep', McGraw-Hill, 1971.

46. Woodford, D.A., Goldhoff, R.M. Mat. Sci and Eng., 5, p 303-324, 1969-70.

47. Penny, R.K. Met. and Mats., 8, p 124, 1974.

48. Robinson, E.L. Trans. A.S.M.E., 60, 1938.

49. Goldhoff, R.M. Trans A.S.M.E., J. Basic Eng., 87, 1965.

50. A.S.T.M., S.T.P. 165, Chicago, 1954.

51. Odquist, F.K.G., Hult, J. Ark. Fys., 19, p 379, 1961.

52. Kachanov, L.M. Contrib. to 'Problems of Continuum Mechanics'. Contributions in honour of 70th birthday of N.I. Muskhelishviti, Philadelphia, 1961.

53. Rabotnov, Yu. N. 'Creep Problems in structural Members' North-Holland publ. co., London, 1969.

54. Odquist, F.K.G., Proc. I.U.T.A.M. Symp., Haifa, Pergammon Press, 1964.

55. Rabotnov., Yu. N., 'Advances in creep design'. Edited by A.I. Smith and A.M. Nicholson, Applied Sciences, 1971.

56. Onat, E.T. Proc. 5th U.S. Nat. Conf. of Appl. Mech. (Minn.) A.S.M.E., pp 42a-434, N.Y., 1966.

57. Greenwood, J.N., Miller, R.R., Suiter, J.W. Acta. Met., 2, p 256, 1954.

58. Hull, D., Rimmer, D.E. Phil. Mag., 4, p 673-383, 1959.

59. Ratcliffe, R.T., Greenwood, G.W. Phil. Mag., 12, July-Dec., 1965.

60. Chang, H.C., Grant, N.J. Trans. Am. Inst. Min., Metall. Engrs., p 206-344, 1965.

61. Mclean, D. Symp. on Vaccancies and other Point Defects in Metals and alloys. Monograph No 23, London Inst. of Metals, 1957.

62. Williams, J.A. Phil. Mag., 15, p 1289, 1967.

63. Langdon, T.G. Phil. Mag., 22, p 945, 1970.

64. Heald, P.T., Williams, J.A. Phil. Mag., 22, p 1095-1100, 1970.

65. Speight, M.V., Harris, J.E. Mel. Sci. J., 1, p 83-85, 1967.

66. Weertman, J. Mets Trans., 5, p 1743, 1974.

67. Raj, R. and Ashby, M.F. Acta. Metall., 23, p 653, 1975.

68. Lindborg, U. J. Mech Phys of Solids., 16, p 328, 1968.

69. Lindborg, U. Acta. Metall., 17, p 521-526, 1969.

70. Taplin, D.M.R. Phil Mag., 20, p 1079, 1969.

71. Söderberg, R. Proc. 2nd Int. Conf. of Fract., Brighton, Paper 38, 1969.

72. Boettner, R.C., Robertson, W.D. Trans. Met. Soc., A.I.M.E., 221, p 613, 1961.

73. Woodford, D.A. Met. Sci. J., 3, 1969.

74. Dyson, B.F., Mclean, D. Met. Sci. J., 6, p 220, 1972.

75. Dyson, B.F., Loveday, M.S., Rodgers, M.J. Proc. R. Soc. London A 349, p 245-259, 1976.

76. Haigh, J.R. Met. Sci. and Engrg., 20, p 225-235, 1975.

77. Williams, J.A., Price, A.T. Trans of the A.S.M.E., p 214-222, 1975.

78. Kenyon, J.L. Ph.D. Thesis University of London, 1976.

79. Popp, H.G. Goles, A. Proc. U.S. Air Force Conf. on Fatigue and Fracture, p 71 (Microfilm AFFDL-TR-70-144(1970)), 1970.

80. Siverns, M., Price, A.T. Int. J. Fract., 9, p 199, 1973.

81. Harrison, C.B., Sandor, G.N. Eng. Fract. Mech., 3, p 403, 1971.

82. James, L.A. Int. J. Fract. Mech., 8, p 347, 1972.

83. Robson, K. Int. Conf of Creep Resistance in Steel, Verein Deutscher Eisenhuettenlente, 1972.

84. Thornton, D.V. G.E.C. Turbine Division, Rep. No. CML(1972)-18, 1972.

85. Pilkington, R., Hutchinson, D., Jones, C. Met. Sci. J., 8, p 237-241, 1974.

86. Ellison, G., Walton, D. Int. Conf. on Creep and Fatigue in Elevated Temperature applications, (Philadelphia (1973)), Sheffield, 1974.

87. Nicholson, R.D., Formby, C.L. Int. J. Fract., 11, 4, p 595-604, 1975.

88. Neate, G., Siverns, M. Int. Conf on Creep and Fatigue in Elevated Temperature applications, (Philadelphia (1973)) Sheffield, 1974.

89. Landes, J., Begley, J. Westinghouse Scientific paper, 74-1E7-FESGT-P1, 1974.

90. Haigh, J. Mat. Sci. and Engrg., 20, p 213-223, 1975.

91. Neate, G., C.E.G.B. Report No. SSD MID/R12/74, 1975.

92. Floreen, S. Metall. Trans., 6A, p 1741-1949, 1975.

93. Nicholson, R.D. C.E.G.B. Report No. RD/B/N2594, 1973.

94. Kaufmann, J.G. Bogardus, K.D., Mauney, D.A., Malcom, R.C. Alcoa Rep. No. 57-74-3, (New Kensington, PA., U.S.A.), 1974.

95. Harper, M. Ph.D. Thesis, University of Bristol, 1976.

96. Outwater, J.O., Murphy, M.C., Kumble, R.G. Berry, J.T., A.S.T.M., S.T.P. 559, p 127-138, 1974.

97. Brown, W.F., Srawley, J.E. A.S.T.M., S.T.P. No 410., 1966.

98. Srawley, J.E., Gross, B. NASA Tech. Note: NASA-TN-D-3820, 1967.

99. Freed, C.M., Krafft, J.M. J. Mat., 1, p 770, 1966.

100. Gilby, D.M., Pearson, S. R.A.E., Tech. Rep. No. 66402, 1966.

101. Neate, G. C.E.G.B. Rep SSD M1D/R34.72, 1972.

102. Haigh, J.R., Richards, C.E. C.E.G.B. rep. no RD/L/N 19/73, 1973.

103. Nicholson, R.D. Formby, C.L. Int. J. Fract., 11, 4, p 595-604, 1975.

104. Leckie, F.A., Hayburst, D.R. Proc. R. Soc. Lond., A.340, p 323-347, 1974.

105. Marriot, D. University of Liverpool, Dept. Mech. Engrg. Report No D/017/70, 1970.

106. Sim, R. J. Mech. Eng. Sci., 13, 1, p 47-50, 1971.

107. Anderson, R.G., Gardner, L.R.T., Holgkins, W.R. J. Mech. Engrg. Sci., 5, p 238-244, 1963.

108. Machenzie, A.C. Int. J. Mech. Sci, 10, p 441-453, 1968.

109. Leckie, F.A., Hayhurst, D., Morrison, C. 2nd Int. Conf. on Structural Mechanics in Reactor Technology, Berlin, 1973.

110. Hayhurst, D., Morrison, C., Leckie, F. J. Appl. Mech., Trans A.S.M.E., No 75-APM-R, 1975.

111. Ponter, A., Leckie, F.A. J. Appl. Mech., Trans A.S.M.E., 92, p 753-758, 1970.

112. Hayhurst, D., J. Mech. Phys. of Solids, 20, p 381-390, 1972.

113. Martin, J., Leckie, F. J. Mech. Phys. Sol., 20, p 223-238, 1972.

114. Hayhurst, D.R. J. Appl. Mechn., 40, p 915, 1973.

115. Haigh, J.R. Ph.D. Thesis, CNAA London, 1973.

116. Ewing, D., Richards, C. J. Mech. Phys. Sol., 22, 1, p 27-36.

117. Goodall, I.W., Chubb, E.J. C.E.G.B. Rep. No. RD/B/N3227, 1974.

118. Nikbin, K.M., Webster, G.A. Joint Metals Soc/IOP/I. Mech.E.Meeting, 'Prediction of Component Life at High Temperatures, 1975.

119. Vítek, V. C.E.G.B. Report No RD/L/N 34/76, 1976.

120. Bilby, B.A. Cottrell, A.H., Swinden, K.H. Proc. Roy. Soc., A272, p 304, 1963.

121. Wells, A.A., McBride, F.H., Canadian Metall.Quart.,6, 4, p 347-367, 1966.

122. Goldman, N.L., Hutchinson, J.W. Internal report Harvard University, 1973.

123. Harper, M.P. Ellison, E.G., University of Bristol Report, to be published in J. Strain Anal., 1976.

124. Haigh, J.R., Richards, C.E. C.E G.B. report RD/L/M 461, 1974.

125 Kenyon, J.L., Webster, G.A., Radon, J.C., Turner, C.E., Int. Conf. on Creep and Fatigue at Elevated Temperature applications, (Philadelphia (1973)), Sheffield, 1974.

126. Turner, C.E., Webster, G.A. Int. J. Fract., 10, p 455, 1974.

127. Webster, G.A. Conf. on Mech. and Phys. of Fract., Inst. Phys. Cambridge, 1975.

128. Nikbin, K.M., Webster, G.A., Turner, C.E. A.S.T.M., S.T.P 601, 1976.

129. Nikbin, K.M., Webster, G.A., Turner, C.E. Int. Conf. on Fract., Waterloo, Canada, 1977. (to be published).

130. Wilson, R.N. RAE. Tech. Rep. No. 73149, 1973

131. Roark, R.J. 'Formulas in Stress and Strain', McGraw-Hill, N.Y., 1959.

132. Cummings, W.M., King, R.H. N.E.L. Report No 448, 1970.

133. Gross, B., Roberts, E., Srawley, J.E. Int. J. of Fract. Mech., 4, No. 3., 1968.

134. Roberts, E. Mat. Res. and Stand., MTRSA, 9, No. 2, 1969.

135. Wilson, R.N. R.A.E. Techn. Rep. No. 76071, 1976.

136. Gooch, D.J. C.E.G.B. Rep. No RD/L/R1900, 1975.

137. Goodall, I.W., Cockcroft, R.D.H., Chubb, E.J., C.E.G.B. Report No. RD/B/N 3059, 1974.

138. Ellison, E.G., Neate, G.J. I.Mech.E., Paper C 110/76, pp 39-46, 1976.

TABLE (1)

List of authors applying fracture mechanics to C.C.G.

Author and Reference	Material Tested	Test Temp °C	Creep Index n	Geometry	Specimen Width (W) mm	Correlating Parameter
Popp and Coles (79)	Inconel (Nikel base)	538	7	CCP	75	K
Siverns and Prince (80)	2¼ Cr-1Mo-V Quenched	568	5.5	SEN-T	25	K
Harrison and Sandor (81)	1 Cr-Mo-V Wrought Steel	538	4.5	CCP	25-60	σ_{net}
James (82)	A1S1-316, steel Cold worked (20%)	538	> 20	CT	30,50	K
Robson (83)	0.2% C Cast steel 0.2% C Wrought steel	400 450	14-20	CT SEN-T	40,50	K
Thornton (84)	1 Cr-Mo-V Cast and wrought steel	565	6-16	SEN-B	50	K
Pilkington (85)	½ Cr-½Mo-¼V Bainitic	550	10-25	SEN-B	18	K, C.O.D.
Ellison and Walton (86)	1 Cr-Mo-V Tempered	565	10	SEN-T SEN-B	40	K
Nicholson and Formby (87)	A1S1 316	740	7	SEN-T CCP	17,35	σ_{net}
Neate and Siverns (88)	2¼ Cr-1Mo-V 1 Cr-½Mo-¼V (ferritic and bainitic)	565	3-5	SEN-T	15-50	K, σ_{net}
Landes and Begley (89)	Discolloy Superalloy (Nickel base)	650	-	CCP CT	50	C*
Haigh (90)	Cr-Mo-V Bainitic and ferritic	550	-	WOL	50	C.O.D. Notional K
Neate (91)	½Cr-½Mo-¼V Various Heat treatments and grain sizes	565	3-7	SEN-T CCP, CT WOL	25-65	K for brittle σ_{net} for ductile

TABLE (1) Cont'd

Author and Reference	Material Tested	Test Temp °C	Creep Index n	Geometry	Specimen Width (W) mm	Correlating Parameter
Floreen (92)	Nickel alloy	500-750	-	CT	25	K
Nicholson (93)	A1S1-316 steel Normalized	600-850	5-12	DEN-T	25	σ_{net}
Kaufmann et al (94)	Aluminium Alloy	150-200	-	CT	100-125	K
Harper (95)	1Cr-Mo-V Ferritic Steel	565	10-15	CT SEN-B	50	C*
Kenyon (78)	Aluminium Alloy (RR58)	100-200	10-30	DCB-C	> 200	K
Nikbin et al (129)	$\frac{1}{2}$Cr-$\frac{1}{2}$Mo-$\frac{1}{4}$V steel	565-615	5-10	DCB-C DCB-P	50-200	K C*
	Aluminium Alloy (RR58)	100-200	10-30	DT CT		

TABLE 2a

Details of Composition and the Mechanical Properties of RR58

Element	Cu	Mg	Fe	Si	Mn	Ti	Zn	Ni
Composition Weight %	2.64	1.64	1.15	0.23	0.03	0.06	0.06	1.15

Temp (T) ^{o}C	Young's Modulus (E) GPa	Yield Stress (σ_y) MPa	U.T.S. MPa	Elongation (ϵ_f) %
R.T.(20)	77.8	332	436	4-4.3
100	68.1	294	408	5.3
125	65.6	-	-	-
150	63.1	265	362	8.4-11.1
175	61.0	-	-	-
200	56.5	240	295	8.6

TABLE 2b

Detail of Composition and the Mechanical Properties of the ¼% Cr, ½% Mo, ¼% V steel

Block	C	Cr	Mo	V	Mn	Al	Ce
3F	.08	.45	.70	.34	.42	.029	.010
4F	.11	.37	.42	.22	.36	.019	.002
7G	.08	.45	.70	.34	.46	.011	.101
8F	.08	.45	.69	.34	.41	.094	.010
10F	.08	.42	.69	.33	.31	.005	.025

Mechanical Properties for the steel heated for ½ hour at 1250°C and Oil Quenched

Temp (T) °C	Young's Modulus (E) GPa	Yield Stress (σ_y) MPa	U.T.S. MPa	Elongation (ϵ_f) %
R.T.(20)	222	670	760	3.3
565	181	595	721	4.8

Mechanical Properties for the Steel heated for ½ hour at 1250°C, Oil Quenched and subsequently tempered for 24 hours at 680°C

Temp (T) °C	Young's Modulus (E) GPa	Yield Stress (σ_y) MPa	U.T.S. MPa	Elongation (ϵ_f) %
R.T.(20)	216	657	749	4.2
565	176	580	708	5.6

TABLE (3a)

Dimensions of the Specimens

Figures of all the specimens shown in this table are illustrated in figure (15)

Geometry: DCB

Material	Thickness (B) (mm)	Net Thickness (B_n) (mm)	Maximum Specimen height (h_{max}) (mm)
RR58	25.0	12.7	38.0
	9.5	7.7	38.0
	25.4	20.0	38.0
Steel	25.0	6.5	35.5
	12.0	6.0	35.5
	12.0	3.0	35.5

Dimension of the taper of the DCB-C with respect to crack length

Crack length (a) (mm)	50.0	70.0	90.0	100.0	110.0	120.0	140.0	150.0
Height (h) (mm)	17.1	20.3	24.0	25.6	27.4	29.0	33.2	35.0

Geometry: DT

Material	B (mm)	B_n (mm)	h_m (mm)	W (mm)
RR58	9.5	7.7	62.5	200

Geometry: CT

Material	B (mm)	B_n (mm)	W (mm)
Steel	25.0	13.1	50

TABLE (3b)

Variation of H_p/e, W/e and W/H_p with $KBW^{\frac{1}{2}}/p$ for the DCB-C Test-piece

In conjunction with figure (30)

H_p/e	W/e	W/H_p	a/W values					
			0.2	0.8	0.4	0.5	0.6	0.7
			$KBW^{\frac{1}{2}}/p$					
0.2	5	25	35.2	36.2	36.0	35.3	34.5	35.0

TABLE (4a)

Uniaxial Creep Data for RR58 (from Kenyon (78))

Specimen	Test Temp °C	Applied Stress MPa	Secondary Creep Rate ($\dot{\epsilon}_s$) (%/H)	t_R (H)
C10	125	301	.0023	946
C11	125	340	.093	34.7
C12	125	388	43.3	.068
C13	125	360	1.73	2.65
C14	175	285	.527	6.8
C15	175	247	.015	111.2
C16	175	319	19.5	.254
C18	200	208	.012	92.3
C19	200	232	.077	23.5
C20	200	263	1.0	2.76
C21	200	295	30.0	.154
C24	175	271	.083	15.9
C25	175	308	3.13	1.37
C28	150	347	12.7	.328
C29	125	370	7.88	.475
C30	175	226	.0037	282
C31	100	388	1.3	2.88
C32	100	355	.022	122.4
C33	100	371	.141	23.4
C34	100	398	3.34	.874
C36	100	338	.0054	607.6
M1	150	337	3.15	1.2
M2	150	322	.96	4.5
M3	150	309	.32	15.0
M4	150	294	.022	92.0
M5	150	280	.0076	275

TABLE (4b)

Uniaxial Creep Data for $\frac{1}{2}$ Cr, $\frac{1}{2}$ Mo, $\frac{1}{4}$ V steel at 565°C

(i) Solution Treated and Quenched

Specimen	Applied Stress MPa	Secondary creep rate ($\dot{\epsilon}_s$) (%/H)x10^{-3}	t_R (H)
E1	360	2.2	18
E2	332	3.3	20.8
E3	305	3.5	25
E4	278	1.56	19.5
E5	263	5.85	14
E6	235	1.1	51
E7	208	.34	109
E8	180	.315	265
E9	442	54.6	1.4
E10	405	14.8	3.3
E12	154	.429	210

(ii) Solution Treated, Quenched and Tempered

Specimen	Applied Stress MPa	Secondary creep rate ($\dot{\epsilon}_s$) (%/H)x10^{-3}	t_R (H)
ET1	278	10.5	53
ET2	244	5.46	80
ET3	228	29.6	68
ET4	500	858.0	2.1
ET5	235	1.95	310
ET6	374	17.9	50
ET7	165	.897	> 400
ET8	225	.234	> 700
ET9	360	.156	8.5
ET10	316	25.7	40
ET11	295	24.6	43

TABLE (5)

The experimental data used in the analysis in Chapter Six is shown in the following pages (155-181), divided into the subsections listed below. The basic information concerning each test and the values of applied load, crack growth rate, transducer displacement rate the slope of the experimental $\frac{\Delta}{a}$ graphs and the experimental value of the stress intensity factor at different increments of crack length are listed. It should be noted that the value of the net thickness B_n is printed as BN in this table.

The subsections are as follows:

ALUMINIUM ALLOY RR58

	B (mm)	Geometry	Test Temp. °C	Page
(a)	25.0	DCB-C	100	155
(b)	25.0	DCB-C	125	156
(c)	25.0	DCB-C	150	157
(d)	25.0	DCB-C	175	162
(e)	25.0	DCB-C	200	165
(f)	9.5	DCB-C	100	166
(g)	9.5	DCB-C	150	167
(h)	25.0	DCB-P	150	169
(i)	9.5	DT	150	171

½% Cr, ½% Mo, ¼% V STEEL

	B (mm)	Geometry	Test Temp. °C	Page
*(j)	25.0	DCB-C	565	172
(k)	25.0	DCB-C	565	174
(l)	12.0	DCB-C	565	176
(m)	25.0	DCB-P	565	178
(n)	25.0	DCB-P	615	180
(o)	12.0	DCB-P	565	180
(p)	25.0	CT	565	181

* N.B. Specimens in table 5(j) were solution treated at 1250°C and quenched in oil. The rest of the steels were subsequently given a tempering treatment at 680°C.

TABLE (5)

5(a)

ALUMINIUM ALLOY RR58	CRACK LENGTH (a) (MM)	APPLIED LOAD (P) NEWTONS	CRACK RATE (ȧ) (MM/H)	TRANS. RATE (ȧ) (MM/H)	Δ/a	STRESS INTENS. (K) 1/2 MPa.m
SPECIMEN B14 GEOMETRY DCB-C TEST TEMP 100 C B (MM) 25.0 BN (MM) 12.7 TEST TIME(H) 350.0	100.0	3914.2	.010	.0004	.023	20.94
	105.0	4003.2	.015	.0007	.023	21.42
SPECIMEN B24 GEOMETRY DCB-C TEST TEMP 100 C B (MM) 25.0 BN (MM) 12.7 TEST TIME(H) 2850.0	102.5	4581.4	.014	.0006	.042	24.51
	105.0	4581.4	.014	.0006	.042	24.51
	107.5	4581.4	.014	.0006	.042	24.51
	110.0	4581.4	.014	.0006	.042	24.51
	115.0	4581.4	.014	.0006	.042	24.51
	117.5	4803.8	.016	.0008	.047	25.70
	120.0	4803.8	.016	.0008	.047	25.70
	125.0	4803.8	.016	.0008	.047	25.70
SPECIMEN B29 GEOMETRY DCB-C TEST TEMP 100 C B (MM) 25.0 BN (MM) 12.7 TEST TIME(H) 900.0	100.0	3780.8	.004	.0005	.040	20.23
	102.5	3780.8	.004	.0005	.040	20.23
	102.5	4047.7	.013	.0005	.040	21.66
	105.0	4047.7	.013	.0005	.040	21.66
	107.5	4047.7	.013	.0005	.040	21.66
	110.0	4270.1	.026	.0009	.040	22.85
	112.5	4270.1	.026	.0009	.040	22.85
	115.0	4270.1	.026	.0009	.040	22.85
SPECIMEN B33 GEOMETRY DCB-C TEST TEMP 100 C B (MM) 25.0 BN (MM) 12.7 TEST TIME(H) 1270.0	105.0	4092.2	.020	.0004	.031	21.90
	107.5	4092.2	.020	.0004	.031	21.90
	110.0	4092.2	.020	.0004	.031	21.90
	112.5	4092.2	.020	.0004	.031	21.90
	115.0	4270.1	.025	.0012	.031	22.85
	117.5	4270.1	.025	.0012	.031	22.85
	117.5	4359.0	.025	.0012	.031	23.32
	120.0	4359.0	.025	.0012	.031	23.32
	125.0	4359.0	.058	.0023	.031	23.32

5(a) Cont.

ALUMINIUM ALLOY RR58	CRACK LENGTH (a) (MM)	APPLIED LOAD (P) NEWTONS	CRACK RATE (ȧ) (MM/H)	TRANS. RATE (ȧ) (MM/H)	Δ/a	STRESS INTENS. (K) 1/2 MPa.m
SPECIMEN B34	75.0	4714.9	.005	.0006	.021	25.23
GEOMETRY DCB-C						
TEST TEMP 100 C	76.0	4714.9	.005	.0006	.021	25.23
B (MM) 25.0						
BN (MM) 12.7	76.0	9340.8	.009	.0006	.021	49.98
TEST TIME(H) 2100.0						
	77.5	9340.8	.009	.0006	.021	49.98
	80.0	9340.8	.009	.0006	.021	49.98
	85.0	4981.8	.010	.0006	.021	26.66
	87.5	4981.8	.010	.0006	.021	26.66

5(b)

ALUMINIUM ALLOY RR58	CRACK LENGTH (a) (MM)	APPLIED LOAD (P) NEWTONS	CRACK RATE (ȧ) (MM/H)	TRANS. RATE (ȧ) (MM/H)	Δ/a	STRESS INTENS. (K) 1/2 MPa.m
SPECIMEN B7	117.5	3691.8	.023	.0006	.023	19.75
GEOMETRY DCB-C						
TEST TEMP 125 C	120.0	3691.8	.023	.0006	.023	19.75
B (MM) 25.4						
BN (MM) 12.7	122.5	3691.8	.023	.0006	.023	19.75
TEST TIME(H) 420.0						
SPECIMEN B22	100.0	3736.3	.052	.0020	.031	19.99
GEOMETRY DCB-C						
TEST TEMP 125 C	105.0	3736.3	.042	.0015	.031	19.99
B (MM) 25.4						
BN (MM) 12.7	110.0	3736.3	.042	.0015	.031	19.99
TEST TIME(H) 530.0						
	115.0	3736.3	.052	.0015	.031	19.99
	120.0	3736.3	.069	.0024	.031	19.99
	125.0	3736.3	.115	.0046	.031	19.99
	130.0	3736.3	.115	.0056	.031	19.99

5(c)

ALUMINIUM ALLOY RR58	CRACK LENGTH (a) (MM)	APPLIED LOAD (P) NEWTONS	CRACK RATE (ȧ) (MM/H)	TRANS. RATE (ȧ) (MM/H)	Δ/a	STRESS INTENS. (K) 1/2 MPa.m
SPECIMEN B3	105.0	3780.8	.145	.0069	.039	20.23
GEOMETRY DCB-C						
TEST TEMP 150 C	110.0	3780.8	.115	.0046	.039	20.23
B (MM) 25.4						
BN (MM) 12.7	115.0	3780.8	.115	.0038	.039	20.23
TEST TIME(H) 600.0						
	120.0	3780.8	.115	.0038	.039	20.23
	125.0	3780.8	.115	.0038	.039	20.23
	130.0	3780.8	.115	.0038	.039	20.23
	135.0	3691.8	.050	.0019	.039	19.75
	140.0	3691.8	.050	.0019	.039	19.75
SPECIMEN B4	100.0	4448.0	1.412	.0638	.042	23.80
GEOMETRY DCB-C						
TEST TEMP 150 C	105.0	4448.0	.983	.0467	.042	23.80
B (MM) 25.4						
BN (MM) 12.7	110.0	4448.0	.638	.0239	.042	23.80
TEST TIME(H) 75.0						
	120.0	4448.0	.638	.0239	.042	23.80
	130.0	4448.0	.638	.0239	.042	23.80
	140.0	4448.0	.774	.0290	.042	23.80
SPECIMEN B5	75.0	3669.6	.183	.0061	.042	19.63
GEOMETRY DCB-C						
TEST TEMP 150 C	77.5	3669.6	.115	.0051	.042	19.63
B (MM) 25.4						
BN (MM) 12.7	80.0	3669.6	.085	.0039	.042	19.63
TEST TIME(H) 2450.0						
	82.5	3669.6	.059	.0021	.042	19.63
	85.0	3669.6	.049	.0016	.042	19.63
	87.5	3669.6	.040	.0007	.042	19.63
	90.0	3669.6	.040	.0007	.042	19.63
	95.0	3669.6	.040	.0007	.042	19.63
	100.0	3669.6	.025	.0006	.042	19.63
	105.0	3669.6	.020	.0005	.042	19.63
	110.0	3669.6	.013	.0005	.042	19.63
	112.5	3469.4	.008	.0004	.042	18.56
	115.0	3469.4	.008	.0004	.042	18.56
	120.0	3469.4	.008	.0004	.042	18.56

5(c) Cont.

ALUMINIUM ALLOY RR58	CRACK LENGTH (a) (MM)	APPLIED LOAD (P) NEWTONS	CRACK RATE (ȧ) (MM/H)	TRANS. RATE (Δ̇) (MM/H)	Δ/a	STRESS INTENS. (K) 1/2 MPa.m
SPECIMEN B6	140.0	3869.8	.274	.0076	.034	20.71
GEOMETRY DCB-C						
TEST TEMP 150 C	145.0	3869.8	.274	.0076	.034	20.71
B (MM) 25.4						
BN (MM) 12.7	150.0	3869.8	.274	.0076	.034	20.71
TEST TIME(H) 59.0						
SPECIMEN B7	105.0	3691.8	.167	.0038	.029	19.75
GEOMETRY DCB-C						
TEST TEMP 150 C	110.0	3691.8	.109	.0028	.029	19.75
B (MM) 25.4						
BN (MM) 12.7	115.0	3691.8	.109	.0028	.029	19.75
TEST TIME(H) 840.0						
	125.0	3691.8	.068	.0019	.029	19.75
	130.0	3691.8	.068	.0019	.029	19.75
	135.0	3691.8	.068	.0019	.029	19.75
SPECIMEN B9	100.0	3558.4	.061	.0024	.049	19.04
GEOMETRY DCB-C						
TEST TEMP 150 C	102.5	3558.4	.036	.0016	.049	19.04
B (MM) 25.4						
BN (MM) 12.7	105.0	3558.4	.025	.0011	.049	19.04
TEST TIME(H) 1400.0						
	108.0	3558.4	.021	.0008	.049	19.04
	110.0	3558.4	.019	.0005	.049	19.04
	115.0	3558.4	.013	.0005	.049	19.04
	115.0	3647.4	.009	.0005	.053	19.52
	117.5	3647.4	.009	.0005	.053	19.52
	117.5	3736.3	.008	.0005	.053	19.99
	120.0	3736.3	.008	.0005	.053	19.99
SPECIMEN B10	105.0	3113.6	.006	.0002	.037	16.66
GEOMETRY DCB-C						
TEST TEMP 150 C	110.0	3113.6	.006	.0002	.037	16.66
B (MM) 25.4						
BN (MM) 12.7	110.0	3558.4	.018	.0013	.037	19.04
TEST TIME(H) 2200.0						
	115.0	3558.4	.018	.0013	.037	19.04
	120.0	3558.4	.018	.0013	.037	19.04
	120.0	4003.2	.197	.0046	.037	21.42
	130.0	4003.2	.197	.0046	.037	21.42
	140.0	4003.2	.197	.0046	.037	21.42

5(c) Cont

ALUMINIUM ALLOY RR58		CRACK LENGTH (a) (MM)	APPLIED LOAD (P) NEWTONS	CRACK RATE (ȧ) (MM/H)	TRANS. RATE (ȧ) (MM/H)	Δ/d	STRESS INTENS. (K) 1/2 MPa.m
SPECIMEN	B15	95.0	3780.8	.240	.0104	.034	20.23
GEOMETRY	DCB-C						
TEST TEMP	150 C	100.0	3780.8	.169	.0094	.034	20.23
B (MM)	25.4						
BN (MM)	12.7	105.0	3780.8	.157	.0079	.034	20.23
TEST TIME(H)	640.0						
		110.0	3780.8	.146	.0053	.034	20.23
		115.0	3780.8	.146	.0044	.034	20.23
		120.0	3780.8	.146	.0022	.034	20.23
		125.0	3780.8	.136	.0022	.034	20.23
		135.0	3780.8	.136	.0022	.034	20.23
		140.0	3780.8	.136	.0022	.034	20.23
SPECIMEN	B16	105.0	3602.9	.036	.0014	.039	19.28
GEOMETRY	DCB-C						
TEST TEMP	150 C	107.5	3602.9	.025	.0010	.039	19.28
B (MM)	25.4						
BN (MM)	12.7	110.0	3602.9	.017	.0008	.039	19.28
TEST TIME(H)	1400.0						
		115.0	3602.9	.017	.0008	.039	19.28
SPECIMEN	B17	105.0	3380.5	.075	.0043	.035	18.09
GEOMETRY	DCB-C						
TEST TEMP	150 C	107.5	3380.5	.064	.0030	.035	18.09
B (MM)	25.4						
BN (MM)	12.7	110.0	3380.5	.035	.0023	.035	18.09
TEST TIME(H)	1160.0						
		112.5	3380.5	.035	.0016	.035	18.09
		115.0	3380.5	.035	.0013	.035	18.09
		120.0	3380.5	.035	.0013	.035	18.09
		122.5	3602.9	.077	.0024	.035	19.28
		130.0	3602.9	.077	.0024	.035	19.28
		137.5	3602.9	.077	.0024	.035	19.28
		140.0	3380.5	.032	.0009	.035	18.09
		145.0	3380.5	.031	.0009	.035	18.09
SPECIMEN	B20	100.0	3558.4	.167	.0071	.047	19.04
GEOMETRY	DCB-C						
TEST TEMP	150 C	105.0	3558.4	.088	.0041	.047	19.04
B (MM)	25.4						
BN (MM)	12.7	110.0	3558.4	.065	.0028	.047	19.04
TEST TIME(H)	800.0						
		115.0	3558.4	.048	.0023	.047	19.04
		120.0	3558.4	.048	.0021	.047	19.04
		125.0	3558.4	.048	.0015	.047	19.04
SPECIMEN	B38	100.0	4136.6	.565	.0310	.056	22.13
GEOMETRY	DCB-C						
TEST TEMP	150 C	105.0	4136.6	.261	.0159	.056	22.13
B (MM)	25.4						
BN (MM)	12.7	110.0	4225.6	.193	.0113	.056	22.61
TEST TIME(H)	66.0						
		115.0	4270.1	.148	.0080	.056	22.85

5(c) Cont.

ALUMINIUM ALLOY RR58	CRACK LENGTH (a) (MM)	APPLIED LOAD (P) NEWTONS	CRACK RATE (da) (MM/H)	TRANS. RATE (da) (MM/H)	Δ/a	STRESS INTENS. (K) 1/2 MPa.M
SPECIMEN B43	115.0	4047.7	.439	.0287	.060	21.66
GEOMETRY DCB-C						
TEST TEMP 150 C	120.0	4047.7	.439	.0231	.060	21.66
B (MM) 25.4						
BN (MM) 12.7	125.0	4136.6	.439	.0231	.060	22.13
TEST TIME(H) 68.0						
	130.0	4136.6	.439	.0231	.060	22.13
	135.0	4225.6	.439	.0231	.060	22.61
	140.0	4270.1	.554	.0249	.060	22.85
SPECIMEN B44	117.5	4003.2	.220	.0107	.046	21.42
GEOMETRY DCB-C						
TEST TEMP 150 C	120.0	4003.2	.220	.0107	.046	21.42
B (MM) 25.4						
BN (MM) 12.7	125.0	4047.7	.220	.0107	.046	21.66
TEST TIME(H) 75.0						
	130.0	4092.2	.251	.0122	.046	21.90
SPECIMEN B45	95.0	3825.3	.167	.0074	.050	20.47
GEOMETRY DCB-C						
TEST TEMP 150 C	100.0	3825.3	.167	.0069	.050	20.47
B (MM) 25.4						
BN (MM) 12.7	105.0	3869.8	.167	.0069	.050	20.71
TEST TIME(H) 240.0						
	110.0	3914.2	.167	.0069	.050	20.94
	115.0	3958.7	.167	.0069	.050	21.18
	120.0	4003.2	.167	.0069	.050	21.42
	125.0	4047.7	.167	.0069	.050	21.66
	130.0	4092.2	.251	.0079	.050	21.90
	135.0	4136.6	.371	.0163	.050	22.13
SPECIMEN B47	80.0	3380.5	.009	.0004	.030	18.09
GEOMETRY DCB-C						
TEST TEMP 150 C	82.0	3380.5	.009	.0004	.030	18.09
B (MM) 25.4						
BN (MM) 12.7	83.0	3380.5	.009	.0004	.030	18.09
TEST TIME(H) 800.0						
	85.0	3558.4	.048	.0007	.030	19.04
	90.0	3558.4	.032	.0005	.030	19.04
	95.0	3558.4	.012	.0004	.030	19.04
SPECIMEN B48	75.0	3202.6	.021	.0007	.028	17.14
GEOMETRY DCB-C						
TEST TEMP 150 C	77.5	3202.6	.021	.0007	.028	17.14
B (MM) 25.4						
BN (MM) 12.7	80.0	3202.6	.021	.0007	.028	17.14
TEST TIME(H) 780.0						
	82.5	3247.0	.021	.0007	.028	17.37
	110.0	3602.9	.058	.0026	.032	19.28
	115.0	3647.4	.050	.0019	.032	19.52
	120.0	3691.8	.043	.0011	.032	19.75
	125.0	3736.3	.030	.0010	.032	19.99

5(c) Cont.

ALUMINIUM ALLOY RR58	CRACK LENGTH (a) (MM)	APPLIED LOAD (P) NEWTONS	CRACK RATE (ȧ) (MM/H)	TRANS. RATE (ȧ) (MM/H)	Δ/a	STRESS INTENS. (K) 1/2 MPa.m
SPECIMEN B2	105.0	5337.6	.096	.0127	.071	22.76
GEOMETRY DCB-C						
TEST TEMP 150 C	110.0	5337.6	.069	.0048	.071	22.76
B (MM) 25.4						
BN (MM) 20.0	115.0	5337.6	.040	.0020	.071	22.76
TEST TIME(H) 1380.0	120.0	5337.6	.016	.0012	.071	22.76
	122.5	5337.6	.012	.0007	.071	22.76
	125.0	5560.0	.010	.0007	.071	23.71
	127.5	5560.0	.010	.0007	.071	23.71
	130.0	5560.0	.010	.0007	.071	23.71

ALUMINIUM ALLOY RR58 Overaged for 600 hours at 200°C	CRACK LENGTH (a) (MM)	APPLIED LOAD (P) NEWTONS	CRACK RATE (ȧ) (MM/H)	TRANS. RATE (ȧ) (MM/H)	Δ/a	STRESS INTENS. (K) 1/2 MPa.m
SPECIMEN B41	80.0	4448.0	.026	.0009	.038	23.80
GEOMETRY DCB-C						
TEST TEMP 150 C	90.0	4448.0	.018	.0005	.038	23.80
B (MM) 25.4						
BN (MM) 12.7	100.0	4448.0	.012	.0004	.038	23.80
TEST TIME(H) 2900.0	110.0	4448.0	.005	.0002	.038	23.80

5(d)

ALUMINIUM ALLOY RR58	CRACK LENGTH (a) (MM)	APPLIED LOAD (P) NEWTONS	CRACK RATE (ȧ) (MM/H)	TRANS. RATE (ȧ) (MM/H)	$\frac{\Delta}{a}$	STRESS INTENS. (K) 1/2 MPa.M
SPECIMEN B7	140.0	3691.8	.157	.0074	.043	19.75
GEOMETRY DCB-C						
TEST TEMP 175 C	142.5	3691.8	.157	.0074	.043	19.75
B (MM) 25.0						
BN (MM) 12.7	145.0	3691.8	.157	.0074	.043	19.75
TEST TIME(H) 720.0						
	147.5	3691.8	.157	.0074	.043	19.75
SPECIMEN B16	115.0	3602.9	.032	.0015	.060	19.28
GEOMETRY DCB-C						
TEST TEMP 175 C	120.0	3602.9	.032	.0015	.060	19.28
B (MM) 25.0						
BN (MM) 12.7	125.0	3602.9	.032	.0015	.060	19.28
TEST TIME(H) 900.0						
SPECIMEN B20	135.0	3558.4	.084	.0053	.060	19.04
GEOMETRY DCB-C						
TEST TEMP 175 C	140.0	3558.4	.084	.0053	.060	19.04
B (MM) 25.0						
BN (MM) 12.7	145.0	3558.4	.084	.0053	.060	19.04
TEST TIME(H) 700.0						
SPECIMEN B21	105.0	3336.0	.115	.0089	.060	17.85
GEOMETRY DCB-C						
TEST TEMP 175 C	110.0	3336.0	.068	.0051	.060	17.85
B (MM) 25.0						
BN (MM) 12.7	115.0	3336.0	.033	.0030	.060	17.85
TEST TIME(H) 960.0						
	120.0	3336.0	.023	.0016	.060	17.85
	125.0	3336.0	.023	.0015	.060	17.85
	127.5	3513.9	.037	.0022	.065	18.80
	130.0	3513.9	.037	.0022	.065	18.80
	132.5	3513.9	.037	.0022	.065	18.80
	135.0	3691.8	.073	.0038	.060	19.75
	140.0	3691.8	.073	.0046	.060	19.75
	145.0	3691.8	.073	.0051	.060	19.75
SPECIMEN B23	120.0	4448.0	.065	.0056	.057	23.80
GEOMETRY DCB-C						
TEST TEMP 175 C	130.0	4448.0	.065	.0056	.057	23.80
B (MM) 25.0						
BN (MM) 12.7	140.0	4448.0	.065	.0056	.057	23.80
TEST TIME(H) 1400.0						
	150.0	4448.0	.065	.0056	.057	23.80

ALUMINIUM ALLOY RR58	CRACK LENGTH (a) (MM)	APPLIED LOAD (P) NEWTONS	CRACK RATE (da/dt) (MM/H)	TRANS. RATE (Δa) (MM/H)	Δ/d	STRESS INTENS. (K) 1/2 MPa.M
SPECIMEN B26	100.0	4448.0	.068	.0079	.066	23.80
GEOMETRY DCB-C						
TEST TEMP 175 C	105.0	4448.0	.068	.0074	.066	23.80
B (MM) 25.0						
BN (MM) 12.7	110.0	4448.0	.068	.0074	.066	23.80
TEST TIME(H) 840.0	115.0	4448.0	.068	.0074	.066	23.80
	135.0	4448.0	.023	.0015	.061	23.80
	140.0	4448.0	.023	.0015	.061	23.80
	142.5	4448.0	.023	.0015	.061	23.80
SPECIMEN B27	110.0	3558.4	.042	.0038	.077	19.04
GEOMETRY DCB-C						
TEST TEMP 175 C	115.0	3558.4	.028	.0019	.077	19.04
B (MM) 25.0						
BN (MM) 12.7	120.0	3558.4	.018	.0008	.077	19.04
TEST TIME(H) 1100.0	122.5	3558.4	.014	.0007	.077	19.04
	125.0	4225.6	.041	.0028	.077	22.61
	130.0	4225.6	.041	.0028	.077	22.61
	135.0	4225.6	.043	.0030	.077	22.61
	140.0	4225.6	.046	.0030	.077	22.61
SPECIMEN B30	100.0	4448.0	.078	.0124	.070	23.80
GEOMETRY DCB-C						
TEST TEMP 175 C	105.0	4448.0	.058	.0058	.070	23.80
B (MM) 25.0						
BN (MM) 12.7	110.0	4448.0	.044	.0033	.070	23.80
TEST TIME(H) 2000.0	115.0	4448.0	.044	.0033	.070	23.80
overaged for 1500 hours at 175°C	120.0	4448.0	.044	.0033	.070	23.80
	125.0	4448.0	.044	.0033	.070	23.80
	125.0	4270.1	.025	.0020	.070	22.85
	130.0	4270.1	.025	.0011	.070	22.85
	135.0	4270.1	.025	.0011	.070	22.85
	140.0	4270.1	.025	.0011	.070	22.85
	145.0	4270.1	.025	.0011	.070	22.85
	150.0	4270.1	.037	.0017	.070	22.85
	160.0	4270.1	.040	.0038	.070	22.85
SPECIMEN B31	125.0	4448.0	.324	.0251	.080	23.80
GEOMETRY DCB-C						
TEST TEMP 175 C	130.0	4448.0	.220	.0180	.080	23.80
B (MM) 25.0						
BN (MM) 12.7	135.0	4448.0	.125	.0135	.080	23.80
TEST TIME(H) 200.0	140.0	4448.0	.098	.0089	.080	23.80
	145.0	4448.0	.098	.0089	.080	23.80
	150.0	4448.0	.130	.0114	.080	23.80

5(d) Cont.

ALUMINIUM ALLOY RR58	CRACK LENGTH (a) (MM)	APPLIED LOAD (P) NEWTONS	CRACK RATE ($\dot{a}$) (MM/H)	TRANS. RATE ($\dot{\Delta}$) (MM/H)	$\frac{\Delta}{a}$	STRESS INTENS. (K) 1/2 MPa.M
SPECIMEN B32	70.0	4537.0	.168	.0191	.066	24.28
GEOMETRY DCB-C						
TEST TEMP 175 C	80.0	4537.0	.168	.0112	.066	24.28
B (MM) 25.0						
BN (MM) 12.7	90.0	4537.0	.168	.0063	.066	24.28
TEST TIME(H) 570.0						
	100.0	4537.0	.168	.0063	.066	24.28
	110.0	4537.0	.168	.0063	.066	24.28
	120.0	4537.0	.168	.0063	.066	24.28
	130.0	4537.0	.168	.0063	.066	24.28
	140.0	4537.0	.168	.0063	.066	24.28
	150.0	4537.0	.168	.0063	.066	24.28
SPECIMEN B36	120.0	4003.2	.171	.0203	.086	21.42
GEOMETRY DCB-C						
TEST TEMP 175 C	125.0	4003.2	.087	.0112	.086	21.42
B (MM) 25.0						
BN (MM) 12.7	130.0	4003.2	.044	.0048	.086	21.42
TEST TIME(H) 720.0						
	135.0	4003.2	.029	.0027	.086	21.42
	140.0	4003.2	.012	.0015	.086	21.42
SPECIMEN B37	95.0	4003.2	.136	.0137	.070	21.42
GEOMETRY DCB-C						
TEST TEMP 175 C	100.0	4003.2	.067	.0050	.070	21.42
B (MM) 25.0						
BN (MM) 12.7	105.0	4003.2	.042	.0030	.070	21.42
TEST TIME(H) 360.0						
	110.0	4003.2	.037	.0025	.070	21.42

5(e)

ALUMINIUM ALLOY RR58

CRACK LENGTH (a) (MM)	APPLIED LOAD (P) NEWTONS	CRACK RATE ($\dot{a}$) (MM/H)	TRANS. RATE ($\dot{\Delta}$) (MM/H)	$\frac{\Delta}{a}$	STRESS INTENS. (K) 1/2 MPa.m
SPECIMEN B26					
GEOMETRY DCB-C					
TEST TEMP 200 C					
B (MM) 25.0					
BN (MM) 12.7					
TEST TIME(H) 450.0					
120.0	4448.0	.115	.0124	.102	23.80
125.0	4448.0	.115	.0124	.102	23.80
130.0	4448.0	.115	.0124	.102	23.80
135.0	4448.0	.115	.0124	.102	23.80
SPECIMEN B28					
GEOMETRY DCB-C					
TEST TEMP 200 C					
B (MM) 25.0					
BN (MM) 12.7					
TEST TIME(H) 600.0					
110.0	4892.8	.157	.0508	.125	26.18
115.0	4892.8	.157	.0381	.125	26.18
120.0	4892.8	.157	.0231	.125	26.18
125.0	4892.8	.115	.0188	.125	26.18
130.0	4892.8	.068	.0157	.125	26.18
135.0	4892.8	.068	.0104	.125	26.18
140.0	4892.8	.068	.0094	.125	26.18
145.0	4892.8	.068	.0076	.125	26.18
150.0	4892.8	.068	.0048	.125	26.18
160.0	4892.8	.068	.0048	.125	26.18

5(f)

ALUMINIUM ALLOY RR58		CRACK LENGTH (a) (MM)	APPLIED LOAD (P) NEWTONS	CRACK RATE (ȧ) (MM/H)	TRANS. RATE (ȧ) (MM/H)	Δ/a	STRESS INTENS. (K) 1/2 MPa.m
SPECIMEN	D54	105.0	1957.1	.010	.0010	.057	23.29
GEOMETRY	DCB-C						
TEST TEMP	100 C	107.5	1957.1	.004	.0003	.057	23.29
B (MM)	9.5						
BN (MM)	7.7	107.0	1957.1	.004	.0003	.057	23.29
TEST TIME(H)	1900.0						
		110.0	2090.6	.008	.0004	.053	24.88
		112.5	2090.6	.008	.0004	.053	24.88
		115.0	2090.6	.008	.0004	.053	24.88
		117.5	2090.6	.008	.0004	.053	24.88
SPECIMEN	D58	100.0	1957.1	.019	.0020	.070	23.29
GEOMETRY	DCB-C						
TEST TEMP	100 C	102.5	1957.1	.015	.0015	.070	23.29
B (MM)	9.5						
BN (MM)	7.7	105.0	1957.1	.009	.0008	.070	23.29
TEST TIME(H)	700.0						
		106.0	1957.1	.006	.0003	.070	23.29
		107.5	2135.0	.042	.0025	.070	25.41
		110.0	2135.0	.042	.0025	.070	25.41
		111.0	2135.0	.042	.0025	.070	25.41
SPECIMEN	D59	105.0	2179.5	.008	.0004	.050	25.94
GEOMETRY	DCB-C						
TEST TEMP	100 C	107.5	2179.5	.008	.0004	.050	25.94
B (MM)	9.5						
BN (MM)	7.7	110.0	2179.5	.008	.0004	.050	25.94
TEST TIME(H)	1300.0						
		112.5	2268.5	.008	.0004	.042	27.00
		115.0	2268.5	.008	.0004	.042	27.00
		117.5	2268.5	.008	.0004	.042	27.00

5(g)

ALUMINIUM ALLOY RR58		CRACK LENGTH (a) (MM)	APPLIED LOAD (P) NEWTONS	CRACK RATE (ȧ) (MM/H)	TRANS. RATE (Δ̇) (MM/H)	Δ/a	STRESS INTENS. (K) 1/2 MPa.m
SPECIMEN	D43	100.0	2135.0	.111	.0062	.083	25.41
GEOMETRY	DCB-C						
TEST TEMP	150 C	105.0	2135.0	.054	.0029	.083	25.41
B (MM)	9.5						
BN (MM)	7.7	110.0	2135.0	.036	.0018	.083	25.41
TEST TIME(H)	3300.0						
		120.0	2135.0	.022	.0011	.083	25.41
		130.0	2135.0	.015	.0008	.083	25.41
		140.0	2135.0	.015	.0008	.083	25.41
		150.0	2135.0	.015	.0008	.083	25.41
SPECIMEN	D44	95.0	1948.2	.125	.0054	.049	23.19
GEOMETRY	DCB-C						
TEST TEMP	150 C	100.0	1948.2	.073	.0042	.049	23.19
B (MM)	9.5						
BN (MM)	7.7	105.0	1948.2	.058	.0020	.049	23.19
TEST TIME(H)	3200.0						
		107.5	1948.2	.038	.0013	.049	23.19
		110.0	1948.2	.018	.0008	.049	23.19
		120.0	1948.2	.014	.0005	.049	23.19
		127.5	1948.2	.012	.0005	.049	23.19
		130.0	2086.1	.018	.0009	.049	24.83
		140.0	2086.1	.022	.0011	.049	24.83
		150.0	2086.1	.026	.0018	.049	24.83
SPECIMEN	D50	105.0	2023.8	.125	.0056	.047	24.09
GEOMETRY	DCB-C						
TEST TEMP	150 C	110.0	2023.8	.073	.0033	.047	24.09
B (MM)	9.5						
BN (MM)	7.7	115.0	2023.8	.047	.0024	.047	24.09
TEST TIME(H)	2700.0						
		117.5	2023.8	.038	.0020	.047	24.09
		120.0	2023.8	.026	.0012	.047	24.09
		130.0	2023.8	.021	.0011	.047	24.09
		140.0	2023.8	.021	.0011	.047	24.09
		150.0	2023.8	.021	.0011	.047	24.09

5(g) Cont.

ALUMINIUM ALLOY RR58	CRACK LENGTH (a) (MM)	APPLIED LOAD (P) NEWTONS	CRACK RATE (ȧ) (MM/H)	TRANS. RATE (Δ̇) (MM/H)	Δ/a	STRESS INTENS. (K) 1/2 MPa.m
SPECIMEN 051 GEOMETRY DCB-C TEST TEMP 150 C B (MM) 9.5 BN (MM) 7.7 TEST TIME(H)1200.0	130.0	2046.1	.038	.0024	.047	24.35
	135.0	2046.1	.027	.0019	.076	24.35
	140.0	2046.1	.016	.0014	.076	24.35
	140.0	2121.7	.019	.0017	.076	25.25
	145.0	2121.7	.019	.0017	.076	25.25
	147.5	2224.0	.025	.0020	.076	26.47
	150.0	2224.0	.058	.0034	.076	26.47
SPECIMEN 061 GEOMETRY DCB-C TEST TEMP 150 C B (MM) 9.5 BN (MM) 7.7 TEST TIME(H)1030.0	105.0	2112.8	.188	.0132	.063	25.15
	110.0	2112.8	.105	.0060	.063	25.15
	115.0	2112.8	.058	.0031	.063	25.15
	120.0	2112.8	.033	.0018	.063	25.15
	125.0	2112.8	.033	.0018	.063	25.15
	127.5	2224.0	.046	.0027	.063	26.47
	130.0	2224.0	.046	.0027	.063	26.47
	135.0	2224.0	.046	.0027	.063	26.47
	140.0	2224.0	.046	.0027	.063	26.47
	145.0	2313.0	.075	.0051	.063	27.53
	150.0	2313.0	.075	.0051	.063	27.53
SPECIMEN 063 GEOMETRY DCB-C TEST TEMP 150 C B (MM) 9.5 BN (MM) 7.7 TEST TIME(H)2100.0	75.0	2090.6	.178	.0109	.056	24.88
	80.0	2090.6	.115	.0089	.056	24.88
	85.0	2090.6	.094	.0079	.056	24.88
	90.0	2090.6	.068	.0056	.056	24.88
	95.0	2090.6	.029	.0015	.056	24.88
	105.0	2046.1	.028	.0025	.066	24.35
	110.0	2046.1	.021	.0016	.066	24.35
	115.0	2046.1	.013	.0010	.066	24.35
	120.0	2046.1	.013	.0010	.066	24.35
	125.0	2135.0	.018	.0011	.066	25.41
	130.0	2135.0	.018	.0011	.066	25.41

5(h)

ALUMINIUM ALLOY RR58		CRACK LENGTH (a) (MM)	APPLIED LOAD (P) NEWTONS	CRACK RATE (ȧ) (MM/H)	TRANS. RATE (ȧ) (MM/H)	$\frac{\Delta}{a}$	STRESS INTENS. (K) 1/2 MPa.m
SPECIMEN	U1	92.5	5337.6	.020	.0005	.012	19.51
GEOMETRY	DCB-P						
TEST TEMP	150 C	95.0	5337.6	.020	.0005	.012	20.86
B (MM)	25.4						
BN (MM)	12.7	97.5	5337.6	.020	.0006	.014	21.50
TEST TIME(H)	1140.0						
		100.0	5337.6	.020	.0007	.028	22.73
		110.0	5337.6	.035	.0016	.042	24.46
		120.0	5337.6	.064	.0036	.051	26.07
		130.0	5337.6	.131	.0099	.066	28.56
		140.0	5337.6	.220	.0174	.114	30.85
SPECIMEN	U2	132.5	3380.5	.016	.0003	.046	18.39
GEOMETRY	DCB-P						
TEST TEMP	150 C	135.0	3336.0	.009	.0003	.046	18.44
B (MM)	25.0						
BN (MM)	12.7	137.5	3202.6	.006	.0003	.046	17.97
TEST TIME(H)	1900.0						
		140.0	3113.6	.004	.0003	.046	17.99
		140.0	4003.2	.019	.0008	.031	23.14
		145.0	4003.2	.031	.0010	.038	24.42
		150.0	4003.2	.044	.0023	.057	25.64
SPECIMEN	U4	67.5	8896.0	.030	.0013	.034	24.58
GEOMETRY	DCB-P						
TEST TEMP	150 C	70.0	8896.0	.030	.0013	.034	26.07
B (MM)	25.0						
BN (MM)	12.7	70.0	6672.0	.006	.0002	.021	19.55
TEST TIME(H)	1500.0						
		72.5	6672.0	.013	.0003	.021	20.61
		75.0	6672.0	.019	.0004	.021	21.62
		80.0	6672.0	.027	.0005	.021	22.58
		85.0	6672.0	.048	.0009	.021	24.39
		90.0	6672.0	.095	.0028	.028	25.24

5(h) Cont.

ALUMINIUM ALLOY RR58

SPECIMEN U5
GEOMETRY DCB-P
TEST TEMP 150 C
B (MM) 25.0
BN (MM) 12.7
TEST TIME(H) 1100.0

CRACK LENGTH (a) (MM)	APPLIED LOAD (P) NEWTONS	CRACK RATE (ȧ) (MM/H)	TRANS. RATE (ȧ) (MM/H)	Δ/a	STRESS INTENS. (K) 1/2 MPa.M
52.5	9340.8	.066	.0008	.025	20.40
55.0	9340.8	.066	.0009	.025	22.35
57.5	9340.8	.066	.0010	.025	22.35
60.0	9340.8	.066	.0011	.025	24.14
60.0	5782.4	.006	.0001	.022	14.95
62.5	5782.4	.007	.0001	.022	14.95
65.0	5782.4	.008	.0002	.022	15.98
65.0	7561.6	.125	.0017	.006	20.89
67.5	7561.6	.125	.0017	.009	20.89
70.0	7561.6	.125	.0018	.012	22.16
72.5	7561.6	.188	.0028	.016	23.36
75.0	7561.6	.261	.0046	.019	24.50
77.5	7561.6	.481	.0097	.022	24.50
80.0	7561.6	.941	.0254	.028	25.59
82.5	7561.6	1.202	.0508	.035	26.63
85.0	7561.6	2.196	.0711	.047	27.64

5(i)

ALUMINIUM ALLOY RR58	CRACK LENGTH (a) (MM)	APPLIED LOAD (P) NEWTONS	CRACK RATE (ȧ) (MM/H)	TRANS. RATE (Δ̇) (MM/H)	Δ/a	STRESS INTENS. (K) 1/2 MPa.M
SPECIMEN DT2	130.0	8273.3	.199	.0017	.010	20.76
GEOMETRY DT						
TEST TEMP 150 C	140.0	8273.3	.199	.0017	.010	20.76
B (MM) 9.5						
BN (MM) 7.7	150.0	8273.3	.199	.0017	.010	20.76
TEST TIME(H) 205.0						
	160.0	8273.3	.199	.0017	.010	20.76
	170.0	8273.3	.199	.0017	.010	20.76
SPECIMEN DT4	60.0	8273.3	.031	.0007	.028	20.76
GEOMETRY DT						
TEST TEMP 150 C	70.0	8807.0	.046	.0010	.028	22.10
B (MM) 9.5						
BN (MM) 7.7	80.0	8807.0	.046	.0010	.028	22.10
TEST TIME(H) 1100.0						
	90.0	9340.8	.071	.0010	.028	23.44
	100.0	9340.8	.071	.0010	.028	23.44
	110.0	9874.6	.088	.0010	.028	24.78
	120.0	9874.6	.088	.0010	.028	24.78
	130.0	9874.6	.088	.0010	.028	24.78
SPECIMEN DT12	40.0	9607.7	.107	.0013	.012	24.11
GEOMETRY DT						
TEST TEMP 150 C	50.0	9607.7	.107	.0013	.012	24.11
B (MM) 9.5						
BN (MM) 7.7	60.0	9607.7	.107	.0013	.012	24.11
TEST TIME(H) 1850.0						
	70.0	9607.7	.107	.0013	.012	24.11
	80.0	8273.3	.022	.0004	.011	20.76
	90.0	8273.3	.022	.0004	.011	20.76
	97.5	8273.3	.022	.0004	.011	20.76
	100.0	9607.7	.058	.0008	.011	24.11
	110.0	9607.7	.058	.0008	.011	24.11
	115.0	9607.7	.058	.0008	.011	24.11
	120.0	10942.1	.157	.0024	.015	27.46
	130.0	10942.1	.157	.0024	.015	27.46

1/2CR 1/2MO 1/4V STEEL,QUENCHED

	CRACK LENGTH (a) (MM)	APPLIED LOAD (P) NEWTONS	CRACK RATE (ȧ) (MM/H)	TRANS. RATE (ȧ) (MM/H)	Δ/a	STRESS INTENS. (K) 1/2 MPa.m
SPECIMEN 3F 2	52.5	3558.4	.014	.0003	.039	28.33
GEOMETRY DCB-C						
TEST TEMP 565 C	52.5	4448.0	.141	.0013	.039	31.92
B (MM) 25.4						
BN (MM) 6.5	60.0	4448.0	.141	.0013	.039	31.92
TEST TIME(H) 300.0						
	62.5	4448.0	.141	.0013	.031	31.92
	65.0	4892.8	.153	.0036	.031	35.12
	70.0	4892.8	.153	.0036	.031	35.12
	75.5	4892.8	.153	.0036	.031	35.12
	80.0	4892.8	.157	.0038	.031	35.12
SPECIMEN 3F 3	80.0	4892.8	.199	.0127	.031	37.54
GEOMETRY DCB-C						
TEST TEMP 565 C	90.0	4892.8	.173	.0046	.031	37.54
B (MM) 25.0						
BN (MM) 7.0	105.0	4892.8	.125	.0033	.031	37.54
TEST TIME(H) 950.0						
	120.0	4892.8	.094	.0033	.031	37.54
	145.0	4892.8	.046	.0030	.031	37.54
	150.0	4892.8	.041	.0025	.031	37.54
SPECIMEN 3F 4	80.0	5560.0	1.297	.0462	.038	46.08
GEOMETRY DCB-C						
TEST TEMP 565 C	90.0	5560.0	.711	.0246	.038	46.08
B (MM) 25.0						
BN (MM) 6.0	100.0	5560.0	.450	.0170	.038	46.08
TEST TIME(H) 280.0						
	110.0	5560.0	.356	.0099	.038	46.08
	120.0	5560.0	.202	.0066	.038	46.08
	130.0	5560.0	.202	.0066	.038	46.08
	140.0	5560.0	.202	.0066	.038	46.08
SPECIMEN 3F 5	90.0	5782.4	.606	.0351	.046	46.04
GEOMETRY DCB-C						
TEST TEMP 565 C	100.0	5782.4	.565	.0279	.046	47.92
B (MM) 25.0						
BN (MM) 6.5	110.0	5782.4	.565	.0282	.046	47.92
TEST TIME(H) 85.0						
	115.0	5782.4	.606	.0213	.046	47.92
	120.0	5782.4	.627	.0213	.046	47.92
	130.0	5782.4	1.150	.0213	.046	47.92
	140.0	5782.4	1.464	.0381	.046	46.04

5(j) Cont.

1/2CR 1/2MO 1/4V STEEL, QUENCHED

	CRACK LENGTH (a) (MM)	APPLIED LOAD (P) NEWTONS	CRACK RATE (ȧ) (MM/H)	TRANS. RATE (ȧ) (MM/H)	Δ/a	STRESS INTENS. (K) 1/2 MPa.m
SPECIMEN 3F 6 GEOMETRY DCB-C TEST TEMP 565 C B (MM) 25.0 BN (MM) 5.0 TEST TIME(H) 33.0	90.0	6227.2	1.997	.0762	.035	56.53
	100.0	6227.2	1.746	.0533	.035	56.53
	110.0	6227.2	1.746	.0533	.035	56.53
	120.0	6227.2	1.746	.0533	.035	56.53
	130.0	6227.2	2.405	.0533	.035	56.53
	140.0	6227.2	2.635	.0724	.035	56.53
SPECIMEN 3F 7 GEOMETRY DCB-C TEST TEMP 565 C B (MM) 25.0 BN (MM) 6.0 TEST TIME(H) 65.0	90.0	5604.5	1.725	.0546	.049	46.45
	100.0	5782.4	1.746	.0533	.049	47.92
	110.0	5960.3	1.725	.0546	.049	49.39
	120.0	6049.3	1.746	.0533	.049	50.13
	125.0	6138.2	1.725	.0546	.049	50.87
	135.0	6227.2	2.823	.1041	.046	49.58

5(k)

1/2CR 1/2MO 1/4V STEEL, QUENCHED AND TEMPERED	CRACK LENGTH (a) (MM)	APPLIED LOAD (P) NEWTONS	CRACK RATE (ȧ) (MM/H)	TRANS. RATE (ȧ) (MM/H)	Δ/a	STRESS INTENS. (K) 1/2 MPa.m
SPECIMEN 8F 1	90.0	5337.6	.545	.0142	.033	42.50
GEOMETRY DCB-C						
TEST TEMP 565 C	100.0	5337.6	.545	.0142	.033	42.50
B (MM) 25.4						
BN (MM) 6.5	110.0	5337.6	.545	.0142	.033	42.50
TEST TIME(H) 160.0						
	120.0	5337.6	.545	.0142	.033	42.50
	130.0	5337.6	.545	.0142	.033	42.50
	140.0	5337.6	.545	.0142	.033	42.50
SPECIMEN 8F 2	90.0	4892.8	.137	.0048	.043	38.96
GEOMETRY DCB-C						
TEST TEMP 565 C	100.0	4892.8	.137	.0036	.043	38.96
B (MM) 25.0						
BN (MM) 6.5	110.0	4892.8	.137	.0036	.043	38.96
TEST TIME(H) 1750.0						
	120.0	4892.8	.137	.0036	.043	38.96
	125.0	3780.8	.009	.0004	.043	30.10
	130.0	3780.8	.022	.0004	.043	30.10
	135.0	3780.8	.022	.0004	.043	30.10
	140.0	3780.8	.022	.0004	.043	30.10
	145.0	3780.8	.029	.0005	.043	30.10
SPECIMEN 8F 3	90.0	4892.8	.326	.0147	.039	38.96
GEOMETRY DCB-C						
TEST TEMP 565 C	100.0	5026.2	.326	.0148	.039	40.02
B (MM) 25.0						
BN (MM) 6.5	110.0	5159.7	.326	.0147	.039	41.08
TEST TIME(H) 156.0						
	120.0	5293.1	.326	.0148	.039	42.14
	130.0	5426.6	.366	.0147	.039	43.21
	140.0	5515.5	.606	.0427	.039	43.92
SPECIMEN 8F 4	90.0	4625.9	.162	.0053	.031	36.83
GEOMETRY DCB-C						
TEST TEMP 565 C	100.0	4625.9	.162	.0053	.031	36.83
B (MM) 25.0						
BN (MM) 6.5	110.0	4937.3	.162	.0053	.031	39.31
TEST TIME(H) 635.0						
	120.0	5026.2	.162	.0053	.031	40.02
	130.0	5204.2	.318	.0145	.031	41.44
	135.0	4003.2	.032	.0011	.028	31.87
	145.0	4003.2	.050	.0013	.028	31.87
	150.0	4003.2	.097	.0022	.028	31.87

5(k) Cont.

1/2CR 1/2MO 1/4V STEEL-QUENCHED AND TEMPERED		CRACK LENGTH (a) (MM)	APPLIED LOAD (P) NEWTONS	CRACK RATE (ȧ) (MM/H)	TRANS. RATE (ȧ) (MM/H)	Δ/a	STRESS INTENS. (K) 1/2 MPa.m
SPECIMEN	8F 5	90.0	4225.6	.235	.0069	.032	33.64
GEOMETRY	DCB-C						
TEST TEMP	565 C	100.0	4270.1	.235	.0071	.032	34.00
B (MM)	25.0						
BN (MM)	6.5	110.0	4448.0	.235	.0074	.032	35.42
TEST TIME(H)	248.0						
		120.0	4581.4	.235	.0076	.032	36.48
		130.0	4714.9	.240	.0079	.032	37.54
		145.0	4937.3	.439	.0193	.032	39.31
SPECIMEN	8F 6	90.0	4492.5	.199	.0074	.034	35.77
GEOMETRY	DCB-C						
TEST TEMP	565 C	100.0	4537.0	.230	.0089	.034	36.12
B (MM)	25.0						
BN (MM)	6.5	110.0	4714.9	.308	.0114	.034	37.54
TEST TIME(H)	165.0						
		120.0	4714.9	.314	.0114	.034	37.54
		130.0	4937.3	.324	.0114	.034	39.31
		140.0	5026.2	.774	.0307	.034	40.02
SPECIMEN	8F 7	90.0	3736.3	.136	.0058	.029	29.75
GEOMETRY	DCB-C						
TEST TEMP	565 C	100.0	3914.2	.115	.0038	.029	31.17
B (MM)	25.0						
BN (MM)	6.5	110.0	3914.2	.115	.0038	.029	31.17
TEST TIME(H)	590.0						
		125.0	4181.1	.115	.0038	.029	33.29
		125.0	3558.4	.038	.0014	.047	28.33
		130.0	3558.4	.038	.0014	.047	28.33
		135.0	3556.4	.038	.0014	.047	28.33
		135.0	6227.2	3.356	.0874	.038	49.58
		140.0	6227.2	3.356	.0874	.038	49.58
		145.0	6227.2	3.356	.0874	.038	49.58
		150.0	6227.2	3.869	.1143	.038	49.58
		155.0	6227.2	4.099	.1201	.038	49.58
SPECIMEN	8F 8	90.0	4047.7	.199	.0061	.030	32.23
GEOMETRY	DCB-C						
TEST TEMP	565 C	100.0	4092.2	.199	.0086	.030	32.58
B (MM)	25.0						
BN (MM)	6.5	110.0	4537.0	.199	.0061	.030	36.12
TEST TIME(H)	325.0						
		120.0	4403.5	.199	.0061	.030	35.06
		130.0	4670.4	.199	.0061	.030	37.19
		140.0	4670.4	.261	.0089	.030	37.19
		145.0	4759.4	.324	.0145	.030	37.89

5(k) Cont.

1/2CR 1/2MO 1/4V STEEL,QUENCHED AND TEMPERED	CRACK LENGTH (a) (MM)	APPLIED LOAD (P) NEWTONS	CRACK RATE (ȧ) (MM/H)	TRANS. RATE (Δ̇) (MM/H)	Δ/a	STRESS INTENS. (K) 1/2 MPa.M
SPECIMEN 8F 9 GEOMETRY DCB-C TEST TEMP 565 C B (MM) 25.0 BN (MM) 6.5 TEST TIME(H) 1110.0	90.0	3291.5	.012	.0007	.048	26.21
	95.0	3291.5	.008	.0005	.048	26.21
	100.0	3291.5	.008	.0005	.048	26.21
	105.0	5826.9	1.704	.0615	.040	46.39
	110.0	5826.9	1.704	.0615	.040	46.39
	120.0	6093.8	1.704	.0615	.040	48.52

5(l)

1/2CR 1/2MO 1/4V STEEL,QUENCHED AND TEMPERED	CRACK LENGTH (a) (MM)	APPLIED LOAD (P) NEWTONS	CRACK RATE (ȧ) (MM/H)	TRANS. RATE (Δ̇) (MM/H)	Δ/a	STRESS INTENS. (K) 1/2 MPa.M
SPECIMEN 7G2 GEOMETRY DCB-C TEST TEMP 565 C B (MM) 12.0 BN (MM) 6.0 TEST TIME(H) 830.0	100.0	3558.4	.115	.0056	.061	41.40
	110.0	3558.4	.105	.0051	.061	41.40
	120.0	3558.4	.094	.0046	.061	41.40
	132.5	4003.2	.523	.0457	.061	46.57
	145.0	4003.2	.523	.0406	.061	46.57
SPECIMEN 8F10 GEOMETRY DCB-C TEST TEMP 565 C B (MM) 12.0 BN (MM) 6.0 TEST TIME(H) 800.0	80.0	2668.8	.038	.0026	.059	31.05
	85.0	2668.8	.038	.0026	.059	31.05
	90.0	2668.8	.038	.0026	.059	31.05
	95.0	2668.8	.038	.0026	.059	31.05
	95.0	3113.6	.157	.0142	.090	36.22
	100.0	3113.6	.157	.0142	.090	36.22
	105.0	3113.6	.157	.0142	.090	36.22
	110.0	3113.6	.157	.0142	.090	36.22
	115.0	3336.0	.125	.0140	.127	38.81
	120.0	3336.0	.125	.0140	.127	38.81
	125.0	3336.0	.125	.0140	.127	38.81
	130.0	3336.0	.125	.0140	.127	38.81

5(1) Cont

1/2CR 1/2MO 1/4V STEEL.QUENCHED AND TEMPERED	CRACK LENGTH (a) (MM)	APPLIED LOAD (P) NEWTONS	CRACK RATE (ȧ) (MM/H)	TRANS. RATE (ȧ) (MM/H)	Δ/a	STRESS INTENS. (K) 1/2 MPa.M
SPECIMEN 7G1	50.0	2668.8	.016	.0014	.071	43.91
GEOMETRY DCB-C						
TEST TEMP 565 C	55.0	2668.8	.015	.0012	.071	43.91
B (MM) 12.0						
BN (MM) 3.0	60.0	2668.8	.012	.0010	.071	43.91
TEST TIME(H) 2060.0						
	65.0	2668.8	.007	.0009	.071	43.91
	65.0	3113.6	.036	.0020	.071	51.23
	70.0	3113.6	.036	.0018	.071	51.23
	75.0	3113.6	.036	.0017	.071	51.23
	80.0	3113.6	.036	.0017	.071	51.23
	80.0	3558.4	.033	.0028	.132	58.54
	85.0	3558.4	.033	.0036	.132	58.54
	90.0	3558.4	.033	.0030	.132	58.54
	95.0	3558.4	.033	.0030	.132	58.54
	97.5	3558.4	.033	.0028	.132	58.54
SPECIMEN 7G5	90.0	3780.8	.711	.0498	.071	62.20
GEOMETRY DCB-C						
TEST TEMP 565 C	95.0	3780.8	.711	.0498	.071	62.20
B (MM) 12.0						
BN (MM) 3.0	105.0	3780.8	.711	.0498	.071	62.20
TEST TIME(H) 130.0						
	115.0	3780.8	.711	.0498	.071	62.20
	120.0	3113.6	.157	.0152	.071	51.23
	125.0	3113.6	.157	.0152	.071	51.23
SPECIMEN 7G6	85.0	4225.6	2.091	.1524	.069	76.16
GEOMETRY DCB-C						
TEST TEMP 565 C	90.0	4225.6	2.091	.1524	.069	76.16
B (MM) 12.0						
BN (MM) 2.5	100.0	4225.6	2.091	.1524	.069	76.16
TEST TIME(H) 28.0						
	110.0	4225.6	2.091	.1524	.069	76.16
	120.0	4225.6	2.091	.1524	.069	76.16
	130.0	4225.6	2.091	.1524	.069	76.16
	140.0	4225.6	2.091	.1524	.069	76.16

5(m)

1/2CR 1/2MO 1/4V STEEL, QUENCHED AND TEMPERED	CRACK LENGTH (a) (MM)	APPLIED LOAD (P) NEWTONS	CRACK RATE (ȧ) (MM/H)	TRANS. RATE (ȧ) (MM/H)	Δ/a	STRESS INTENS. (K) 1/2 MPa.√m
SPECIMEN 10F 2	55.0	11564.8	.073	.0008	.005	38.68
GEOMETRY DCB-P						
TEST TEMP 565 C	60.0	11564.8	.137	.0006	.006	47.64
B (MM) 25.4						
BN (MM) 6.5	70.0	11564.8	.181	.0018	.006	54.02
TEST TIME(H) 90.0						
	80.0	11564.8	.252	.0028	.014	62.37
	90.0	11564.8	.408	.0067	.018	69.73
	100.0	11564.8	.727	.0189	.026	78.48
	110.0	11564.8	.795	.0223	.029	84.45
	120.0	11564.8	1.129	.0386	.044	90.03
	120.0	8896.0	.240	.0063	.025	69.25
	130.0	8896.0	.288	.0070	.035	75.86
	140.0	8896.0	.382	.0112	.040	81.94
	150.0	8896.0	1.171	.0401	.049	90.82
	160.0	8896.0	2.426	.0538	.054	100.83
SPECIMEN 10F 3	55.0	10675.2	.094	.0018	.008	40.71
GEOMETRY DCB-P						
TEST TEMP 565 C	60.0	10675.2	.158	.0028	.008	43.97
B (MM) 25.0						
BN (MM) 5.0	70.0	10675.2	.214	.0034	.016	49.86
TEST TIME(H) 270.0						
	80.0	10675.2	.335	.0061	.026	57.57
	90.0	10675.2	.451	.0218	.039	64.37
	100.0	10675.2	.742	.0663	.072	72.45
	110.0	10675.2	1.851	.1031	.084	77.96

5(m) Cont.

1/2CR 1/2MO 1/4V STEEL,QUENCHED AND TEMPERED	CRACK LENGTH (a) (MM)	APPLIED LOAD (P) NEWTONS	CRACK RATE (ȧ) (MM/H)	TRANS. RATE (ȧ) (MM/H)	Δ/a	STRESS INTENS. (K) 1/2 MPa.m
SPECIMEN 10F 4	50.0	10008.0	.007	.0001	.007	30.56
GEOMETRY DCB-P						
TEST TEMP 565 C	55.0	10008.0	.007	.0001	.007	33.47
B (MM) 25.0						
BN (MM) 6.5	60.0	10008.0	.015	.0001	.013	36.16
TEST TIME(H) 2030.0						
	65.0	10897.6	.029	.0005	.014	42.09
	70.0	10897.6	.056	.0008	.015	44.64
	80.0	10897.6	.107	.0016	.017	51.55
	90.0	10897.6	.171	.0030	.021	57.63
	100.0	10897.6	.185	.0079	.023	64.86
	100.0	10008.0	.130	.0025	.023	59.57
	110.0	10008.0	.293	.0112	.024	64.10
	120.0	10008.0	.878	.0340	.029	68.33
	130.0	10008.0	1.171	.0660	.033	74.85
	130.0	4670.4	.020	.0003	.014	34.93
	132.5	4670.4	.032	.0003	.014	35.51
	135.0	5782.4	.078	.0007	.017	44.67
	140.0	5782.4	.092	.0012	.023	46.71
	150.0	5782.4	.220	.0079	.028	51.78
	155.0	5782.4	.397	.0249	.035	53.55
SPECIMEN 10F 5	55.0	17792.0	.293	.0063	.006	59.51
GEOMETRY DCB-P						
TEST TEMP 565 C	60.0	17792.0	1.202	.0114	.008	64.28
B (MM) 25.0						
BN (MM) 6.5	70.0	17792.0	3.252	.0317	.018	72.88
TEST TIME(H) 515.0						
	80.0	17792.0	4.062	.1123	.021	84.16
	90.0	17792.0	6.002	.2123	.024	94.09
	110.0	8896.0	.152	.0009	.013	56.98
	120.0	8896.0	.230	.0019	.021	60.74
	130.0	8896.0	.387	.0039	.027	63.12
	132.5	6672.0	.073	.0010	.008	50.73
	140.0	6672.0	.129	.0027	.012	53.90
	150.0	6672.0	.329	.0137	.039	59.74

5(n)

1/2CR 1/2MO 1/4V STEEL, QUENCHED AND TEMPERED

SPECIMEN 10F 7
GEOMETRY DCB-P
TEST TEMP 615 C
B (MM) 25.0
BN (MM) 8.0
TEST TIME(H) 1025.0

CRACK LENGTH (a) (MM)	APPLIED LOAD (P) NEWTONS	CRACK RATE (ȧ) (MM/H)	TRANS. RATE (ȧ) (MM/H)	Δ/a	STRESS INTENS. (K) 1/2 MPa.m
55.0	8896.0	.021	.0011	.043	32.85
60.0	8896.0	.030	.0014	.043	34.63
70.0	8896.0	.094	.0025	.043	37.93
80.0	8896.0	.136	.0030	.043	40.97
90.0	8896.0	.188	.0035	.043	40.97
100.0	8896.0	.230	.0046	.043	47.73
110.0	8896.0	.303	.0076	.043	51.36

5(o)

1/2CR 1/2MO 1/4V STEEL, QUENCHED AND TEMPERED

SPECIMEN 7G11
GEOMETRY DCB-P
TEST TEMP 565 C
B (MM) 12.0
BN (MM) 3.0
TEST TIME(H) 204.5

CRACK LENGTH (a) (MM)	APPLIED LOAD (P) NEWTONS	CRACK RATE (ȧ) (MM/H)	TRANS. RATE (ȧ) (MM/H)	Δ/a	STRESS INTENS. (K) 1/2 MPa.m
50.0	8896.0	.784	.0406	.051	66.90
60.0	8896.0	1.778	.1118	.051	75.86
70.0	8896.0	3.346	.2007	.051	81.94
80.0	8896.0	5.123	.4064	.051	91.17
90.0	8896.0	7.528	.5588	.061	99.56
100.0	8896.0	10.979	.8890	.061	104.26
110.0	8896.0	12.965	.9652	.071	115.88
125.0	4448.0	.627	.0122	.039	64.47
130.0	4448.0	1.004	.0325	.034	68.09
140.0	4448.0	1.568	.1626	.056	74.26
150.0	4448.0	2.300	.2794	.066	83.87
160.0	4448.0	3.137	.4801	.086	99.56

SPECIMEN 7G13
GEOMETRY DCB-P
TEST TEMP 565 C
B (MM) 12.0
BN (MM) 3.0
TEST TIME(H) 890.0

CRACK LENGTH (a) (MM)	APPLIED LOAD (P) NEWTONS	CRACK RATE (ȧ) (MM/H)	TRANS. RATE (ȧ) (MM/H)	Δ/a	STRESS INTENS. (K) 1/2 MPa.m
55.0	4448.0	.046	.0011	.021	34.63
60.0	4448.0	.097	.0019	.021	37.93
70.0	4448.0	.136	.0025	.021	40.97
80.0	4448.0	.282	.0036	.021	45.59
85.0	3113.6	.029	.0003	.012	33.70
90.0	3113.6	.064	.0006	.012	34.84
100.0	3113.6	.084	.0008	.012	36.49
110.0	3113.6	.115	.0011	.012	40.56

5(o) Cont

1/2CR 1/2MO 1/4V STEEL, QUENCHED AND TEMPERED		CRACK LENGTH (a) (MM)	APPLIED LOAD (P) NEWTONS	CRACK RATE (ȧ) (MM/H)	TRANS. RATE (ȧ) (MM/H)	Δ/a	STRESS INTENS. (K) 1/2 MPa.m
SPECIMEN	7G8	65.0	8896.0	.450	.0305	.066	55.11
GEOMETRY	DCB-P						
TEST TEMP	565 C	70.0	8896.0	.627	.0432	.066	57.94
B (MM)	12.0						
BN (MM)	6.0	75.0	8896.0	.993	.0610	.066	61.94
TEST TIME(H)	31.0						
		80.0	8896.0	1.778	.0940	.066	64.47
		85.0	8896.0	2.719	.1118	.066	66.90
		90.0	8896.0	4.705	.2362	.066	70.40
SPECIMEN	7G9	85.0	6672.0	.105	.0061	.061	50.18
GEOMETRY	DCB-P						
TEST TEMP	565 C	90.0	6672.0	.188	.0130	.071	52.80
B (MM)	12.0						
BN (MM)	6.0	100.0	6672.0	.335	.0279	.091	55.29
TEST TIME(H)	750.0						
		110.0	6672.0	.502	.0376	.101	61.45
		115.0	6672.0	.816	.0554	.112	62.90
		120.0	4448.0	.014	.0007	.032	42.88
		130.0	4448.0	.086	.0034	.062	43.00
		140.0	4448.0	.283	.0179	.096	52.51

5(P)

1/2CR 1/2MO 1/4V STEEL, QUENCHED AND TEMPERED		CRACK LENGTH (a) (MM)	APPLIED LOAD (P) NEWTONS	CRACK RATE (ȧ) (MM/H)	TRANS. RATE (ȧ) (MM/H)	Δ/a	STRESS INTENS. (K) 1/2 MPa.m
SPECIMEN	4F1	15.2	11342.4	.398	.0025	.007	17.07
GEOMETRY	CT						
TEST TEMP	565 C	15.5	11342.4	.531	.0038	.008	17.26
B (MM)	25.4						
BN (MM)	13.1	17.5	11342.4	.797	.0043	.006	18.75
TEST TIME(H)	35.0						
		19.0	11342.4	.930	.0051	.006	20.08
		19.8	11342.4	1.062	.0076	.007	20.87
		20.8	11342.4	1.328	.0089	.007	21.92
		21.8	11342.4	1.593	.0114	.008	23.06
		23.4	11342.4	1.859	.0127	.007	25.08
		24.9	11342.4	2.257	.0191	.009	27.26
		26.9	11342.4	2.921	.0635	.013	30.75
SPECIMEN	4F2	17.3	9785.6	.014	.0001	.005	16.04
GEOMETRY	CT						
TEST TEMP	565 C	18.5	9785.6	.019	.0001	.005	16.93
B (MM)	25.4						
BN (MM)	13.1	19.0	9785.6	.038	.0001	.003	17.33
TEST TIME(H)	420.0						
		20.0	9785.6	.044	.0002	.005	18.18
		21.6	9785.6	.066	.0003	.004	19.69
		22.6	9785.6	.125	.0005	.004	20.74
		24.1	9785.6	.186	.0009	.005	22.48
		27.2	9785.6	.292	.0025	.009	27.04

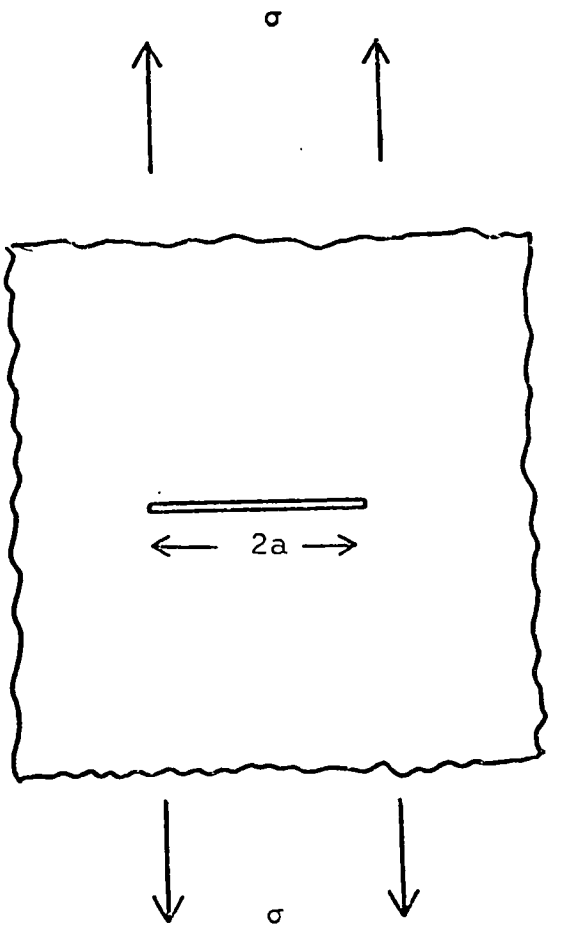

Figure (1): Infinite plate of crack length 2a subjected to a remote stress σ

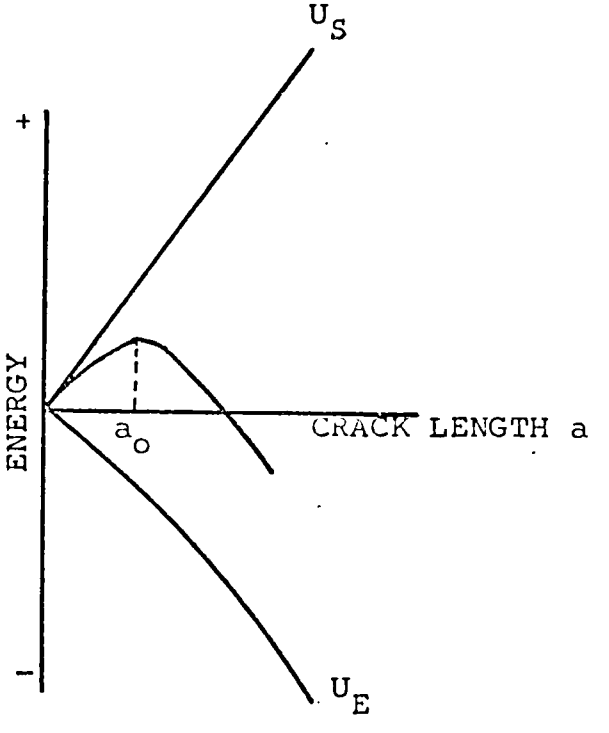

Figure (2): Variation of Energy with crack length where a_o is the critical Griffith crack length

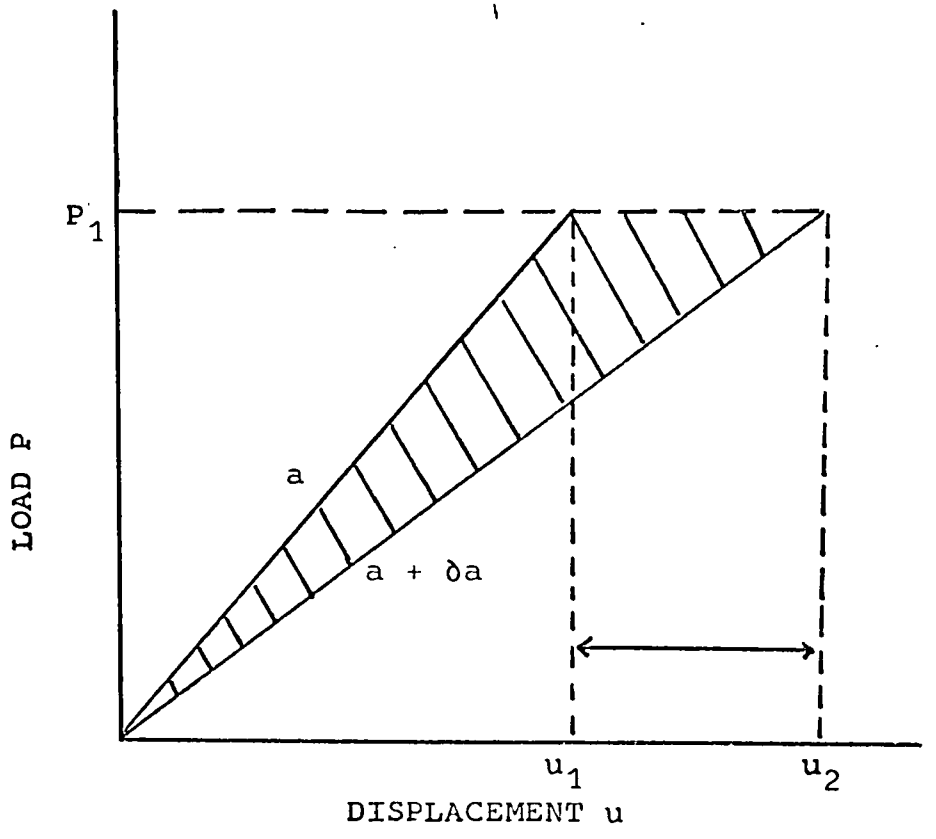

Figure (3): Elastic loading at constant load for a crack length of a and a + δa

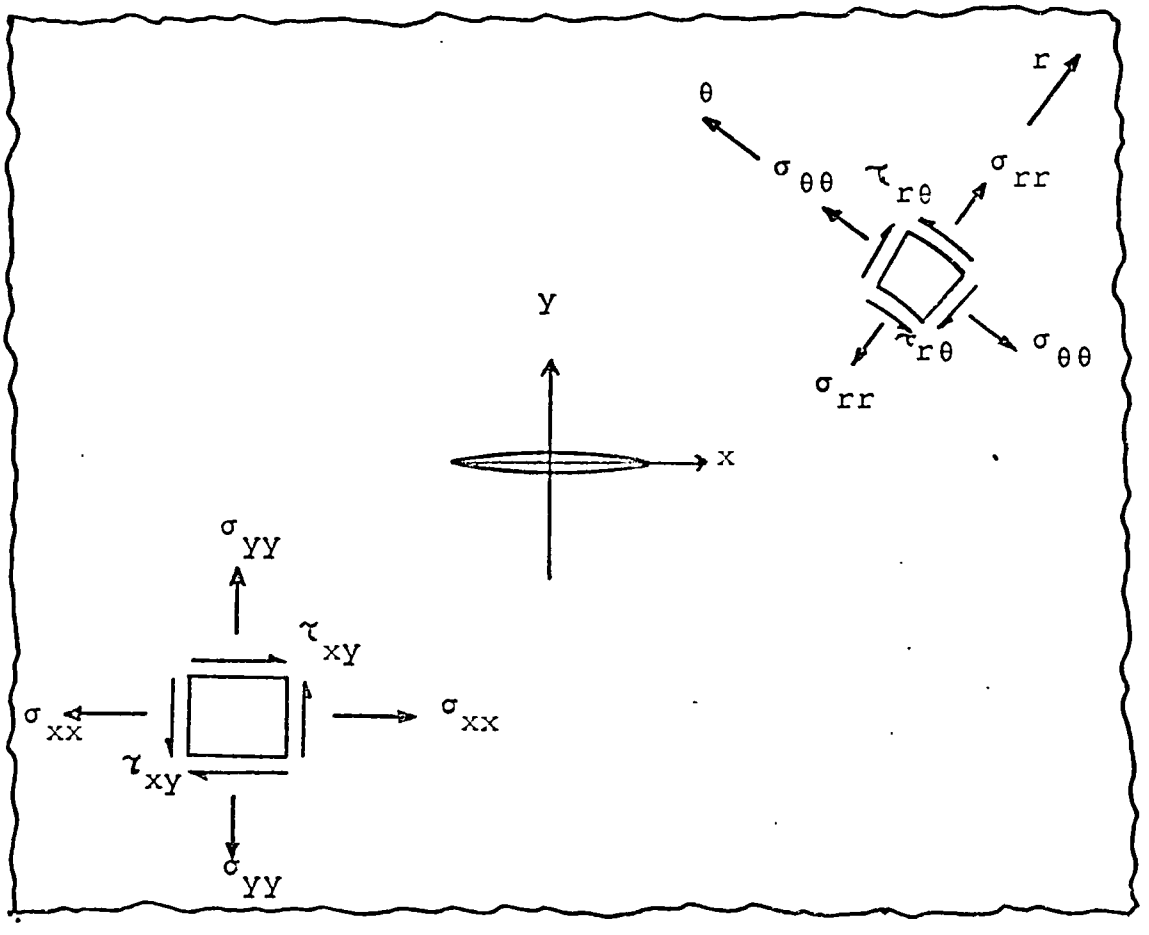

Figure (4): Coordinate system of a cracked body.

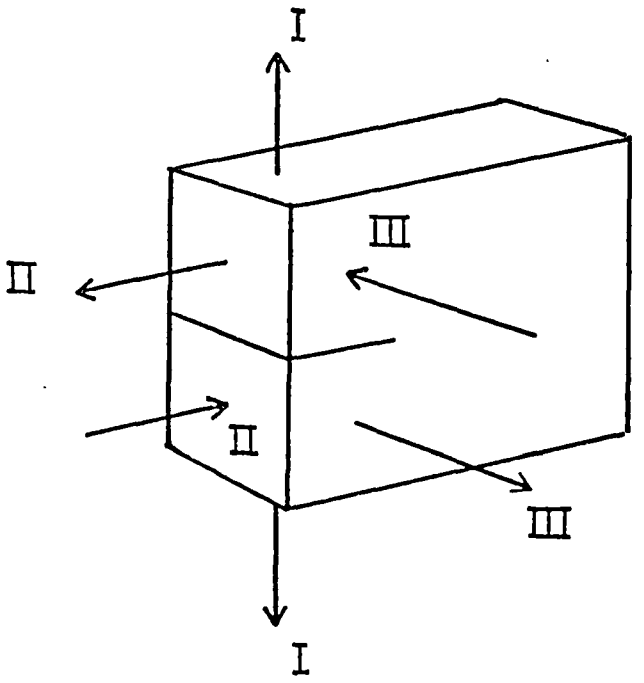

Figure (5): The different modes of cracking

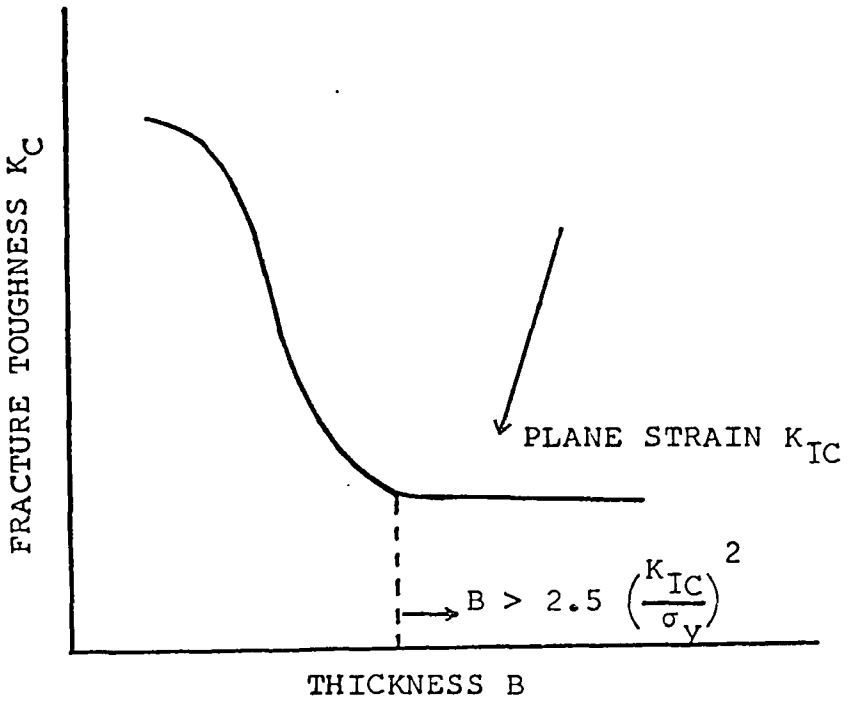

Figure (6): Variation of fracture toughness with thickness. Minimum value is plane strain fracture toughness K_{IC}

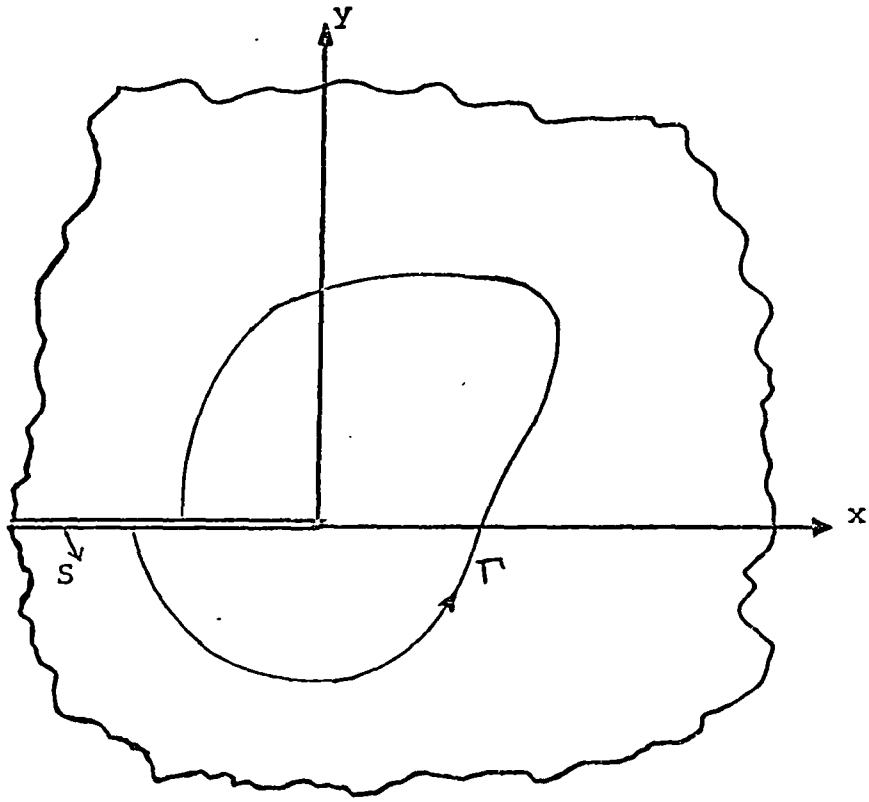

Figure (7): Arbitary Contour over which J integral may be evaluated

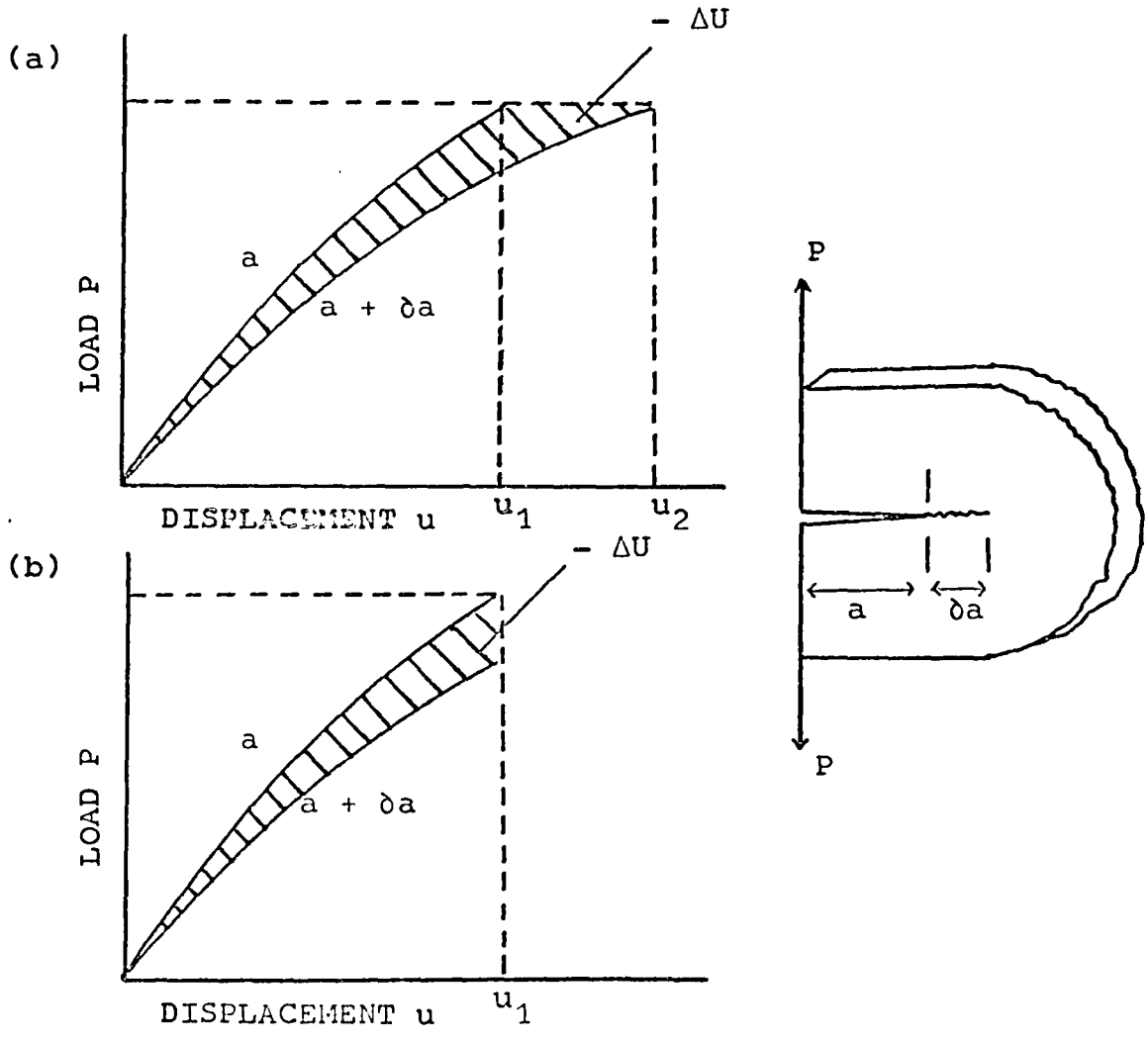

Figure (8): Generalized load deflection diagrams (a) for constant load (b) for constant displacement

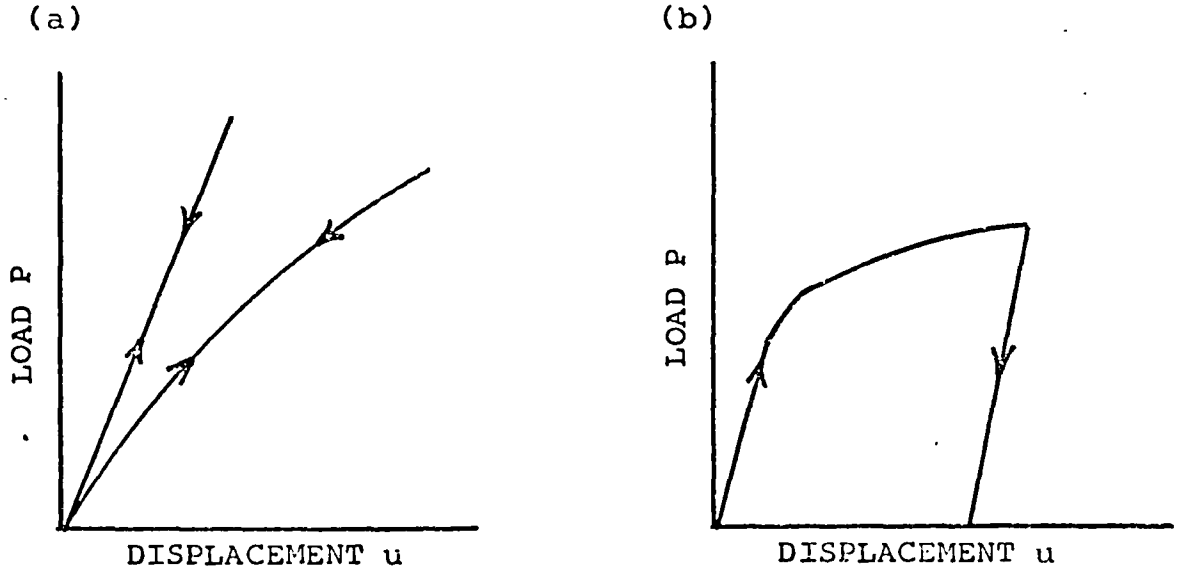

Figure (9): Loading and unloading of (a) a linear and non-linear elastic material (b) an elastic-plastic material

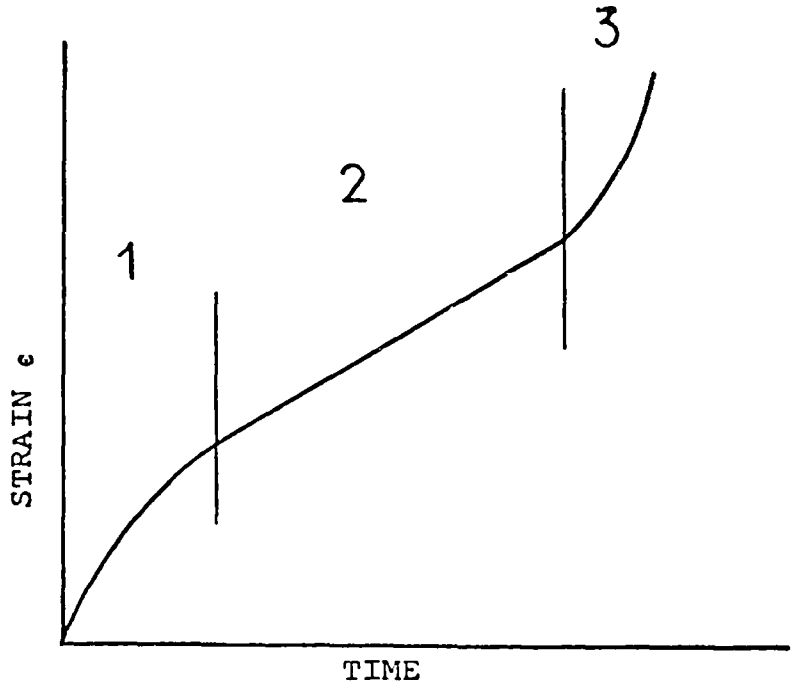

Figure (10): An Idealized Uniaxial Creep curve showing the Primary (1), Secondary (2) and Tertiary (3), stages of Creep

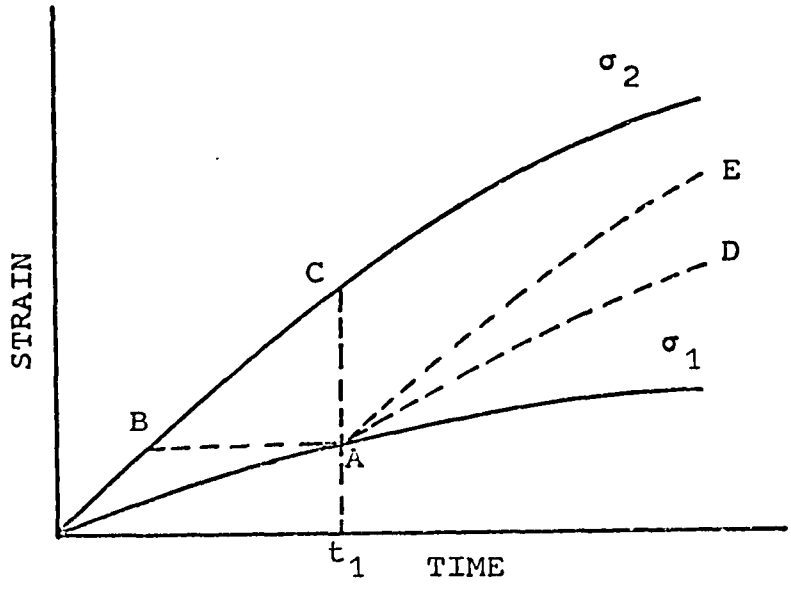

Figure (11): Comparison of predictions of Time-Hardening and Strain-Hardening theory

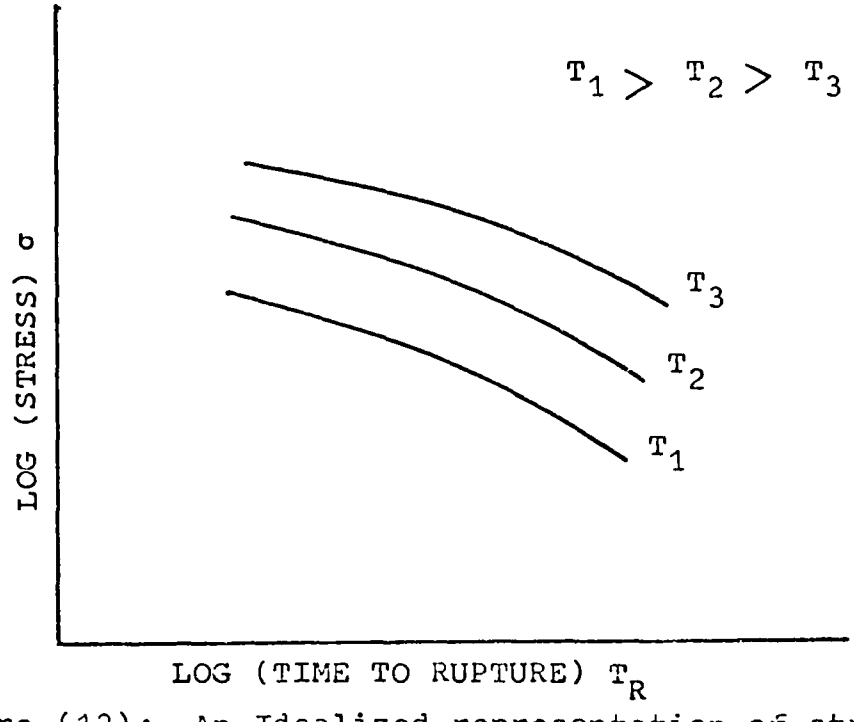

Figure (12): An Idealized representation of stress versus time to rupture for uniaxial creep specimens at three different temperatures

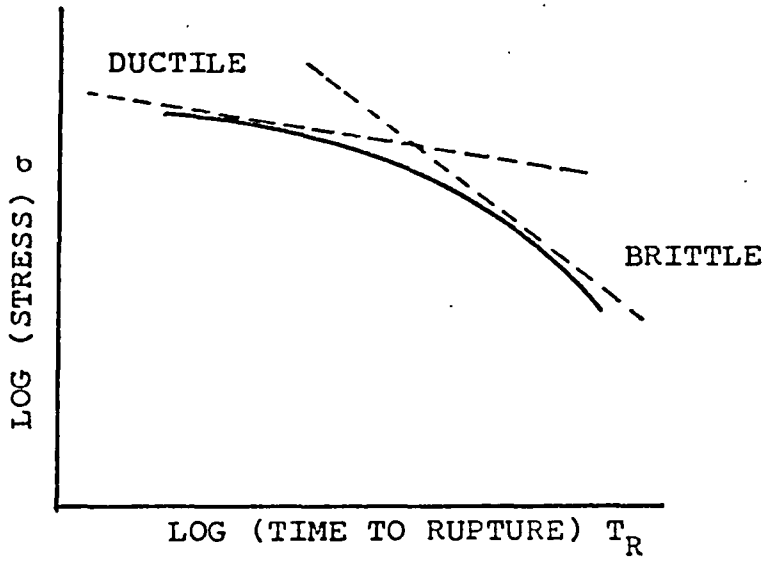

Figure (13): An Idealized representation of a ductile-brittle transition of the creep fracture mode

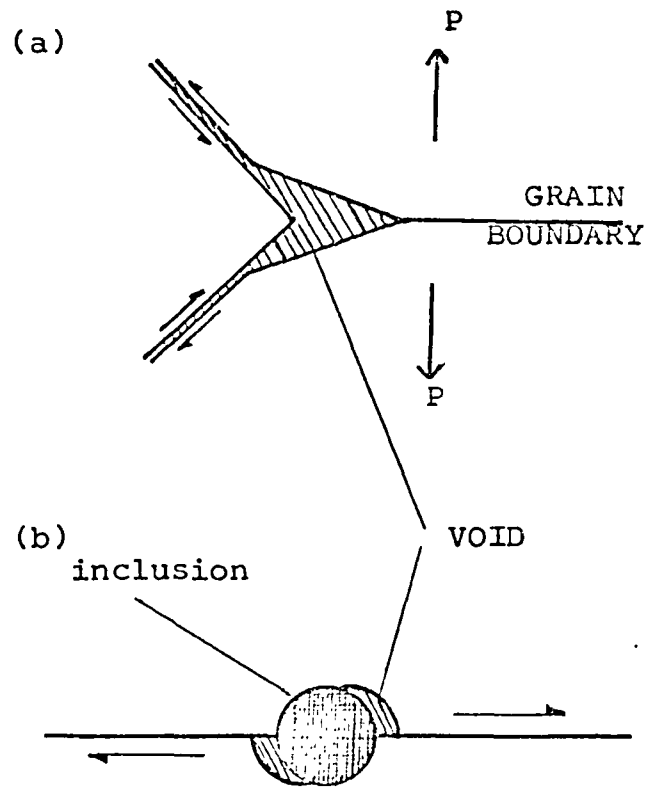

Figure (14): Nucleation of (a) a wedge-type crack at a grain corner by grain boundary sliding and (b) a crack near an inclusion

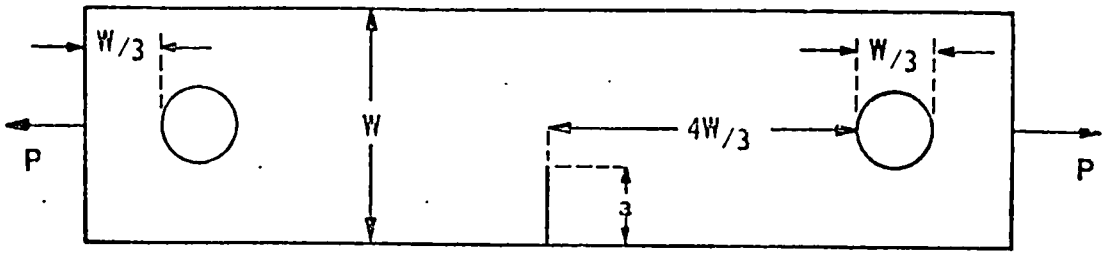

1. SEN-T

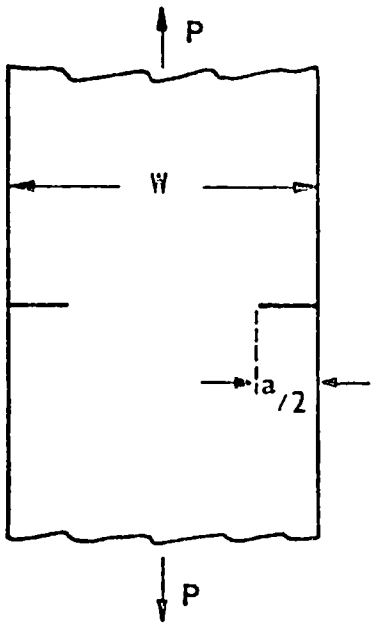

2. DEN-T

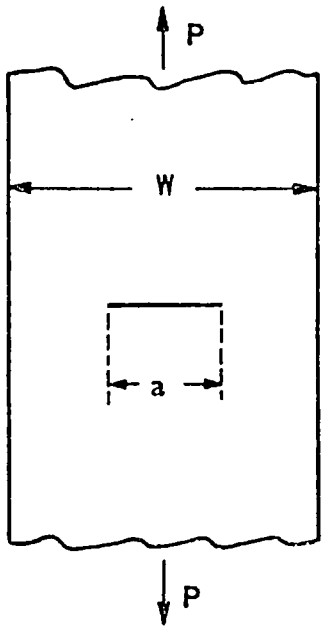

3. CCP

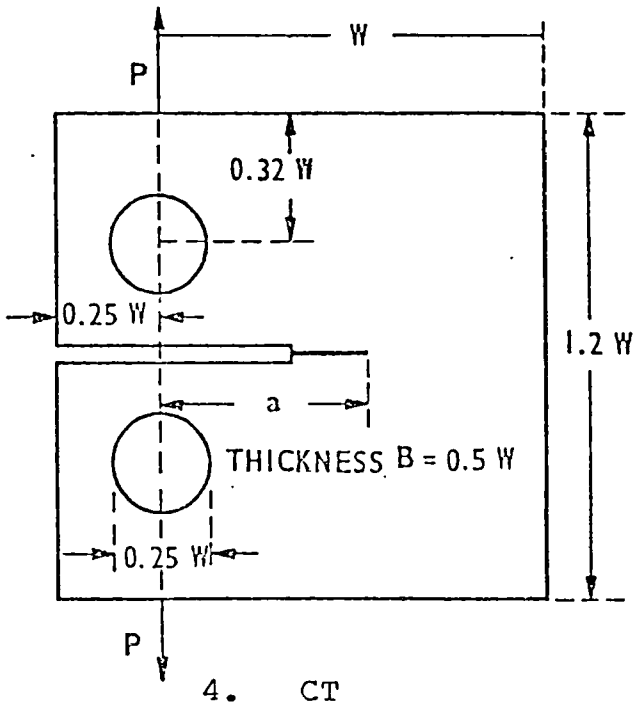

4. CT

Figure (15): Dimensions of various specimen geometries used in creep crack growth studies

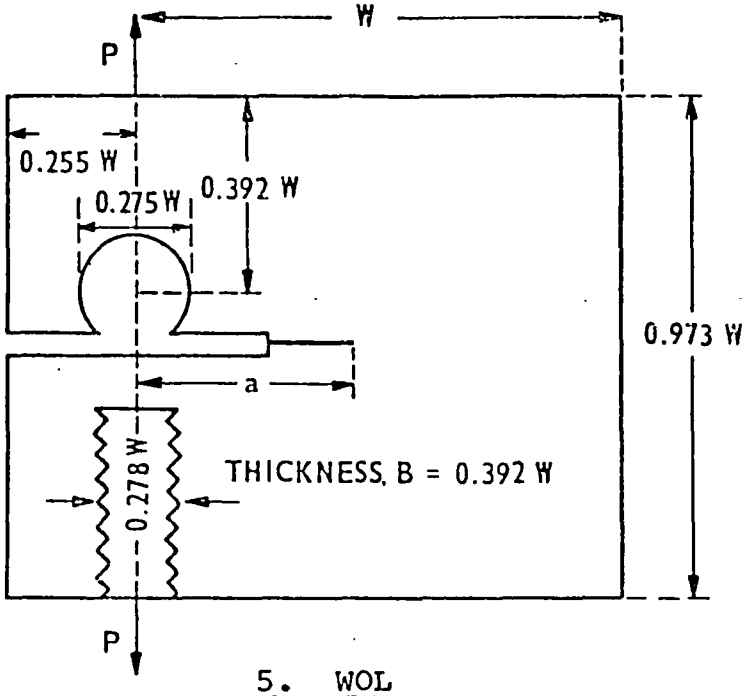

5. WOL

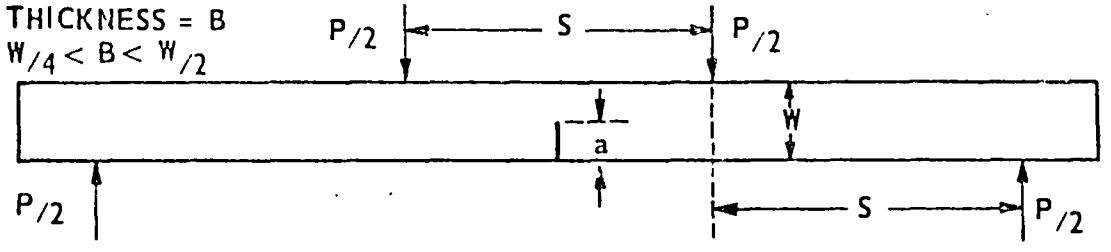

6. SEN-T (4-Point Bend)

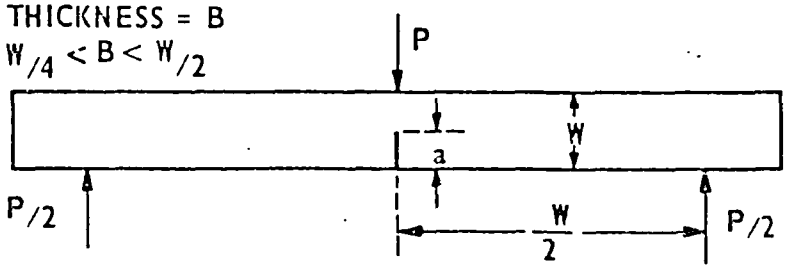

6. SEN-T (Three point Bend)

Figure (15): Continued

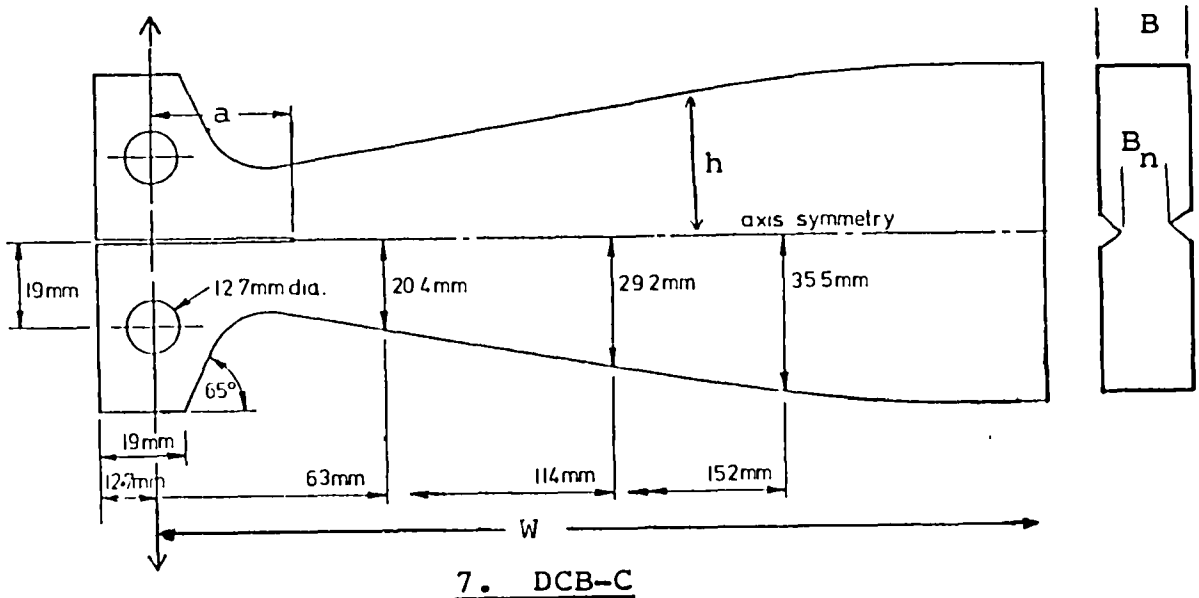

7. DCB-C

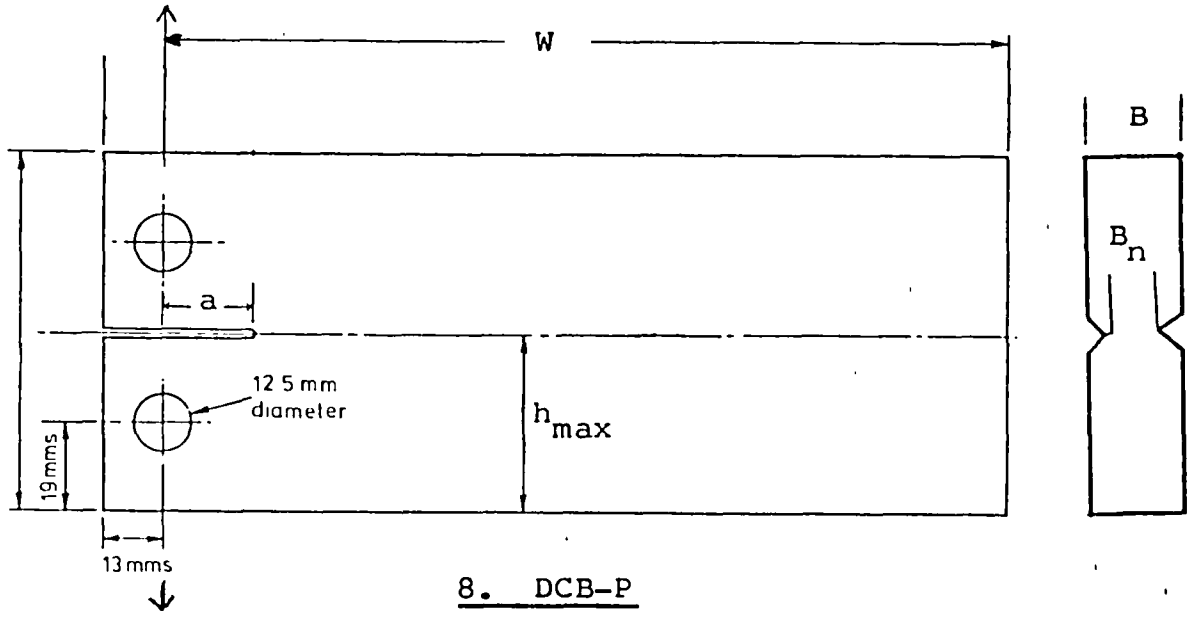

8. DCB-P

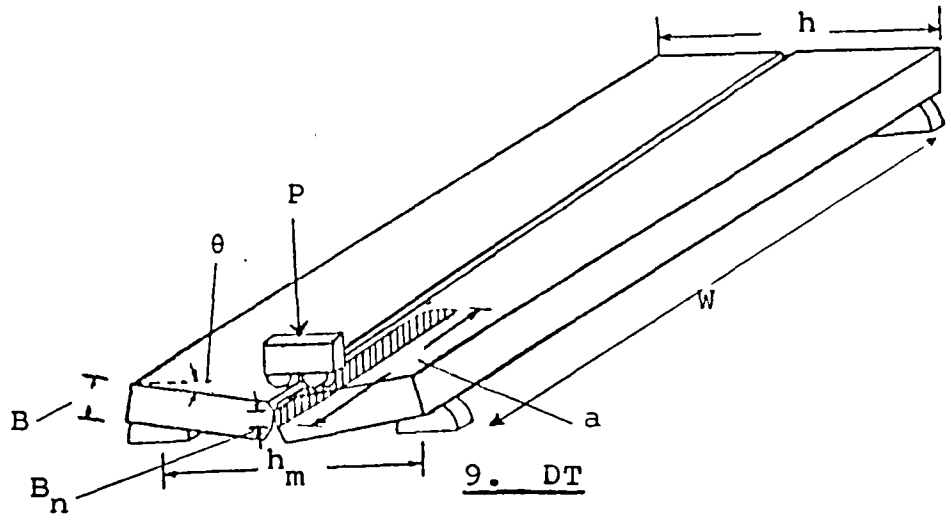

9. DT

Figure (15): Continued

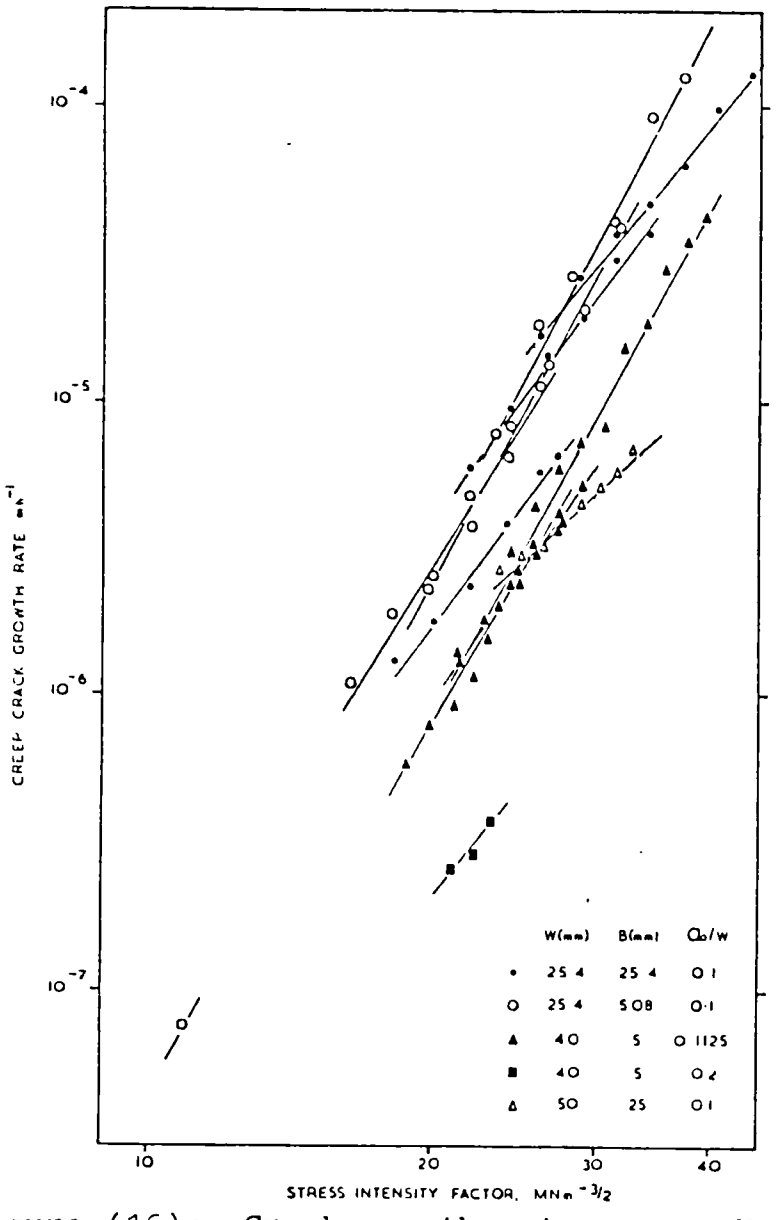

Figure (16): Crack growth rate versus K for $\frac{1}{2}$ Cr - $\frac{1}{2}$ Mo - $\frac{1}{4}$ V normalized and tempered (From Neate (91))

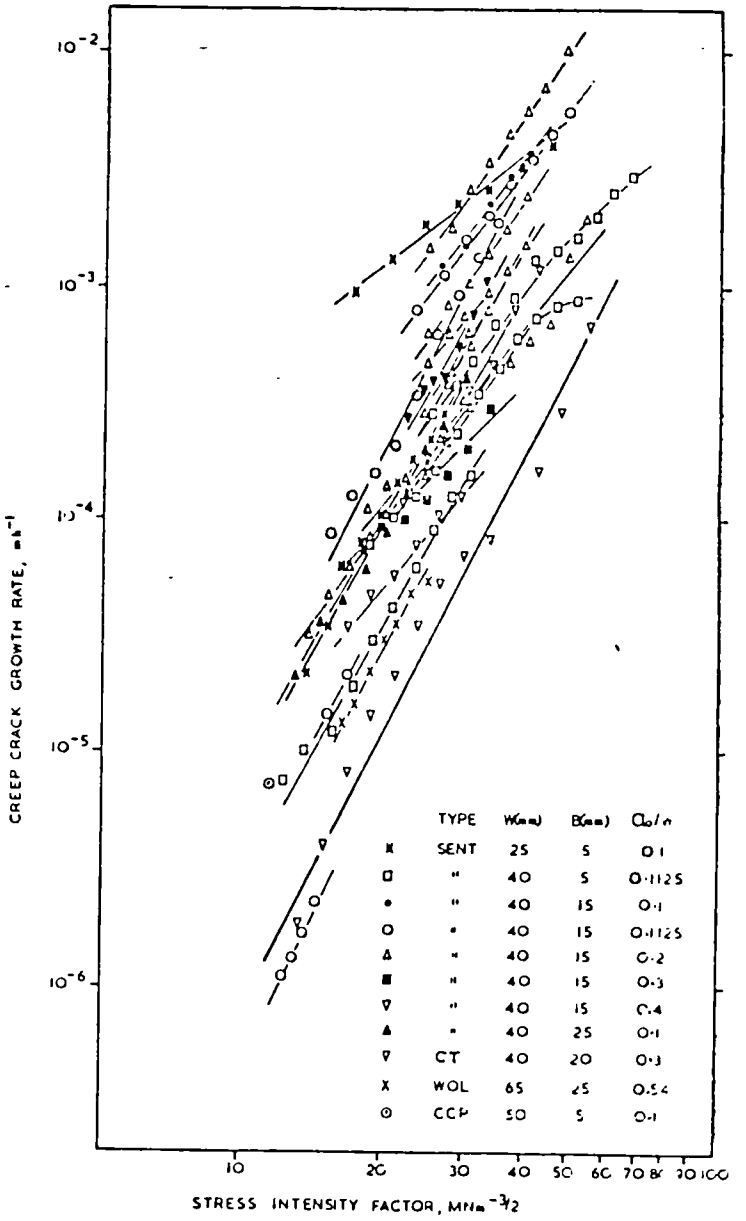

Figure (17): Crack growth rate versus K for $\frac{1}{2}$ Cr- $\frac{1}{2}$ Mo - $\frac{1}{4}$ V Quenched steel (From Neate (91))

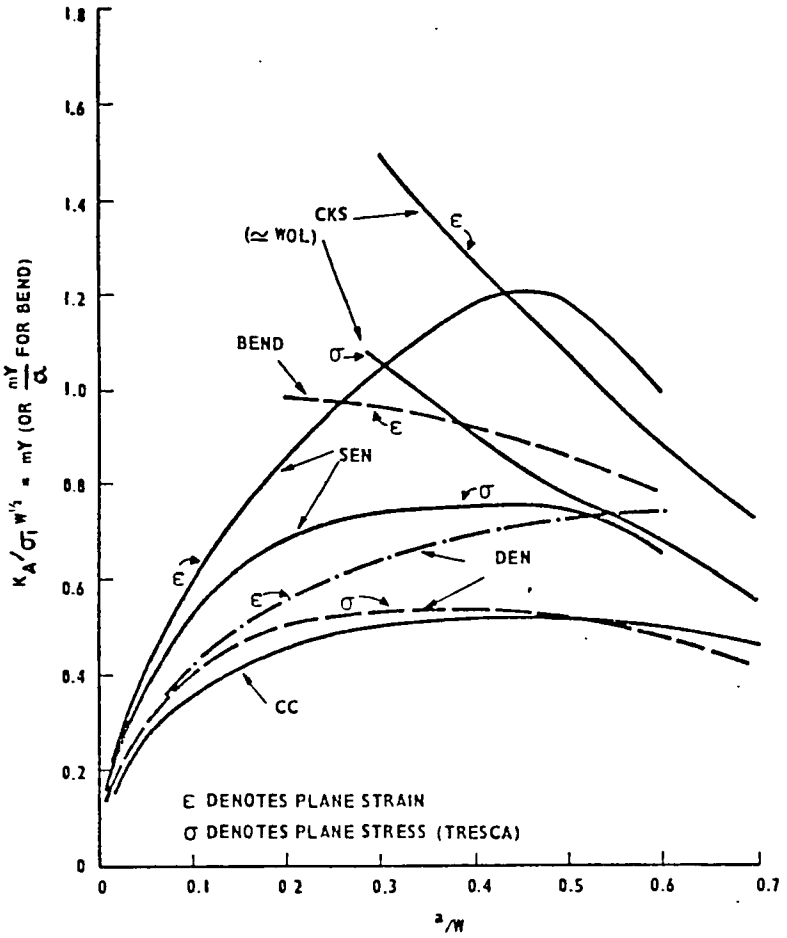

Figure (18): Notional stress intensities at general yield (from Haigh and Richards (124))

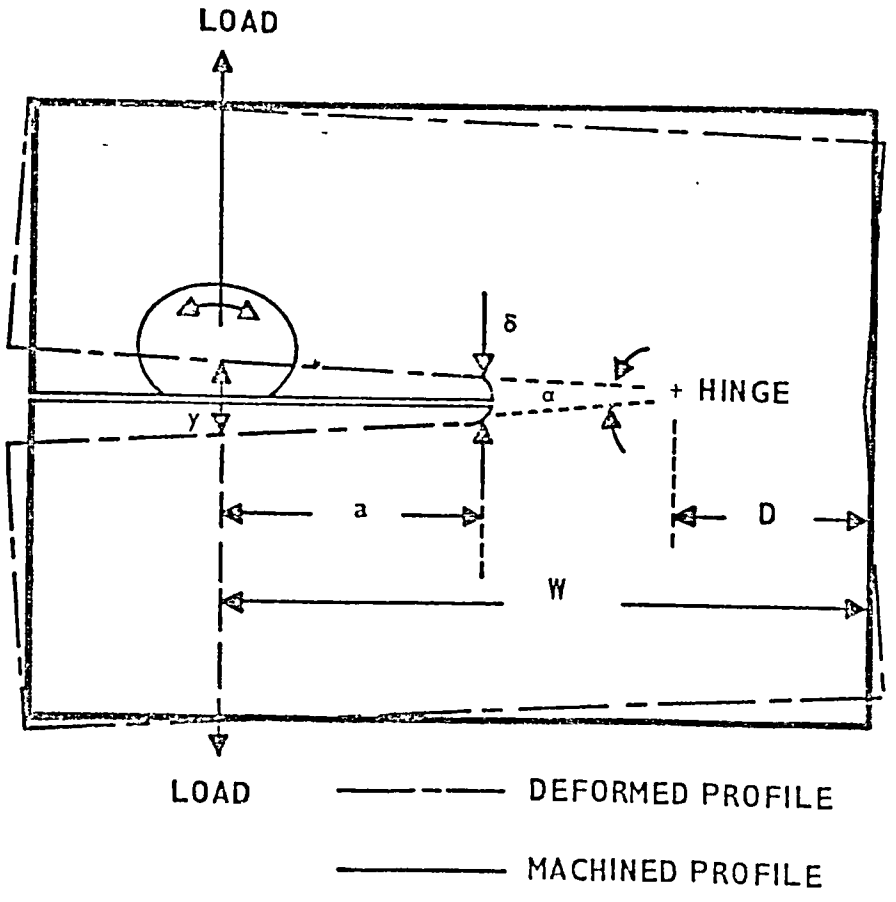

Figure (19): Plastic Hinge Points in WOL Specimens (from Haigh and Richards (124))

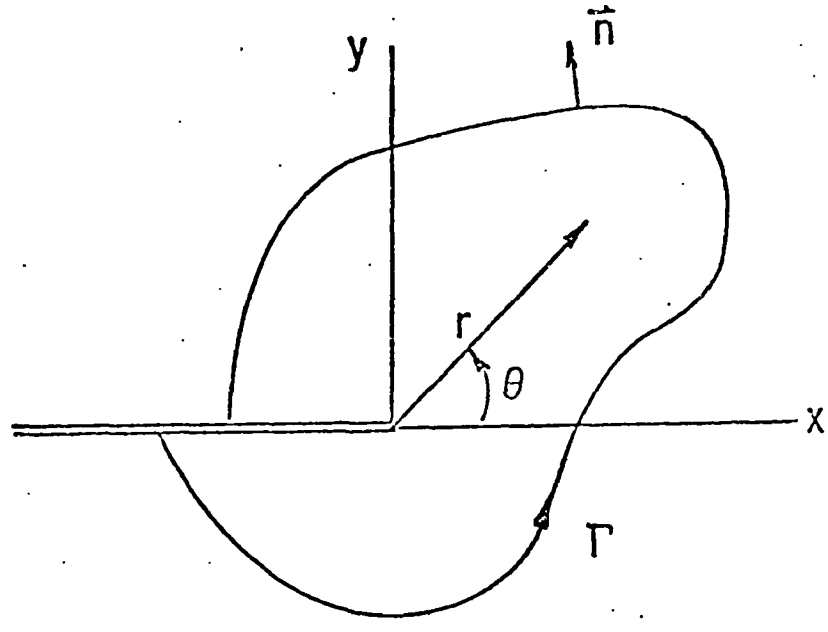

Figure (20): Crack tip coordinate system and arbitary line integral contour

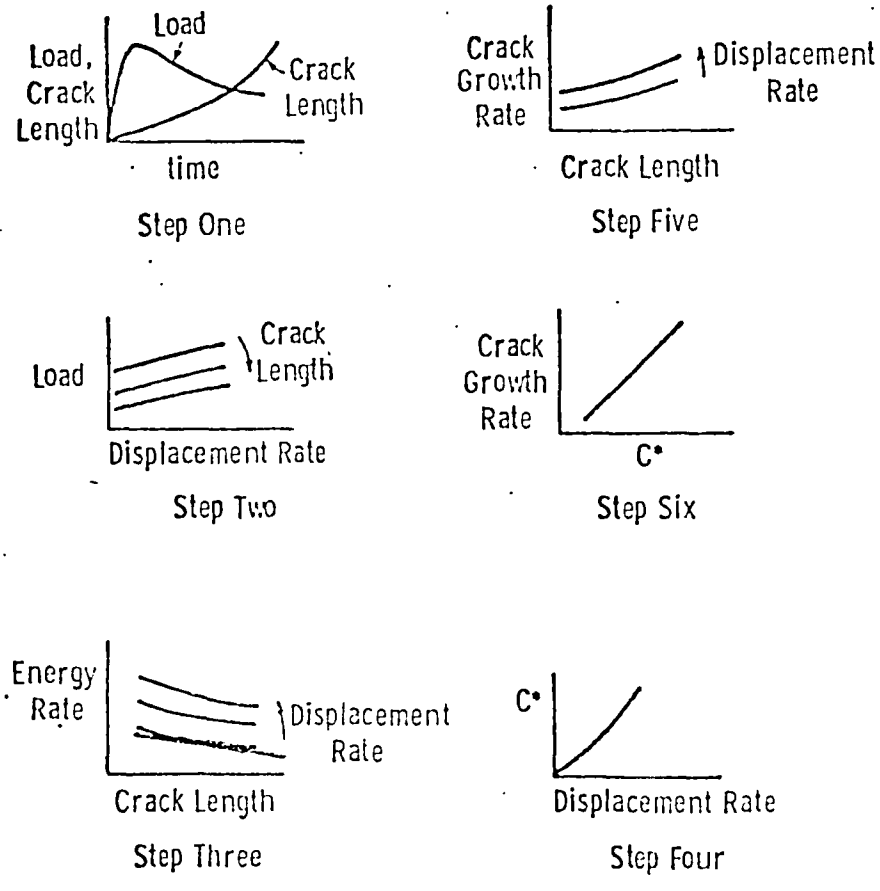

Figure (21): Schematic illustration of the six steps involved in C* data reduction (from Landes and Begley (89

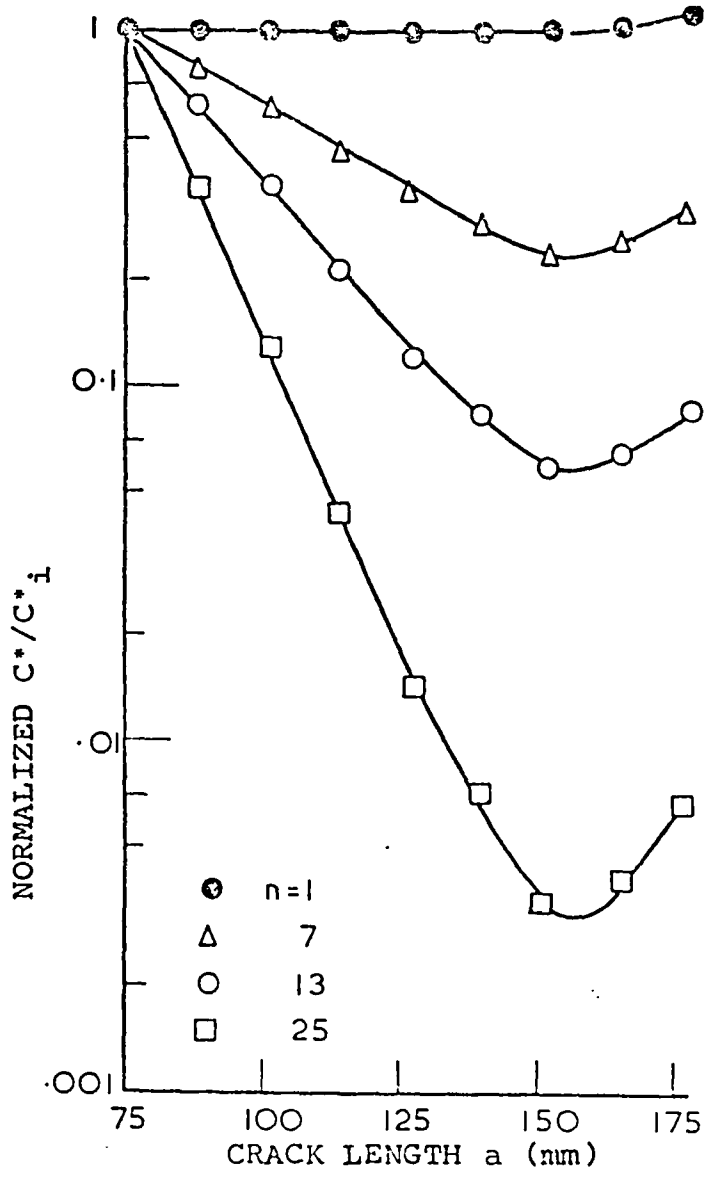

Figure (22): Variation of the analytical C* with crack length and creep index n for the DCB-C test-piece

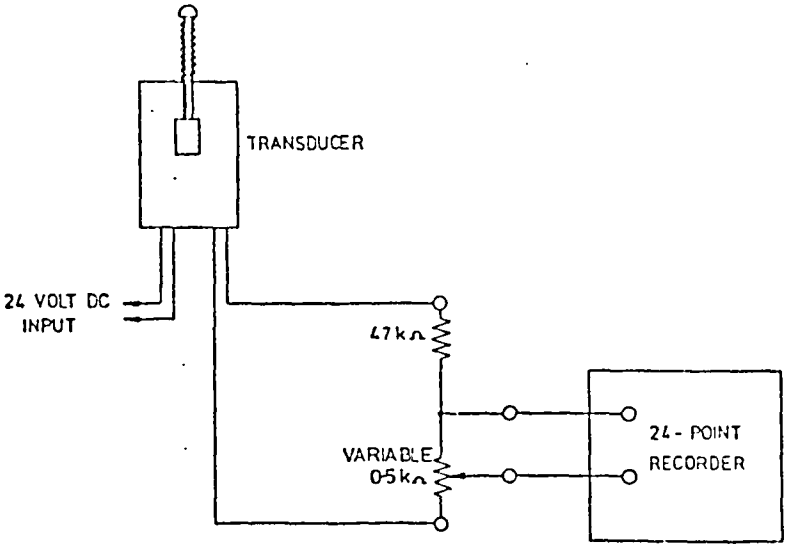

Figure (23): Strain measuring circuit for creep tests

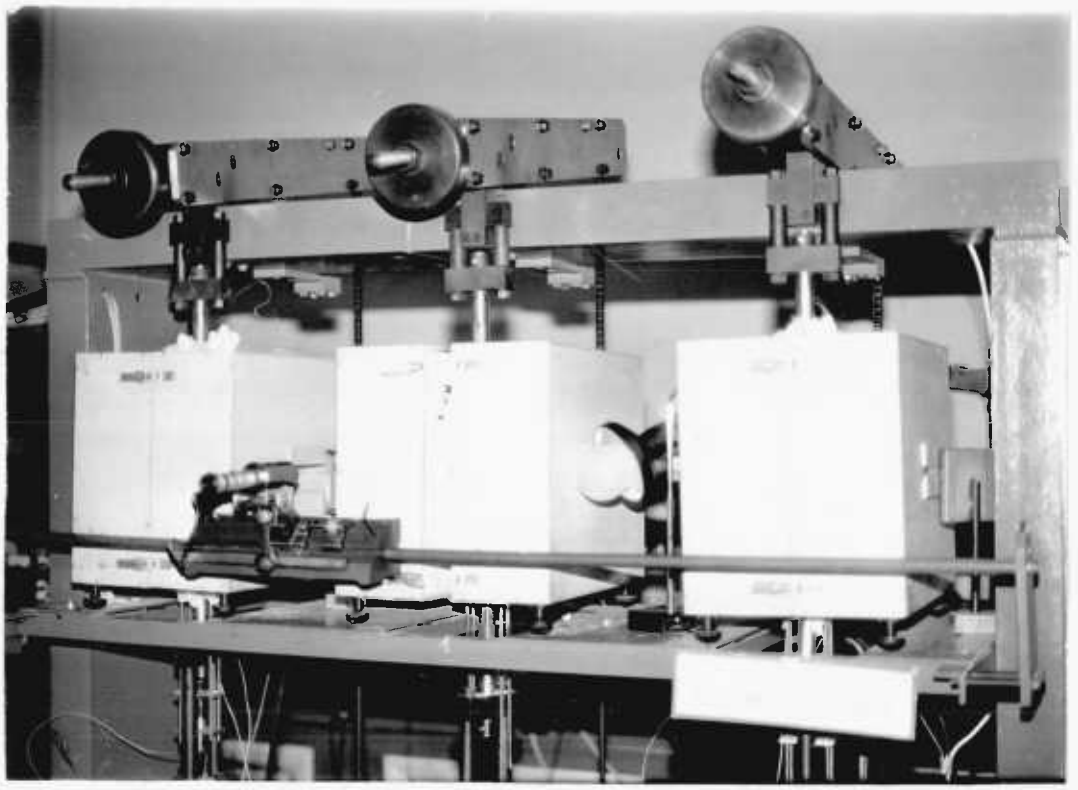

Figure (24): Set of three machines used for creep cracking tests

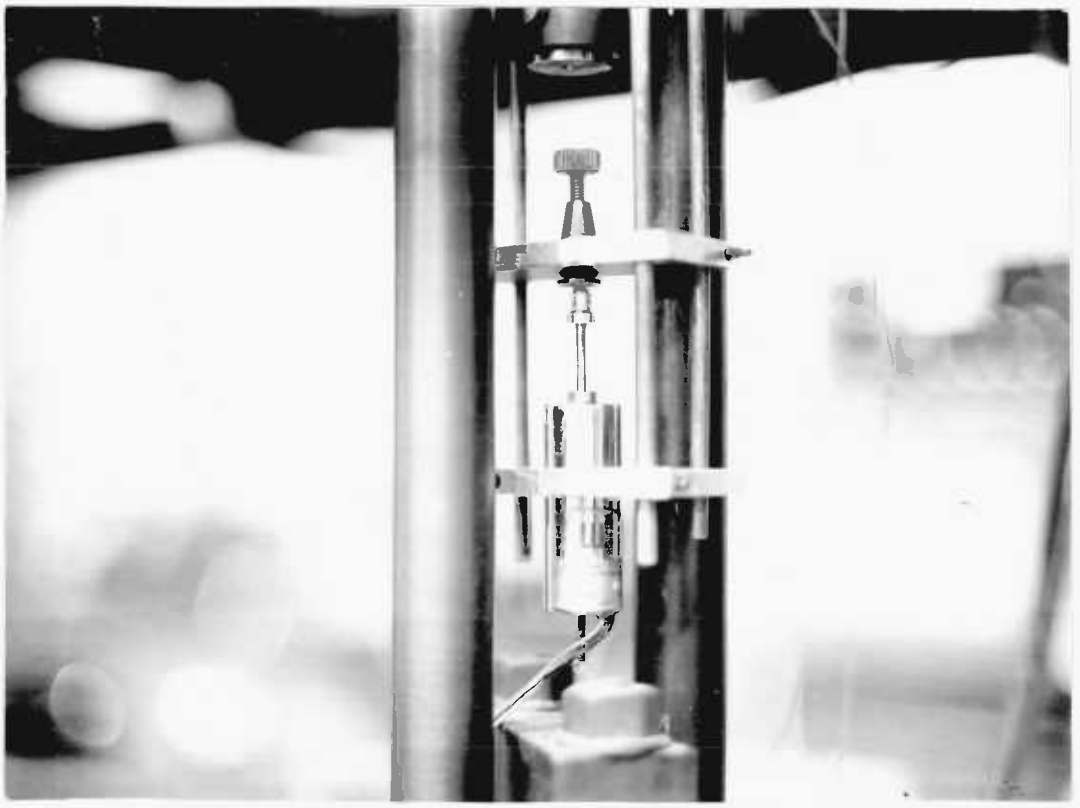

Figure (25): View of the transducer set-up, below the furnace, used to measure the displacement at the loading line of specimens

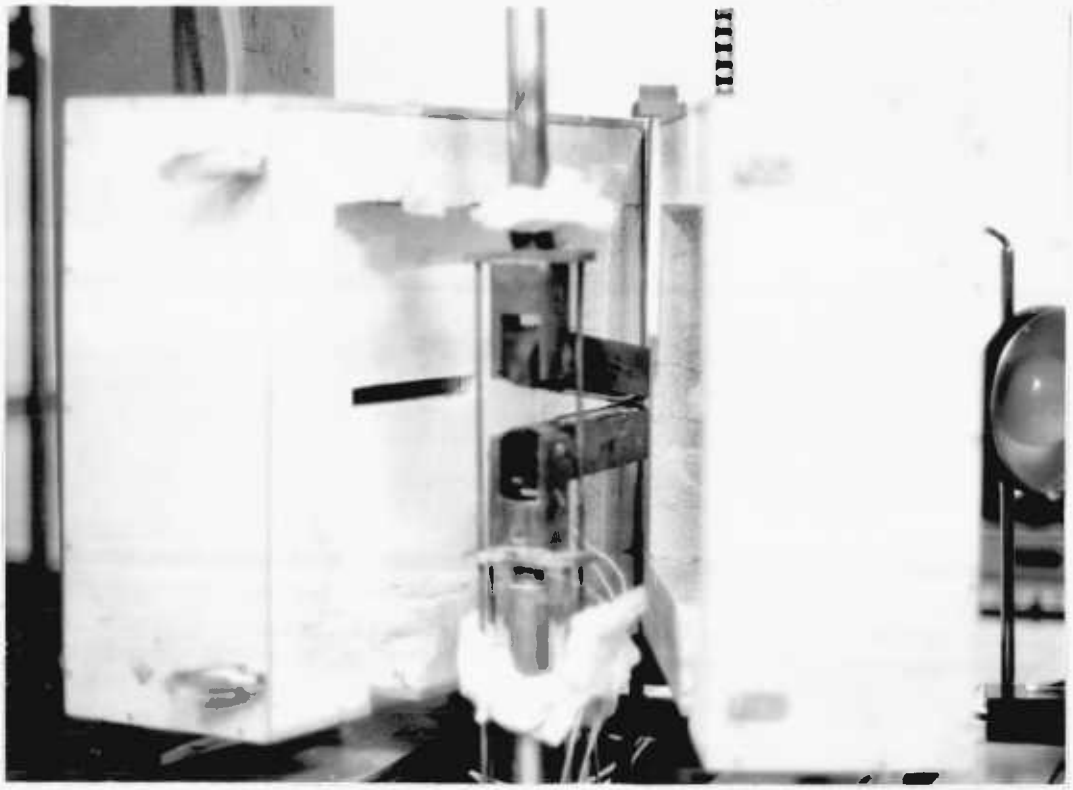

Figure (26): Front view of an open furnace showing a tested DCB-P, steel specimen.

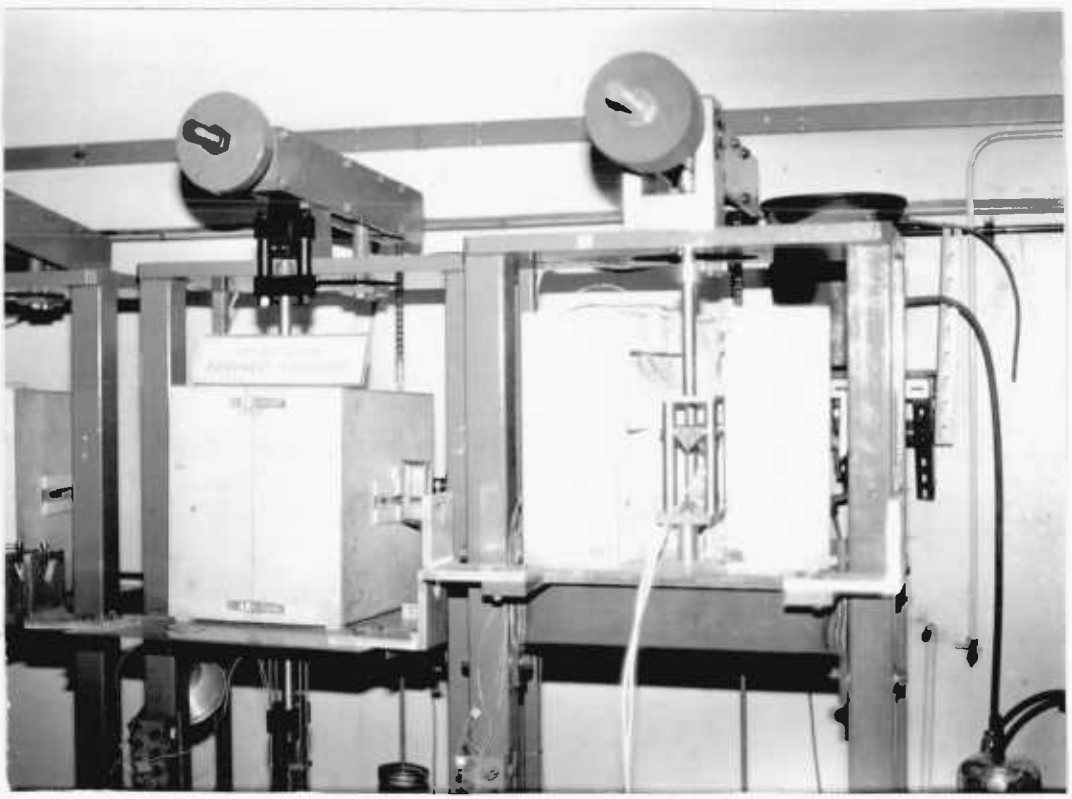

Figure (27): Front view of the machine used to test Double Torsion (DT) test-pieces

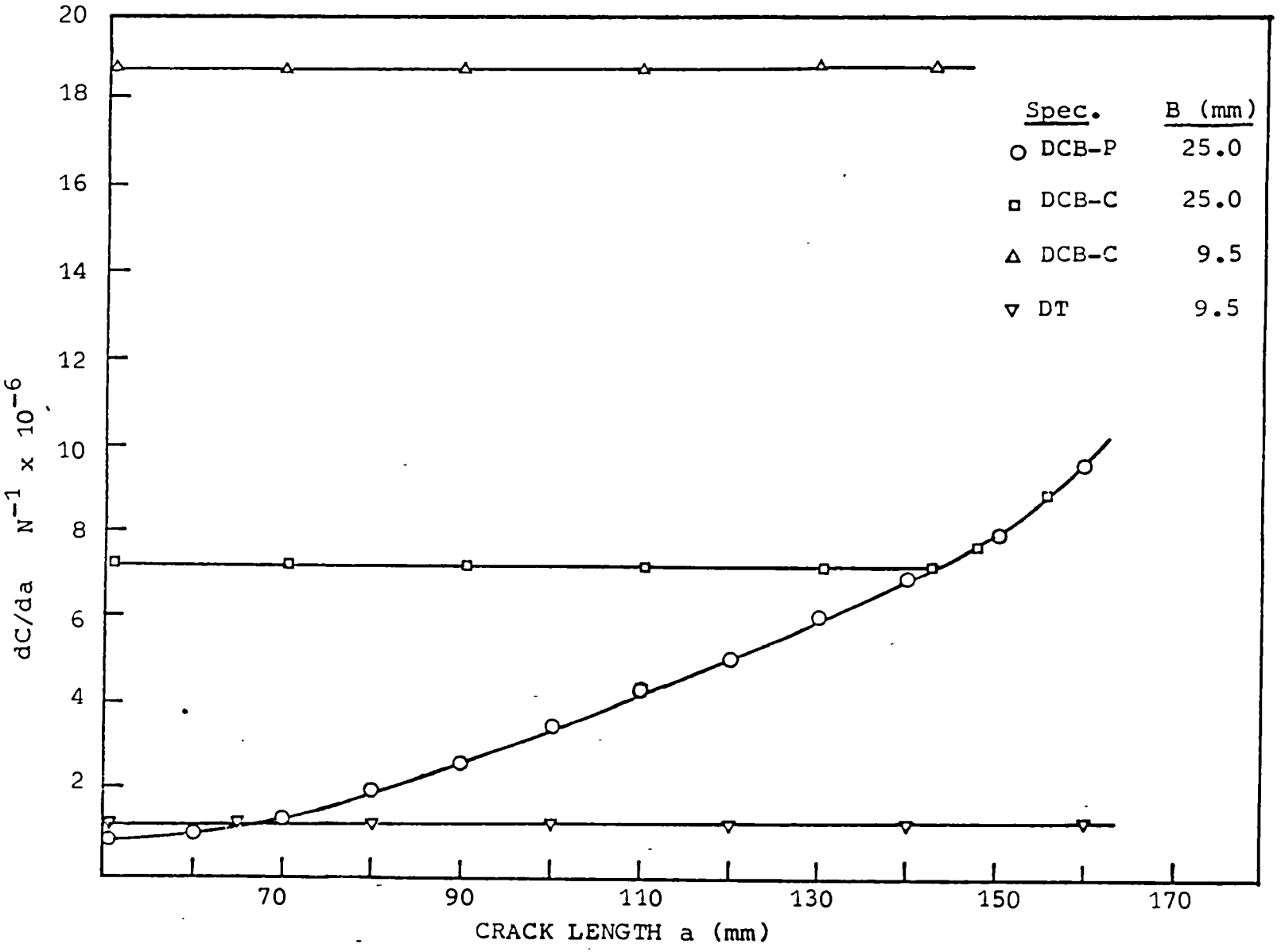

Figure (28): Experimental room temperature dC/da graph versus crack length for various DCB and DT, RR58 specimens

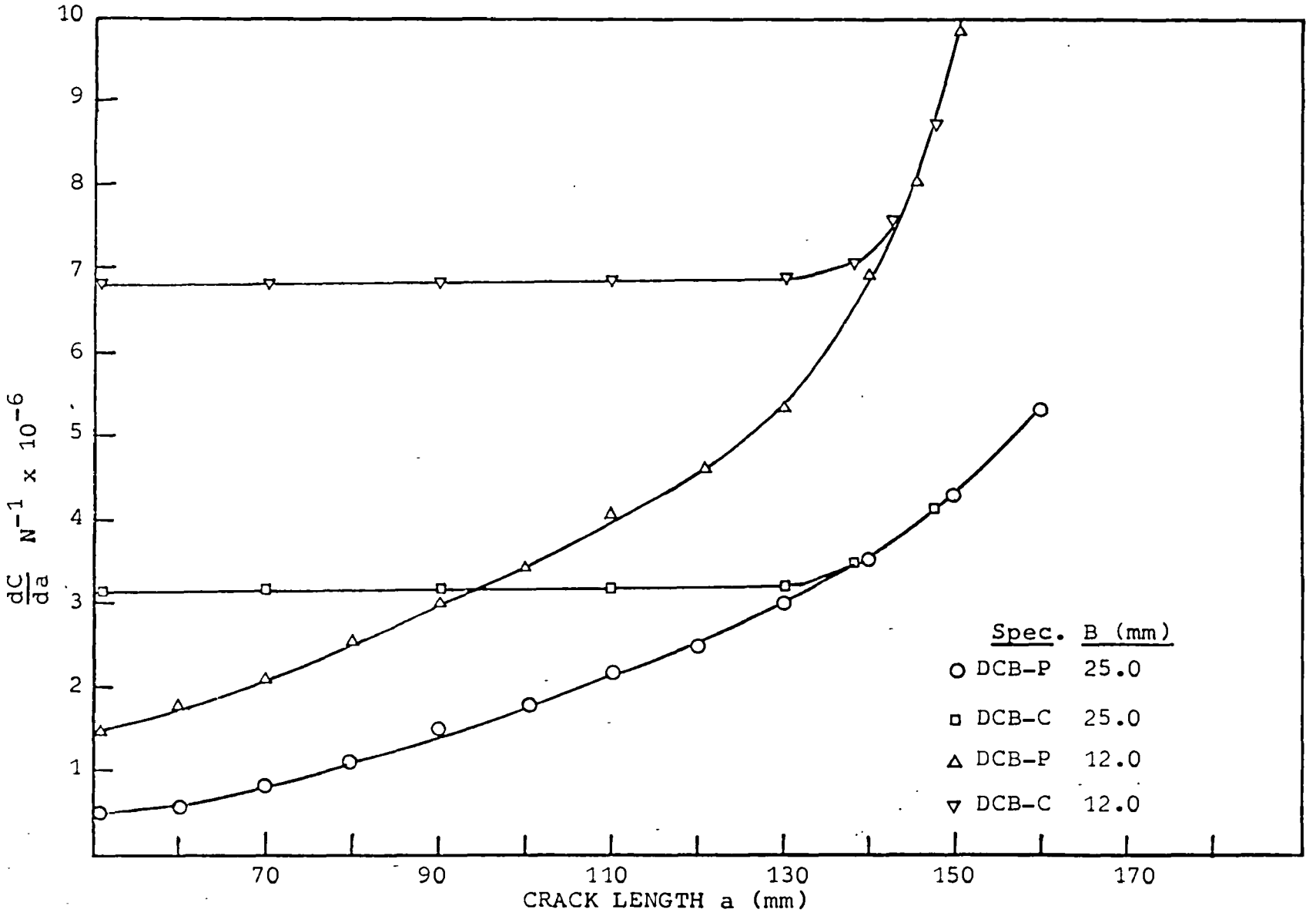

Figure (29): Experimental room temperature dc/da graph versus crack length for various thicknesses of DCB specimens of $\frac{1}{2}$ Cr - $\frac{1}{2}$ Mo - $\frac{1}{4}$ V steel

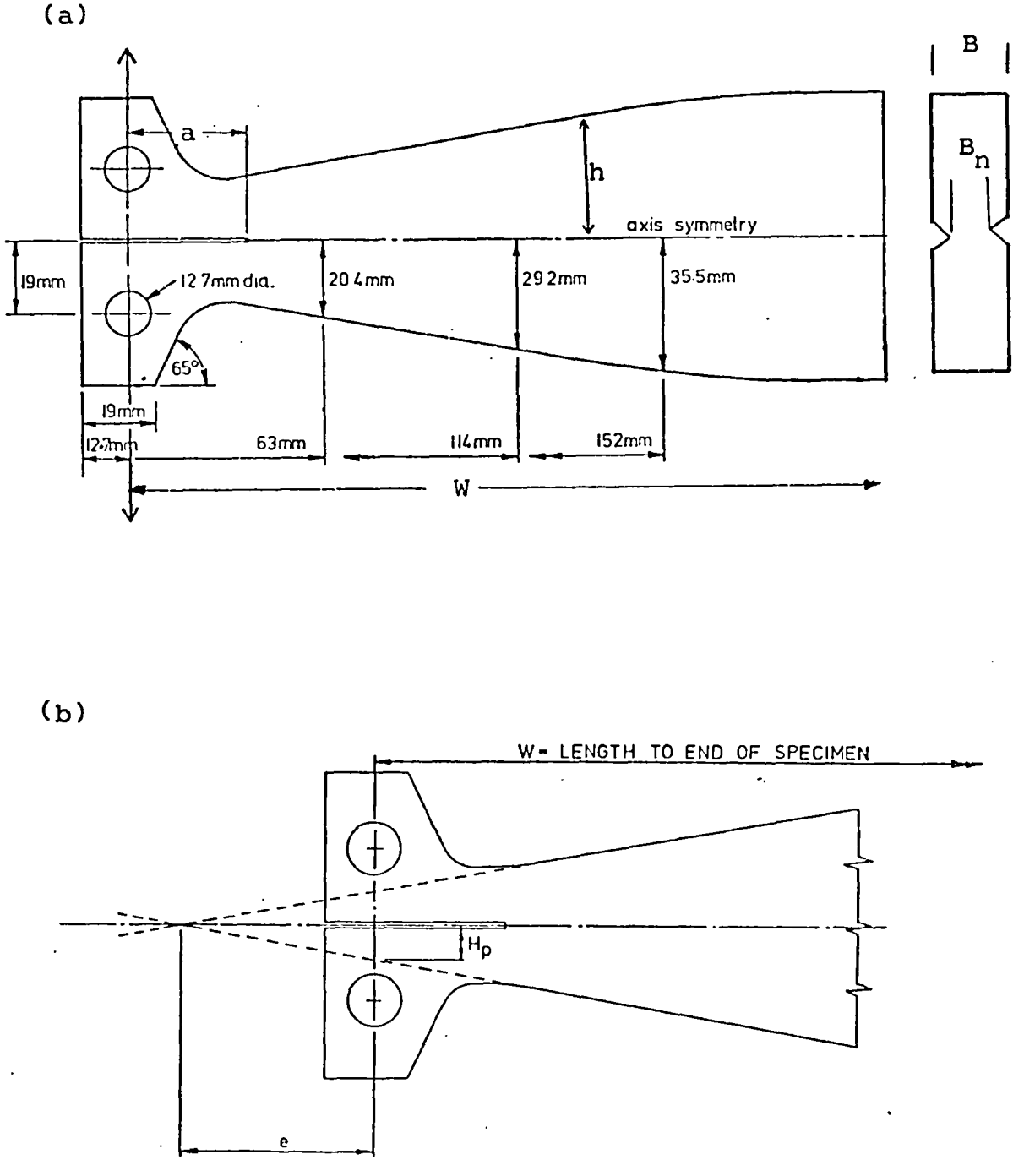

Figure (30): (a) The actual dimensions of the DCB-C test-pieces used.
(b) An explanation of parameters used in the design of the DCB-C specimen

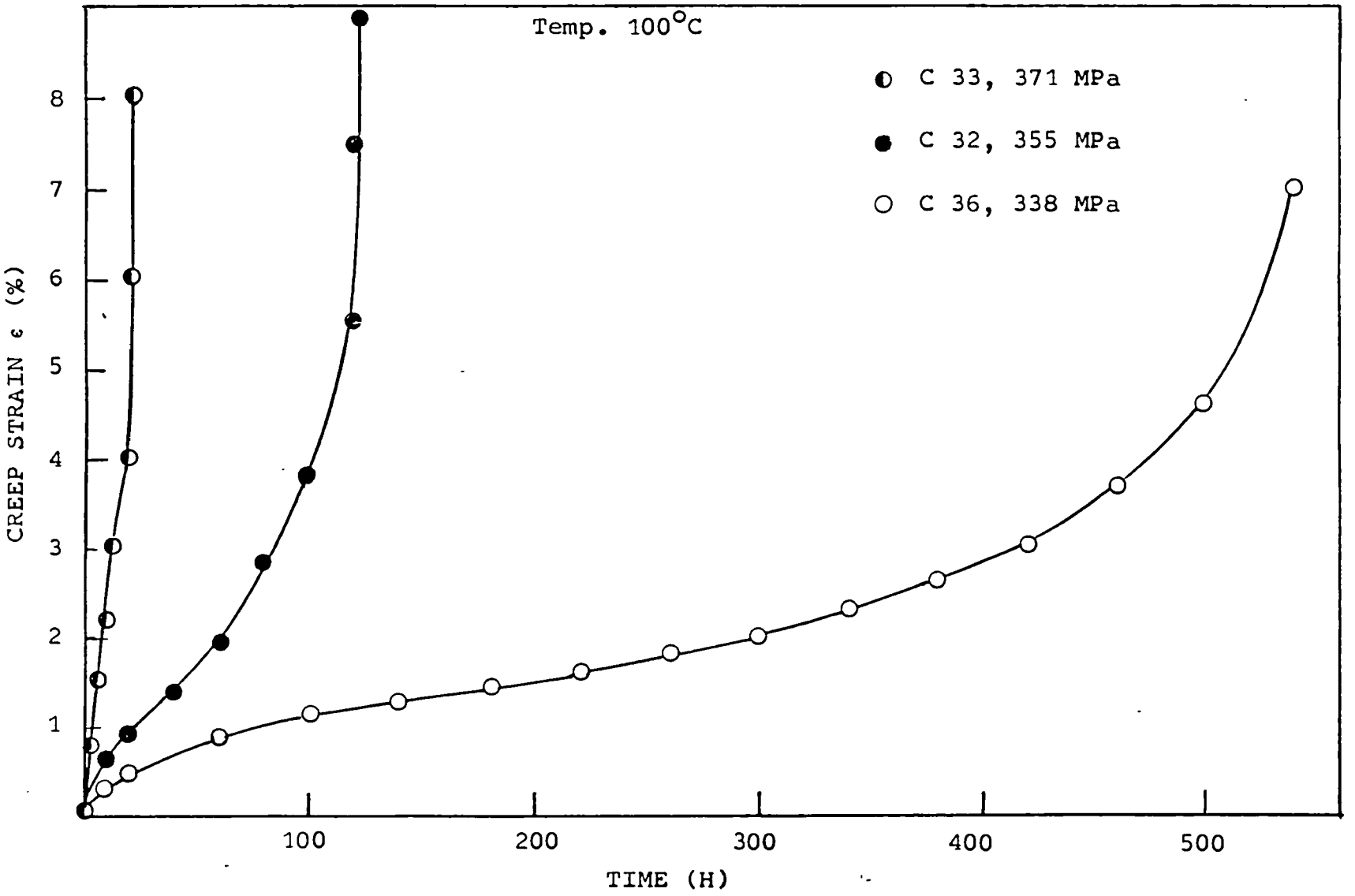

Figure (31): The effect of increase in stress on the uniaxial creep curve of RR58 tested at 100°C.

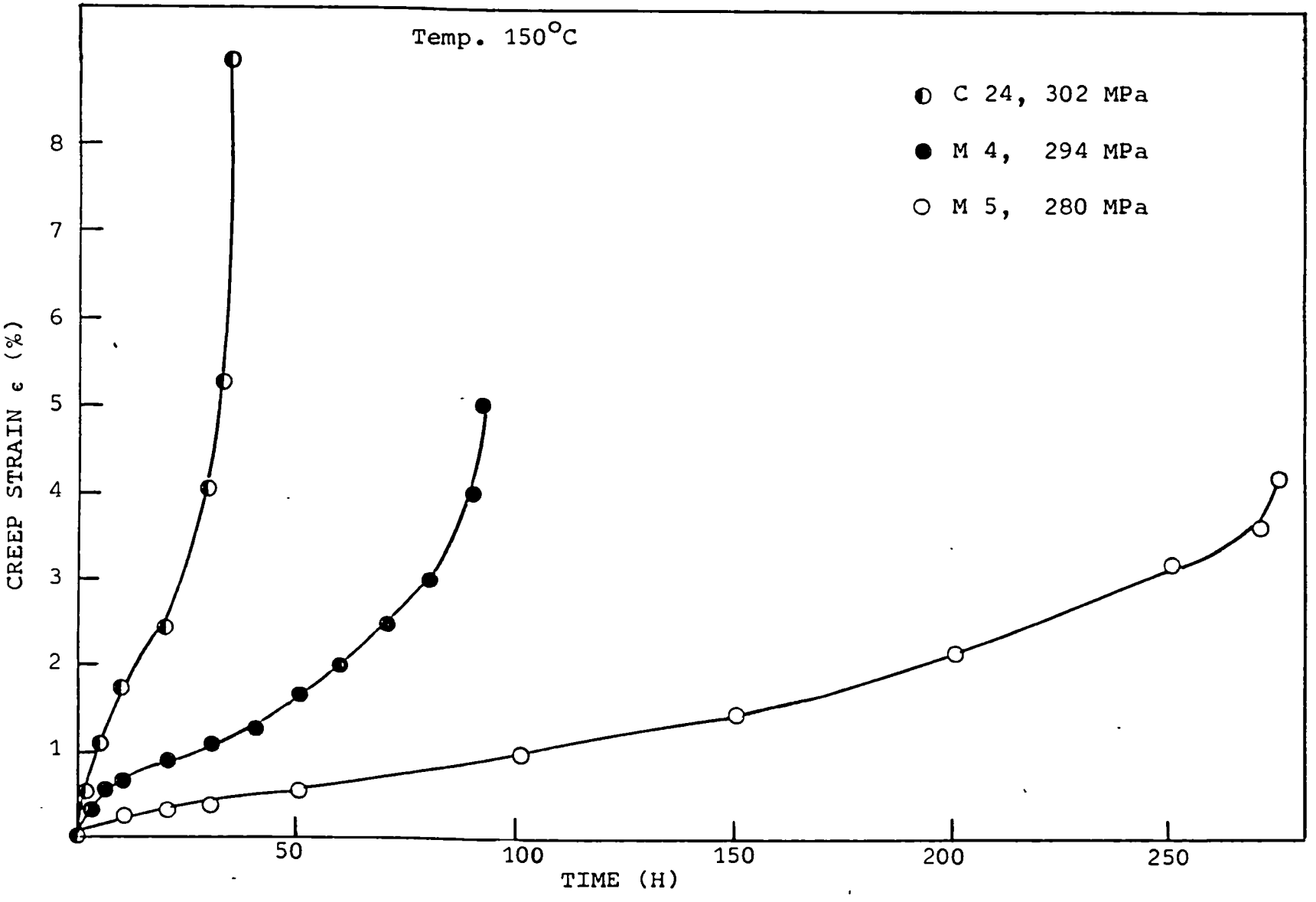

Figure (32): The effect of increase in stress on the uniaxial creep curve of RR58 tested at 150°C.

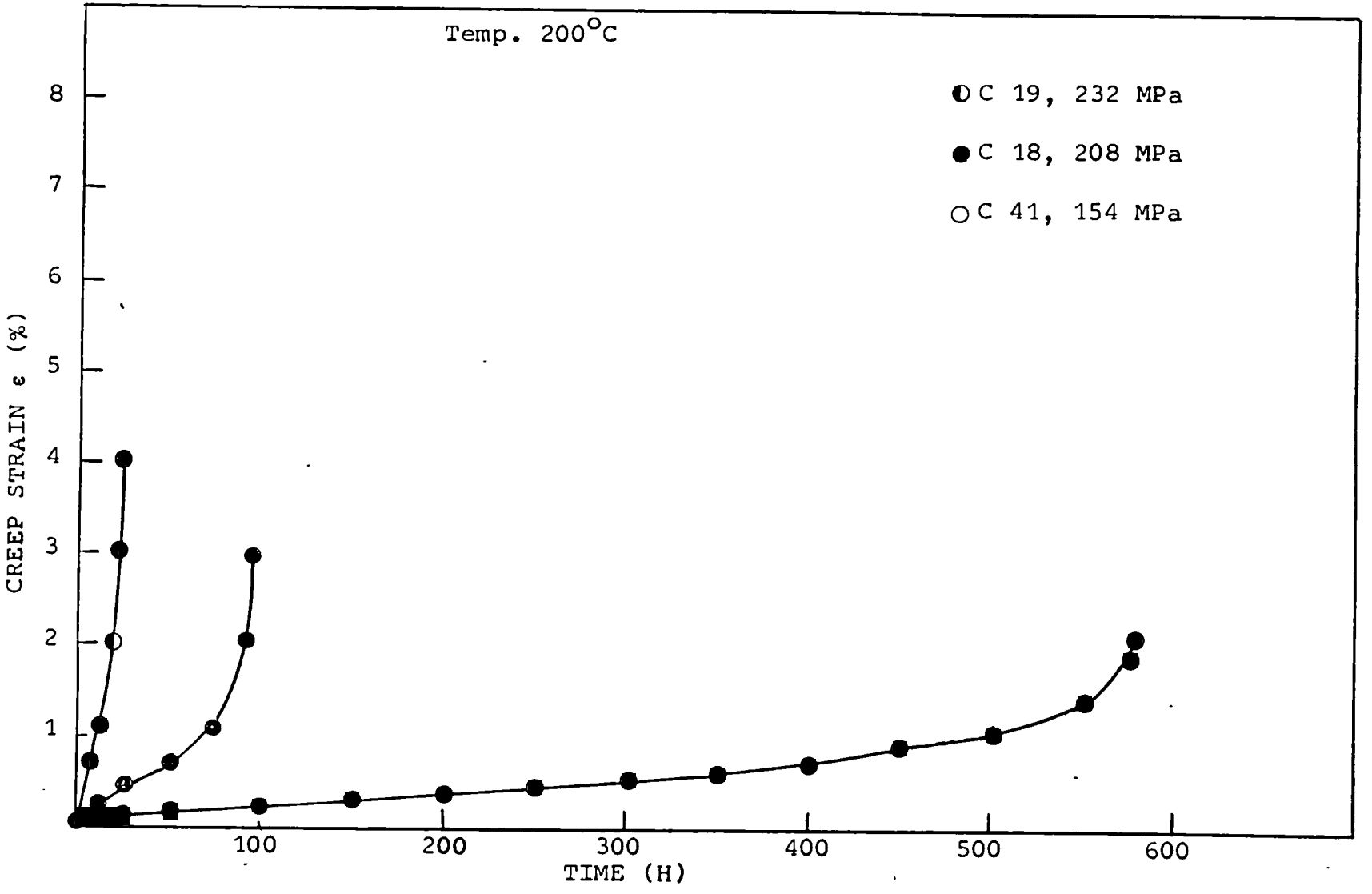

Figure (33): The effect of increase in stress on the uniaxial creep curve of RR58 tested at 200°C.

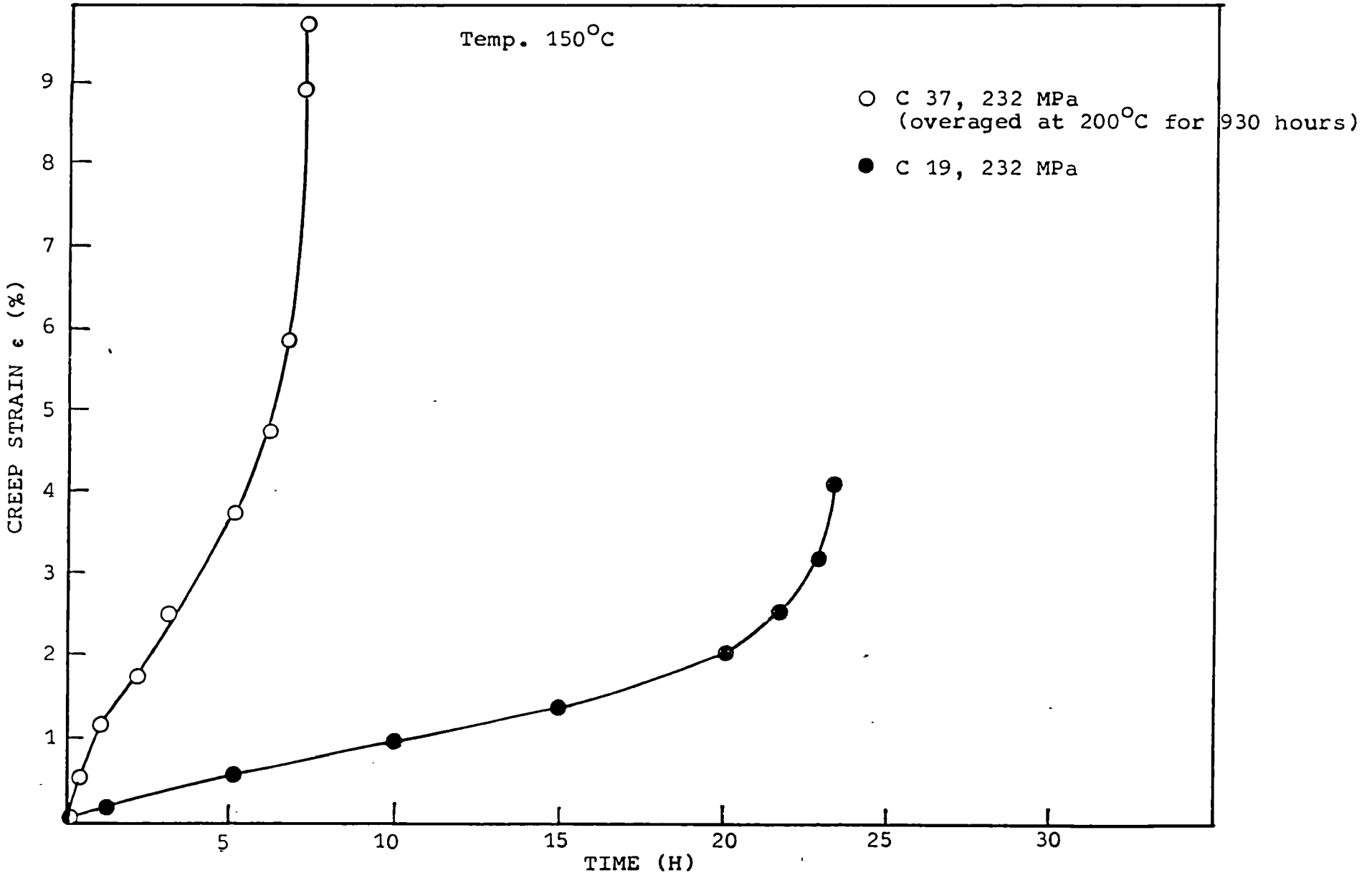

Figure (34): The effect of overaging at 200°C on the uniaxial creep curve of RR58 tested at 150°C.

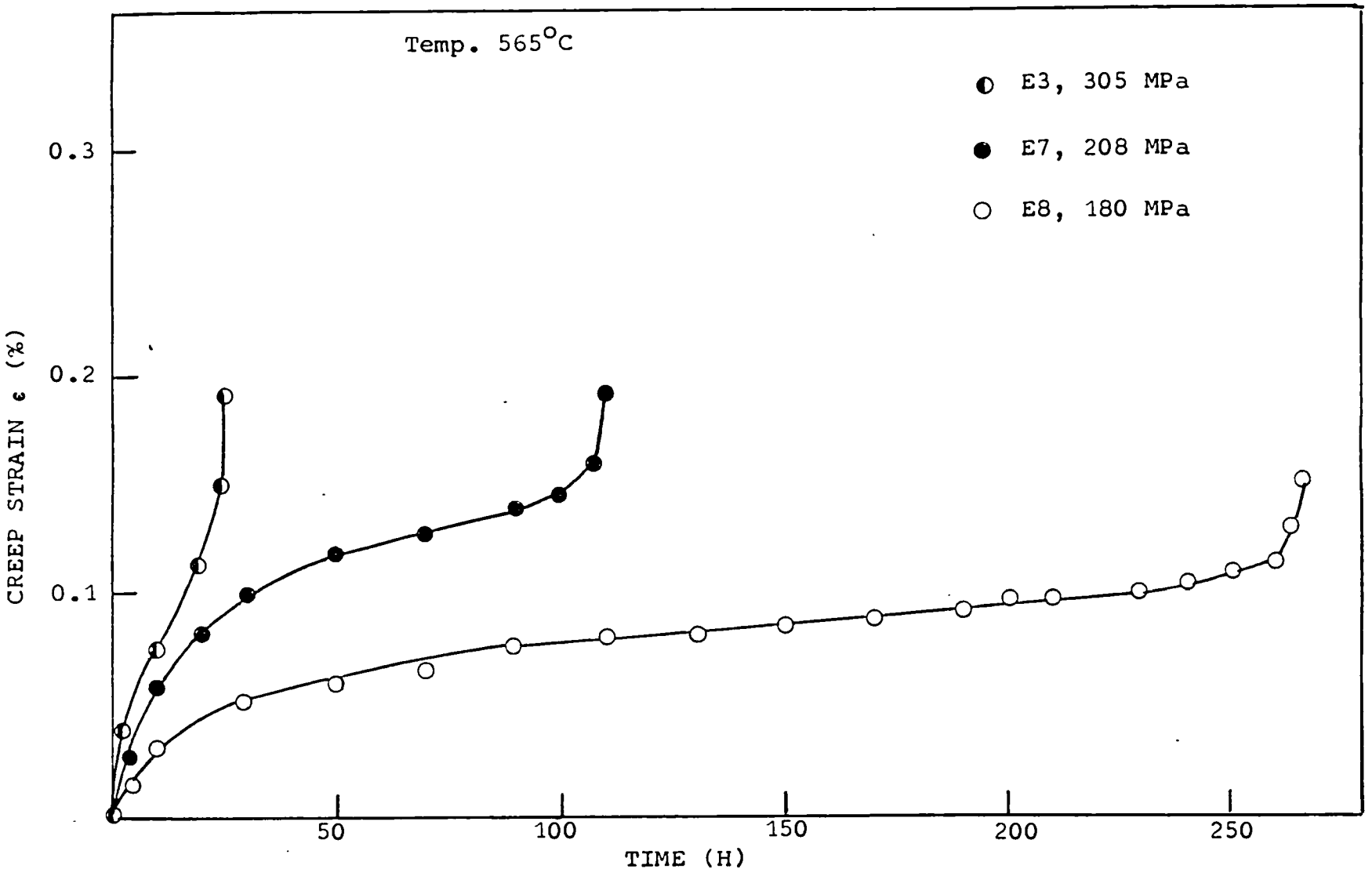

Figure (35): The effect of increase in stress on the uniaxial creep curve of the quenched steel tested at 565°C.

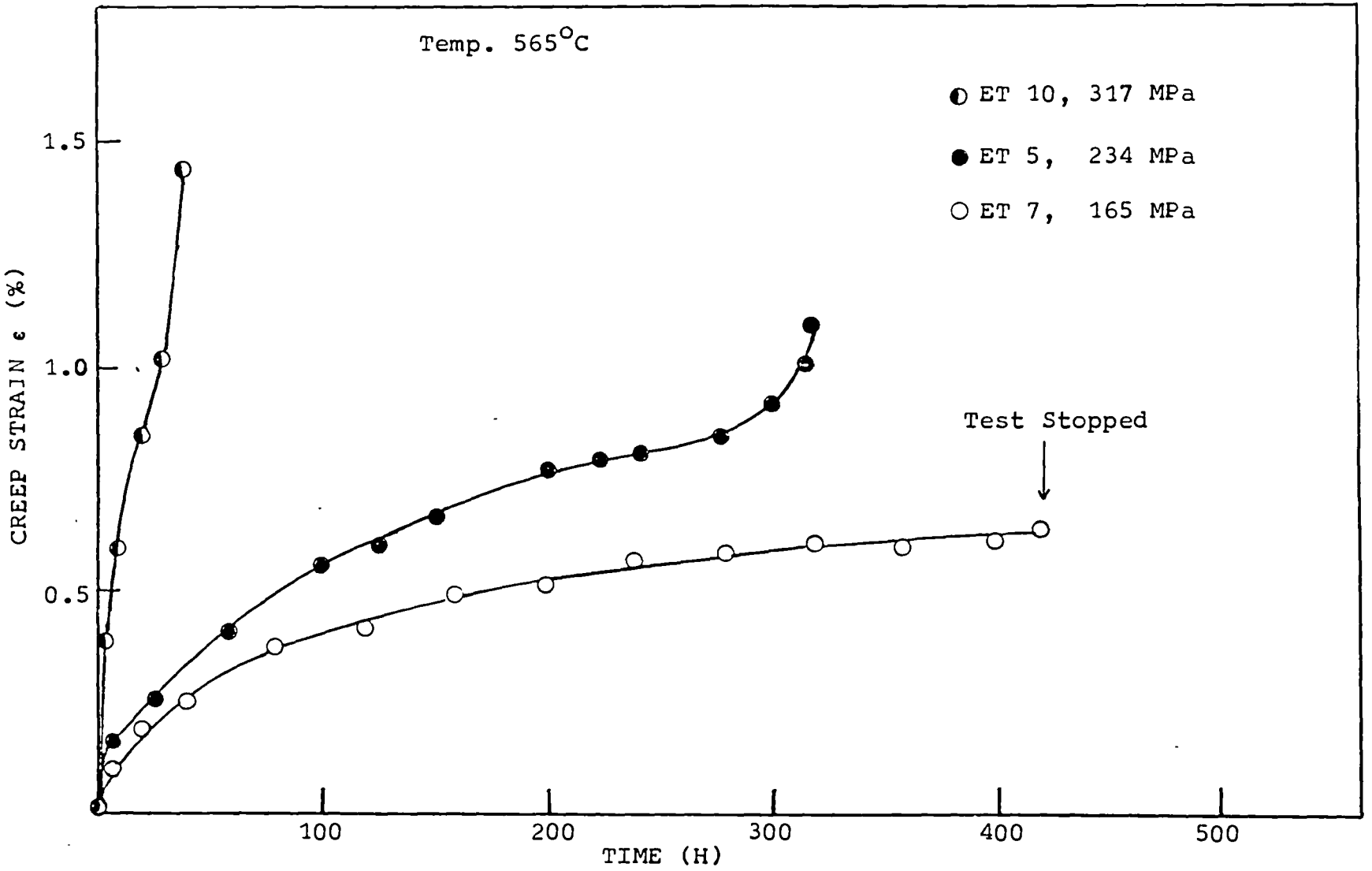

Figure (36): The effect of increase in stress on the uniaxial creep curve of the quenched and tempered steel tested at 565°C.

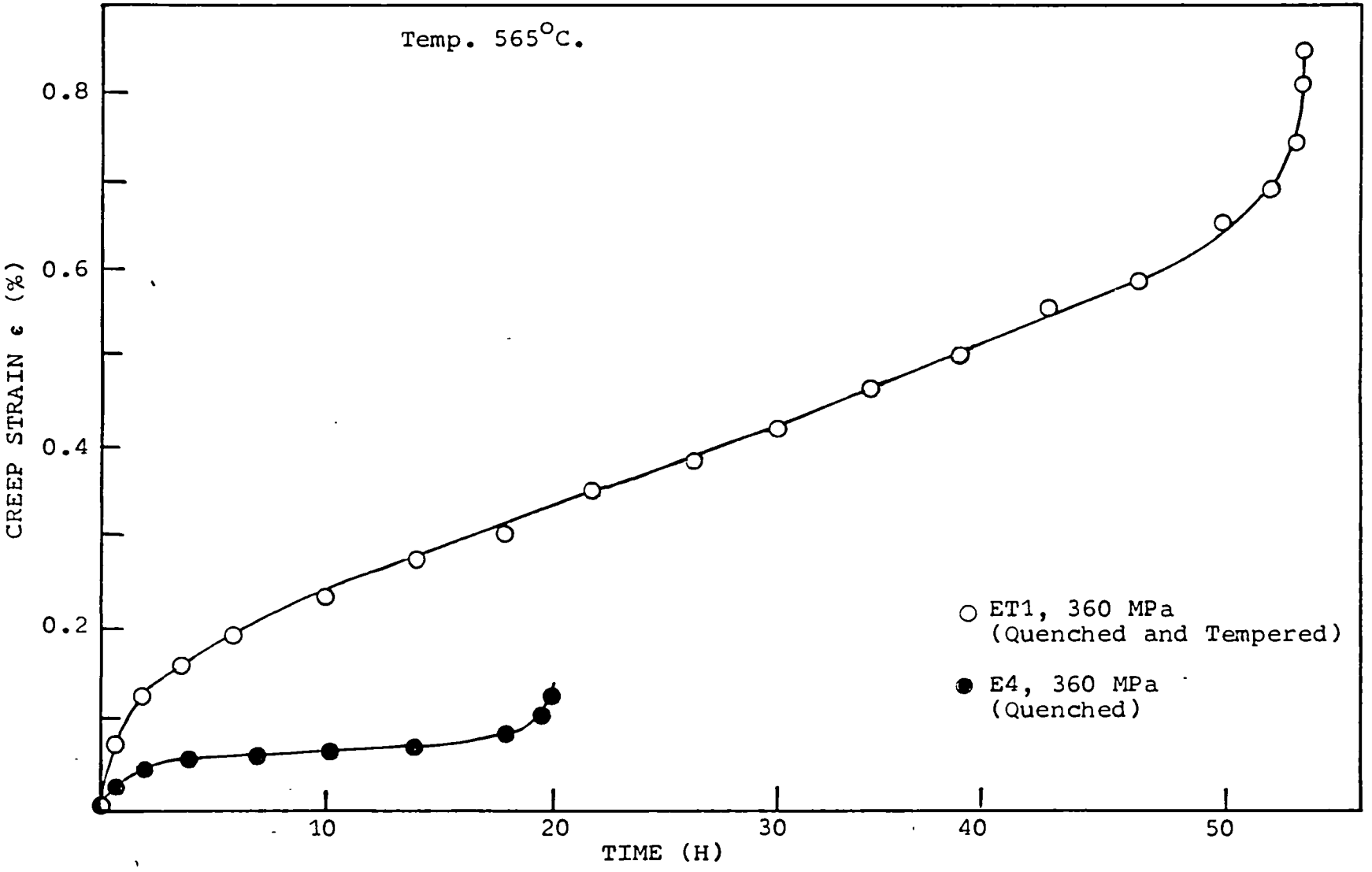

Figure (37): The effect of prior tempering at 680°C on the uniaxial creep curve of the steel tested at 565°C.

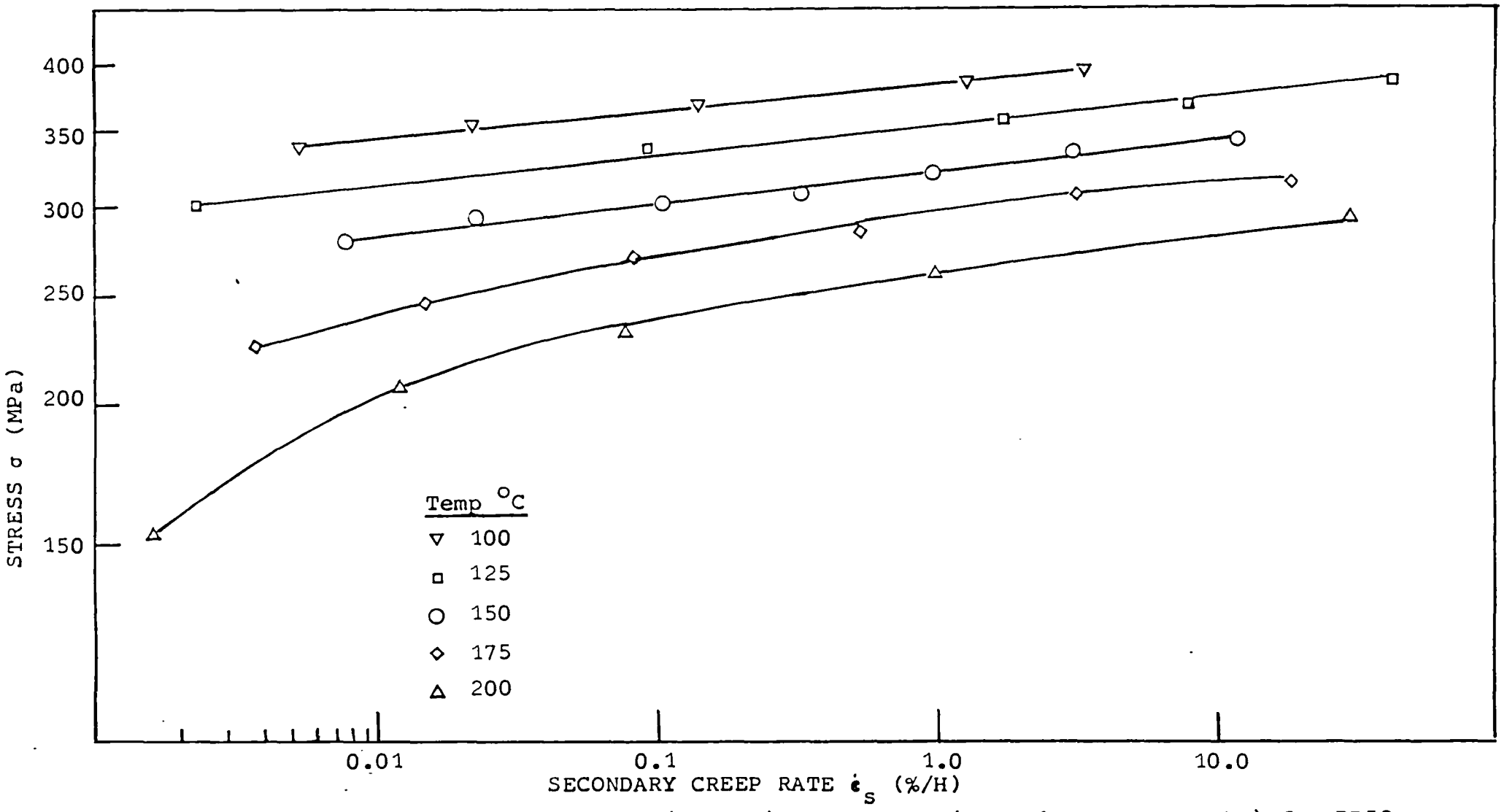

Figure (38): Effect of temperature on log (stress) versus log (secondary creep rate) for RR58

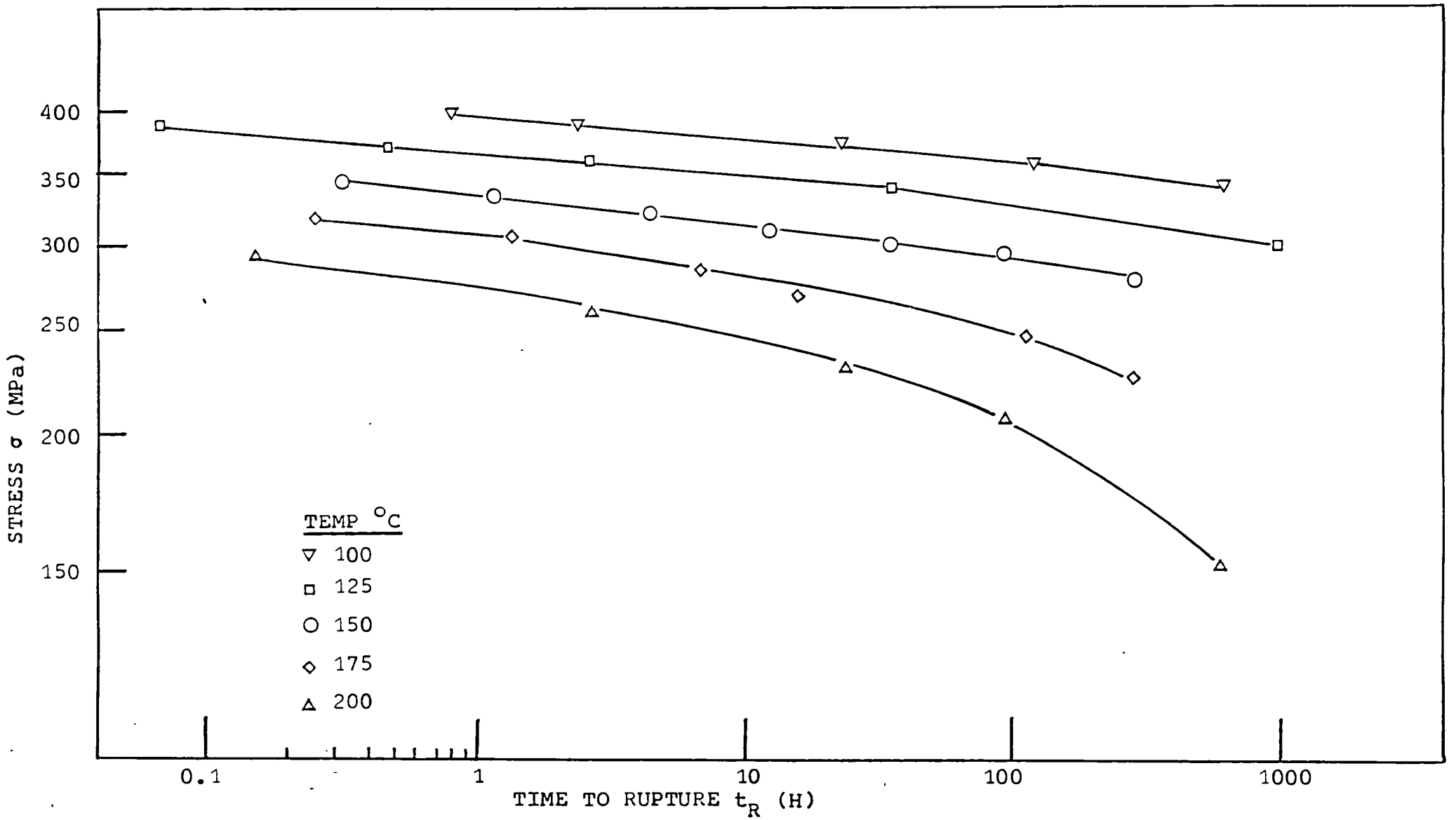

Figure (39): The effect of temperature on log (stress) versus log (time to rupture) of RR58.

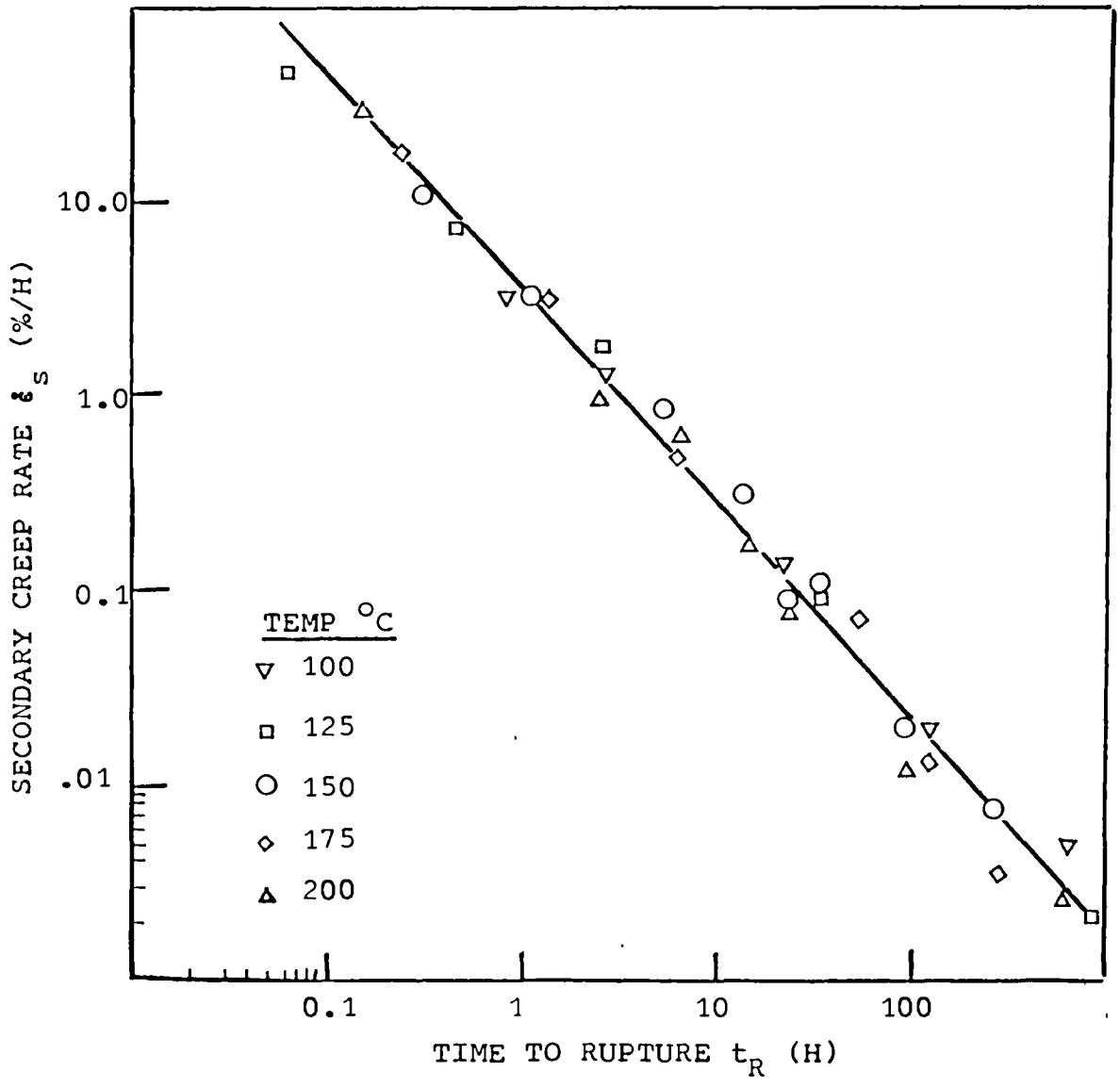

Figure (40): Graph of log (Secondary Creep rate) versus log (time to rupture) of RR58 for various temperatures

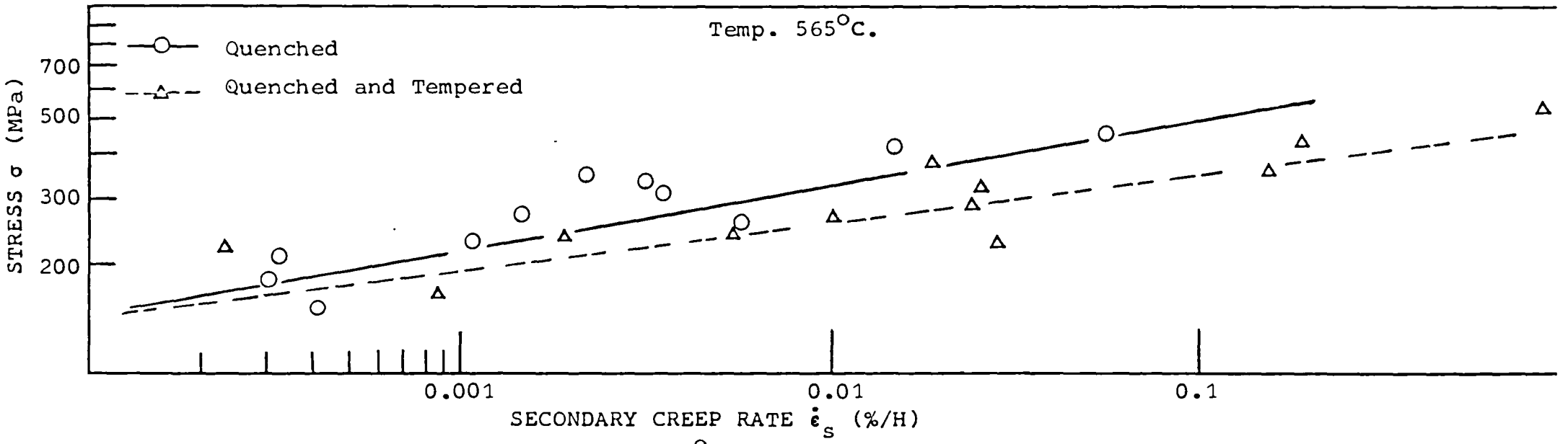

Figure (41): Effect of prior tempering at 680°C on the log (stress) versus log (secondary creep rate) graph of the steel tested at 565°C.

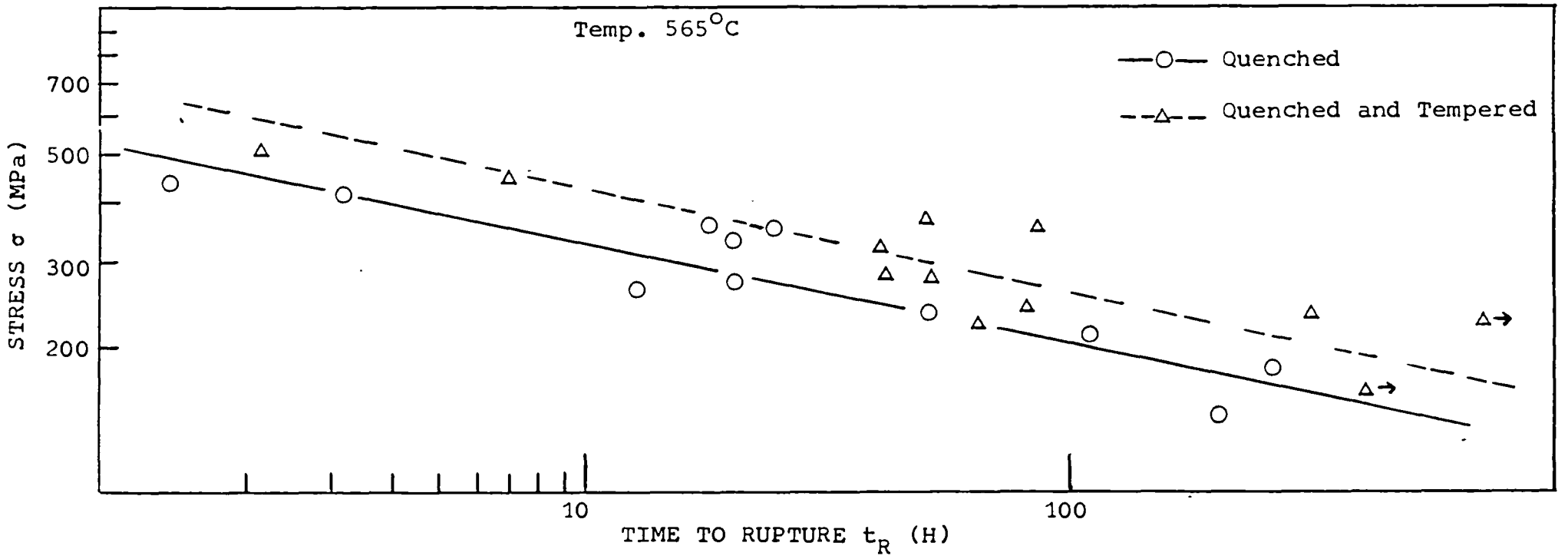

Figure (42): The effect of prior tempering at 680°C on the log (stress) versus log (time to rupture) graph of the steel tested at 565°C.

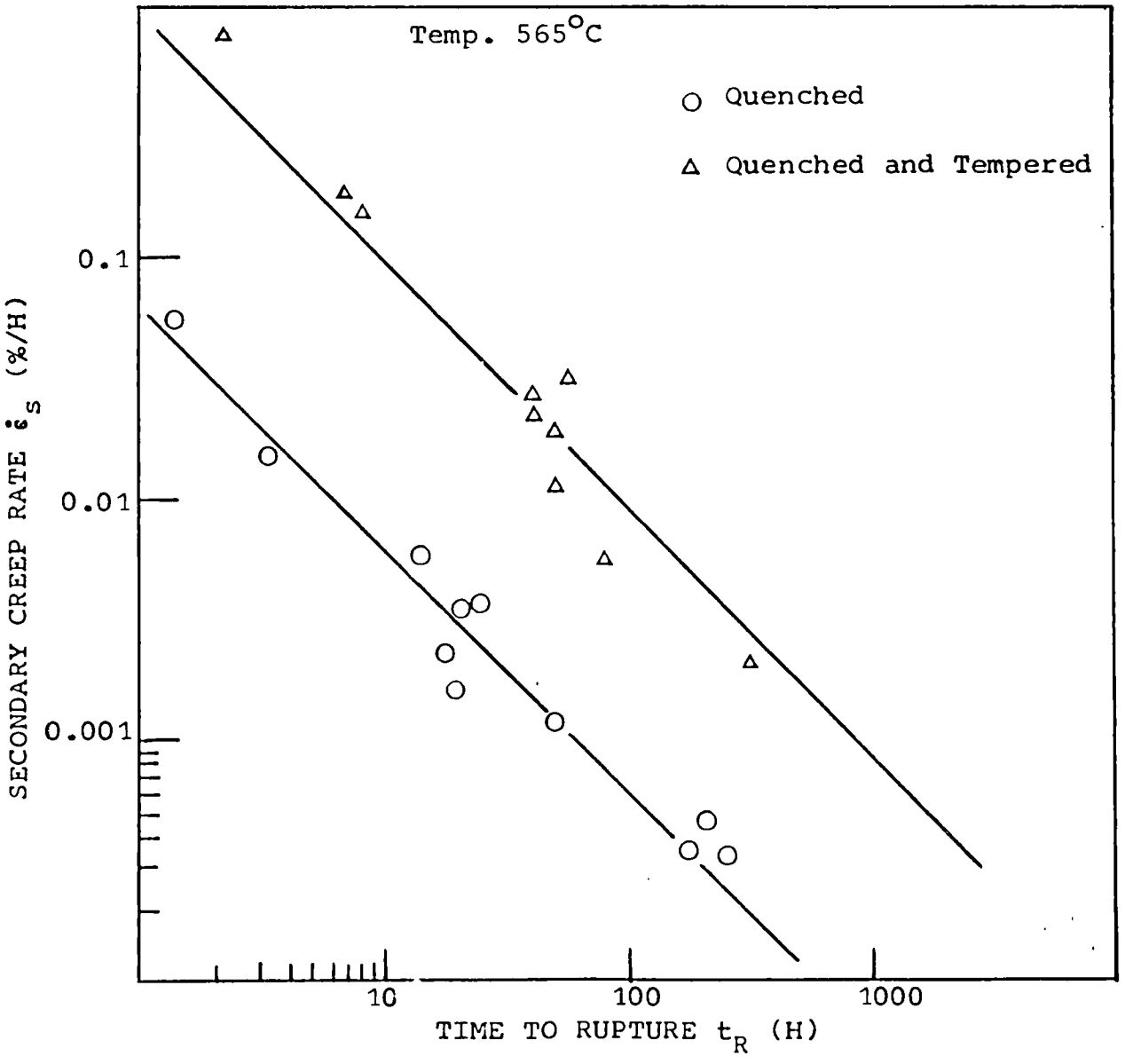

Figure (43): The effect of prior tempering at 680°C on the log (secondary creep rate) versus log (time to rupture) graph of the steel tested at 565°C.

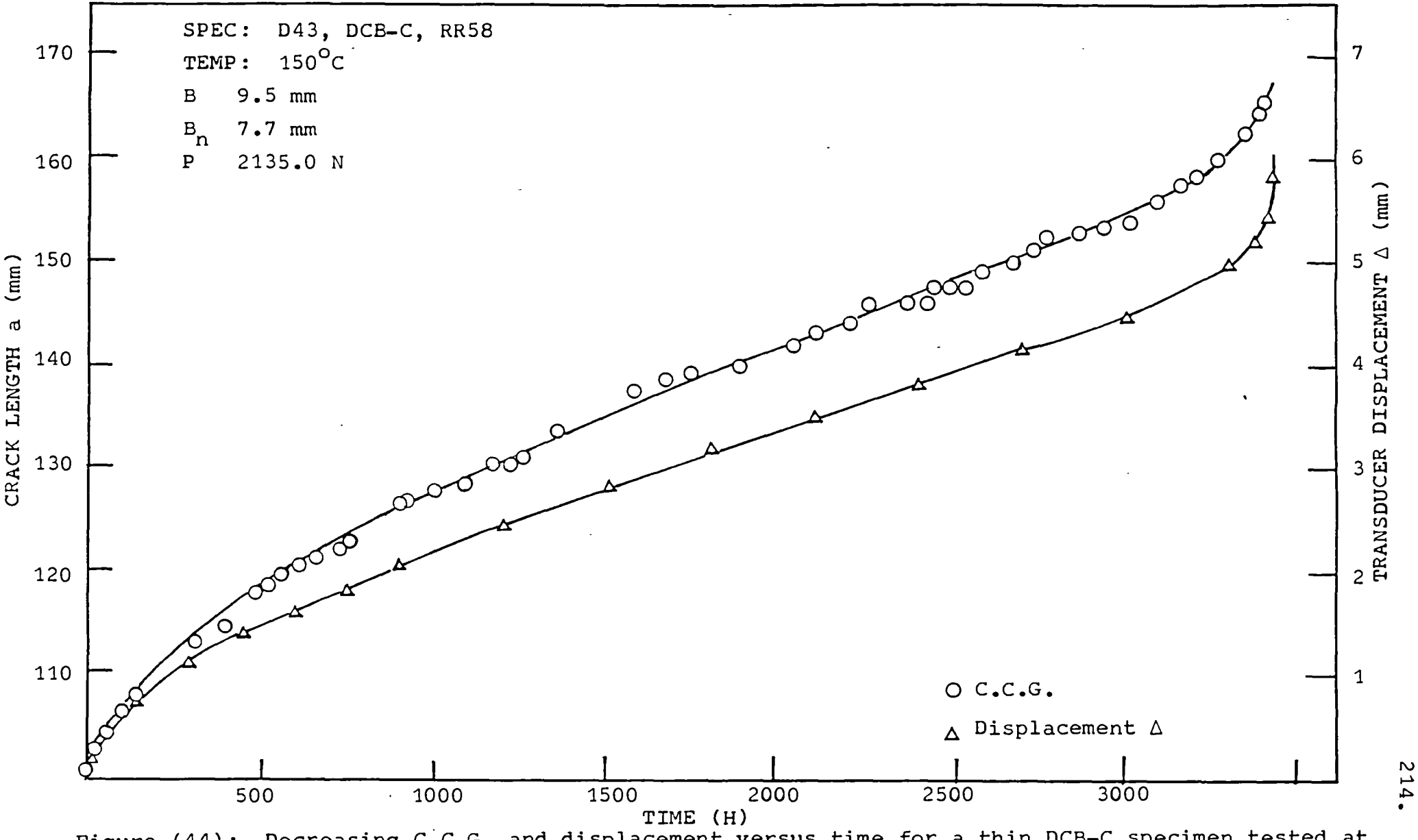

Figure (44): Decreasing C.C.G. and displacement versus time for a thin DCB-C specimen tested at 150°C.

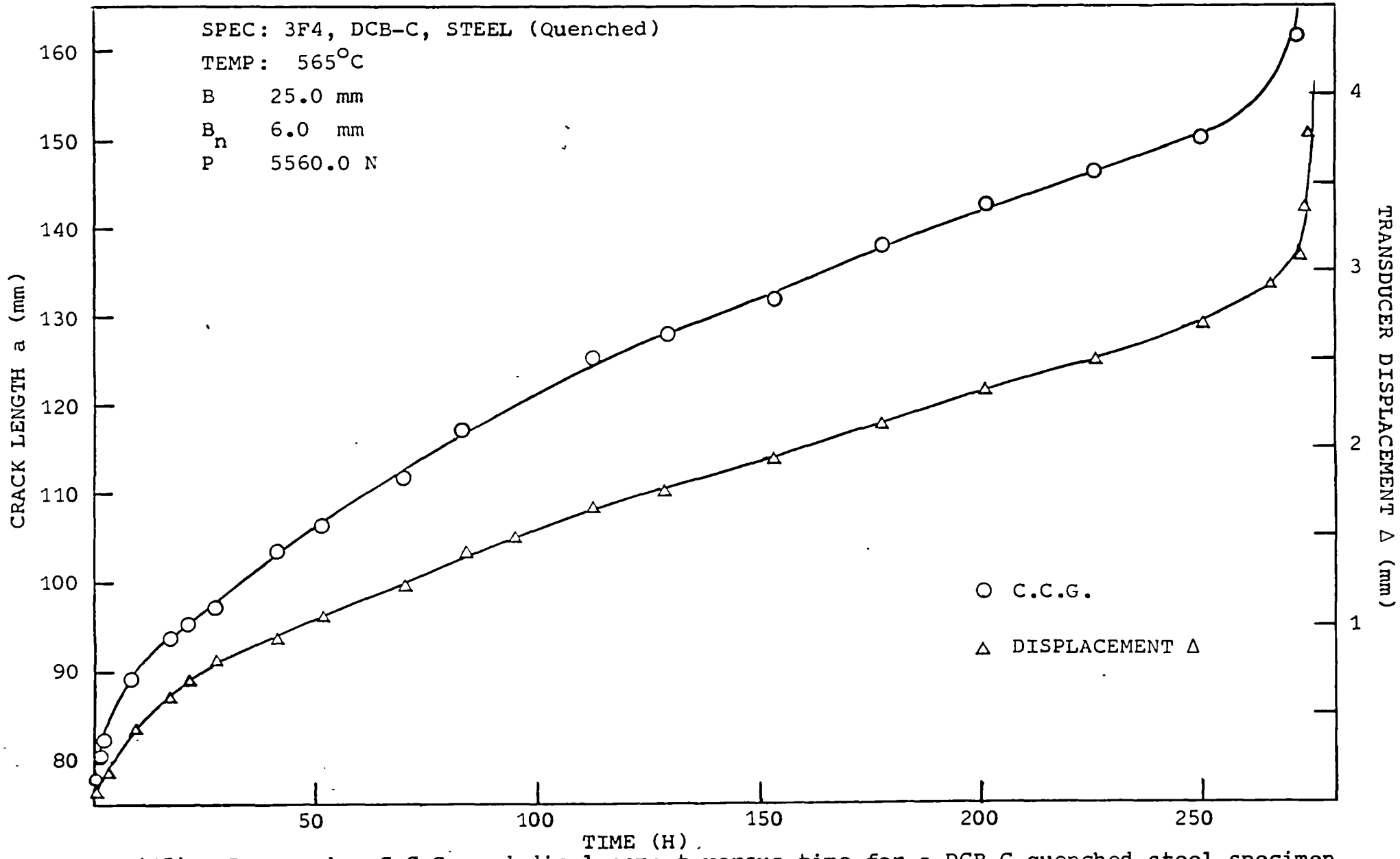

Figure (45): Decreasing C.C.G. and displacement versus time for a DCB-C quenched steel specimen

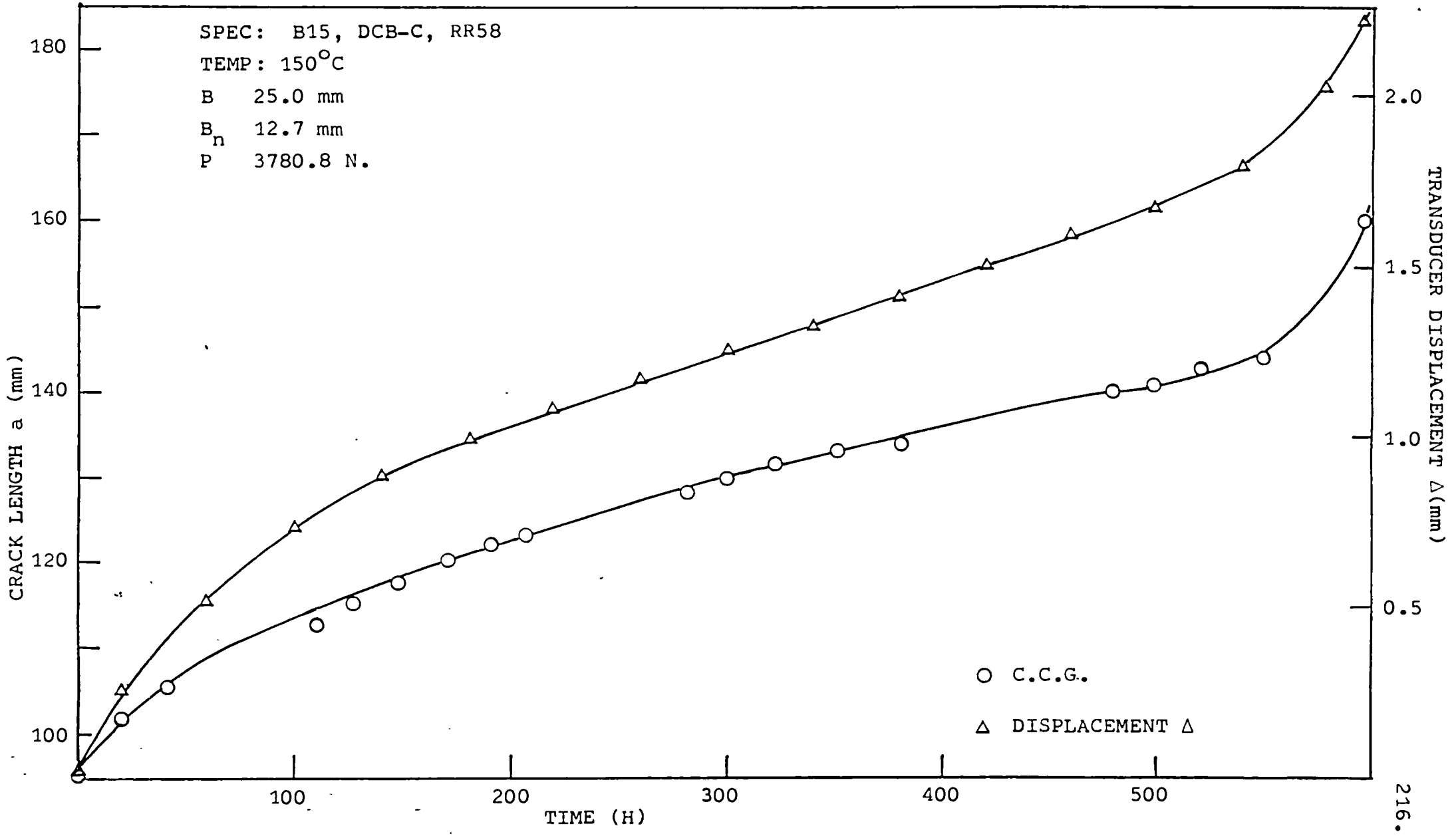

Figure (46): Decreasing C.C.G. and displacement versus time for a thick DCB-C RR58 specimen tested at 150°C.

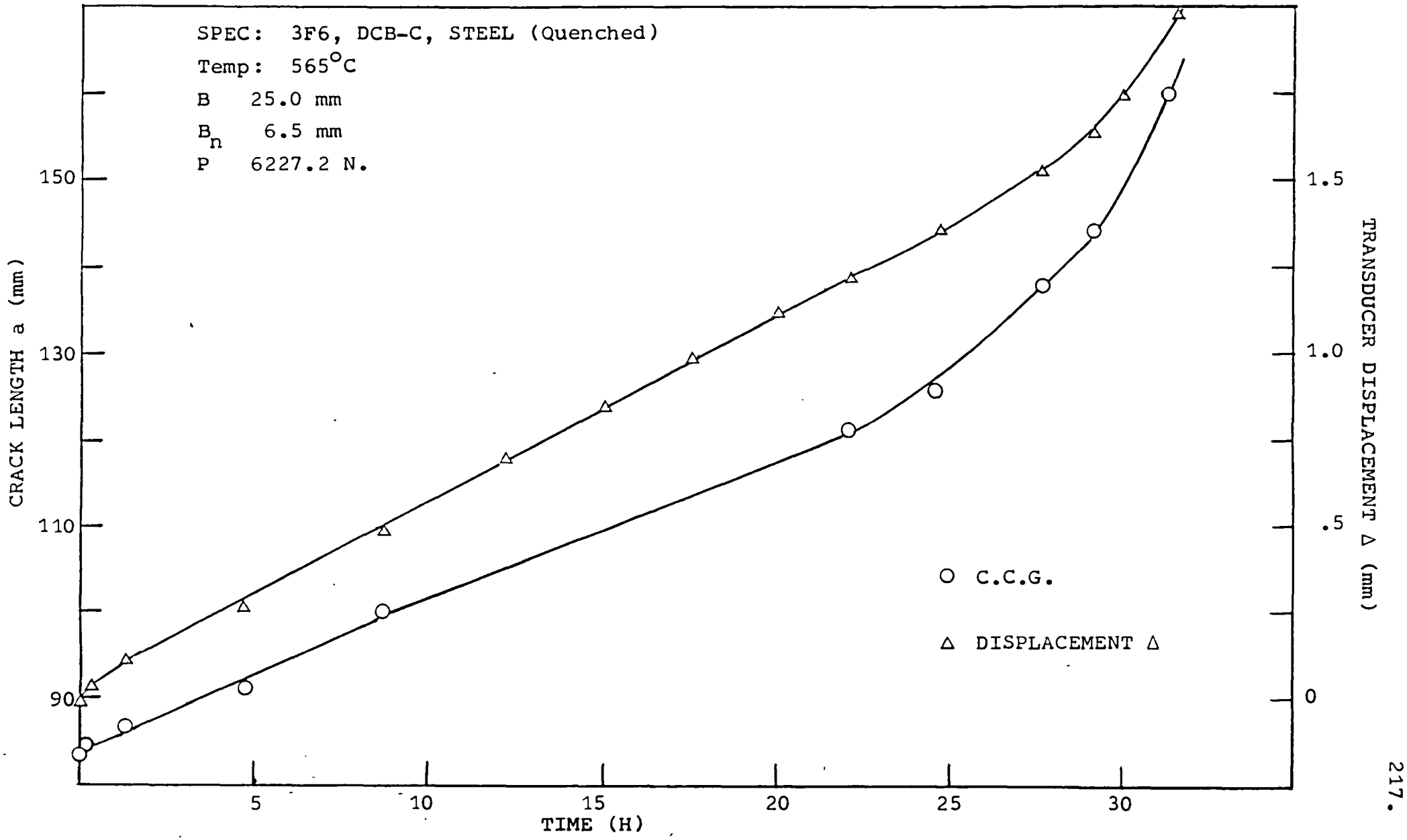

Figure (47): Graph of C.C.G. and displacement for a short term test on a DCB-C quenched steel

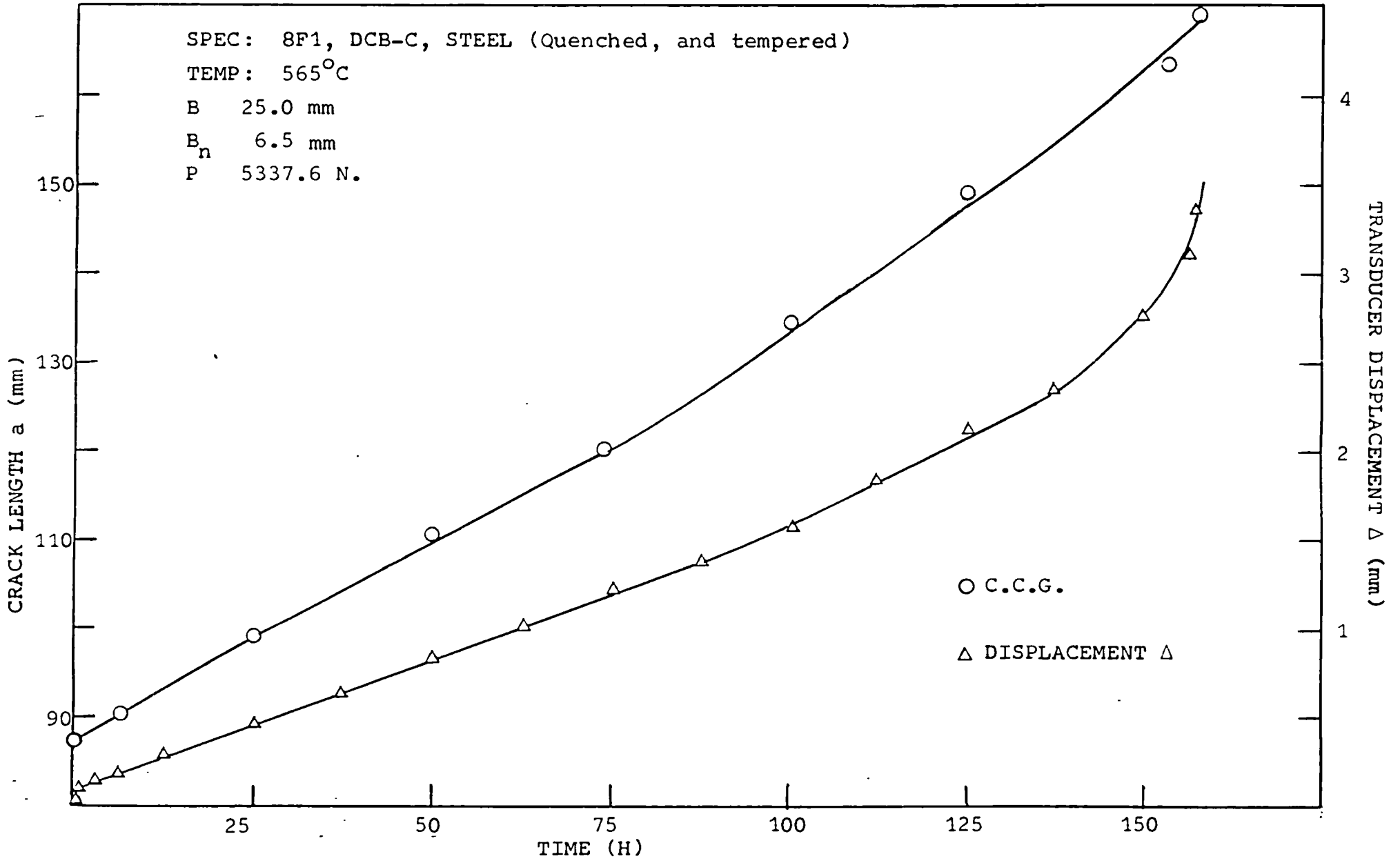

Figure (48): Graph of C.C.G. and displacement for a short term test on a DCB-C quenched and tempered steel

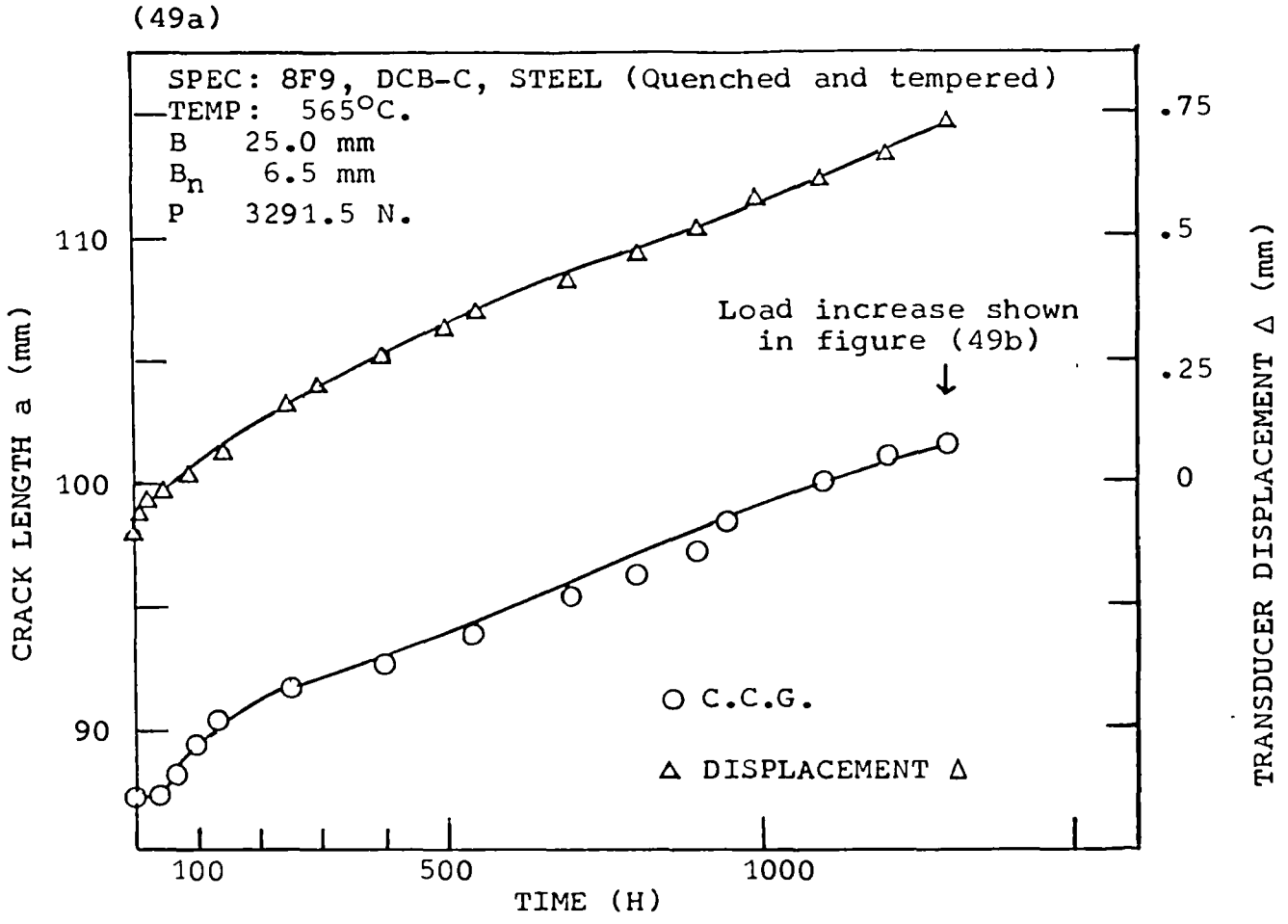

Figure (49a, 49b): The effect of load increase on C.C.G. and displacement of a thick DCB-C quenched and tempered steel

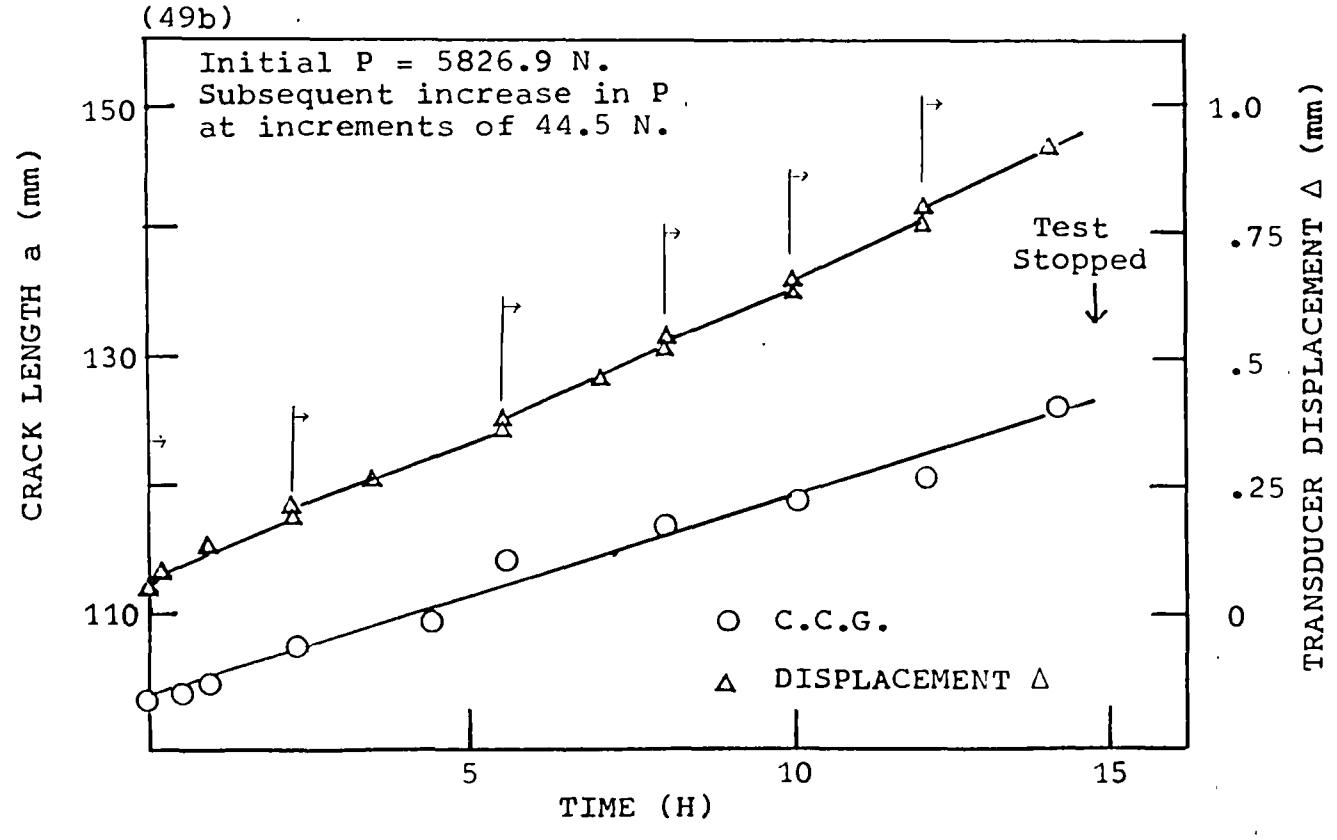

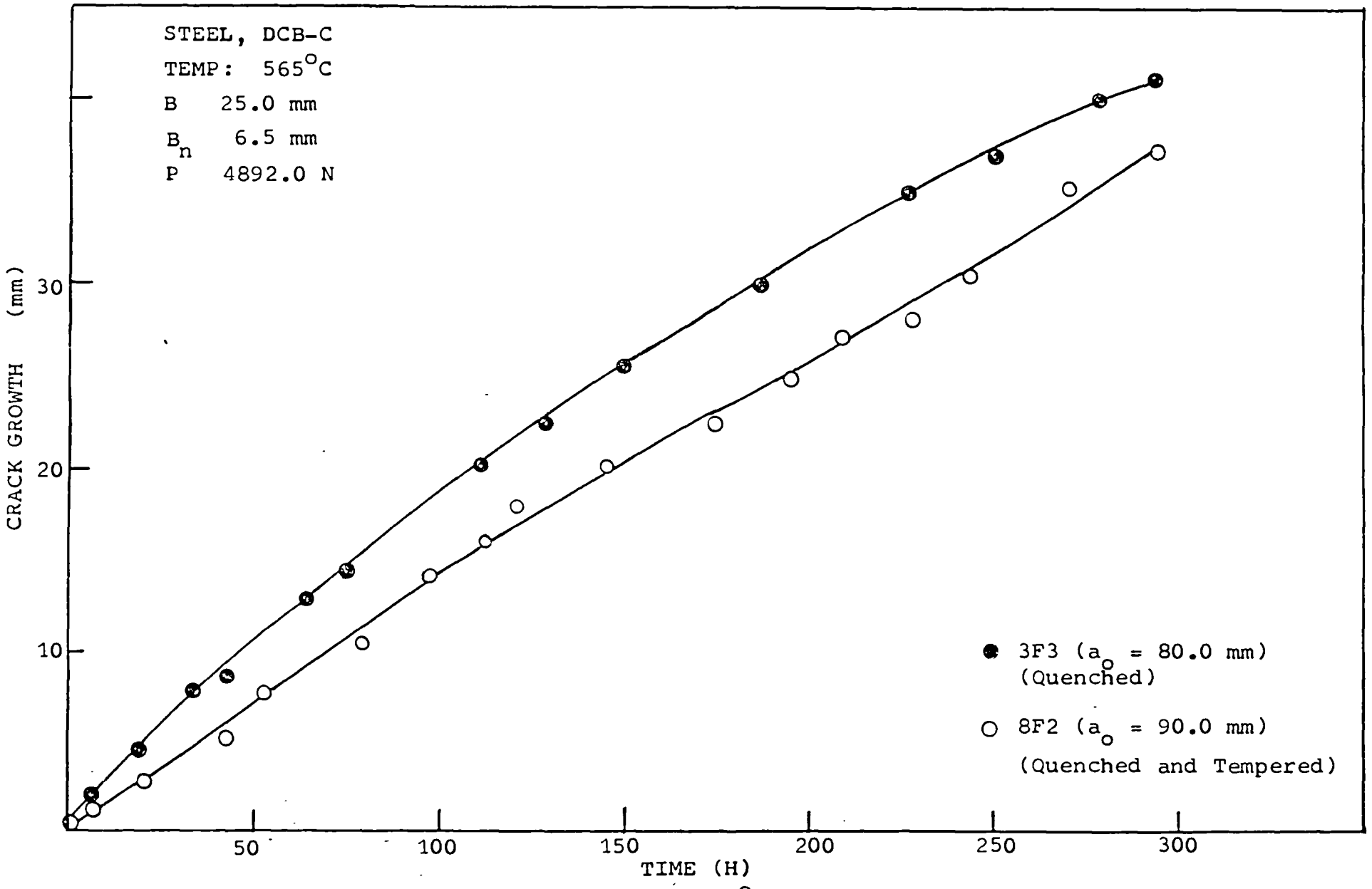

Figure (50): The effect of prior tempering at 680°C on the C.C.G. of DCB-C steel specimens

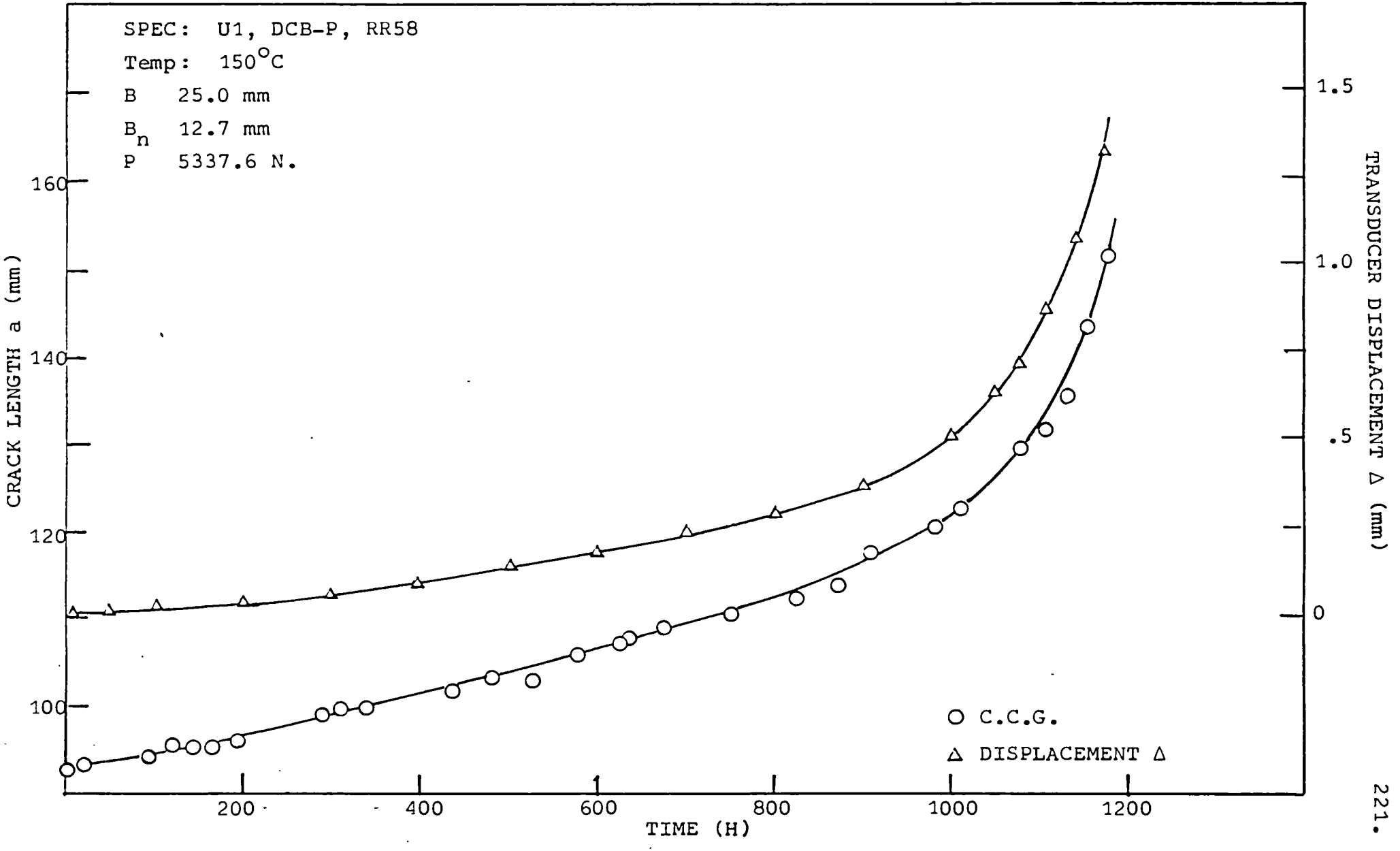

Figure (51): Typical C.C.G. and displacement versus time for a DCB-P, RR58 tested at constant load

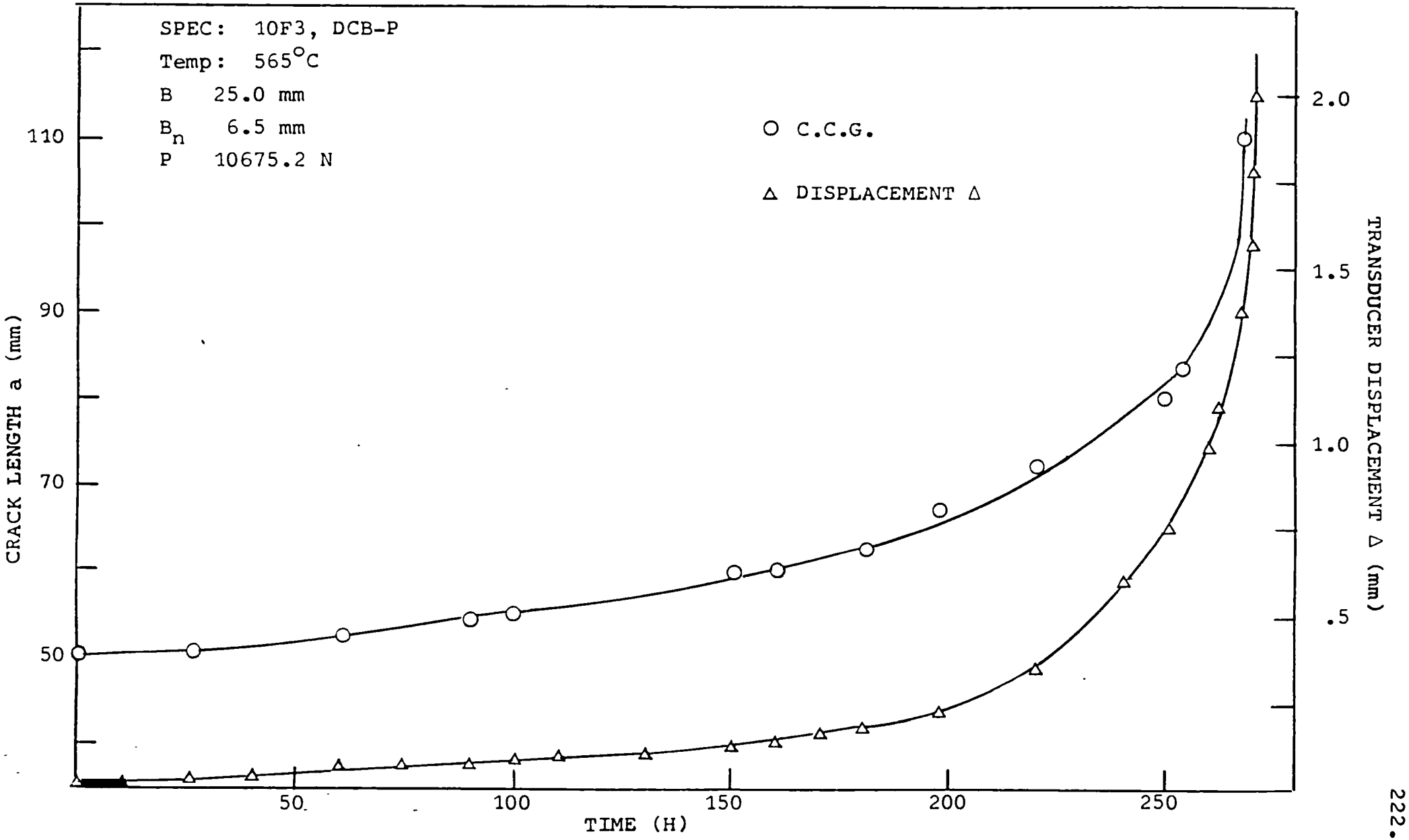

Figure (52): Typical C.C.G. and displacement versus time for a DCB-P, steel tested at constant load

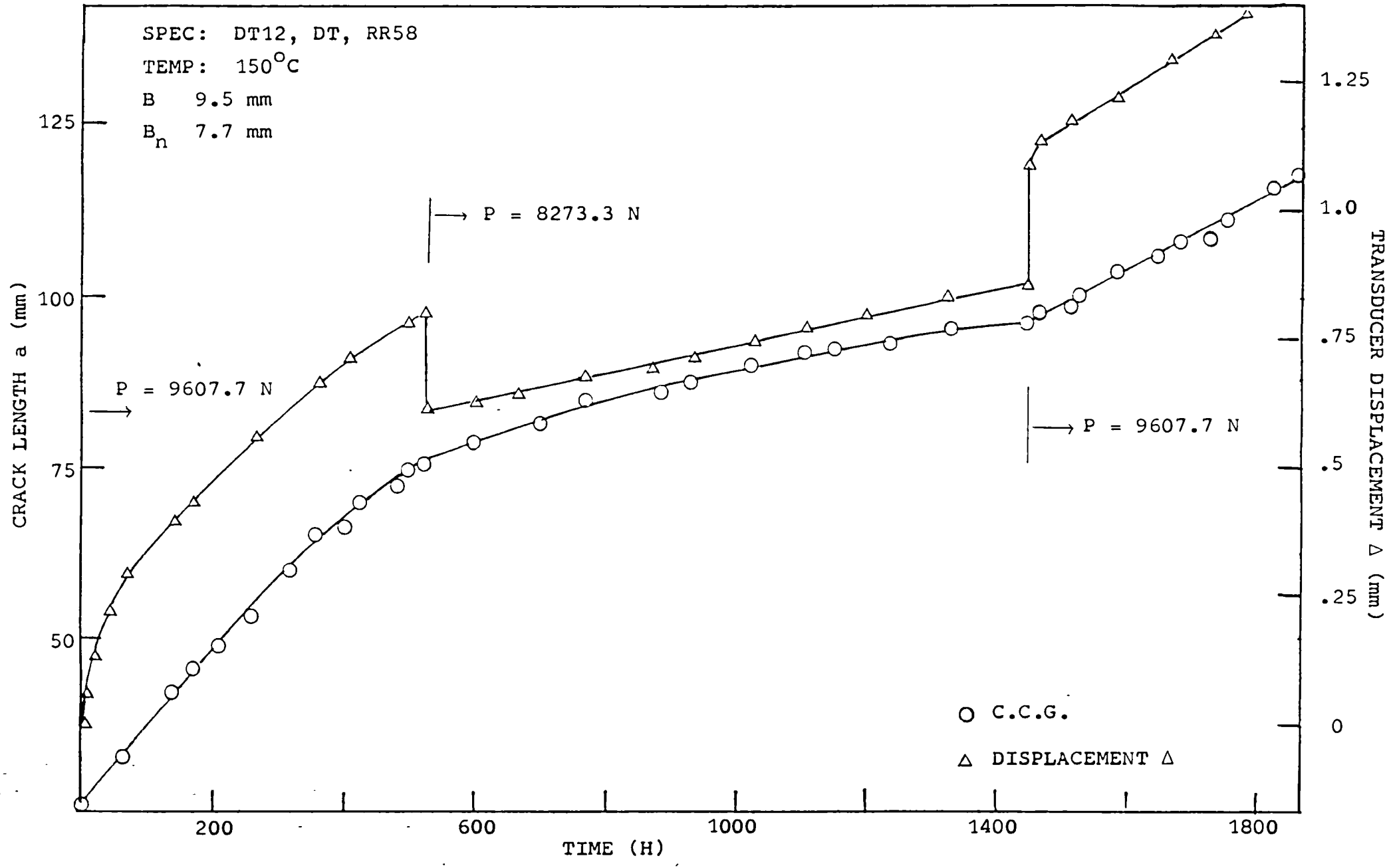

Figure (53): Typical C.C.G. and displacement for a DT, RR58 specimen, with load changes at various crack lengths

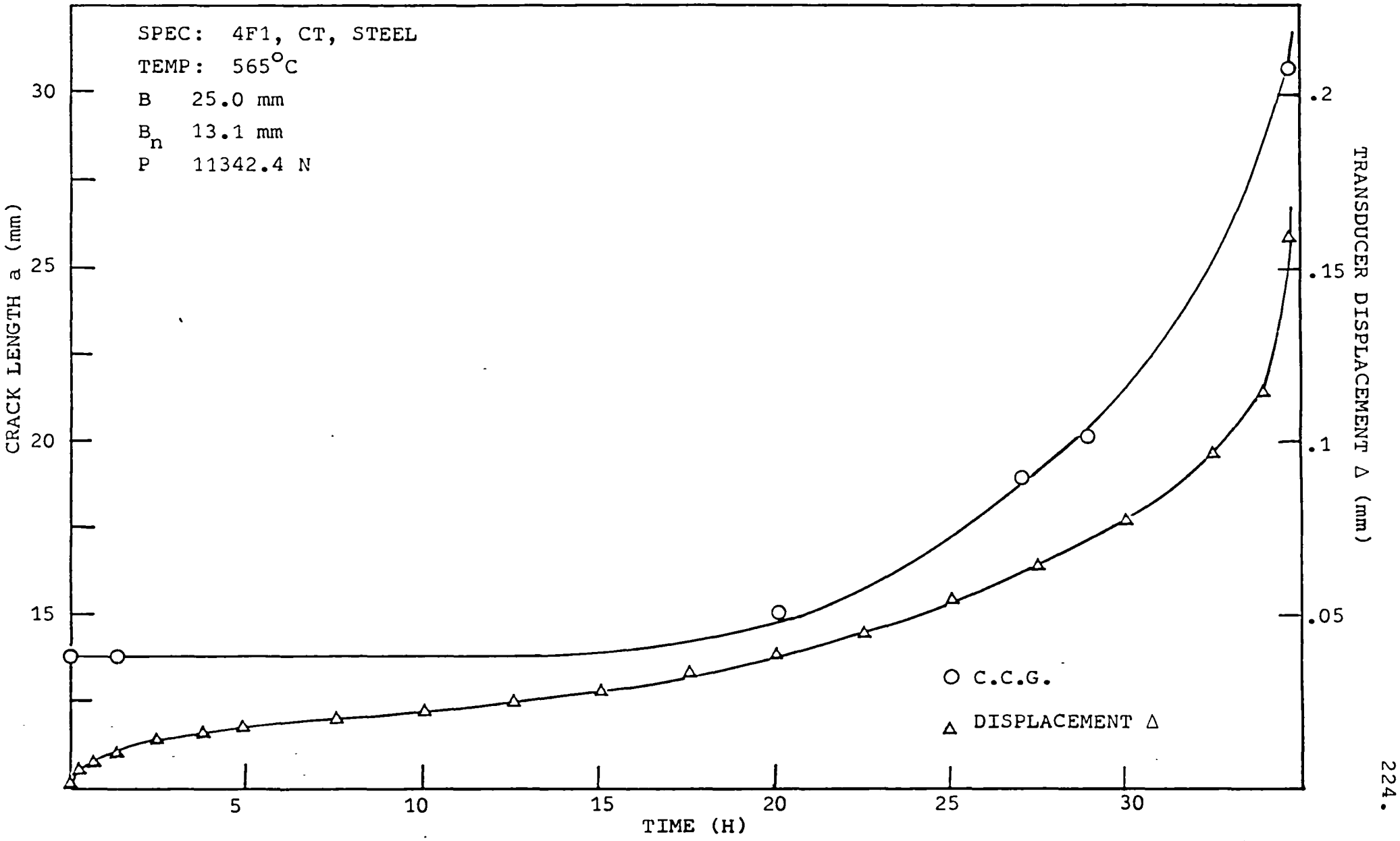

Figure (54): Typical graph of C.C.G. and displacement for a CT steel specimen tested at 565°C

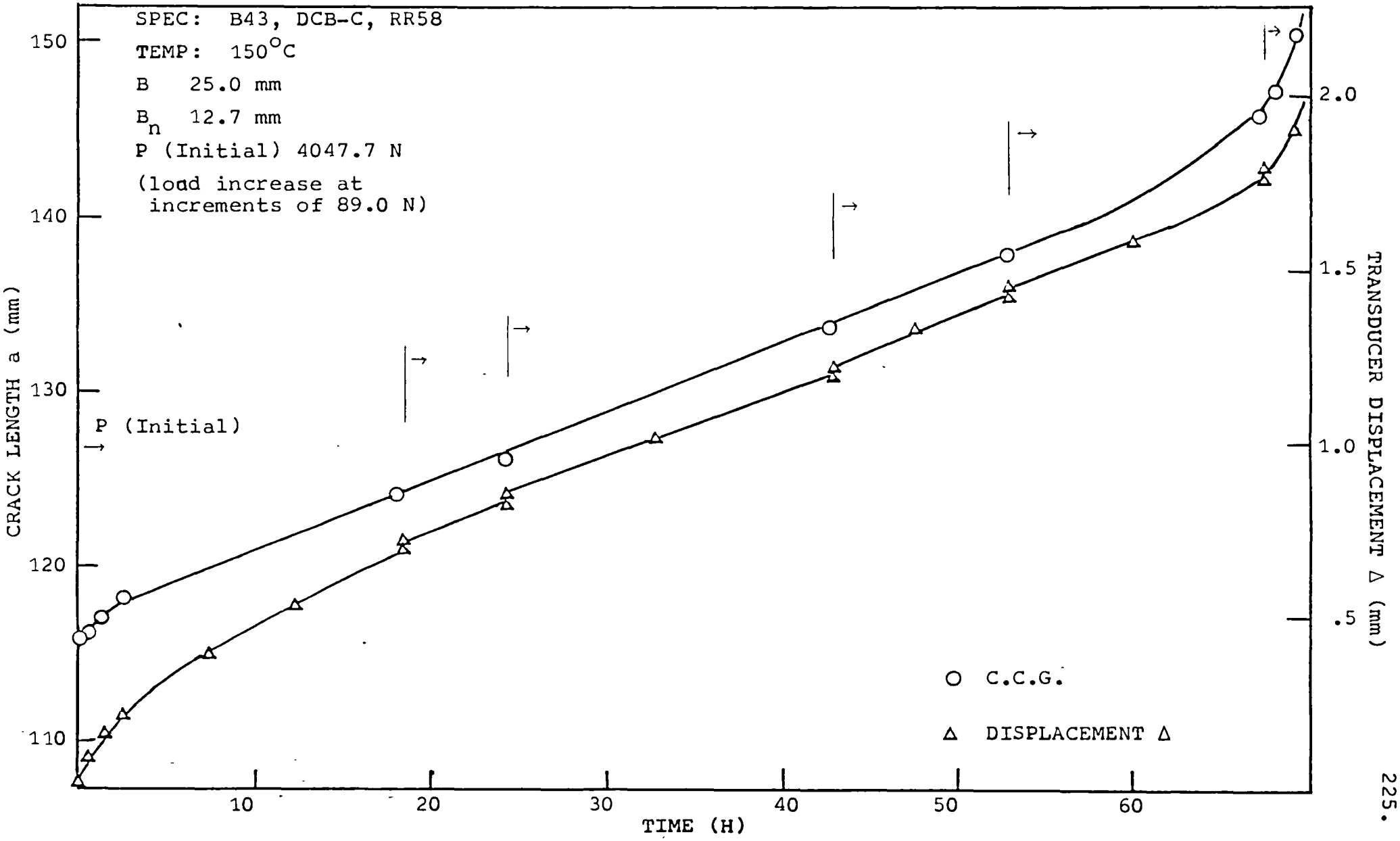

Figure (55): Graph of constant C* (Analytical) test for a DCB-C, RR58 tested at 150°C.

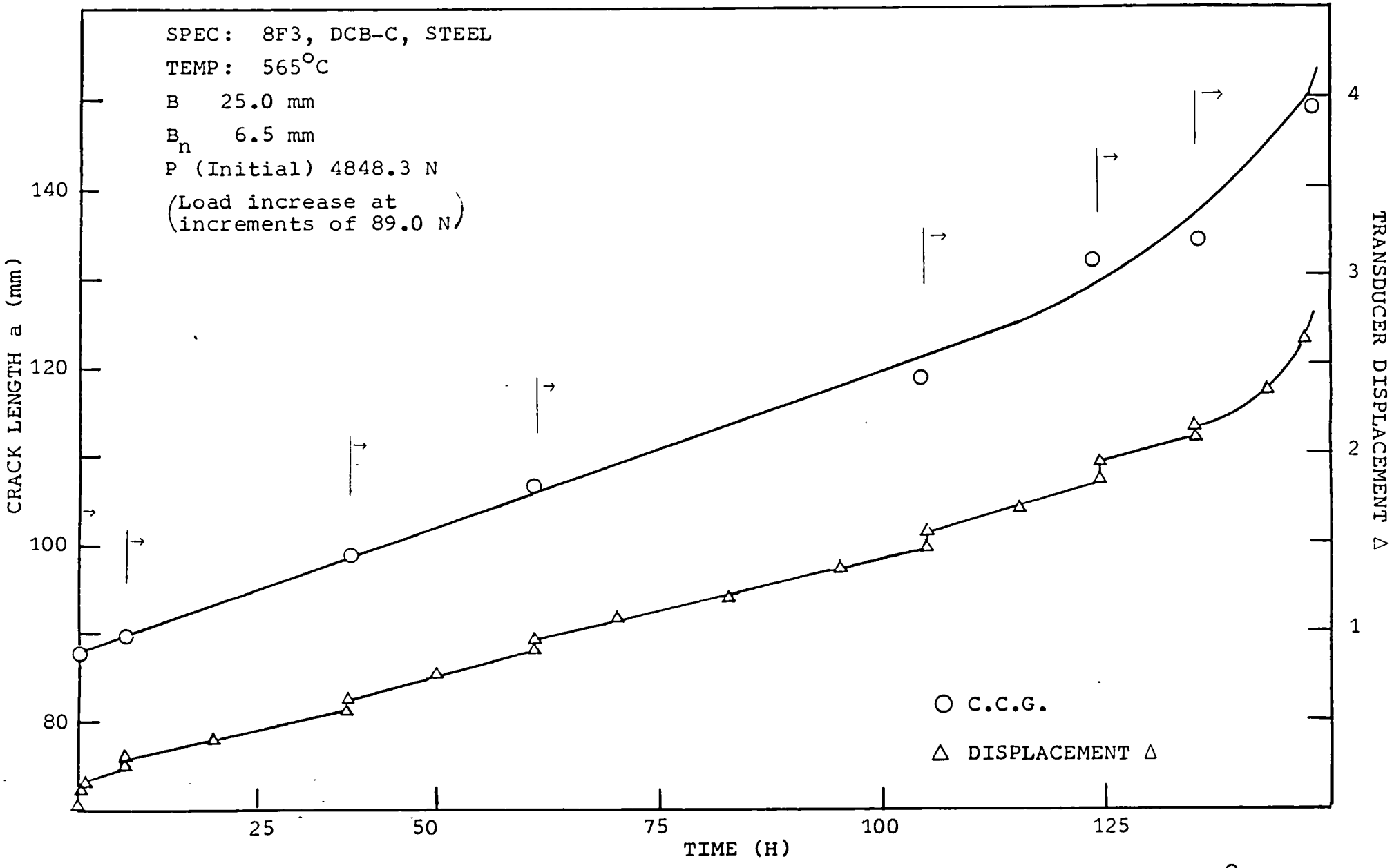

Figure (56): Graph of constant C* (Analytical) test for a DCB-C, steel tested at 565°C

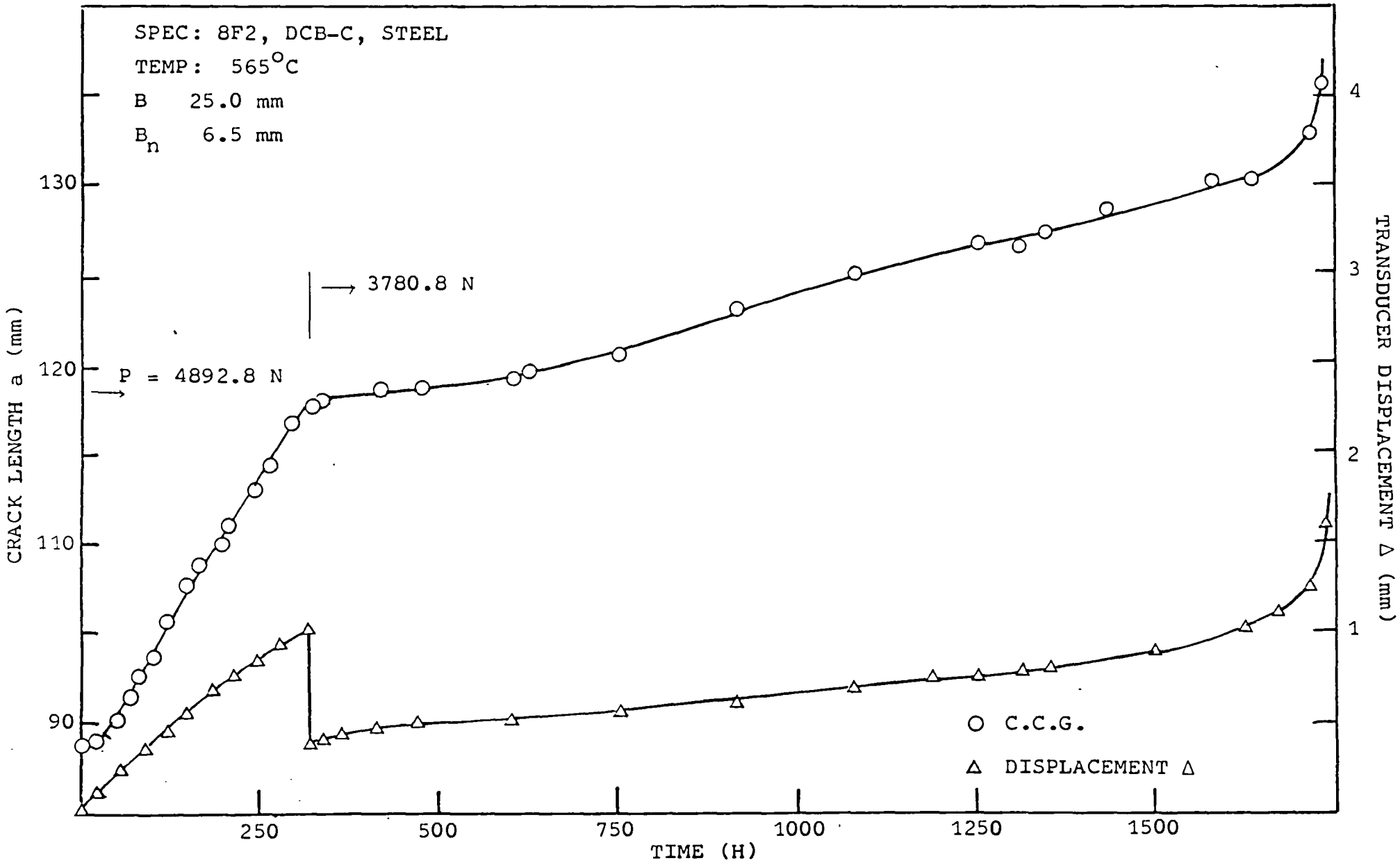

Figure (57): Effect of Load decrease on the C.C.G. of a 25 mm thick DCB-C steel

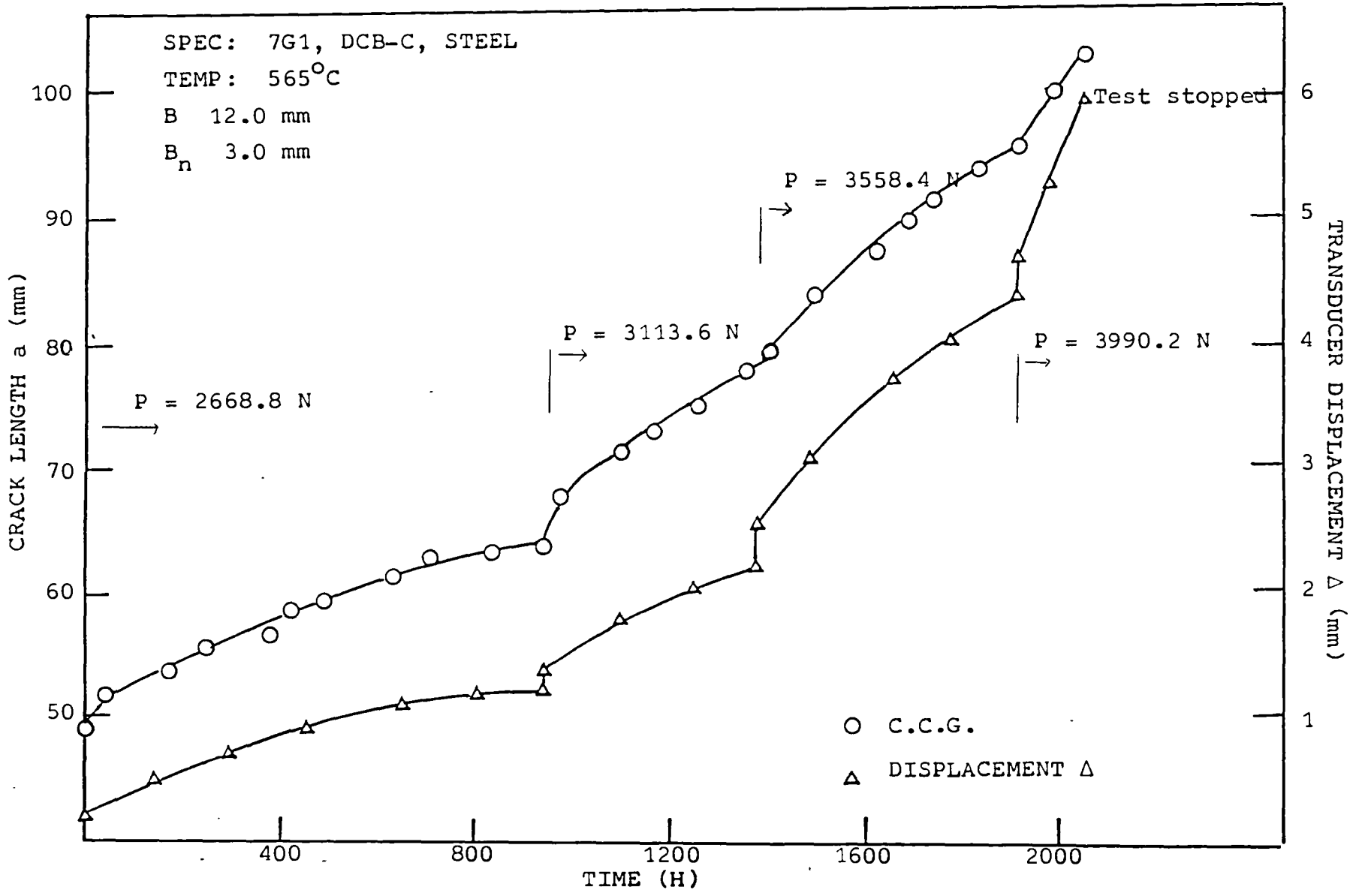

Figure (58): Effect of load increase on the C.C.G. of a 12 mm thick DCB-C steel

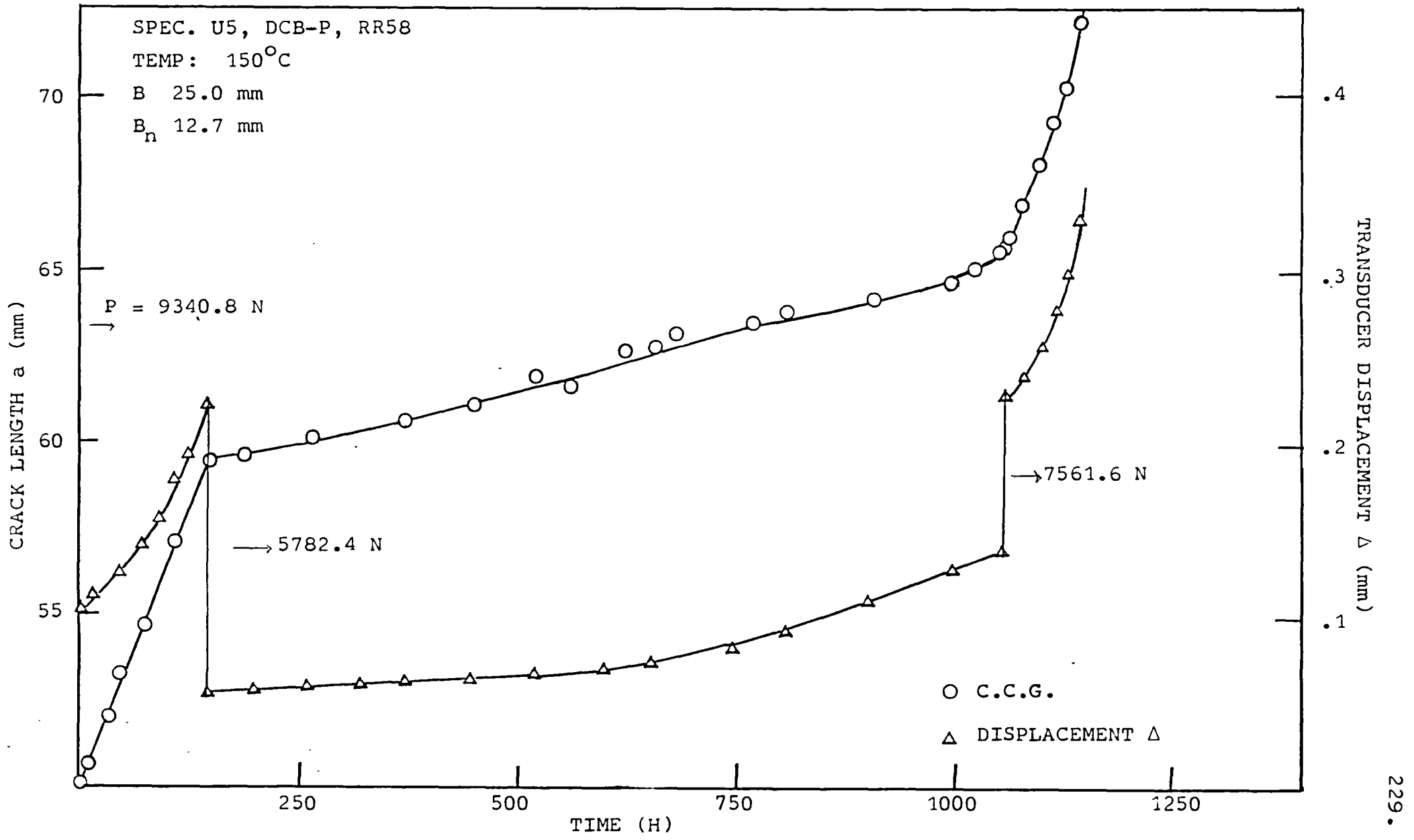

Figure (59): Effect of Load change on C.C.G. and Displacement of a DCB-P, RR58 tested at 150°C.

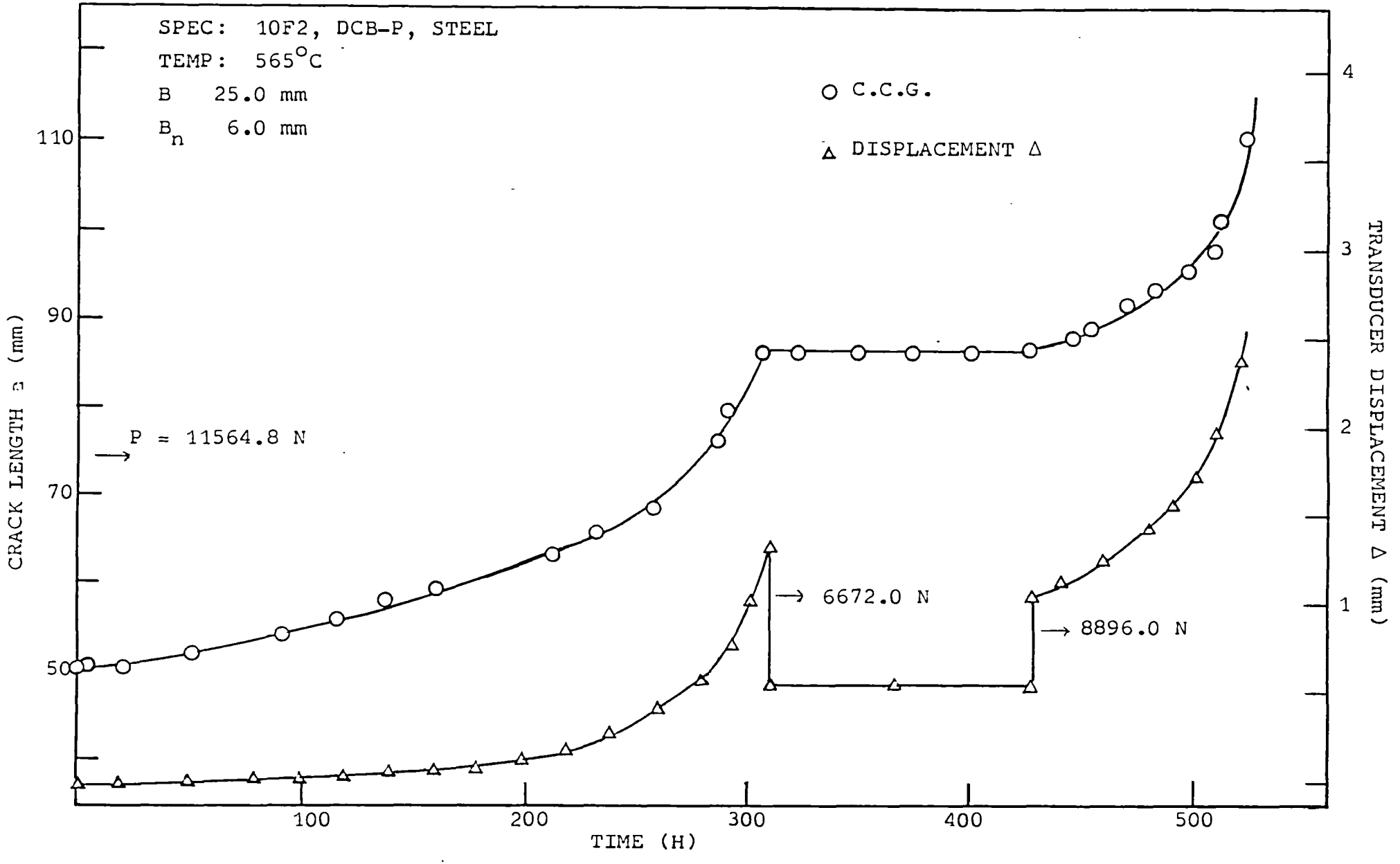

Figure (60): Effect of load change on C.C.G. and displacement for a DCB-P steel specimen tested at 565°C

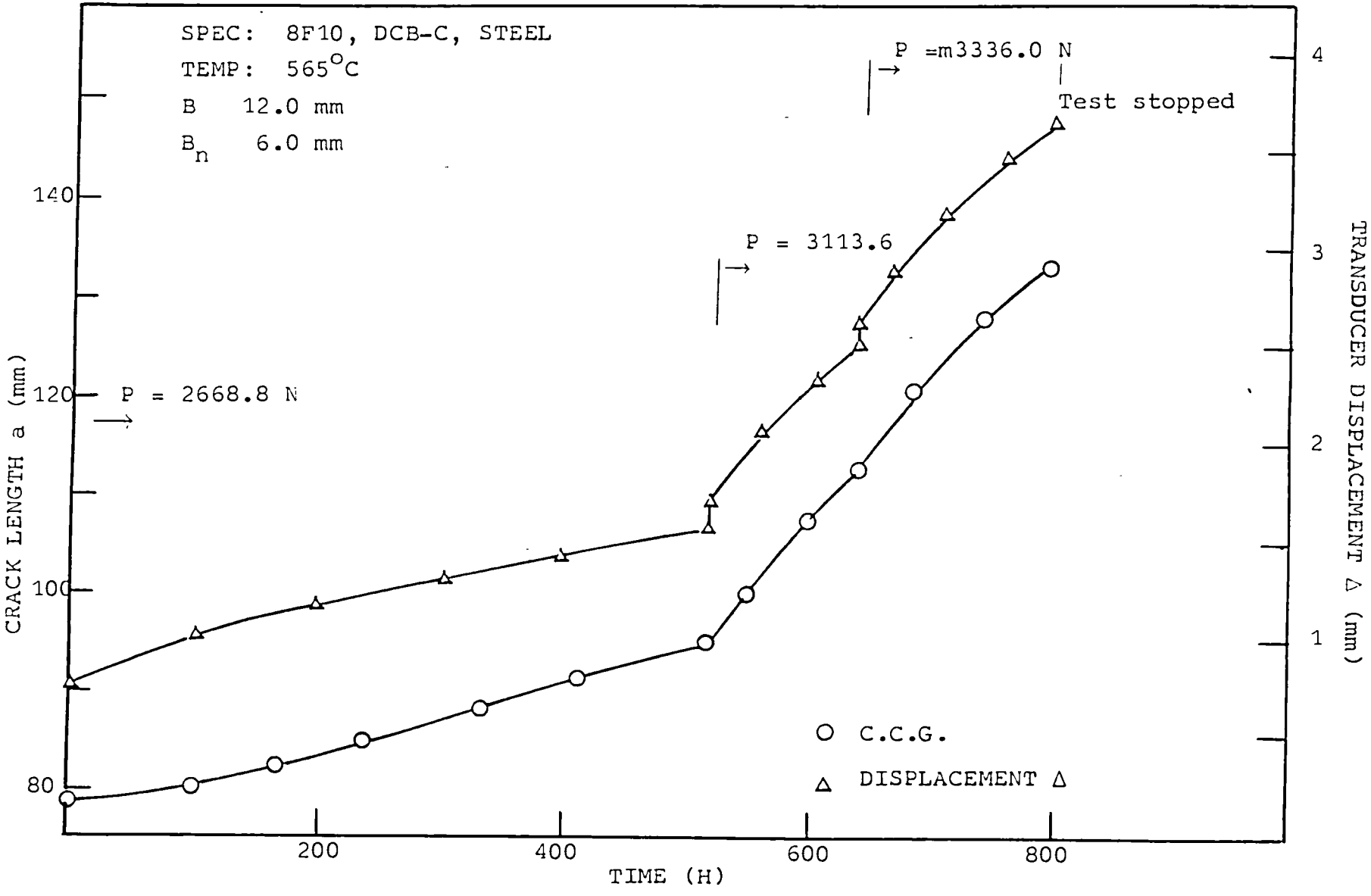

Figure (61): Effect of load increase on C.C.G. and displacement for a DCB-C, thin steel specimen

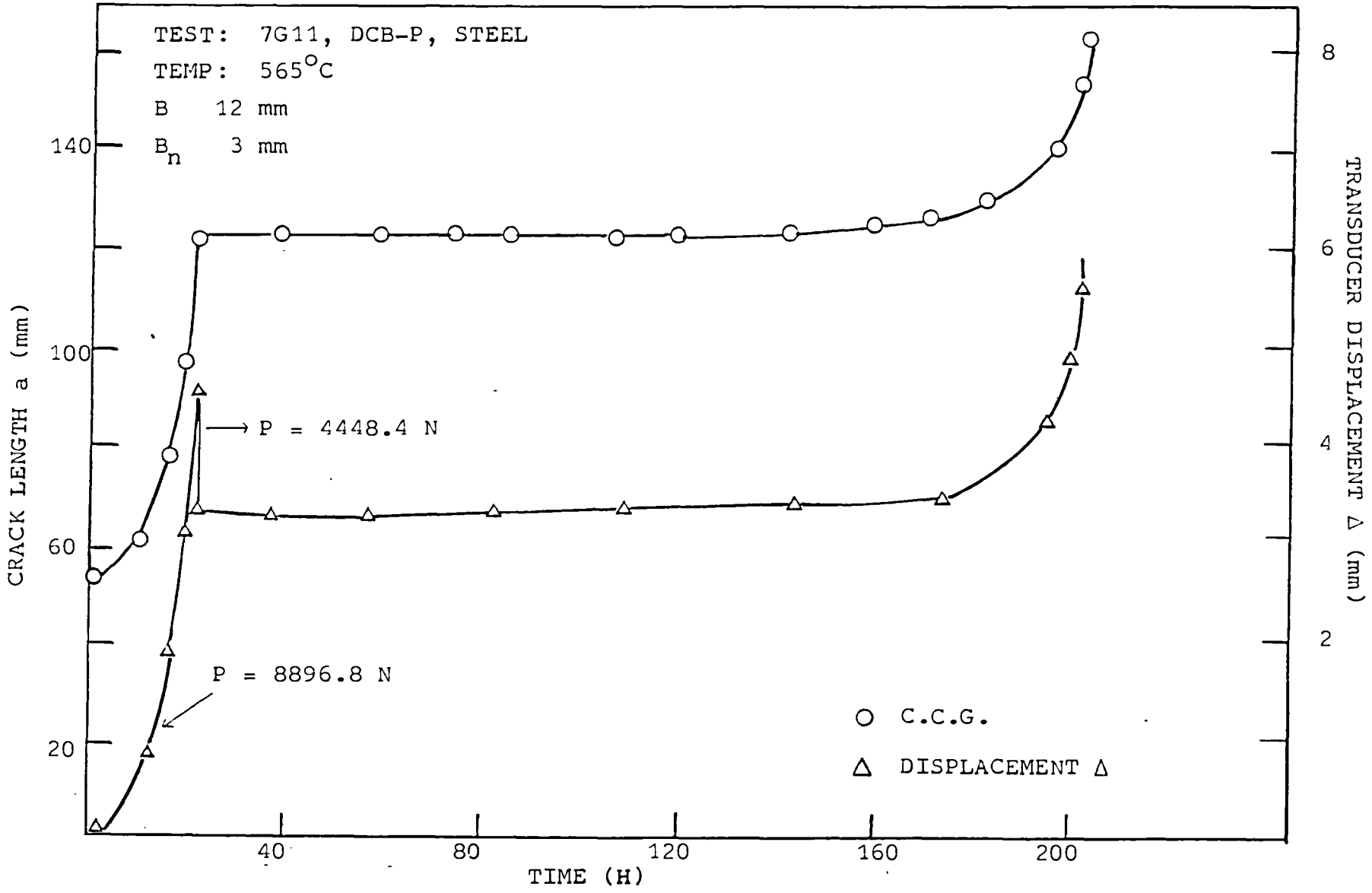

Figure (62): Effect of load change on C.C.G. and displacement of a thin DCB-P, steel specimen with B_n = 3.0 mm

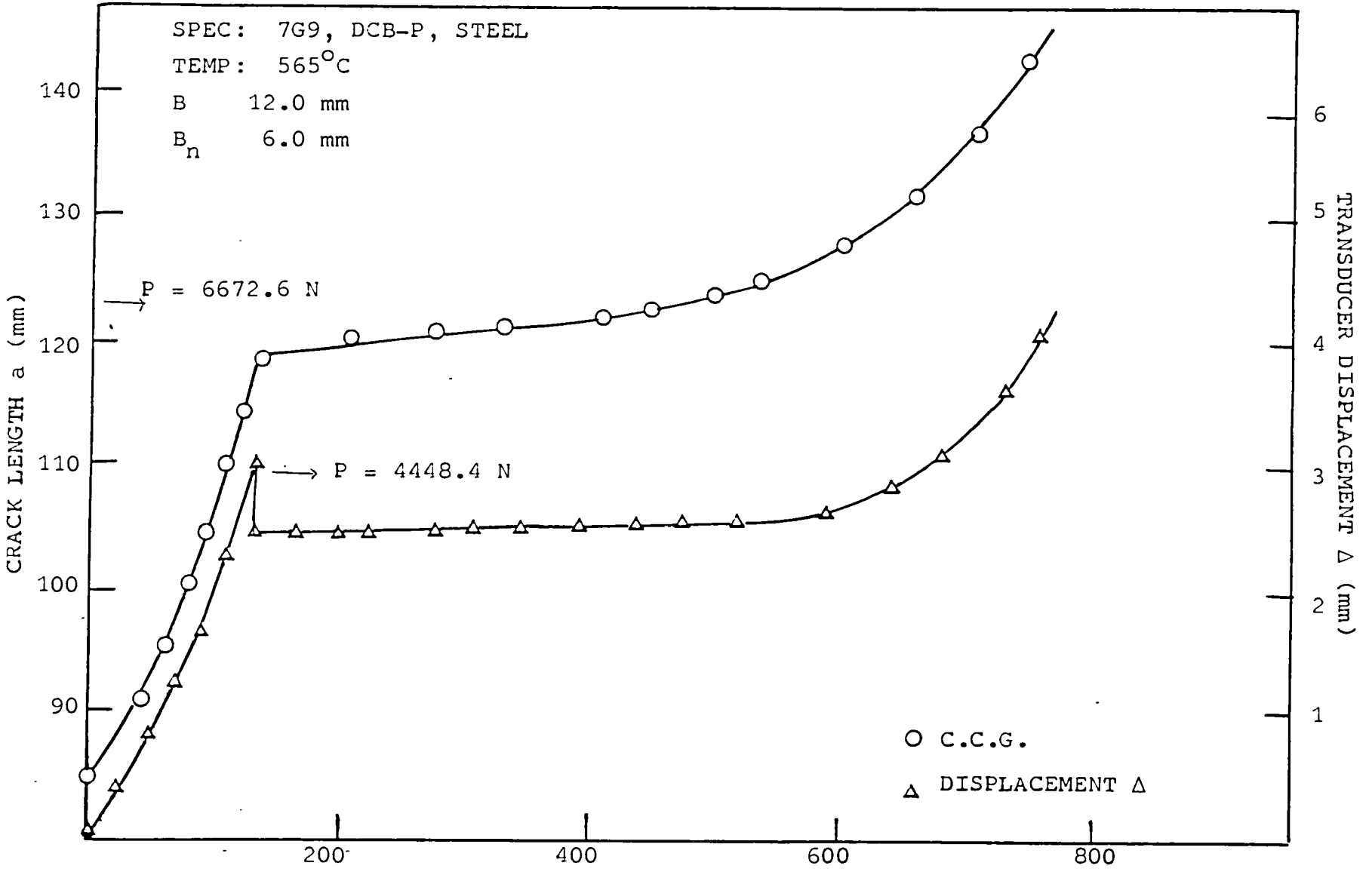

Figure (63): Effect of load change on C.C.G. and displacement of a thin DCB-P, steel specimen with B_n = 6.0 mm

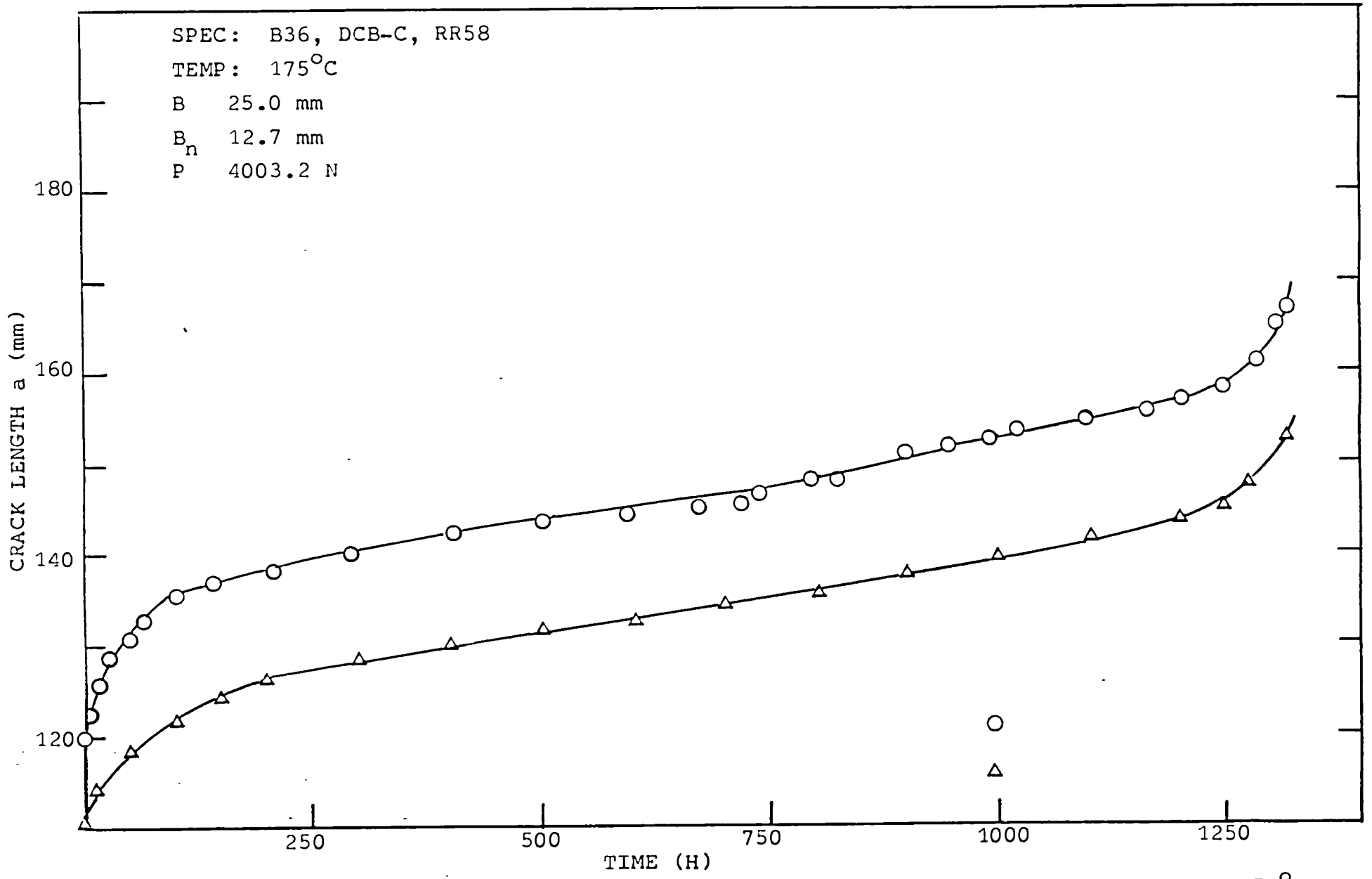

Figure (64): Typical C.C.G. and displacement versus time for DCB-C, RR58 tested at 175°C

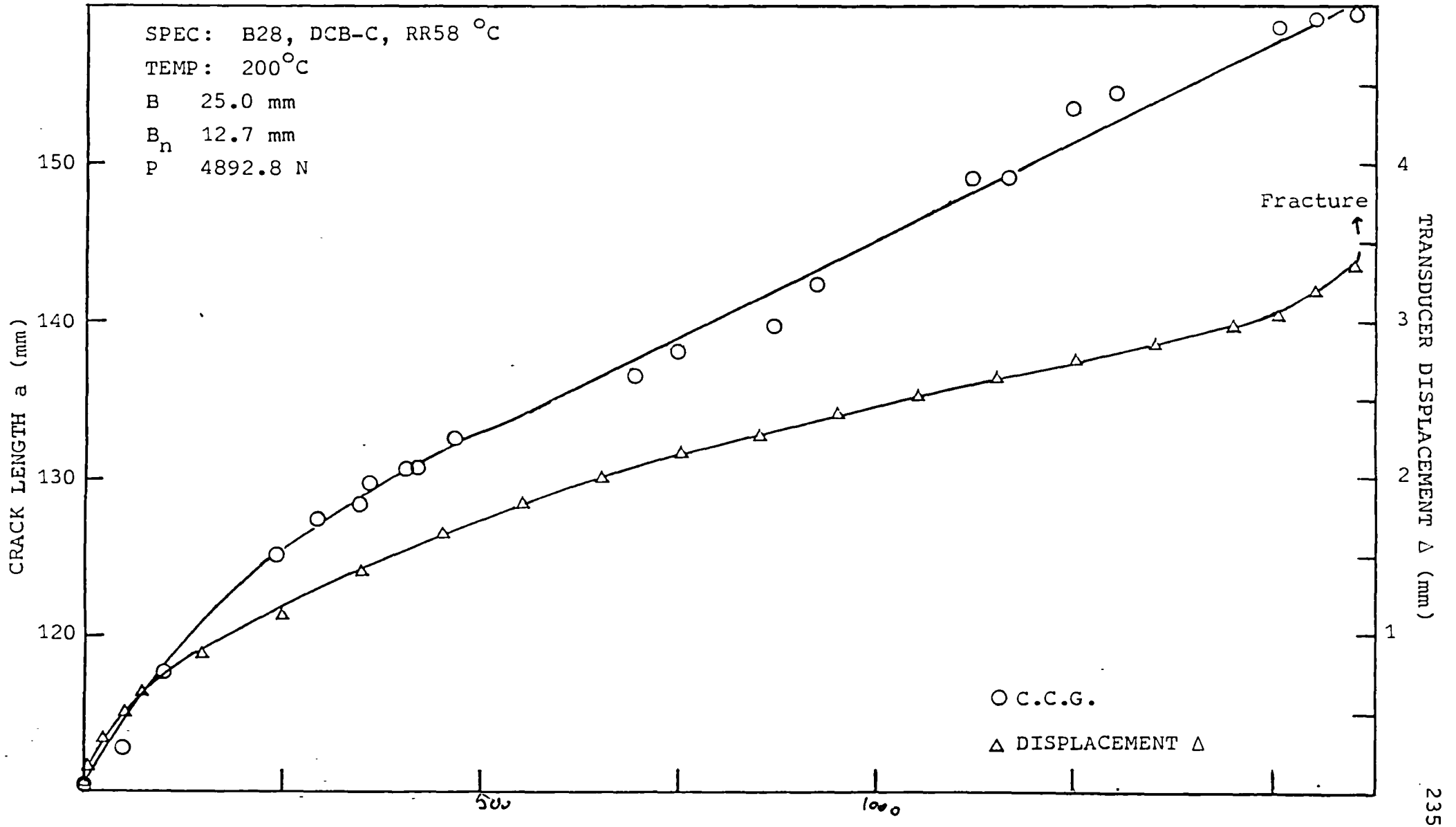

Figure (65): Typical C.C.G. and displacement versus time for DCB-C, RR58 tested at 200°C.

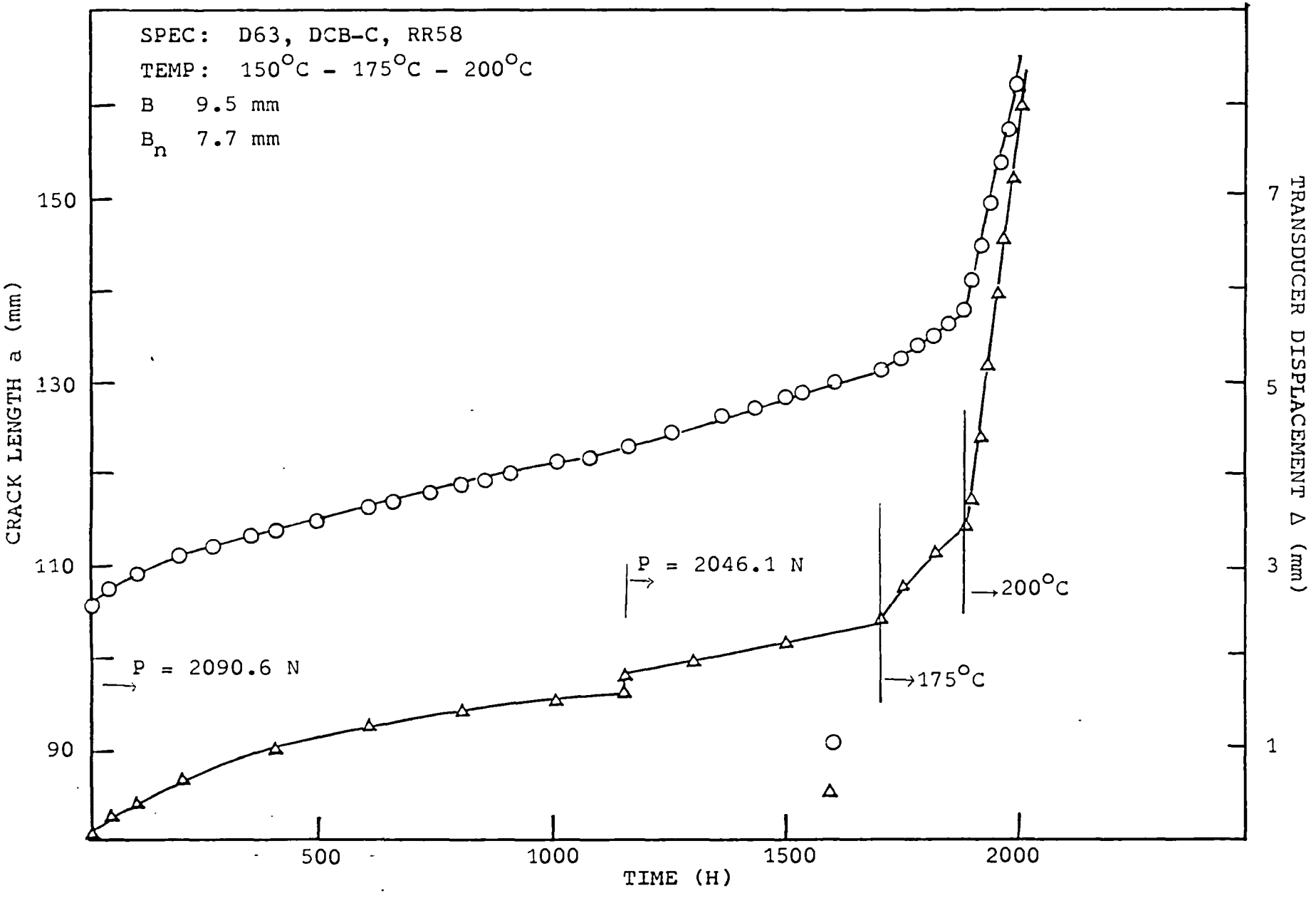

Figure (66): Effect of load and temperature change of the C.C.G. and displacement of a DCB-C, RR58 specimen

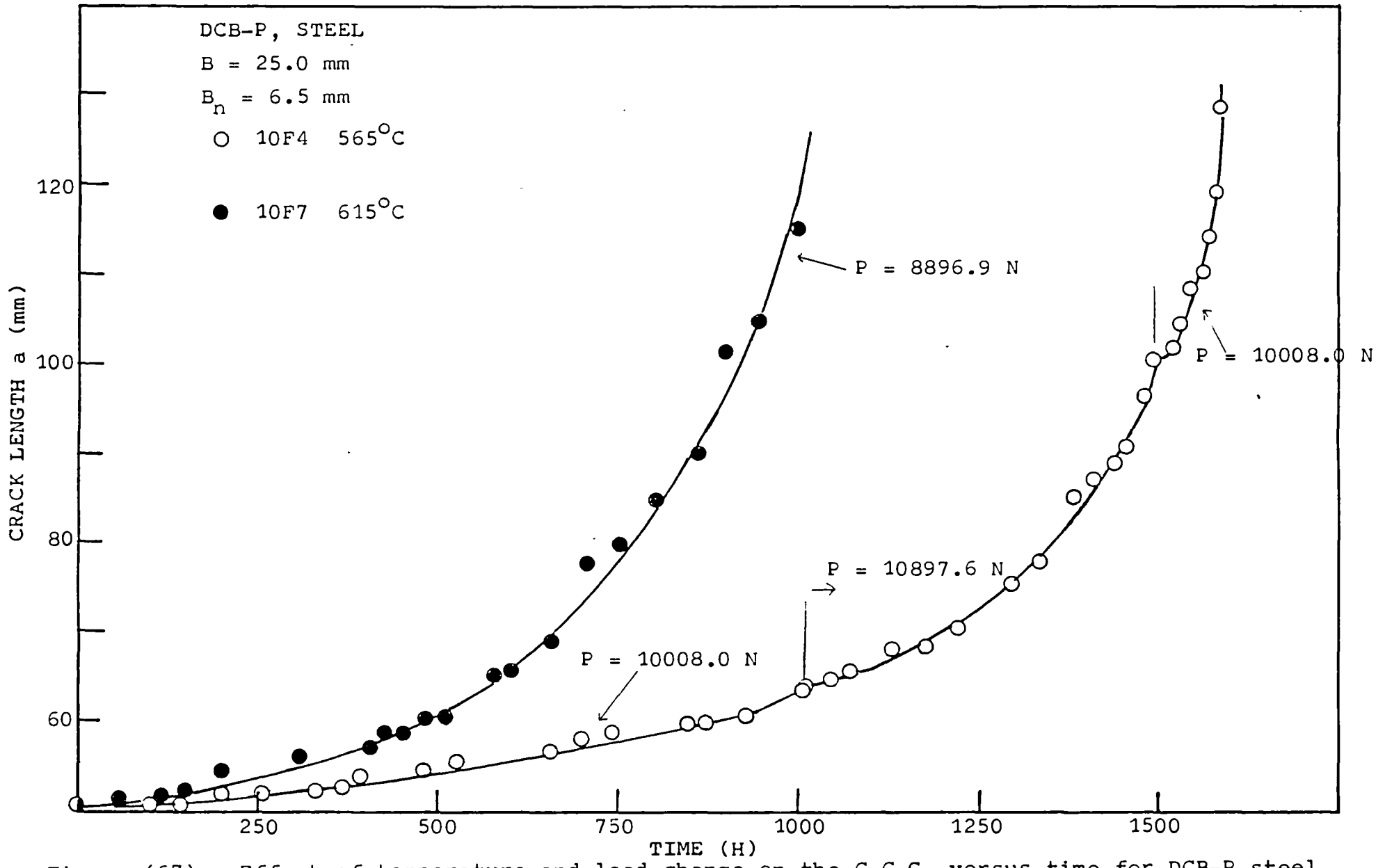

Figure (67): Effect of temperature and load change on the C.C.G. versus time for DCB-P steel specimens

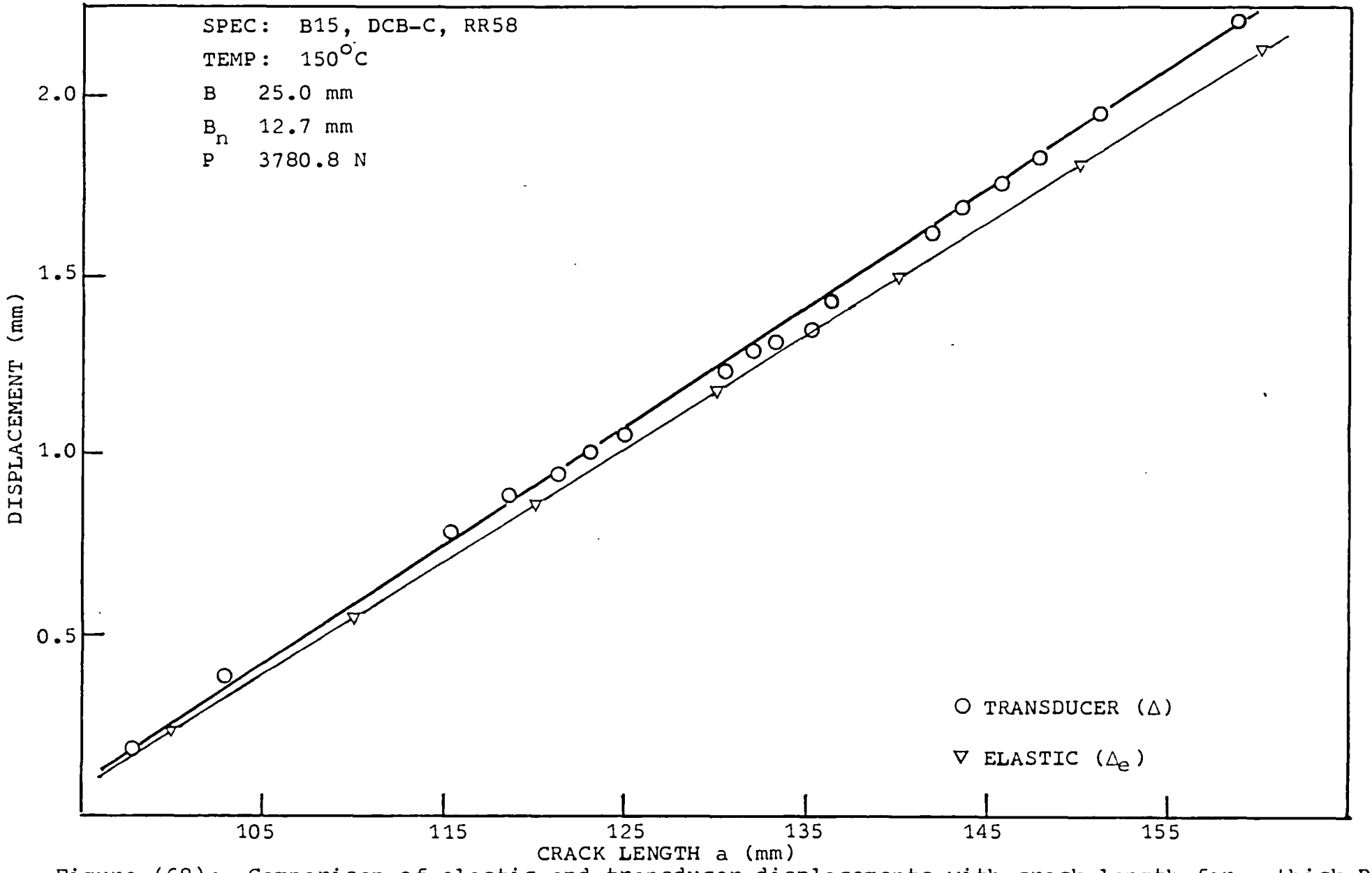

Figure (68): Comparison of elastic and transducer displacements with crack length for a thick DCB-C, RR58 specimen

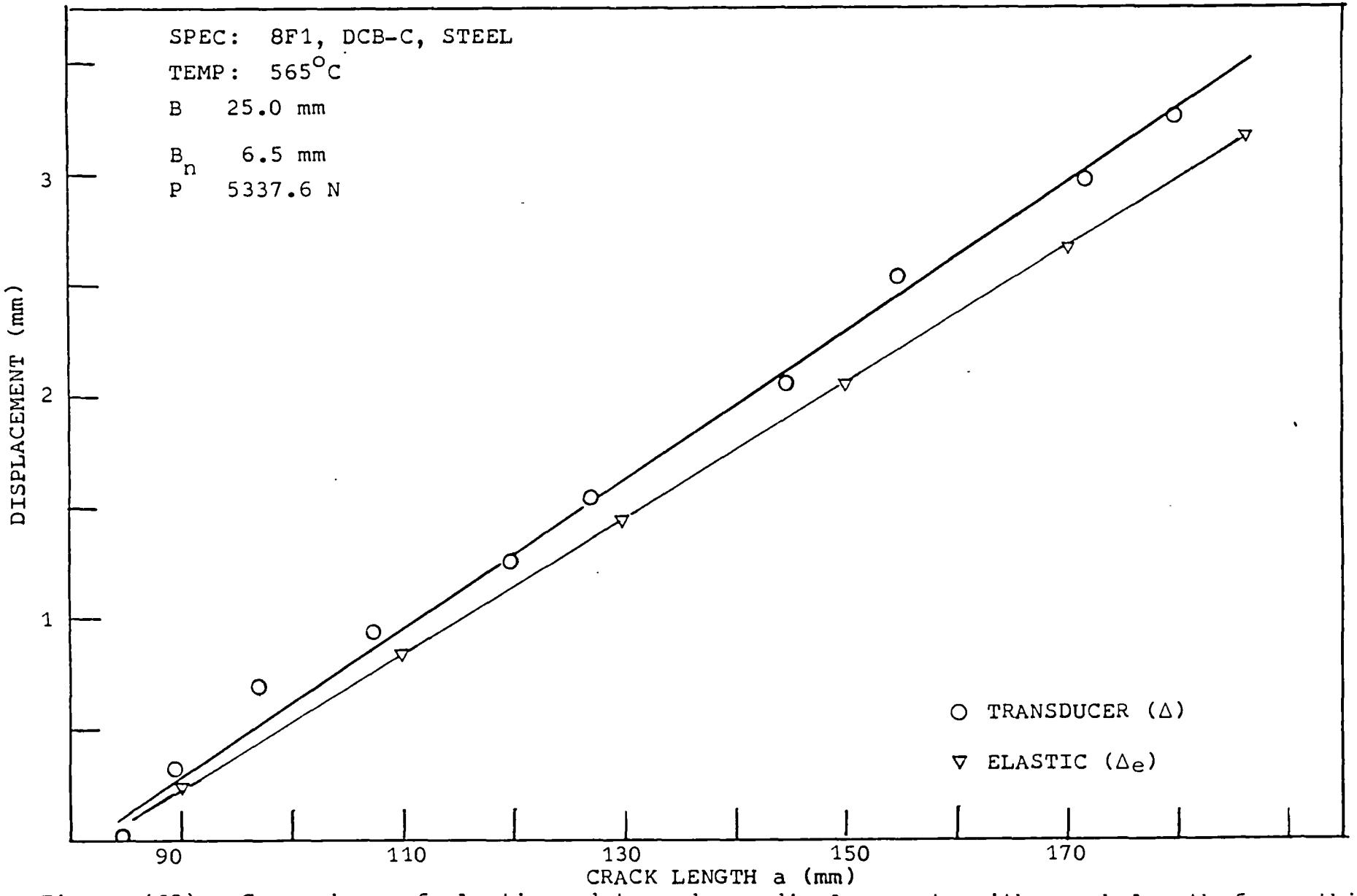

Figure (69): Comparison of elastic and transducer displacements with crack length for a thick DCB-C steel specimen

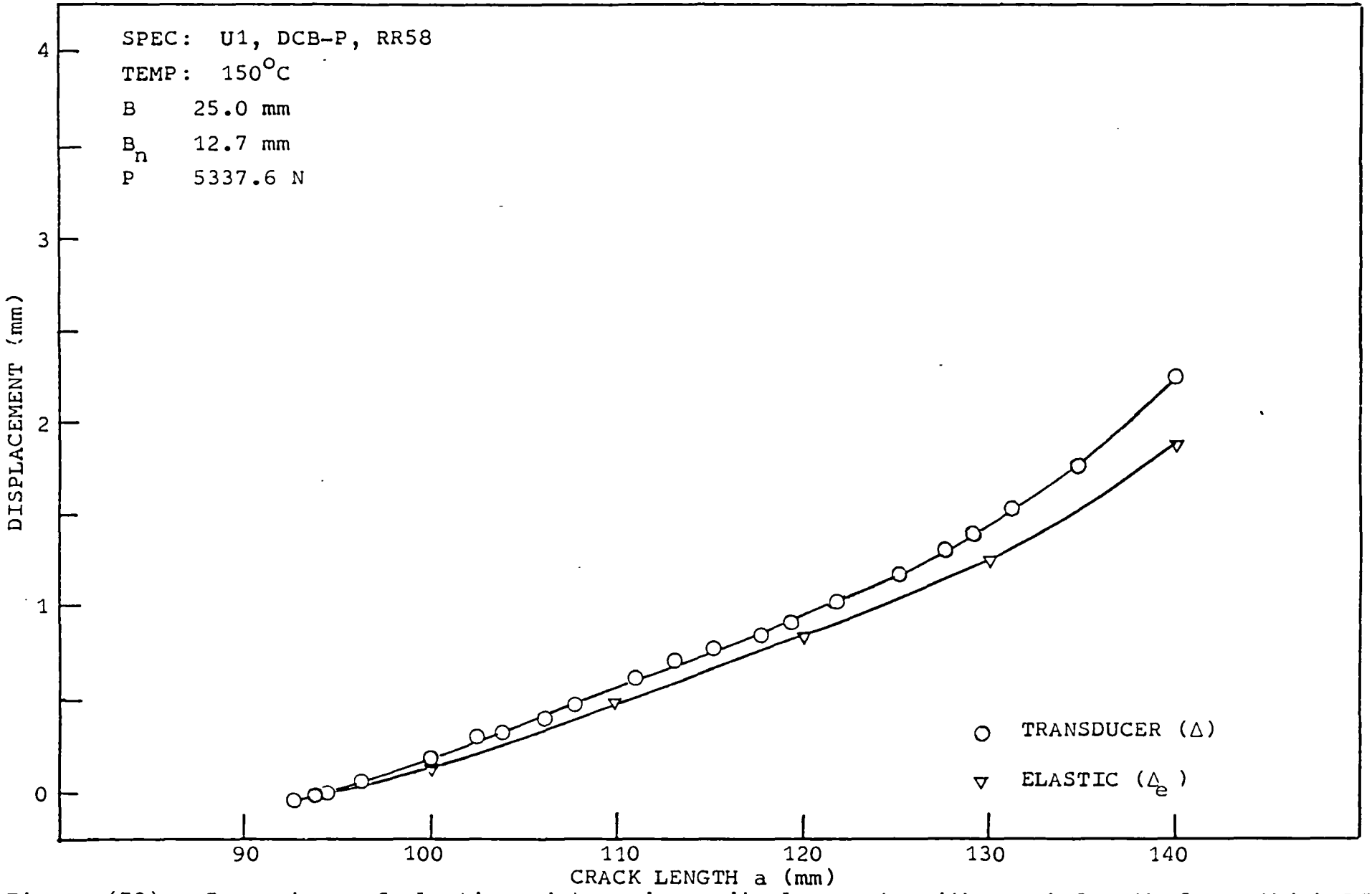

Figure (70): Comparison of elastic and transducer displacements with crack length for a thick DCB-P, RR58 specimen

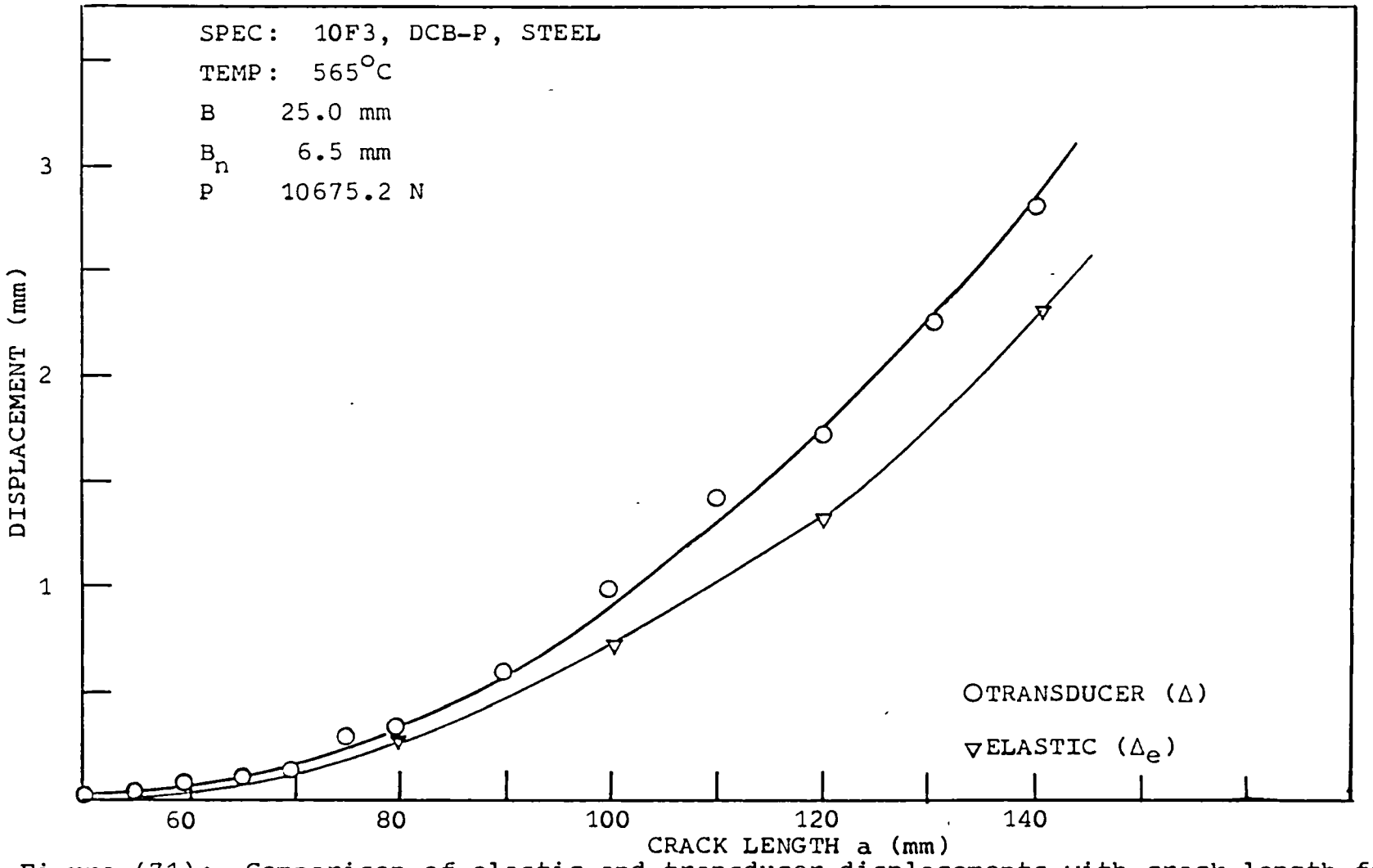

Figure (71): Comparison of elastic and transducer displacements with crack length for a thick DCB-P steel specimen

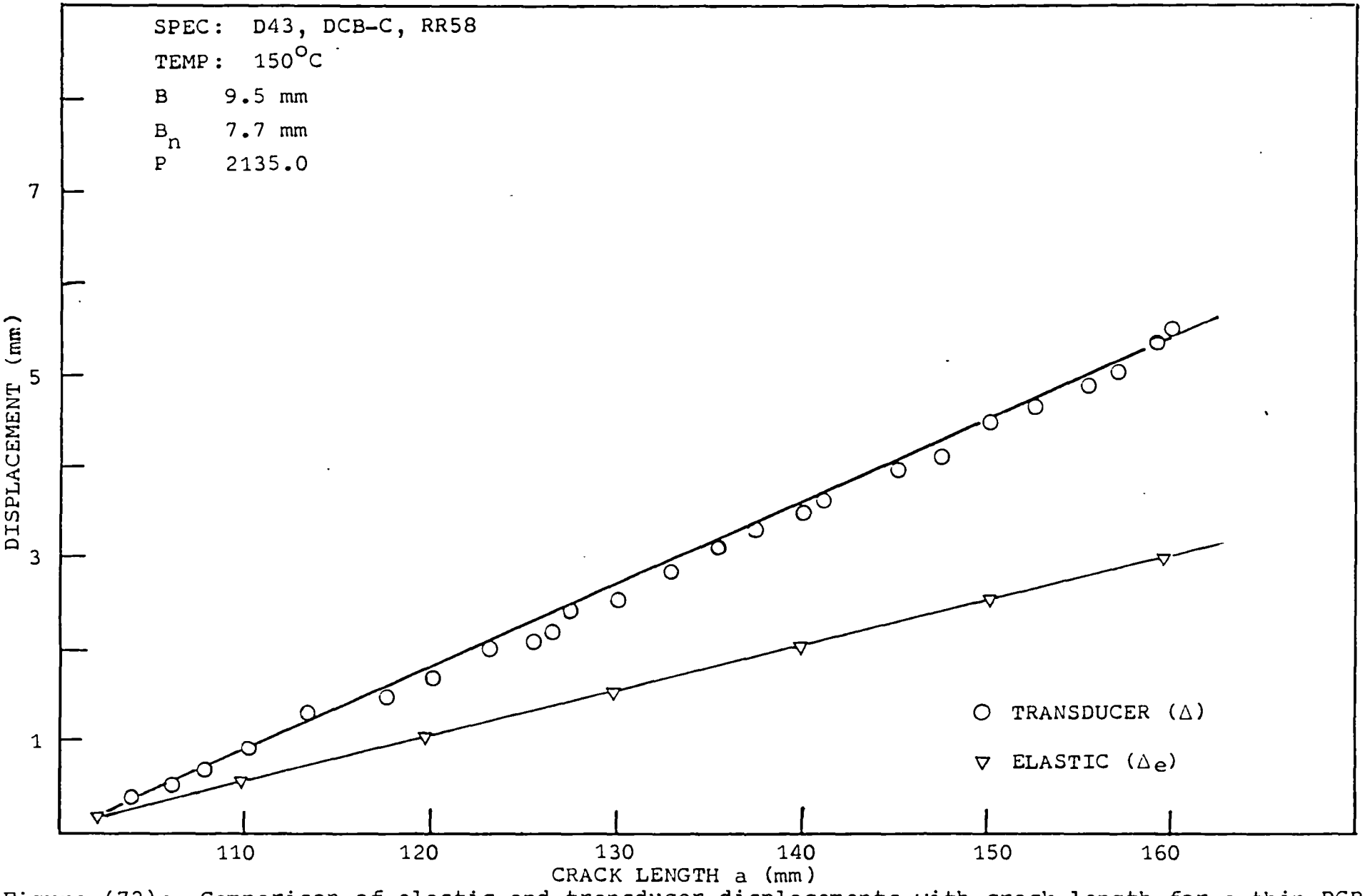

Figure (72): Comparison of elastic and transducer displacements with crack length for a thin DCB-C RR58 specimen

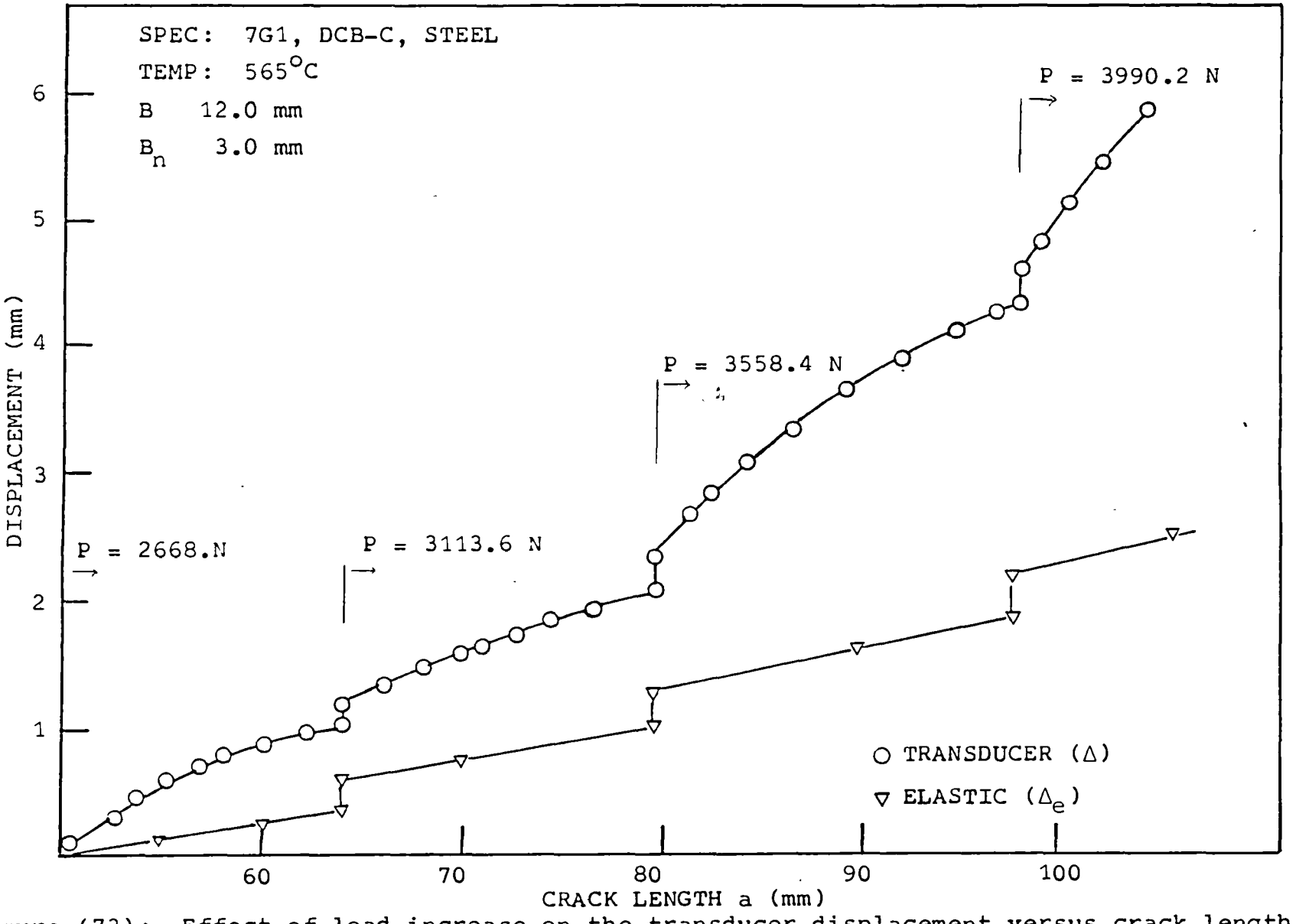

Figure (73): Effect of load increase on the transducer displacement versus crack length for a thin DCB-C, steel specimen with B_n = 3 mm

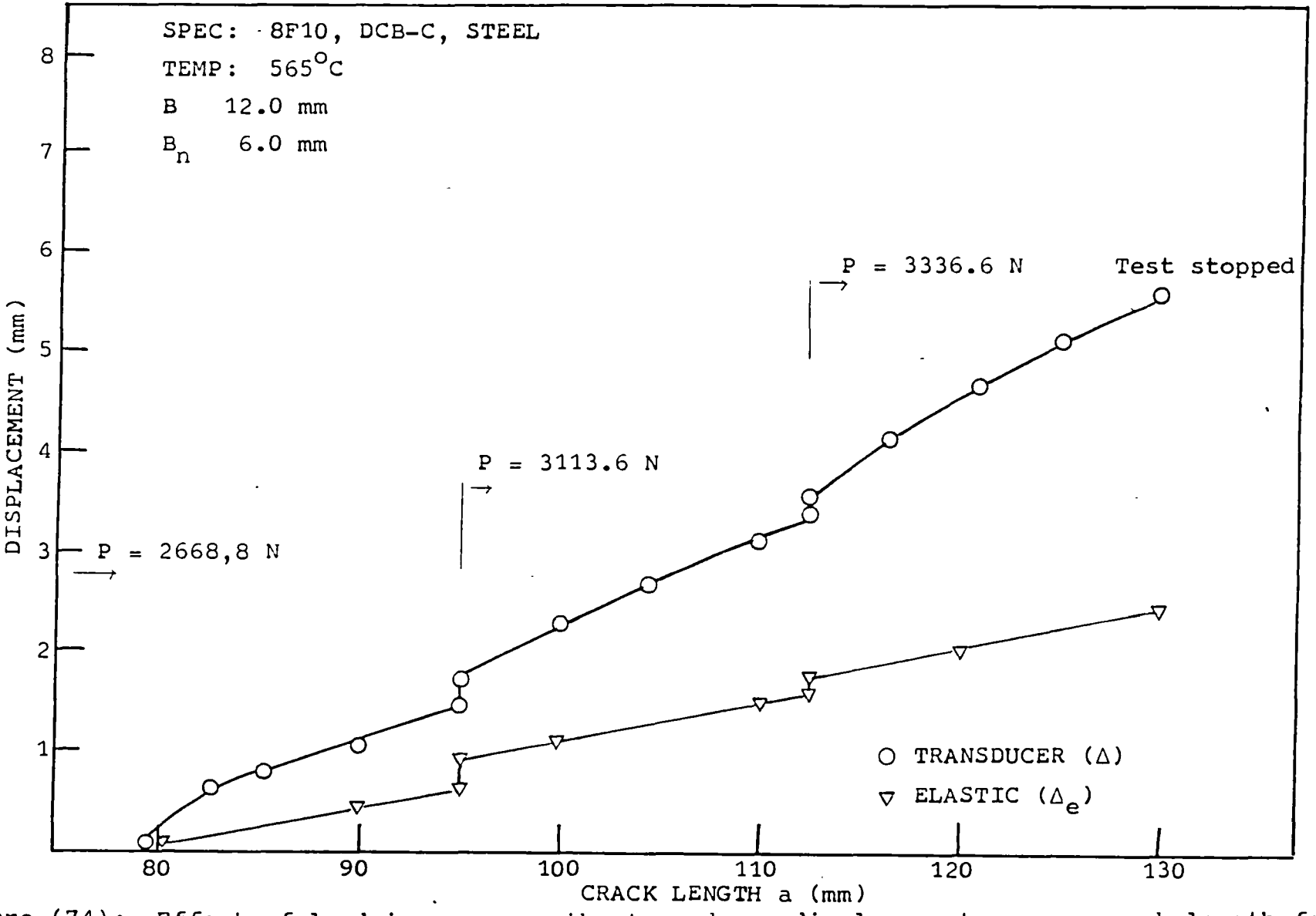

Figure (74): Effect of load increase on the transducer displacement versus crack length for a thin DCB-C steel specimen with B_n = 6 mm

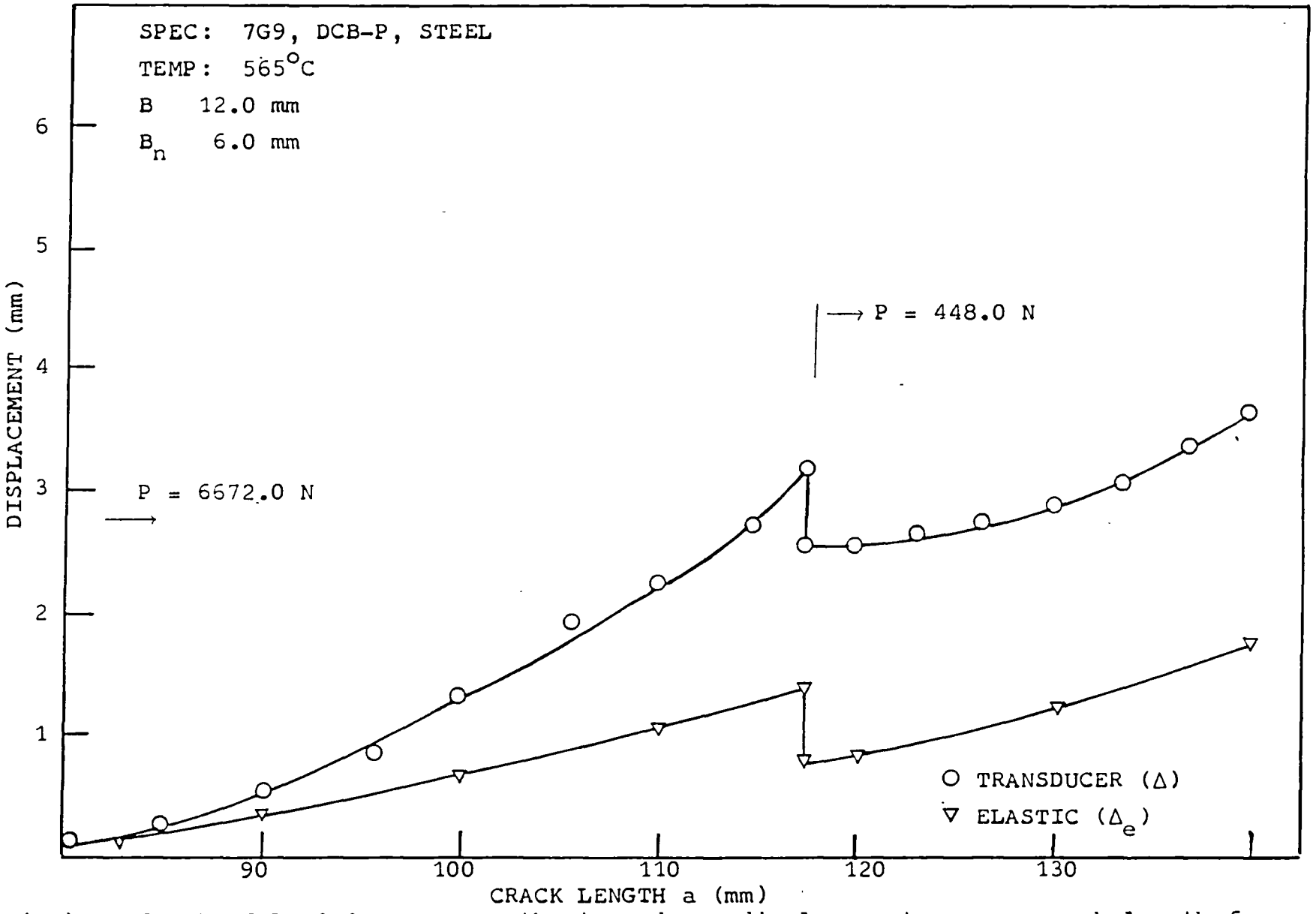

Figure (75): Effect of load decrease on the transducer displacement versus crack length for a thin DCB-P steel specimen with B_n = 6 mm

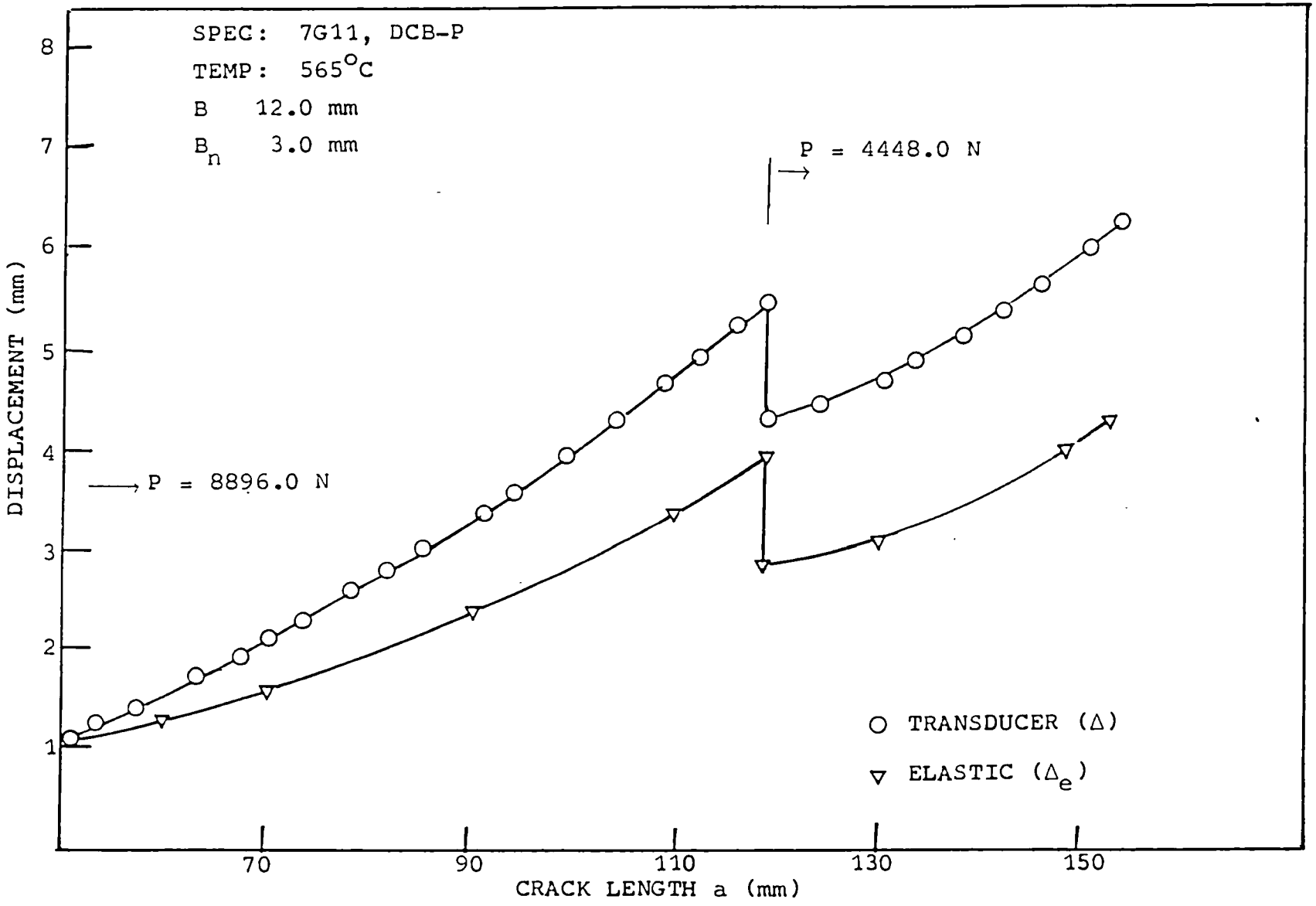

Figure (76): Effect of load decrease on the transducer displacement versus crack length for a thin DCB-P steel specimen with B_n = 3 mm

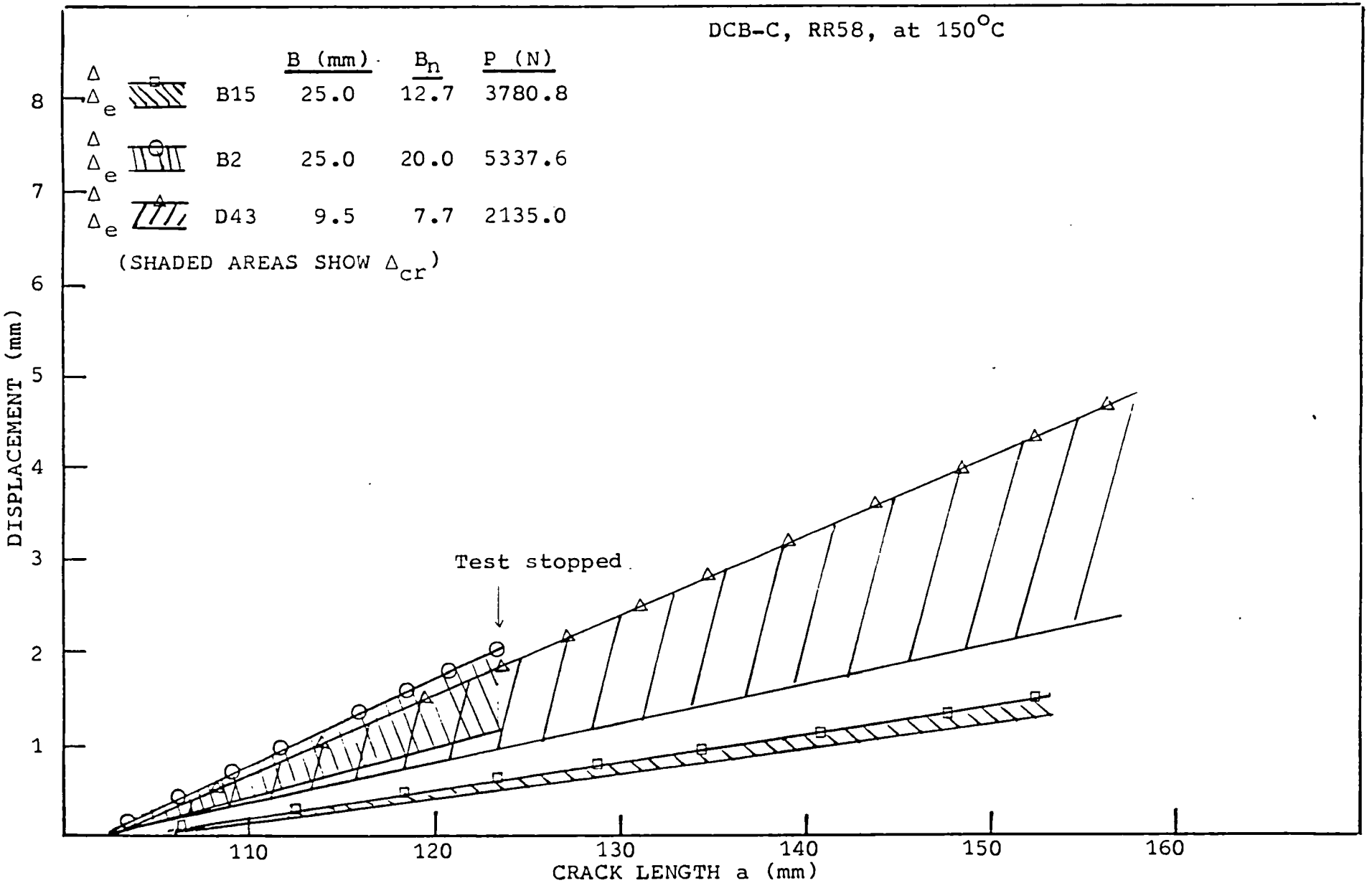

Figure (77): Extent of creep displacement (Δ_c) with crack length for different thickness and side grooving of DCB-C, RR58 tested at 150°C.

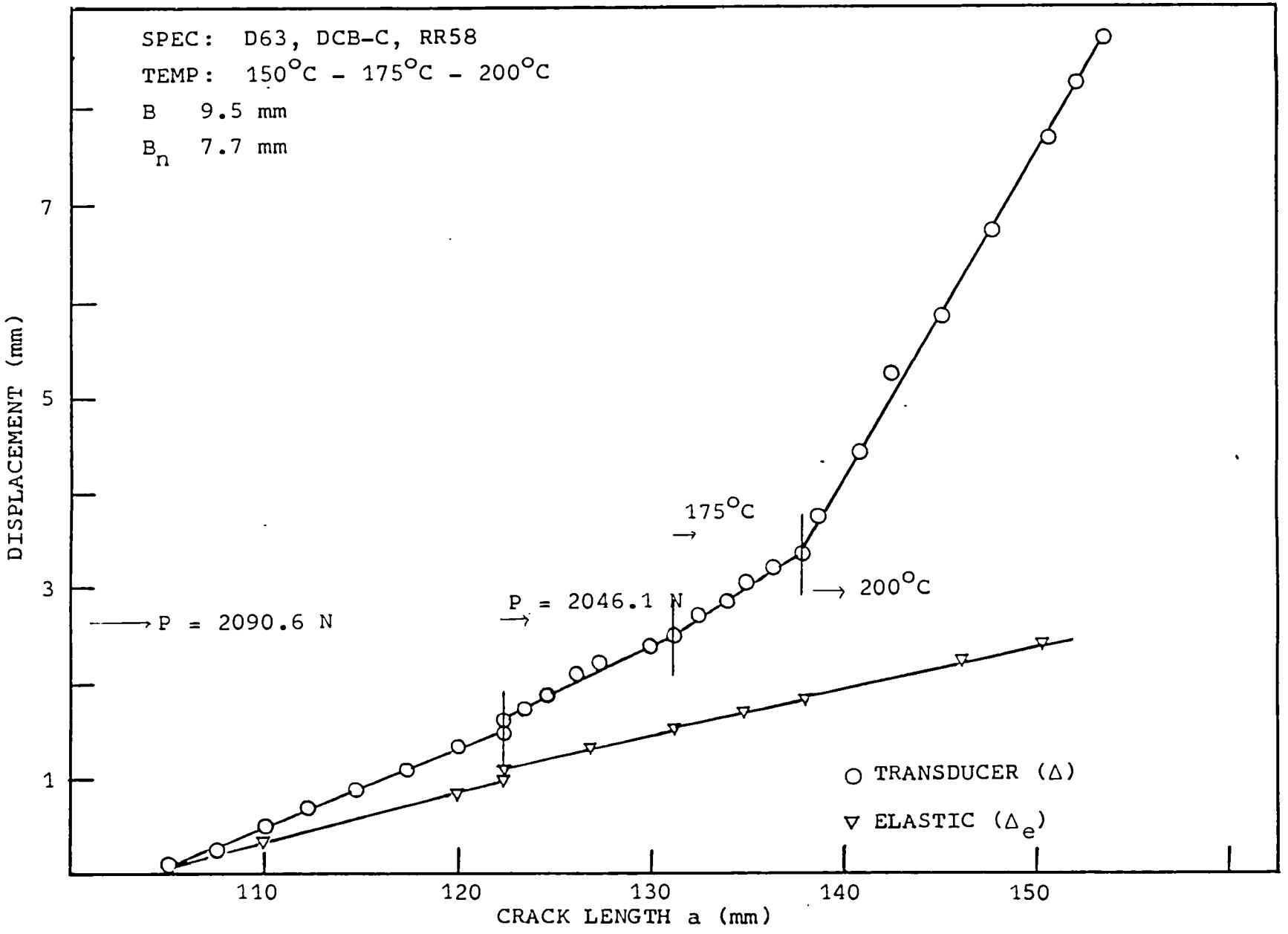

Figure (78): Effect of load and temperature increase on displacement versus crack length for a DCB-C, RR58

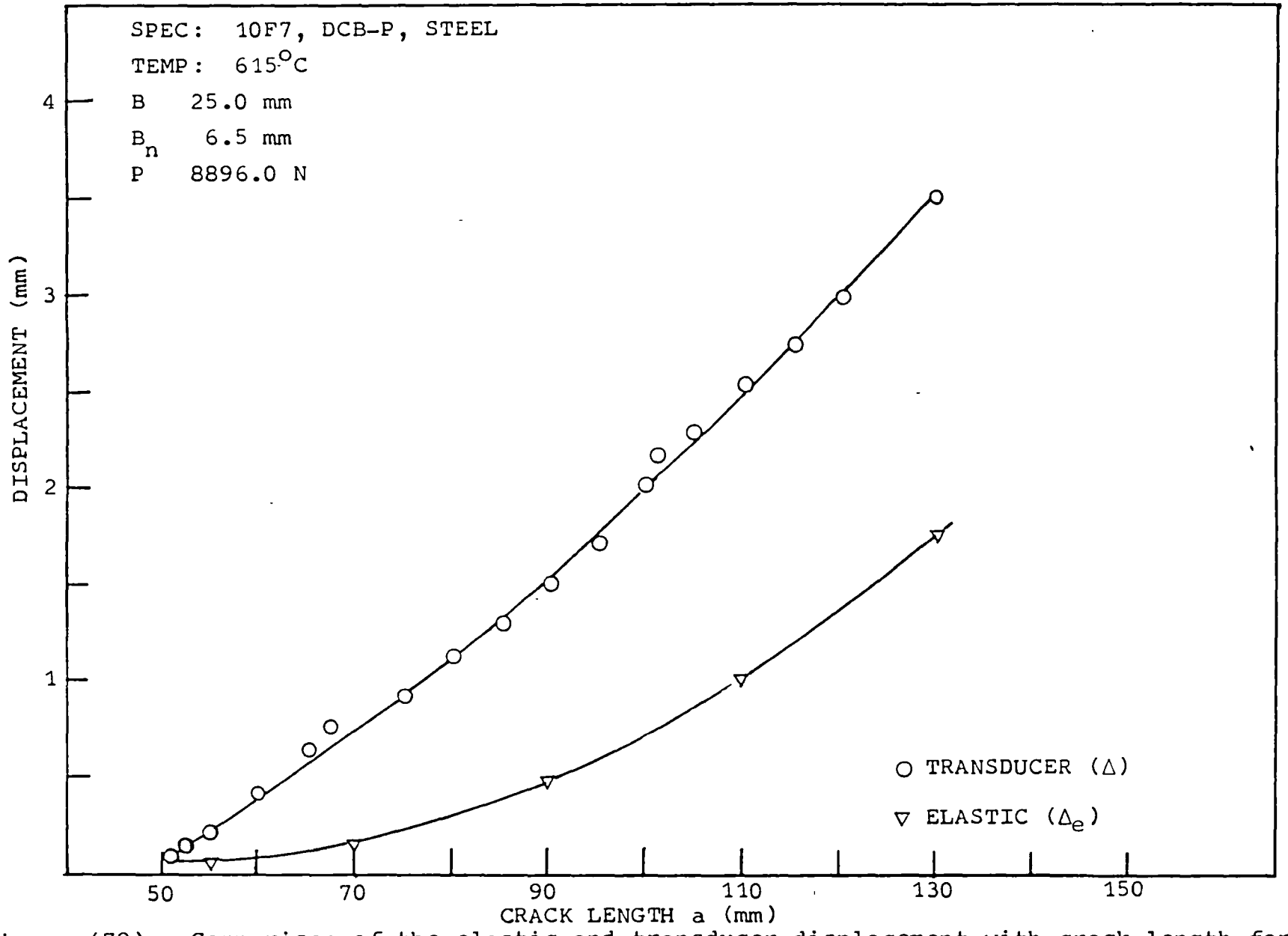

Figure (79): Comparison of the elastic and transducer displacement with crack length for a DCB-P, steel specimen tested at 615°C.

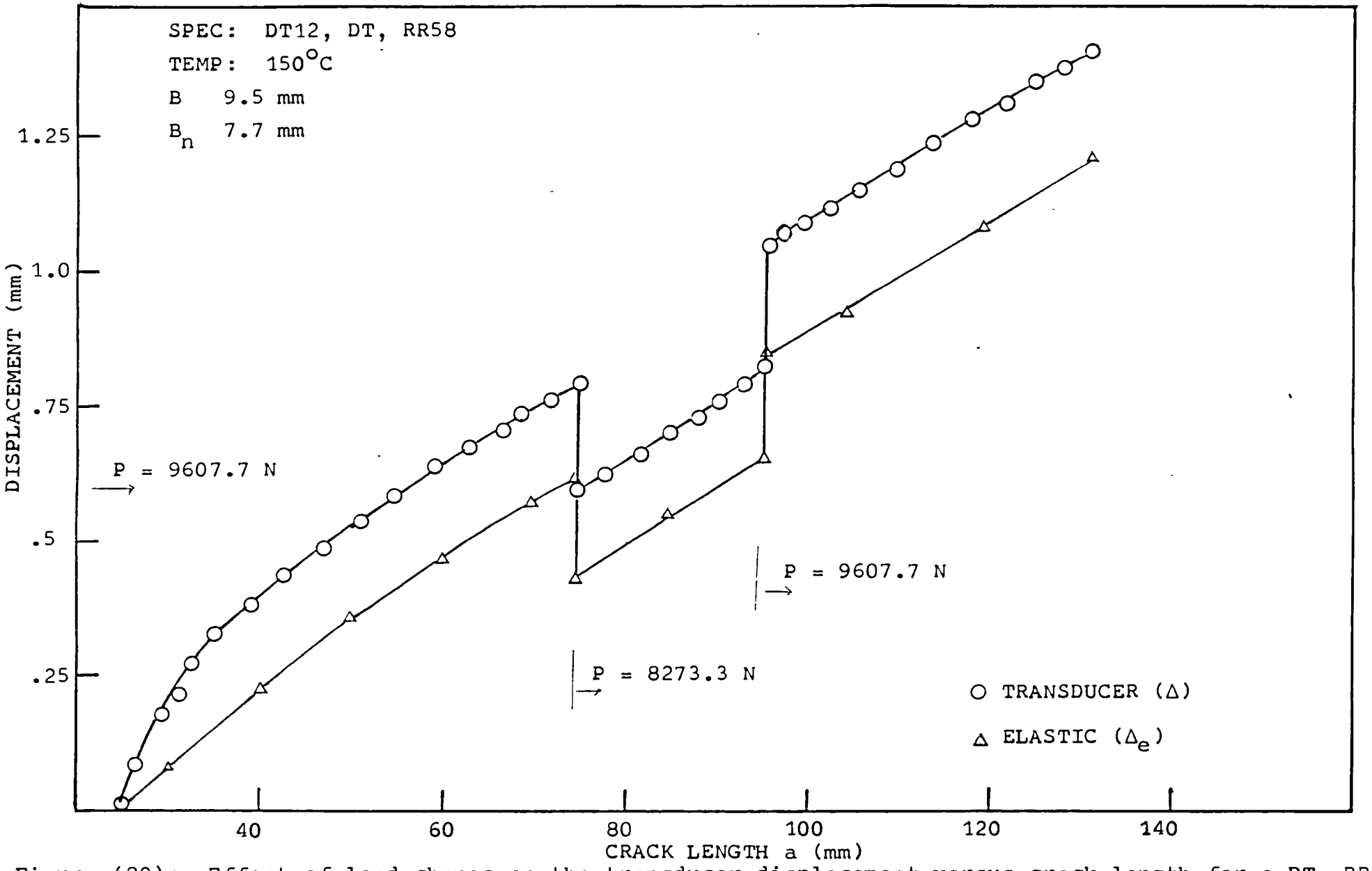

Figure (80): Effect of load change on the transducer displacement versus crack length for a DT, RR58 specimen tested at 150°C

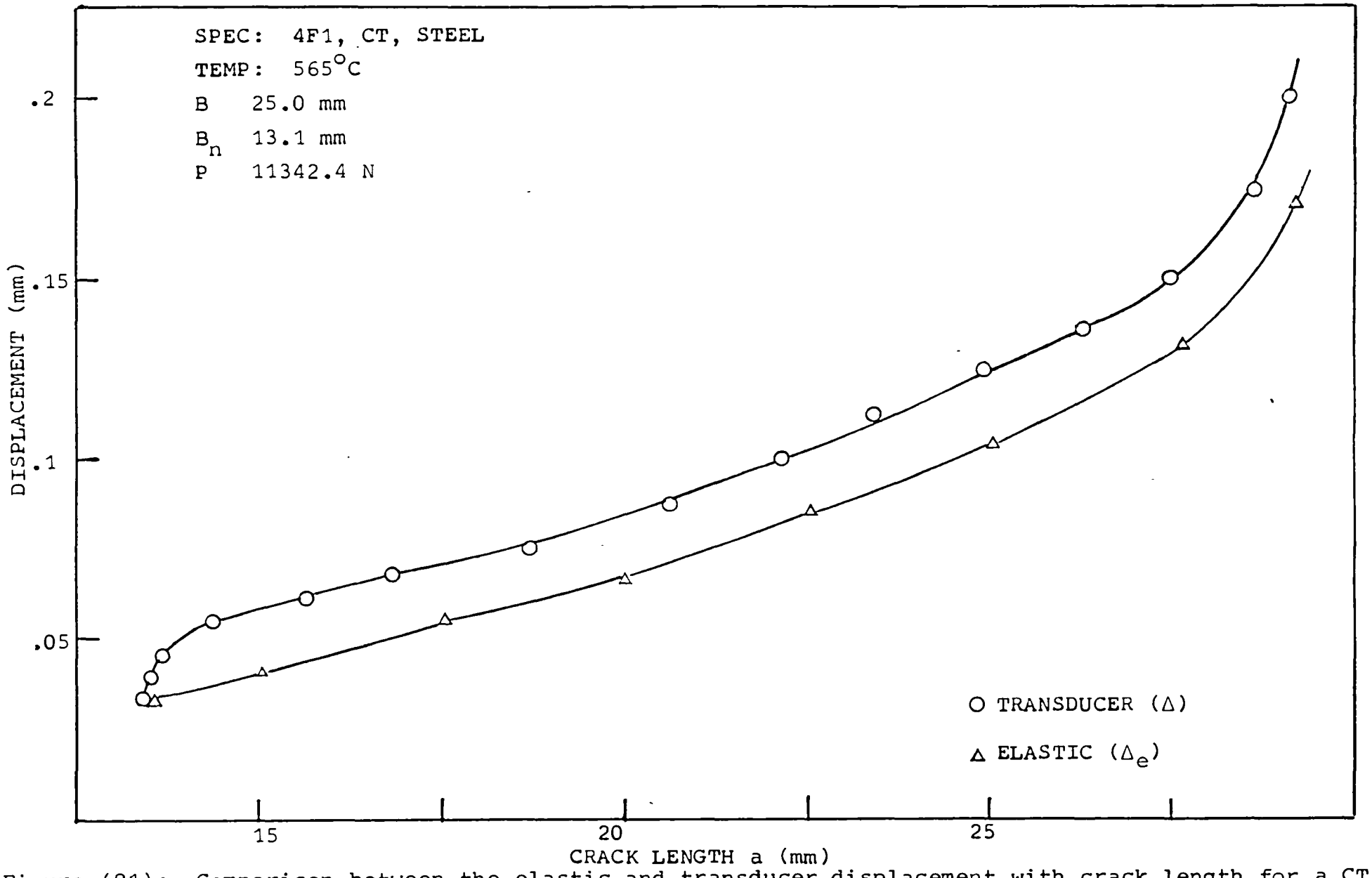

Figure (81): Comparison between the elastic and transducer displacement with crack length for a CT, steel specimen

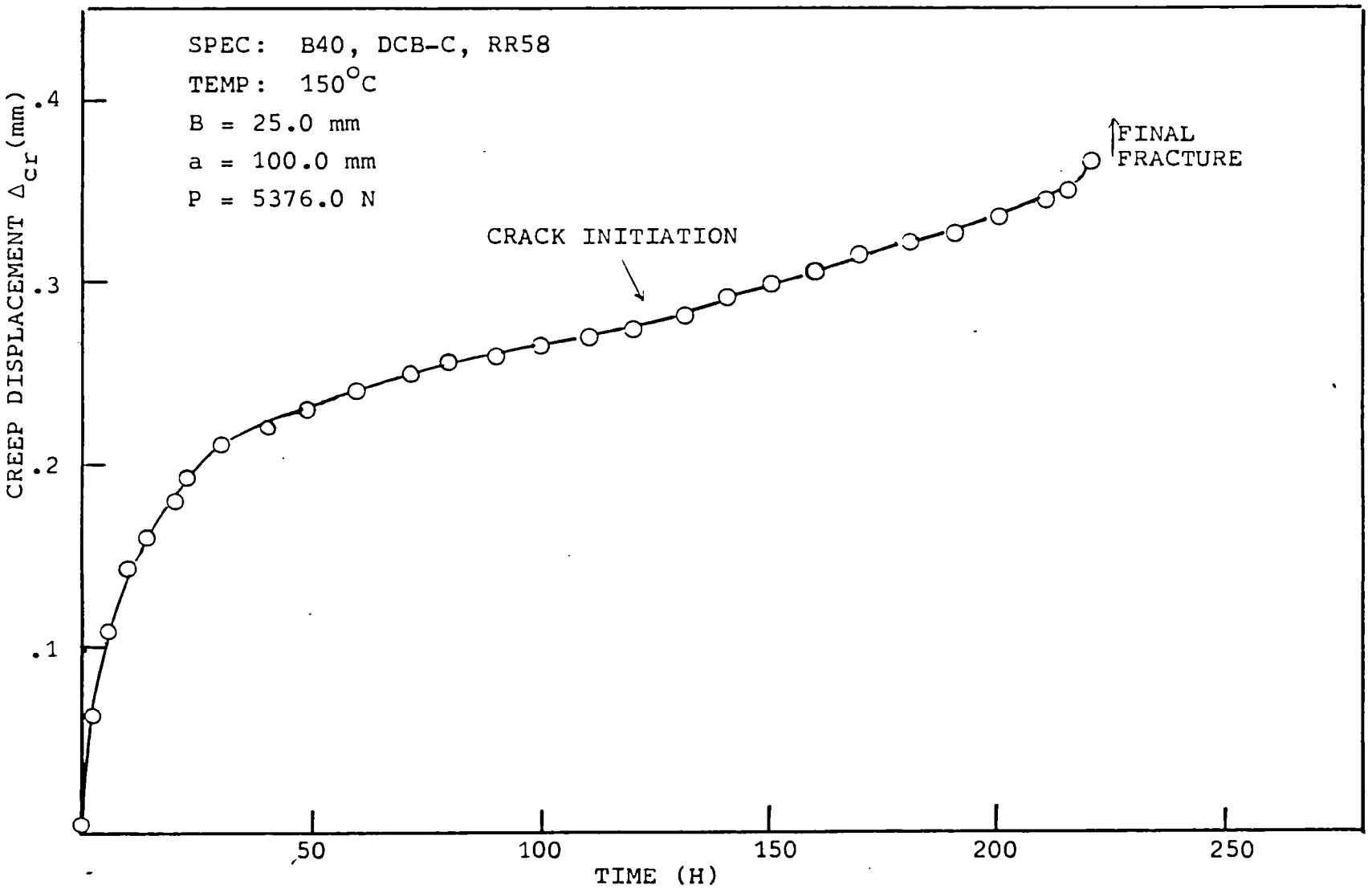

Figure (82): Creep displacement of the arms versus time for a thick DCB-C, RR58 specimen

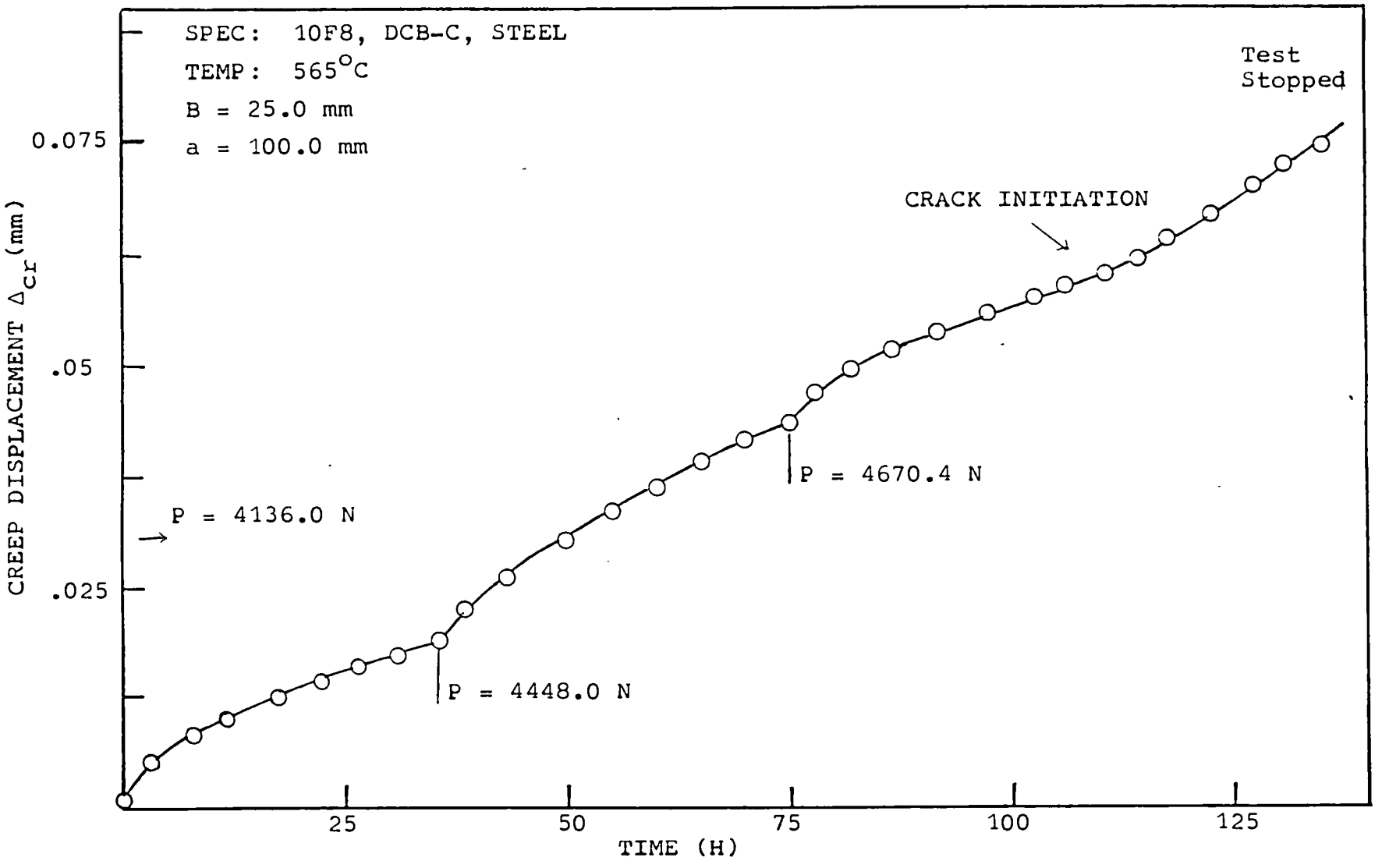

Figure (83): Effect of load increase on the creep displacement of the arms of a DCB-C steel tested at 565°C

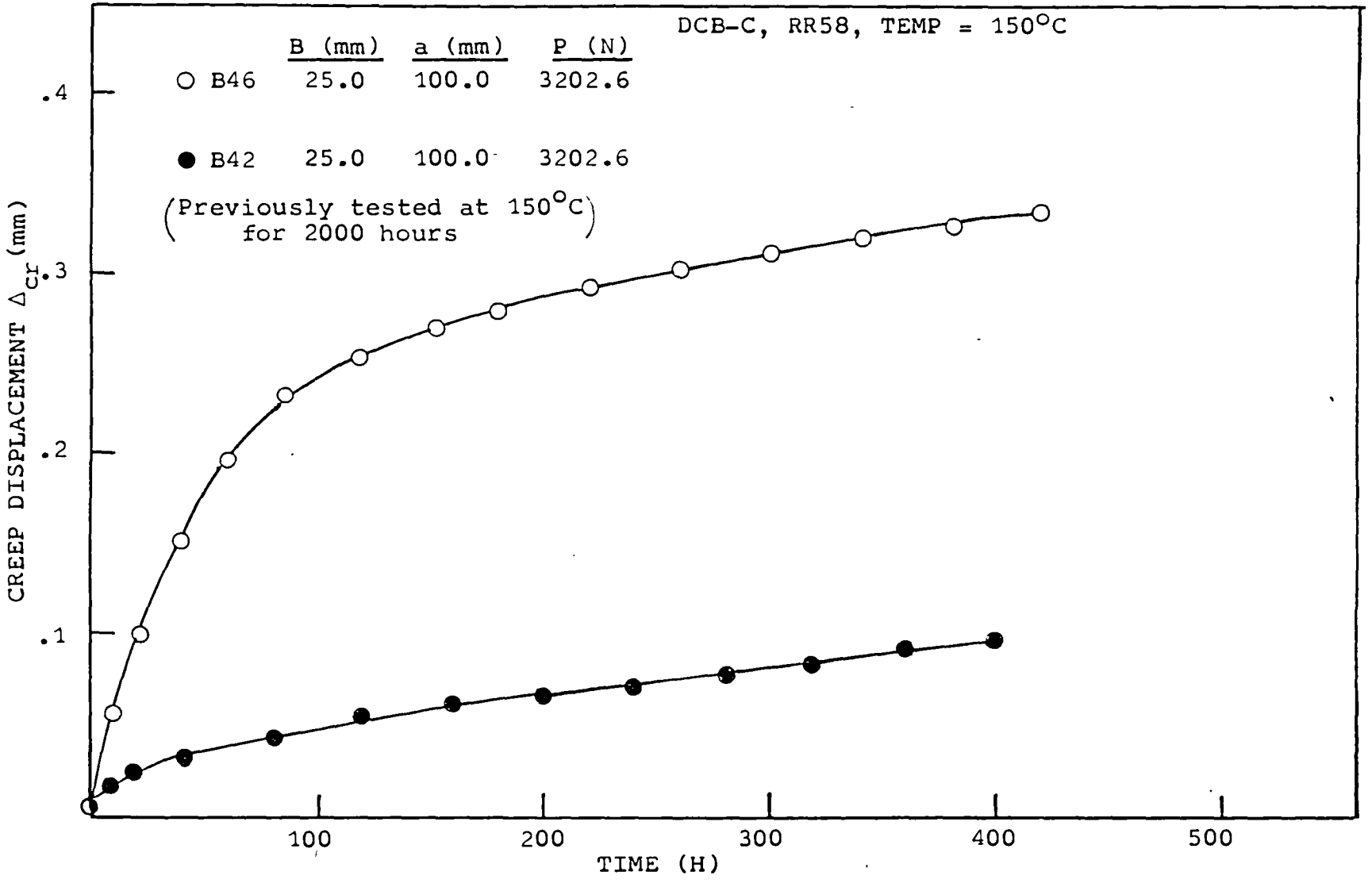

Figure (84): Effect of Previous load and overaging history on the creep displacement of the DCB-C, RR58

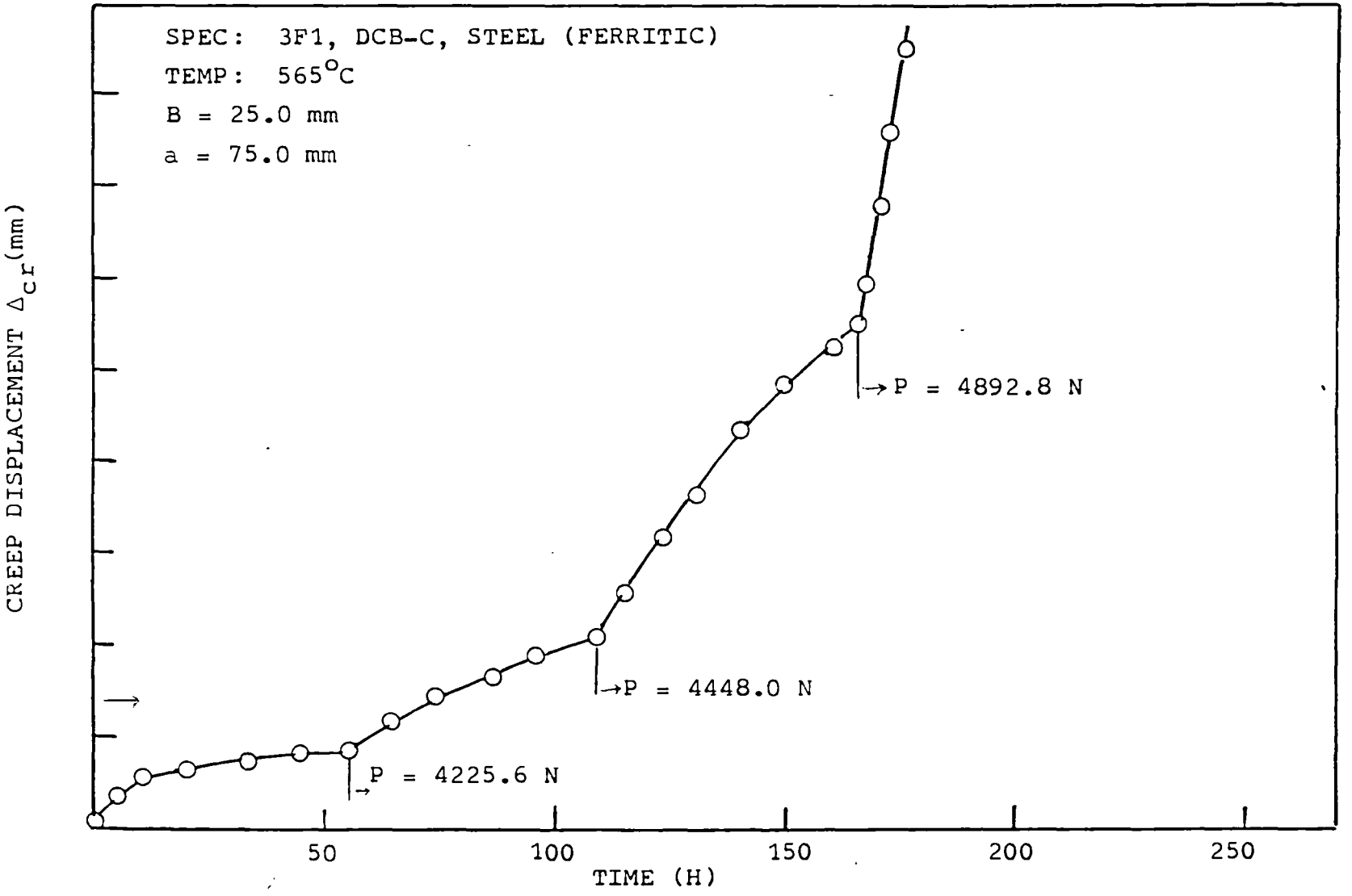

Figure (85): Creep displacement versus time for a DCB-C steel in the normalized ferritic condition

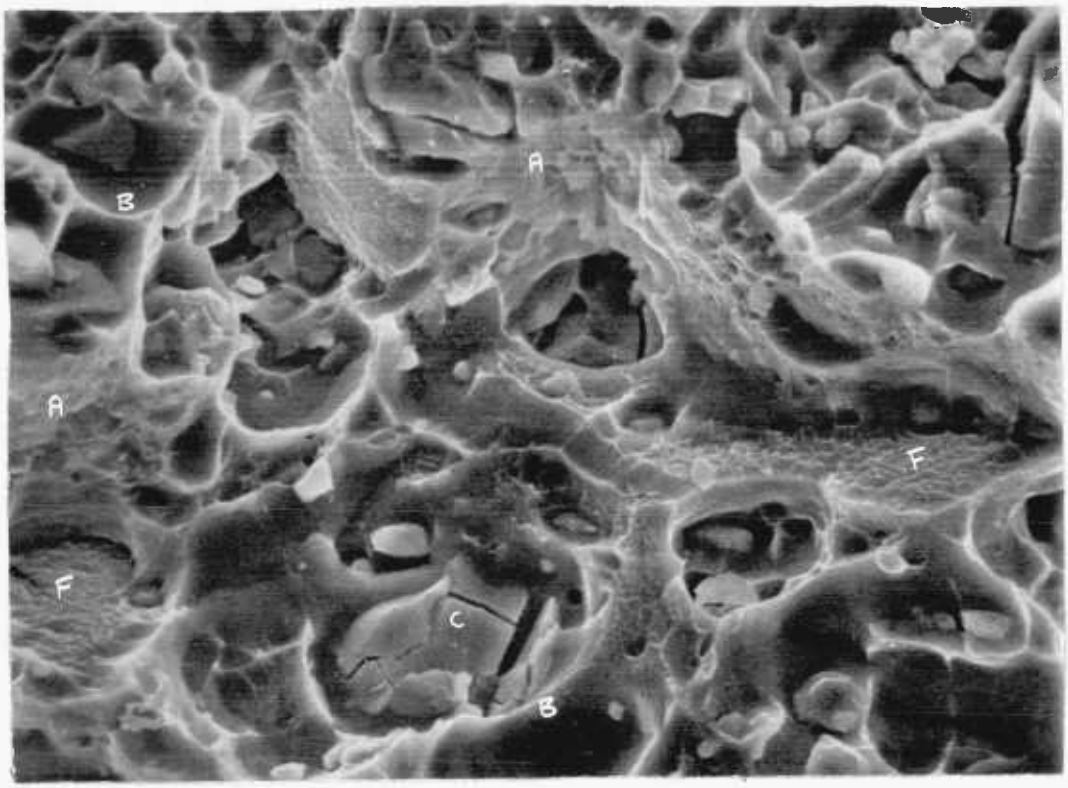

Figure (86): Fracture surface of RR58 precracked at room temperature (A) Ductile tearing, (B) Large dimples, (C) Intermetallic particles, (D) Fine dimples, (F) Grain boundary fracture. (Mag x1100)

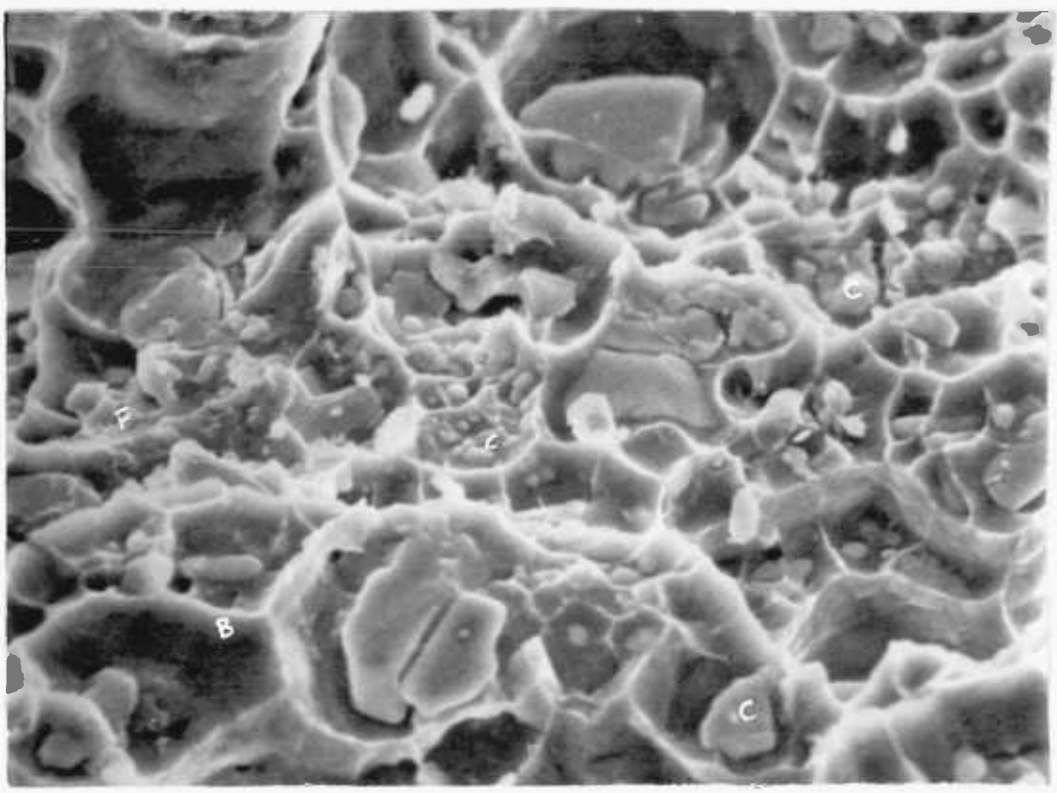

Figure (87): Fracture surface of RR58 creep cracked at 150°C. (A) Ductile tearing, (B) Large dimples, (C) Intermetallic particles, (D) Fine dimples, (F) Grain boundary fracture (Mag x1100)

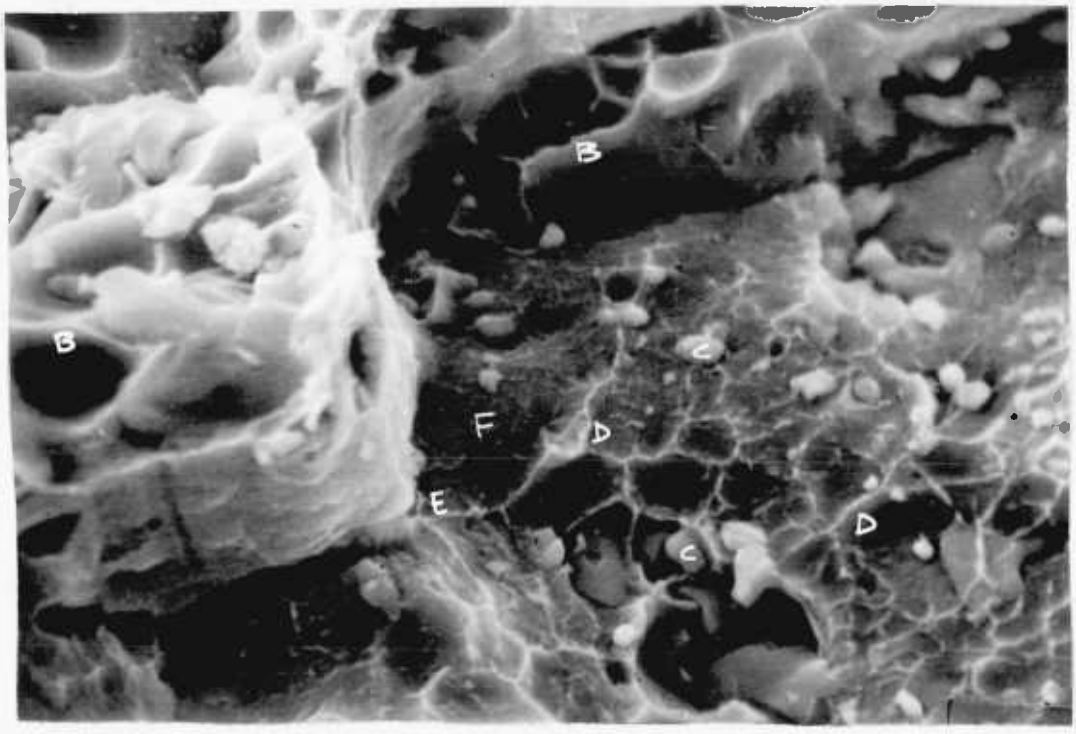

Figure (88): Fracture surface of RR58 Creep cracked at 150°C showing the ductile grain boundary fracture
(B) Large dimples, (C) Intermetallic particles, (D) Fine dimples, (E) Triple point, (F) Grain boundary fracture
(Mag x1800)

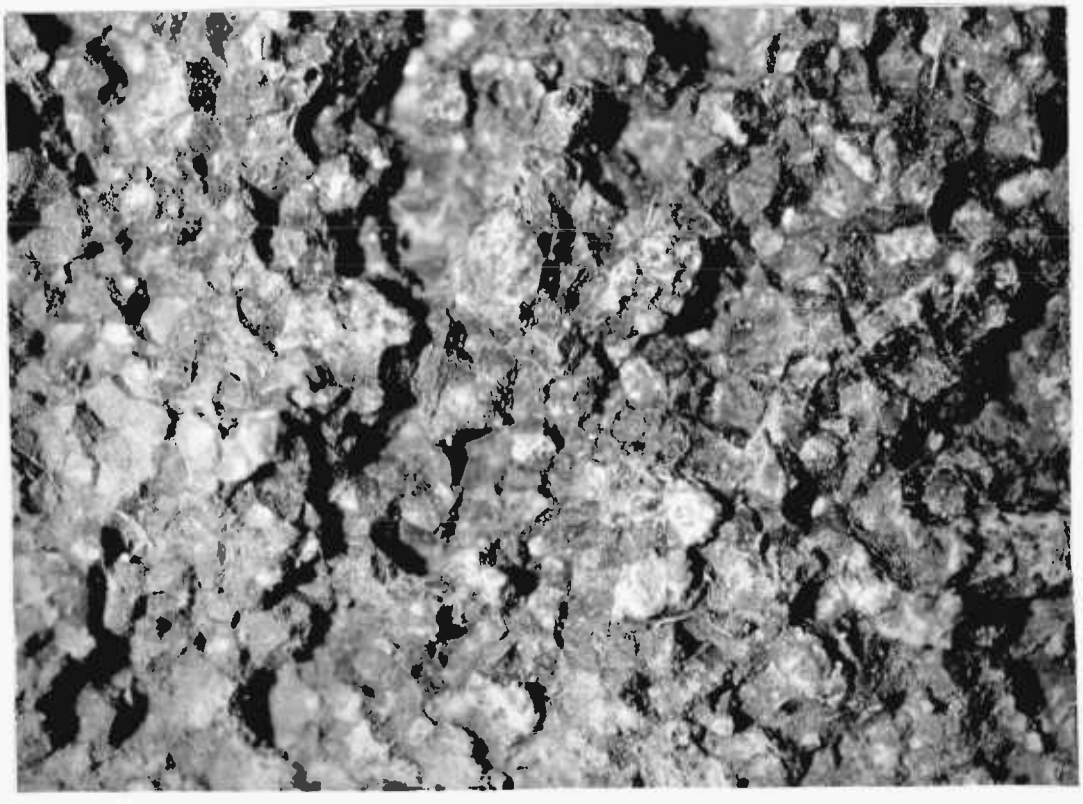

Figure (89): Fracture Surface of the Quenched Steel Creep Cracked at 565°C in air
(Mag x14)

(a) Further back along the crack

(b) Crack tip region

Figure (90): Creep Crack of a 9.5 mm DCB, RR58 tested at 150°C, showing predominantly intergranular fracture and also disconnected cracking in the vicinity of the crack tip

(Mag x70)

(a) Further back along the crack

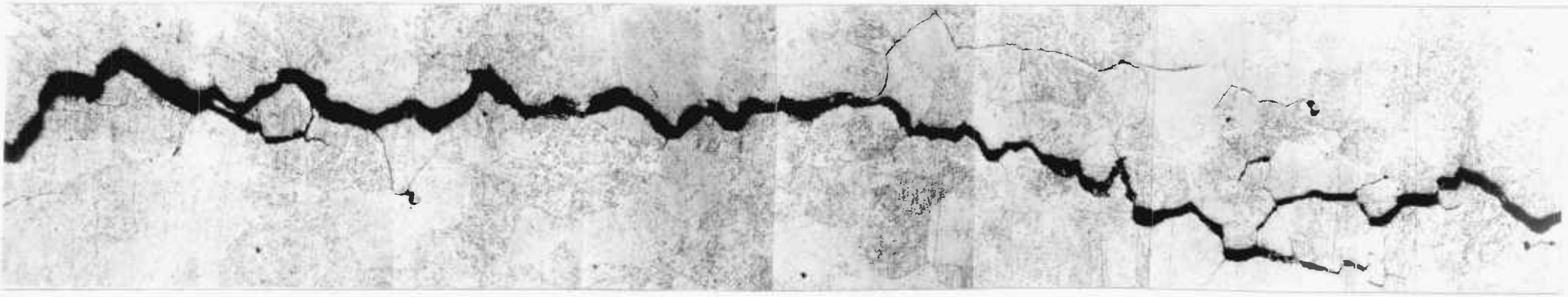

(b) Crack tip region

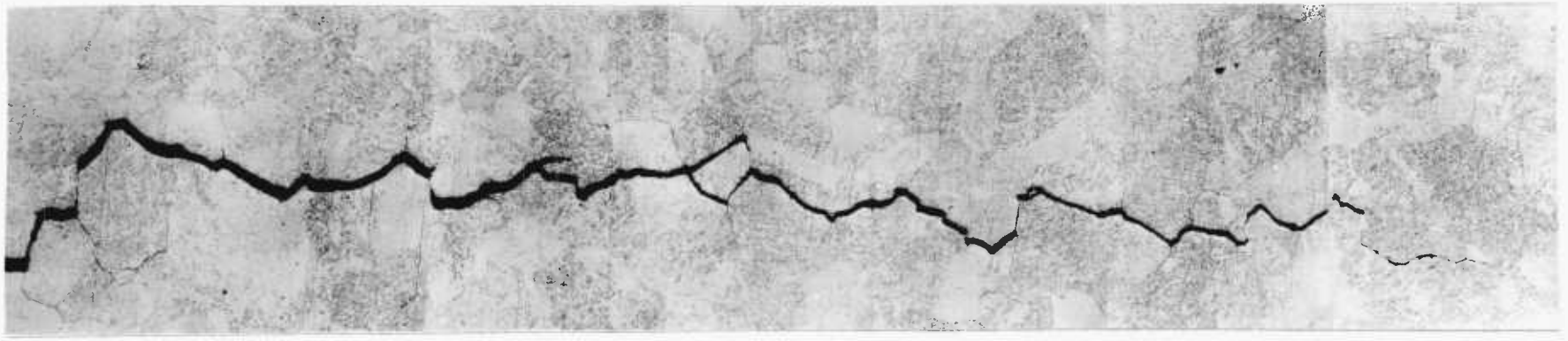

Figure (91): Creep Crack of a 25 mm thick DCB, Quenched steel tested at 565^{o}C showing sharp intergranular fracture at the prior austenite grain boundaries (Mag x20)

(a) Further back along the crack

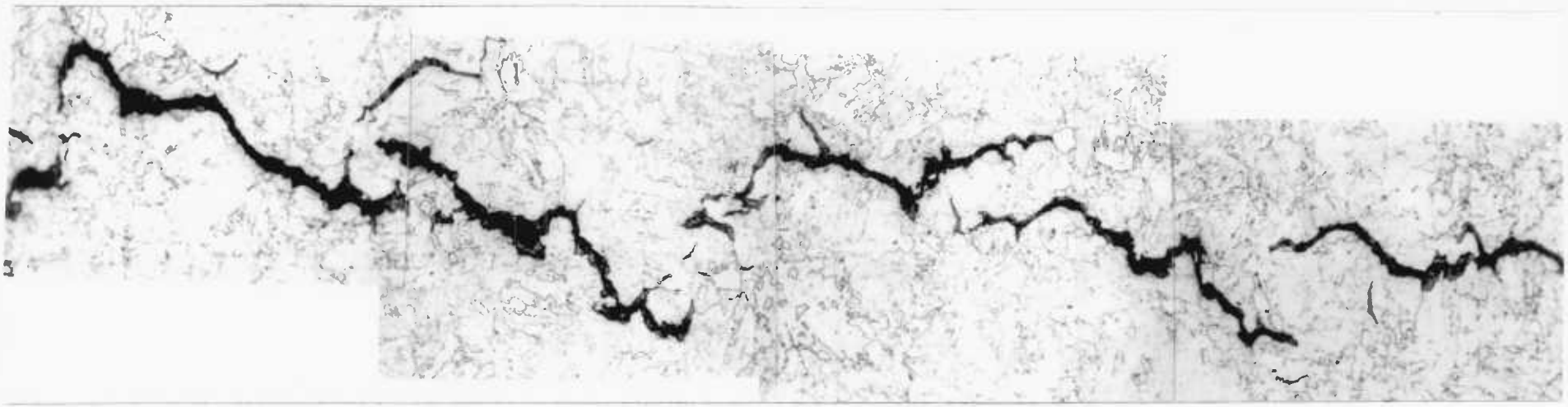

(b) Crack tip region

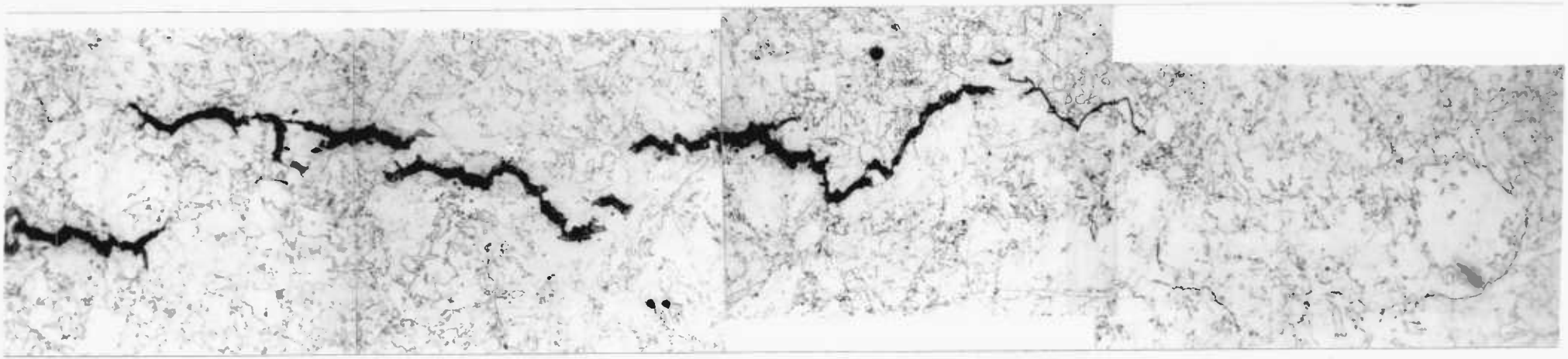

Figure (92): Creep Crack of a 12 mm thick DCB Quenched and tempered steel tested at 565oC showing a tempered matrix with disconnected cracking at the crack tip (Mag x150)

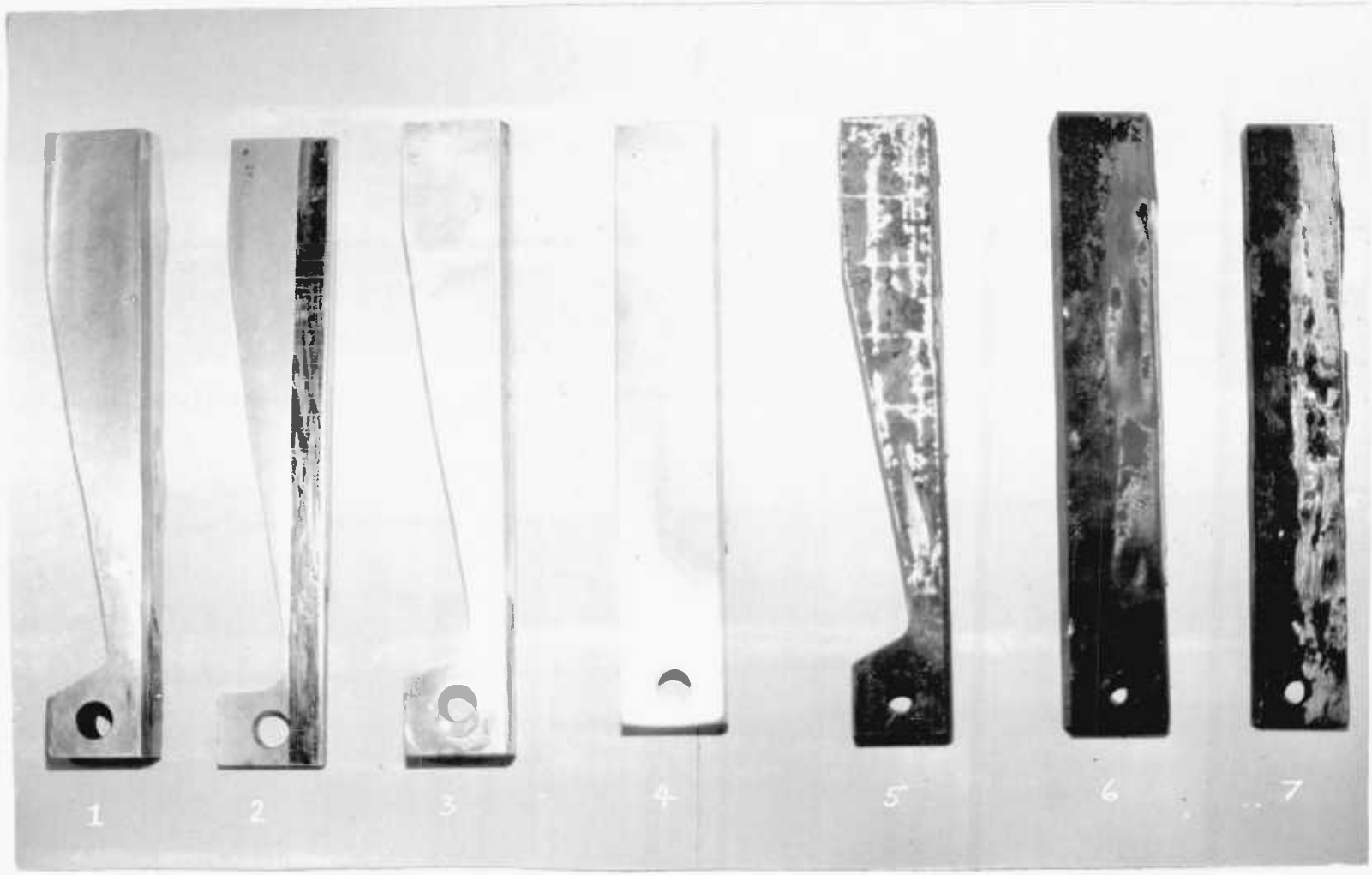

Figure (93): The side view of seven cracked DCB specimens (1) RR58, 25 mm thick, tested at 200°C, (2) RR58, 9.5 mm thick tested at 175°C, (3) RR58, 25 mm thick tested at 150°C, (4) RR58, 25 mm thick tested at 150°C, (5) steel, 12 mm thick, tested at 565°C, (6) steel, 25 mm thick, tested at 565°C, (7) steel, 12 mm thick, tested at 565°C

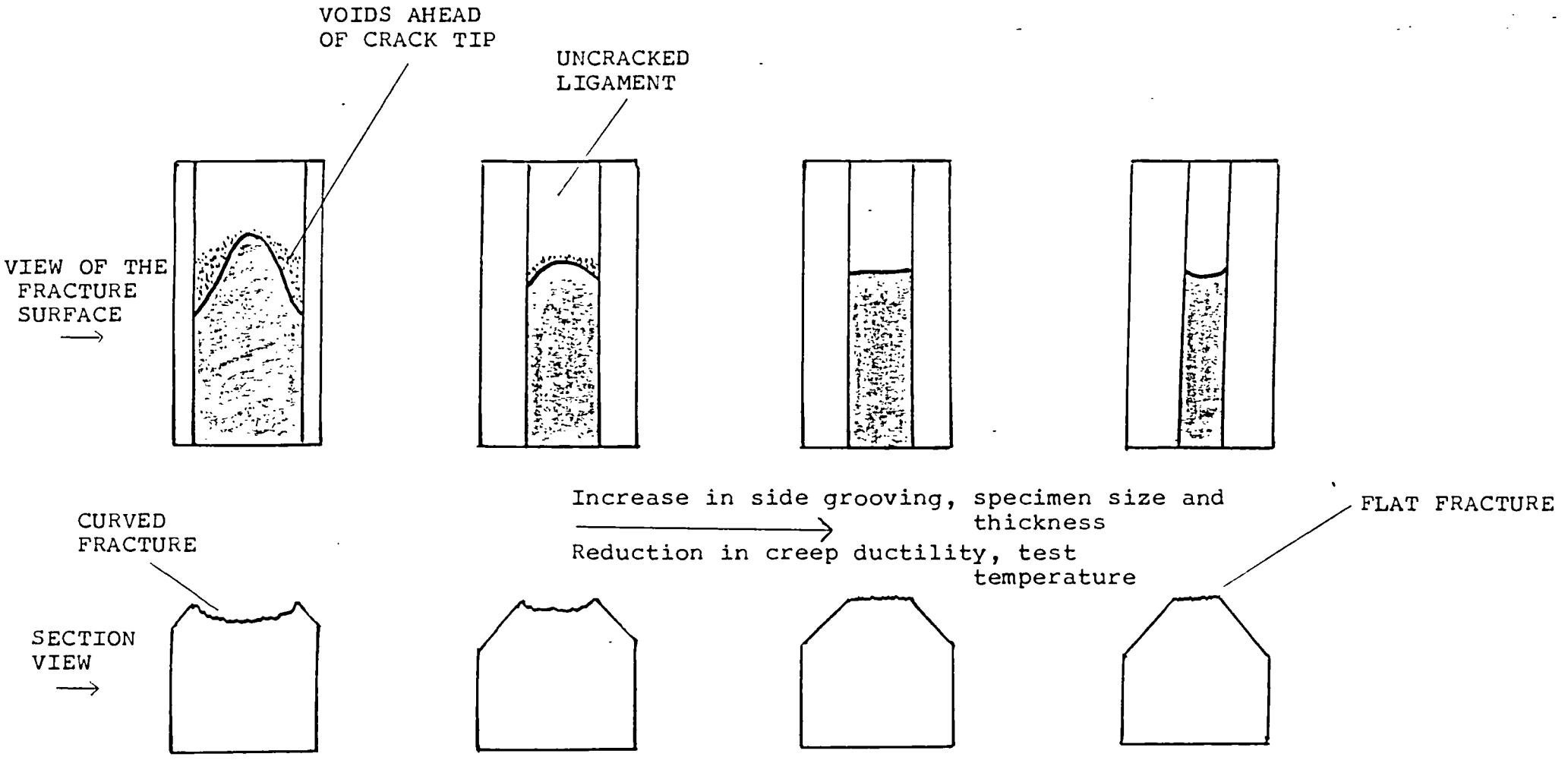

Figure (94): Schematic representations of crack fronts and profiles and the possible tests variables that may effect them

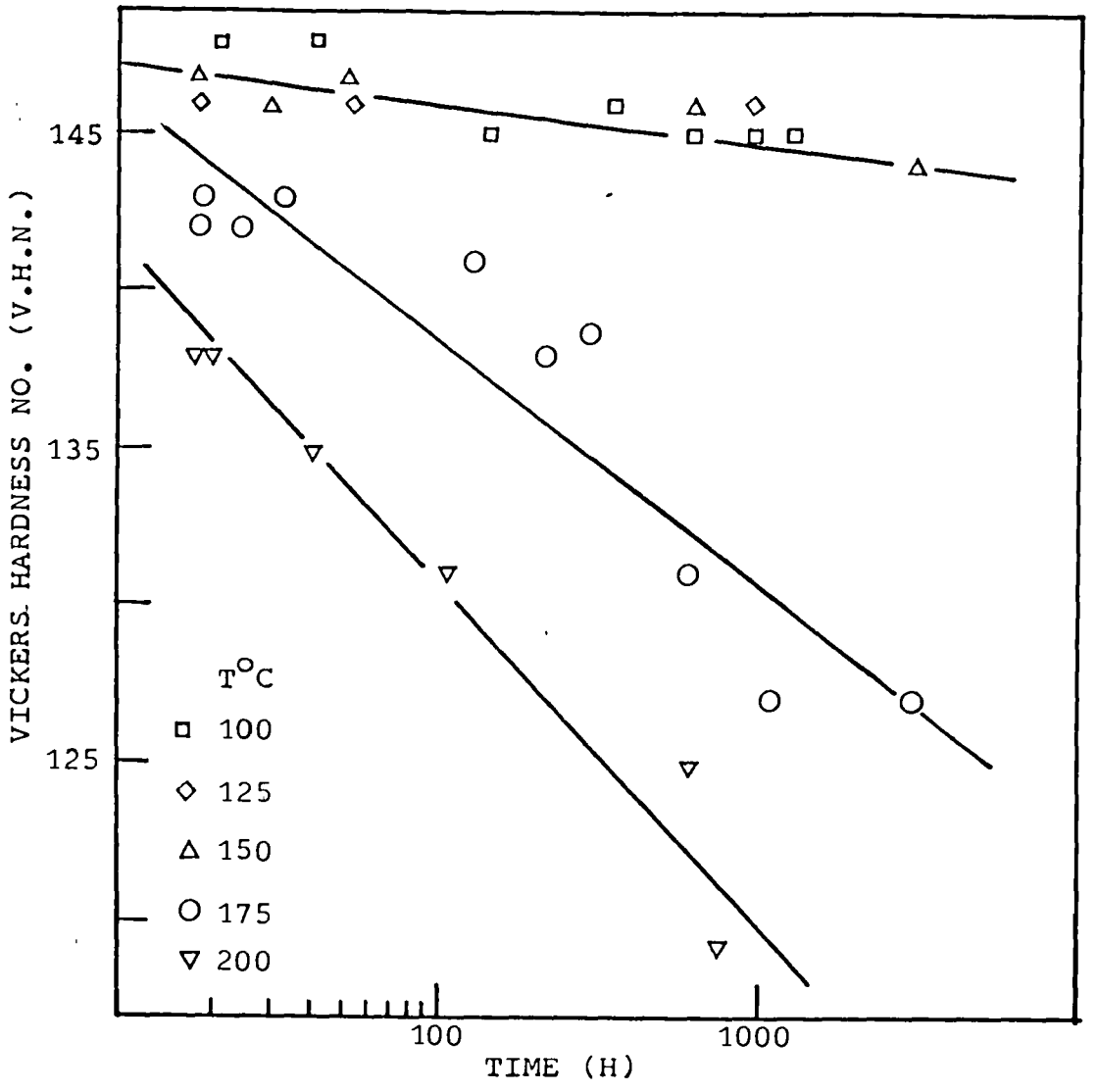

Figure (95): Hardness of RR58 specimens after various test times and temperatures

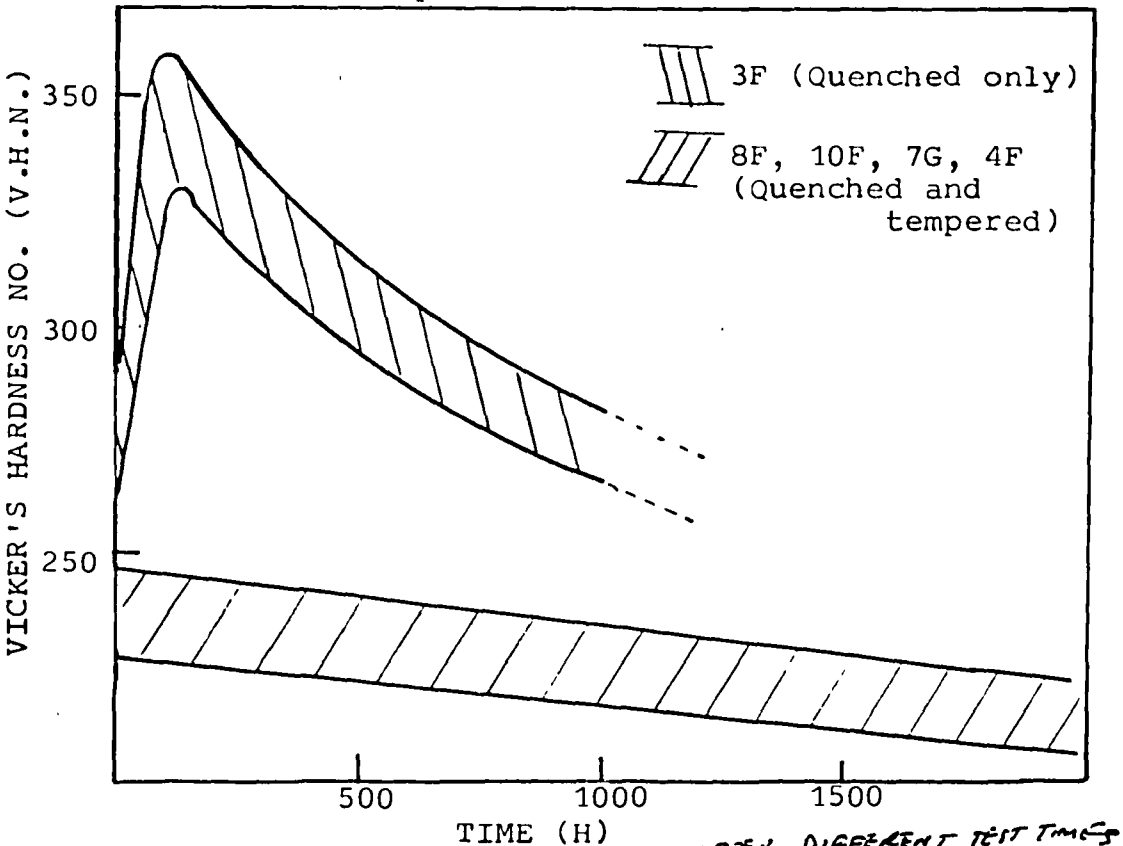

Figure (96) HARDNESS VALUES OF SPECIMENS AFTER DIFFERENT TEST TIMES AT 585°C

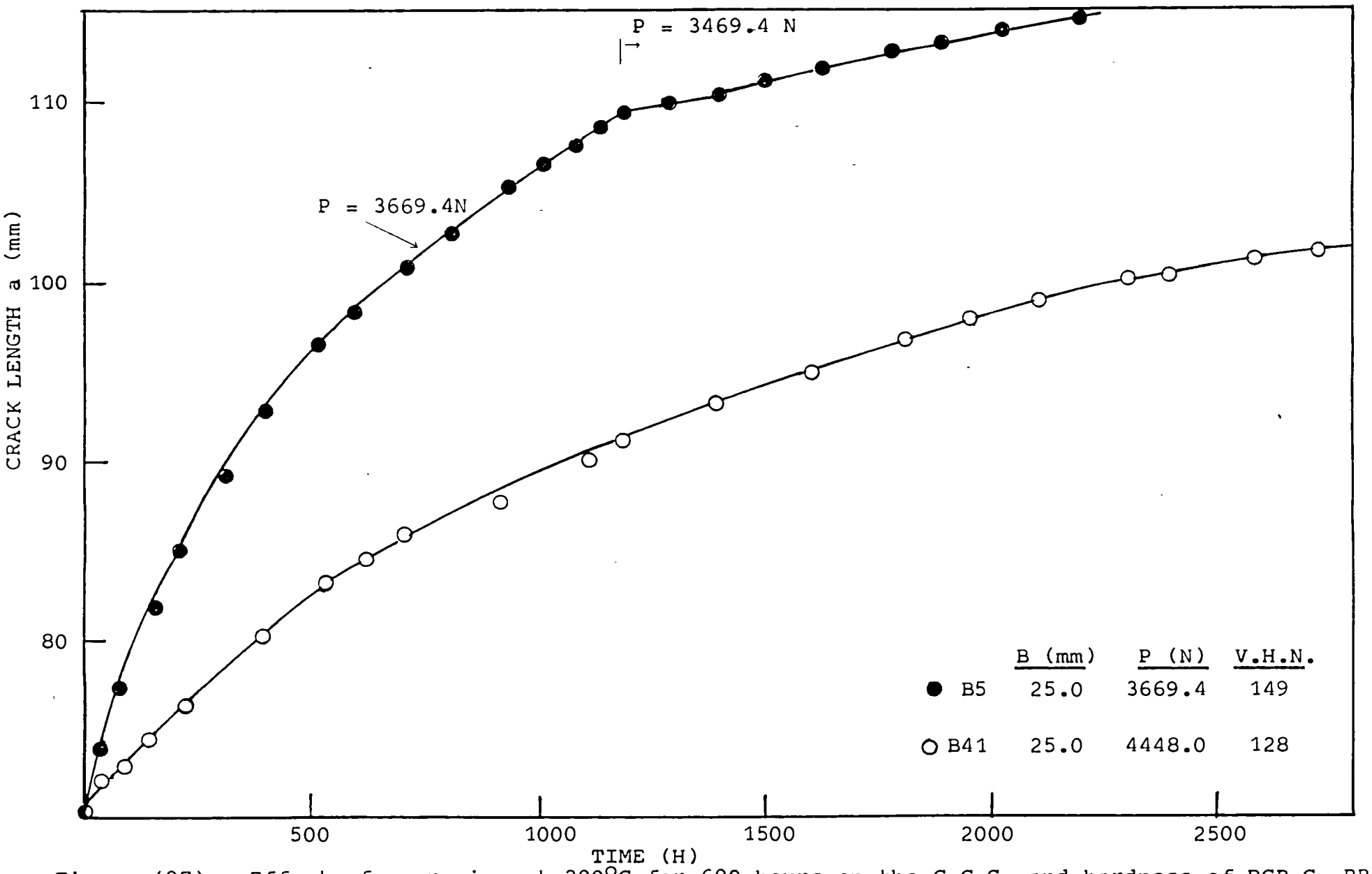

Figure (97): Effect of overaging at 200°C for 600 hours on the C.C.G. and hardness of DCB-C, RR58 specimens tested at 150°C.

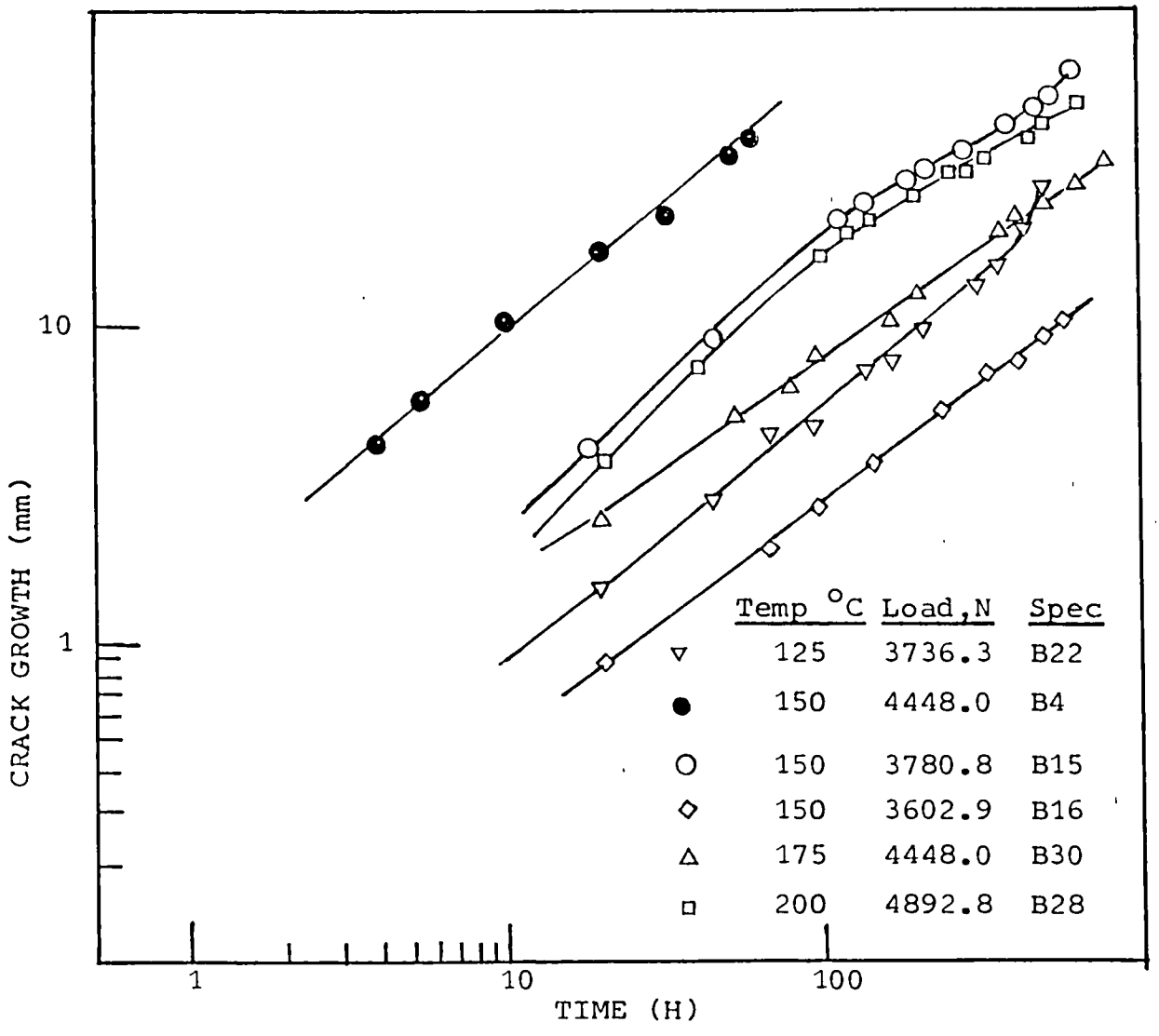

Figure (98): Effect of temperature and load on the C.C.G. of DCB-C RR58 specimens

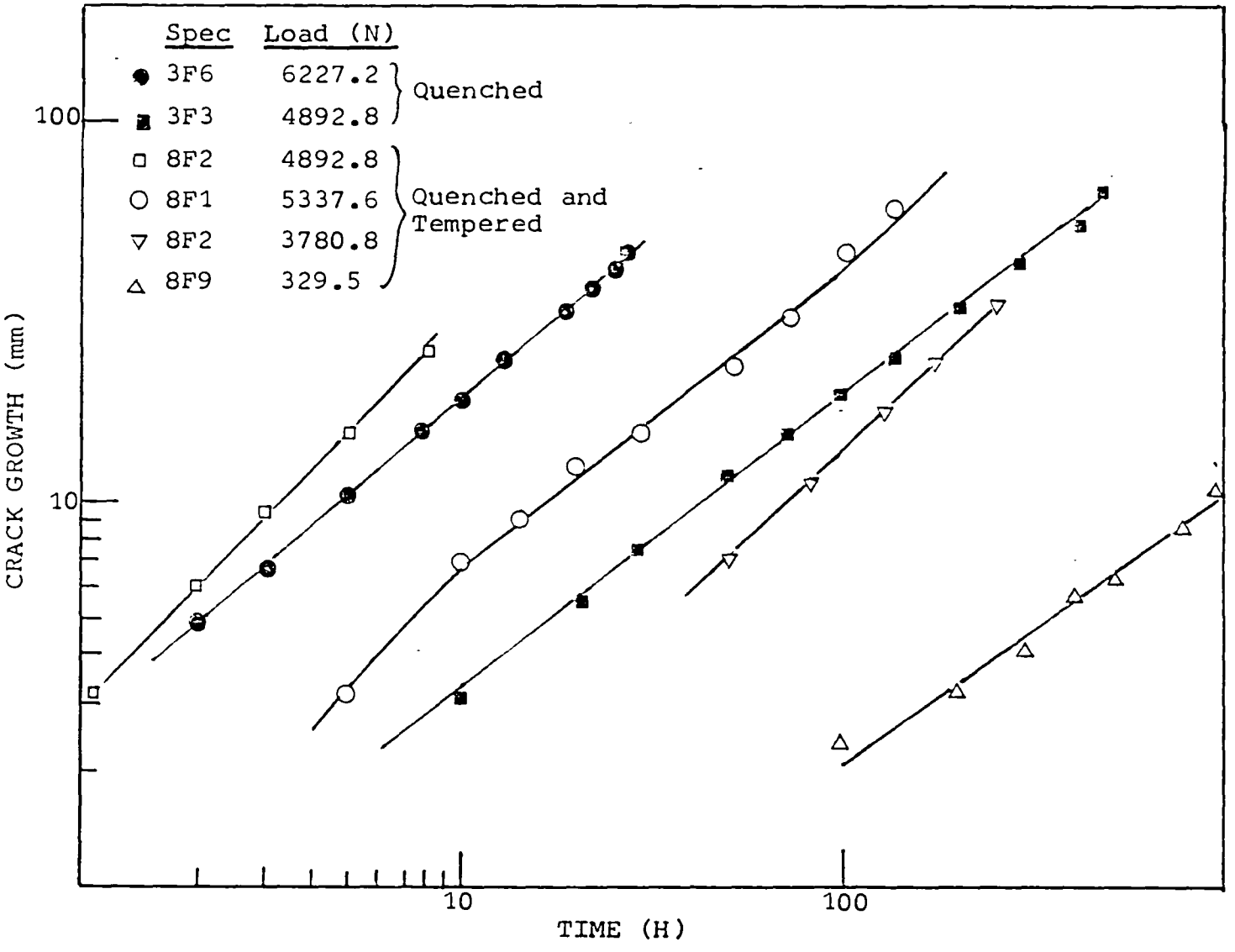

Figure (99): Effect of load and heat treatment on the C.C.G. of DCB-C steel specimens

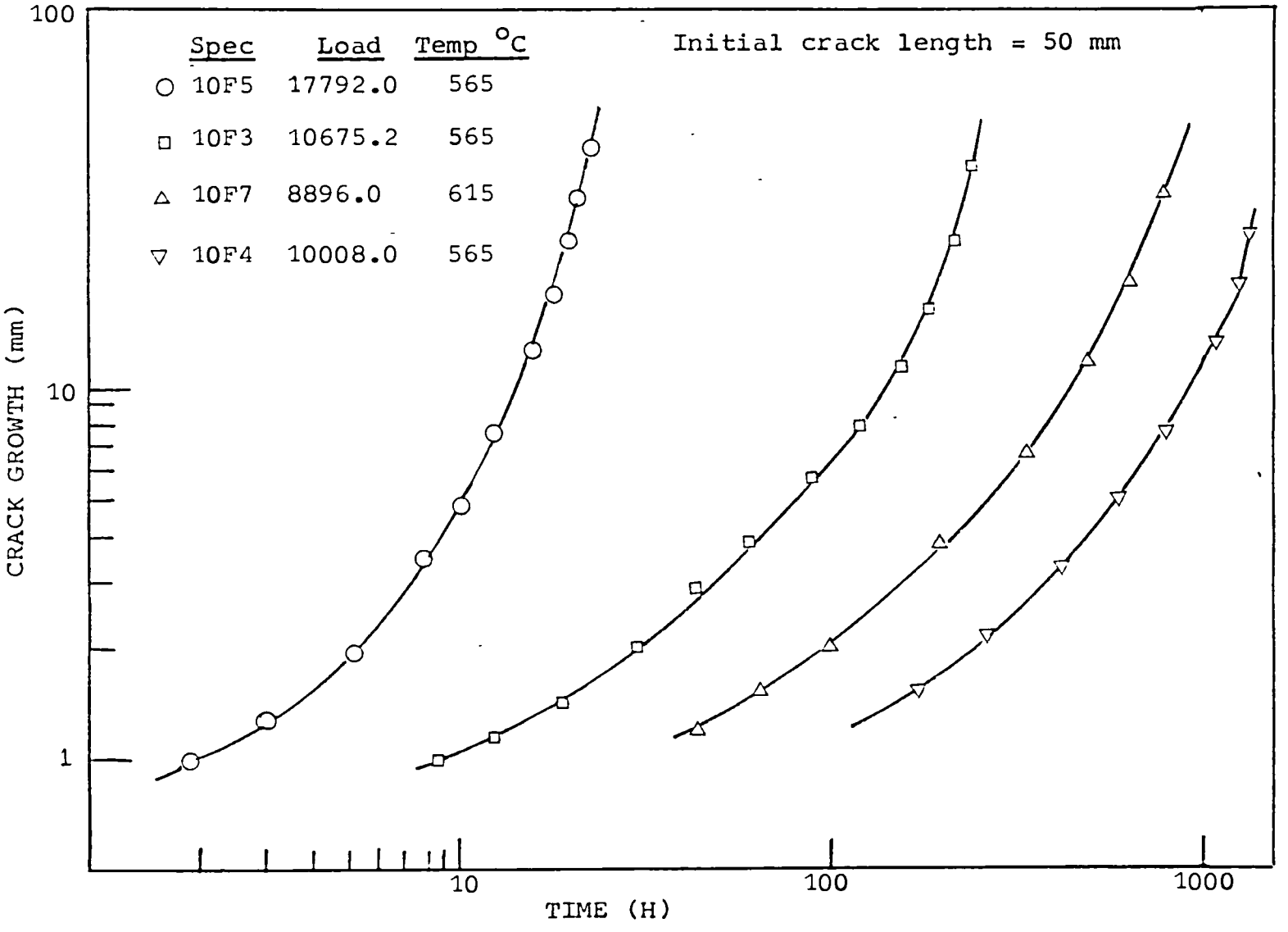

Figure (100): Effect of load and temperature on the C.C.G. of DCB-P steel specimens

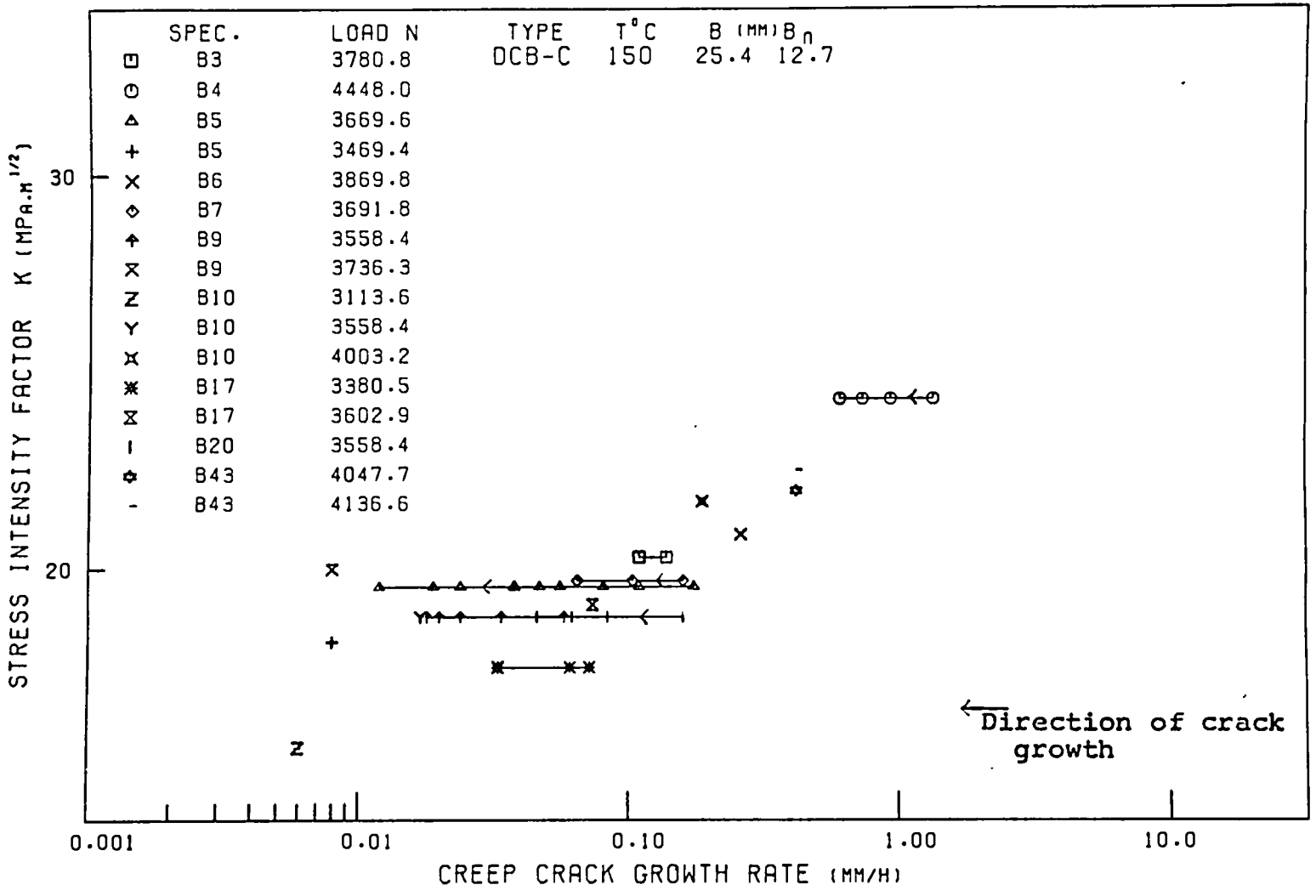

Figure (101): The effect of load change on the correlation of C.C.G. rate with K for DCB-C RR58 specimens

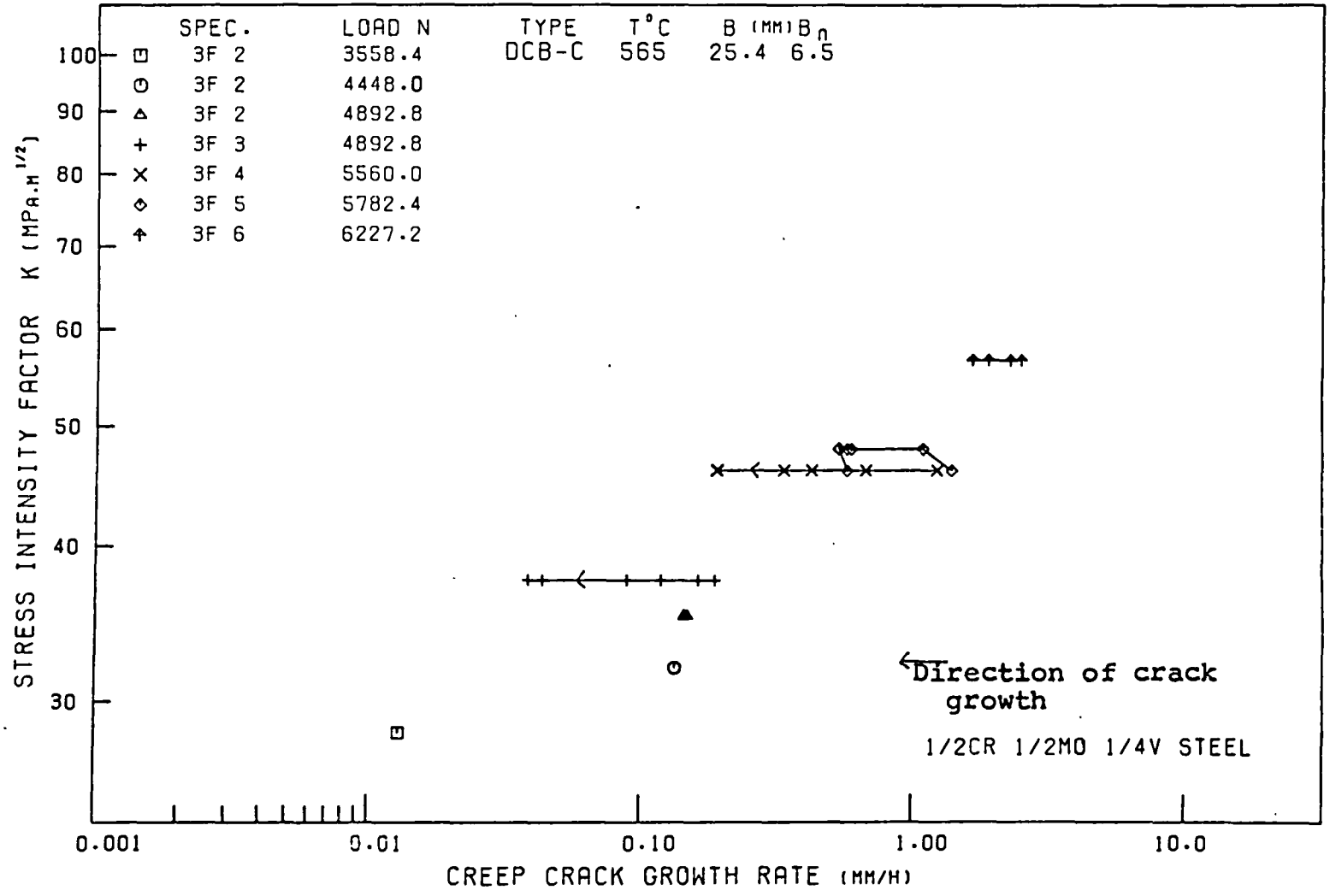

Figure (102): The effect of load change on the correlation of C.C.G. rate with K for DCB-C quenched steel specimens

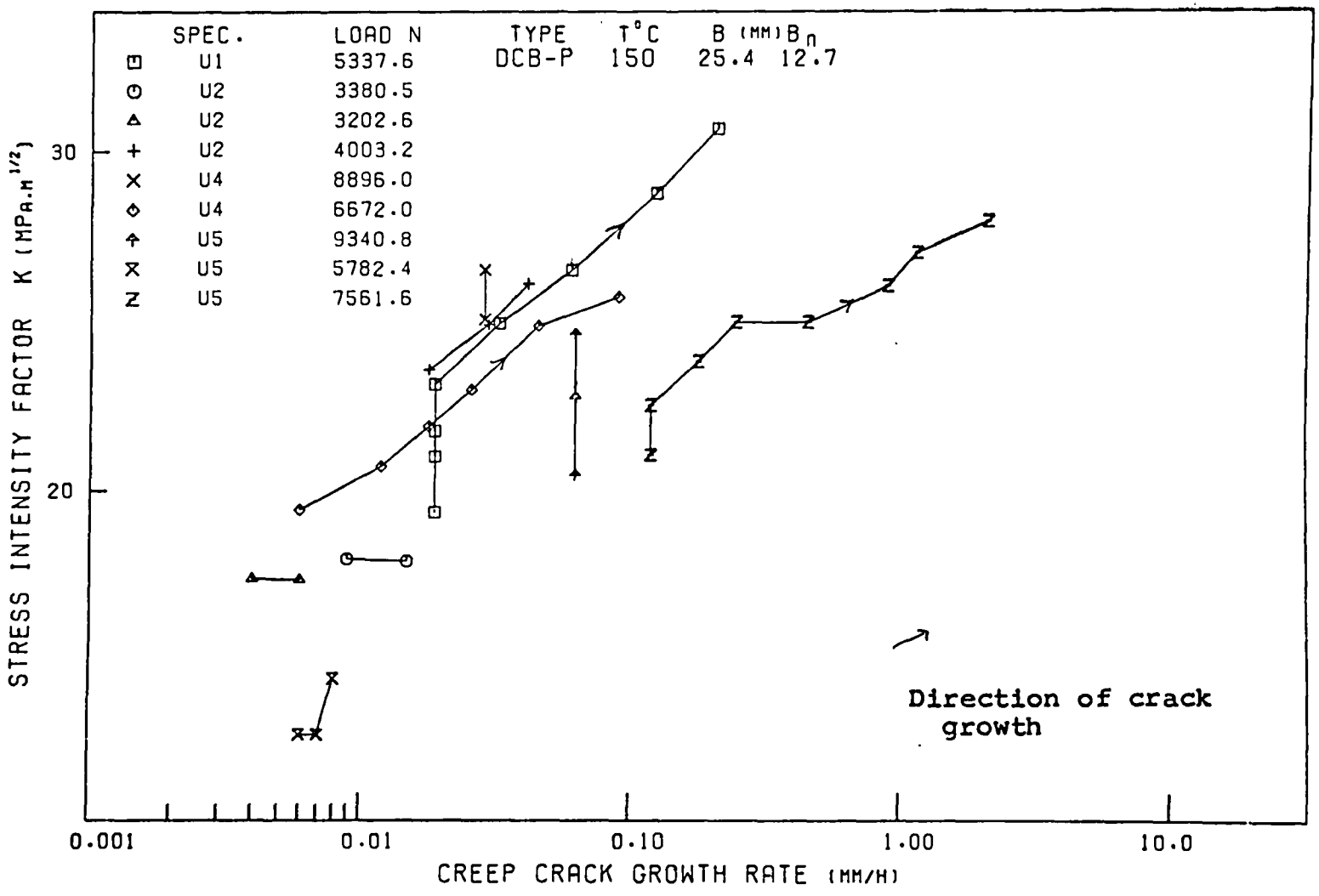

Figure (104): The effect of load change on the correlation of C.C.G. rate with K for the DCB-P, RR58 specimens

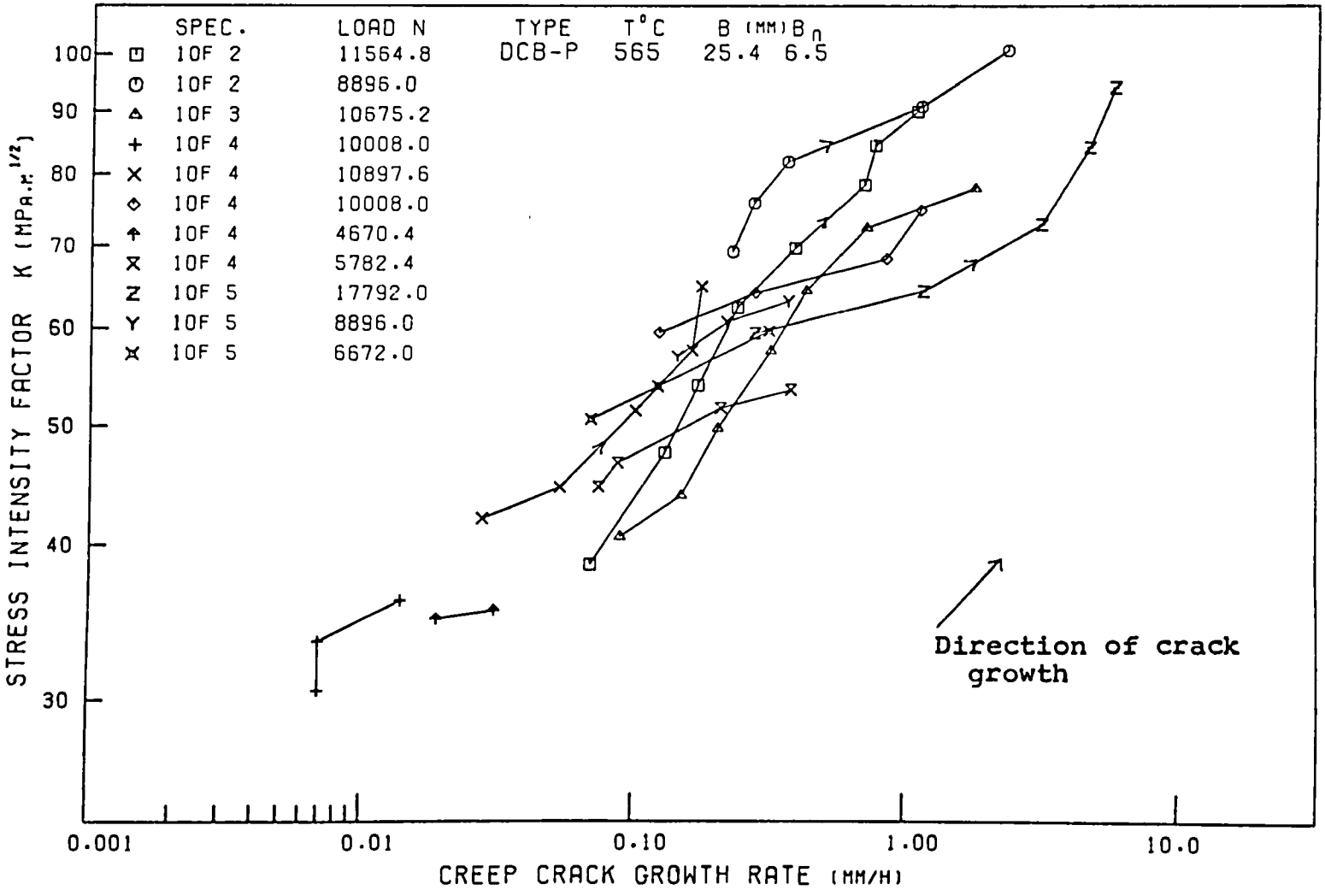

Figure (105): The effect of load change on the correlation of C.C.G. rate with K for DCB-P, steel specimens

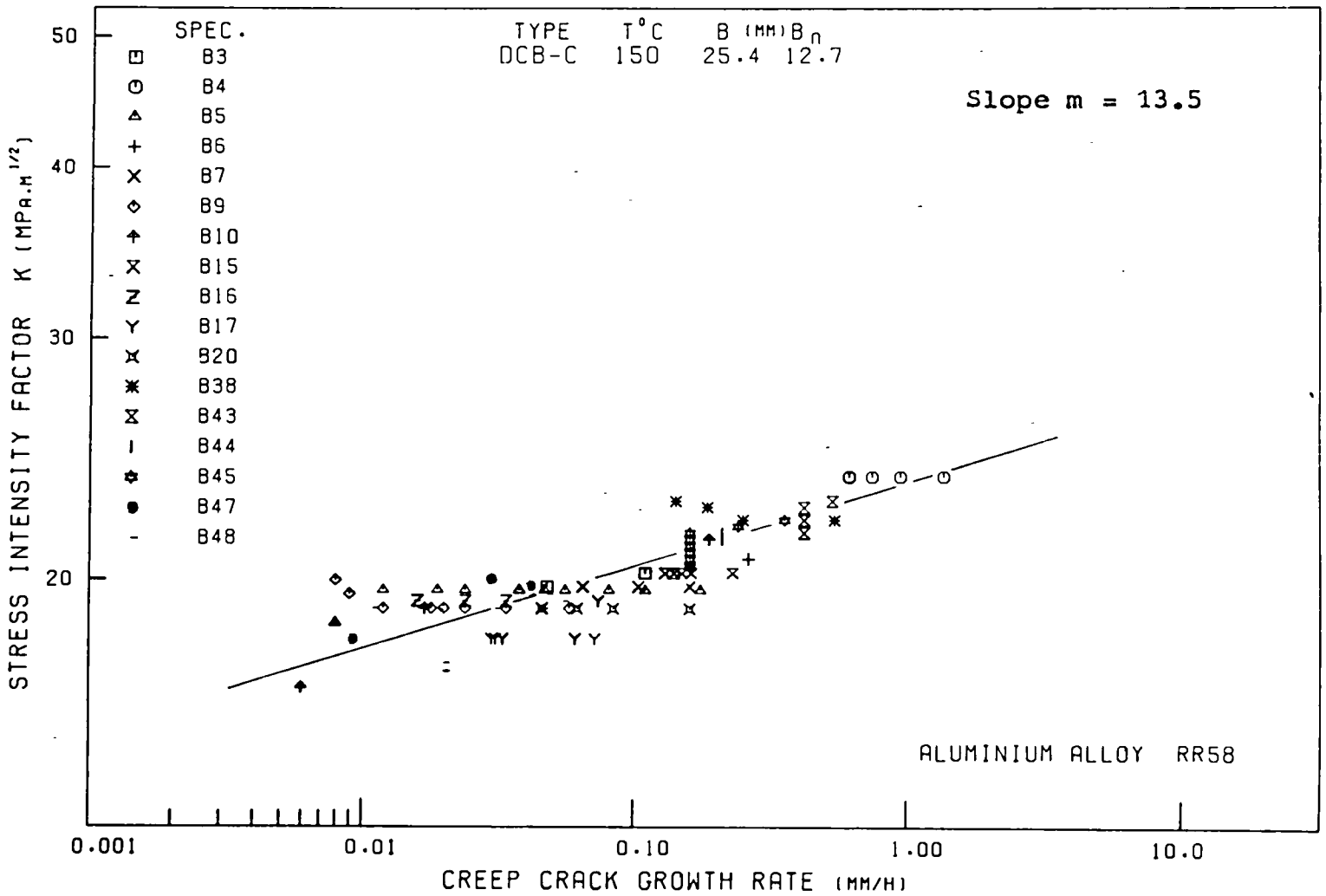

Figure (106): Correlation of C.C.G. rate with K for all the DCB-C, RR58 data tested

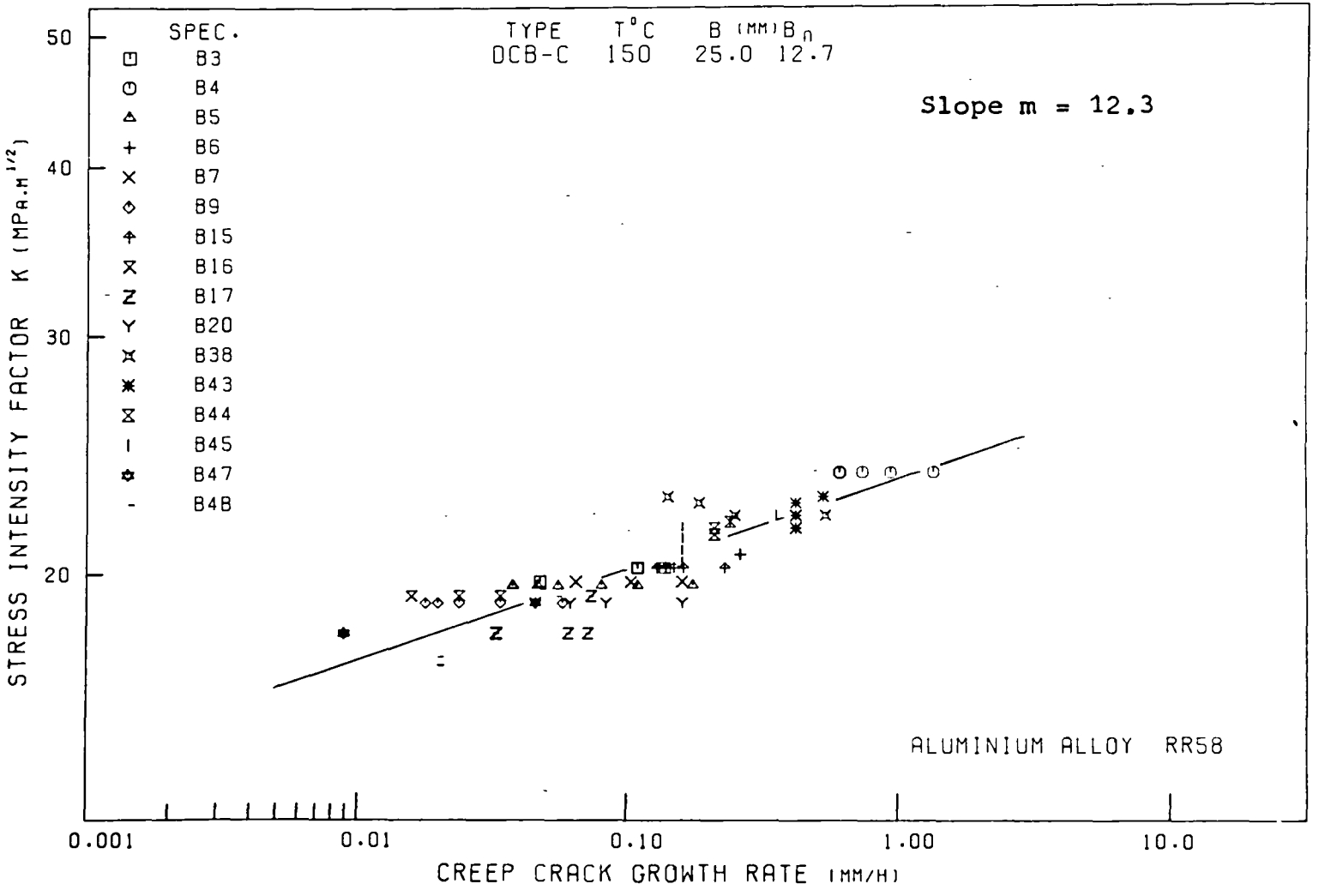

Figure (107): Correlation of C.C.G. rate with K for the DCB-C, RR58 data for test times of less than 500 hours

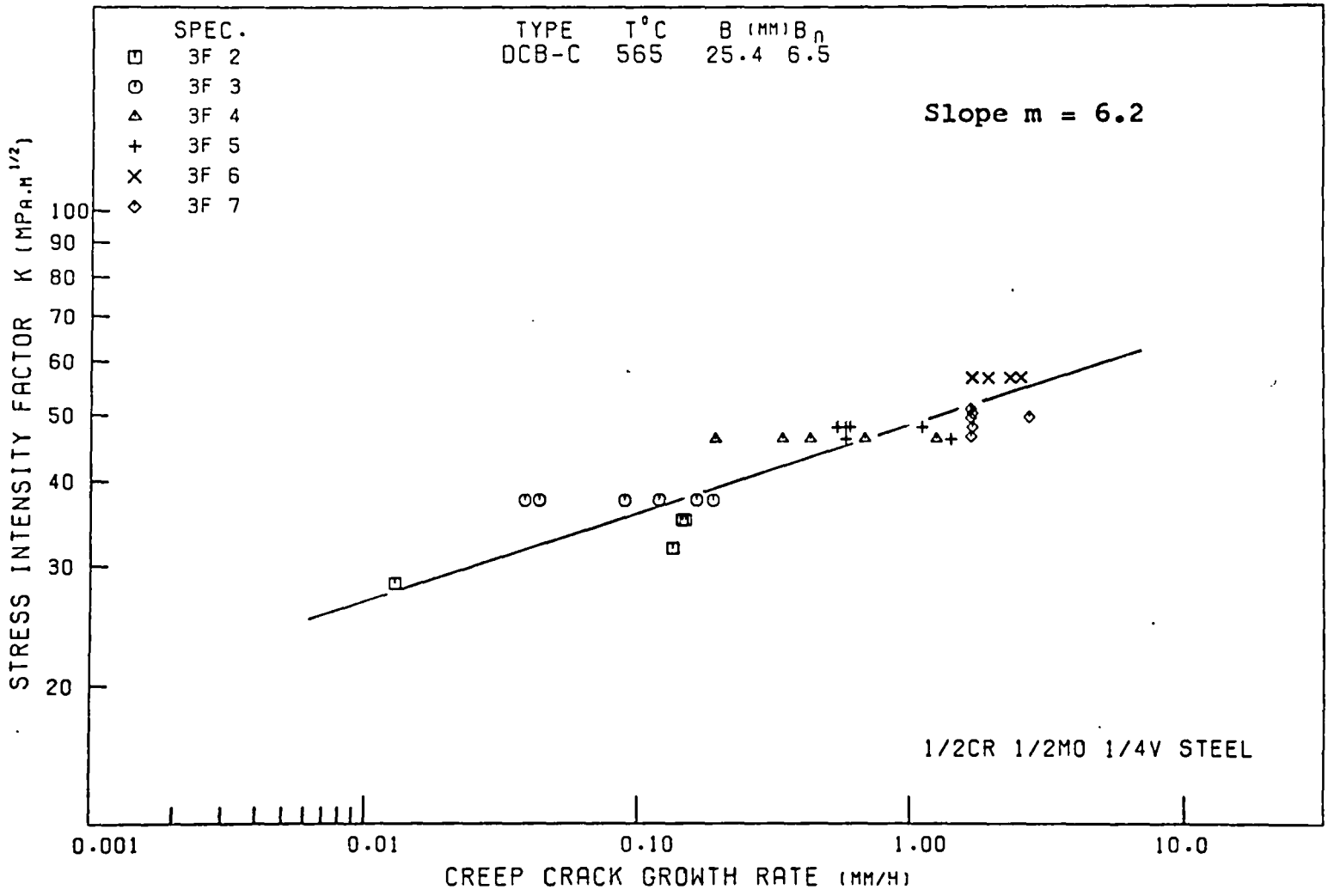

Figure (108): Correlation of C.C.G. rate with K for all the DCB-C, steel quenched data

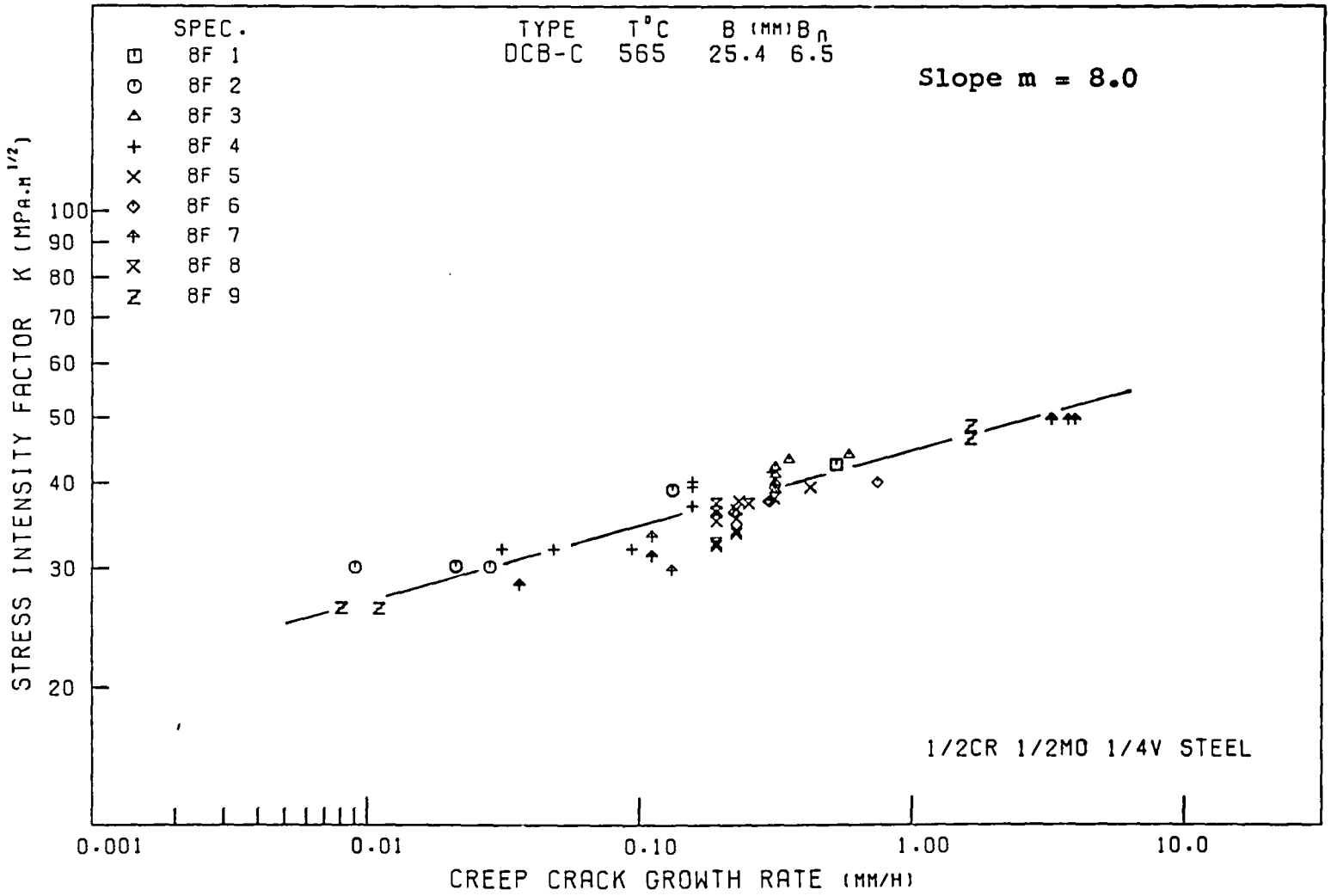

Figure (109): Correlation of C.C.G. rate with K for the 25 mm thick DCB-C, steel quenched and tempered data

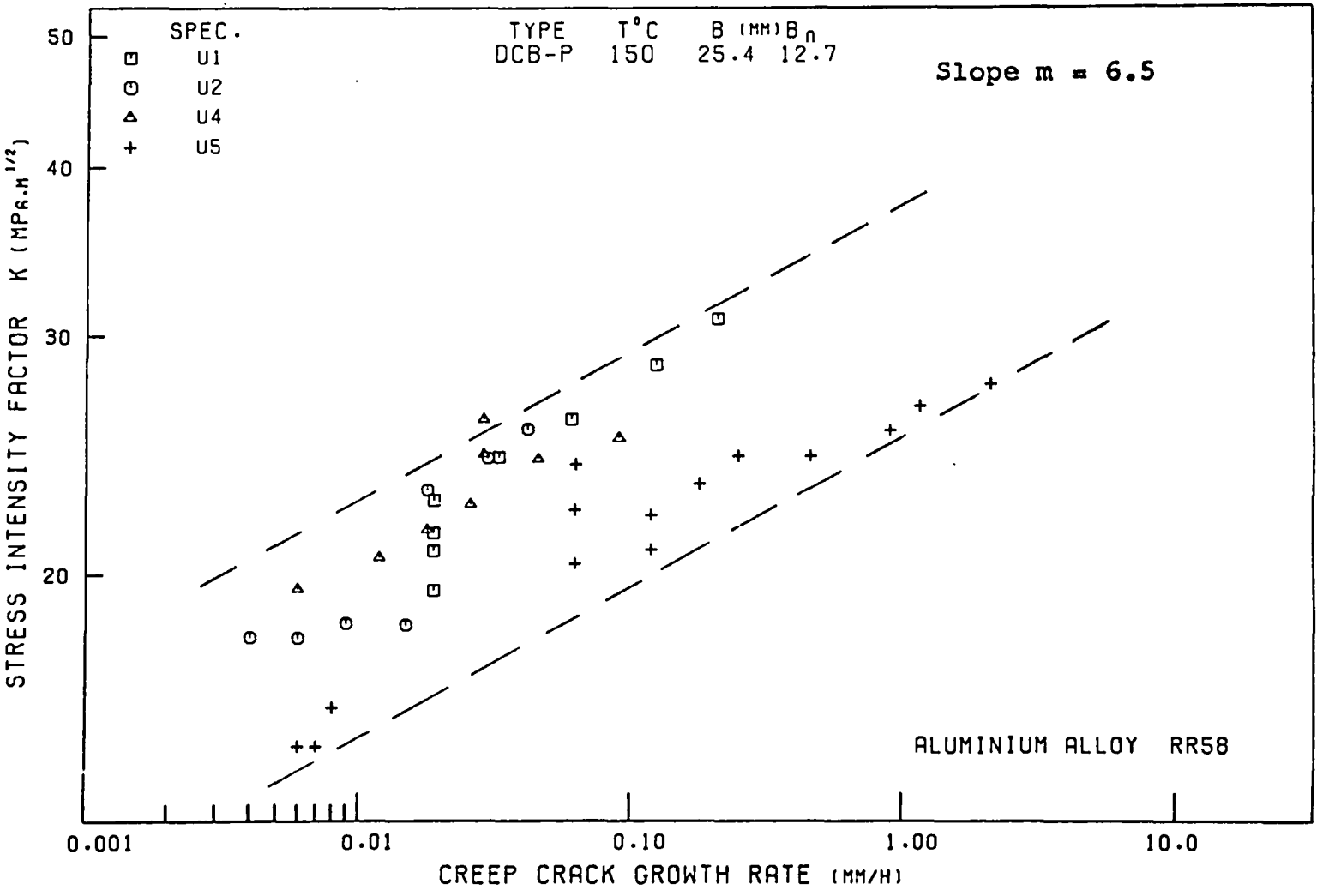

Figure (110): Correlation of C.C.G. rate with K for all the DCB-P, RR58 data tested at 150°C.

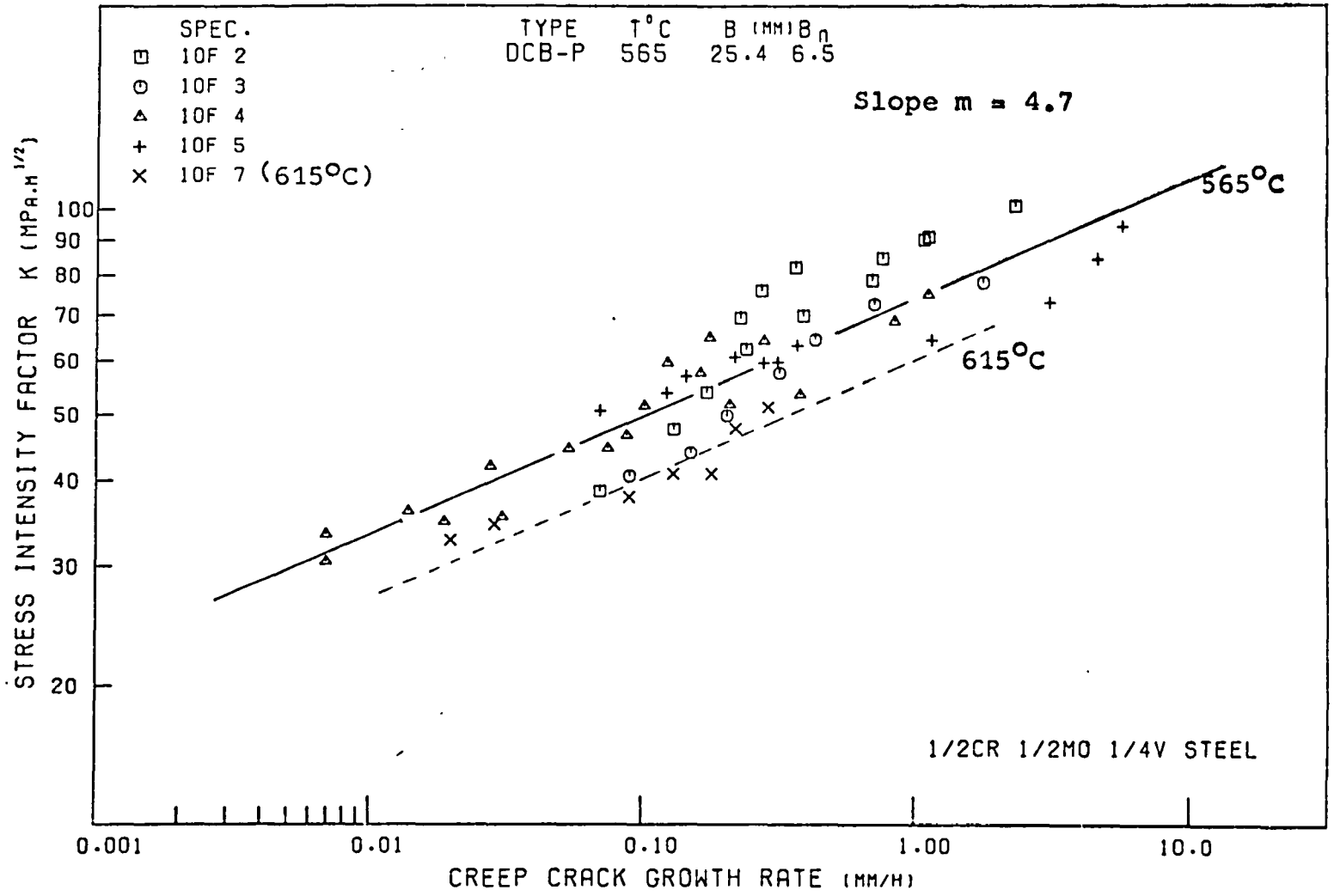

Figure (111): Correlation of C.C.G. rate with K for DCB-P, steel specimens tested at 565°C and 615°C.

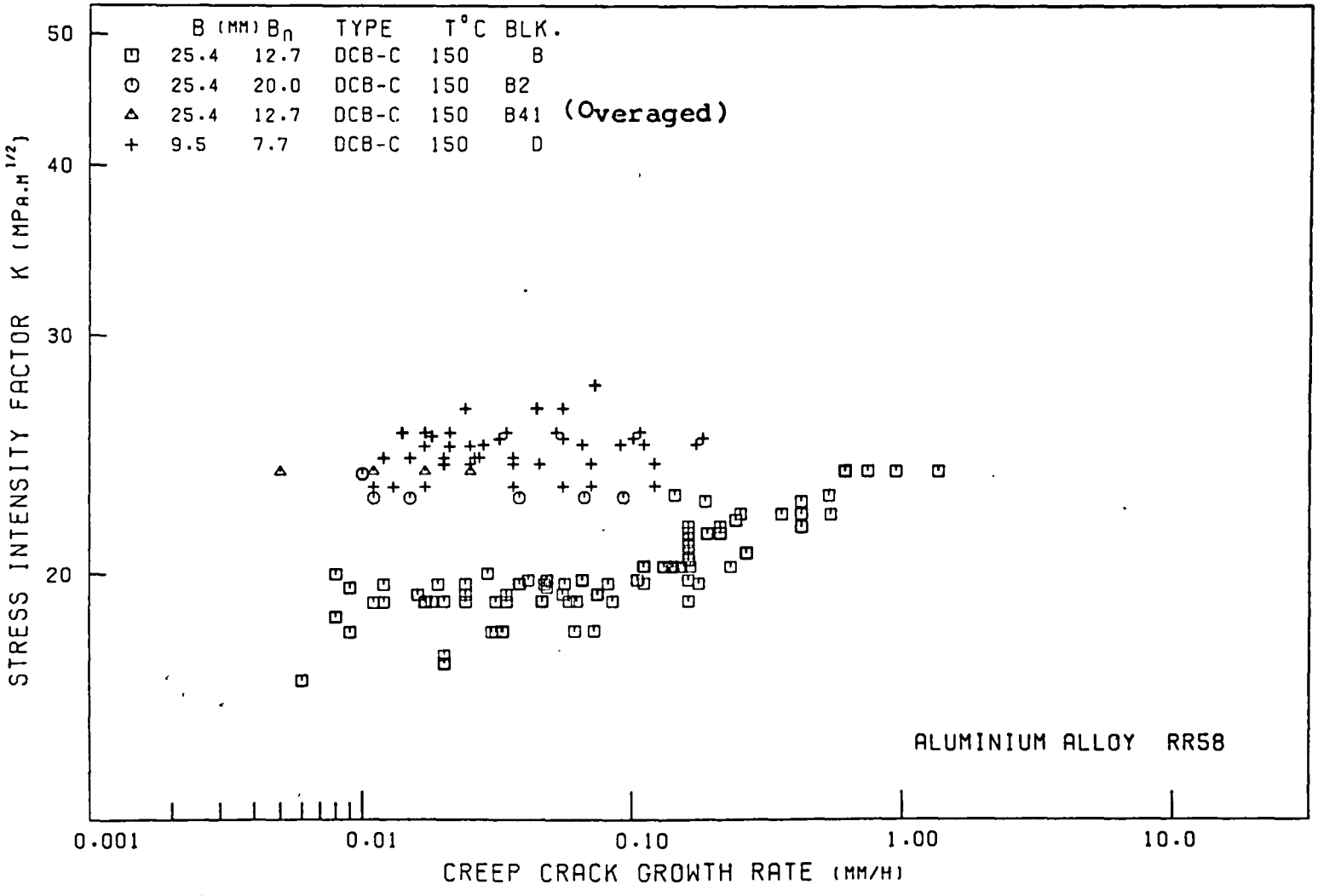

Figure (112): The Effect of Thickness, Sidegrooving and overaging on the correlation of C.C.G. rate with K for DCB-C, RR58 specimen tested at 150°C.

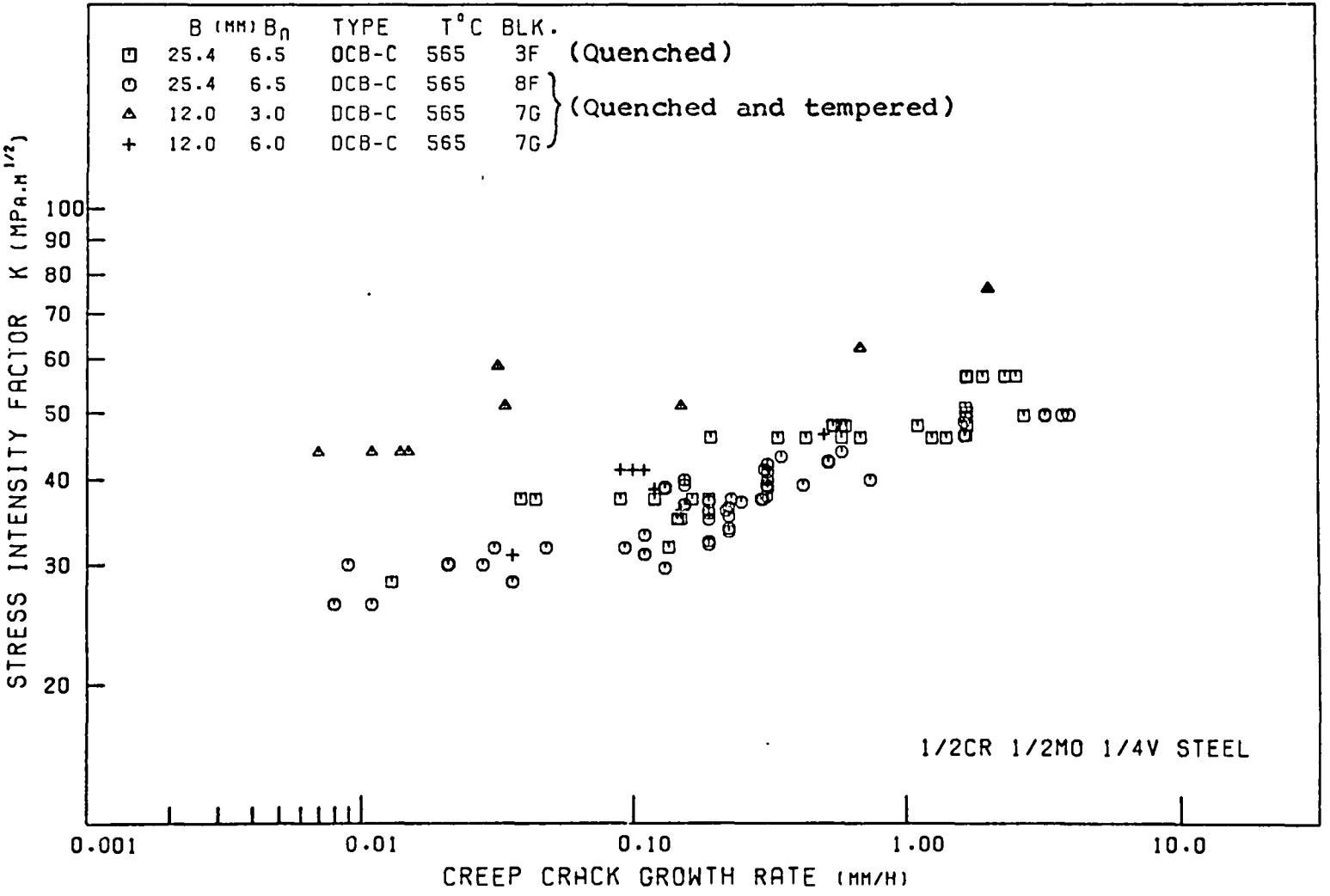

Figure (113): The effect of Heat treatment, and thickness on the correlation of C.C.G. rate with K for DCB-C steel specimens

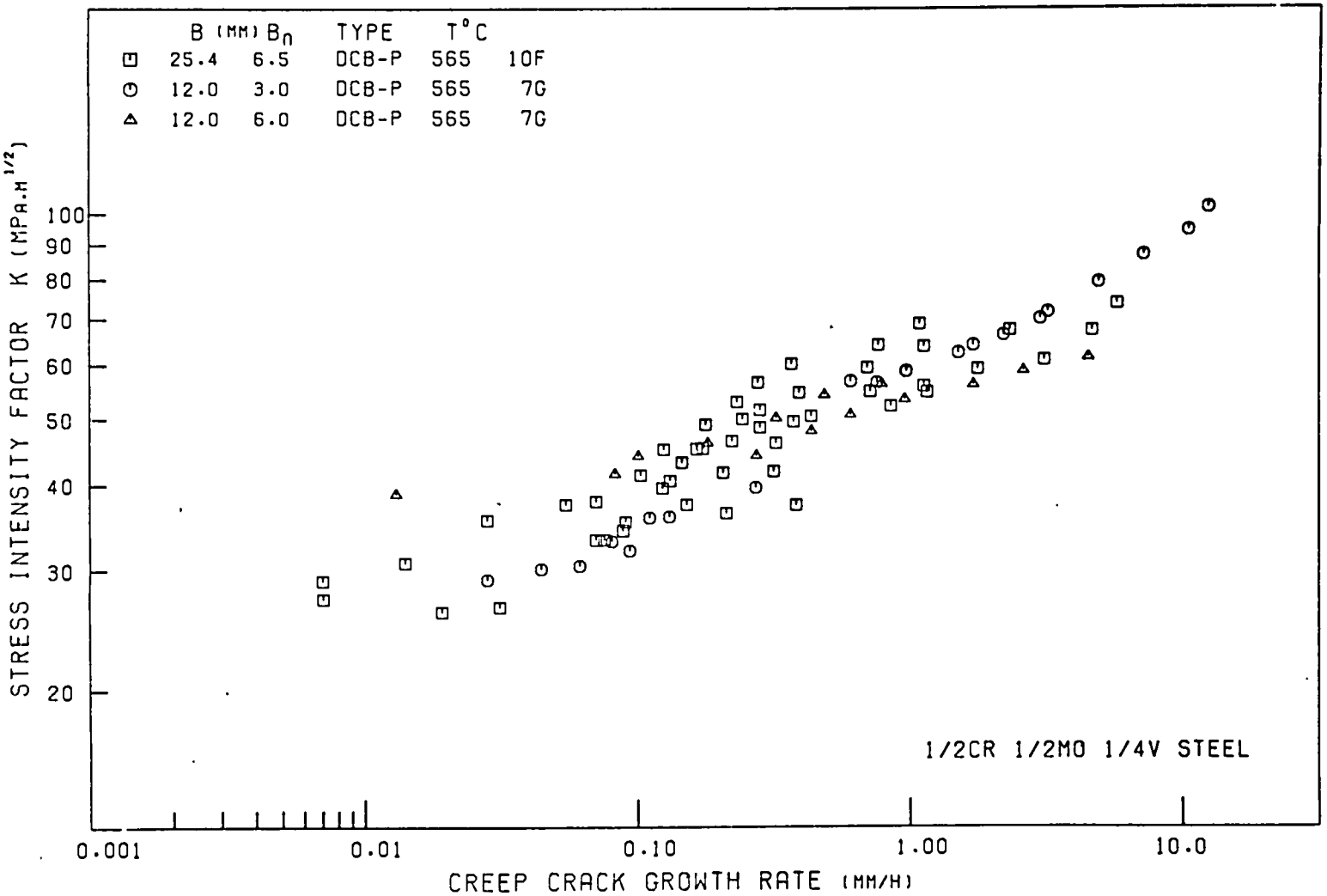

Figure (114): The effect of thickness on the correlation of C.C.G. rate with K for the DCB-P steel specimens

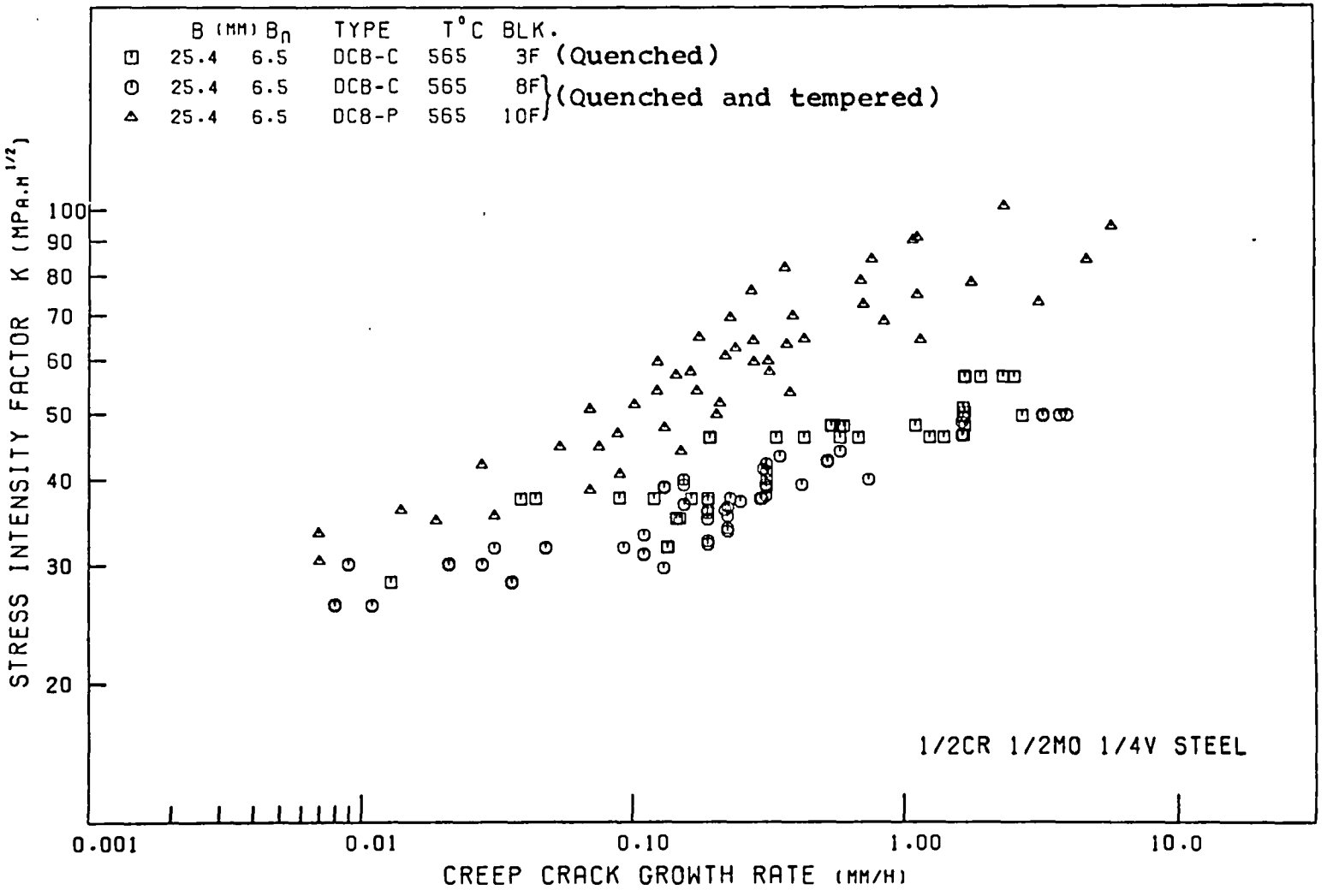

Figure (115): Comparison of the C.C.G. rate between DCB-C and DCB-P 25 mm thick steel specimens

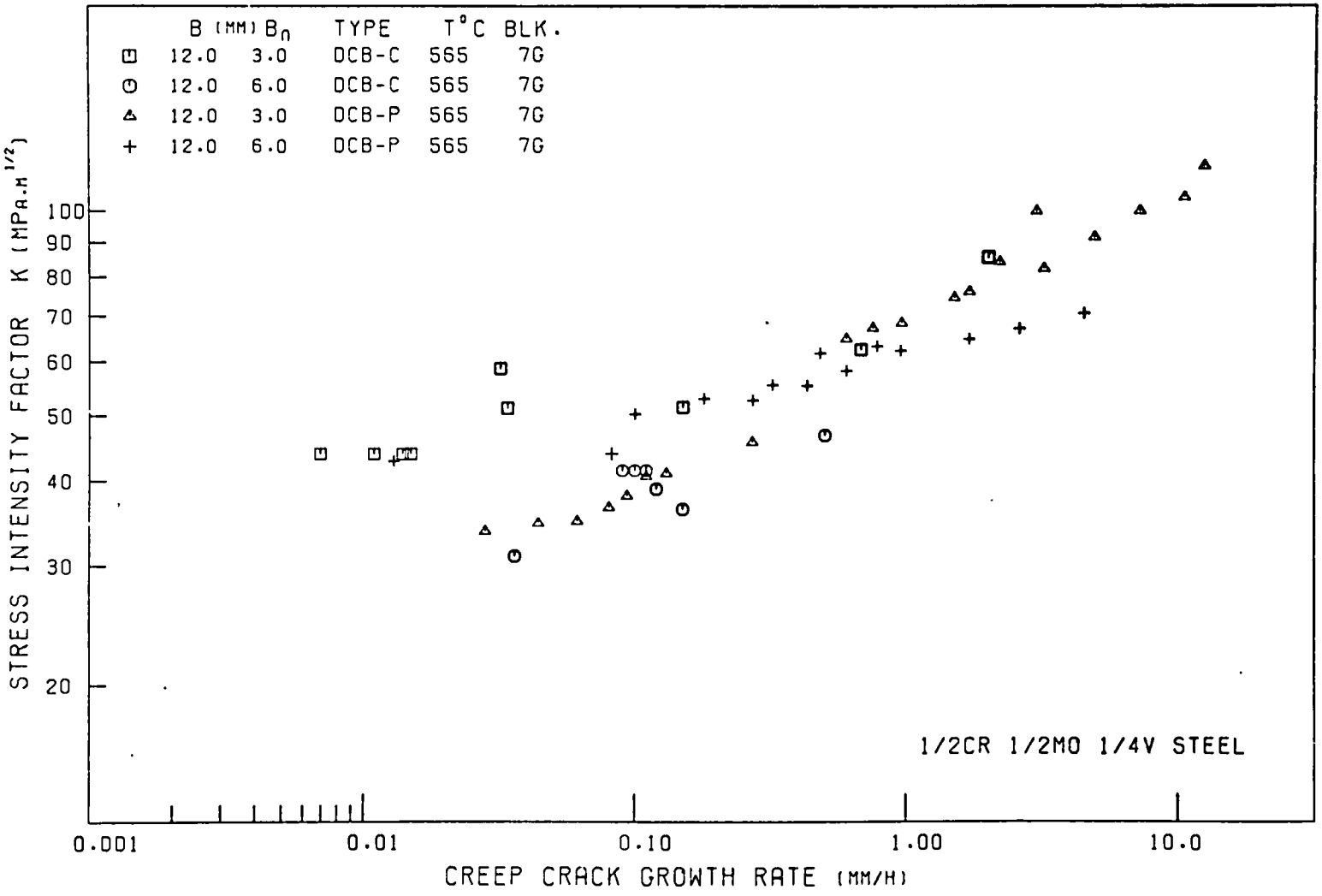

Figure (116): Comparison of the C.C.G. rate between DCB-C and DCB-P 12 mm thick steel specimen with various extent of side grooving

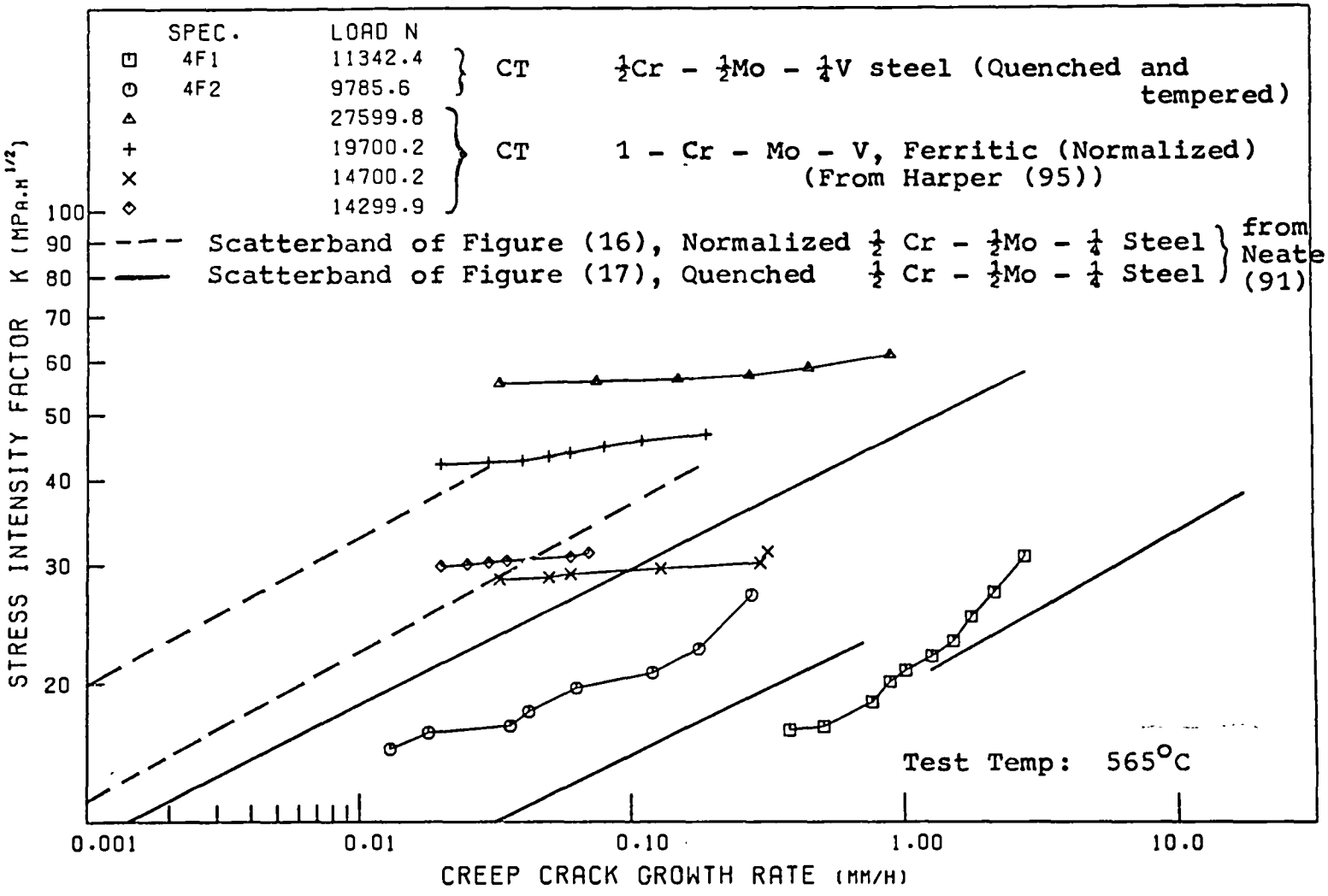

Figure (117): Effect of Creep ductility on the correlation of C.C.G. rate with K for CT, low alloy steels of various heat treatments

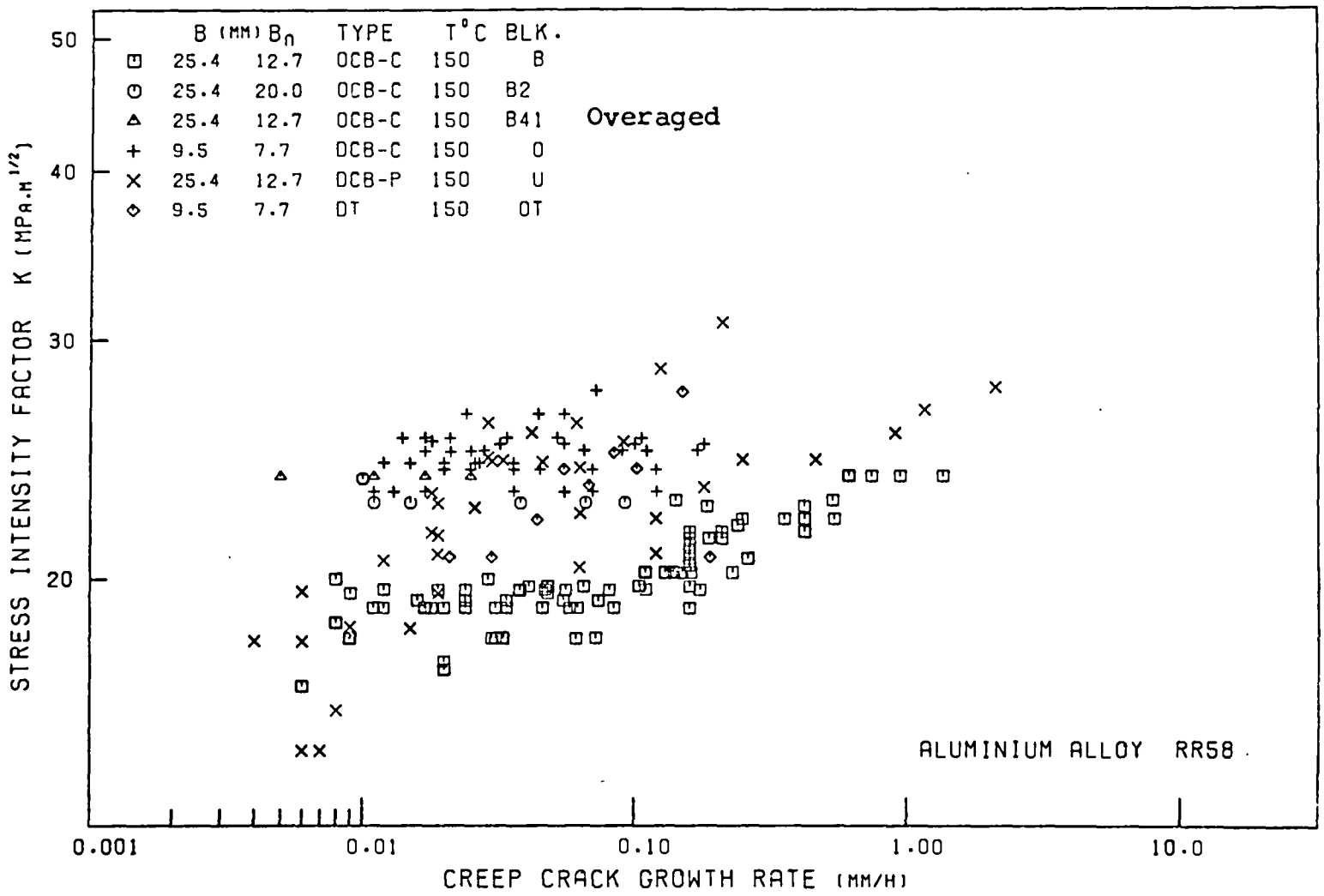

Figure (118): The effect of various geometries and thicknesses on the correlation of C.C.G. rate with K for RR58 at 150°C.

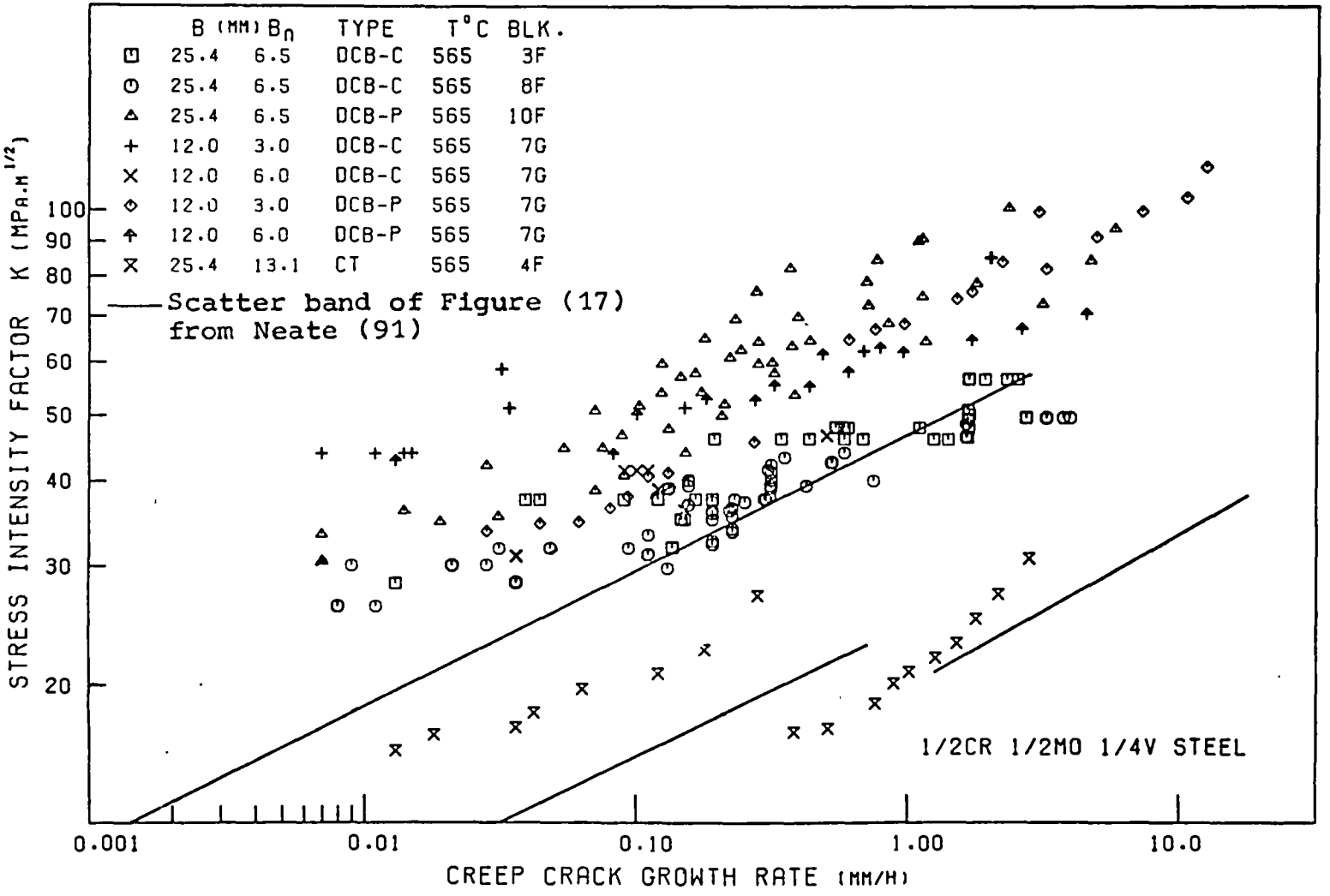

Figure (119): The effect of various geometries and thicknesses on the correlation of C.C.G. rate with K for low alloy steels tested at 565°C.

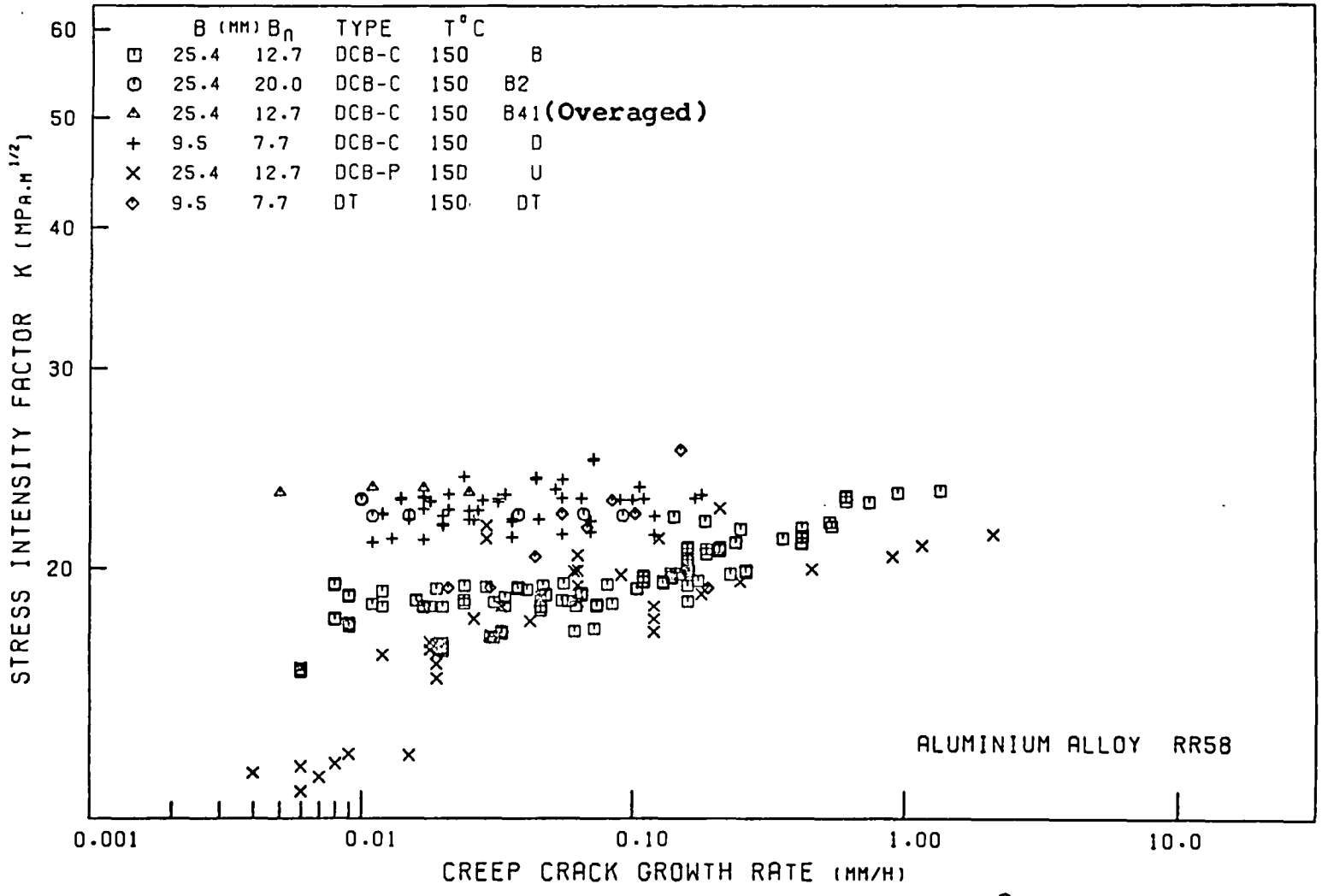

Figure (120): Correlation of the C.C.G. rate of RR58 at 150°C with the theoretically evaluated K (in comparison to the experimental derivation of K shown in figure (118))

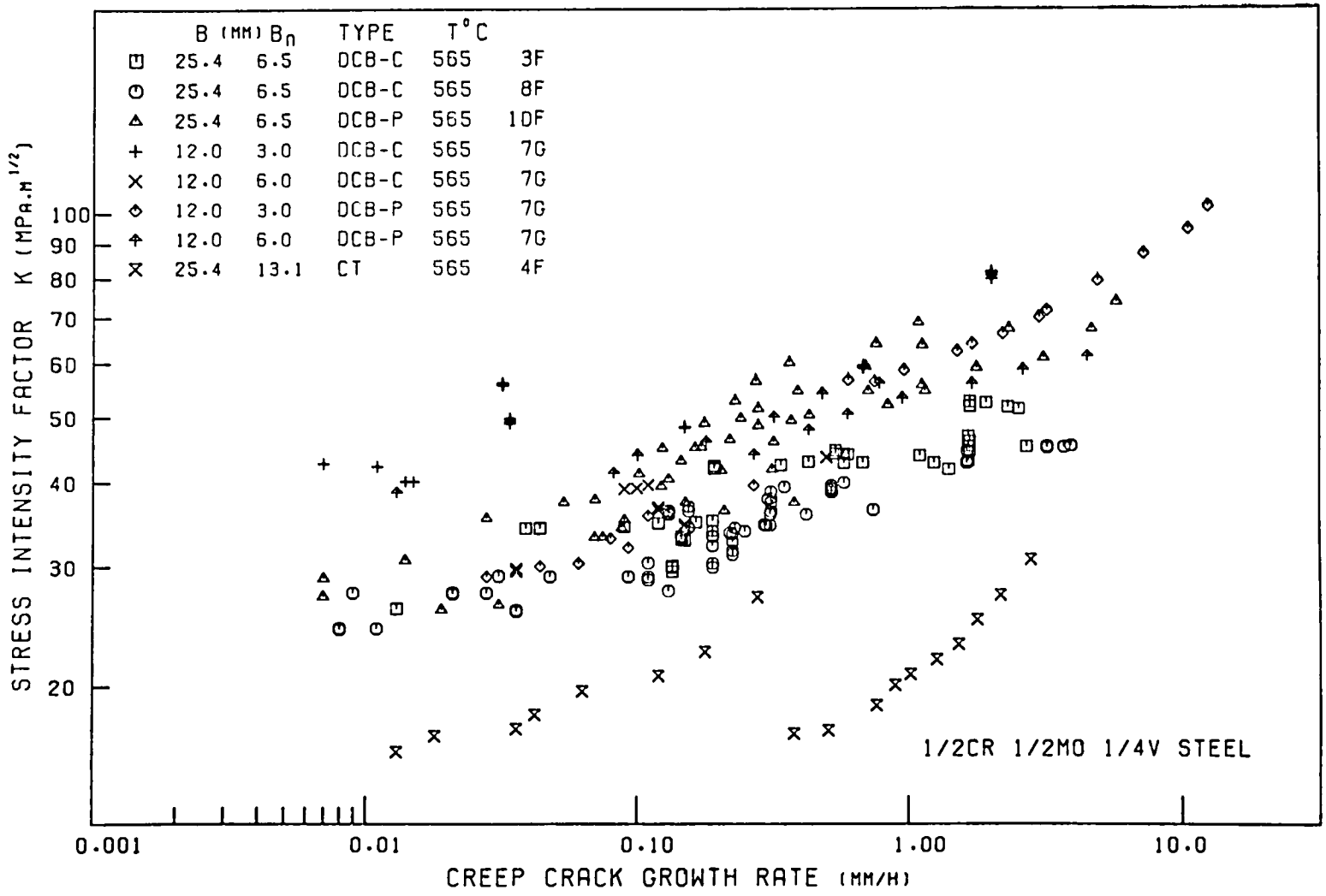

Figure (121): Correlation of the C.C.G. rate of steel at 565°C with the theoretically evaluated K (In comparison to the experimental derivation of K shown in figure (119))

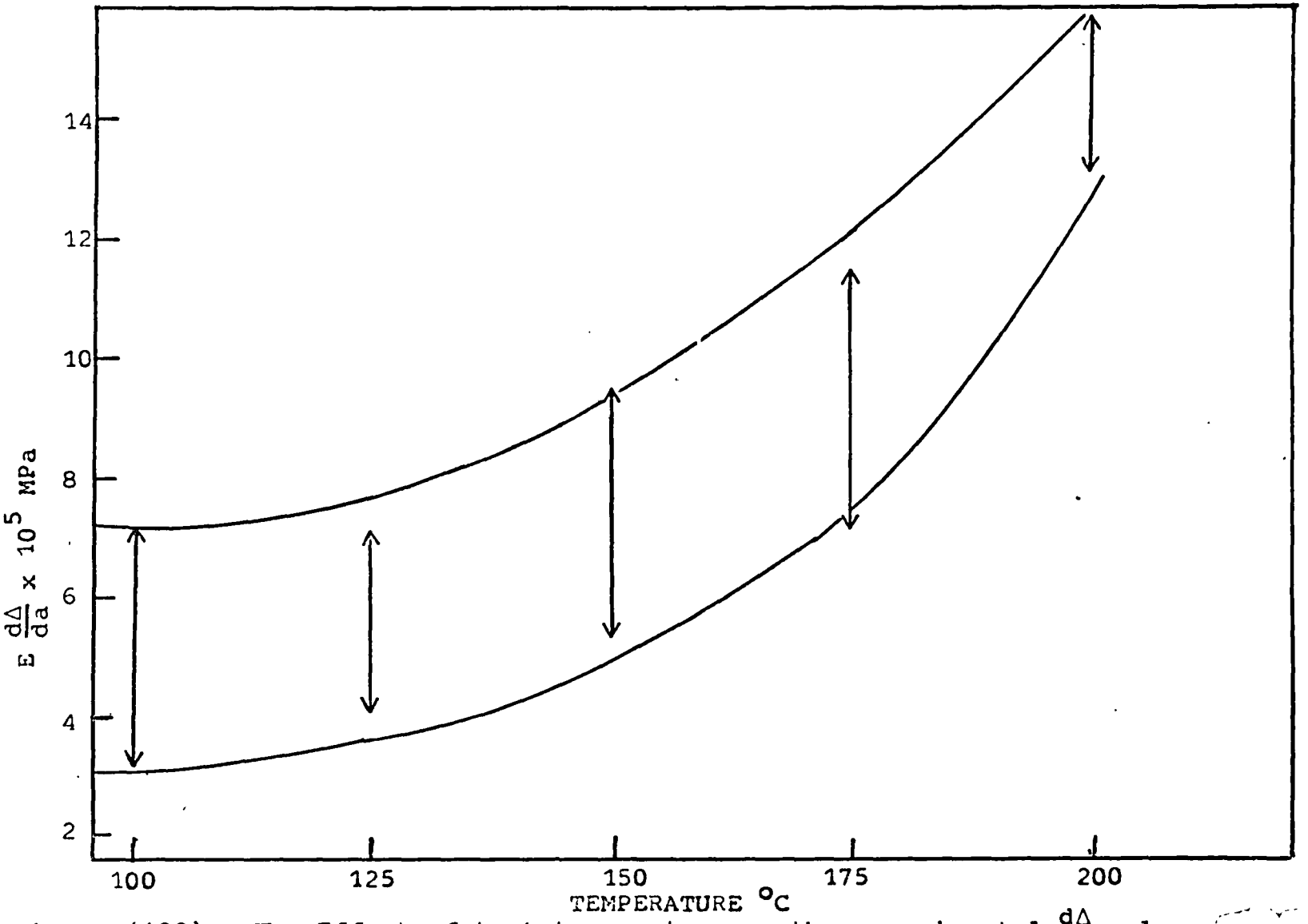

Figure (122): The Effect of test temperature on the experimental $\frac{d\Delta}{da}$ values for DCB-C 25 mm thick RR58 specimens

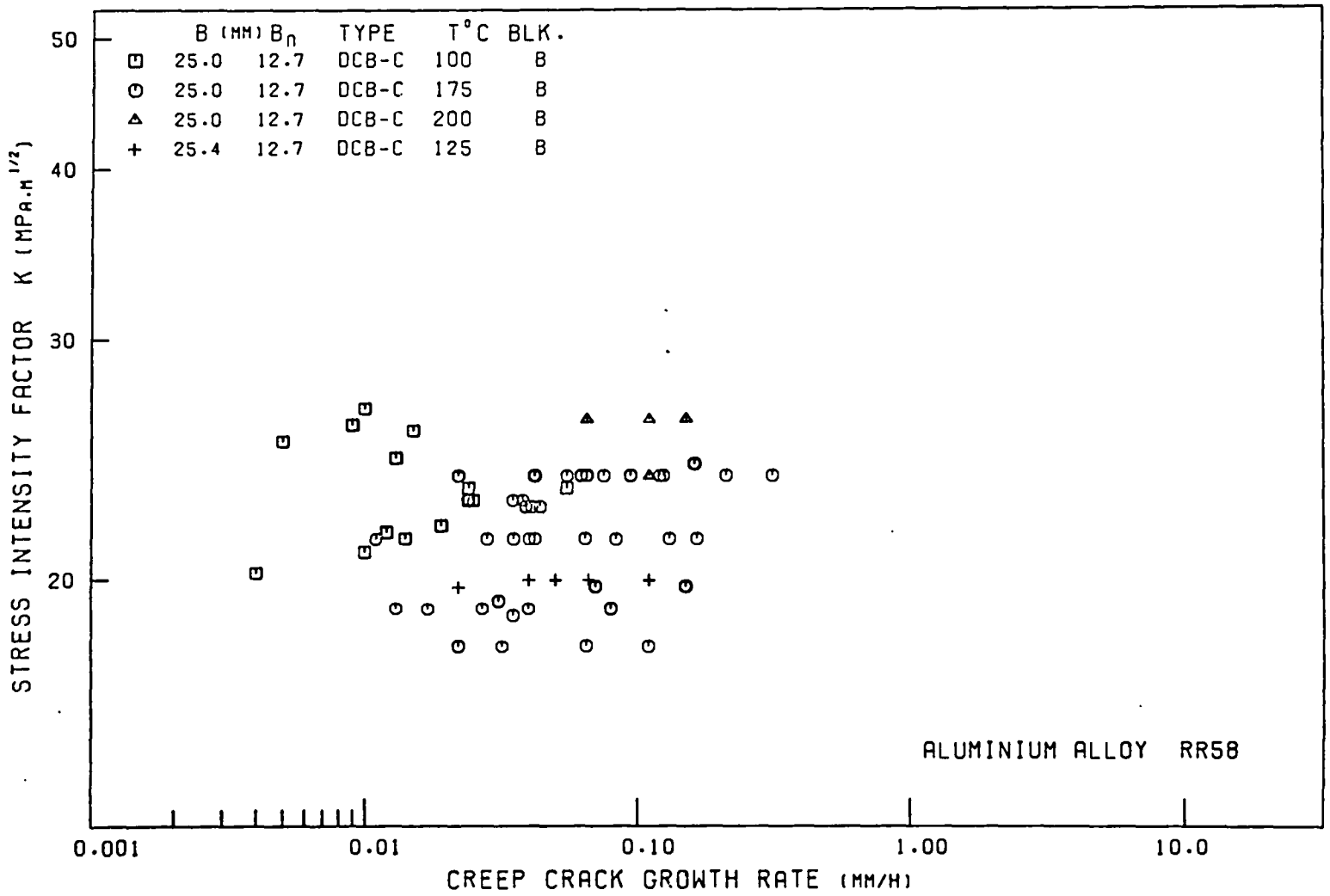

Figure (123): The effect of temperature on the correlation of C.C.G. rate with K for 25 mm thick DCB-C, RR58 specimens

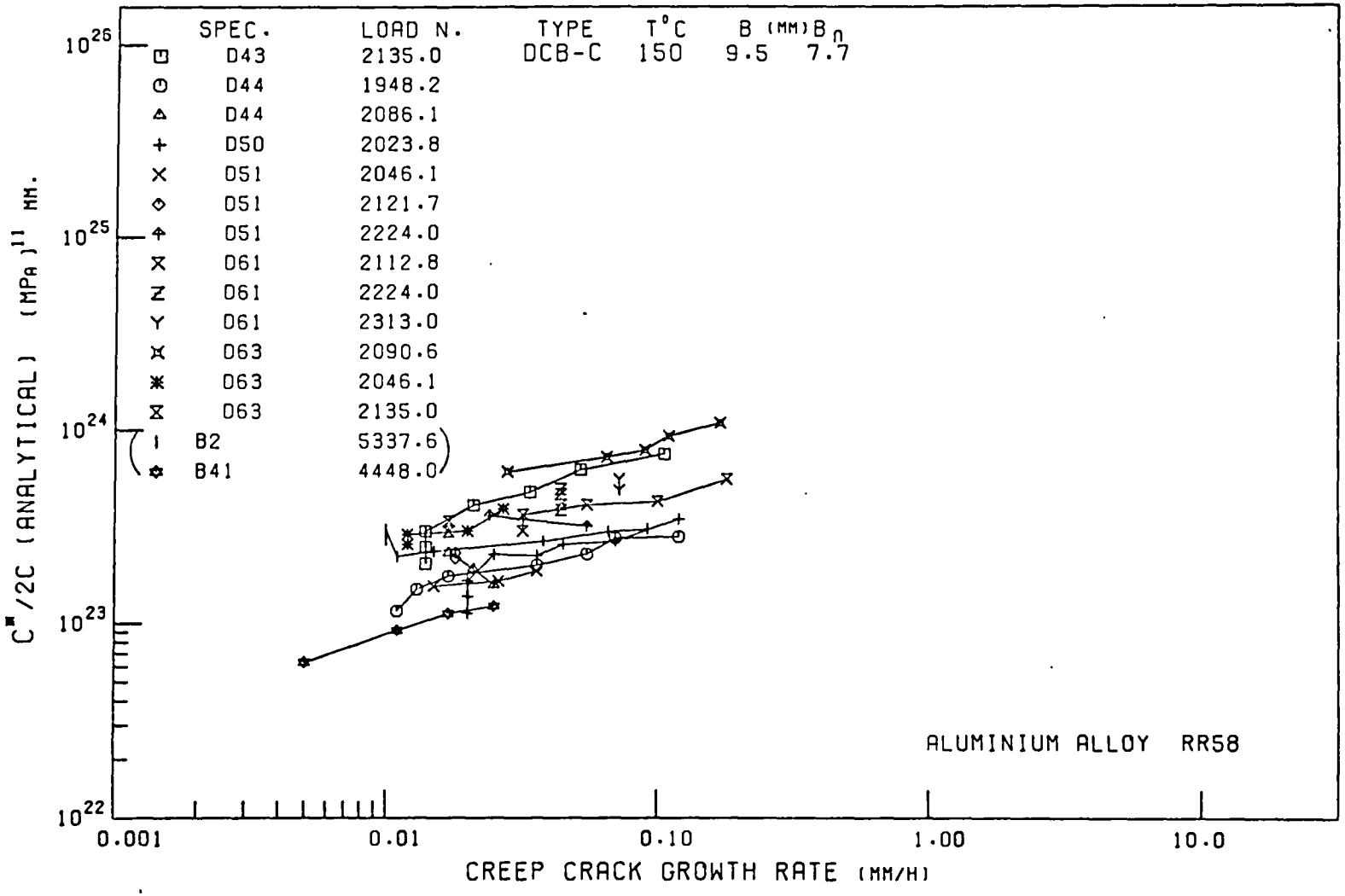

Figure (124): Correlation of C.C.G. rate with the analytical C* for the DCB-C RR58 specimens

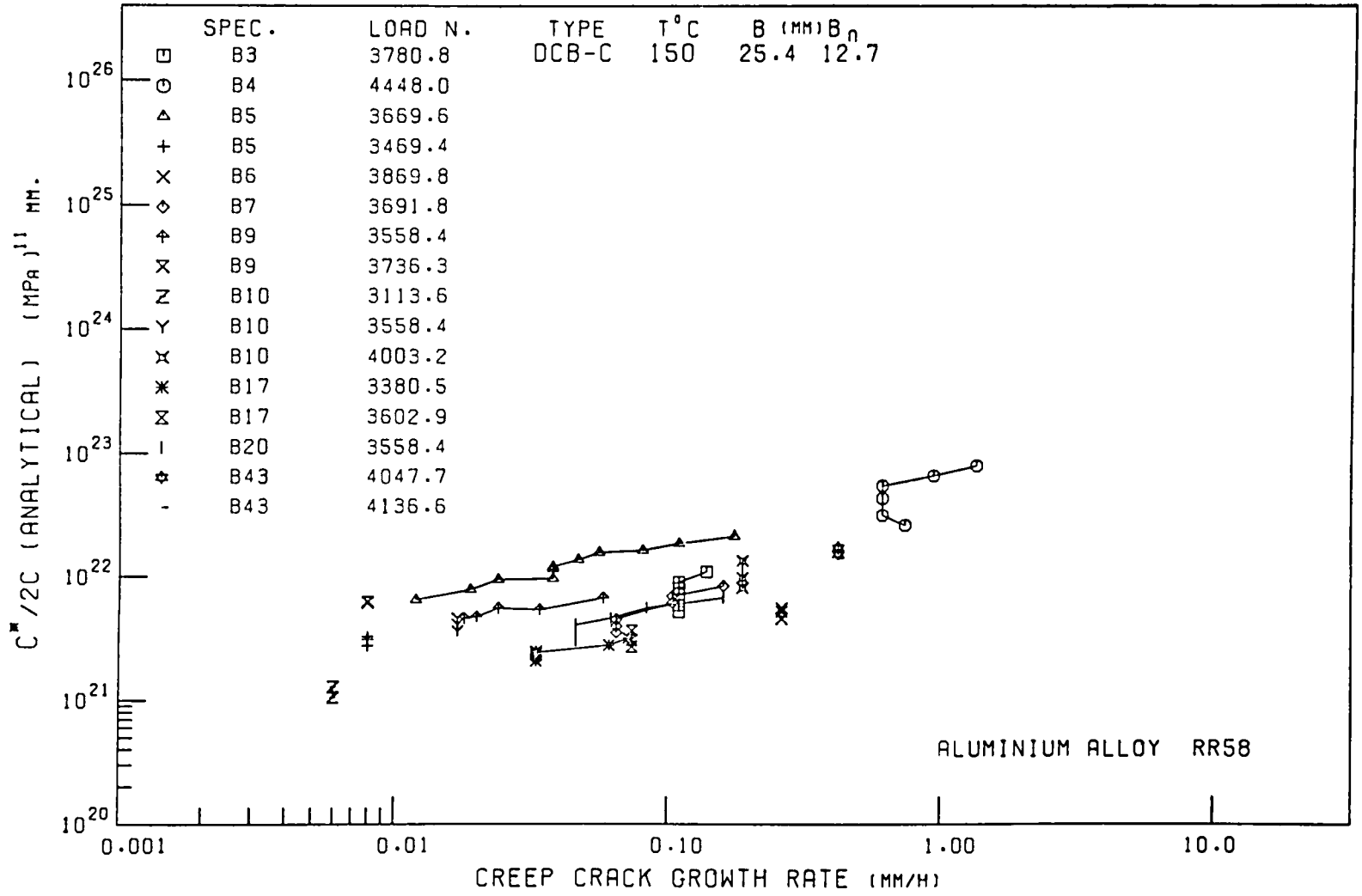

Figure (125): Correlation of C.C.G. rate with the analytical C* for the thick DCB-C RR58 specimens

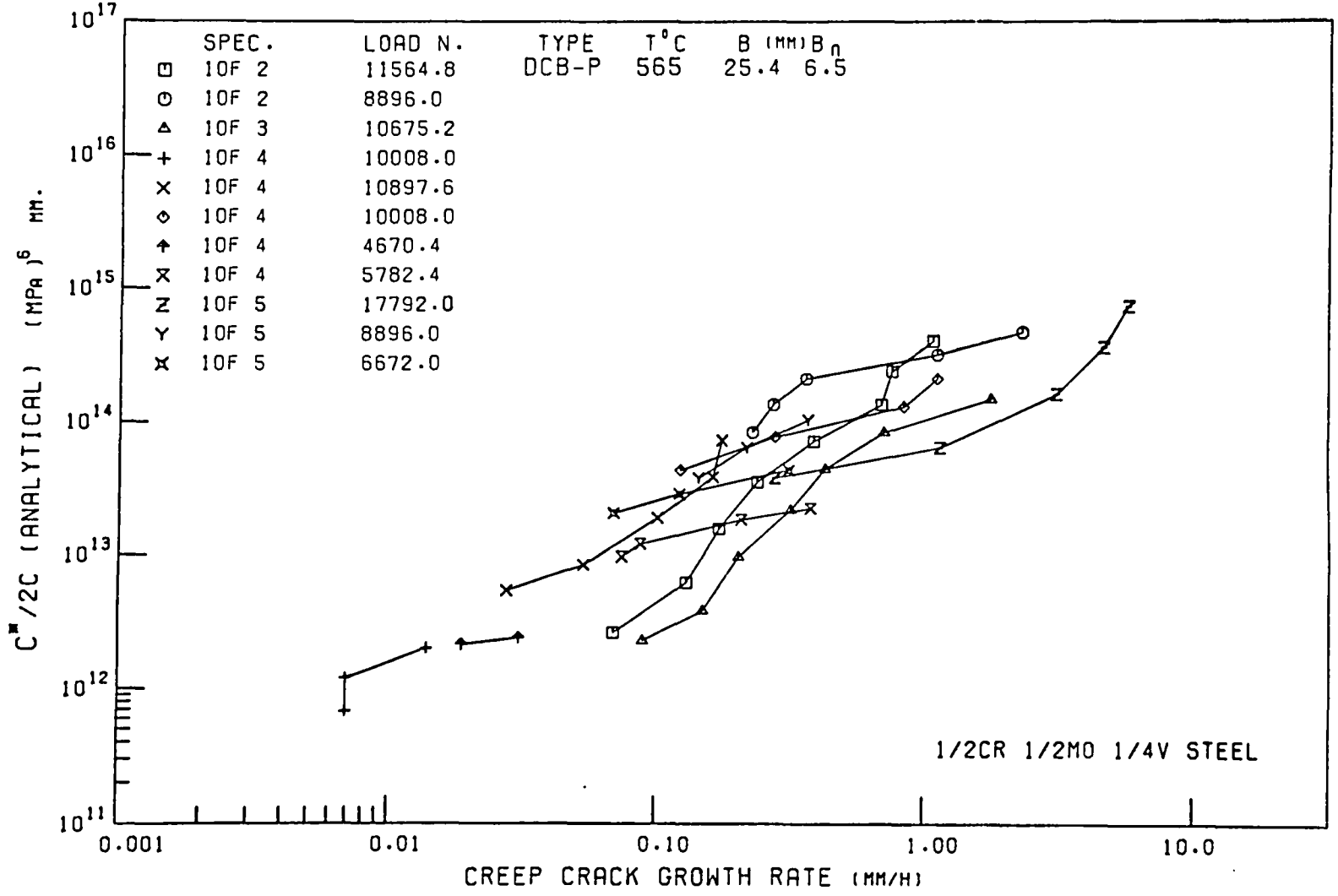

Figure (126): Correlation of C.C.G. rate with the analytical C* for the DCB-P steel specimens

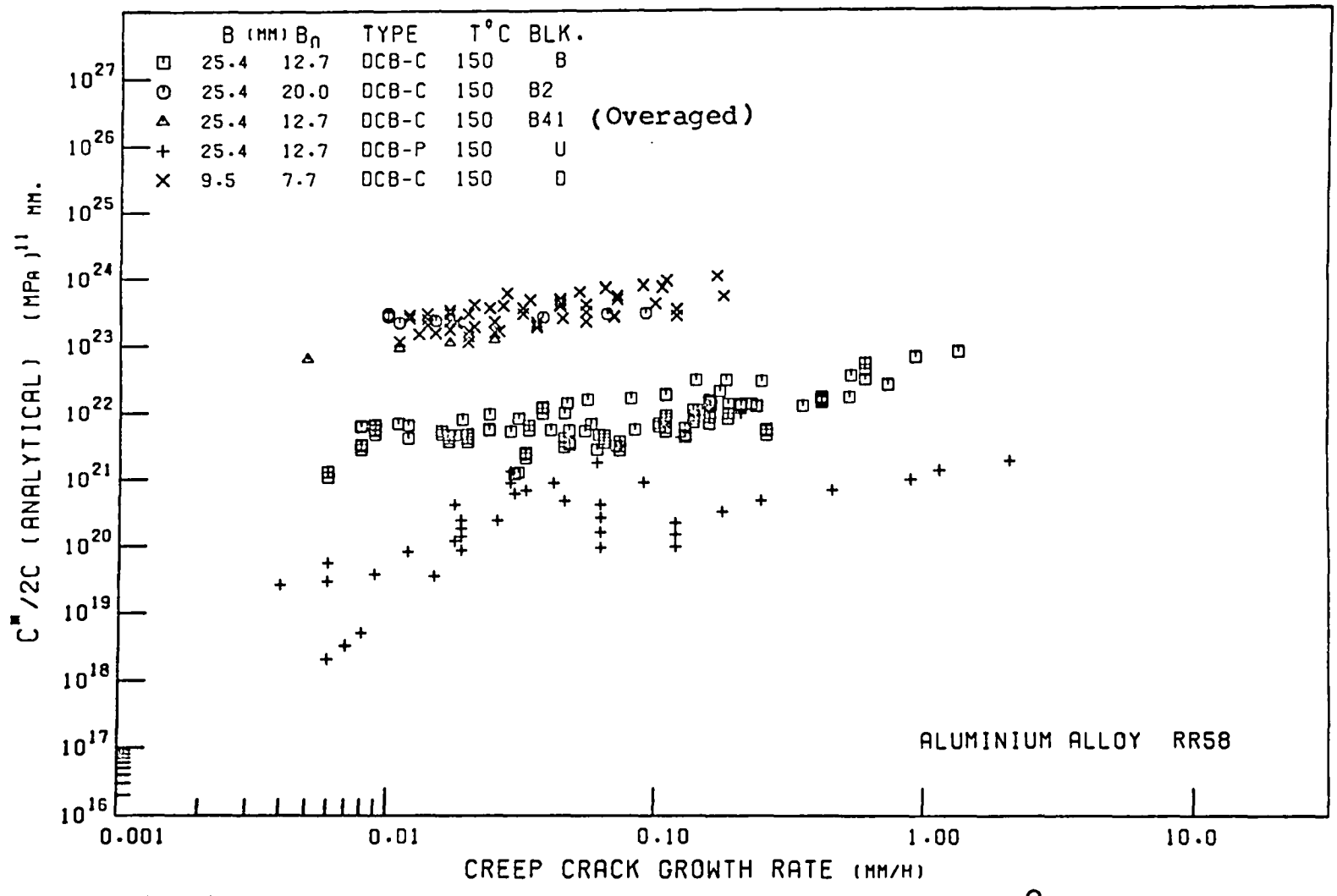

Figure (127): Comparison of all the C.C.G. rate data at 150°C with C* (analytical) for various thicknesses of DCB-C and DCB-P, RR58 specimens

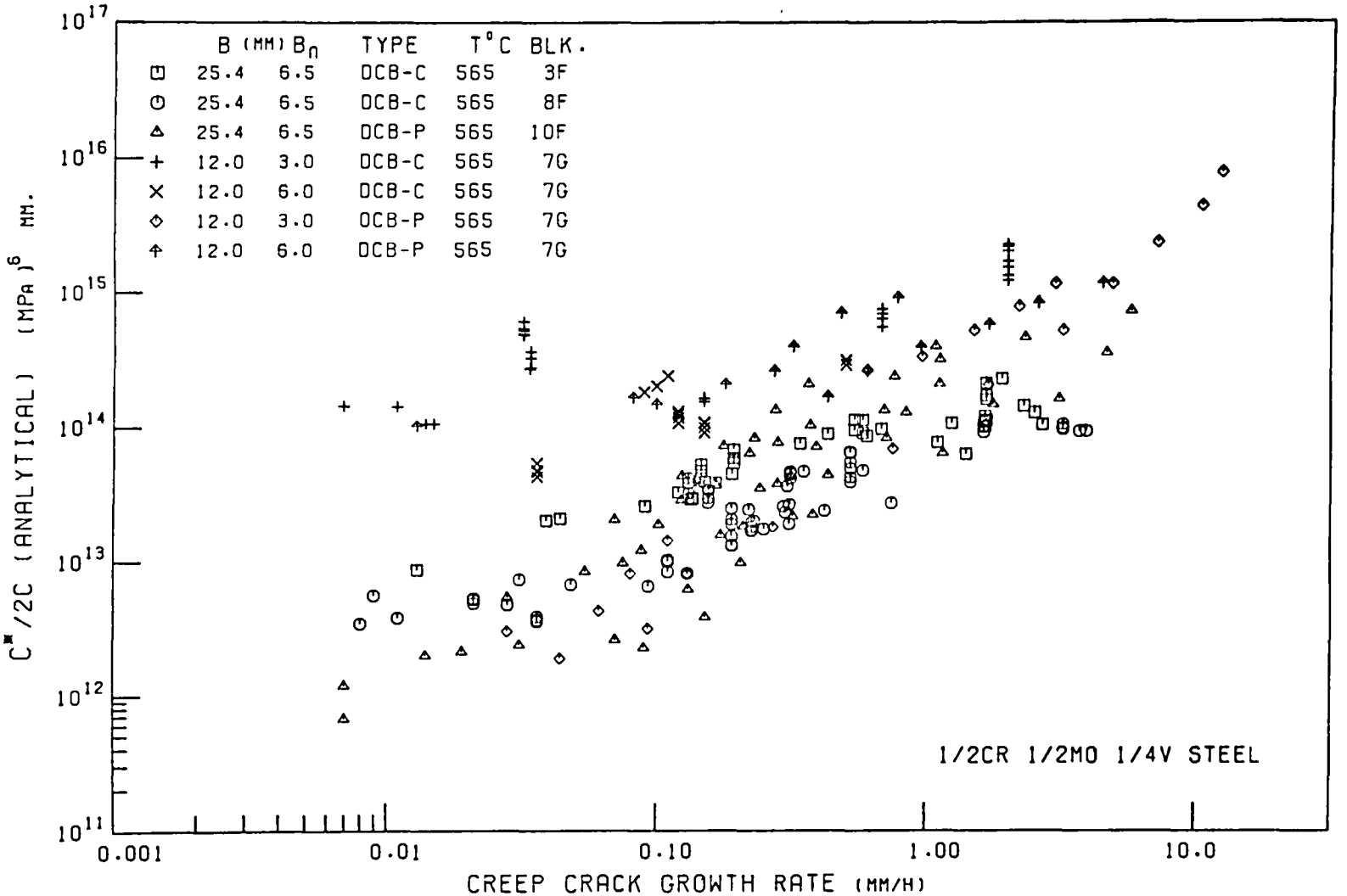

Figure (128): Comparison of all the C.C.G. rate data at 565°C with C* (analytical) for various thicknesses of DCB-C and DCB-P, steel specimens

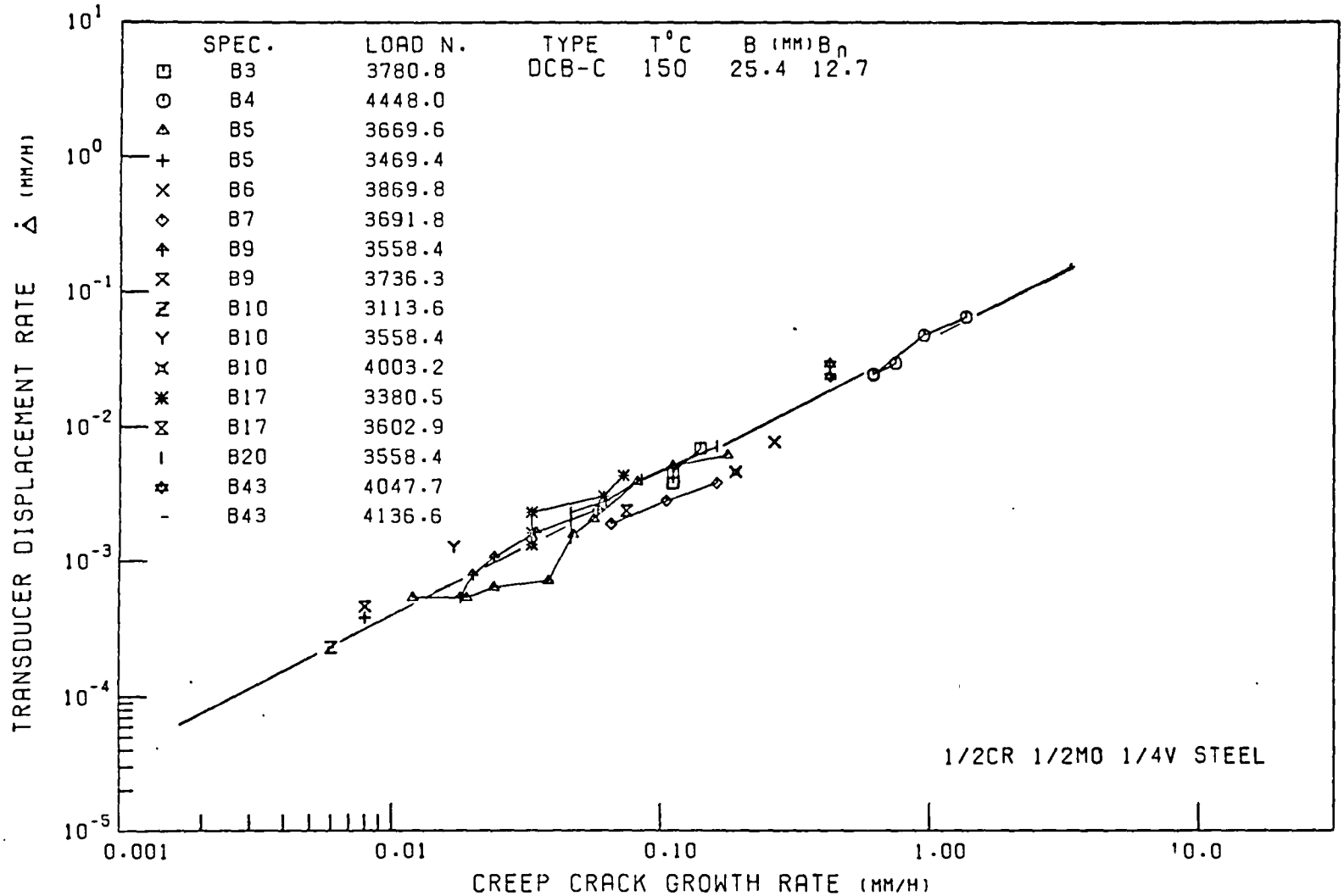

Figure (129): Correlation of C.C.G. rate with the experimental $\dot{\Delta}$ for the DCB-C, RR58 specimens

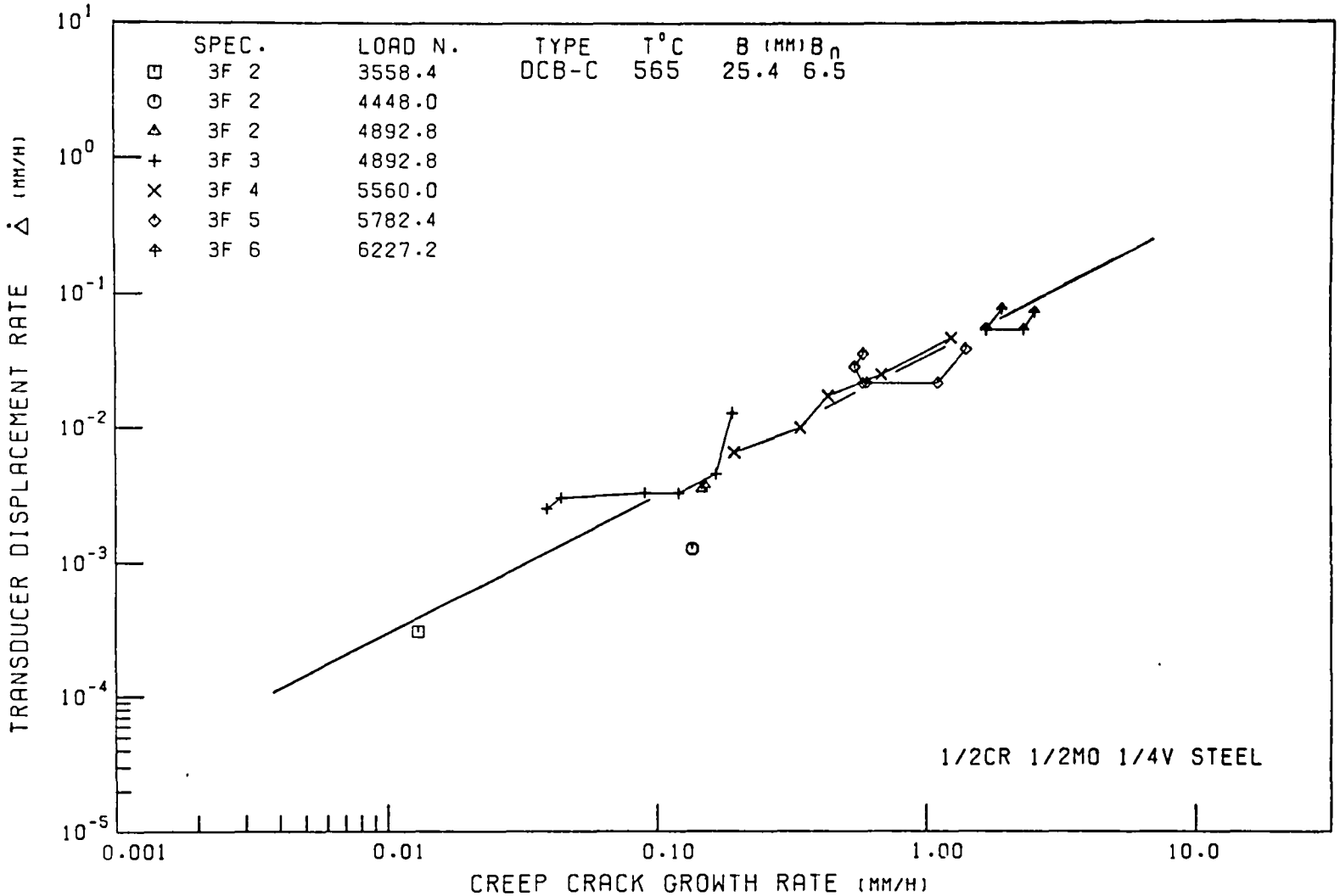

Figure (130): Correlation of C.C.G. rate with the experimental Å for the DCB-C quenched steel specimens

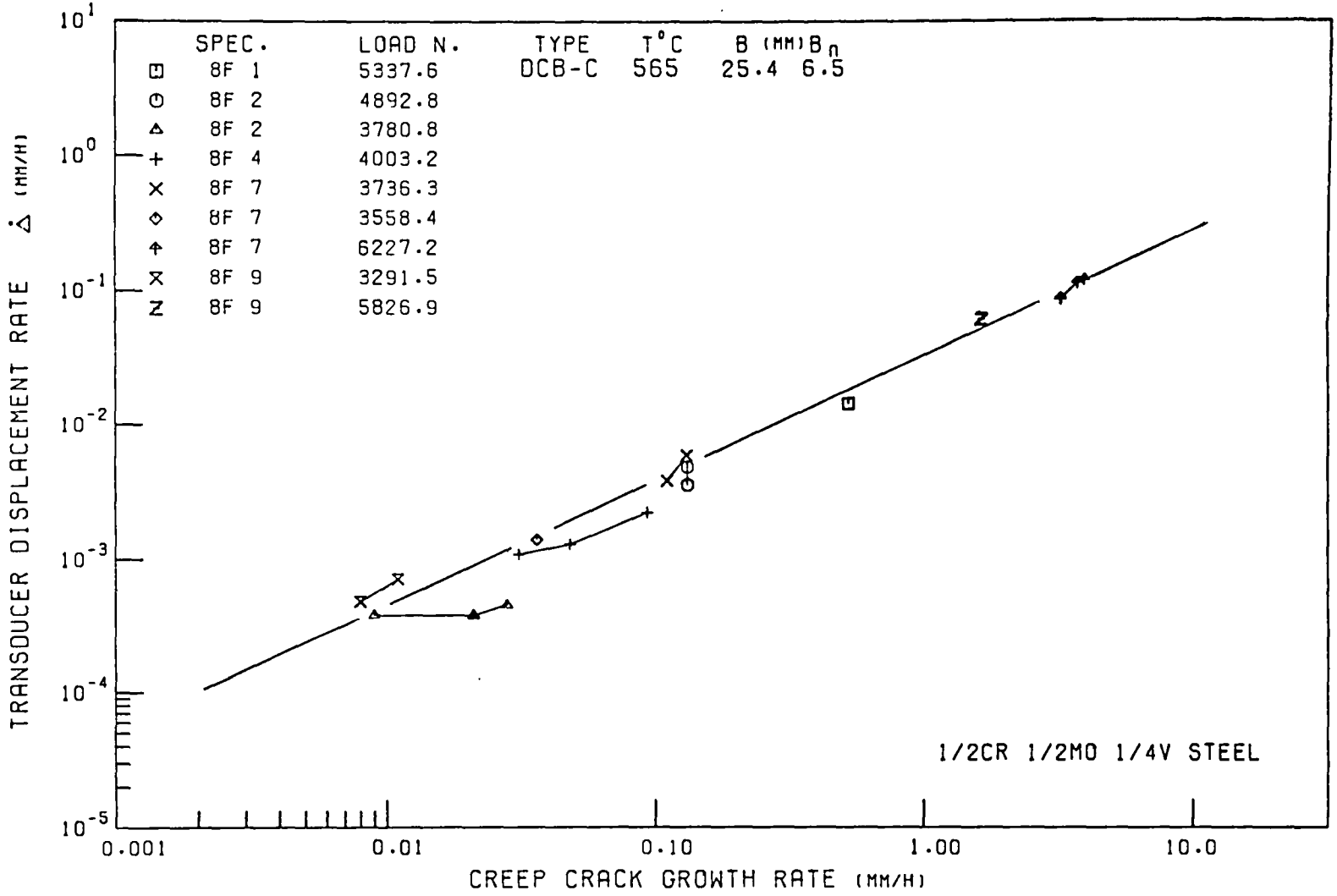

Figure (131): Correlation of C.C.G. rate with the experimental $\dot{\Delta}$ for the DCB-C quenched and tempered steel specimens

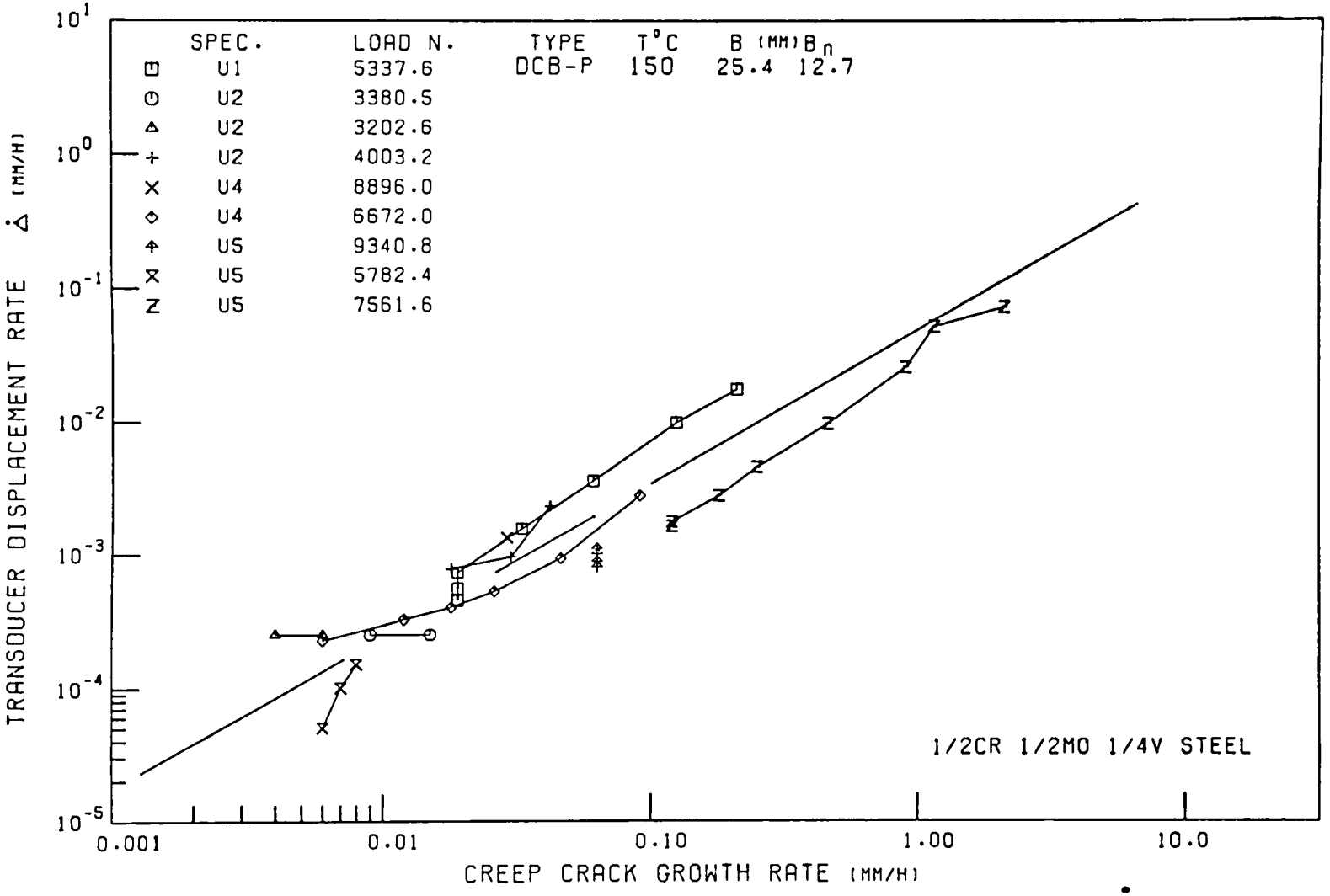

Figure (132): Correlation of C.C.G. rate with the experimental $\dot{\Delta}$ for the DCB-P RR58 specimens

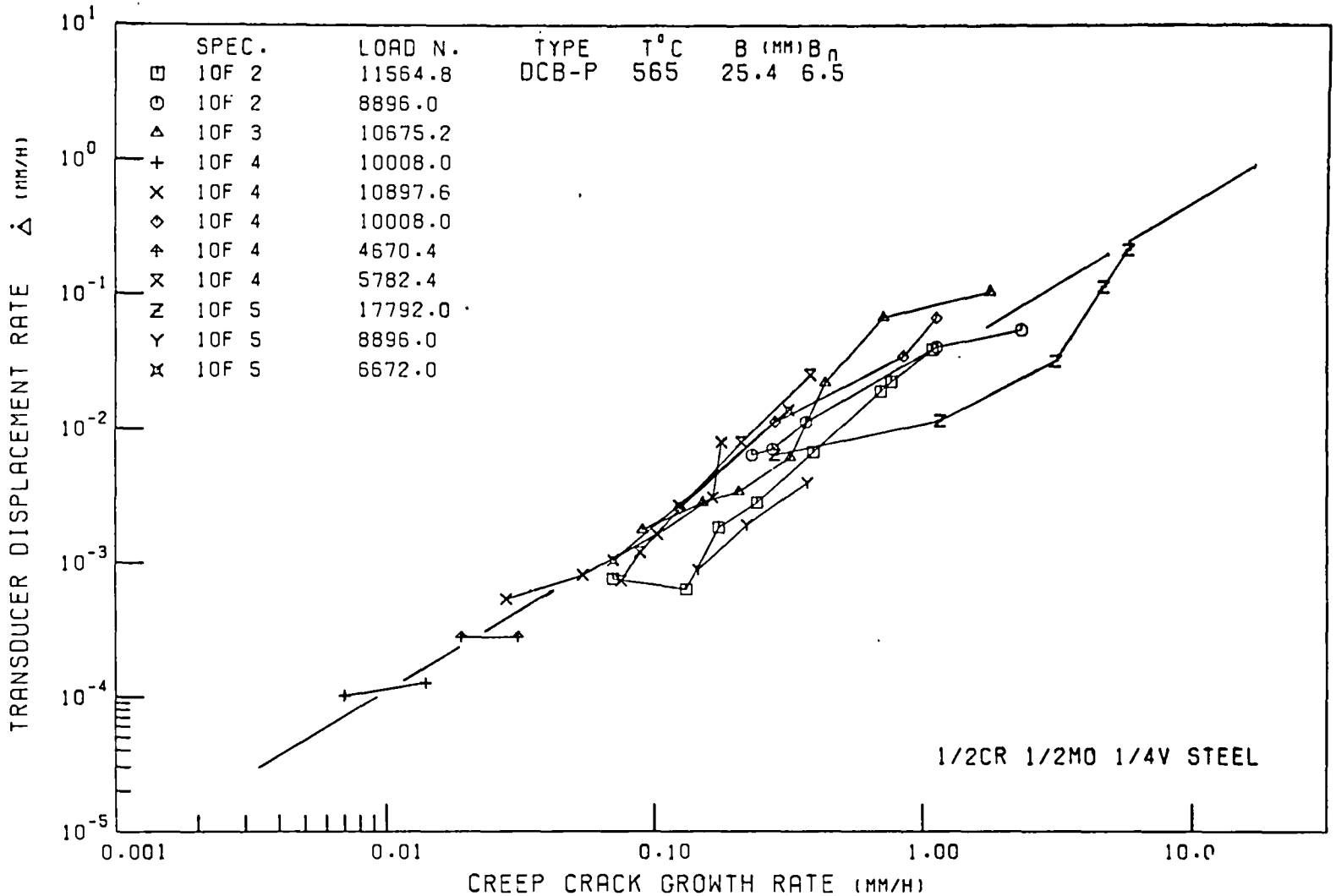

Figure (133): Correlation of C.C.G. rate with the experimental $\dot{\Delta}$ for the DCB-P, steel specimens

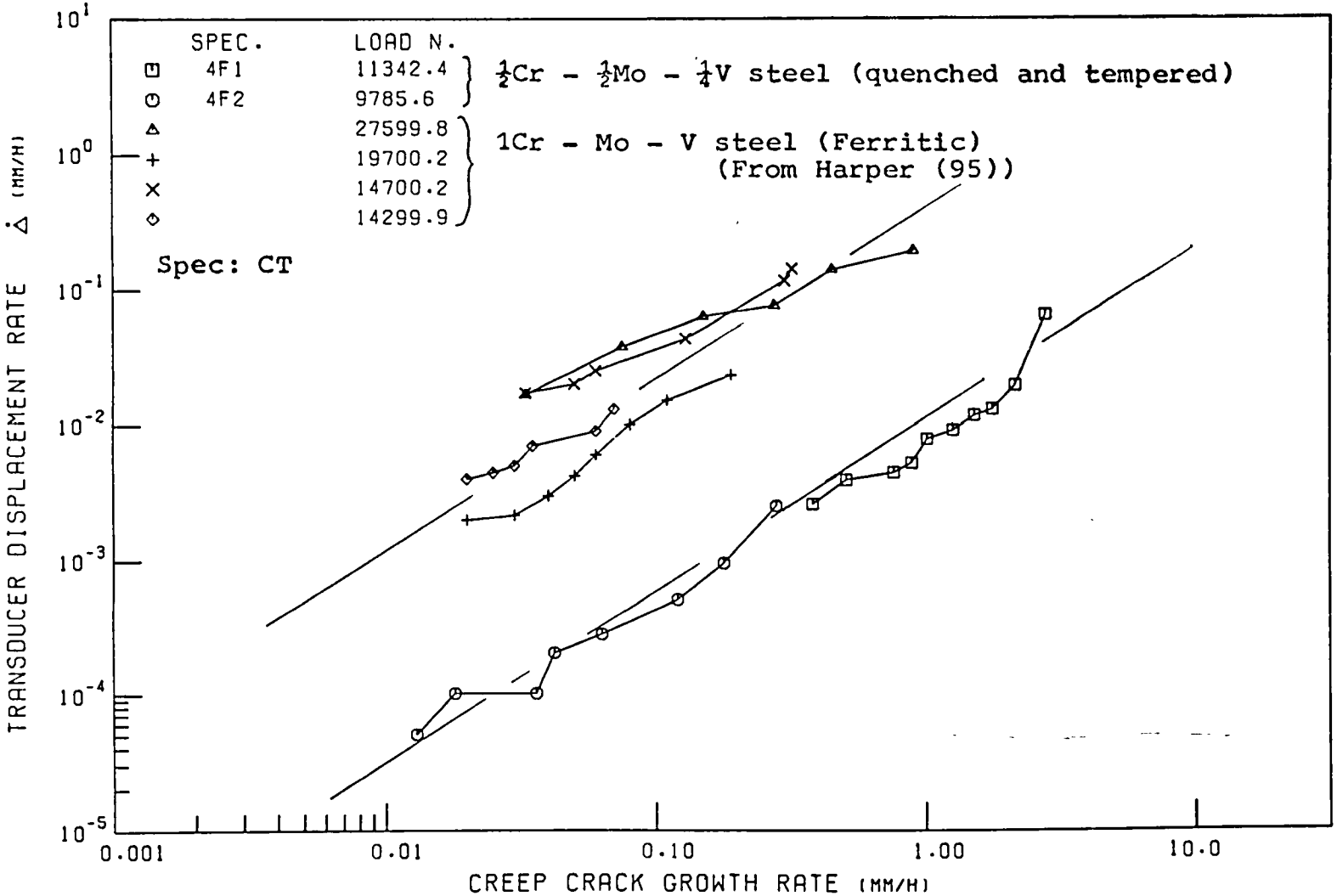

Figure (134): The effect of creep ductility of the experimental $\dot{\Delta}$ of low alloy steel, CT specimens

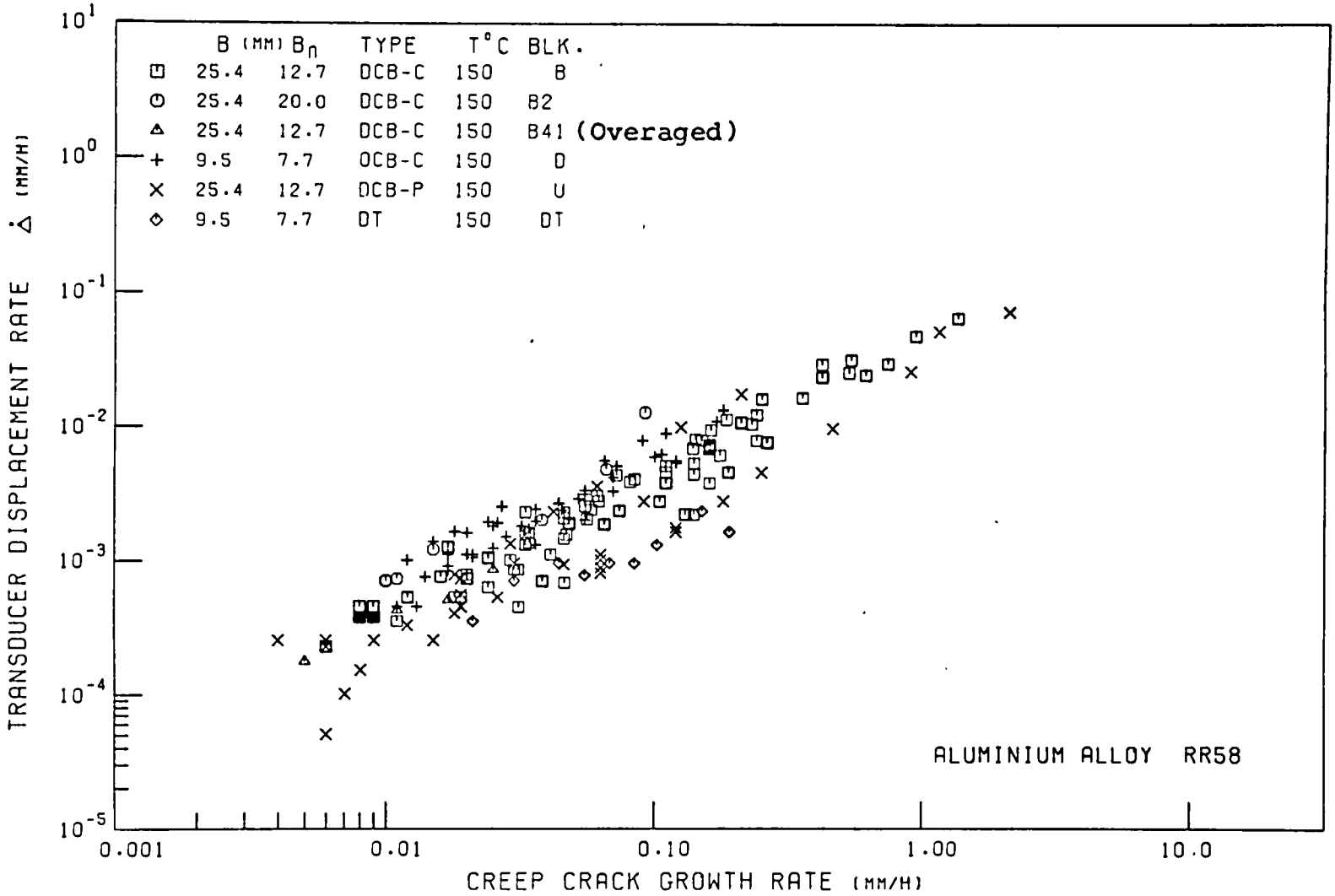

Figure (135): The effect of Geometry and Thickness on the correlation of C.C.G. rate with the experimental $\dot{\Delta}$ for RR58 at 150°C.

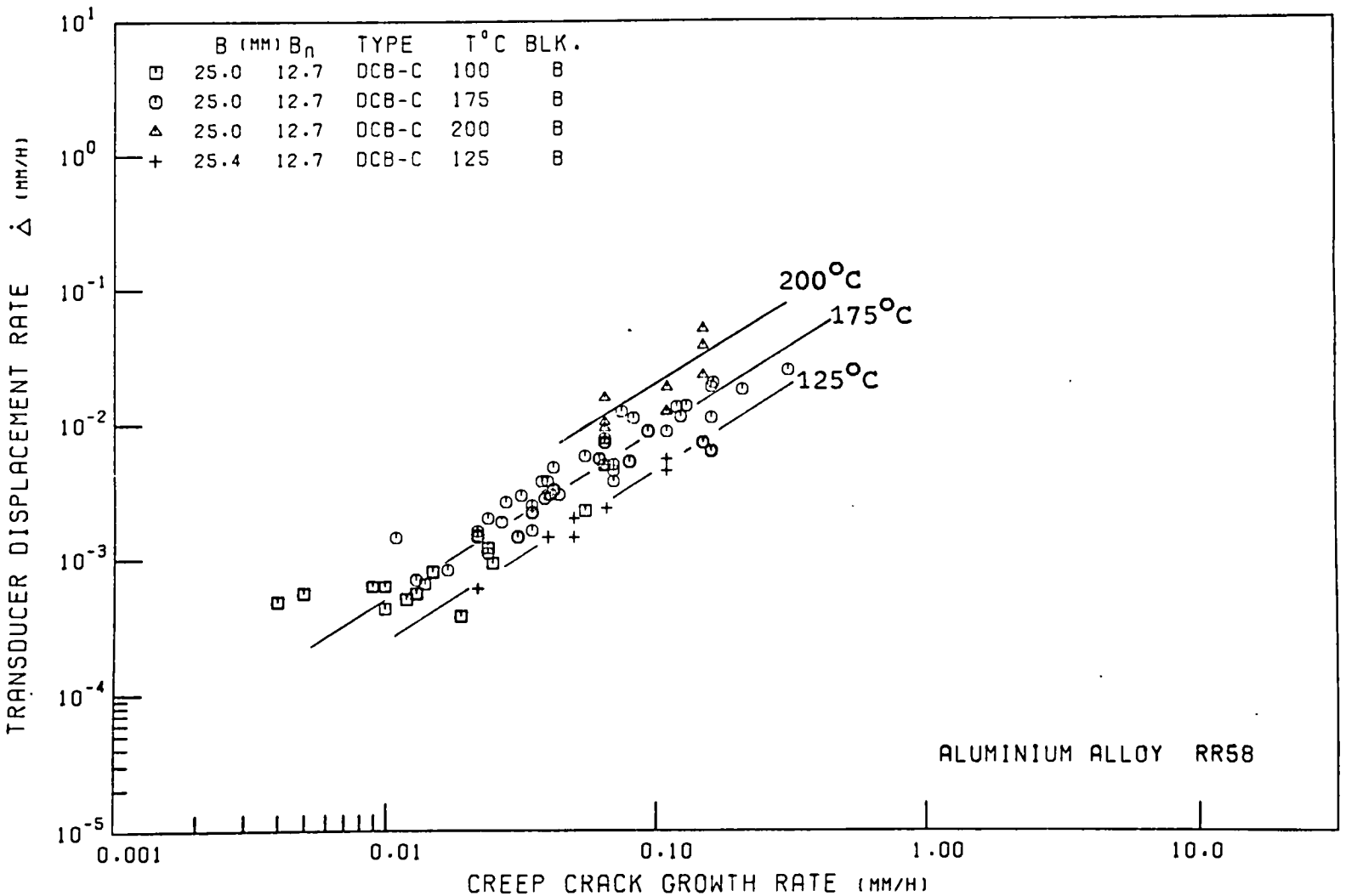

Figure (136): The effect of temperature on the correlation of the C.C.G. rate with the experimental $\dot{\Delta}$ for DCB-C, RR58 specimens

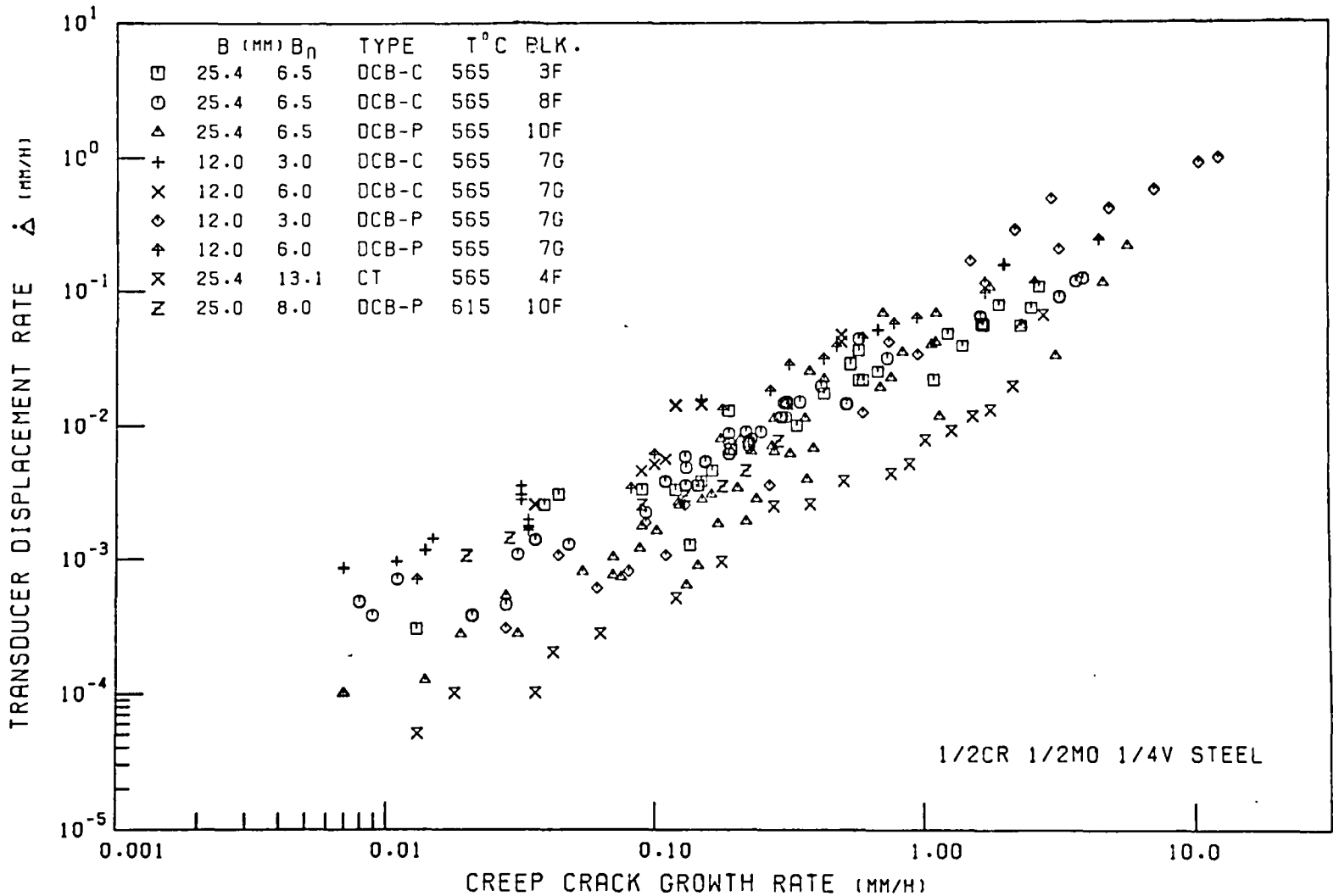

Figure (137): The effect of geometry and thickness on the correlation of C.C.G. rate with the experimental Δ for the steel at 565°C.

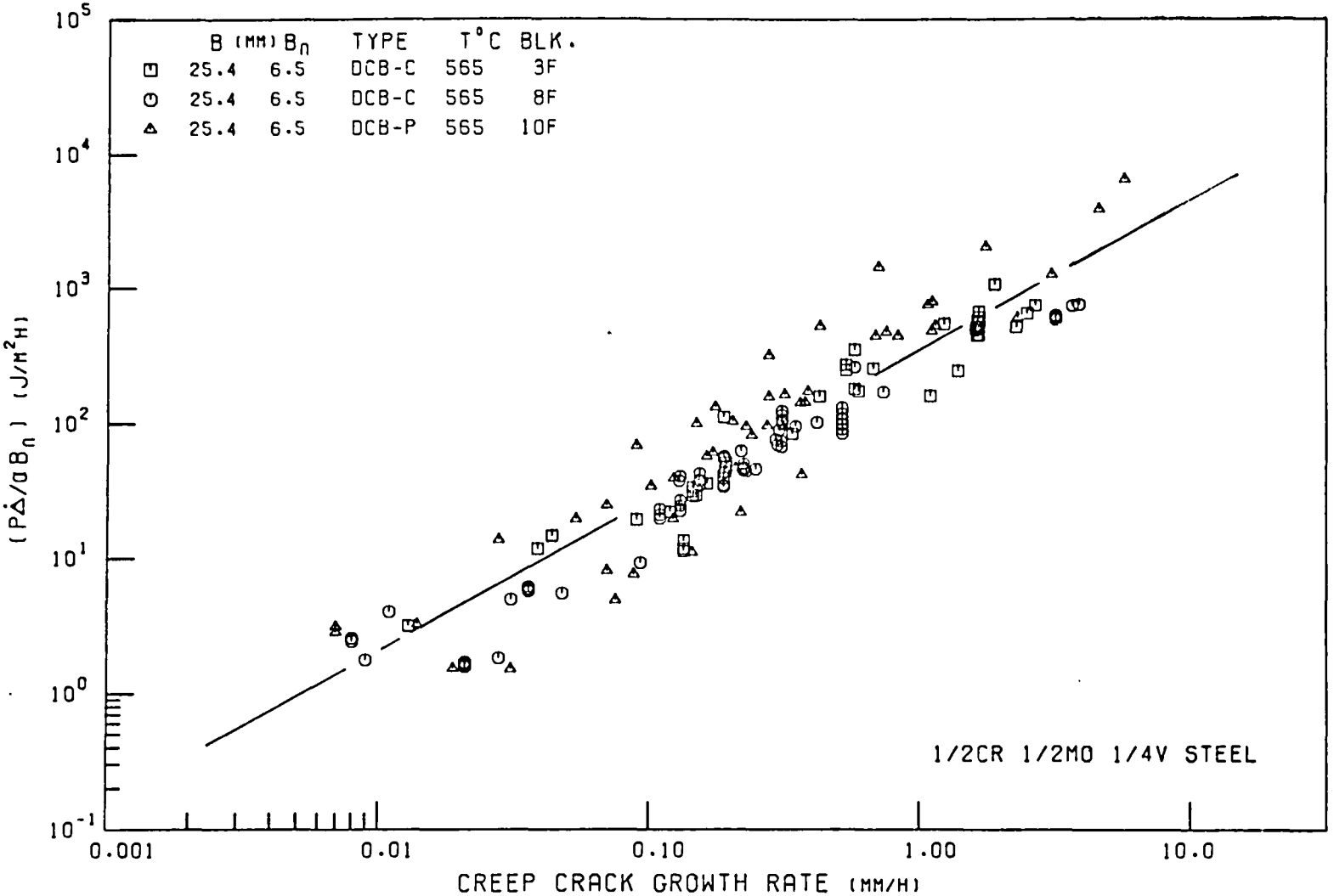

Figure (138): Correlation of C.C.G. rate with C^*_T for the thick DCB-C and DCB-P steel specimens

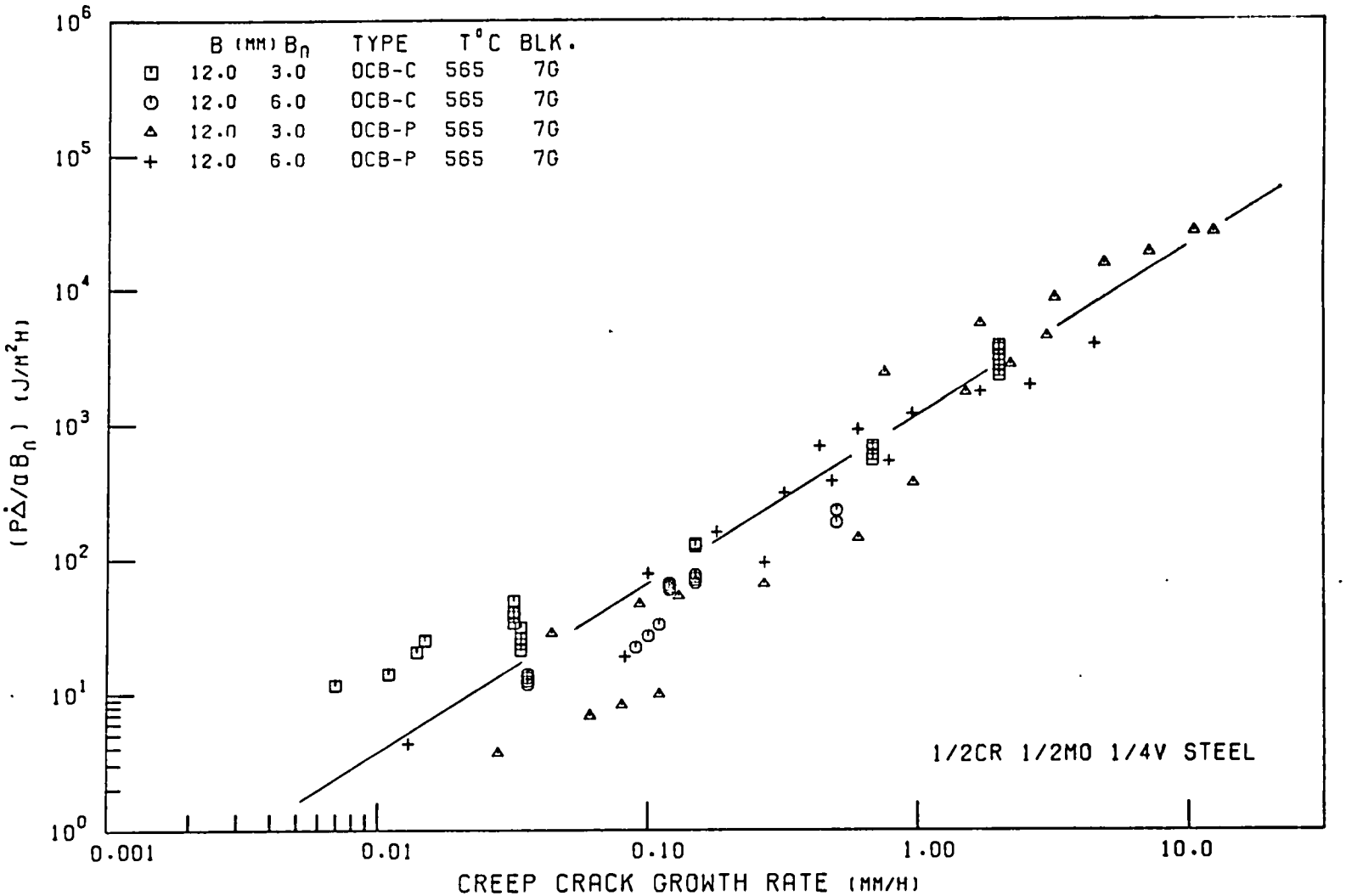

Figure (139): Correlation of C.C.G. rate with C^*_T for the thin DCB-C and DCB-P steel specimens

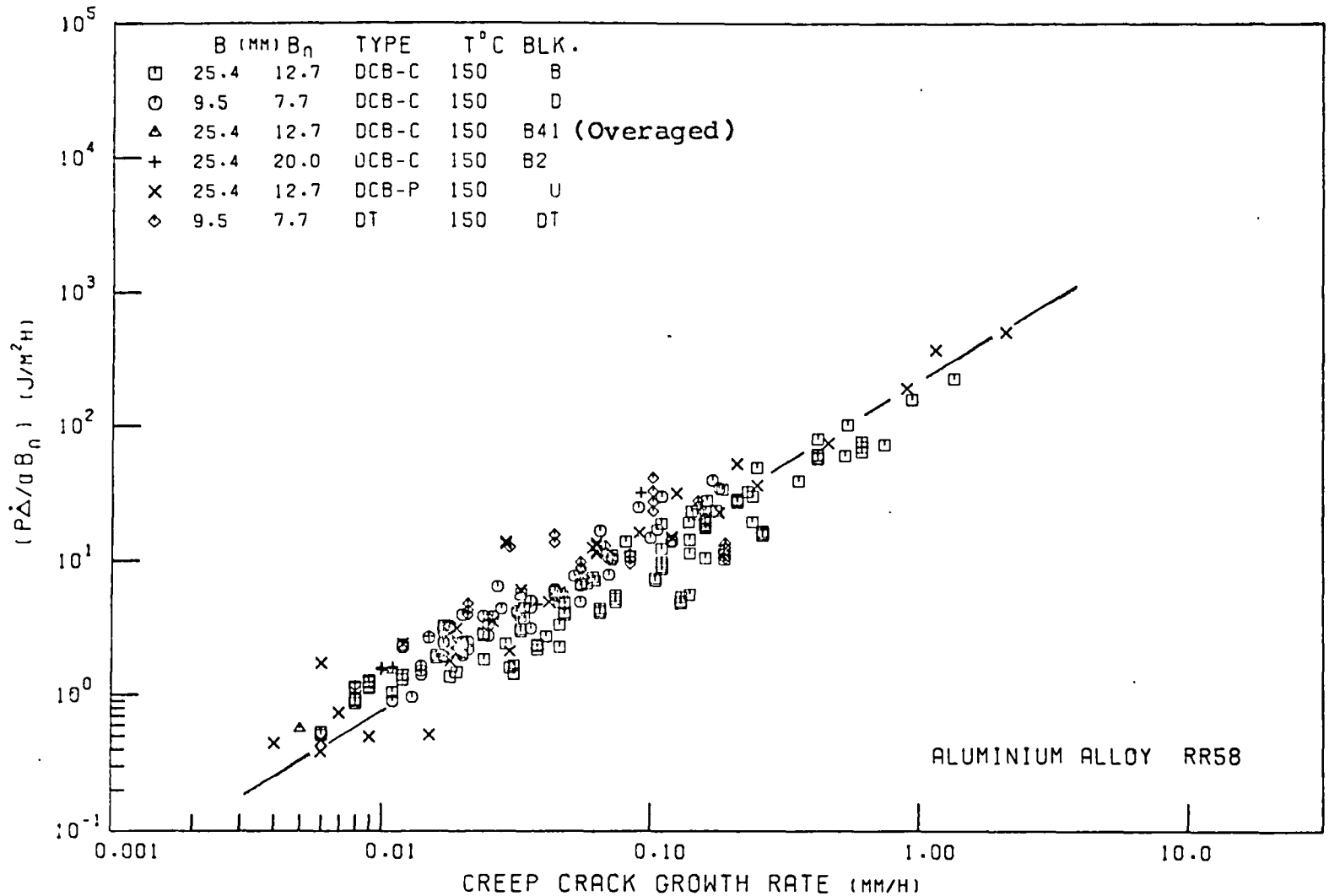

Figure (140): Correlation of C.C.G. rate with C^*_T for various geometries and thicknesses of RR58 specimens tested at 150°C.

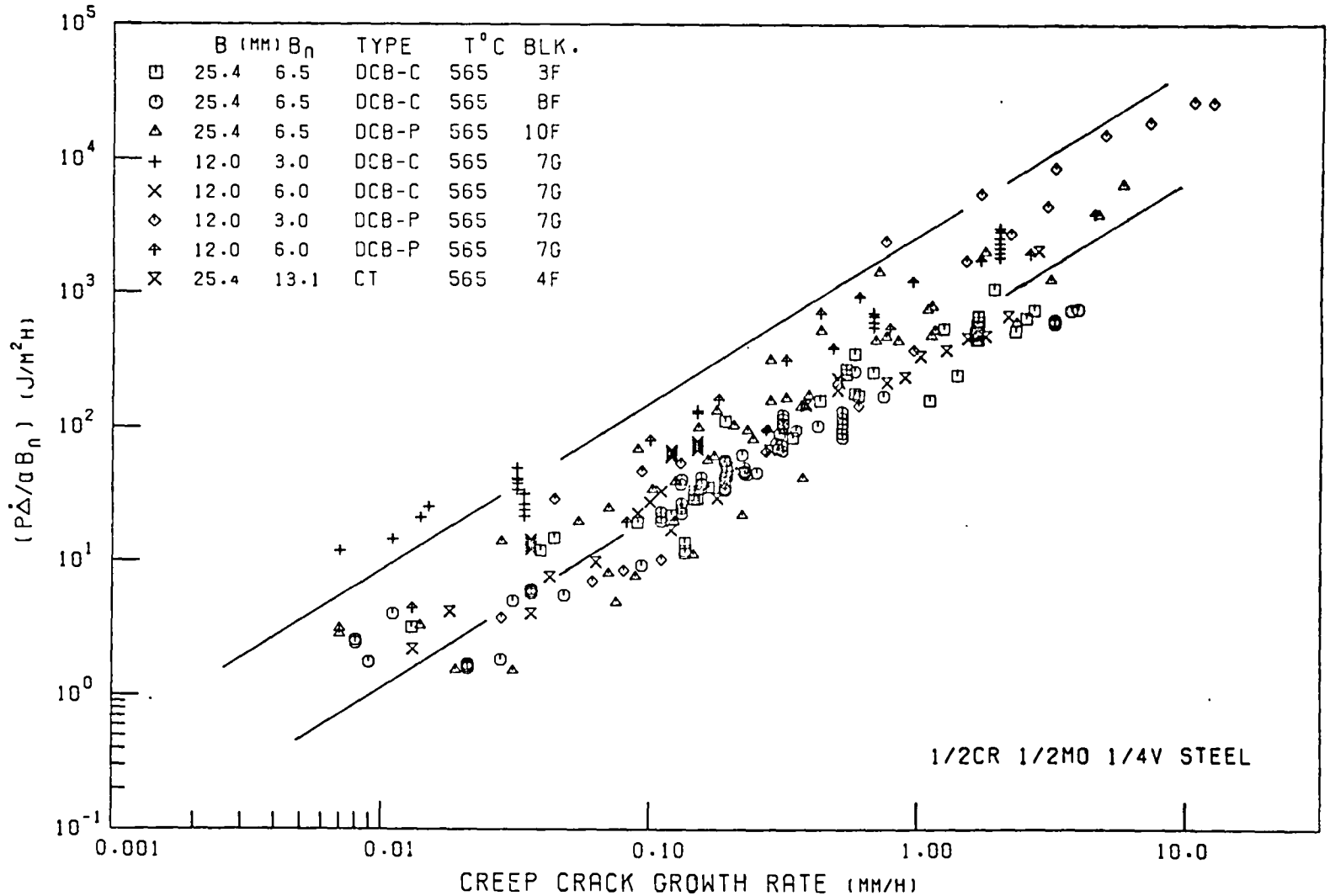

Figure (141): Correlation of C.C.G. rate with C^*_T for various geometries and thicknesses of steel tested at 565°C.

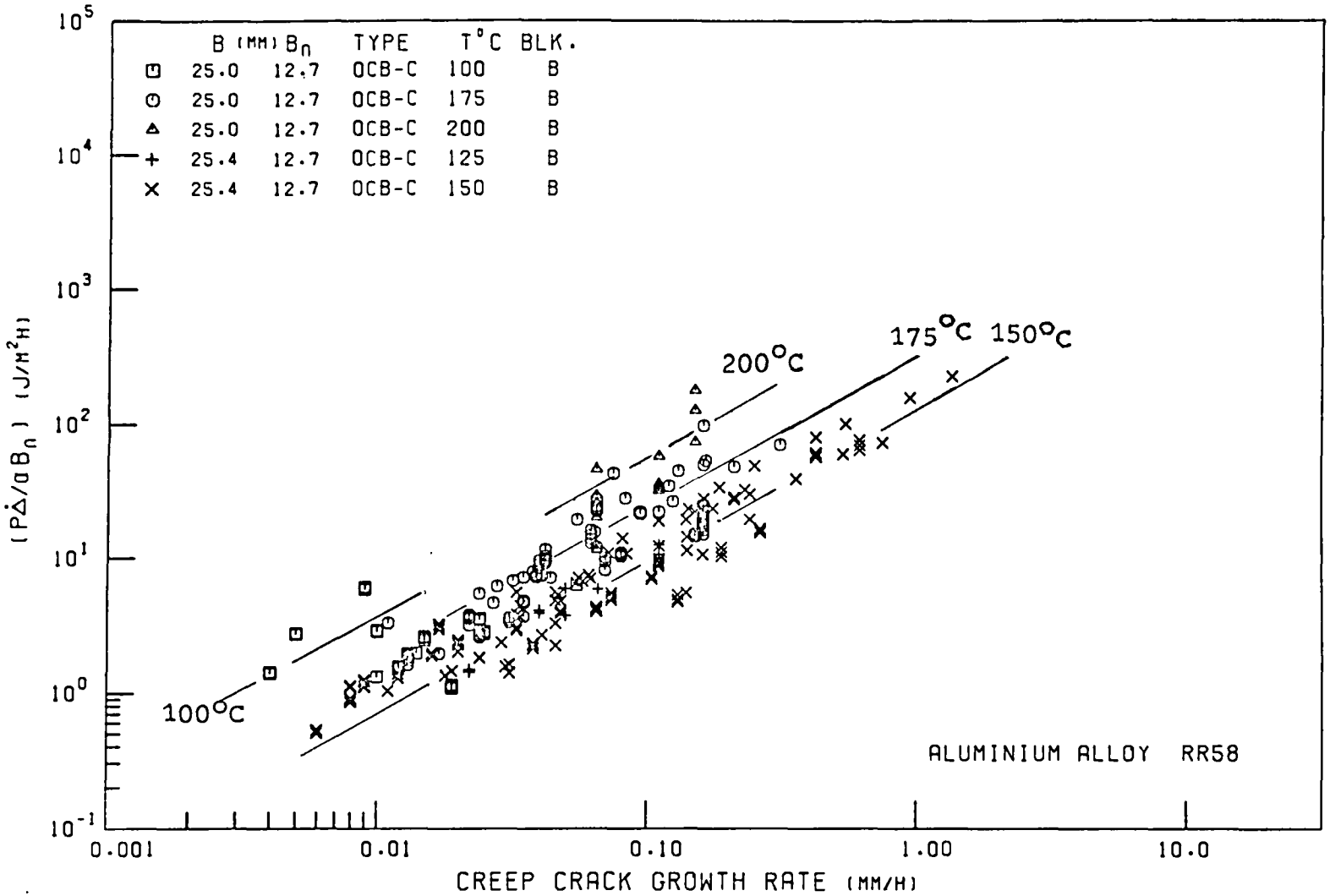

Figure (142): The effect of temperature on the correlation of C.C.G. rate with C^*_T for DCB-C, RR58 specimens

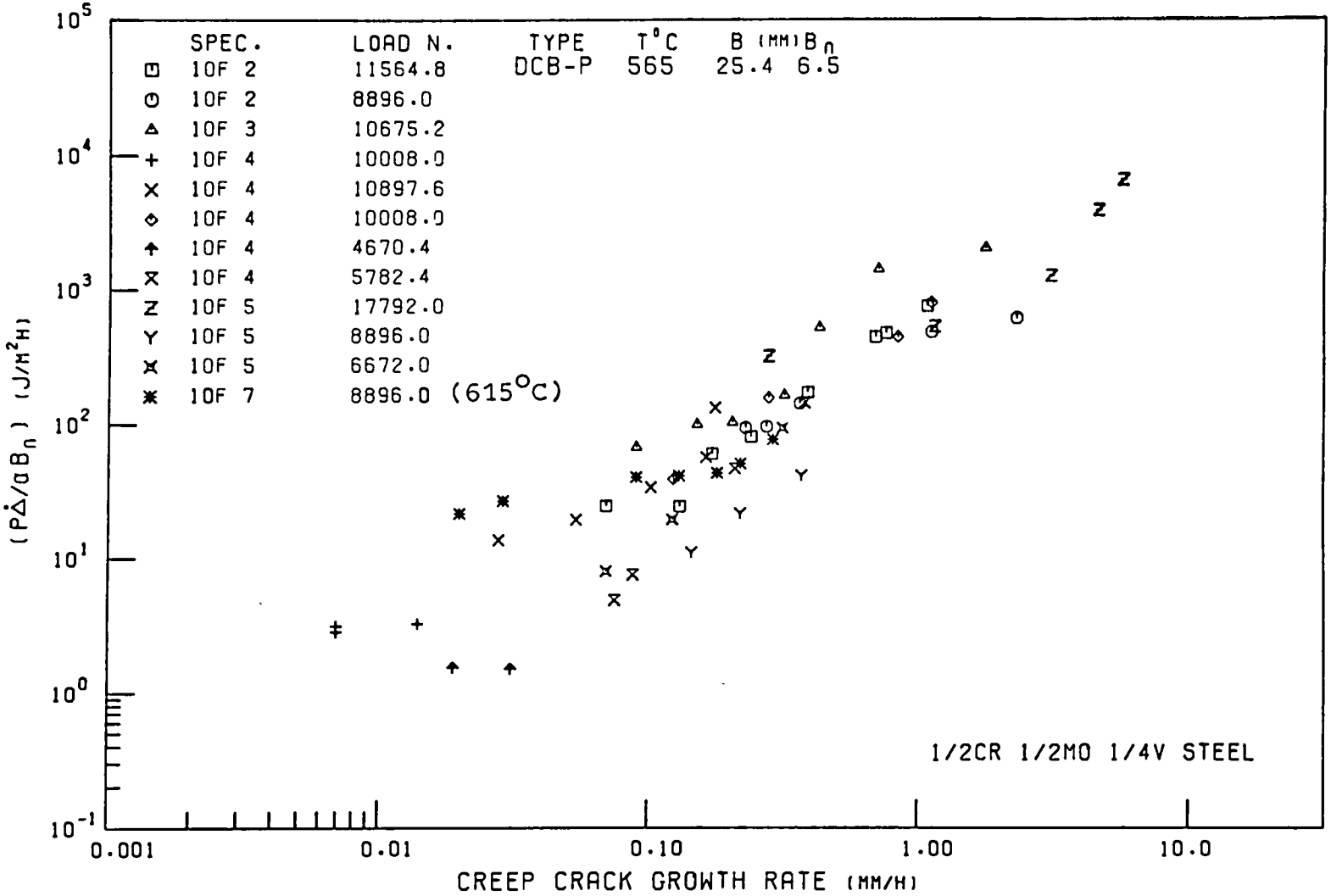

Figure (143): Effect of temperature on C.C.G. rate for the DCB-P steel specimens tested at 565 and 615°C.

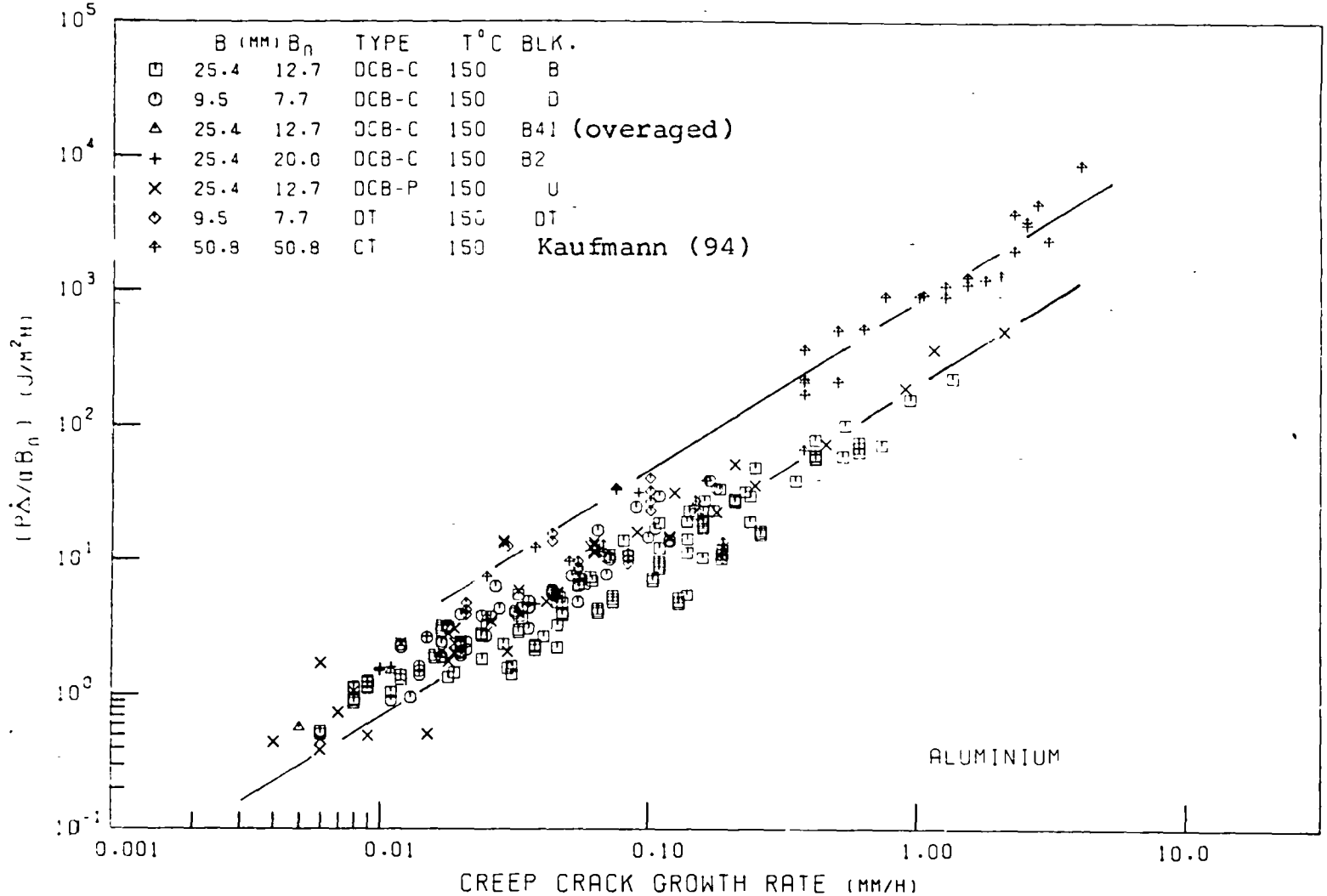

Figure (144): The effect of various geometries on the correlation of C.C.G. rate with C^*_T (also including the CT data on an aluminium alloy from Kaufmann (94))

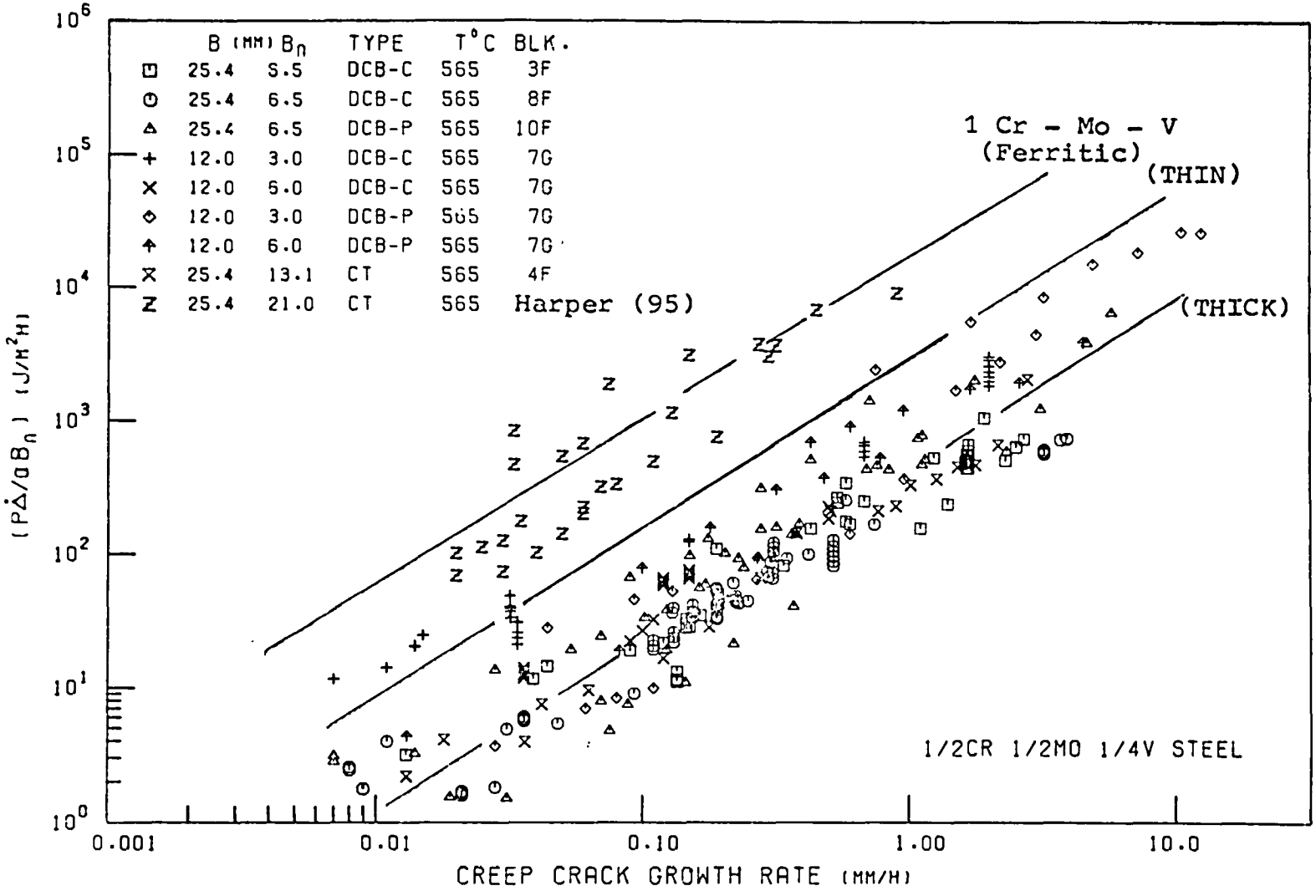

Figure (145): The effect of creep ductility, thickness, and differing geometries on the correlation of C.C.G. rate with C^*_T for low alloy steels

LIST OF PUBLISHED PAPERS

1. Nikbin, K.M., Webster, G.A.
Joint Metals Soc., I.Mech.E. Meeting, 'Prediction of Component Life at high temperatures', 1976.

2. Nikbin, K.M., Webster, G.A., Turner, C.E.
A.S.T.M. S.T.P., 601, 1976.

3. Nikbin, K.M., Webster, G.A., Turner, C.E.
Int. Conf. on Fract., Waterloo, Canada, 1977.
(To be published)

APPLICATION OF FRACTURE MECHANICS TO CREEP CRACKING

by

K.M. Nikbin and G.A. Webster

Department of Mechanical Engineering,
Imperial College.

It cannot be ensured that engineering components will not contain pre-existing flaws or develop cracks during use. For those components operating at elevated temperatures it is possible that any cracks present may grow by creep. In order to produce a reliable design, therefore, it is necessary to know the factors affecting the rate of propagation of cracks by creep.

Attempts have been made, with varying degrees of success, to apply fracture mechanics concepts to creep cracking. It has been shown in appropriate circumstances that crack growth rate, $\dot{a}$, can be correlated in terms of stress intensity factor, K, according to

$$\dot{a} \alpha K^n \qquad (1)$$

where n is usually very close to the stress sensitivity of secondary creep rate or time to rupture, although in some cases better agreement is claimed with net section or a reference stress. In most instances cracks were only propagated over relatively short distances. Despite the applicability of equation (1), Kenyon et al [1] showed (using a contoured DCB test piece, Fig.1) for aluminium alloy RR58 that a constant crack growth rate was not obtained over long distances at constant K. Fig.2a shows apparent primary, secondary and tertiary stages of cracking. Results are presented here on a ½%Cr ½%Mo 1/4%V steel which indicate that the observations are not peculiar to the aluminium alloy.

The same test piece geometry was used as before [1] except that the depth of the side grooves was deepened to eliminate arm bending. All the specimens were heated to 1250°C for ½ hour and oil quenched (to produce

a martensitic structure with grains approximately 300 μm in diameter prior to testing at 565°C. The side grooves were coated with a high temperature paint to prevent oxidation and enable crack growth to be monitored visually.

Fig.2b shows a typical crack growth curve. Like the aluminium alloy primary, secondary and tertiary stages of cracking are observed. Fig.3 shows the dependence of secondary crack growth rate, $\dot{a}_s$, against K. Over most of the range it can be described by equation (1) with n approximately 10 close to the stress dependence of time to rupture for this material [2].

Also shown on Fig.3 are the results of Pilkington et al [3] and Neate and Siverns [4] who tested the same steel but with different heat treatments and test-piece geometries. Pilkington et al's results are in complete agreement with the present data although their specimens were tempered to a bainitic structure prior to testing. The results of Neate and Siverns straddle the present data and show a difference depending on heat-treatment. Some tempering of the quenched samples will be expected during testing and could be an explanation of the agreement of the present results with the tempered data at long times (i.e. slow cracking rates).

The micrograph (Fig.4) shows a section through the tip of an advancing crack. The cracking is predominantly intercrystalline, following the prior austenite grain boundaries with considerable branching of the crack behind the crack tip.

Although the present results reinforce the linear elastic fracture mechanics interpretation of creep cracking an explanation of the primary and tertiary regions is still required. The tertiary stage can be attributed to increasing K as the crack approached the end of the test piece. The decreasing crack growth rate in the primary region can be explained by introducing non-linear fracture mechanics concepts [5,6].

For a material obeying the secondary creep law

$$\dot{\varepsilon} \alpha \sigma^n \tag{2}$$

where σ is stress, it can be shown [6] that a contour integral $\dot{J}$ (equivalent to J for a work hardening material) can be defined which varies with crack length for a DCB test piece such that,

$$\dot{J} \alpha \frac{(aP)^{n+1}}{(h/2)^{2n+1}} \tag{3}$$

At constant load, P, for a constant K geometry, $\dot{J}$ first decreases and then increases with increase in crack length and could therefore characterise the primary, secondary and tertiary regions of cracking. This possibility was examined by carrying out tests in which the load was adjusted to keep $\dot{J}$ constant. The results are shown in Figs.5 and 6. The primary region has virtually been eliminated indicating that $\dot{J}$ (rather than K) is the true characterising parameter.

For a particular geometry $\dot{J}$ and K are related. Consequently expression (1) is consistent with the above interpretation over short crack growths. When n is large $\dot{J}$ is proportional to net section stress and correlation with this term would be expected in this case.

Further experiments are required over a wider range of testing conditions to determine whether non-linear fracture mechanics concepts can be extended to predict creep crack growth in practical situations.

References

1. Kenyon, J.L., Webster, G.A., Radon, J.C. and Turner, C.E.
Int.Conf. on Creep and Fatigue at Elevated Temperatures, I.Mech.E., Sept.1973/April 1974

2. Cummings, W.M. and King, R.H.
Proc.I.Mech.E., V.185, 1970/71, p.285

3. Pilkington, R., Hutchinson, D. and Jones, C.L.
Metal Sci.J., Vol.8, No.8, August 1974, pp.237

4. Neate, G.J. and Siverns, M.J.
Int.Conf. on Creep and Fatigue at Elevated Temperatures, I.Mech.E., Sept.1973/April 1974

5. Turner, C.E. and Webster, G.A.
Int.J.Fracture, Vol.10, Sept.1974, p.455

6. Webster, G.A.
Conf. The Mechanics and Physics of Fracture, Inst.Physics, Cambridge, Jan.1975

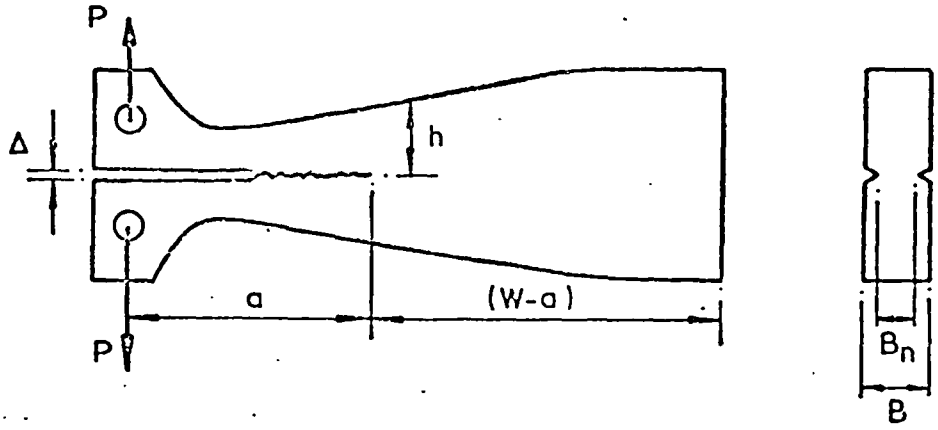

FIG. 1 : TYPICAL CONTOURED DCB GEOMETRY.

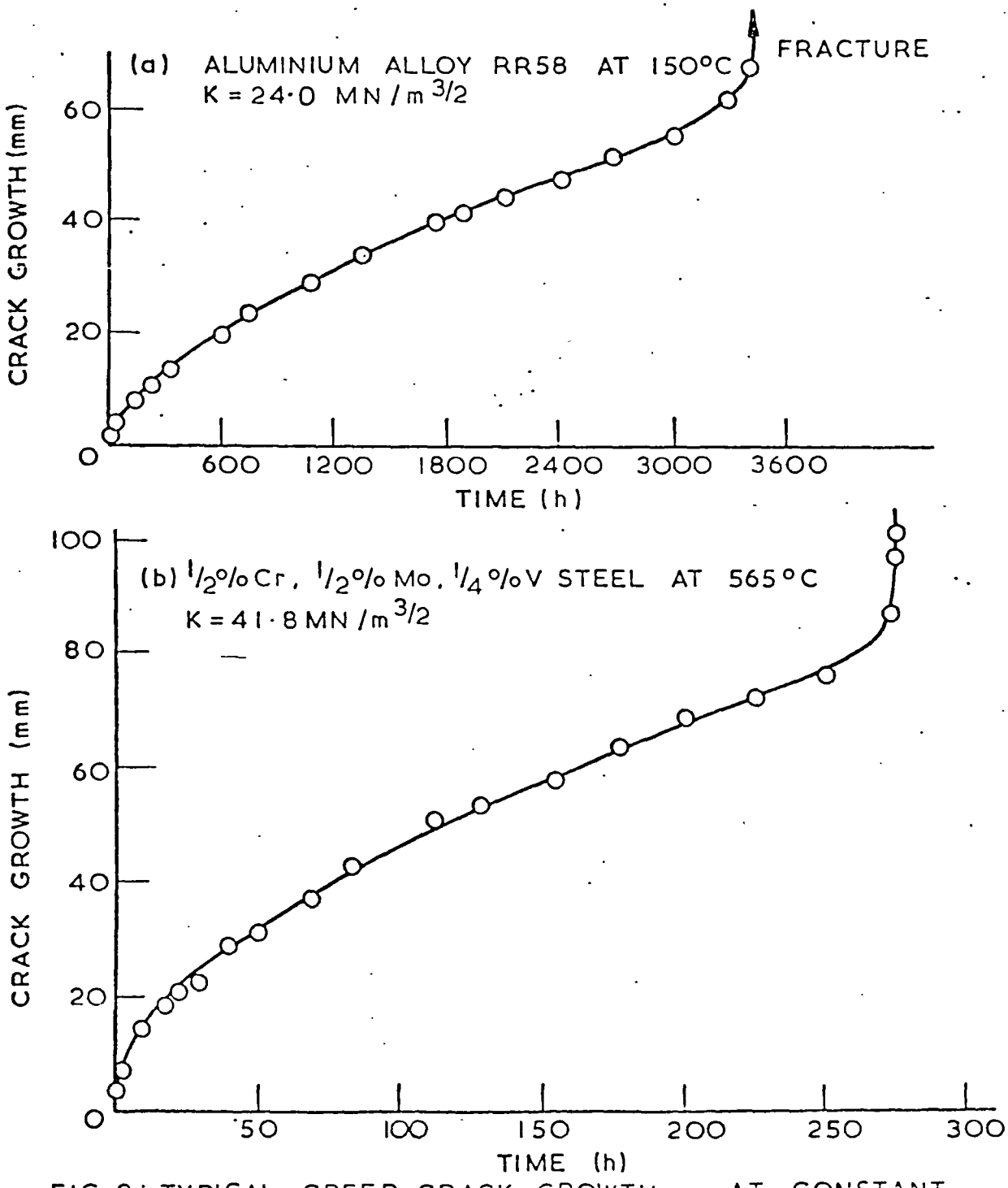

FIG. 2 : TYPICAL CREEP CRACK GROWTH, a, AT CONSTANT STRESS INTENSITY FACTOR K.

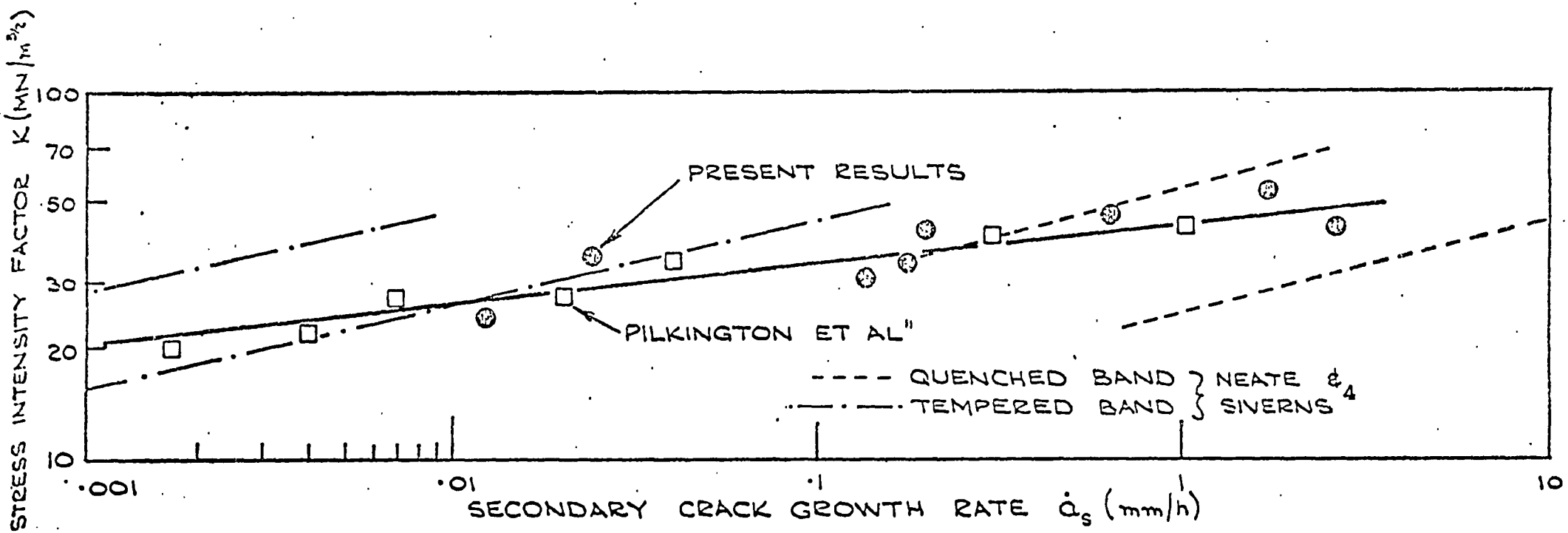

FIG.3. CRACK GROWTH RATE AS A FUNCTION OF STRESS INTENSITY FACTOR FOR ½% Cr ½% Mo ¼% V, STEEL AT 565° C.

(a)

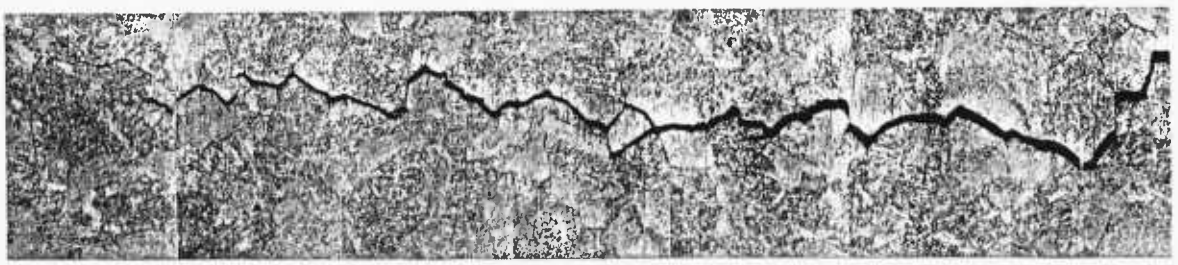

(b)

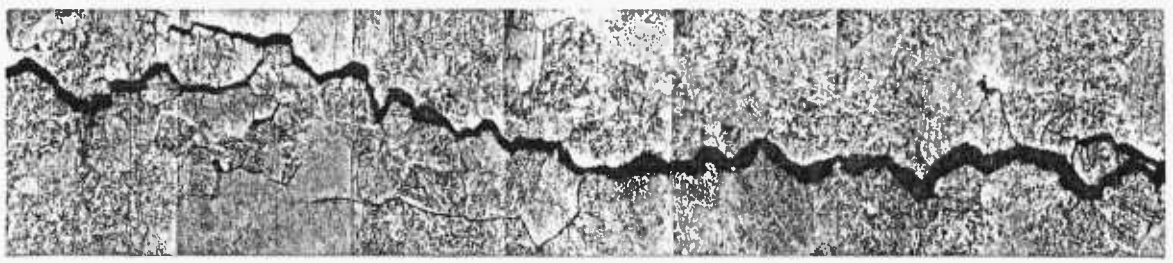

FIG.4 CREEP CRACK AT 565°C IN ½% Cr, ½% Mo, ¼% V STEEL SHOWING (a) CRACK TIP REGION AND (b) FURTHER BACK ALONG THE CRACK

mag x 13

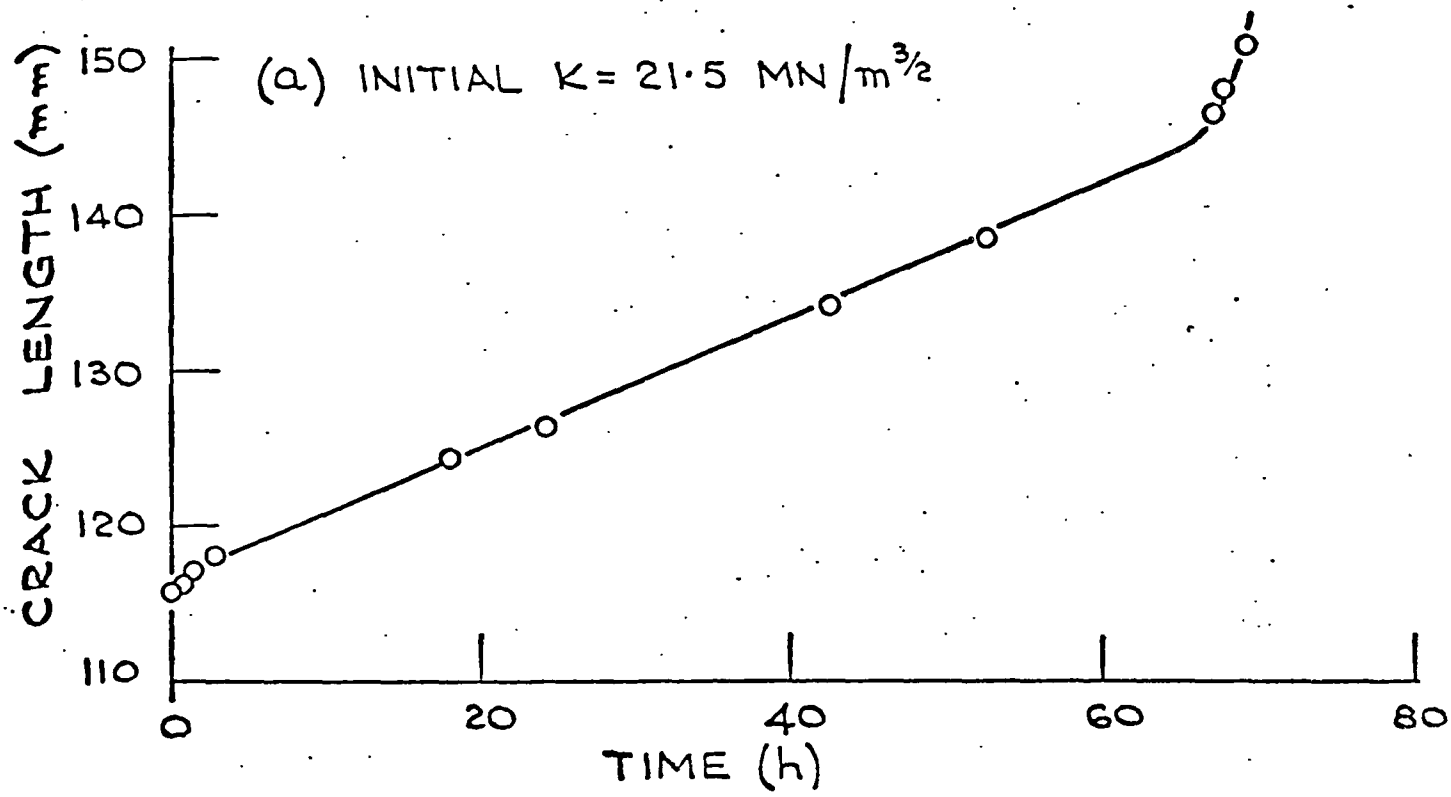

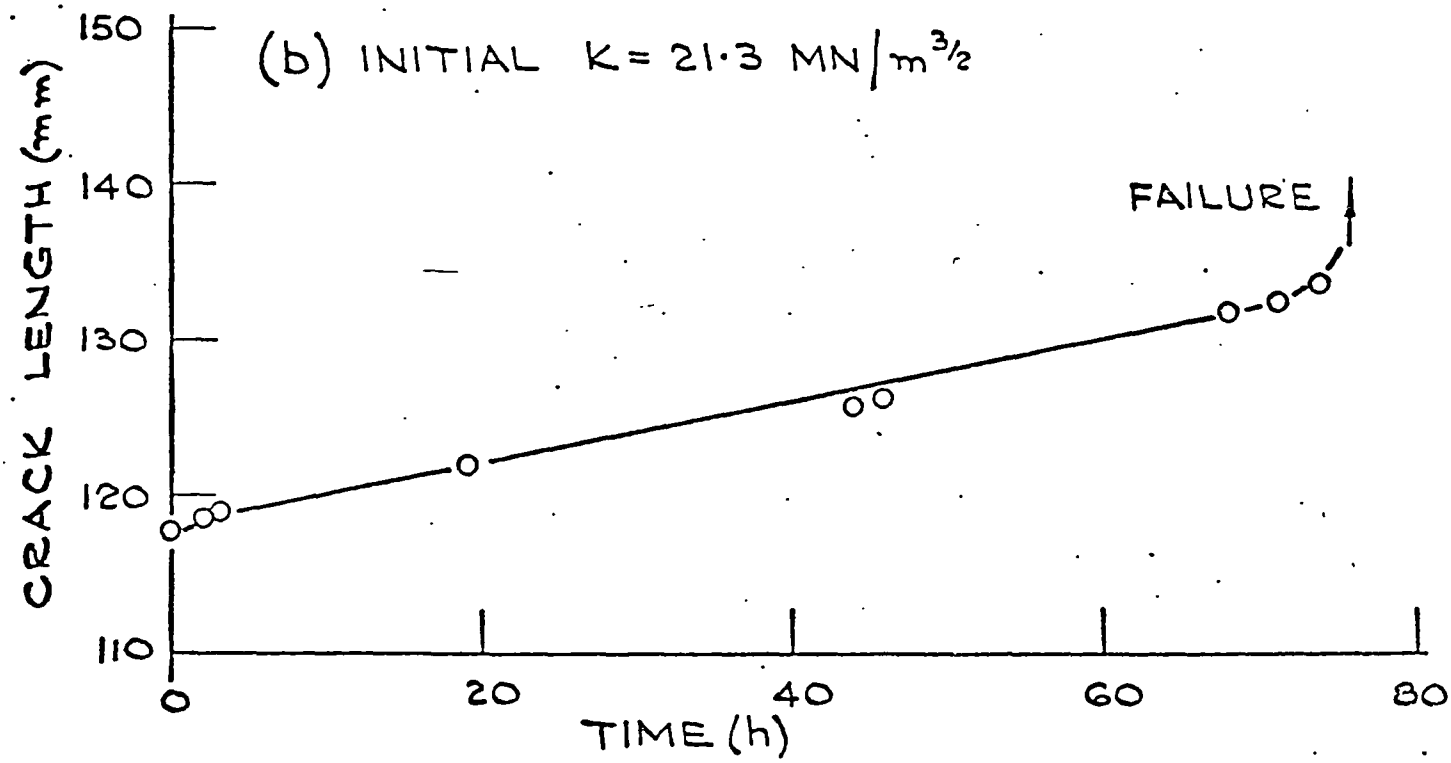

CREEP CRACK GROWTH IN ALUMINIUM ALLOY RR 58 AT 150°C AT CONSTANT $\dot{J}$ TAKING $n = 14$

FIG.5.

Authorized Reprint from
Special Technical Publication 601

American Society for Testing and Materials
1916 Race Street, Philadelphia, Pa. 19103
1976

K. M. Nikbin,[1] *G. A. Webster,*[1] *and C. E. Turner*

Relevance of Nonlinear Fracture Mechanics to Creep Cracking

REFERENCE: Nikbin, K. M., Webster, G. A., and Turner, C. E., **"Relevance of Nonlinear Fracture Mechanics to Creep Cracking,"** *Cracks and Fracture, ASTM STP 601,* American Society for Testing and Materials, 1976, pp. 47–62.

ABSTRACT: Creep crack growth tests, conducted on contoured double cantilever beam (DCB) specimens are described for aluminium alloy RR58 and a chromium-molybdenum-vanadium steel. The results are analyzed in terms of $\dot{J}$, the rate equivalent of the J contour integral, which is a nonlinear fracture mechanics parameter. Direct proportionality is found between crack growth rate, $\dot{a}$ and $\dot{J}$. The treatment is shown to reveal a unification of the linear elastic fracture mechanics and net section or reference stress descriptions of creep cracking.

KEY WORDS: crack propagation, mechanical properties, temperature, creep, properties, J contour integral, linear elastic fracture mechanics

It cannot be ensured that engineering components will not contain preexisting flaws or develop cracks during use. For those components operating at elevated temperatures, it is possible that any cracks present may grow by creep. In order to produce a reliable design, therefore, it is necessary to establish the factors controlling the rate of propagation of cracks by creep.

Creep failure is predominantly intercrystalline [*1–3*][2] and usually occurs by the linking up of many individual cracks [*4–6*] (rather than the propagation of one major crack), when the true stress in the material approaches its ultimate tensile strength [*5*]. Observations indicate that cavities and triple point cracks can be present from the early stages of creep [*4–6*] and that they continue to grow with deformation. Mechanisms for the growth of individual cavities and triple point cracks by grain boundary sliding and vacancy diffusion have been proposed by a number of authors [*6–8*]. However, difficulties arise in applying these

[1] Research student, senior lecturer, and professor of materials in mechanical engineering, Department of Mechanical Engineering, Imperial College, London, S. W. 7, England.

[2] The italic numbers in brackets refer to the list of references appended to this paper.

theories to creep rupture when cracking is extensive and nucleation is occurring throughout creep.

There is much evidence from conventional tensile creep tests carried out on round bars at constant stress (or load) to show that creep deformation and time to failure are related [*1,2*]. Because of this relation, attempts [*9,10*] have been made to explain tertiary creep and fracture by incorporating a damage factor into conventional secondary creep laws to allow for the progressive loss in area due to cracking. However it is not certain that theories which predict creep fracture where failure is by linking up of many cracks will be satisfactory where failure is by propagation from a single large preexisting flaw. More recently a number of investigators [*11–19*] have attempted to establish the relevance of fracture mechanics to creep cracking in this situation. Their data where obtained over a range of specimen geometries and materials with creep ductilities from <2 percent to 75 percent. It was assumed that creep strain rate $\dot{\epsilon}$ could be described by the secondary creep law written in the form

$$\dot{\epsilon} = C\,\sigma^n \tag{1}$$

where

σ = stress,
n = indication of the stress sensitivity of creep, and
C = function of temperature.

In most instances crack growth rate, $\dot{a}$, could be expressed in terms of stress intensity factory, K, by

$$\dot{a} \propto K^{\beta} \tag{2}$$

although some investigators claim better correlations with net-section stress [*12*] or with a reference stress [*17*]. Generally, the higher strength low ductility materials correlated better with K and the lower strength high ductility materials, with net-section stress. The values of β were found to lie between approximately 3 and 30, typical of the stress sensitivity, n, of secondary creep rate suggesting that the values of n for creep deformation and β for cracking are closely related.

In most instances, Eq 2 was determined from results which were obtained under conditions of continuously rising K. One series of experi-

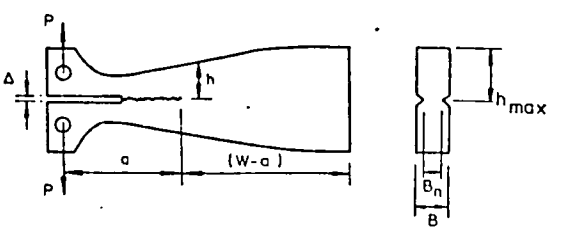

FIG. 1—*Typical contoured DCB geometry.*

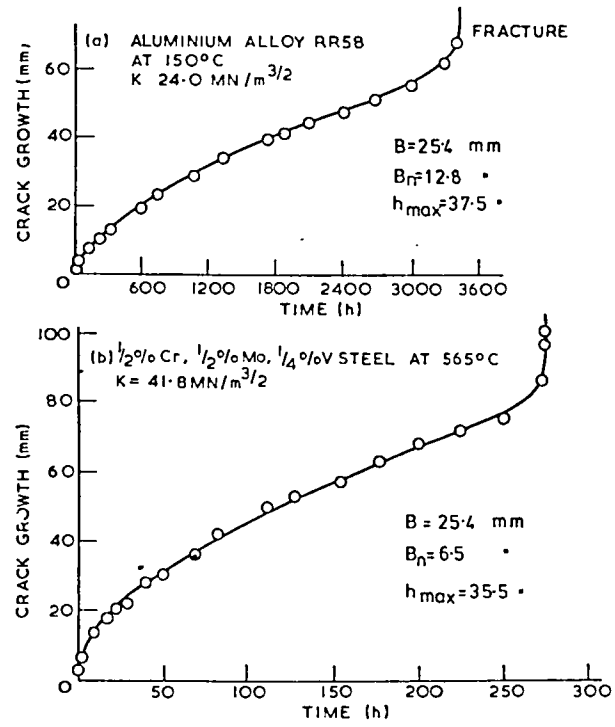

FIG. 2—*Typical creep crack growth,* a, *at constant stress intensity factor,* K.

ments [*18*] was carried out on contoured double cantilever beam (DCB) specimens, Fig. 1, which gave K constant at constant load independent of crack length. The results showed that despite the correlation of Eq 2 a constant crack growth rate was not obtained for aluminium alloy RR 58 (Fig. 2*a*). Apparent primary, secondary, and tertiary regions were observed. The tertiary stage was attributed to increasing K as the crack approached the end of the specimen. The primary region was found to be reduced by increasing the initial crack length and by soaking the specimen at the test temperature before loading, indicating both geometry and aging complications [*19*].

More recent results [*20*], Fig. 2*b*, on a ½Cr-½Mo-¼V steel which had been heat treated at 1250°C for ½ h and oil quenched to simulate a heat affected zone (HAZ) structure have shown that the just mentioned effects are not peculiar to the aluminum alloy. Again primary, secondary, and tertiary cracking was observed. In spite of the change in crack growth rate at constant K, Fig. 3 shows that the crack growth rate in the secondary region, $\dot{a}_s$, when treated as constant, can still be expressed in terms of Eq 2, with a value of β close to n for this material [*21*]. The results are also consistent with other published data [*11,15*] on the same material.

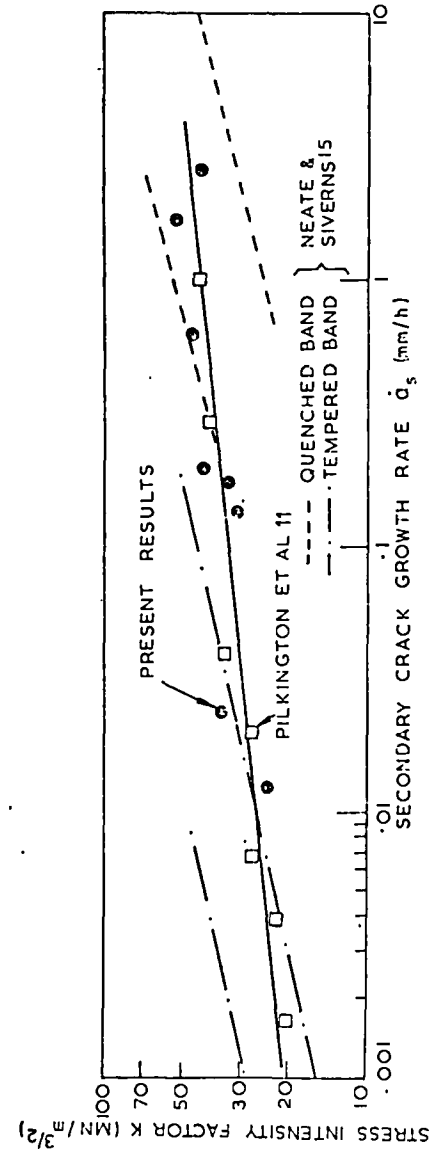

FIG. 3—*Crack growth rate as a function of stress intensity factor for 1/2Cr-1/2Mo-1/4V steel at 565°C.*

It is shown here that the decreasing crack growth rate in the primary region, and the linear elastic fracture mechanics and net section stress approaches to creep cracking, can be rationalized by introducing nonlinear fracture mechanics concepts as suggested by Turner and Webster [*20,22*]. The approach is consistent with that recently reported by Landes and Begley [*23*].

Application of Nonlinear Fracture Mechanics to Creep Cracking

The viewpoint of the present paper is that the inadequacy of linear elastic concepts in correlating crack growth rate data under creep conditions at constant stress intensity factor, K, may be due to the nonlinear nature of the constitutive laws for the highly deformed region around the crack tip. The J contour integral has been used to describe the singular terms of stress or strain for a nonlinear elastic material [*24,25*]. Possible application to the onset of cracking in materials obeying the laws of incremental plasticity has been implied by many workers recently studying elastic-plastic fracture problems although a sure foundation to this approach has not been established. Essential steps in the argument are the retention of the property of path independence, to the extent demonstrated by finite element computation [*26–29*], and the apparent success of preliminary tests to establish a critical value of the contour integral J_{Ic}, for the onset of cracking in pieces of different geometry [*30,31*]. If these demonstrations of the usefulness of J for plastic (as distinct from nonlinear elastic) materials are taken to warrant further more extensive studies of the concept then it is here argued that for *steady state creep*, there should likewise be a relevance of J to creep crack growth. The authors are not aware of a proper energy rate balance for the time dependent processes of creep and creep crack growth. The use of J (in a modified form, $\dot{J}$, for reasons of dimensional analysis) as proposed here rests on being able to carry over to steady state creep the characterizing role of J in describing the singular stress and strain rates at the crack tip. As creep rupture in conventional creep testing is related to secondary creep strain rate [*1,2*], it may be expected that crack growth rate will also depend on secondary creep rate. Following Hutchinson [*24*], McClintock [*32*] showed that for nonlinear elastic materials obeying power law hardening of the form

$$\epsilon = A\ \sigma^n \tag{3}$$

the stresses and strains around a crack tip are characterized by

$$\sigma \alpha\ (J/A)^{1/n+1} \tag{4}$$

$$\epsilon \alpha\ A(J/A)^{n/n+1} \tag{5}$$

For a material obeying the secondary creep rate law, Eq 1, it follows by analogy that the stress and strain rates around a crack tip in a material subjected to steady state creep are

$$\sigma \propto (\dot{J}/C)^{1/n+1} \tag{6}$$

$$\dot{\epsilon} \propto C(\dot{J}/C)^{n/n+1} \tag{7}$$

where $\dot{J}$ is the characterizing parameter for creep. It has the dimensions of J divided by time in order to accommodate the different dimensions of C (Eq 1) and A (Eq 3).

For the case of nonlinear elasticity it has been shown, as reviewed by Rice [*33*], that for a crack of thickness, B_n, and length, a, the numerical value of J can be found from the expression

$$J = -\frac{1}{B_n}\frac{dU}{da} \tag{8}$$

where U is potential energy.

In elasticity, this energy is available to grow the crack. With plasticity, Eq 8 remains a means of evaluating the crack tip parameter J but J is no longer the energy potentially available to grow the crack. This method of evaluating J was used experimentally for plasticity by Begley and Landes [*30*]. For a nonlinear material obeying power law hardening, Eq 3, it is shown [*20*] that for a DCB specimen subjected to a constant load, P

$$J = \frac{P}{B_n\,(n+1)}\cdot\frac{d\Delta}{da} \tag{9}$$

where Δ is deflection at the loading line (Fig. 1).

Evaluation of $d\Delta/da$ as the crack propagates along the length of the specimen will therefore give J as a function of crack length. Provided the crack length is long enough, shear deflections can be neglected and $d\Delta/da$ obtained from nonlinear bending theory as shown in the Appendix. Substituting in Eq 9 gives

$$J = \frac{2A}{B_n\,(n+1)}\left[\frac{(2n+1)}{2nB}\right]^n \frac{(aP)^{n+1}}{(h/2)^{2n+1}} \tag{10}$$

This equation enables the instantaneous value of J to be calculated for a nonlinear material for any crack length, provided the geometry of the specimen is known. It applies to any DCB specimen contour for which it may be assumed that bending stresses dominate and shear deflections can be ignored. For linear elasticity, $n = 1$, $A = 1/E$, and $J = G$, the elastic strain energy release rate. For plane stress

$$G = K^2/E \tag{11}$$

and for plane strain

$$G = (1 - \nu)^2 K^2/E \tag{12}$$

where ν is Poisson's ratio.

Now consider a material obeying the secondary creep law, Eq 1. The above analysis can obviously be repeated with ϵ replaced by $\dot{\epsilon}$, A by C, and Δ by $\dot{\Delta}$.

For creep, we can define a term with the dimensions of power, $\dot{U}$, and by analogy with Eq 8 a term corresponding to potential power release rate, $\dot{J}$

$$\dot{J} = -\frac{1}{B_n}\frac{d\dot{U}}{da}$$

$$= \frac{2C}{B_n(n+1)}\left[\frac{(2n+1)}{2nB}\right]^n \frac{(aP)^{n+1}}{(h/2)^{2n+1}} \tag{13}$$

This equation is exactly the same as Eq 10 except that J has dimensions of power whereas J has dimensions of energy. It is equivalent to replacing ϵ by $\dot{\epsilon}$ in the experimental plasticity evaluation of J as discussed by Landes and Begley [*23*].

Comparison with Experimental Data

The profile of the contoured DCB specimen used by Kenyon et al [*18*] was chosen to give a constant K at constant load independent of crack length. This necessarily implies from Eq 13, however, that $\dot{J}$ will vary with crack length. Figure 4*a* shows the relationship between $\dot{J}$ and crack length for the geometry tested by Kenyon et al for values of n in the range 1 to 25. The ordinate has been normalized with respect to $\dot{J}_i$ the value of $\dot{J}$ at a crack length of 75 mm (the shortest initial crack length used) for ease of comparison. The graph indicates that from the present analysis with $n = 1$, $\dot{J}$ is constant (as it should be for a constant K geometry) until a crack length of 155 mm, after which it rises. For all other values of n, $\dot{J}$ decreases with crack length until 155 mm when it rises again. The decrease is most marked the higher the value of n. Sufficient data have not been obtained yet to enable $\dot{J}$ to be evaluated experimentally to check this trend.

Figure 4*b* shows how crack growth rate decreases experimentally with crack length for the two tests shown in Fig. 2. No truly constant secondary rate exists. The shapes compare very favorably with those shown in Fig. 4*a*, suggesting that the primary stage of cracking may be caused by the decrease in $\dot{J}$ with crack length. Both the experimental and calculated curves have a minimum at a crack length of 155 mm. For crack lengths longer than this, the elastic analysis for this geometry becomes invalid

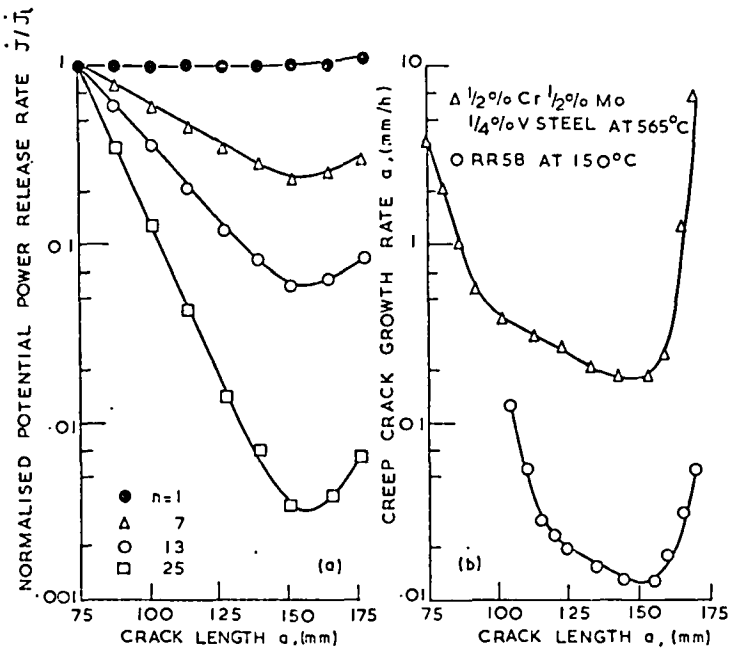

FIG. 4—*Comparison of the change in* (a) *potential power release rate and* (b) *creep crack growth rate with crack length.*

due to the effect of the "remote" free end of the specimen. It is assumed that the same limitation applies to the analysis for J and $\dot{J}$.

Before it is possible to plot crack growth rate against $\dot{J}$, it is necessary to know the value of n in Eq 1 for each material. A value of 10 for n has been estimated for the steel from the tensile creep data of Cummings and King [*21*] and 14 for the aluminum alloy from the results of Kenyon [*19*]. Figure 5 shows the dependence of crack growth rate in the primary and secondary regions on $\dot{J}$ calculated using these values of n. Except in the very early stages of cracking, the results tend to suggest that crack growth rate is approximately proportional to $\dot{J}$. The analysis neglects elastic strains and assumes that both materials exhibit only secondary creep deformation when in fact some primary creep was observed [*19*]. Consequently, some deviation would be anticipated in the early stages of cracking as the stress distribution changes from the initial elastic stress distribution to the settled steady state creep stress distribution. For both materials, this settling down period extended over a crack growth of approximately 5 mm.

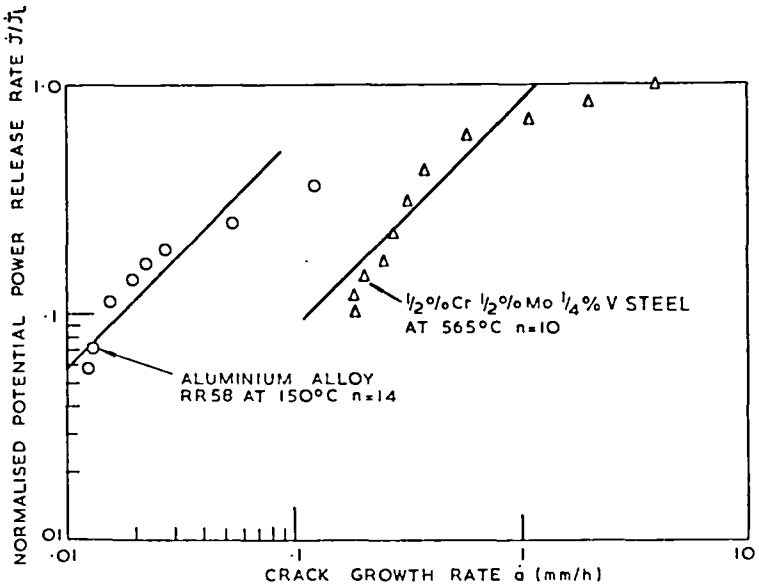

FIG. 5—*Change in crack growth rate with J during primary and secondary regions.*

Additional experiments have been carried out to establish more firmly the dependence of crack growth rate on $\dot{J}$. The same experimental procedure as reported by Kenyon et al was used except that fatigue precracking was adopted. All the specimens were 25 mm thick but the groove of the steel specimens was deepened to leave a net thickness of 6.5 mm (compared with 12.6 mm for the aluminum alloy) to prevent breaking off of the specimen leg perpendicular to the crack path. The aluminum alloy was tested at 150°C and the steel, at 565°C. The surfaces of the side grooves in the steel were coated with an alumina-based paint resistant to high temperatures to prevent oxidation and enable crack growth to be monitored visually with the aid of a travelling telescope.

Most of the tests were performed at constant K, but in some instances the load was adjusted during the test to keep $\dot{J}$ constant with crack growth. The results of 9 tests are summarized in Figs. 6 and 7. Figure 6 confirms the trend indicated in Fig. 5. It shows that all the results fall on one straight line with a slope of unity with comparatively little scatter (the points furthest from the line are usually those for the early stages of cracking before a settled state has been reached) indicating

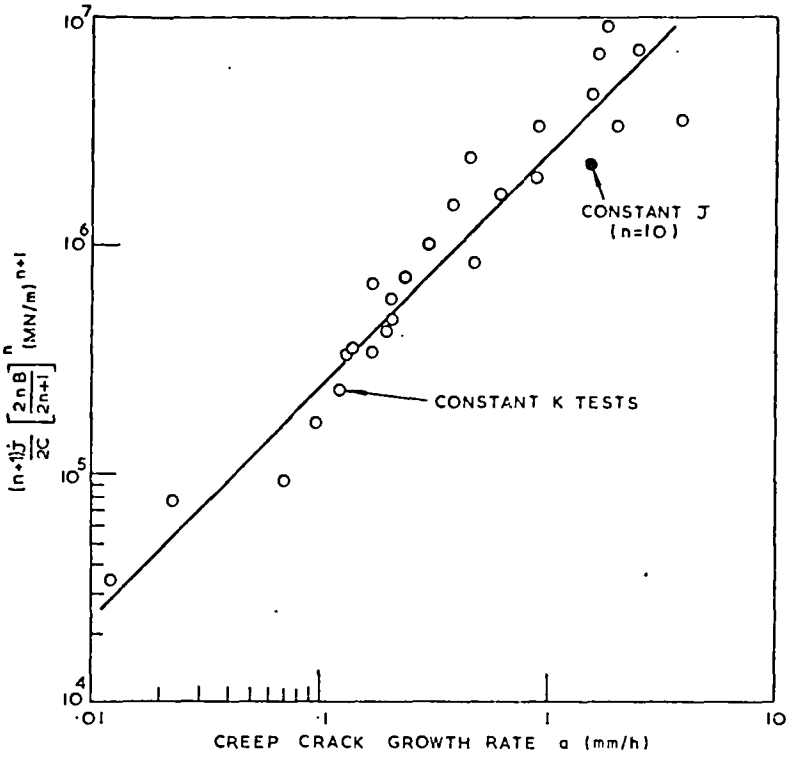

FIG. 6—*Crack growth rate as a function of potential power release rate* $\dot{J}$ *for 1/2Cr-1/2Mo-1/4V steel at 565°C.*

that creep crack growth rate throughout the primary and secondary regions can be expressed by

$$\dot{a} = F\,\dot{J} \tag{14}$$

where F is a proportionality factor which could be a function of temperature, since in the creep law, Eq 1, C is, of course, a function of temperature.

A similar observation can be made from the data of Landes and Begley [*23*] on a superalloy. The characterizing parameter, C^*, used in their paper is equivalent to the J used here. Although they show a change in slope in some of their graphs, to a good approximation all their results can be described by Eq 14.

In the present investigation, all the individual constant K tests exhibited primary, secondary, and tertiary regions of cracking whereas Eq 2 predicts a constant crack growth rate. If $\dot{J}$ (rather than K) is the true characterizing parameter, a constant crack growth rate would be expected throughout a test at constant $\dot{J}$. Examples of crack growth curves obtained when load was altered to keep $\dot{J}$ constant are shown in Fig 7. This figure confirms that for both the aluminum alloy and the steel, after a slight curvature

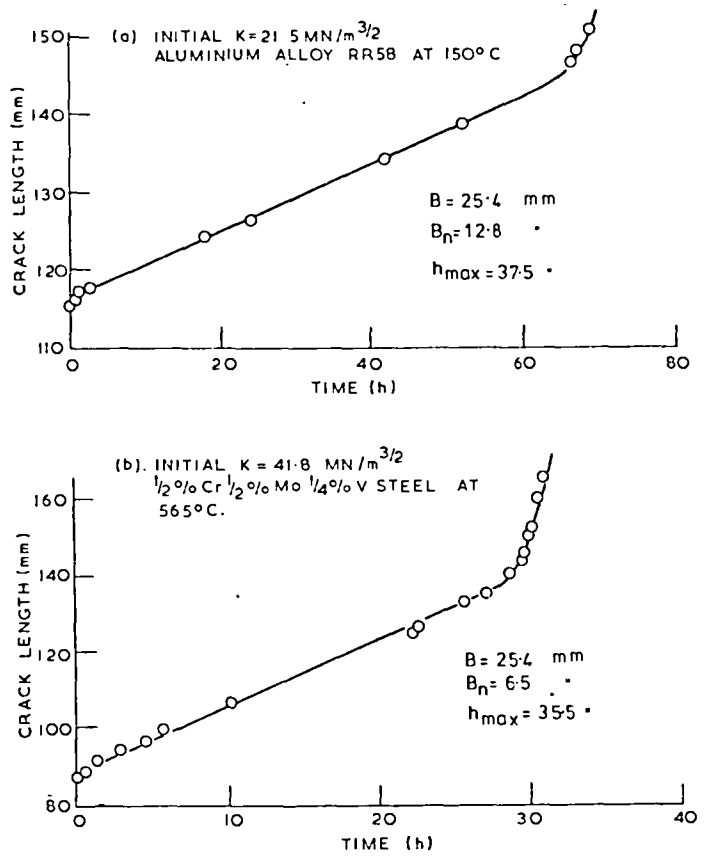

FIG. 7—*Creep crack growth curves at constant* $\dot{J}$.

during an initial settling down stage, the crack growth rate is constant until the test is no longer valid at long crack lengths. The initial K value for the constant $\dot{J}$ test of Fig. 7*b* was deliberately chosen to be the same as that of the constant K test of Fig. 2*b* for comparison purposes. The initial crack growth rate of the two tests is the same. However, if after the same initial starting conditions the load is either maintained constant to keep K constant or alternatively increased to maintain $\dot{J}$ constant for a total crack growth of 50 mm, two quite different behaviors result. In the former case (constant K), the crack growth rate decreases gradually (see Fig. 4*b*) by nearly an order of magnitude thus extending the test time to 300 h, whereas in the latter case (constant $\dot{J}$) the growth rate remains constant (Fig. 7) over a crack growth of 50 mm and final fracture is reached in only 30 h. These observations, therefore, reinforce the interpretation of creep crack growth in terms of $\dot{J}$, the creep equivalent of the J contour integral.

Discussion

It has been shown that nonlinear fracture mechanics can be used to explain creep crack growth quantitatively. It describes the apparent primary region of cracking which cannot be explained by linear mechanics arguments. No doubt, in some cases, as reported [*19*] for the aluminium alloy, metallurgical changes may also play a role and influence the so-called primary stage of cracking.

Further insight into the cracking process can be obtained by comparing Eq 7 which characterizes the creep strain rates around a crack tip, with the experimental correlation shown in Eq 14. For the materials tested, n was found to be 10 for the steel and 14 for the aluminum alloy. Thus, it is difficult in practice to the distinguish between the ratio $n/n + 1$ and 1. Consequently, although proportionality between crack growth rate and J is indicated by the data, it is also clear that a satisfactory correlation could be obtained with $J^{n/n+1}$ to give proportionality between secondary creep rate and creep crack growth at least for the values of n found here.

The successful correlation of creep crack growth with K already reported in the literature calls for comment. Using elastic fracture mechanics $K \alpha P$. From Eq 13

$$\dot{J} \quad \alpha \quad P^{n+1} \tag{15}$$

therefore

$$\dot{J} \quad \alpha \quad K^{n+1} \tag{16}$$

Thus Eq 2 could be rewritten

$$\dot{a} \quad \alpha \quad J^{\beta/n+1} \tag{17}$$

Taking β as n gives the correlation with creep strain rate and $J^{n/n+1}$ or K^n. Taking $\beta = n + 1$ gives direct correlation with $\dot{J}$ or K^{n+1}. As already discussed, the difference between these powers cannot be resolved with the present data. It must be noted, however, that the dependence of J on crack length, a, (Eq 13) is a function of n so that in general J and K will be different functions of crack length. The above discussion holds strictly only for a fixed crack length. It appears that experimental results so far published have been obtained over small changes in crack length and thus do not discriminate between the linear or nonlinear correlations. Another circumstance where K might be more relevant than J is where creep ductility is small. The present analysis ignores elastic strains and primary creep. It assumes that sufficient creep occurs to allow a secondary creep stress distribution to be established by redistribution of elastic stresses at the crack tip. For a material of very limited creep ductility this may not happen.

The adoption of nonlinear fracture mechanics can also be used to explain the better agreement of crack growth with net section stress than with K reported by some authors [*12,17*]. It can be shown that the

maximum bending stress (neglecting the singularity) at the crack tip in each leg of the DCB specimen is

$$\sigma_{max} = \frac{(2n+1)aP}{2nB \times (h/2)^2} \tag{18}$$

Substituting $n = 1$ in this expression gives the net section stress [*12*], and $n = \infty$, the reference stress. Whichever definition of stress is used it will change with crack length in the same way. Comparison of this equation with the expression for J (Eq 13), reveals that when $n >> 1$

$$J \alpha (\sigma_{max})^n$$

Hence, correlation with net section stress or with the reference stress for materials exhibiting high values of n are in agreement with nonlinear fracture mechanics. The value of n for cracking should be the same as that required to describe creep deformation behavior.

Fracture mechanics also provides an explanation of extensive cracking in conventional uncracked creep specimens. By using the infinite plate solution

$$K = \sigma\sqrt{\pi a}$$

an estimate can be made of the size of cracks that will be propagated in these specimens. The lowest value of K at which creep crack growth has been observed in steels and aluminium alloy RR58 is approximately 15 $MN/m^{3/2}$. A typical creep stress for these materials is 300 MN/m^2 giving a crack length $2a = 1.6$ mm. This is far in excess of the sizes of cracks measured [*4,5*]. Even close to fracture, individual cracks seldom exceed a grain facet in length and in aluminium alloy RR58 are typically 30 μm long [*5*]. These figures indicate why, in most materials, crack nucleation is easier than crack propagation and why final creep failure occurs by the linking up of many small cracks when the net section stress approaches the ultimate tensile strength of the material. For creep failure, if a grain facet can be regarded as an incipient flaw, it is likely that grain sizes as large as approximately 1 mm can be tolerated in conventional creep specimens before failure will be by the propagation of one dominant crack. Conversely where large defects exist, such as in weldments or at a major inclusion, good creep toughness in conventional tensile creep tests may not guard against crack growth by creep from the preexisting defect.

Conclusions

Microstructural evidence of the development of voids and triple point cracks during creep deformation suggests that final failure occurs by ligament tearing when the ultimate tensile strength of the material is approached. The stress intensity factors required to propagate creep cracks are sufficiently high that the individual voids or triple point cracks

will not be propagated by creep until they reach a size of approximately 1 mm. It is unlikely, therefore, that the failure of round bar creep specimens will be described by fracture mechanics. The creep fracture toughnesses of most materials are too high in relation to their creep strengths for this to happen.

It has been shown that initial flaws which are sufficiently large can be extended by creep. The resulting creep crack growth rate can, for a particular geometry, be correlated in terms of the crack tip characterizing parameter, $\dot{J}$, which corresponds to the J contour integral as used in plasticity for a work-hardening material. Experimental results suggest that creep crack growth rate is approximately proportional to $\dot{J}$. Nonlinear fracture mechanics can describe the previously unexplained apparent primary region of cracking. It is also capable of unifying the linear elastic fracture mechanics and net section stress correlations of creep cracking reported previously.

Acknowledgments

The authors wish to thank the Science Research Council who supported much of the work, The Royal Aircraft Establishment and English Electric for supplying the materials, and their colleague, J. C. Radon, for helpful discussions.

APPENDIX

Analysis of Deflection of DCB Specimen

Consider a cross section of the DCB specimen to be a distance $x < a$ from the loading line. Let the curvature at this section under load, P, be k. Then for plane sections to remain plane, the strain at any distance y from the neutral axis is

$$\varepsilon = ky \tag{19}$$

For moment equilibrium

$$M = \int_{-h/2}^{h/2} \sigma B \, y \, dy$$

Therefore, substituting from Eqs 3 and 19

$$M = B \left(\frac{k}{A}\right)^{1/n} \int_{-h/2}^{h/2} y^{1+1/n} dy$$

$$= \frac{2nB}{(2n+1)} \left(\frac{k}{A}\right)^{1/n} \left(\frac{h}{2}\right)^{2+1/n} \tag{20}$$

For small deflections δ, Eq 20 can be rearranged to give

$$k = \frac{d^2\delta}{dx^2} = \left[\frac{(2n+1)M}{2nB}\right]^n \frac{A}{(h/2)^{2n+1}}$$

But $M = Px$, therefore

$$\frac{d^2\delta}{dx^2} = \left[\frac{(2n+1)P}{2nB}\right]^n A \frac{x^n}{(h/2)^{2n+1}}$$

Integrating twice and using the boundary condition $d\delta/dx = 0$ and $\delta = 0$ at $x = a$, the crack tip, gives

$$\delta = \left[\frac{(2n+1)P}{2nB}\right]^n A \left[I_x{}^{**} - I_a{}^{**} - I_a{}^{*}(x-a)\right] \tag{21}$$

where

$$I^* = \int \frac{x^n}{(h/2)^{2n+1}}\,dx$$

and

$$I^{**} = \int\int \frac{x^n}{(h/2)^{2n+1}}\,dx$$

and the subscripts x and a indicate the values of the integrals at x and a, respectively. For the contoured geometry, h is a function of x.

The loading pin displacement, Δ, required for the evaluation of J, Eqs 4 and 5, is given by

$$\Delta = 2\delta$$

evaluated at $x = 0$; therefore

$$\Delta = \left[\frac{(2n+1)P}{2nB}\right]^n 2A \left[I_0^{**} - I_a^{**} + I_a^{*}\,a\right]$$

where I_0^{**} is the value of I^{**} at $x = 0$. Therefore

$$\frac{d\Delta}{da} = \left[\frac{(2n+1)P}{2nB}\right]^n 2A \left[-I_a^{*} + I_a^{*} + a\frac{dI_a^{*}}{da}\right]$$

$$= \left[\frac{(2n+1)P}{2nB}\right]^n 2A \frac{a^{n+1}}{(h/2)^{2n+1}} \tag{22}$$

This expression can be substituted into Eq 9 to give J.

References

[1] Garofalo, F., *Fundamentals of Creep and Creep-Rupture in Metals*, Macmillan, New York, 1965.

[2] Penny, R. K., and Marriott, D. L., *Design for Creep*, McGraw-Hill, New York, 1971.

[3] Sullivan, C. P., "A Review of Some Microstructural Aspects of Fracture in Crystalline Materials," *Welding Research Council Bulletin*, No. 122, 1967.

[4] Dyson, B. F. and McLean, D., *Metal Science Journal*, Vol. 6, 1972, pp. 220–223.

[5] Wilson, R. N. and Peel, C. J., RAE Technical Report No. 73149, Royal Aircraft Establishment, Feb. 1974.

[6] Greenwood, G. W., *Philosophical Magazine*, Vol. 19, 1969, pp. 423–427.
[7] Langdon, T. G., *Philosophical Magazine*, Vol. 22, 1970, pp. 945–948.
[8] Heald, P. T. and Williams, J. A., *Philosophical Magazine*, Vol. 24, 1971, pp. 1215–1220.
[9] Kachanov, L. M., *Izvestiia Akademii Nauk*, No. 8, 1958, pp. 26–31.
[10] Rabatnov, Yn. N., *Creep Problems In Structural Members*, North-Holland, London, 1969.
[11] Pilkington, R., Hutchinson, D., and Jones, C. L., *Metal Science Journal*, Vol. 8, 1974, pp. 237–241.
[12] Harrison, C. B. and Sandor, G. N., *Engineering Fracture Mechanics*, Vol. 3, 1971, pp. 403–420.
[13] Robson, K., "Crack Growth in Two Carbon Steels at 450°C," International Conference on Creep Resistance in Steel, Verein Deutscher Eisenhuttenleute, May 1972.
[14] Siverns, M. J. and Price, A. T., *International Journal of Fracture*, Vol. 9, 1973, pp. 199–207.
[15] Neate, G. J. and Siverns, M. J., "The Application of Fracture Mechanics to Creep Crack Growth," International Conference on Creep and Fracture in Elevated Temperature Applications, Institution of Mechanical Engineers, Sept. 1973/April 1974.
[16] Ellison, E. G. and Walton, D., "Fatigue Creep and Cyclic Creep Crack Propagation in a 1 Cr-Mo-V Steel," Institution of Mechanical Engineers, Sept. 1973/April 1974.
[17] Haigh, J. R. and Richards, C. E., "Limits in the Application of Fracture Mechanics to High Temperature Fatigue Crack Propagation in a Turbine Steel," Institution of Mechanical Engineers, Sept. 1973/April 1974.
[18] Kenyon, J. L., Webster, G. A., Radon, J. C., and Turner, C. E., "An Investigation of the Application of Fracture Mechanics to Creep Cracking," Institution of Mechanical Engineers, Sept. 1973/April 1974.
[19] Kenyon, J. L., "Application of Linear Elastic Fracture Mechanics to Creep Cracking," Ph.D. thesis, University of London, 1975.
[20] Webster, G. A., "The Application of Fracture Mechanics to Creep Cracking," Conference on Mechanics and Physics of Fracture, Institute of Physics, Cambridge, England Jan. 1975.
[21] Cummings, W. M. and King, R. H., *Proceedings*, Institution of Mechanical Engineers, Vol. 185, 1970/71, pp. 285–299.
[22] Turner, C. E. and Webster, G. A., *International Journal of Fracture*, Vol. 10, Sept. 1974.
[23] Landes, J. D. and Begley, J. A., "A Fracture Mechanics Approach to Creep Crack Growth," Report 74-1E7-FESGT-P1, Westinghouse Research Laboratory, Dec. 1974.
[24] Hutchinson, J. W., *Journal of Mechanics and Physics of Solids*, Vol. 16, 1968, p. 13–31.
[25] Rice, J. R. and Rosengren, G. F., *Journal of Mechanics and Physics of Solids*, Vol. 16, 1968, p. 1–12.
[26] Hayes, D. J., "Some Applications of Elastic-Plastic Analysis to Fracture Mechanics," Ph.D. thesis, University of London, 1970.
[27] Boyle, E. F., "Calculations of Elastic and Plastic Crack Extension Forces," Ph.D. thesis, Queen's University, Belfast, 1972.
[28] Sumpter, J. D. G., "Elastic-Plastic Fracture Analysis and Design Using the Finite-Element Method," Ph.D. thesis, University of London, 1973/1974.
[29] Sumpter, J. D. G. and Turner, C. E., "Remarks on the Characterising Role of the *J* Contour Integral in Elastic-Plastic Fracture Studies," to be published in *Journal of Mechanical Engineering Science*, April 1976.
[30] Begley, J. A. and Landes, J. D. in *Fracture Toughness, ASTM STP 514*, American Society for Testing and Material, 1972, p. 1.
[31] Landes, J. D. and Begley, J. A. in *Fracture Toughness, ASTM STP 514*, American Society for Testing and Materials, 1972, p. 24.
[32] McClintock, F., *Fracture, An Advanced Treatise*, Vol. 3, H. Leibowitz, Ed., Academic Press, New York, 1971, Chapter 2.
[33] Rice, J. R., *Mathematical Analysis in the Mechanics of Fracture*, H. Liebowitz, Ed., Vol. 2, Academic Press, New York, 1968.

A COMPARISON OF METHODS OF CORRELATING CREEP CRACK GROWTH

K.M. Nikbin*, G.A. Webster*, C.E. Turner*

INTRODUCTION

With the use of materials under increasingly arduous conditions at elevated temperatures increasing attention has been devoted recently to establishing the circumstances under which cracks could be extended by creep. Some experimenters [1-5] have claimed that creep crack growth rate $\dot{a}$, can be expressed in terms of stress intensity factor, K, in the form;

$$\dot{a} = D\, K^{\beta} \tag{1}$$

whereas others [6-8] claim better correlations with the nett section stress, σ_{nett}, remaining on the uncracked ligament or with a reference stress [9-10].

i.e.
$$\dot{a} = F\, \sigma_{nett}^{\alpha} \tag{2}$$

where D, F, α and β are coefficients which in general will depend on the material and test temperature. Values of α and β reported range from 3 to 30 but for a particular material are usually close to the value of the stress sensitivity, n, of secondary creep strain rate, $\dot{\varepsilon}$, in the creep law,

$$\dot{\varepsilon} = C\, \sigma^{n} \tag{3}$$

where C is a temperature dependent material parameter. Generally, the data indicate that for relatively brittle materials creep crack growth rate correlates best with Eqn(1) and where substantial creep deformation is possible with Eqn.(2). This is not surprising as creep will cause redistribution of the elastic stresses at the crack tip and for sufficient creep ductility and high enough values of n the stresses at the crack tip will approach the nett section stress.

It may be expected that because of the non-linear nature of the creep law non-linear mechanics should be more relevant than linear mechanics. Recently a number of authors [11-15] have attempted to extend the J contour integral concept used to describe the stress and strain distributions around a crack tip in a non-linear elastic material to the creep circumstance. For a non-linear material the numerical value of J can be obtained from the expression

$$J = -\frac{1}{B_n}\frac{dU}{da} \tag{4}$$

where B_n is the thickness of the crack and U is potential energy. Although in the presence of plasticity J is no longer the energy potentially available to grow the crack its value can still be evaluated from Eqn.(4). For a non-linear material obeying the work hardening law,

$$\varepsilon = A\, \sigma^{n} \tag{5}$$

and for test pieces in which the primary mode of displacement is by bending it can be shown [14] that for a constant load P,

*Res.Stud., Sen.Lect.,Prof., Dept.Mech.Eng., Imperial College, London, S.W.7.

$$J = \frac{P}{B_n(n+1)} \frac{d\Delta}{da} \quad (6)$$

where Δ is the deflection at the loading points.

An analogy can be drawn between a material obeying the work-hardening law Eqn.(5) and one obeying the creep law Eqn.(3). It is possible to define a contour integral like J, in which ε is replaced by $\dot{\varepsilon}$, A by C and Δ by the displacement rate $\dot{\Delta}$, which will describe the state of stress and strain rate around a crack tip in a creeping material. This creep equivalent of the J contour integral has been called C* by Landes and Begley [12] and J by others [13,14] because it has the dimensions of J divided by time. It is not, however, dJ/dt and to avoid any possible ambiguity it will be called C* here. It can be evaluated in the same way as J, except with U replaced by a term $\dot{U}$ which has the dimensions of power,

i.e. $$C^* = -\frac{1}{B_n} \cdot \frac{d\dot{U}}{da} \quad (7)$$

$$= \frac{P}{B_n(n+1)} \frac{d\dot{\Delta}}{da} \quad (8)$$

when bending displacements dominate. Some success has been achieved in characterising creep crack growth with this parameter. In most instances approximate proportionality between $\dot{a}$ and C* was observed [12-15]. Since the state of strain rate around a crack tip varies according to [14].

$$\dot{\varepsilon} \alpha C(C^*/C)^{n/(n+1)} \quad (9)$$

this suggests that creep crack growth may be directly proportional to the strain rate at the crack tip as for most materials $n >> 1$ and $n/(n+1)$ will be close to unity. An attraction of the C* approach is that it is consistent with the K approach for creep brittle circumstances and with the nett section stress description when creep strains dominate and $n >> 1$.

In the previous investigation of C* by Nikbin et al [14] only one geometry of test piece was examined. In this paper, the work is extended to cover a range of geometries and a critical assessment is made of the K and C* characterisations.

EXPERIMENTS

The materials investigated were aluminium alloy RR58 and a ½%Cr, ½%Mo, 1/4%V steel. Details of their composition and heat treatment, and of the experimental procedure have been given previously [2,5,14]. In these series of experiments the aluminium alloy was tested at 150°C and the steel at 565°C. Displacements were measured automatically with a transducer and crack growth measurements made visually with the aid of a telescope. The geometries of test pieces used included the contoured DCB (C-DCB) geometry having a constant compliance with crack length used previously [2,5,14], parallel edge DCB (P-DCB), compact tension (CT) and double torsion (DT) shapes. Each specimen was provided with side grooves to control the direction of crack growth. Two thicknesses B, of the aluminium alloy and two thicknesses of steel samples, each with different notch depth ratios were tested. Compliance calibration experiments were performed on each geometry. Most of the creep cracking tests were carried out at constant load but in some cases load changes were made to investigate history effects.

RESULTS

The following general observations can be made concerning the creep crack growth against time curves for both materials. In most instances at constant load, crack growth rate decreased progressively with time (and crack length) in the constant K contoured DCB test-pieces (as was reported previously [2,5,14], decreased or remained approximately constant in the double torsion samples and increased in the remaining geometries. Comparisons of the data with K are shown in Figs.1 and 2. The symbols in brackets, which represent test-pieces with the same values of B and B_n but different shapes, show that although there is some correlation of the results within one geometry there is little agreement between the different geometries suggesting that K is not an adequate characterising parameter in these circumstances. This is emphasised by the observation that crack growth rate decreased and did not remain constant in the constant K tests although previously [5,14] this decelerating rate had been partially attributed to overageing. Comparisons of the results from specimens with the same geometry but different thicknesses and notch depth ratios indicate that at the same value of K crack growth rate increases with increase in thickness and side groove ratio suggesting that increase in degree of constraint increases creep crack growth rate.

Comparisons of the same data with analytical estimates (where these were possible) of C*, made in the same manner as reported by Nikbin et al [14] are shown in Figs.3 and 4. The values of n used to calculate C* were those which gave the best fit of Eqn.(3) to the creep data and were respectively for the aluminium alloy and steel 10 and 5. Although there is better correlation of the data than there is with K for individual geometries of the same thickness and notch depths there is again lack of agreement between specimens of different geometries particularly for the aluminium alloy. For the same geometry crack growth rate again increases with degree of constraint at constant C*.

DISCUSSION

Because of the satisfactory correlations of the cracking data for one geometry with C* shown in Figs.3 and 4, reasons for the discrepancies between geometries were sought. In making the analytical estimates of C* it was assumed that any elastic strains and displacements were small compared to the corresponding creep values. Checks of the experimental displacements however showed that this was not the case. In some instances the creep component of the deflection was found to be almost negligible and in no case was it appreciably greater than the elastic value. Consequently the assumption that creep strains were dominant is not valid.

An alternative approximate estimate of C* which avoids the necessity of making the above assumption and which enables values of C* to be obtained for a wider range of geometries than is possible analytically is as follows. The problem is one of estimating $d\dot{\Delta}/da$ in Eqn.(8).

For any circumstance where bending displacements dominate it may be expected that $\dot{\Delta}$ can be written as

$$\dot{\Delta} = \frac{1}{B} f(a) g(P) \qquad (10)$$

where f and g are functions. Therefore at constant load

$$\frac{d\dot{\Delta}}{da} = \frac{1}{B} d \frac{f(a)}{da} \cdot g(P) \qquad (11)$$

Furthermore, if f(a) can be approximated over a limited range of crack lengths by a simple power law function $f(a) = a^{\eta}$, Eqn.(11) becomes

$$\frac{d\dot{\Delta}}{da} = \eta \frac{\dot{\Delta}}{a} \qquad (12)$$

and

$$C^* = \frac{\eta P \dot{\Delta}}{a B_n (n + 1)}$$

Eqn.(12) provides an approximate method of estimating C* from the experimental data. It is analagous to estimating J for plasticity by the well known formula $J = 2U/B(W - a)$ for deep notch three point bend test pieces where U is work done in this instance. Provided η does not vary appreciably (by more than a factor of about 2) for different geometries C* will be proportional approximately to $P\dot{\Delta}/aB_n$.

Comparisons of the cracking data with $P\dot{\Delta}/aB_n$ are shown in Figs.5 and 6. These figures show satisfactory correlations for all test-piece geometries with the same values of B and B_n indicating that the lack of agreement on Figs.3 and 4 was probably caused by inadequate estimates of C*. No effect of constraint is apparent on Fig.5 for the aluminium alloy but Fig.6 shows that for the steel cracking rate is accelerated with increase in degree of constraint. The data on Figs.5 and 6 can be described satisfactorily by a straight line relationship giving

$$\dot{a} \alpha \left(\frac{P\dot{\Delta}}{aB_n}\right)^{\phi} \alpha \left[\frac{(n + 1)C^*}{\eta}\right]^{\phi} \alpha (C^*)^{\phi}$$

where $\phi = 0.86$ for the aluminium alloy and 0.82 for the steel. Both these values are close to the respective $n/(n + 1)$ values for each material adding weight to the possibility that creep crack growth rate may be directly proportional to the rate of straining at the crack tip, Eqn.(9), suggested earlier [14].

REFERENCES

1. NEATE, G.J., SIVERNS, M.J. Int.Conf. on Creep and Fracture in Elevated Temperature Applications. I.Mech.E., 1973/74.
2. KENYON, J.L., WEBSTER, G.A., RADON, J.C., TURNER, C.E. ibid.
3. ROBSON, K. Int.Conf. on Creep Resistance in Steel. Verein Deutscher Eisenhuttenleute, May 1972.
4. THORNTON, D.V. ibid.
5. KENYON, J.L. Ph.D.Thesis, University of London, 1975.
6. HARRISON, C.B., SANDOR, G.N. Eng.Fract.Mech., 3, 1971, 403.
7. NICHOLSON, R.D., FORMBY, C.L. Int.J.Fract., 11, 1975, 595.
8. NICHOLSON, R.D. Mat.Sci. and Eng., 22, 1976, 1.
9. HAIGH, J.R. Mat.Sci. and Eng., 20, 1975, 225.
10. WILLIAMS, A.J., PRICE, A.T. J.Eng.Mats. and Tech., 97, 1975, 214.
11. TURNER, C.E., WEBSTER, G.A. Int.J.Fract., 10, 1974, 455.
12. LANDES, J.D., BEGLEY, J.A. Westinghouse Res.Lab.Rep.74-1E7-FESGT-P1, 1974.
13. WEBSTER, G.A. Conf. on Mechanics and Physics of Fracture, Inst.Phys., Cambridge,January 1975.

14. NIKBIN, K.M., WEBSTER, G.A., TURNER, C.E. ASTM STP 601, 1976, 47.
15. HARPER, M. Ph.D.Thesis, University of Bristol, 1976.

FIGURE CAPTIONS

Fig.1 Correlation of creep crack growth with stress intensity factor K for aluminium alloy RR58 at 150°C.

Fig.2 Correlation of creep crack growth with stress intensity factor K for ½%Cr ½%Mo 1/4%V steel at 565°C.

Fig.3 Dependence of creep crack growth rate on analytical estimate of C* for aluminium alloy RR58 at 150°C.

Fig.4 Dependence of creep crack growth rate on analytical estimate of C* for ½%Cr ½%Mo 1/4%V steel at 565°C.

Fig.5 Comparison of creep crack growth rate with experimental estimate of C* for aluminium alloy RR58 at 150°C.

Fig.6 Comparison of creep crack growth rate with experimental estimate of C* for ½%Cr ½%Mo 1/4%V steel at 565°C.

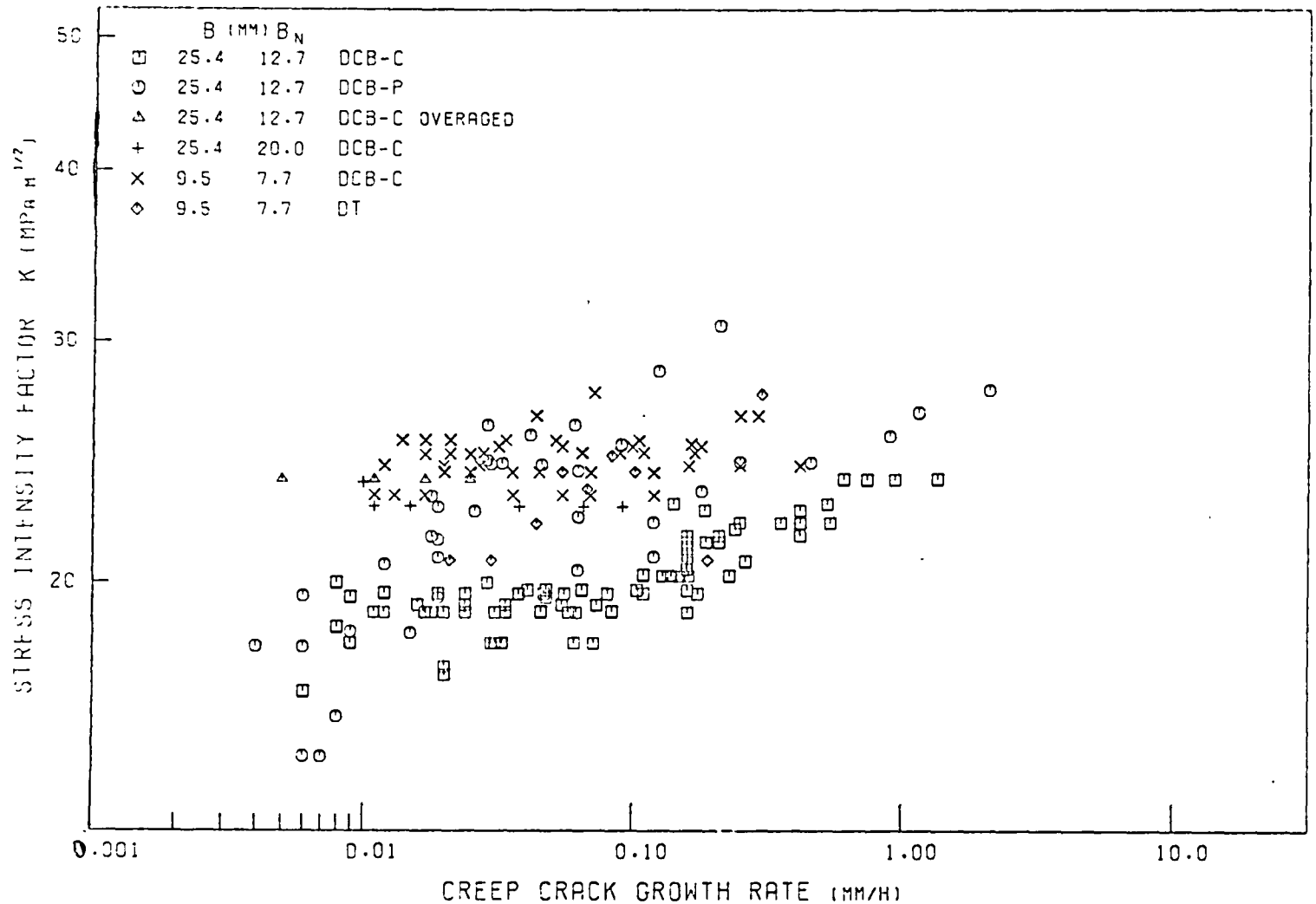

Fig.1 Correlation of creep crack growth with stress intensity factor K for aluminium alloy RR58 at 150°C.

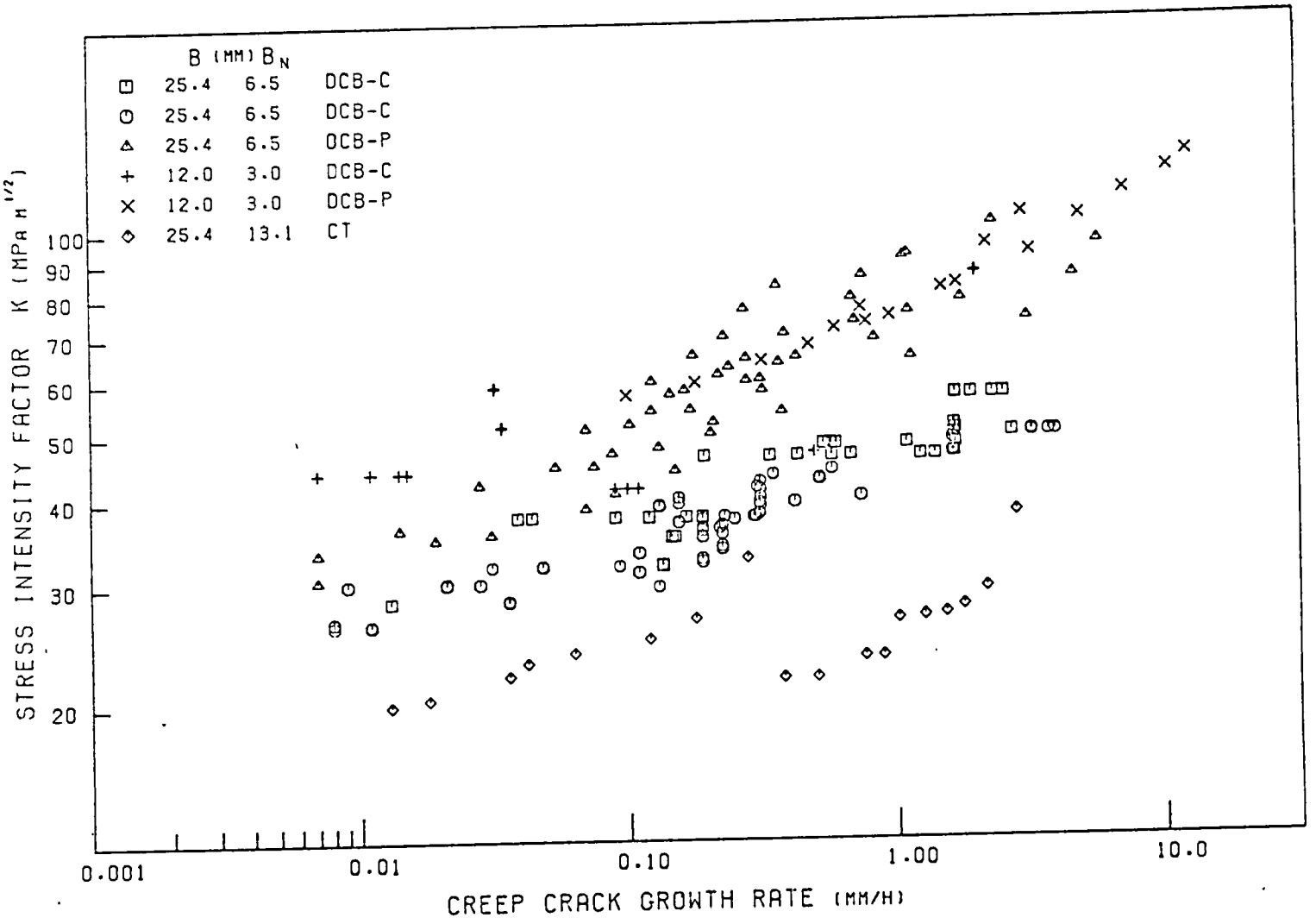

Fig.2 Correlation of creep crack growth with stress intensity factor K for ½%Cr ½%Mo 1/4%V steel at 565 °C.

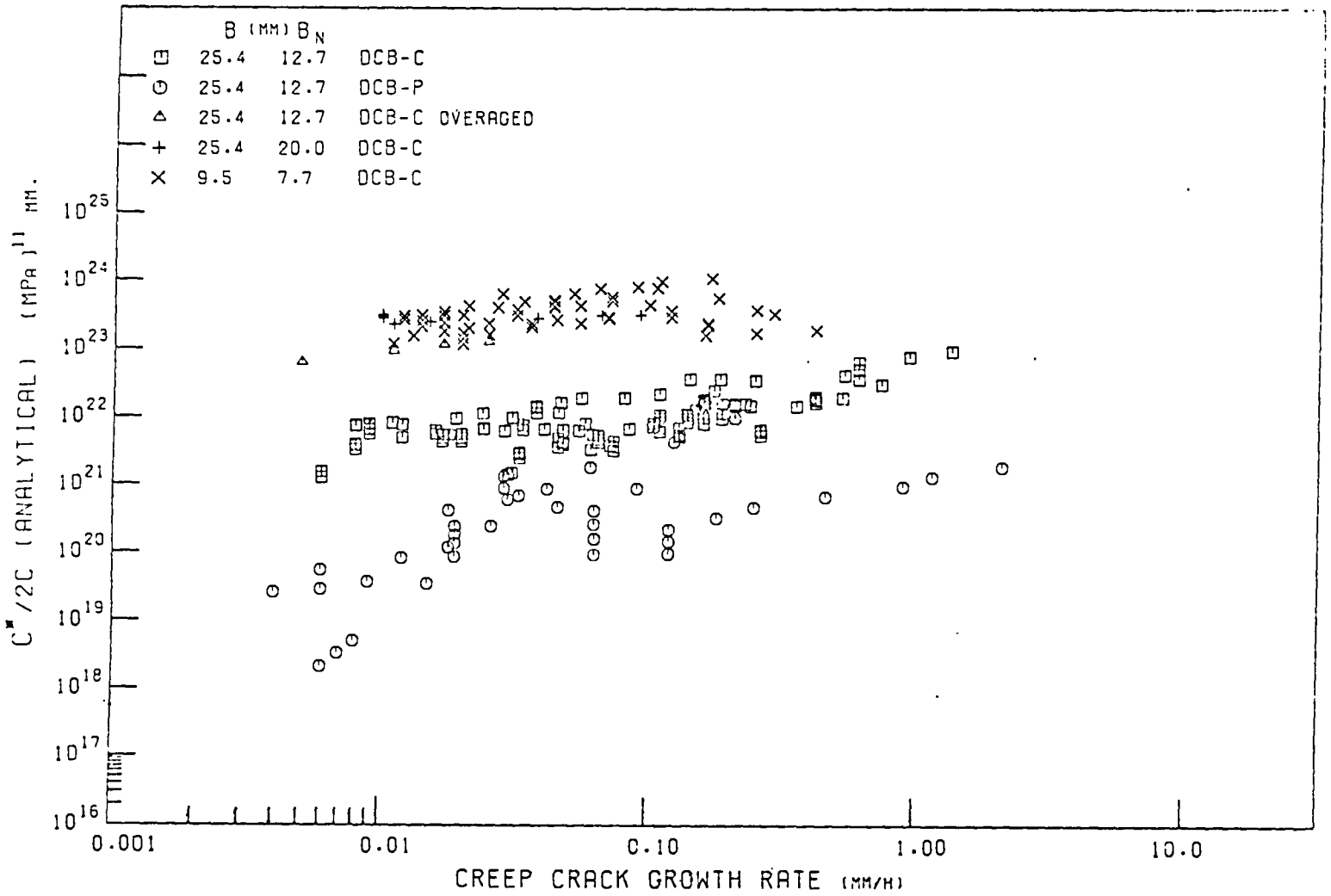

Fig.3 Dependence of creep crack growth rate on analytical estimate of C* for aluminium alloy RR58 at 150°C.

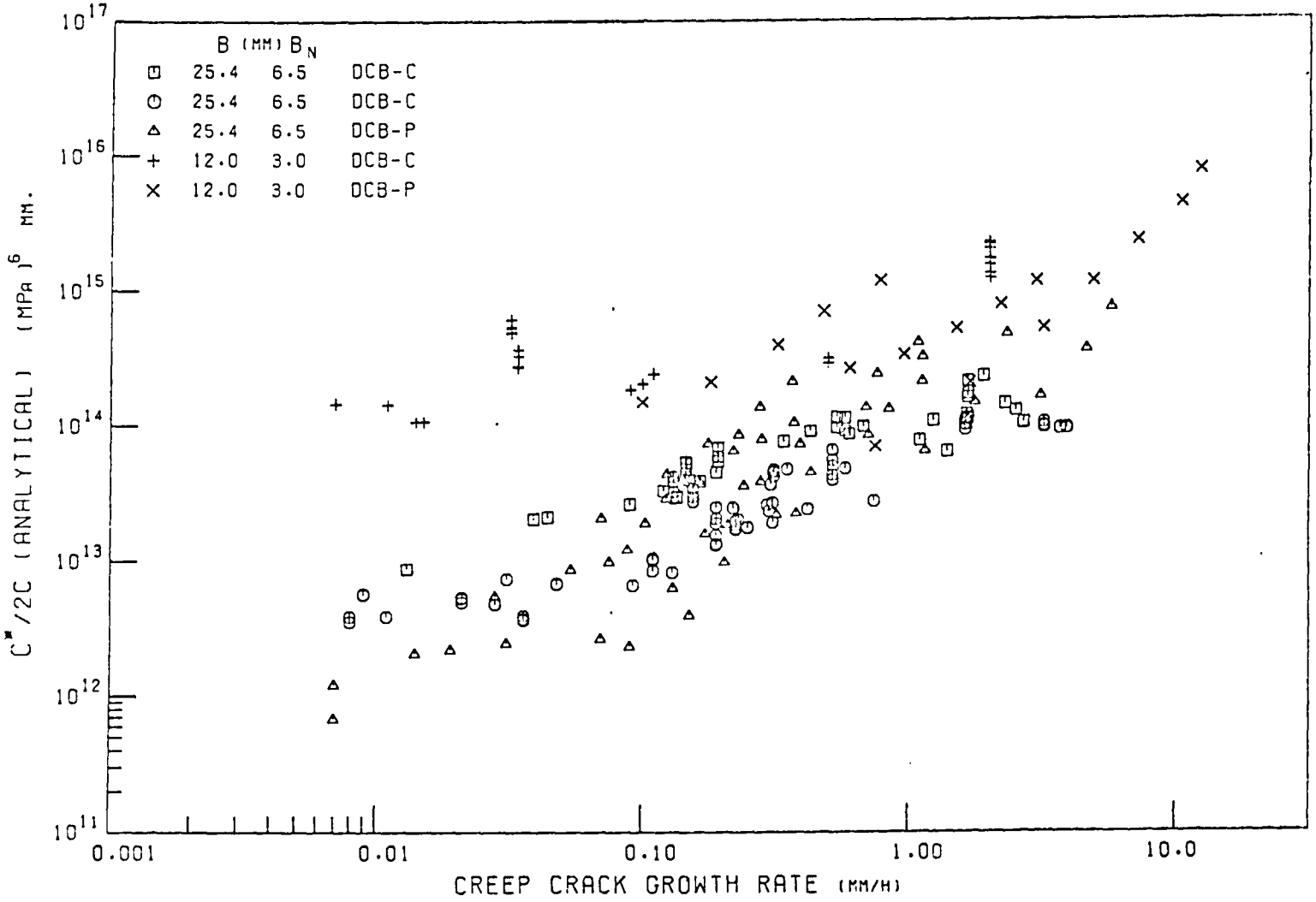

Fig.4 Dependence of creep crack growth rate on analytical estimate of C* for ½%Cr ½%Mo 1/4%V steel at 565°C.

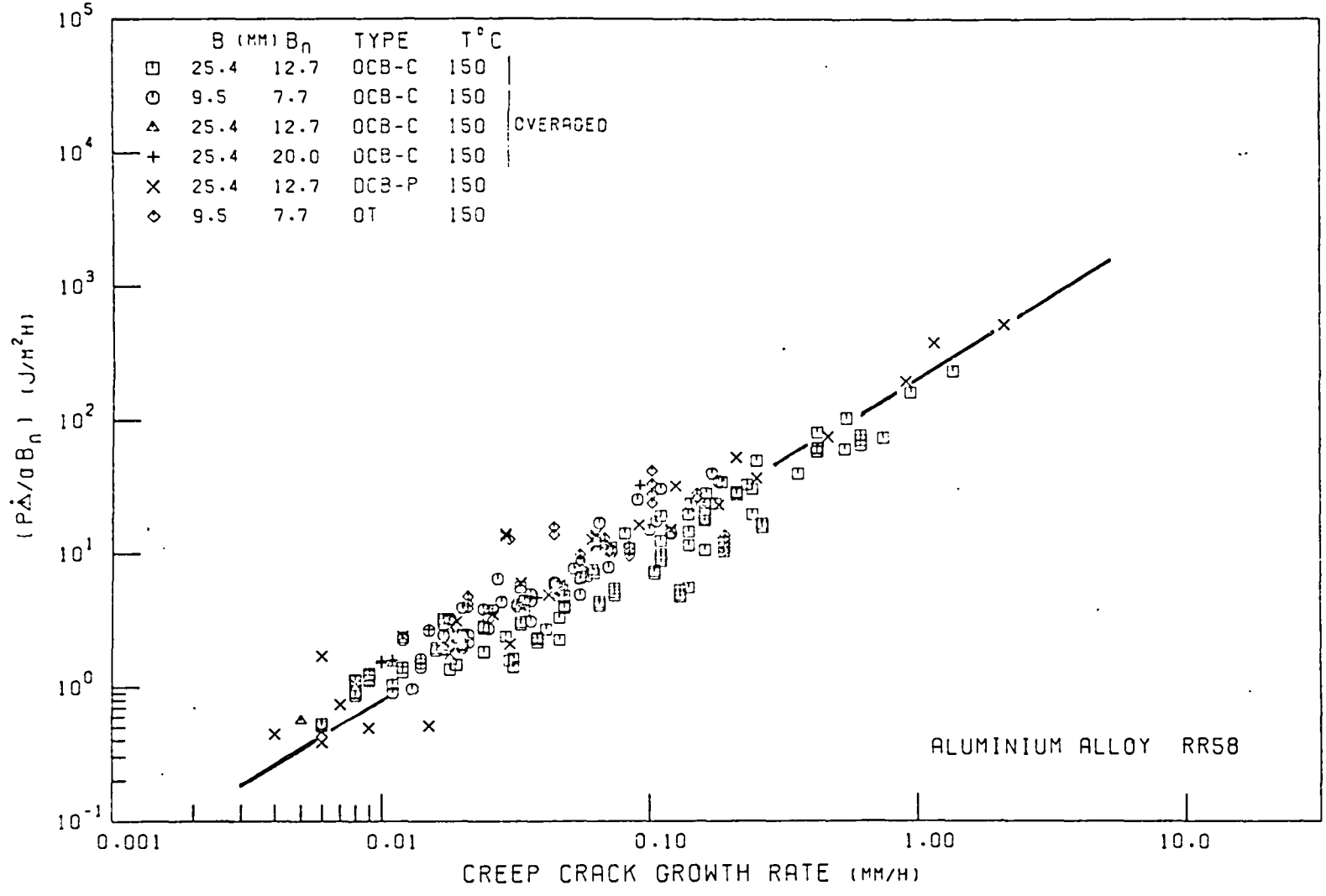

Fig.5 Comparison of creep crack growth rate with experimental estimate of C* for aluminium alloy RR58 at 150°C.

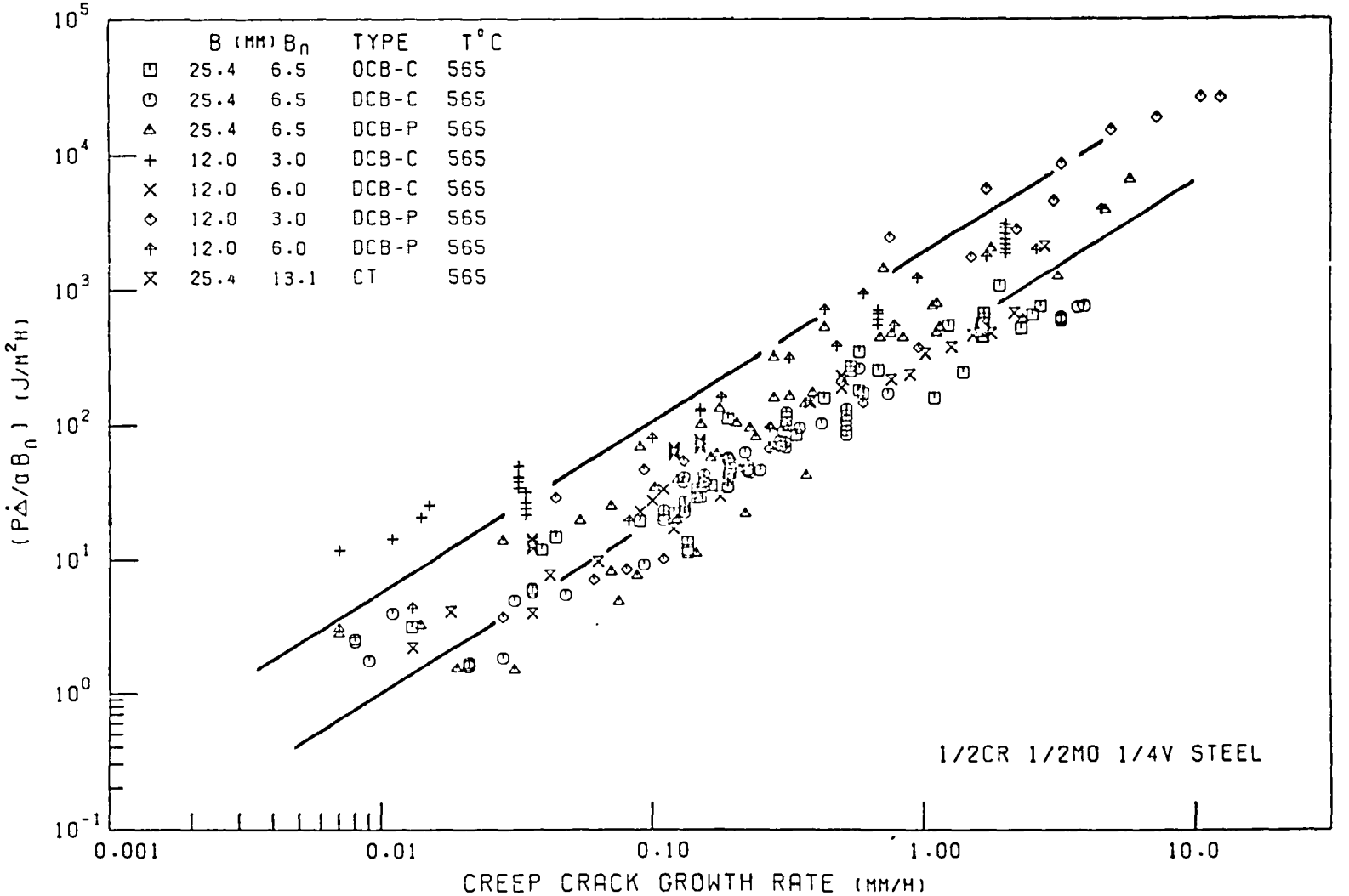

Fig.6 Comparison of creep crack growth rate with experimental estimate of C* for ½Cr ½Mo 1/4V steel at 565°C.